

**Ongoing Face Recognition
Vendor Test (FRVT)**
Part 1: Verification

Patrick Grother
Mei Ngan
Kayee Hanaoka
*Information Access Division
Information Technology Laboratory*

This publication is available free of charge from:
<https://www.nist.gov/programs-projects/face-recognition-vendor-test-frvt-ongoing>

2021/06/28

ACKNOWLEDGMENTS

The authors are grateful to staff in the NIST Biometrics Research Laboratory for infrastructure supporting rapid evaluation of algorithms.

DISCLAIMER

Specific hardware and software products identified in this report were used in order to perform the evaluations described in this document. In no case does identification of any commercial product, trade name, or vendor, imply recommendation or endorsement by the National Institute of Standards and Technology, nor does it imply that the products and equipment identified are necessarily the best available for the purpose.

INSTITUTIONAL REVIEW BOARD

The National Institute of Standards and Technology's Research Protections Office reviewed the protocol for this project and determined it is not human subjects research as defined in Department of Commerce Regulations, 15 CFR 27, also known as the Common Rule for the Protection of Human Subjects (45 CFR 46, Subpart A).

FRVT STATUS

This report is a draft NIST Interagency Report, and is open for comment. It is the twenty first edition of the report since the first was published in June 2017. Prior editions of this report are maintained on the FRVT [website](#), and may contain useful information about older algorithms and datasets no longer used in FRVT.

FRVT remains open: All [four tracks](#) of the FRVT are open to new algorithm submissions.

Changes since May 21, 2021:

- ▷ We have added results for first algorithms from six new developers: Alice Biometrics, BOE Technology Group, Fincore, Neosecu, Sodec App, and Yuntu Data and Technology.
- ▷ We have added results for new algorithms from seven returning developers: Incode Technologies, HyperVerge, Mobbeel Solutions, Guangzhou Pixel Solutions, Remark Holdings, Sensetime, and Vietnam Posts and Telecommunications Group.
- ▷ We have retired results for four algorithms per our policy to only list results for two algorithms per developer. Results for retired algorithms appear in prior versions of this report in the [archive](#).

Changes since April 26, 2021:

- ▷ We have added results for first algorithms from five new developers: Ekin Smart City Technologies, Suprema ID, Tripleize, Taiwan-Certificate Authority, and Vision Intelligence Center of Meituan.
- ▷ We have added results for new algorithms from eight returning developers: ID3 Technology, Imagus Technology, Momentum Digital, N-Tech Lab, NSENSE, Shanghai Jiao Tong University, Vision-Box, and Yuan High-Tech Development
- ▷ We have retired results for seven algorithms per our policy to only list results for two algorithms per developer. Results for retired algorithms appear in prior versions of this report in the [archive](#).

Changes since April 16, 2021:

- ▷ We have added results for first algorithms from three new developers: Quantasoft, Rendip, and NEO Systems.
- ▷ We have added results for new algorithms from four returning developers: 3Divi, Realnetworks, Veridas Digital Authentication Solutions, and Universidade de Coimbra.
- ▷ We have retired results for three algorithms per our policy to only list results for two algorithms per developer. Results for retired algorithms appear in prior versions of this report in the [archive](#).

Changes since March 5, 2021:

- ▷ We have added results for first algorithms from six new developers: 20Face, Beijing DeepSense Technologies, BitCenter UK, Enface, FaceTag, InsightFace AI, Line Corporation, Lema Labs, Nanjing Kiwi Network Technology, Omnidarde, Regula Forensics, and Suprema.
- ▷ We have added results for new algorithms from ten returning developers: CloudSmart Consulting, Dermalog, GeoVision, Neurotechnology, Panasonic R+D Center Singapore, Samsung S1, Securif AI, Trueface.ai, Vigilant Solutions, and Visidon.

- ▷ We have retired results for ten algorithms per our policy to only list results for two algorithms per developer. Results for retired algorithms appear in prior versions of this report in the [archive](#).

Changes since March 5, 2021:

- ▷ We have added results for first algorithms from six new developers: Ajou University, AuthenMetric, Code Everest, Corsight, Papilon Savunma, and NHN Corp
- ▷ We have added results for new algorithms from seven returning developers: Alchera, Deepglint, Fiber-home Telecommunication Technologies, Kakao Enterprise, Kookmin University, Megvii/Face++, and NotionTag Technologies.
- ▷ We have updated many of the hyperlinked HTML report-cards to include seven figures on demographic dependence. Figures of this kind first appeared, and are documented in, the December 2019 document, [NIST Interagency Report 8280](#) on demographic differentials in face recognition. The figures quantify false negative dependence on demographics using “visa-border” comparisons, and false positive dependence using comparisons of “application” photos that uniformly of quality and similar to visa photos.

Changes since January 19, 2021:

- ▷ We have added results for first algorithms from three new developers: IVA Cognitive, Mobbeel, and MoreDian Technology.
- ▷ We have added results for new algorithms from returning developers: Ability Enterprise - Andro Video, ACI Software, Adera Global, AnyVision, BioID Technologies, China Electronics Import-Export, Cognitec Systems, Fujitsu Research and Development Center, Glory, Guangzhou Pixel Solutions, Hengrui AI Technology, Incode Technologies, Intel Research, iQIYI, Mobai, Oz Forensics, Paravision, VisionLabs, and Xforward AI Technology.
- ▷ We have added a new “resources” tab to the main [webpage](#). It includes sortable columns for data related to speed, model size, storage, and memory consumption.
- ▷ We have retired results for 13 algorithms per our policy to only list results for two algorithms per developer. Results for retired algorithms appear in prior versions of this report in the [archive](#).

Changes since December 18, 2020:

- ▷ This report adds results for first algorithms from four developers: Herta Security, Irax AI, Shenzhen Univeristy-Macau University of Science and Technology, and Vietnam Posts and Telecommunications Group. See Table 5 for more information.
- ▷ The report also includes results for thirteen developers who have previously submitted algorithms: Bresee Technology, Canon (previously Canon Information Technology (Beijing)), Cyberlink, CSA IntelliCloud Technology, Dahua Technology, ID3 Technology, Imagus Technology (Vixvization), Moontime Smart Technology, N-Tech Lab, Thales Cogent, Veridas Digital Authentication Solutions, Vocord, and Yuan High-Tech Development.
- ▷ We have retired results for ten algorithms per our policy to only list results for two algorithms per developer. Results for retired algorithms appear in prior versions of this report in the [archive](#).

Changes since October 9, 2020:

- ▷ This report adds results for first algorithms from ten developers: BitCenter UK, CloudSmart Consulting, Cubox, Institute of Computing Technology, Naver Corp, Minivision, NSENSE Corp, Viettel Group, Visage Technologies, and Xiamen University. See Table 5 for more information.
- ▷ The report also includes results for eighteen developers who have previously submitted algorithms: ADVANCE.AI, Awidit Systems, Chosun University, Dermalog, GeoVision, ICM Airport Technics, Idemia, Institute of Information Technologies, Kakao Enterprise, Neurotechnology, Panasonic R+D Center Singapore, Rank One Computing, Sensetime Group, Shanghai Jiao Tong University, TigerIT Americas LLC, Vigilant Solutions, Winsense, and YooniK
- ▷ We have retired results for twelve algorithms per our policy to only list results for two algorithms per developer. Results for retired algorithms appear in prior versions of this report in the [archive](#).

Changes since September 18, 2020:

- ▷ This report adds results for first algorithms from five developers: Aigen, Cortica, Kookmin University, Securif AI and Vinai.
- ▷ The report also includes results for three developers who have previously submitted algorithms: Fujitsu Laboratories, Hengrui AI, and X-Forward AI.
- ▷ In the per-algorithm report-cards linked from tables and the main webpage, we have added a chart to showing reduction in error rates over the course of FRVT i.e. from 2017 onwards for all algorithms supplied by that developer. Similarly we have added a chart showing error rate reductions for our test of protective face mask verification.
- ▷ We plan to continue evaluating algorithms on various mask datasets. We hold that algorithms should be capable of detecting masks and verifying identity of all combinations of masked and unmasked faces. We have accordingly increased the amount of time allowed to extract those features from 1.0 to 1.5 seconds.

Changes since August 25, 2020:

- ▷ This report adds results for first algorithms from eight new developers. Akurat Satu Indonesia, Cybercore, Decatur Industries, Innef Labs, Satellite Innovation/Eocortex, Expasoft, and Mobai.
- ▷ The report includes results for seven developers who have previously submitted algorithms: 3Divi, BioID Technologies, Incode Technologies, Innovatrics, iSAP Solution, Synology, and Tevian.
- ▷ We have retired results for five algorithms per our policy to only list results for two algorithms per developer. Results for retired algorithms appear in prior versions of this report in the [archive](#).

Changes since July 27, 2020:

- ▷ We have introduced per-algorithm report sheets. These are HTML documents linked from the accuracy tables in this report (i.e. Table 21) and on the FRVT 1:1 [homepage](#). The sheets contain interactive graphics allowing, for example, mouseover exploration of FNMR(T) and FMR(T). Some of their content had previously appeared in this document.
- ▷ This report adds results for algorithms from six new developers. ACI Software, Bresee Technology, Fiberhome Telecommunication Technologies, Imageware Systems, Oz Forensics, and Pensees.
- ▷ The report includes results for thirteen developers who have previously submitted algorithms: Canon Information Technology (Beijing), Cyberlink, Dahua Technology, Gorilla Technology, ID3 Technology, Intel Research Group, iQIYI Inc, Momentum Digital, Netbridge Technology, Tech5 SA, Shenzhen AiMall Tech, Vigilant Solutions, and VisionLabs.

- ▷ We have retired results for nine algorithms per our policy to only list results for two algorithms per developer. Results for retired algorithms appear in prior versions of this report in the [archive](#).

Changes since May 18, 2020:

- ▷ The report is the first FRVT update since the pandemic closed it from March to June 2020.
- ▷ This report includes results for algorithms from nine new developers: GeoVision Inc, Su Zhou NaZhi-TianDi Intelligent Technology, YooniK, AYF Technology, PXL Vision AG, Yuan High-Tech Development, Beihang University-ERCACAT, ICM Airport Technics, and Staqu Technologies
- ▷ This report includes results for algorithms from 15 returning developers Acer Incorporated, Antheus Technologia, Chosun University, Chunghwa Telecom, Idemia, Moontime Smart Technology, Neurotechnology, Guangzhou Pixel Solutions, Panasonic R+D Center Singapore, Rank One Computing, Scanovate, Shanghai Universiy - Shanghai Film Academy, Synesis, Trueface.ai, and Veridas Digital Authentication Solutions
- ▷ We have retired results for ten algorithms per our policy to only list results for two algorithms per developer. Results for retired algorithms appear in prior versions of this report in the [archive](#).
- ▷ We separated timing and other resource consumption from the main participation table. The new Table [13](#) includes template generation durations for four kinds of images, not just mugshots.
- ▷ We have published a separate report, [NIST Interagency Report 8311](#) on accuracy of pre-pandemic algorithms on subjects wearing face masks. We plan to track improvements in accuracy on masked images going forward. In particular, we invite submission of algorithms that can detect whether a person is wearing a mask, extract features from the full face or the exposed periocular region, and do appropriate comparison. We do not intend to evaluate algorithms that assume 100% of images will be of masked individuals.

Changes since March 25, 2020:

- ▷ The report is a maintenance release - it does not add any new algorithms, and FRVT has been closed to new algorithms since mid March 2020.
- ▷ We modified the primary accuracy summary, Table [21](#), as follows:
 - ▷▷ For visa images, the column for FNMR at FMR = 0.0001 has been removed. The visa images are so highly controlled that the error rates for the most accurate algorithms are dominated by false rejection of very young children and by the presence of a few noisy greyscale images. For now, two visa columns remain: FNMR at $FMR = 10^{-6}$ and, for matched covariates, FNMR at $FMR = 10^{-4}$.
 - ▷▷ We have inserted a new column labelled "BORDER" giving accuracy for comparison of moderately poor webcam border-crossing photos that exhibit pose variations, poor compression, and low contrast due to strong background illumination. The accuracies are the worst from all cooperative image datasets used in FRVT.
- ▷ Accordingly, we updated the failure-to-template rates in Table [27](#).
- ▷ We withdrew a figure showing how false matches are concentrated in certain visa images used in cross-comparison, because it didn't attempt to include demographic information.

Changes since February 27, 2020:

- ▷ The report adds results algorithms from two new developers: Beijing Alleyes Technology, and the Chinese University of Hong Kong. Results for newly submitted algorithms from two other developers will appear in the next report.
- ▷ The report adds results for algorithms from thirteen returning developers: ASUSTek Computer, Aware, Cyberlink Corp, Gorilla Technology, Innovative Technology, Kakao Enterprise, Lomonosov Moscow State University, Panasonic R+D Center Singapore, Shenzhen AiMall Technology, Shenzhen Intellifusion Technologies, Synology, Tech5 SA, and Via Technologies.
- ▷ Per policy to only list results for two algorithms per developer, we have dropped results for algorithms from Aware, Cyberlink, Gorilla Technology, Kakao Enterprise, Lomonosov Moscow State University, Panasonic R+D Center Singapore, and Tech5 SA.

Changes since January 20, 2020:

- ▷ The report adds results for five new developers: Ability Enterprise (Andro Video), Chosun University, Fujitsu Research and Development Center, University of Coimbra, and Xforward AI Technology.
- ▷ The report adds results for algorithms from six returning developers: AlphaSSTG, Incode Technologies, Kneron, Shanghai Jiao Tong University, Vocord, and X-Laboratory.
- ▷ We have corrected template comparison timing numbers for algorithms submitted September 2019 to January 2020. The values reported previously were slower due to a software bug.
- ▷ We have dropped results for algorithms from Vocord and Incode per policy to only list results for two algorithms per developer.
- ▷ The [FRVT 1:1 homepage](#) has been updated with latest accuracy results.
- ▷ The [FRVT 1:N homepage](#) now includes an update to the September 2019 NIST Interagency Report 8271. The new report adds results for one-to-many search algorithms submitted to NIST from June 2019 to January 2020.

Changes since January 6, 2020:

- ▷ Section 2 has been updated to better describe the Visa and Border images. The caption for Table 21 has been updated to better relate the accuracy values to particular image comparisons.
- ▷ The report adds results for five new developers: Acer, Advance.AI, Expasoft, Netbridge Technology, and Videmo Intelligent Videoanalyse.
- ▷ The report adds results for algorithms from 7 returning developers: China Electronics Import-Export Corp, Intel Research Group, ITMO University, Neurotechnology, N-Tech Lab, Rokid, and VisionLabs.
- ▷ We have dropped results from this edition of the report per policy to only list results for two algorithms per developer: N-Tech Lab, Neurotechnology, ITMO, Visionlabs, and CEIEC.
- ▷ The [FRVT homepage](#) has been updated with latest accuracy results.

Changes since November 11, 2019:

- ▷ Table 13 has been updated to include runtime memory usage. This is the first time such a quantity has been reported. The value is the peak size of the resident set size logged during enrollment of single images.
- ▷ We have migrated summary results table to a new platform that supports sortable tables:
<https://pages.nist.gov/frvt/html/frvt11.html>

- ▷ The report adds results for four new developers: Antheus Technologia, BioID Technologies SA, Canon Information Tech. (Beijing), Samsung S1 (listed in the tables as S1), and Taiwan AI Labs.
- ▷ The report adds results for algorithms from 13 returning developers: Anke Investments, Chunghwa Telecom, Deepglint, Institute of Information Technologies, iQIYI, Kneron, Ping An Technology, Paravision, KanKan Ai, Rokid Corporation, Shanghai Universiy - Shanghai Film Academy, Veridas Digital Authentication Solutions, and Videometrics Technology.
- ▷ We have dropped results from this edition of the report per policy to only list results for two algorithms per developer: remarkai-000, veridas-001, sensetime-001, iit-000, anke-003, and everai-002. Results for these are available in prior editions of this report linked from the FRVT page.
- ▷ We issued [NIST Interagency Report 8280: FRVT Part 3: Demographics](#) on 2019-12-19. It includes results for many of the algorithms covered by this report.

Changes since October 16, 2019:

- ▷ The report adds results for ten new developers: Ai-Union Technology, ASUSTek Computer, DiDi ChuXing Technology, Innovative Technology, Luxand, MVision, Pyramid Cyber Security + Forensic, Scanovate, Shenzhen AiMall Tech, and TUPU Technology.
- ▷ The report adds results for 12 returning developers: CTBC Bank Glory Gorilla Technology Guangzhou Pixel Solutions Imagus Technology Incode Technologies Lomonosov Moscow State University Rank One Computing Samtech InfoNet Shanghai Ulucu Electronics Technology Synesis, and Winsense.
- ▷ We have dropped results from this edition of the report per policy to only list results for two algorithms per developer: glory-000, gorilla-002, incode-003, rankone-006, and synesis-004.
- ▷ Results for five recently submitted algorithms will appear in the next report.

Changes since September 11, 2019:

- ▷ The report adds results for five new participants: Awidit Systems (Awiros), Momemtum Digital (Sertis), Trueface AI, Shanghai Jiao Tong University, and X-Laboratory.
- ▷ The reports adds results for five new algorithms from returning developers: Cyberlink, Hengrui AI Technology, Idemia, Panasonic R+D Singapore, and Tevian. This causes three algorithm, to be de-listed from the report per policy to list results for two algorithms per developer.

Changes since July 31 2019:

- ▷ The HTML table on the [FRVT 1:1 homepage](#) has been updated to include a column for cross-domain Visa-Border verification. Results for this new dataset appeared in the July 29 report under the name "CrossEV" - these are now renamed "Visa-Border".
- ▷ The [FRVT 1:1 homepage](#) lists algorithms according to lowest mean rank accuracy:

$$\begin{aligned} & \text{Rank(FNMR}_{\text{VISA}}\text{ at FMR = 0.000001}) + \\ & \text{Rank(FNMR}_{\text{VISA-BORDER}}\text{ at FMR = 0.000001}) + \\ & \text{Rank(FNMR}_{\text{MUGSHOT}}\text{ at FMR = 0.00001 after 14 years}) + \\ & \text{Rank(FNMR}_{\text{WILD}}\text{ at FMR = 0.00001}) \end{aligned}$$

This ordering rewards high accuracy across all datasets.
- ▷ The main results in Table 21 is now in landscape format to accomodate extra columns for the Visa-Border set, and mugshot comparisons after at least 12 years.
- ▷ The report adds results for nine new participants: Alpha SSTG, Intel Research, ULSee, Chungwa Telecon, iSAP Solution, Rokid, Shenzhen EI Networks, CSA Intellicloud, Shenzhen Intellifusion Technologies.

- ▷ The report adds results for six new algorithms from returning developers: Innovatrics, Dahua Technology, Tech5 SA, Intellivision, Nodeflux and Imperial College, London. One algorithm, from Imperial has been retired, per policy to list results for two algorithms per developer.
- ▷ The cross-country false match rate heatmaps have been replotted to reveal more structure by listing countries by region instead of alphabetically.
- ▷ The next version of this report will be posted around October 18, 2019.

Changes since July 3 2019:

- ▷ The HTML table on the [FRVT 1:1 homepage](#) has been updated to list the 20 most accurate developers rather than algorithms, choosing the most accurate algorithm from each developer based on visa and mugshot results. Also, the algorithms are ordered in terms of lowest mean rank across mugshot, visa and wild datasets, rewarding broad accuracy over a good result on one particular dataset.
- ▷ This report includes results for a new dataset - see the column labelled "visa-border" in Table 5. It compares a new set of high quality visa-like portraits with a set webcam border-crossing photos that exhibit moderately poor pose variations and background illumination. The two new sets are described in sections [2.3](#) and [2.4](#). The comparisons are "cross-domain" in that the algorithm must compare "visa" and "wild" images. Results for other algorithms will be added in future reports as they become available.
- ▷ This report adds results for algorithms from 9 developers submitted in early July 2019. These are from 3DiVi, Camvi, EverAI-Paravision, Facesoft, Farbar (F8), Institute of Information Technologies, Shanghai U. Film Academy, Via Technologies, and Ulucu Electronics Tech. Six of these are new participants.
- ▷ Several other algorithms have been submitted and are being evaluated. Results will be released in the next report, scheduled for September 5. That report will include results for new datasets.
- ▷ Older algorithms from Everai, Camvi and 3DiVi, have been retired, per the policy to list only two algorithms per developer.

Changes since June 20 2019:

- ▷ This report adds results for algorithms from 18 developers submitted in early June 2019. These are from CTBC Bank, Deep Glint, Thales Cogent, Ever AI Paravision, Gorilla Technology, Imagus, Incode, Kneron, N-Tech Lab, Neurotechnology, Notiontag Technologies, Star Hybrid, Videogenetics, Vigilant Solutions, Winsense, Anke Investments, CEIEC, and DSK. Nine of these are new participants.
- ▷ Several other algorithms have been submitted and are being evaluated. Results will be released in the next report, scheduled for August 1.
- ▷ Older algorithms from Everai, Thales Cogent, Gorilla Technology, Incode, Neurotechnology, N-Tech Lab and Vigilant Solutions have been retired, per the policy to list only two algorithms per developer.

Changes since April 2019:

- ▷ This report adds results for nine algorithms from nine developers submitted in early June 2019. These are from Tencent Deepsea, Hengrui, Kedacom, Moontime, Guangzhou Pixel, Rank One Computing, Synesis, Sensetime and Vocord.
- ▷ Another 23 algorithms have been submitted and are being evaluated. Results will be released in the next report, scheduled for July 3.
- ▷ Older algorithms for Rank One, Synesis, and Vocord have been retired, per the policy to list only two algorithms per developer.

Changes since February 2019:

- ▷ This report adds results for 49 algorithms from 42 developers submitted in early March 2019.

- ▷ This report omits results for algorithms that we retired. We retired for three reasons: 1. The developer submitted a new algorithm, and we only list two. 2. The algorithm needs a GPU, and we no longer allow GPU-based algorithms. 3. Inoperable algorithms.
- ▷ Previous results for retired algorithms are available in older editions of this report linked [here](#).
- ▷ The mugshot database used from February 2017 to January 2019 has been replaced with an extract of the mugshot database documented in NIST Interagency Report 8238, November 2018. The new mugshot set is described in section [2.5](#) and is adopted because:
 - ▷▷ It has much better identity label integrity, so that false non-match rates are substantially lower than those reported in FRVT 1:1 reports to date - see Figure [66](#).
 - ▷▷ It includes images collected over a 17 year period such that ageing can be much better characterized - - see Figure [243](#).
- ▷ Using the new mugshot database, Figure [243](#) shows accuracy for four demographic groups identified in the biographic metadata that accompanies the data: black females, black males, white females and white males.
- ▷ The report adds Figure [17](#) with results for the twenty human-difficult pairs used in the May 2018 paper *Face recognition accuracy of forensic examiners, superrecognizers, and face recognition algorithms* by Phillips et al. [[1](#)].
- ▷ The report uses an update to the wild image database that corrects some ground truth labels.
- ▷ Some results for the child exploitation database are not complete. They are typically updated less frequently than for other image sets.

Contents

ACKNOWLEDGMENTS	1
DISCLAIMER	1
INSTITUTIONAL REVIEW BOARD	1
1 METRICS	40
1.1 CORE ACCURACY	40
2 DATASETS	41
2.1 CHILD EXPLOITATION IMAGES	41
2.2 VISA IMAGES	41
2.3 APPLICATION IMAGES	41
2.4 BORDER CROSSING IMAGES	42
2.5 MUGSHOT IMAGES	42
2.6 WILD IMAGES	42
3 RESULTS	43
3.1 TEST GOALS	43
3.2 TEST DESIGN	43
3.3 FAILURE TO ENROLL	46
3.4 RECOGNITION ACCURACY	52
3.5 GENUINE DISTRIBUTION STABILITY	246
3.5.1 EFFECT OF BIRTH PLACE ON THE GENUINE DISTRIBUTION	246
3.5.2 EFFECT OF AGEING	274
3.5.3 EFFECT OF AGE ON GENUINE SUBJECTS	295
3.6 IMPOSTOR DISTRIBUTION STABILITY	324
3.6.1 EFFECT OF BIRTH PLACE ON THE IMPOSTOR DISTRIBUTION	324
3.6.2 EFFECT OF AGE ON IMPOSTORS	328

List of Tables

1 PARTICIPANT INFORMATION	17
2 PARTICIPANT INFORMATION	18
3 PARTICIPANT INFORMATION	19
4 PARTICIPANT INFORMATION	20
5 PARTICIPANT INFORMATION	21
6 ALGORITHM SUMMARY	22
7 ALGORITHM SUMMARY	23
8 ALGORITHM SUMMARY	24
9 ALGORITHM SUMMARY	25
10 ALGORITHM SUMMARY	26
11 ALGORITHM SUMMARY	27
12 ALGORITHM SUMMARY	28
13 ALGORITHM SUMMARY	29
14 FALSE NON-MATCH RATE	30
15 FALSE NON-MATCH RATE	31
16 FALSE NON-MATCH RATE	32
17 FALSE NON-MATCH RATE	33
18 FALSE NON-MATCH RATE	34
19 FALSE NON-MATCH RATE	35
20 FALSE NON-MATCH RATE	36

21	FALSE NON-MATCH RATE	37
22	FAILURE TO ENROL RATES	46
23	FAILURE TO ENROL RATES	47
24	FAILURE TO ENROL RATES	48
25	FAILURE TO ENROL RATES	49
26	FAILURE TO ENROL RATES	50
27	FAILURE TO ENROL RATES	51

List of Figures

1	PERFORMANCE SUMMARY: FNMR VS. TEMPLATE SIZE TRADEOFF	38
2	PERFORMANCE SUMMARY: FNMR VS. TEMPLATE TIME TRADEOFF	39
3	EXAMPLE IMAGES	43
(A)	VISA	43
(B)	MUGSHOT	43
(C)	WILD	43
(D)	BORDER	43
4	PERFORMANCE ON 20 HUMAN-DIFFICULT PAIRS	53
5	PERFORMANCE ON 20 HUMAN-DIFFICULT PAIRS	54
6	PERFORMANCE ON 20 HUMAN-DIFFICULT PAIRS	55
7	PERFORMANCE ON 20 HUMAN-DIFFICULT PAIRS	56
8	PERFORMANCE ON 20 HUMAN-DIFFICULT PAIRS	57
9	PERFORMANCE ON 20 HUMAN-DIFFICULT PAIRS	58
10	PERFORMANCE ON 20 HUMAN-DIFFICULT PAIRS	59
11	PERFORMANCE ON 20 HUMAN-DIFFICULT PAIRS	60
12	PERFORMANCE ON 20 HUMAN-DIFFICULT PAIRS	61
13	PERFORMANCE ON 20 HUMAN-DIFFICULT PAIRS	62
14	PERFORMANCE ON 20 HUMAN-DIFFICULT PAIRS	63
15	PERFORMANCE ON 20 HUMAN-DIFFICULT PAIRS	64
16	PERFORMANCE ON 20 HUMAN-DIFFICULT PAIRS	65
17	PERFORMANCE ON 20 HUMAN-DIFFICULT PAIRS	66
18	ERROR TRADEOFF CHARACTERISTIC: VISA IMAGES	67
19	ERROR TRADEOFF CHARACTERISTIC: VISA IMAGES	68
20	ERROR TRADEOFF CHARACTERISTIC: VISA IMAGES	69
21	ERROR TRADEOFF CHARACTERISTIC: VISA IMAGES	70
22	ERROR TRADEOFF CHARACTERISTIC: VISA IMAGES	71
23	ERROR TRADEOFF CHARACTERISTIC: VISA IMAGES	72
24	ERROR TRADEOFF CHARACTERISTIC: VISA IMAGES	73
25	ERROR TRADEOFF CHARACTERISTIC: VISA IMAGES	74
26	ERROR TRADEOFF CHARACTERISTIC: VISA IMAGES	75
27	ERROR TRADEOFF CHARACTERISTIC: VISA IMAGES	76
28	ERROR TRADEOFF CHARACTERISTIC: VISA IMAGES	77
29	ERROR TRADEOFF CHARACTERISTIC: VISA IMAGES	78
30	ERROR TRADEOFF CHARACTERISTIC: VISA IMAGES	79
31	ERROR TRADEOFF CHARACTERISTIC: VISA IMAGES	80
32	ERROR TRADEOFF CHARACTERISTIC: VISA IMAGES	81
33	ERROR TRADEOFF CHARACTERISTIC: VISA IMAGES	82
34	ERROR TRADEOFF CHARACTERISTIC: VISA IMAGES	83
35	ERROR TRADEOFF CHARACTERISTIC: VISA IMAGES	84
36	ERROR TRADEOFF CHARACTERISTIC: VISA IMAGES	85
37	ERROR TRADEOFF CHARACTERISTIC: VISA IMAGES	86
38	ERROR TRADEOFF CHARACTERISTIC: VISA IMAGES	87
39	ERROR TRADEOFF CHARACTERISTIC: VISA IMAGES	88
40	ERROR TRADEOFF CHARACTERISTIC: VISA IMAGES	89
41	ERROR TRADEOFF CHARACTERISTIC: VISA IMAGES	90

42	ERROR TRADEOFF CHARACTERISTIC: VISA IMAGES	91
43	ERROR TRADEOFF CHARACTERISTIC: VISA IMAGES	92
44	ERROR TRADEOFF CHARACTERISTIC: VISA IMAGES	93
45	ERROR TRADEOFF CHARACTERISTIC: VISA IMAGES	94
46	ERROR TRADEOFF CHARACTERISTIC: VISA IMAGES	95
47	ERROR TRADEOFF CHARACTERISTIC: VISA IMAGES	96
48	ERROR TRADEOFF CHARACTERISTIC: VISA IMAGES	97
49	ERROR TRADEOFF CHARACTERISTIC: VISA IMAGES	98
50	ERROR TRADEOFF CHARACTERISTIC: VISA IMAGES	99
51	ERROR TRADEOFF CHARACTERISTIC: MUGSHOT IMAGES	100
52	ERROR TRADEOFF CHARACTERISTIC: MUGSHOT IMAGES	101
53	ERROR TRADEOFF CHARACTERISTIC: MUGSHOT IMAGES	102
54	ERROR TRADEOFF CHARACTERISTIC: MUGSHOT IMAGES	103
55	ERROR TRADEOFF CHARACTERISTIC: MUGSHOT IMAGES	104
56	ERROR TRADEOFF CHARACTERISTIC: MUGSHOT IMAGES	105
57	ERROR TRADEOFF CHARACTERISTIC: MUGSHOT IMAGES	106
58	ERROR TRADEOFF CHARACTERISTIC: MUGSHOT IMAGES	107
59	ERROR TRADEOFF CHARACTERISTIC: MUGSHOT IMAGES	108
60	ERROR TRADEOFF CHARACTERISTIC: MUGSHOT IMAGES	109
61	ERROR TRADEOFF CHARACTERISTIC: MUGSHOT IMAGES	110
62	ERROR TRADEOFF CHARACTERISTIC: MUGSHOT IMAGES	111
63	ERROR TRADEOFF CHARACTERISTIC: MUGSHOT IMAGES	112
64	ERROR TRADEOFF CHARACTERISTIC: MUGSHOT IMAGES	113
65	ERROR TRADEOFF CHARACTERISTIC: MUGSHOT IMAGES	114
66	ERROR TRADEOFF CHARACTERISTIC: MUGSHOT IMAGES	115
67	ERROR TRADEOFF CHARACTERISTIC: WILD IMAGES	116
68	ERROR TRADEOFF CHARACTERISTIC: WILD IMAGES	117
69	ERROR TRADEOFF CHARACTERISTIC: WILD IMAGES	118
70	ERROR TRADEOFF CHARACTERISTIC: WILD IMAGES	119
71	ERROR TRADEOFF CHARACTERISTIC: WILD IMAGES	120
72	ERROR TRADEOFF CHARACTERISTIC: WILD IMAGES	121
73	ERROR TRADEOFF CHARACTERISTIC: WILD IMAGES	122
74	ERROR TRADEOFF CHARACTERISTIC: WILD IMAGES	123
75	ERROR TRADEOFF CHARACTERISTIC: WILD IMAGES	124
76	ERROR TRADEOFF CHARACTERISTIC: WILD IMAGES	125
77	ERROR TRADEOFF CHARACTERISTIC: WILD IMAGES	126
78	ERROR TRADEOFF CHARACTERISTIC: WILD IMAGES	127
79	ERROR TRADEOFF CHARACTERISTIC: WILD IMAGES	128
80	ERROR TRADEOFF CHARACTERISTIC: WILD IMAGES	129
81	ERROR TRADEOFF CHARACTERISTICS: CHILD EXPLOITATION IMAGES	130
82	ERROR TRADEOFF CHARACTERISTICS: CHILD EXPLOITATION IMAGES	131
83	ERROR TRADEOFF CHARACTERISTICS: CHILD EXPLOITATION IMAGES	132
84	CMC CHARACTERISTICS: CHILD EXPLOITATION IMAGES	133
85	CMC CHARACTERISTICS: CHILD EXPLOITATION IMAGES	134
86	CMC CHARACTERISTICS: CHILD EXPLOITATION IMAGES	135
87	CMC CHARACTERISTICS: CHILD EXPLOITATION IMAGES	136
88	CMC CHARACTERISTICS: CHILD EXPLOITATION IMAGES	137
89	FALSE MATCH RATES WITHIN AND ACROSS DEMOGRAPHIC GROUPS	138
90	FALSE MATCH RATES WITHIN AND ACROSS DEMOGRAPHIC GROUPS	139
91	FALSE MATCH RATES WITHIN AND ACROSS DEMOGRAPHIC GROUPS	140
92	FALSE MATCH RATES WITHIN AND ACROSS DEMOGRAPHIC GROUPS	141
93	FALSE MATCH RATES WITHIN AND ACROSS DEMOGRAPHIC GROUPS	142
94	FALSE MATCH RATES WITHIN AND ACROSS DEMOGRAPHIC GROUPS	143
95	FALSE MATCH RATES WITHIN AND ACROSS DEMOGRAPHIC GROUPS	144
96	FALSE MATCH RATES WITHIN AND ACROSS DEMOGRAPHIC GROUPS	145
97	FALSE MATCH RATES WITHIN AND ACROSS DEMOGRAPHIC GROUPS	146
98	FALSE MATCH RATES WITHIN AND ACROSS DEMOGRAPHIC GROUPS	147

99	FALSE MATCH RATES WITHIN AND ACROSS DEMOGRAPHIC GROUPS	148
100	FALSE MATCH RATES WITHIN AND ACROSS DEMOGRAPHIC GROUPS	149
101	FALSE MATCH RATES WITHIN AND ACROSS DEMOGRAPHIC GROUPS	150
102	FALSE MATCH RATES WITHIN AND ACROSS DEMOGRAPHIC GROUPS	151
103	FALSE MATCH RATES WITHIN AND ACROSS DEMOGRAPHIC GROUPS	152
104	FALSE MATCH RATES WITHIN AND ACROSS DEMOGRAPHIC GROUPS	153
105	SEX AND RACE EFFECTS: MUGSHOT IMAGES	154
106	SEX AND RACE EFFECTS: MUGSHOT IMAGES	155
107	SEX AND RACE EFFECTS: MUGSHOT IMAGES	156
108	SEX AND RACE EFFECTS: MUGSHOT IMAGES	157
109	SEX AND RACE EFFECTS: MUGSHOT IMAGES	158
110	SEX AND RACE EFFECTS: MUGSHOT IMAGES	159
111	SEX AND RACE EFFECTS: MUGSHOT IMAGES	160
112	SEX AND RACE EFFECTS: MUGSHOT IMAGES	161
113	SEX AND RACE EFFECTS: MUGSHOT IMAGES	162
114	SEX AND RACE EFFECTS: MUGSHOT IMAGES	163
115	SEX AND RACE EFFECTS: MUGSHOT IMAGES	164
116	SEX AND RACE EFFECTS: MUGSHOT IMAGES	165
117	SEX AND RACE EFFECTS: MUGSHOT IMAGES	166
118	SEX AND RACE EFFECTS: MUGSHOT IMAGES	167
119	SEX AND RACE EFFECTS: MUGSHOT IMAGES	168
120	SEX AND RACE EFFECTS: MUGSHOT IMAGES	169
121	SEX EFFECTS: VISA IMAGES	170
122	SEX EFFECTS: VISA IMAGES	171
123	SEX EFFECTS: VISA IMAGES	172
124	SEX EFFECTS: VISA IMAGES	173
125	SEX EFFECTS: VISA IMAGES	174
126	SEX EFFECTS: VISA IMAGES	175
127	SEX EFFECTS: VISA IMAGES	176
128	SEX EFFECTS: VISA IMAGES	177
129	SEX EFFECTS: VISA IMAGES	178
130	SEX EFFECTS: VISA IMAGES	179
131	SEX EFFECTS: VISA IMAGES	180
132	SEX EFFECTS: VISA IMAGES	181
133	SEX EFFECTS: VISA IMAGES	182
134	SEX EFFECTS: VISA IMAGES	183
135	SEX EFFECTS: VISA IMAGES	184
136	SEX EFFECTS: VISA IMAGES	185
137	SEX EFFECTS: VISA IMAGES	186
138	SEX EFFECTS: VISA IMAGES	187
139	SEX EFFECTS: VISA IMAGES	188
140	SEX EFFECTS: VISA IMAGES	189
141	SEX EFFECTS: VISA IMAGES	190
142	SEX EFFECTS: VISA IMAGES	191
143	SEX EFFECTS: VISA IMAGES	192
144	SEX EFFECTS: VISA IMAGES	193
145	SEX EFFECTS: VISA IMAGES	194
146	SEX EFFECTS: VISA IMAGES	195
147	SEX EFFECTS: VISA IMAGES	196
148	FALSE MATCH RATE CALIBRATION: MUGSHOT IMAGES	197
149	FALSE MATCH RATE CALIBRATION: MUGSHOT IMAGES	198
150	FALSE MATCH RATE CALIBRATION: MUGSHOT IMAGES	199
151	FALSE MATCH RATE CALIBRATION: MUGSHOT IMAGES	200
152	FALSE MATCH RATE CALIBRATION: MUGSHOT IMAGES	201
153	FALSE MATCH RATE CALIBRATION: MUGSHOT IMAGES	202
154	FALSE MATCH RATE CALIBRATION: MUGSHOT IMAGES	203

155	FALSE MATCH RATE CALIBRATION: MUGSHOT IMAGES	204
156	FALSE MATCH RATE CALIBRATION: MUGSHOT IMAGES	205
157	FALSE MATCH RATE CALIBRATION: MUGSHOT IMAGES	206
158	FALSE MATCH RATE CALIBRATION: MUGSHOT IMAGES	207
159	FALSE MATCH RATE CALIBRATION: MUGSHOT IMAGES	208
160	FALSE MATCH RATE CALIBRATION: MUGSHOT IMAGES	209
161	FALSE MATCH RATE CALIBRATION: MUGSHOT IMAGES	210
162	FALSE MATCH RATE CALIBRATION: MUGSHOT IMAGES	211
163	FALSE MATCH RATE CALIBRATION: MUGSHOT IMAGES	212
164	FALSE MATCH RATE CALIBRATION: VISA IMAGES	213
165	FALSE MATCH RATE CALIBRATION: VISA IMAGES	214
166	FALSE MATCH RATE CALIBRATION: VISA IMAGES	215
167	FALSE MATCH RATE CALIBRATION: VISA IMAGES	216
168	FALSE MATCH RATE CALIBRATION: VISA IMAGES	217
169	FALSE MATCH RATE CALIBRATION: VISA IMAGES	218
170	FALSE MATCH RATE CALIBRATION: VISA IMAGES	219
171	FALSE MATCH RATE CALIBRATION: VISA IMAGES	220
172	FALSE MATCH RATE CALIBRATION: VISA IMAGES	221
173	FALSE MATCH RATE CALIBRATION: VISA IMAGES	222
174	FALSE MATCH RATE CALIBRATION: VISA IMAGES	223
175	FALSE MATCH RATE CALIBRATION: VISA IMAGES	224
176	FALSE MATCH RATE CALIBRATION: VISA IMAGES	225
177	FALSE MATCH RATE CALIBRATION: VISA IMAGES	226
178	FALSE MATCH RATE CALIBRATION: VISA IMAGES	227
179	FALSE MATCH RATE CALIBRATION: VISA IMAGES	228
180	FALSE MATCH RATE CALIBRATION: VISA IMAGES	229
181	FALSE MATCH RATE CALIBRATION: VISA IMAGES	230
182	FALSE MATCH RATE CALIBRATION: VISA IMAGES	231
183	FALSE MATCH RATE CALIBRATION: VISA IMAGES	232
184	FALSE MATCH RATE CALIBRATION: VISA IMAGES	233
185	FALSE MATCH RATE CALIBRATION: VISA IMAGES	234
186	FALSE MATCH RATE CALIBRATION: VISA IMAGES	235
187	FALSE MATCH RATE CALIBRATION: VISA IMAGES	236
188	FALSE MATCH RATE CALIBRATION: VISA IMAGES	237
189	FALSE MATCH RATE CALIBRATION: VISA IMAGES	238
190	FALSE MATCH RATE CALIBRATION: VISA IMAGES	239
191	FALSE MATCH RATE CALIBRATION: VISA IMAGES	240
192	FALSE MATCH RATE CALIBRATION: VISA IMAGES	241
193	FALSE MATCH RATE CALIBRATION: VISA IMAGES	242
194	FALSE MATCH RATE CALIBRATION: VISA IMAGES	243
195	FALSE MATCH RATE CALIBRATION: VISA IMAGES	244
196	FALSE MATCH RATE CALIBRATION: VISA IMAGES	245
197	EFFECT OF COUNTRY OF BIRTH ON FNMR	247
198	EFFECT OF COUNTRY OF BIRTH ON FNMR	248
199	EFFECT OF COUNTRY OF BIRTH ON FNMR	249
200	EFFECT OF COUNTRY OF BIRTH ON FNMR	250
201	EFFECT OF COUNTRY OF BIRTH ON FNMR	251
202	EFFECT OF COUNTRY OF BIRTH ON FNMR	252
203	EFFECT OF COUNTRY OF BIRTH ON FNMR	253
204	EFFECT OF COUNTRY OF BIRTH ON FNMR	254
205	EFFECT OF COUNTRY OF BIRTH ON FNMR	255
206	EFFECT OF COUNTRY OF BIRTH ON FNMR	256
207	EFFECT OF COUNTRY OF BIRTH ON FNMR	257
208	EFFECT OF COUNTRY OF BIRTH ON FNMR	258
209	EFFECT OF COUNTRY OF BIRTH ON FNMR	259
210	EFFECT OF COUNTRY OF BIRTH ON FNMR	260
211	EFFECT OF COUNTRY OF BIRTH ON FNMR	261

212	EFFECT OF COUNTRY OF BIRTH ON FNMR	262
213	EFFECT OF COUNTRY OF BIRTH ON FNMR	263
214	EFFECT OF COUNTRY OF BIRTH ON FNMR	264
215	EFFECT OF COUNTRY OF BIRTH ON FNMR	265
216	EFFECT OF COUNTRY OF BIRTH ON FNMR	266
217	EFFECT OF COUNTRY OF BIRTH ON FNMR	267
218	EFFECT OF COUNTRY OF BIRTH ON FNMR	268
219	EFFECT OF COUNTRY OF BIRTH ON FNMR	269
220	EFFECT OF COUNTRY OF BIRTH ON FNMR	270
221	EFFECT OF COUNTRY OF BIRTH ON FNMR	271
222	EFFECT OF COUNTRY OF BIRTH ON FNMR	272
223	EFFECT OF COUNTRY OF BIRTH ON FNMR	273
224	ERROR TRADEOFF CHARACTERISTIC: MUGSHOT IMAGES	275
225	ERROR TRADEOFF CHARACTERISTIC: MUGSHOT IMAGES	276
226	ERROR TRADEOFF CHARACTERISTIC: MUGSHOT IMAGES	277
227	ERROR TRADEOFF CHARACTERISTIC: MUGSHOT IMAGES	278
228	ERROR TRADEOFF CHARACTERISTIC: MUGSHOT IMAGES	279
229	ERROR TRADEOFF CHARACTERISTIC: MUGSHOT IMAGES	280
230	ERROR TRADEOFF CHARACTERISTIC: MUGSHOT IMAGES	281
231	ERROR TRADEOFF CHARACTERISTIC: MUGSHOT IMAGES	282
232	ERROR TRADEOFF CHARACTERISTIC: MUGSHOT IMAGES	283
233	ERROR TRADEOFF CHARACTERISTIC: MUGSHOT IMAGES	284
234	ERROR TRADEOFF CHARACTERISTIC: MUGSHOT IMAGES	285
235	ERROR TRADEOFF CHARACTERISTIC: MUGSHOT IMAGES	286
236	ERROR TRADEOFF CHARACTERISTIC: MUGSHOT IMAGES	287
237	ERROR TRADEOFF CHARACTERISTIC: MUGSHOT IMAGES	288
238	ERROR TRADEOFF CHARACTERISTIC: MUGSHOT IMAGES	289
239	ERROR TRADEOFF CHARACTERISTIC: MUGSHOT IMAGES	290
240	ERROR TRADEOFF CHARACTERISTIC: MUGSHOT IMAGES	291
241	ERROR TRADEOFF CHARACTERISTIC: MUGSHOT IMAGES	292
242	ERROR TRADEOFF CHARACTERISTIC: MUGSHOT IMAGES	293
243	ERROR TRADEOFF CHARACTERISTIC: MUGSHOT IMAGES	294
244	EFFECT OF SUBJECT AGE ON FNMR	296
245	EFFECT OF SUBJECT AGE ON FNMR	297
246	EFFECT OF SUBJECT AGE ON FNMR	298
247	EFFECT OF SUBJECT AGE ON FNMR	299
248	EFFECT OF SUBJECT AGE ON FNMR	300
249	EFFECT OF SUBJECT AGE ON FNMR	301
250	EFFECT OF SUBJECT AGE ON FNMR	302
251	EFFECT OF SUBJECT AGE ON FNMR	303
252	EFFECT OF SUBJECT AGE ON FNMR	304
253	EFFECT OF SUBJECT AGE ON FNMR	305
254	EFFECT OF SUBJECT AGE ON FNMR	306
255	EFFECT OF SUBJECT AGE ON FNMR	307
256	EFFECT OF SUBJECT AGE ON FNMR	308
257	EFFECT OF SUBJECT AGE ON FNMR	309
258	EFFECT OF SUBJECT AGE ON FNMR	310
259	EFFECT OF SUBJECT AGE ON FNMR	311
260	EFFECT OF SUBJECT AGE ON FNMR	312
261	EFFECT OF SUBJECT AGE ON FNMR	313
262	EFFECT OF SUBJECT AGE ON FNMR	314
263	EFFECT OF SUBJECT AGE ON FNMR	315
264	EFFECT OF SUBJECT AGE ON FNMR	316
265	EFFECT OF SUBJECT AGE ON FNMR	317

266	EFFECT OF SUBJECT AGE ON FNMR	318
267	EFFECT OF SUBJECT AGE ON FNMR	319
268	EFFECT OF SUBJECT AGE ON FNMR	320
269	EFFECT OF SUBJECT AGE ON FNMR	321
270	EFFECT OF SUBJECT AGE ON FNMR	322
271	WORST CASE REGIONAL EFFECT FNMR	325
272	IMPOSTOR DISTRIBUTION SHIFTS FOR SELECT COUNTRY PAIRS	327

	Location	Developer Name	Short Name	Seq. Num.	Validation Date
1	NL	20Face	20face-000	000	2021-04-12
2	US	3Divi	3divi-005	005	2020-08-28
3	US	3Divi	3divi-006	006	2021-04-14
4	TH	ACI Software	acisw-003	003	2020-08-03
5	TH	ACI Software	acisw-006	006	2021-02-25
6	SG	ADVANCE.AI	advance-002	002	2019-12-19
7	TW	ASUSTek Computer Inc	asusaics-000	000	2019-10-24
8	TW	ASUSTek Computer Inc	asusaics-001	001	2020-02-25
9	CN	AYF Technology	ayftech-001	001	2020-07-06
10	TW	Ability Enterprise - Andro Video	androvideo-000	000	2021-01-25
11	TW	Acer Incorporated	acer-000	000	2020-01-08
12	TW	Acer Incorporated	acer-001	001	2020-06-30
13	SG	Adera Global PTE	adera-001	001	2019-06-17
14	SG	Adera Global PTE	adera-002	002	2021-02-16
15	TH	Ai First	aifirst-001	001	2019-11-21
16	TW	AiUnion Technology	aiunionface-000	000	2019-10-22
17	TH	Aigen	aigen-001	001	2020-10-06
18	TH	Aigen	aigen-002	002	2021-03-15
19	KR	Ajou University	ajou-001	001	2021-03-08
20	ID	Akurat Satu Indonesia	ptakuratsatu-000	000	2020-09-11
21	KR	Alchera Inc	alchera-000	000	2019-03-01
22	KR	Alchera Inc	alchera-002	002	2021-03-05
23	ES	Alice Biometrics	alice-000	000	2021-06-15
24	RU	Alivia / Innovation Sys	isystems-001	001	2018-06-12
25	RU	Alivia / Innovation Sys	isystems-002	002	2018-10-18
26	IN	AllGoVision	allgovision-000	000	2019-03-01
27	CN	AlphaSSTG	alphaface-001	001	2019-09-03
28	CN	AlphaSSTG	alphaface-002	002	2020-02-20
29	GB	Amplified Group	amplifiedgroup-001	001	2019-03-01
30	CN	Anke Investments	anke-004	004	2019-06-27
31	CN	Anke Investments	anke-005	005	2019-11-21
32	BR	Antheus Technologia	antheus-000	000	2019-12-05
33	BR	Antheus Technologia	antheus-001	001	2020-06-25
34	GB	AnyVision	anyvision-004	004	2018-06-15
35	GB	AnyVision	anyvision-005	005	2021-02-03
36	CN	AuthenMetric	authenmetric-002	002	2021-03-10
37	US	Aware	aware-004	004	2019-03-01
38	US	Aware	aware-005	005	2020-02-27
39	IN	Awidit Systems	awiros-001	001	2019-09-23
40	IN	Awidit Systems	awiros-002	002	2020-10-28
41	JP	Ayonix	ayonix-000	000	2017-06-22
42	CN	BOE Technology Group	boetech-001	001	2021-06-22
43	CN	Beihang University-ERCACAT	ercacat-001	001	2020-07-06
44	CN	Beijing Alleyes Technology	alleyes-000	000	2020-03-09
45	CN	Beijing DeepSense Technologies	deepsense-000	000	2021-03-19
46	CN	Beijing Vion Technology Inc	vion-000	000	2018-10-19
47	CH	BioID Technologies SA	bioidechswiss-001	001	2020-08-28
48	CH	BioID Technologies SA	bioidechswiss-002	002	2021-02-17
49	UK	BitCenter UK	farfaces-001	001	2021-04-09
50	CN	Bitmain	bm-001	001	2018-10-17
51	CN	Bresee Technology	bresee-000	000	2020-08-07
52	CN	Bresee Technology	bresee-001	001	2020-12-30
53	CN	CSA IntelliCloud Technology	intellicloudai-001	001	2019-08-13
54	CN	CSA IntelliCloud Technology	intellicloudai-002	002	2020-12-17
55	TW	CTBC Bank	ctbcbank-000	000	2019-06-28
56	TW	CTBC Bank	ctbcbank-001	001	2019-10-28
57	US	Camvi Technologies	camvi-002	002	2018-10-19
58	US	Camvi Technologies	camvi-004	004	2019-07-12
59	CN	Canon Inc	canon-002	002	2020-12-29
60	CN	Canon Inc	cib-001	001	2020-08-05
61	CN	China Electronics Import-Export Corp	ceiec-003	003	2020-01-06
62	CN	China Electronics Import-Export Corp	ceiec-004	004	2021-01-18
63	CN	China University of Petroleum	upc-001	001	2019-06-05
64	CN	Chinese University of Hong Kong	cuhkee-001	001	2020-03-18
65	KR	Chosun University	chosun-001	001	2020-07-01
66	KR	Chosun University	chosun-002	002	2020-11-25
67	TW	Chunghwa Telecom	chtface-002	002	2019-12-07
68	TW	Chunghwa Telecom	chtface-003	003	2020-06-24
69	US	CloudSmart Consulting LLC	csc-001	001	2020-11-20
70	US	CloudSmart Consulting LLC	csc-002	002	2021-03-24

Table 1: Summary of participant information included in this report.

	Location	Developer Name	Short Name	Seq. Num.	Validation Date
71	CN	Cloudwalk - Hengrui AI Technology	cloudwalk-hr-003	003	2020-09-25
72	CN	Cloudwalk - Hengrui AI Technology	cloudwalk-hr-004	004	2021-02-10
73	CN	Cloudwalk - Moontime Smart Technology	cloudwalk-mt-002	002	2020-07-02
74	CN	Cloudwalk - Moontime Smart Technology	cloudwalk-mt-003	003	2020-12-22
75	IN	Code Everest Pvt	facex-001	001	2021-03-08
76	DE	Cognitec Systems GmbH	cognitec-000	000	2018-10-19
77	DE	Cognitec Systems GmbH	cognitec-002	002	2021-02-24
78	IL	Corsight	corsight-001	001	2021-03-11
79	IL	Cortica	cor-001	001	2020-09-24
80	KR	Cubox	cubox-001	001	2020-12-07
81	JP	Cybercore	cybercore-000	000	2020-08-26
82	US	Cyberextruder	cyberextruder-001	001	2017-08-02
83	US	Cyberextruder	cyberextruder-002	002	2018-01-30
84	TW	Cyberlink Corp	cyberlink-005	005	2020-07-31
85	TW	Cyberlink Corp	cyberlink-006	006	2021-01-08
86	CN	DSK	dsk-000	000	2019-06-28
87	CN	Dahua Technology	dahua-005	005	2020-08-13
88	CN	Dahua Technology	dahua-006	006	2020-12-30
89	US	Decatur Industries Inc	decatur-000	000	2020-08-18
90	CN	Deepglint	deepglint-002	002	2019-11-15
91	CN	Deepglint	deepglint-003	003	2021-03-03
92	DE	Dermalog	dermalog-006	006	2018-10-18
93	DE	Dermalog	dermalog-008	008	2021-03-25
94	CN	DiDi ChuXing Technology	didiglobalface-001	001	2019-10-23
95	GB	Digital Barriers	digitalbarriers-002	002	2019-03-01
96	TR	Ekin Smart City Technologies	ekin-002	002	2021-05-04
97	RU	Enface	enface-000	000	2021-04-09
98	RU	Expasoft LLC	expasoft-000	000	2020-01-06
99	RU	Expasoft LLC	expasoft-001	001	2020-09-03
100	GB	FaceSoft	facesoft-000	000	2019-07-10
101	KR	FaceTag Co	facetag-000	000	2021-03-22
102	TW	FarBar Inc	f8-001	001	2019-07-11
103	UK	Fincore Ltd	fincore-000	000	2021-06-07
104	CN	Fujitsu Research and Development Center	fujitsulab-001	001	2020-09-30
105	CN	Fujitsu Research and Development Center	fujitsulab-002	002	2021-02-24
106	US	Gemalto Cogent	cogent-004	004	2019-06-14
107	US	Gemalto Cogent	cogent-005	005	2020-12-29
108	TW	GeoVision Inc	geo-001	001	2020-10-30
109	TW	GeoVision Inc	geo-002	002	2021-04-01
110	JP	Glory	glory-002	002	2019-11-12
111	JP	Glory	glory-003	003	2021-01-15
112	TW	Gorilla Technology	gorilla-005	005	2020-03-11
113	TW	Gorilla Technology	gorilla-006	006	2020-07-31
114	CN	Guangzhou Pixel Solutions	pixelall-005	005	2021-02-05
115	CN	Guangzhou Pixel Solutions	pixelall-006	006	2021-06-17
116	ES	Herta Security	hertasecurity-000	000	2021-01-05
117	CN	Hikvision Research Institute	hik-001	001	2019-03-01
118	IN	HyperVerge Inc	hyperverge-001	001	2020-12-13
119	IN	HyperVerge Inc	hyperverge-002	002	2021-05-27
120	AU	ICM Airport Technics	icm-002	002	2020-11-13
121	FR	ID3 Technology	id3-006	006	2020-12-17
122	FR	ID3 Technology	id3-007	007	2021-05-17
123	RU	ITMO University	itmo-006	006	2019-03-01
124	RU	ITMO University	itmo-007	007	2020-01-06
125	RU	IVA Cognitive	ivacognitive-001	001	2021-01-29
126	FR	Idemia	idemia-006	006	2020-07-06
127	FR	Idemia	idemia-007	007	2020-12-04
128	US	Imageware Systems	iws-000	000	2020-08-12
129	AU	Imagus Technology Pty	imagus-002	002	2020-12-31
130	AU	Imagus Technology Pty	imagus-003	003	2021-05-18
131	GB	Imperial College London	imperial-000	000	2019-03-01
132	GB	Imperial College London	imperial-002	002	2019-08-28
133	US	Incode Technologies Inc	incode-007	007	2020-08-25
134	US	Incode Technologies Inc	incode-008	008	2021-01-19
135	US	Incode Technologies Inc	incode-009	009	2021-06-22
136	IN	Innef Labs	inneflabs-000	000	2020-09-04
137	GB	Innovative Technology	innovativetechnologyltd-001	001	2019-10-22
138	GB	Innovative Technology	innovativetechnologyltd-002	002	2020-02-26
139	SK	Innovatrics	innovatrics-006	006	2019-08-13
140	SK	Innovatrics	innovatrics-007	007	2020-08-19

Table 2: Summary of participant information included in this report.

	Location	Developer Name	Short Name	Seq. Num.	Validation Date
141	CN	InsightFace AI	insightface-000	000	2021-03-17
142	CN	Institute of Computing Technology	icthtc-000	000	2020-11-29
143	RU	Institute of Information Technologies	iit-002	002	2019-12-04
144	RU	Institute of Information Technologies	iit-003	003	2020-12-01
145	IS	Intel Research Group	intelresearch-002	002	2020-07-24
146	IS	Intel Research Group	intelresearch-003	003	2021-01-18
147	US	Intellivision	intellivision-001	001	2017-10-10
148	US	Intellivision	intellivision-002	002	2019-08-23
149	US	IrexAI	irex-000	000	2020-12-17
150	IL	Is It You	isityou-000	000	2017-06-26
151	KR	Kakao Enterprise	kakao-004	004	2020-10-28
152	KR	Kakao Enterprise	kakao-005	005	2021-03-09
153	SG	Kedacom International Pte	kedacom-000	000	2019-06-03
154	US	Kneron Inc	kneron-003	003	2019-07-01
155	US	Kneron Inc	kneron-005	005	2020-02-21
156	KR	Kookmin University	kookmin-001	001	2020-09-28
157	KR	Kookmin University	kookmin-002	002	2021-03-05
158	IN	Lema Labs	lemalabs-001	001	2021-04-13
159	JP	Line Corporation	line-000	000	2021-03-31
160	RU	Lomonosov Moscow State University	intsysmsu-001	001	2019-10-22
161	RU	Lomonosov Moscow State University	intsysmsu-002	002	2020-03-12
162	IN	Lookman Electroplast Industries	lookman-002	002	2018-06-13
163	IN	Lookman Electroplast Industries	lookman-004	004	2019-06-03
164	US	Luxand Inc	luxand-000	000	2019-11-07
165	RU	MVision	mvision-001	001	2019-11-12
166	CN	Megvii/Face++	megvii-002	002	2018-10-19
167	CN	Megvii/Face++	megvii-003	003	2021-03-08
168	GB	MicroFocus	microfocus-001	001	2018-06-13
169	GB	MicroFocus	microfocus-002	002	2018-10-17
170	CN	Minivision	minivision-000	000	2020-10-28
171	NO	Mobai	mobai-000	000	2020-08-26
172	NO	Mobai	mobai-001	001	2021-02-17
173	ES	Mobbeel Solutions	mobbl-000	000	2021-01-28
174	ES	Mobbeel Solutions	mobbl-001	001	2021-06-16
175	TH	Momentum Digital	sertis-000	000	2019-10-07
176	TH	Momentum Digital	sertis-002	002	2021-05-13
177	CN	MoreDian Technology	moreedian-000	000	2021-02-24
178	RU	N-Tech Lab	ntechlab-009	009	2020-12-30
179	RU	N-Tech Lab	ntechlab-010	010	2021-04-30
180	CA	NEO Systems	neosystems-001	001	2021-03-02
181	KR	NHN Corp	rhn-001	001	2021-03-15
182	KR	NSENSE Corp	nsensecorp-001	001	2020-10-20
183	KR	NSENSE Corp	nsensecorp-002	002	2021-05-06
184	CN	Nanjing Kiwi Network Technology	kiwitech-000	000	2021-03-19
185	KR	Naver Corp	clova-000	000	2020-10-21
186	KR	Neosecu Co	openface-001	001	2021-06-15
187	TW	Netbridge Technology Incoporation	netbridgetech-001	001	2020-01-08
188	TW	Netbridge Technology Incoporation	netbridgetech-002	002	2020-08-11
189	LT	Neurotechnology	neurotechnology-010	010	2020-11-26
190	LT	Neurotechnology	neurotechnology-011	011	2021-03-26
191	ID	Nodeflux	nodeflux-002	002	2019-08-13
192	IN	NotionTag Technologies Private Limited	notiontag-000	000	2019-06-12
193	IN	NotionTag Technologies Private Limited	notiontag-001	001	2021-03-04
194	US	Omnigarde Ltd	omnigarde-000	000	2021-04-05
195	RU	Oz Forensics LLC	oz-001	001	2020-07-29
196	RU	Oz Forensics LLC	oz-002	002	2021-01-18
197	CH	PXL Vision AG	pxl-001	001	2020-06-30
198	SG	Panasonic R+D Center Singapore	psl-006	006	2020-11-13
199	SG	Panasonic R+D Center Singapore	psl-007	007	2021-03-19
200	TR	Papilon Savunma	papsav1923-001	001	2021-03-10
201	US	Paravision (EverAI)	paravision-004	004	2019-12-11
202	US	Paravision (EverAI)	paravision-006	006	2021-02-01
203	SG	Pensees Pte	pensees-001	001	2020-08-17
204	IN	Pyramid Cyber Security + Forensic (P)	pyramid-000	000	2019-11-04
205	CZ	Quantasoft	quantasoft-003	003	2021-04-19
206	US	Rank One Computing	rankone-009	009	2020-06-26
207	US	Rank One Computing	rankone-010	010	2020-11-05
208	US	Realnetworks Inc	realnetworks-002	002	2019-02-28
209	US	Realnetworks Inc	realnetworks-004	004	2021-04-15
210	US	Regula Forensics	regula-000	000	2021-04-13

Table 3: Summary of participant information included in this report.

	Location	Developer Name	Short Name	Seq. Num.	Validation Date
211	CN	Remark Holdings	remarkai-001	001	2019-03-01
212	CN	Remark Holdings	remarkai-002	002	2019-11-21
213	CN	Remark Holdings	remarkai-003	003	2021-06-22
214	SG	Rendip	rendip-000	000	2021-04-19
215	CN	Rokid Corporation	rokid-000	000	2019-08-01
216	CN	Rokid Corporation	rokid-001	001	2019-12-13
217	DE	Saffe	saffe-001	001	2018-10-19
218	DE	Saffe	saffe-002	002	2019-03-01
219	KR	Samsung S1 Corp	s1-001	001	2019-12-06
220	KR	Samsung S1 Corp	s1-002	002	2021-03-24
221	IN	Samtech InfoNet Limited	samtech-001	001	2019-10-15
222	RU	Satellite Innovation/Eocortex	eocortex-000	000	2020-08-26
223	IL	Scanovate	scanovate-001	001	2019-11-12
224	IL	Scanovate	scanovate-002	002	2020-06-26
225	RO	Securif AI	securifai-001	001	2020-10-06
226	RO	Securif AI	securifai-002	002	2021-03-19
227	CN	Sensetime Group	sensetime-004	004	2020-11-20
228	CN	Sensetime Group	sensetime-005	005	2021-05-24
229	US	Shaman Software	shaman-000	000	2017-12-05
230	US	Shaman Software	shaman-001	001	2018-01-13
231	CN	Shanghai Jiao Tong University	sjtu-003	003	2020-11-02
232	CN	Shanghai Jiao Tong University	sjtu-004	004	2021-05-13
233	CN	Shanghai Ulucu Electronics Technology	uluface-002	002	2019-07-10
234	CN	Shanghai Ulucu Electronics Technology	uluface-003	003	2019-11-12
235	CN	Shanghai University - Shanghai Film Academy	shu-002	002	2019-12-10
236	CN	Shanghai University - Shanghai Film Academy	shu-003	003	2020-06-24
237	CN	Shanghai Yitu Technology	yitu-003	003	2019-03-01
238	CN	Shenzhen AiMall Tech	aimall-002	002	2020-03-12
239	CN	Shenzhen AiMall Tech	aimall-003	003	2020-08-12
240	CN	Shenzhen EI Networks	einetworks-000	000	2019-08-13
241	CN	Shenzhen Inst Adv Integrated Tech CAS	siat-002	002	2018-06-13
242	CN	Shenzhen Inst Adv Integrated Tech CAS	siat-004	004	2019-03-01
243	CN	Shenzhen Intellifusion Technologies	intellifusion-001	001	2019-08-22
244	CN	Shenzhen Intellifusion Technologies	intellifusion-002	002	2020-03-18
245	CN	Shenzhen University-Macau University of Science and Technology	sztu-000	000	2020-12-17
246	DE	Smilart	smilart-002	002	2018-02-06
247	DE	Smilart	smilart-003	003	2018-06-18
248	TR	Sodec App Inc	sodec-000	000	2021-06-02
249	IN	Staqua Technologies	staqua-000	000	2020-07-15
250	CN	Star Hybrid Limited	starhybrid-001	001	2019-06-19
251	CN	Su Zhou NaZhiTianDi intelligent technology	nazhai-000	000	2020-06-25
252	KR	Suprema	suprema-000	000	2021-03-31
253	KR	Suprema ID Inc	supremaid-001	001	2021-05-04
254	RU	Synesis	synesis-006	006	2019-10-10
255	RU	Synesis	synesis-007	007	2020-06-24
256	TW	Synology Inc	synology-000	000	2019-10-23
257	TW	Synology Inc	synology-002	002	2020-08-20
258	CN	TUPU Technology	tuputech-000	000	2019-10-11
259	TW	Taiwan AI Labs	ailabs-001	001	2019-12-18
260	TW	Taiwan-Certificate Authority Incorporatio)	twface-000	000	2021-05-14
261	CH	Tech5 SA	tech5-004	004	2020-03-09
262	CH	Tech5 SA	tech5-005	005	2020-07-24
263	CN	Tencent Deepsea Lab	deepsea-001	001	2019-06-03
264	RU	Tevian	tevian-005	005	2019-09-21
265	RU	Tevian	tevian-006	006	2020-09-11
266	US	TigerIT Americas LLC	tiger-003	003	2018-10-16
267	US	TigerIT Americas LLC	tiger-004	004	2020-12-01
268	CN	Tong Yi Transportation Technology	tongyi-005	005	2019-06-12
269	JP	Toshiba	toshiba-002	002	2018-10-19
270	JP	Toshiba	toshiba-003	003	2019-03-01
271	JP	Tripleize	aize-001	001	2021-04-23
272	US	Trueface.ai	trueface-001	001	2020-07-20
273	US	Trueface.ai	trueface-002	002	2021-03-29
274	CN	ULSee Inc	ulsee-001	001	2019-07-31
275	PT	Universidade de Coimbra	visteam-000	000	2020-01-14
276	PT	Universidade de Coimbra	visteam-001	001	2021-03-16
277	US	VCognition	vcog-002	002	2017-06-12
278	ES	Veridas Digital Authentication Solutions S.L.	veridas-004	004	2020-07-21
279	ES	Veridas Digital Authentication Solutions S.L.	veridas-006	006	2021-04-15
280	TW	Via Technologies Inc	via-000	000	2019-07-08

Table 4: Summary of participant information included in this report.

	Location	Developer Name	Short Name	Seq. Num.	Validation Date
281	TW	Via Technologies Inc	via-001	001	2020-01-08
282	DE	Videmo Intelligent Videoanalyse	videmo-000	000	2019-12-19
283	IN	Videonetics Technology Pvt	videonetics-001	001	2019-06-19
284	IN	Videonetics Technology Pvt	videonetics-002	002	2019-11-21
285	VN	Vietnam Posts and Telecommunications Group	vnpt-001	001	2021-01-08
286	VN	Vietnam Posts and Telecommunications Group	vnpt-002	002	2021-06-08
287	VN	Viettel Group	vts-000	000	2020-11-04
288	US	Vigilant Solutions	vigilantsolutions-009	009	2020-12-07
289	US	Vigilant Solutions	vigilantsolutions-010	010	2021-04-07
290	VN	VinAI Research VietNam	vina-000	000	2020-09-24
291	SE	Visage Technologies	visage-000	000	2020-12-09
292	FI	Visidon	vd-001	001	2019-02-26
293	FI	Visidon	vd-002	002	2021-04-12
294	CN	Vision Intelligence Center of Meituan	meituan-000	000	2021-05-14
295	PT	Vision-Box	visionbox-001	001	2019-03-01
296	PT	Vision-Box	visionbox-002	002	2021-04-29
297	RU	VisionLabs	visionlabs-009	009	2020-07-27
298	RU	VisionLabs	visionlabs-010	010	2021-01-25
299	RU	Vocord	vocord-008	008	2020-01-31
300	RU	Vocord	vocord-009	009	2020-12-28
301	CN	Winsense	winsense-001	001	2019-10-16
302	CN	Winsense	winsense-002	002	2020-11-20
303	CN	Xforward AI Technology	xforwardai-001	001	2020-09-25
304	CN	Xforward AI Technology	xforwardai-002	002	2021-02-10
305	CN	Xiamen Meiya Pico Information	meiya-001	001	2019-03-01
306	CN	Xiamen University	xm-000	000	2020-10-19
307	PT	YooniK	yoonik-000	000	2020-06-24
308	PT	YooniK	yoonik-001	001	2020-10-26
309	TW	Yuan High-Tech Development	yuan-001	001	2021-01-08
310	TW	Yuan High-Tech Development	yuan-002	002	2021-05-17
311	CN	Yuntu Data and Technology	ytu-000	000	2021-06-16
312	CN	Zhuhai Yisheng Electronics Technology	yisheng-004	004	2018-06-12
313	CN	iQIYI Inc	iqface-000	000	2019-06-04
314	CN	iQIYI Inc	iqface-003	003	2021-02-23
315	TW	iSAP Solution Corporation	isap-001	001	2019-08-07
316	TW	iSAP Solution Corporation	isap-002	002	2020-09-01

Table 5: Summary of participant information included in this report.

				TEMPLATE								COMPARISON ⁴									
ALGORITHM		CONFIG	LIBRARY	GENERATION TIME (ms) ⁴								TIME (ns) ⁵									
NAME		DATA	DATA	MEMORY	SIZE	(B)	MUGSHOT	480x720	960x1440	1600x2400	3000x4500	GENUINE	IMPOSTOR								
		(KB) ¹	(KB) ²	(MB) ³																	
1	20face-000	119967175	324083	167	905	139	2048 ± 0	37	232 ± 1	19	223 ± 1	14	226 ± 4	12	222 ± 1	11	224 ± 1	296	44880 ± 134	295	44462 ± 163
2	3divi-005	270436716	53870	60	431	124	2048 ± 0	263	993 ± 83	231	1136 ± 88	239	1309 ± 137	218	1348 ± 131	198	1671 ± 166	77	790 ± 20	75	791 ± 23
3	3divi-006	280439478	52656	71	472	213	2048 ± 0	160	654 ± 1	110	651 ± 0	98	660 ± 1	81	678 ± 2	79	759 ± 13	74	775 ± 19	74	770 ± 22
4	acer-000	112369572	88323	74	478	149	2048 ± 0	34	222 ± 0	21	233 ± 4	17	238 ± 4	16	262 ± 18	19	356 ± 46	97	1065 ± 40	109	1109 ± 35
5	acer-001	37530576	66086	57	417	22	512 ± 0	30	199 ± 0	22	237 ± 28	15	229 ± 26	15	242 ± 37	13	259 ± 21	182	2453 ± 44	184	2461 ± 62
6	acisw-003	288798384	35664	40	282	318	18467 ± 8	36	232 ± 1	27	267 ± 22	54	488 ± 28	138	990 ± 24	231	2977 ± 129	319	847908 ± 16757	319	851850 ± 17018
7	acisw-006	288798384	36107	43	303	317	18465 ± 8	33	219 ± 0	20	227 ± 0	34	410 ± 1	123	838 ± 1	222	2532 ± 10	316	548137 ± 16513	316	549586 ± 9238
8	ader-a-001	0	79272	29	190	263	2560 ± 0	10	97 ± 0	-	-	-	-	-	-	136	1604 ± 71	138	1649 ± 56		
9	ader-a-002	0	749797	171	921	311	5120 ± 0	311	1394 ± 11	257	1381 ± 1	249	1393 ± 1	223	1403 ± 1	188	1464 ± 2	171	2163 ± 32	172	2158 ± 28
10	advance-002	263345868	20434	42	295	142	2048 ± 0	209	811 ± 2	158	803 ± 2	109	696 ± 2	85	699 ± 4	69	718 ± 1	91	987 ± 10	90	988 ± 45
11	aifirst-001	229537224	808777	76	485	126	2048 ± 0	131	587 ± 2	89	568 ± 2	76	584 ± 3	62	601 ± 6	78	755 ± 5	105	1099 ± 14	108	1087 ± 45
12	aigen-001	263125848	595227	207	1136	194	2048 ± 0	318	1448 ± 9	264	1451 ± 8	262	1759 ± 6	257	2594 ± 4	247	5691 ± 44	220	3772 ± 57	217	3736 ± 56
13	aigen-002	210228007	1316138	161	874	152	2048 ± 0	128	586 ± 24	92	582 ± 4	162	920 ± 4	241	1758 ± 5	245	5427 ± 17	217	3678 ± 44	216	3646 ± 48
14	ailabs-001	1079975494	338989	216	1252	115	2048 ± 0	165	664 ± 4	149	774 ± 50	215	1145 ± 12	249	1972 ± 74	243	5205 ± 272	307	104034 ± 661	307	103415 ± 722
15	aimall-002	379040058	25210	250	1576	106	2048 ± 0	199	776 ± 4	189	927 ± 27	168	940 ± 21	150	955 ± 34	126	1003 ± 75	306	72811 ± 7399	305	71216 ± 6286
16	aimall-003	516428479	171935	265	1913	53	1024 ± 0	164	662 ± 1	139	740 ± 51	125	752 ± 62	98	741 ± 46	89	807 ± 47	291	34565 ± 93	292	34598 ± 118
17	aiunionface-000	247442204	840295	52	402	95	2048 ± 0	153	637 ± 13	144	754 ± 41	189	1025 ± 28	191	1179 ± 29	196	1639 ± 47	99	1072 ± 19	105	1080 ± 47
18	aize-001	274899563	168970	239	1436	208	2048 ± 0	80	437 ± 10	54	440 ± 8	69	542 ± 17	105	756 ± 27	193	1583 ± 53	161	1937 ± 22	159	1919 ± 23
19	ajou-001	317975940	31734	63	442	196	2048 ± 0	107	530 ± 0	81	536 ± 0	68	535 ± 0	53	549 ± 0	41	577 ± 0	37	597 ± 19	41	596 ± 13
20	alchera-000	264653474	18848	116	614	215	2048 ± 0	130	587 ± 13	126	706 ± 48	248	1389 ± 58	259	2722 ± 123	255	9011 ± 455	207	3189 ± 32	202	3031 ± 142
21	alchera-002	415139706	22275	214	1233	129	2048 ± 0	257	968 ± 1	200	976 ± 2	179	979 ± 1	157	988 ± 1	129	1025 ± 2	214	3488 ± 63	214	3430 ± 63
22	alice-000	1783085023	19355	257	1732	283	4096 ± 0	251	950 ± 2	191	933 ± 1	172	949 ± 1	163	1011 ± 3	164	1264 ± 8	273	14975 ± 201	272	14890 ± 229
23	alleyes-000	519819601	997090	159	857	197	2048 ± 0	201	784 ± 1	198	970 ± 61	177	974 ± 62	147	943 ± 69	135	1057 ± 23	123	1298 ± 34	125	1303 ± 51
24	allgovision-000	176649434	155862	103	561	216	2048 ± 0	69	384 ± 8	47	395 ± 17	36	413 ± 14	34	471 ± 14	66	710 ± 21	289	29903 ± 406	290	29735 ± 194
25	alphaface-001	266086261	81636	94	527	176	2048 ± 0	141	612 ± 1	99	613 ± 3	83	612 ± 1	66	619 ± 1	54	640 ± 2	94	1008 ± 10	94	1002 ± 19
26	alphaface-002	787451788	70692	238	1434	120	2048 ± 0	149	628 ± 2	140	746 ± 19	124	751 ± 18	112	779 ± 22	95	828 ± 40	84	945 ± 25	86	935 ± 17
27	amplifiedgroup-001	0	47053	9	81	48	866 ± 2	8	93 ± 0	-	-	-	-	-	-	-	303	57803 ± 4210	301	56365 ± 196	
28	androvideo-000	179043623	585063	53	403	210	2048 ± 0	45	277 ± 0	33	285 ± 0	22	314 ± 0	22	372 ± 1	49	620 ± 0	196	2860 ± 28	197	2847 ± 22
29	anke-004	357773976	410776	129	706	248	2056 ± 0	147	625 ± 2	103	627 ± 2	93	635 ± 3	75	653 ± 2	122	982 ± 8	49	633 ± 22	54	632 ± 34
30	anke-005	336438306	429160	206	1134	245	2056 ± 0	132	590 ± 2	94	594 ± 5	80	601 ± 3	71	638 ± 4	94	821 ± 24	57	685 ± 19	63	687 ± 26
31	antheus-000	122319905	41994	18	116	37	520 ± 0	14	109 ± 1	16	187 ± 1	12	189 ± 1	9	195 ± 1	12	236 ± 2	251	6901 ± 268	250	6936 ± 103
32	antheus-001	122319905	41962	19	118	36	520 ± 0	17	120 ± 1	25	265 ± 13	47	468 ± 22	199	1223 ± 27	223	2660 ± 87	248	6218 ± 47	246	6216 ± 45
33	anyvision-004	410625029	630797	203	1102	58	1024 ± 0	63	355 ± 1	-	-	-	-	-	-	-	159	1891 ± 51	154	1829 ± 85	
34	anyvision-005	195563434	116595	180	963	51	1024 ± 0	260	985 ± 1	202	997 ± 1	187	1004 ± 1	159	995 ± 1	124	995 ± 1	67	733 ± 14	70	733 ± 16
35	asusaics-000	263596044	245320	113	605	137	2048 ± 0	93	484 ± 13	74	506 ± 21	144	850 ± 26	243	1789 ± 61	249	6305 ± 188	234	5455 ± 78	234	5422 ± 112
36	asusaics-001	263596114	245330	109	595	288	4096 ± 0	222	842 ± 17	203	1008 ± 20	247	1377 ± 28	256	2423 ± 90	252	7284 ± 277	260	8618 ± 42	260	8638 ± 136
37	authenmetric-002	460742912	91489	205	1112	99	2048 ± 0	247	942 ± 1	195	950 ± 1	175	960 ± 1	152	960 ± 1	123	991 ± 2	143	1712 ± 20	144	1719 ± 19
38	aware-004	438097834	28219	261	1820	256	2084 ± 0	239	900 ± 10	225	1105 ± 10	225	1226 ± 25	236	1585 ± 72	230	2937 ± 166	121	1279 ± 50	124	1287 ± 100
39	aware-005	307217546	26320	219	1265	76	1572 ± 0	237	886 ± 23	213	1038 ± 21	212	1121 ± 22	216	1337 ± 58	210	2195 ± 144	131	1475 ± 63	130	1427 ± 115
40	awiros-001	15871971	87480	13	88	20	512 ± 0	11	97 ± 6	6	98 ± 4	8	138 ± 6	13	225 ± 7	38	556 ± 8	101	1079 ± 44	99	1050 ± 45
41	awiros-002	295953108	203723	104	562	108	2048 ± 0	90	479 ± 0	72	500 ± 0	67	534 ± 0	65	618 ± 0	117	946 ± 1	163	1966 ± 31	164	1957 ± 25
42	ayftech-001	200113346	43580	134	731	26	512 ± 0	76	408 ± 23	60	476 ± 52	133	814 ± 108	244	1827 ± 384	244	5412 ± 1029	43	615 ± 16	84	883 ± 44
43	ayonix-000	59909936	5252	5	69	63	1036 ± 0	2	18 ± 2	-	-	-	-	-	-	-	46	621 ± 23	50	620 ± 26	
44	bioidtechswiss-001	1207059515	120811	242	1455	19	512 ± 0	256	966 ± 4	250	1270 ± 270	236	1294 ± 96	224	1409 ± 157	204	1793 ± 79	189	2610 ± 25	191	2624 ± 32

Table 6: Summary of algorithms and properties included in this report. The red superscripts give ranking for the quantity in that column.

Notes	
1	The configuration size does not capture static data included in libraries.
2	The library size is the combined total of all files provided in the submission lib folder. These libraries e.g. OpenCV may or may not be installed on any end user's platform natively and would not need to be installed with the algorithm. Some developers put neural network models in their libraries.
3	The memory usage is the peak resident set size reported by the ps system call during template generation.
4	The median template creation times are measured on Intel®Xeon®CPU E5-2630 v4 @ 2.20GHz processors.
5	The comparison durations, in nanoseconds, are estimated using std::chrono::high_resolution_clock which on the machine in (2) counts 1ns clock ticks. Precision is somewhat worse than that however. The ± value is the median absolute deviation times 1.48 for Normal consistency.

ALGORITHM		CONFIG	LIBRARY	TEMPLATE								COMPARISON ⁴		
NAME		DATA	DATA	MEMORY	SIZE	GENERATION TIME (ms) ⁴				TIME (ns) ⁵				
		(KB) ¹	(KB) ²	(MB) ³	(B)	MUGSHOT	480x720	960x1440	1600x2400	3000x4500	GENUINE	IMPOSTOR		
45	boidtechswiss-002	762660868	114842	188 ⁹⁹³	27512 ± 0	242917 ± 2	190930 ± 2	173952 ± 2	149947 ± 3	1361058 ± 11	1722177 ± 29	1732170 ± 31		
46	bm-001	294640228	38076	22148	164 ± 0	82444 ± 88	-	-	-	-	1581887 ± 31	1581877 ± 26		
47	boetech-001	267649084	88710	2301384	842048 ± 0	44271 ± 1	28268 ± 1	18273 ± 0	17286 ± 1	15318 ± 1	30468519 ± 1921	30467648 ± 822		
48	bresee-000	294790072	22872	45333	1042048 ± 0	3081309 ± 1	2672126 ± 1	2431330 ± 0	2151312 ± 0	1751333 ± 0	29745317 ± 228	30048256 ± 425		
49	bresee-001	294790077	23227	2121214	1352048 ± 0	2971223 ± 3	2421216 ± 1	2441331 ± 1	2011227 ± 1	1771360 ± 1	29237240 ± 655	29337167 ± 584		
50	camvi-002	241949538	225285	135737	591024 ± 0	170677 ± 7	134726 ± 36	148869 ± 28	1841129 ± 43	2272785 ± 113	41612 ± 26	44603 ± 20		
51	camvi-004	287471548	615819	170919	1662048 ± 0	193759 ± 10	172861 ± 17	182986 ± 34	2091279 ± 51	2292891 ± 158	85948 ± 40	87963 ± 31		
52	canon-002	457207046	130232	165891	2784096 ± 0	3071308 ± 2	2561315 ± 1	2421326 ± 2	2171345 ± 1	2476211 ± 25	2456194 ± 25			
53	ceiec-003	266620201	88707	59430	1282048 ± 0	213817 ± 4	180883 ± 57	156897 ± 60	141899 ± 72	116944 ± 72	1762256 ± 38	1772241 ± 54		
54	ceiec-004	269799940	67011	54408	1162048 ± 0	2691024 ± 1	2081027 ± 1	1911027 ± 1	1671030 ± 1	1341055 ± 1	1551844 ± 26	1551836 ± 20		
55	chosun-001	783990750	707	80491	942048 ± 0	200783 ± 2	162826 ± 4	2611662 ± 13	2623679 ± 67	25911694 ± 243	92998 ± 25	981035 ± 11		
56	chosun-002	239617968	31875	66450	2112048 ± 0	38248 ± 3	29273 ± 3	2571495 ± 14	2657920 ± 90	26280302 ± 1349	47623 ± 17	56634 ± 13		
57	chtface-002	371869498	369529	2021100	1632048 ± 0	126584 ± 14	129712 ± 41	1971038 ± 42	2451861 ± 75	2424661 ± 232	1772264 ± 26	1762234 ± 103		
58	chtface-003	371869498	369529	2091178	1472048 ± 0	136594 ± 16	133720 ± 33	2001050 ± 41	2481884 ± 90	2465606 ± 334	1692110 ± 37	1752219 ± 65		
59	cib-001	446723681	133766	151836	1742048 ± 0	156651 ± 2	127707 ± 13	117716 ± 15	95728 ± 3	93820 ± 5	2213783 ± 38	2193765 ± 37		
60	cloudwalk-hr-003	392949139	144263	186984	2492057 ± 0	138606 ± 0	93588 ± 0	77594 ± 0	64612 ± 1	-	2526982 ± 80	2516972 ± 84		
61	cloudwalk-hr-004	514986414	520169	2321394	2232049 ± 0	231873 ± 1	178877 ± 1	152876 ± 1	136879 ± 1	109902 ± 3	26411652 ± 127	26311608 ± 123		
62	cloudwalk-mt-002	297731560	145340	154844	2212049 ± 0	122573 ± 1	132717 ± 78	112700 ± 66	101749 ± 96	83770 ± 80	2577205 ± 204	2557211 ± 244		
63	cloudwalk-mt-003	502133796	494959	2251342	2222049 ± 0	243923 ± 1	187918 ± 1	166926 ± 1	144925 ± 1	115936 ± 1	26311620 ± 179	26411661 ± 128		
64	clova-000	203182777	6824	69464	1502048 ± 0	81437 ± 0	50431 ± 0	39435 ± 0	31452 ± 2	25508 ± 7	1491794 ± 16	1531795 ± 19		
65	cogent-004	740269228	389164	1951059	801983 ± 0	262987 ± 50	-	-	-	-	27515536 ± 75	27515964 ± 708		
66	cogent-005	1921839276	75276	2892806	2622523 ± 0	2961221 ± 2	2451236 ± 1	2321289 ± 2	2261420 ± 4	1941602 ± 5	28624854 ± 69	28524858 ± 71		
67	cognitec-000	486154134	27371	81495	2252052 ± 0	35224 ± 1	-	-	-	-	2223835 ± 108	2203782 ± 83		
68	cognitec-002	403546749	62354	117624	2332052 ± 0	28192 ± 6	18219 ± 6	16233 ± 8	14241 ± 6	14314 ± 10	2093250 ± 41	2103241 ± 48		
69	cor-001	1223627342	11240	2151249	2522060 ± 0	182699 ± 3	173863 ± 76	147865 ± 80	132872 ± 89	119952 ± 39	314270145 ± 2259	314282686 ± 11788		
70	corsight-001	1472269967	31525	2722040	2532064 ± 0	3041291 ± 3	2511285 ± 1	2341293 ± 1	2111303 ± 2	1781379 ± 3	313249340 ± 1713	313248929 ± 1909		
71	csc-001	0	240698	102557	41544 ± 0	53302 ± 1	35303 ± 0	20304 ± 0	18309 ± 1	17341 ± 4	16354 ± 8	18344 ± 11		
72	csc-002	0	519768	2291376	40544 ± 0	88473 ± 0	69494 ± 0	50481 ± 1	40490 ± 1	28514 ± 5	17367 ± 11	19371 ± 10		
73	ctcbank-000	263381717	599238	106570	1712048 ± 0	120568 ± 43	97606 ± 38	106690 ± 53	90711 ± 50	97831 ± 51	2163551 ± 87	2284805 ± 209		
74	ctcbank-001	282123885	599238	111603	972048 ± 0	158652 ± 35	151781 ± 30	151875 ± 43	140898 ± 51	1301030 ± 47	2233926 ± 45	2223924 ± 56		
75	cubox-001	378498689	75427	121649	1352048 ± 0	240907 ± 1	186902 ± 1	158903 ± 0	143917 ± 0	113931 ± 0	1241379 ± 37	1291417 ± 38		
76	cukee-001	806762318	74917	2832515	2272052 ± 0	258977 ± 31	-	-	-	-	1922719 ± 60	1942783 ± 56		
77	cybercore-000	88073082	55441	32200	25512 ± 0	162655 ± 3	119689 ± 71	96649 ± 6	72648 ± 8	62680 ± 6	27214800 ± 75	27415757 ± 782		
78	cyberextruder-001	124120800	13629	26178	4256 ± 0	238893 ± 25	-	-	-	-	1021083 ± 16	1041079 ± 19		
79	cyberextruder-002	172963574	13924	31194	852048 ± 0	111532 ± 6	-	-	-	-	1521803 ± 14	1511779 ± 22		
80	cyberlink-005	349881011	111358	1921037	3044140 ± 0	187721 ± 1	142752 ± 2	126754 ± 2	104755 ± 1	85791 ± 3	2183680 ± 37	2234021 ± 97		
81	cyberlink-006	349866738	102456	2331400	3156212 ± 0	178690 ± 1	123702 ± 0	113703 ± 0	91712 ± 0	75741 ± 0	9270 ± 13	12271 ± 13		
82	dahua-005	1624985571	169478	3137360	2864096 ± 0	3141418 ± 34	-	-	-	-	87957 ± 23	89969 ± 19		
83	dahua-006	851600617	119261	3105068	1902048 ± 0	3121398 ± 2	2591397 ± 1	2501404 ± 1	2221402 ± 1	1821402 ± 1	7249 ± 13	9250 ± 11		
84	decatur-000	358907752	171271	168907	2954100 ± 0	2681024 ± 2	-	-	-	-	26211439 ± 80	26211418 ± 112		
85	deepglint-002	470673814	272878	2541614	2814096 ± 0	171677 ± 2	161826 ± 74	142848 ± 42	126849 ± 55	105886 ± 27	27113633 ± 87	26912905 ± 440		
86	deepglint-003	858178673	262081	2782374	3136144 ± 0	2861159 ± 1	2331145 ± 1	2161148 ± 1	1891148 ± 1	1531163 ± 1	27717227 ± 41	27717210 ± 51		
87	deepsea-001	151037339	336250	48358	521024 ± 0	150630 ± 7	143752 ± 37	123746 ± 30	94727 ± 32	92820 ± 32	1271401 ± 37	1311467 ± 50		
88	deepsense-000	365684327	936618	3147618	1102048 ± 0	166664 ± 3	109645 ± 1	97660 ± 2	83687 ± 2	90808 ± 3	23480 ± 22	25459 ± 34		

Notes

- 1 The configuration size does not capture static data included in libraries.
- 2 The library size is the combined total of all files provided in the submission lib folder. These libraries e.g. OpenCV may or may not be installed on any end user's platform natively and would not need to be installed with the algorithm. Some developers put neural network models in their libraries.
- 3 The memory usage is the peak resident set size reported by the ps system call during template generation.
- 4 The median template creation times are measured on Intel®Xeon®CPU E5-2630 v4 @ 2.20GHz processors.
- 5 The comparison durations, in nanoseconds, are estimated using std::chrono::high_resolution_clock which on the machine in (2) counts 1ns clock ticks. Precision is somewhat worse than that however. The ± value is the median absolute deviation times 1.48 for Normal consistency.

	ALGORITHM	CONFIG	LIBRARY	TEMPLATE								COMPARISON ⁴		
	NAME	DATA	DATA	MEMORY	SIZE	GENERATION TIME (ms) ⁴				TIME (ns) ⁵				
		(KB) ¹	(KB) ²	(MB) ³	(B)	MUGSHOT	480x720	960x1440	1600x2400	3000x4500	GENUINE	IMPOSTOR		
89	dermalog-006	0	452387	183970	2128 ± 0	110532 ± 12	-	-	-	-	27506 ± 23	26459 ± 23		
90	dermalog-008	0	937895	3094989	21512 ± 0	72404 ± 2	48410 ± 3	38424 ± 5	29430 ± 5	23477 ± 5	22468 ± 31	16328 ± 13		
91	didiglobalface-001	266086235	70680	93527	1572048 ± 0	142612 ± 1	107633 ± 3	92634 ± 3	74650 ± 15	60666 ± 4	89973 ± 20	91988 ± 20		
92	digitalbarriers-002	84994577	598577	2671930	2392056 ± 0	31209 ± 11	24250 ± 19	35411 ± 37	116808 ± 72	2122236 ± 123	26913409 ± 228	27013267 ± 206		
93	dsk-000	12254510	782905	35252	18512 ± 0	54304 ± 47	36317 ± 33	1861001 ± 96	2582660 ± 170	25810451 ± 832	2567152 ± 115	2547134 ± 111		
94	einetworks-000	381551539	219883	163880	2362056 ± 0	156645 ± 3	-	-	-	-	2304876 ± 66	2295156 ± 77		
95	ekin-002	52668576	278	20139	2673072 ± 0	2911186 ± 13	2361180 ± 12	2181181 ± 11	1951191 ± 11	1581207 ± 8	2274294 ± 80	2355569 ± 12		
96	enface-000	378468370	153781	124662	561024 ± 0	119555 ± 4	87558 ± 4	100669 ± 6	156987 ± 15	2152349 ± 54	2547059 ± 62	2526980 ± 65		
97	eocortex-000	262080175	59432	34224	1652048 ± 0	55305 ± 22	41341 ± 25	43440 ± 47	33464 ± 45	27513 ± 44	83923 ± 11	85918 ± 11		
98	ercacat-001	831102356	58012	2902816	2292052 ± 0	2751052 ± 3	-	-	-	-	1852551 ± 62	1852501 ± 81		
99	expasoft-000	15709925	240451	17100	1032048 ± 0	568 ± 0	271 ± 0	275 ± 0	271 ± 0	272 ± 1	1481779 ± 26	1461757 ± 97		
100	expasoft-001	39994987	983064	21142	1482048 ± 0	670 ± 0	374 ± 0	377 ± 0	373 ± 0	374 ± 0	1391660 ± 35	1401676 ± 48		
101	f8-001	279529297	19668	2201276	902048 ± 0	218822 ± 39	-	-	-	-	27415262 ± 139	27315277 ± 21		
102	facesoft-000	379002927	10612	141796	1822048 ± 0	169675 ± 18	113669 ± 3	104686 ± 3	79675 ± 5	63687 ± 2	1752239 ± 28	1782277 ± 96		
103	facetag-000	1261907727	4022	189965	47684 ± 0	64355 ± 17	45369 ± 8	184989 ± 33	252408 ± 91	2537930 ± 316	30272003 ± 625	30671912 ± 61		
104	facex-001	312396751	930372	2932931	892048 ± 0	77422 ± 4	52434 ± 4	65520 ± 7	97737 ± 13	1971670 ± 27	1561871 ± 23	1561846 ± 29		
105	farfaces-001	354810878	44581	36261	14512 ± 0	2881179 ± 1	2381180 ± 1	2171180 ± 0	1921185 ± 1	1591209 ± 2	81855 ± 25	81860 ± 31		
106	fiberhome-nanjing-002	212375748	596827	148826	541024 ± 0	2951217 ± 2	2541294 ± 30	2401312 ± 12	2321477 ± 14	1721326 ± 11	1351582 ± 57	1351560 ± 58		
107	fiberhome-nanjing-003	361365058	1482309	156845	1862048 ± 0	2831136 ± 7	2301134 ± 4	2141132 ± 3	1881139 ± 3	1501154 ± 5	1041097 ± 38	1071083 ± 13		
108	fincore-000	262774045	19409	96535	1402048 ± 0	102508 ± 3	73505 ± 0	60508 ± 1	46513 ± 2	33535 ± 1	1461765 ± 31	1471763 ± 21		
109	fujitsulab-001	63	548917	2171252	2994104 ± 0	3061300 ± 5	2531291 ± 2	2371295 ± 2	2121304 ± 2	1791382 ± 2	1952853 ± 16	1962847 ± 47		
110	fujitsulab-002	0	1088887	2531613	3004104 ± 0	3011237 ± 2	2431222 ± 2	2261236 ± 1	2041251 ± 2	1741327 ± 2	1942836 ± 25	1952809 ± 44		
111	geo-001	264721293	70163	47344	1642048 ± 0	2781079 ± 0	2181076 ± 0	2031076 ± 0	1771078 ± 0	1441102 ± 0	2063163 ± 47	2073158 ± 38		
112	geo-002	378781240	98667	1891018	2012048 ± 0	203791 ± 1	153793 ± 0	129794 ± 0	113795 ± 1	87803 ± 1	2113407 ± 45	2133422 ± 65		
113	glory-002	0	385177	184982	2592106 ± 0	135594 ± 3	137740 ± 3	171948 ± 3	2512168 ± 6	9191 ± 15	2506787 ± 85	2486551 ± 24		
114	glory-003	0	536910	2341400	3054234 ± 0	95489 ± 0	88565 ± 0	120732 ± 0	2471876 ± 2	2548941 ± 20	2436020 ± 90	2446003 ± 72		
115	gorilla-005	103100834	1297614	119629	2612192 ± 0	74407 ± 3	53437 ± 2	45448 ± 4	35473 ± 4	43589 ± 15	1912678 ± 42	1932770 ± 1		
116	gorilla-006	176888996	1318812	162874	3064240 ± 0	83454 ± 3	64484 ± 3	58497 ± 5	52543 ± 25	112928 ± 60	2193755 ± 38	2183737 ± 44		
117	hertasecurity-000	5	780014	90516	6256 ± 0	1299 ± 0	598 ± 0	5100 ± 0	5107 ± 0	6139 ± 0	63710 ± 31	59667 ± 28		
118	hik-001	683894884	9290	3126597	701408 ± 0	157651 ± 0	112667 ± 8	102677 ± 16	82686 ± 13	73737 ± 12	24488 ± 19	247477 ± 24		
119	hyperverge-001	267079500	88624	85507	862048 ± 0	174682 ± 20	120695 ± 17	2221196 ± 37	2542400 ± 68	2517178 ± 204	2456026 ± 40	2435984 ± 88		
120	hyperverge-002	3022745705	198832	2691975	551024 ± 0	245938 ± 1	194939 ± 1	170941 ± 1	148945 ± 1	121975 ± 1	2446023 ± 37	2425966 ± 40		
121	icm-002	636504686	903	75484	1602048 ± 0	2711031 ± 7	-	-	-	-	28524052 ± 118	28424049 ± 124		
122	icthtc-000	176598609	1471004	2601805	1462048 ± 0	62338 ± 11	40338 ± 9	40437 ± 16	88705 ± 24	2011719 ± 44	2335284 ± 63	2335290 ± 54		
123	id3-006	215159624	7706	185982	35520 ± 0	175683 ± 0	2191088 ± 1	2201192 ± 1	1981209 ± 1	1651270 ± 1	2375547 ± 34	2365563 ± 34		
124	id3-007	189471032	7728	187988	9264 ± 0	2661016 ± 1	2321139 ± 1	2673911 ± 2	26710752 ± 12	263135182 ± 1912	2355500 ± 29	2355486 ± 35		
125	idemlia-006	584260076	115633	173932	46668 ± 0	173679 ± 4	188926 ± 54	119728 ± 7	108760 ± 29	96830 ± 31	2315223 ± 80	2305193 ± 12		
126	idemlia-007	361720312	67485	1931051	12468 ± 0	70384 ± 0	46389 ± 0	32393 ± 1	25405 ± 2	22441 ± 8	2083243 ± 63	2093202 ± 63		
127	iit-002	265809599	52070	133731	832048 ± 0	103514 ± 1	77531 ± 2	72547 ± 1	56583 ± 1	71733 ± 2	951023 ± 7	951011 ± 6		
128	iit-003	267559145	53791	146817	2072048 ± 0	91482 ± 0	66493 ± 0	61509 ± 0	51541 ± 0	58661 ± 0	14324 ± 17	15326 ± 8		
129	imagus-002	233233236	318409	56411	1362048 ± 0	202786 ± 1	146766 ± 2	154885 ± 3	2271430 ± 3	2394080 ± 10	53676 ± 16	52630 ± 20		
130	imagus-003	260977219	378019	83498	1052048 ± 0	227865 ± 2	193938 ± 1	2601577 ± 1	2603002 ± 3	2509521 ± 16	69738 ± 26	61683 ± 25		
131	imperial-000	379002927	10623	142796	1782048 ± 0	167669 ± 1	116675 ± 3	103683 ± 17	80676 ± 2	64689 ± 2	1702130 ± 32	1682052 ± 100		
132	imperial-002	483663560	16134	2621826	1312048 ± 0	121569 ± 1	91581 ± 15	75575 ± 5	55576 ± 2	42588 ± 3	1782278 ± 90	1702131 ± 14		

Notes

- 1 The configuration size does not capture static data included in libraries.
- 2 The library size is the combined total of all files provided in the submission lib folder. These libraries e.g. OpenCV may or may not be installed on any end user's platform natively and would not need to be installed with the algorithm. Some developers put neural network models in their libraries.
- 3 The memory usage is the peak resident set size reported by the ps system call during template generation.
- 4 The median template creation times are measured on Intel®Xeon®CPU E5-2630 v4 @ 2.20GHz processors.
- 5 The comparison durations, in nanoseconds, are estimated using std::chrono::high_resolution_clock which on the machine in (2) counts 1ns clock ticks. Precision is somewhat worse than that however. The ± value is the median absolute deviation times 1.48 for Normal consistency.

Table 8: Summary of algorithms and properties included in this report. The red superscripts give ranking for the quantity in that column.

	ALGORITHM	CONFIG	LIBRARY	TEMPLATE								COMPARISON ⁴			
				NAME		DATA		MEMORY		SIZE		GENERATION TIME (ms) ⁴			
				(KB) ¹	(KB) ²	(MB) ³	(B)	MUGSHOT	480x720	960x1440	1600x2400	3000x4500	GENUINE	IMPOSTOR	
133	incode-007	272489724	63524	¹⁴⁷ 818	¹⁸¹ 2048 ± 0	⁸⁷ 470 ± 1	⁷⁵ 516 ± 0	⁶³ 518 ± 1	⁴⁸ 530 ± 2	⁴⁵ 603 ± 4	¹⁵¹ 1799 ± 35	¹⁵² 789 ± 59			
134	incode-008	272489716	21014	²⁴⁴ 1469	¹²¹ 2048 ± 0	⁹⁸ 500 ± 0	⁶⁷ 493 ± 0	⁵⁷ 496 ± 0	⁴⁵ 506 ± 1	³⁴ 537 ± 0	⁹⁸ 1070 ± 28	¹⁰⁶ 1081 ± 34			
135	incode-009	272489716	21014	¹⁷⁶ 939	²⁰⁰ 2048 ± 0	⁹⁹ 503 ± 0	⁶⁵ 490 ± 1	⁵⁹ 498 ± 0	⁴⁴ 505 ± 0	³⁵ 537 ± 0	¹⁰⁶ 1102 ± 28	¹¹¹ 113 ± 29			
136	innefulabs-000	379482783	162172	⁶¹ 439	¹⁵¹ 2048 ± 0	²⁶⁴ 1006 ± 3	²⁰⁶ 1025 ± 3	¹⁹³ 1030 ± 4	¹⁷¹ 1041 ± 2	¹⁴⁷ 1135 ± 3	²³⁹ 5782 ± 41	²⁴¹ 3741 ± 45			
137	innovativetechnologyltd-001	181485901	335757	⁴⁰ 341	¹⁷⁷ 2048 ± 0	⁷⁸ 433 ± 7	⁵⁰ 446 ± 8	⁴¹ 439 ± 4	³⁰ 452 ± 4	²⁴ 485 ± 7	¹⁵⁷ 1877 ± 42	¹⁶⁰ 1924 ± 97			
138	innovativetechnologyltd-002	178114027	372324	¹⁶⁹ 912	¹⁵⁴ 2048 ± 0	¹⁶³ 661 ± 2	¹³⁵ 726 ± 4	¹⁸⁰ 981 ± 27	¹⁶⁰ 997 ± 40	⁸² 766 ± 3	¹⁵⁴ 1841 ± 50	¹⁵⁷ 1857 ± 59			
139	innovatrics-006	74	466269	²⁰⁴ 1107	³⁹ 538 ± 0	²¹⁴ 820 ± 5	¹⁵⁶ 799 ± 4	¹³¹ 805 ± 3	¹¹⁴ 796 ± 9	¹⁰⁶ 890 ± 15	²⁴⁰ 5855 ± 204	²³¹ 5266 ± 118			
140	innovatrics-007	74	493269	²⁶⁸ 1937	⁶⁶ 1064 ± 0	³²⁰ 1485 ± 7	²⁶⁶ 1785 ± 184	²⁶⁴ 2078 ± 24	²⁵⁰ 2123 ± 15	²¹¹ 2210 ± 42	²⁴² 5978 ± 88	²⁴⁰ 5690 ± 102			
141	insightface-000	826320727	16606	³⁰² 3912	²⁷⁹ 4096 ± 0	²⁰⁵ 1009 ± 1	²⁰⁵ 1019 ± 2	¹⁸⁸ 1017 ± 2	¹⁶⁴ 1020 ± 2	¹³¹ 1032 ± 2	¹⁴⁷ 1778 ± 31	¹⁴⁸ 773 ± 35			
142	intelliloudai-001	226131619	868246	¹²² 655	¹⁵⁶ 2048 ± 0	⁸⁶ 468 ± 2	⁵⁷ 456 ± 1	⁴⁶ 466 ± 3	⁴¹ 492 ± 1	⁵⁰ 632 ± 2	⁹⁶ 1056 ± 4	¹⁰⁰ 1051 ± 72			
143	intelliloudai-002	265264200	58559	²⁹⁷ 3584	²⁹⁸ 4100 ± 0	²²³ 847 ± 1	¹⁶⁷ 847 ± 2	¹⁴³ 849 ± 1	¹²⁸ 853 ± 1	¹⁰⁴ 878 ± 4	⁷⁹ 822 ± 28	⁷⁹ 818 ± 23			
144	intellifusion-001	278397082	289387	¹³⁶ 762	²⁰⁶ 2048 ± 0	¹⁹⁴ 764 ± 38	¹⁴⁸ 774 ± 39	¹³⁰ 797 ± 42	¹¹⁵ 803 ± 34	⁸⁸ 805 ± 33	¹⁰⁷ 1112 ± 28	¹¹² 128 ± 41			
145	intellifusion-002	781037413	385841	¹⁷⁷ 941	²⁸⁰ 4096 ± 0	²⁵² 950 ± 2	²²³ 1096 ± 42	²⁰⁶ 1088 ± 33	¹⁹⁰ 1168 ± 31	¹⁵⁴ 1171 ± 10	¹⁴⁴ 1713 ± 57	¹³⁹ 665 ± 87			
146	intellivision-001	44741184	11649	⁷ 74	²⁴³ 2056 ± 0	⁴ 62 ± 2	-	-	-	-	¹⁸⁸ 2573 ± 91	¹⁸⁸ 454 ± 38			
147	intellivision-002	44741184	14505	¹⁰ 81	²⁴⁶ 2056 ± 0	⁵⁷ 322 ± 1	⁴² 355 ± 2	²⁹ 372 ± 1	²⁸ 422 ± 2	⁴⁴ 600 ± 1	²⁷⁰ 13525 ± 134	²⁶⁸ 12782 ± 278			
148	intelresearch-002	463719162	86454	²³⁶ 1420	⁹⁸ 2048 ± 0	¹⁸⁵ 707 ± 2	¹⁵² 790 ± 33	¹²⁸ 788 ± 26	¹²¹ 831 ± 29	¹⁰² 862 ± 22	²²⁵ 4204 ± 91	²²⁴ 453 ± 93			
149	intelresearch-003	410975551	85085	²⁰⁸ 1177	¹⁴⁴ 2048 ± 0	²⁹⁹ 1232 ± 3	²⁴⁶ 1237 ± 2	²²⁸ 1242 ± 2	²⁰⁷ 1263 ± 2	¹⁷¹ 1324 ± 3	²²⁸ 4443 ± 75	²²⁶ 474 ± 77			
150	intsy whole-001	393635676	172480	¹⁴⁰ 789	¹⁹⁹ 2048 ± 0	¹⁴³ 614 ± 2	¹⁰¹ 615 ± 2	⁹⁵ 642 ± 2	¹⁰² 750 ± 3	¹⁵² 1159 ± 4	⁴⁵ 621 ± 8	⁶¹ 61 ± 31			
151	intsy whole-002	784303912	172298	¹³⁹ 786	⁴⁹ 1024 ± 0	¹³⁴ 593 ± 1	¹⁵⁴ 793 ± 2	¹³⁶ 827 ± 1	¹³⁴ 875 ± 104	¹⁶⁷ 1293 ± 3	²⁹ 549 ± 25	³² 548 ± 29			
152	iqface-000	275271315	596337	¹²⁸ 704	³⁰⁸ 4750 ± 32	¹¹² 538 ± 26	⁶⁸ 494 ± 2	⁷⁰ 543 ± 3	⁹⁶ 734 ± 4	¹⁸⁰ 1393 ± 4	³¹⁸ 636433 ± 38446	³¹⁸ 632654 ± 85615			
153	iqface-003	379702979	963398	¹⁴⁵ 817	³⁰⁹ 4763 ± 37	¹⁰⁶ 529 ± 1	⁷⁹ 532 ± 2	⁷⁹ 599 ± 8	¹²⁷ 850 ± 2	¹⁹⁹ 1694 ± 2	³¹⁷ 575924 ± 2601	³¹⁷ 576633 ± 2051			
154	irex-000	759705187	47419	²⁷³ 2086	²⁶⁸ 3080 ± 0	²²⁴ 852 ± 2	¹⁶⁹ 850 ± 1	¹⁵⁰ 874 ± 2	¹⁴⁵ 939 ± 1	¹⁶³ 1249 ± 5	⁴ 201 ± 11	⁵ 208 ± 8			
155	isap-001	101427082	204201	¹ 18	²⁸⁹ 4096 ± 0	¹ 0 ± 0	-	-	-	-	²¹ 459 ± 17	²⁴ 456 ± 11			
156	isap-002	262928187	49931	⁴¹ 288	²¹⁸ 2048 ± 0	¹⁹⁷ 769 ± 3	²⁰⁷ 1027 ± 2	¹⁵³ 877 ± 2	¹⁰⁹ 761 ± 1	¹¹¹ 912 ± 2	²⁰² 3045 ± 94	¹⁹⁸ 4923 ± 66			
157	isityou-000	49163234	36621	¹⁶ 110	³¹⁹ 19200 ± 0	¹⁵ 113 ± 5	-	-	-	-	³¹² 237517 ± 1318	³¹² 237374 ± 1279			
158	isystems-001	281212446	639268	²⁰¹ 1091	²⁰⁵ 2048 ± 0	⁵⁰ 291 ± 9	-	-	-	-	³⁰ 557 ± 16	³⁵ 564 ± 22			
159	isystems-002	367599646	803389	²⁵² 1595	¹²² 2048 ± 0	²¹⁷ 822 ± 8	-	-	-	-	⁷⁰ 749 ± 31	⁵³ 522 ± 28			
160	itm0-006	613567913	96762	²⁴⁶ 1489	²⁶⁰ 2121 ± 0	²¹¹ 814 ± 1	¹⁶⁴ 831 ± 26	¹³⁸ 830 ± 17	¹²⁰ 830 ± 3	¹¹⁸ 952 ± 38	²⁸⁸ 26154 ± 148	²⁸⁷ 26124 ± 260			
161	itm0-007	425962652	245376	²⁷⁷ 2199	¹⁷⁰ 2048 ± 0	¹⁹⁰ 741 ± 2	-	-	-	-	¹⁸⁶ 2551 ± 50	¹⁸⁷ 4529 ± 80			
162	ivacognitive-001	263125888	62791	¹⁷⁸ 947	¹¹⁹ 2048 ± 0	³⁰⁵ 1292 ± 3	²⁵² 1289 ± 4	²³³ 1292 ± 4	²¹⁰ 1292 ± 3	¹⁷⁰ 1321 ± 4	²²⁶ 4228 ± 41	²²⁵ 426 ± 41			
163	iws-000	31616555	3063	⁸ 77	¹⁵ 512 ± 0	⁴⁶ 277 ± 5	³² 283 ± 1	⁵⁵ 494 ± 3	¹⁵⁵ 984 ± 3	²³² 2987 ± 39	⁹³ 999 ± 40	⁹³ 992 ± 22			
164	kakao-004	424357647	135270	²⁵⁹ 1783	¹⁰¹ 2048 ± 0	²²⁵ 856 ± 1	¹⁷⁰ 855 ± 0	¹⁴⁵ 857 ± 0	¹³⁰ 858 ± 0	¹⁰¹ 860 ± 1	¹⁶² 1957 ± 28	¹⁶³ 1953 ± 37			
165	kakao-005	424259623	152216	²⁵¹ 1581	²³⁰ 2052 ± 0	²⁷⁷ 1068 ± 1	²¹⁷ 1073 ± 1	²⁰⁴ 1079 ± 0	¹⁷⁶ 1077 ± 1	¹⁴² 1089 ± 1	¹⁶⁸ 2067 ± 26	¹⁶⁷ 4043 ± 34			
166	kedacom-000	251179996	37401	³¹⁸ 23574	¹⁰ 292 ± 0	¹⁰⁰ 506 ± 3	⁸⁵ 547 ± 10	⁸⁵ 614 ± 9	⁵⁸ 588 ± 10	⁵⁹ 665 ± 24	⁵⁶ 684 ± 14	⁶⁰ 682 ± 16			
167	kiwitech-000	378584700	21375	¹⁴⁴ 808	¹⁴³ 2048 ± 0	¹³³ 591 ± 0	⁹⁵ 594 ± 0	⁷⁸ 595 ± 1	⁶¹ 596 ± 0	⁴⁶ 609 ± 0	¹⁴⁵ 1755 ± 20	¹⁴⁵ 724 ± 16			
168	kneron-003	59767577	1747	²⁷ 188	¹³⁸ 2048 ± 0	⁴⁸ 281 ± 3	³¹ 280 ± 1	²³ 315 ± 13	²¹ 365 ± 7	¹⁶¹ 1224 ± 30	²³² 5237 ± 63	²³² 3244 ± 99			
169	kneron-005	384383985	13633	⁶⁸ 457	¹⁷² 2048 ± 0	¹⁰⁵ 518 ± 2	⁷⁶ 522 ± 4	⁷⁴ 556 ± 5	¹⁰⁶ 757 ± 19	²⁰² 1760 ± 25	¹⁶⁰ 1922 ± 11	¹⁶¹ 926 ± 20			
170	kookmin-001	239617968	31875	⁶² 439	¹⁰² 2048 ± 0	¹⁶ 114 ± 1	⁹ 110 ± 1	⁶ 116 ± 1	⁷ 128 ± 1	⁸ 172 ± 1	⁴⁸ 629 ± 35	⁴⁹ 616 ± 11			
171	kookmin-002	380693533	30734	¹⁴⁹ 827	¹⁶⁷ 2048 ± 0	²⁷³ 1038 ± 2	²¹⁵ 1047 ± 1	¹⁹⁸ 1045 ± 1	¹⁷⁵ 1061 ± 1	¹⁴⁵ 1116 ± 1	⁵¹ 638 ± 19	⁵² 636 ± 20			
172	lemalabs-001	766361714	198794	²⁸⁸ 2738	¹⁰⁰ 2048 ± 0	²⁰⁸ 810 ± 0	-	-	-	-	²⁶⁶ 11930 ± 35	²⁶⁶ 11913 ± 37			
173	line-000	270789845	407003	¹⁰⁸ 590	¹⁷⁵ 2048 ± 0	¹²⁷ 586 ± 0	⁹⁸ 612 ± 0	⁸² 609 ± 1	⁶³ 611 ± 0	⁴⁸ 618 ± 1	¹⁹³ 2753 ± 19	¹⁹² 2745 ± 23			
174	lookman-002	141516916	25410	³¹⁶ 16518	⁴² 548 ± 0	²³ 173 ± 1	-	-	-	-	⁴⁰ 610 ± 19	⁴⁸ 612 ± 22			
175	lookman-004	250650528	37401	³¹⁷ 23548	⁴³ 548 ± 0	¹⁰¹ 507 ± 5	⁸³ 545 ± 12	⁸⁴ 613 ± 12	⁵⁹ 590 ± 11	⁵⁸ 656 ± 16	⁸² 871 ± 29	⁸³ 878 ± 29			
176	luxand-000	0	57908	²²⁷ 1366	⁶⁴ 1040 ± 0	⁷³ 407 ± 23	⁵¹ 433 ± 11	⁴⁴ 444 ± 14	³² 464 ± 14	³⁹ 562 ± 25	⁸⁰ 828 ± 28	⁸⁰ 828 ± 32			

Notes

- 1 The configuration size does not capture static data included in libraries.
- 2 The library size is the combined total of all files provided in the submission lib folder. These libraries e.g. OpenCV may or may not be installed on any end user's platform natively and would not need to be installed with the algorithm. Some developers put neural network models in their libraries.
- 3 The memory usage is the peak resident set size reported by the ps system call during template generation.
- 4 The median template creation times are measured on Intel®Xeon®CPU E5-2630 v4 @ 2.20GHz processors.
- 5 The comparison durations, in nanoseconds, are estimated using std::chrono::high_resolution_clock which on the machine in (2) counts 1ns clock ticks. Precision is somewhat worse than that however. The ± value is the median absolute deviation times 1.48 for Normal consistency.

Table 9: Summary of algorithms and properties included in this report. The red superscripts give ranking for the quantity in that column.

	ALGORITHM	CONFIG	LIBRARY	TEMPLATE								COMPARISON ⁴									
				NAME	DATA	DATA	MEMORY	SIZE	GENERATION TIME (ms) ⁴				TIME (ns) ⁵								
									(KB) ¹	(KB) ²	(MB) ³	(B)	MUGSHOT	480x720	960x1440	1600x2400	3000x4500	GENUINE	IMPOSTOR		
177	megvii-002	1852993999	16491	264	1879	297	4100 ± 0	154	644 ± 0	-	-	-	-	-	-	300	50630 ± 183	299	47591 ± 116		
178	megvii-003	4536617822	42790	308	4878	277	4096 ± 0	293	1210 ± 1	244	1223 ± 0	245	1356 ± 4	235	1582 ± 7	224	2727 ± 23	310	225342 ± 3574	311	225413 ± 6344
179	meituhan-000	265743335	333178	99	554	184	2048 ± 0	79	436 ± 4	55	441 ± 1	86	626 ± 5	178	1098 ± 15	234	3126 ± 53	52	638 ± 17	55	633 ± 16
180	meiya-001	286777340	264913	86	507	220	2049 ± 0	146	622 ± 12	-	-	-	-	-	-	259	8356 ± 615	259	8134 ± 97		
181	microfocus-001	107032902	27242	28	190	3256 ± 0	43	264 ± 18	-	-	-	-	-	-	-	6	215 ± 8	6	217 ± 10		
182	microfocus-002	98599914	27362	25	176	5256 ± 0	40	259 ± 18	-	-	-	-	-	-	-	15	337 ± 34	7	230 ± 25		
183	minivision-000	856777875	16597	303	4013	274	4096 ± 0	272	1035 ± 1	212	1033 ± 2	195	1035 ± 1	170	1037 ± 1	137	1059 ± 2	183	2466 ± 26	183	2460 ± 25
184	mobai-000	374222377	80573	138	786	314	6144 ± 0	196	766 ± 8	173	869 ± 6	224	1205 ± 31	246	1867 ± 45	237	3549 ± 190	276	16458 ± 333	276	16423 ± 1473
185	mobai-001	271664763	60164	95	534	204	2048 ± 0	140	612 ± 3	100	614 ± 3	103	687 ± 9	137	886 ± 31	200	1707 ± 103	125	1386 ± 25	126	1377 ± 26
186	mobbl-000	186421478	58727	37	262	168	2048 ± 0	41	261 ± 16	26	267 ± 22	30	375 ± 92	76	655 ± 273	207	2059 ± 1129	268	12061 ± 142	267	12050 ± 133
187	mobbl-001	236708614	58706	33	223	192	2048 ± 0	27	183 ± 32	15	184 ± 25	26	354 ± 76	119	823 ± 396	226	2781 ± 1166	265	11832 ± 109	265	11851 ± 88
188	moreedian-000	537865562	21374	174	932	153	2048 ± 0	180	694 ± 0	121	698 ± 0	111	699 ± 0	86	700 ± 0	68	713 ± 1	153	1803 ± 11	150	1779 ± 23
189	mvision-001	232962922	149531	131	723	29	512 ± 0	179	691 ± 21	122	702 ± 19	110	697 ± 24	89	708 ± 29	67	710 ± 27	110	1123 ± 40	116	1154 ± 38
190	nazhiai-000	560624381	16141	285	2716	82	2048 ± 0	176	683 ± 3	118	687 ± 2	140	835 ± 27	128	840 ± 31	99	834 ± 34	174	2230 ± 34	171	2133 ± 84
191	neosystems-001	589102173	349959	211	1214	202	2048 ± 0	284	1137 ± 4	224	1098 ± 1	263	1767 ± 4	242	1769 ± 3	203	1765 ± 4	279	18557 ± 189	280	18640 ± 192
192	netbridgeTech-001	136302786	205875	87	508	292	4096 ± 0	785	1 ± 1	483	80 ± 0	484	80 ± 0	492	0 ± 0	4	113 ± 4	261	9280 ± 74	261	9446 ± 312
193	netbridgeTech-002	263871604	49931	43	299	159	2048 ± 0	221	838 ± 6	160	838 ± 2	141	839 ± 1	124	839 ± 3	100	859 ± 3	197	2893 ± 65	203	3050 ± 123
194	neurotechnology-010	370835979	50226	241	1451	32	514 ± 0	204	796 ± 1	158	796 ± 1	134	815 ± 3	129	853 ± 1	127	1006 ± 11	210	120 ± 8	2115	15
195	neurotechnology-011	372877031	51141	243	1462	33	514 ± 0	205	798 ± 1	157	802 ± 1	137	827 ± 3	133	873 ± 2	138	1059 ± 15	1	114 ± 11	114	114 ± 8
196	nhn-001	344464916	817674	123	662	285	4096 ± 0	270	1027 ± 3	210	1029 ± 1	192	1029 ± 1	172	1044 ± 1	143	1090 ± 1	301	56650 ± 260	302	56639 ± 18
197	nodeflux-002	793260136	690213	70	466	118	2048 ± 0	186	708 ± 4	128	709 ± 4	116	716 ± 5	93	716 ± 7	72	736 ± 3	213	3475 ± 62	212	3408 ± 142
198	notiontag-000	94979467	406791	92	525	45	584 ± 0	116	548 ± 64	86	548 ± 35	255	1450 ± 99	263	3771 ± 251	260	13146 ± 792	295	44672 ± 269	296	44593 ± 38
199	notiontag-001	94979467	427967	105	566	44	584 ± 0	244	929 ± 35	220	1092 ± 39	266	3709 ± 81	260	10233 ± 180	-	294	43636 ± 286	294	43724 ± 39	
200	nsensecorp-001	191919164	258593	100	554	198	2048 ± 0	61	336 ± 0	39	335 ± 0	24	336 ± 0	19	335 ± 0	16	337 ± 0	299	46605 ± 93	298	46613 ± 12
201	nsensecorp-002	191919991	122407	101	554	96	2048 ± 0	60	333 ± 0	37	333 ± 0	25	337 ± 0	20	338 ± 0	18	351 ± 0	298	45965 ± 213	297	45988 ± 158
202	ntechlab-009	1789996893	43730	306	4135	79	1940 ± 0	282	1115 ± 2	226	1114 ± 1	209	1119 ± 1	185	1130 ± 2	156	1202 ± 4	42	614 ± 20	40	595 ± 28
203	ntechlab-010	715357382	217167	294	2991	68	1280 ± 0	287	1177 ± 2	237	1180 ± 2	223	1197 ± 2	200	1224 ± 1	173	1326 ± 3	19	405 ± 13	21	416 ± 33
204	omnigarde-000	270395030	32882	91	523	57	1024 ± 0	249	944 ± 0	182	887 ± 0	159	888 ± 1	139	892 ± 0	110	902 ± 0	190	2671 ± 35	260	2620 ± 29
205	openface-001	0	40111	14	100	88	2048 ± 0	21	148 ± 1	13	154 ± 0	28	365 ± 3	27	409 ± 9	47	616 ± 31	39	608 ± 14	49	604 ± 15
206	oz-001	311012472	238311	190	1021	303	4125 ± 0	285	1147 ± 3	240	1182 ± 3	231	1273 ± 4	237	1617 ± 7	228	2890 ± 19	311	228011 ± 5455	310	220746 ± 53
207	oz-002	733207161	170261	296	3561	254	2065 ± 0	276	1064 ± 3	234	1171 ± 3	265	2953 ± 6	264	7352 ± 13	261	26658 ± 29	309	126758 ± 913	309	126758 ± 913
208	papsav1923-001	285911345	52652	73	473	93	2048 ± 0	148	626 ± 1	104	628 ± 1	87	630 ± 1	73	648 ± 2	76	744 ± 3	65	725 ± 25	69	731 ± 28
209	paravision-004	570030501	145440	249	1572	282	4096 ± 0	219	829 ± 2	168	834 ± 6	139	832 ± 2	122	833 ± 4	98	833 ± 2	68	737 ± 31	67	718 ± 38
210	paravision-006	555441987	202234	235	1404	287	4096 ± 0	183	700 ± 1	128	704 ± 0	114	705 ± 0	87	704 ± 0	69	705 ± 0	13	321 ± 16	13	315 ± 14
211	pensees-001	1658297650	408932	266	1922	316	8200 ± 0	280	1108 ± 3	263	1448 ± 17	254	1439 ± 10	231	1464 ± 5	192	1546 ± 9	205	3151 ± 34	206	3143 ± 29
212	pixelall-005	0	1001355	222	1292	310	5120 ± 0	281	1112 ± 3	227	1115 ± 1	210	1120 ± 1	183	1124 ± 2	149	1143 ± 2	119	1259 ± 29	120	1243 ± 23
213	pixelall-006	0	746305	175	934	264	2560 ± 0	267	1024 ± 3	209	1028 ± 2	194	1033 ± 1	168	1032 ± 1	133	1054 ± 2	71	754 ± 14	68	722 ± 10
214	psl-006	1240655589	524525	305	4134	271	3144 ± 0	317	1438 ± 6	262	1434 ± 4	253	1434 ± 4	229	1434 ± 5	186	1437 ± 5	11	291 ± 34	11	268 ± 25
215	psl-007	977255992	524521	304	4042	270	3144 ± 0	313	1408 ± 5	260	1417 ± 3	252	1418 ± 3	225	1419 ± 2	184	1422 ± 3	8	265 ± 22	10	258 ± 17
216	ptakuratsatu-000	29	585434	226	1347	38	538 ± 0	233	875 ± 3	174	863 ± 48	167	928 ± 9	151	958 ± 17	140	1066 ± 26	241	5900 ± 103	239	5687 ± 167
217	pxl-001	112759507	78231	23	168	16	512 ± 0	13	101 ± 5	8	104 ± 5	11	189 ± 12	26	408 ± 27	189	1470 ± 144	238	5598 ± 45	238	5590 ± 68
218	pyramid-000	381551539	219883	143	804	238	2056 ± 0	125	583 ± 2	-	-	-	-	-	-	255	7147 ± 59	257	7586 ± 425		
219	quantasoft-003	379410922	211354	194	1058	217	2048 ± 0	161	632 ± 2	108	634 ± 0	91	632 ± 0	68	631 ± 1	52	634 ± 0	5	201 ± 7	4	203 ± 8
220	rankone-009	441	107688	341	260	25	179 ± 4	-	-	-	-	-	-	-	-	62	710 ± 32	33	552 ± 25		

Table 10: Summary of algorithms and properties included in this report. The red superscripts give ranking for the quantity in that column.

Notes

- 1 The configuration size does not capture static data included in libraries.
- 2 The library size is the combined total of all files provided in the submission lib folder. These libraries e.g. OpenCV may or may not be installed on any end user's platform natively and would not need to be installed with the algorithm. Some developers put neural network models in their libraries.
- 3 The memory usage is the peak resident set size reported by the ps system call during template generation.
- 4 The median template creation times are measured on Intel®Xeon®CPU E5-2630 v4 @ 2.20GHz processors.
- 5 The comparison durations, in nanoseconds, are estimated using std::chrono::high_resolution_clock which on the machine in (2) counts 1ns clock ticks. Precision is somewhat worse than that however. The ± value is the median absolute deviation times 1.48 for Normal consistency.

	ALGORITHM	CONFIG	LIBRARY	TEMPLATE								COMPARISON ⁴									
				NAME	DATA	DATA	MEMORY	SIZE	GENERATION TIME (ms) ⁴				TIME (ns) ⁵								
									(KB) ¹	(KB) ²	(MB) ³	(B)	MUGSHOT	480x720	960x1440	1600x2400	3000x4500	GENUINE	IMPOSTOR		
221	rankone-010	441	138435	11	83	8	261 ± 0	29	193 ± 1	-	-	-	-	-	-	10	282 ± 13	8	234 ± 16		
222	realnetworks-002	97616019	107088	49	370	77	1848 ± 0	39	250 ± 2	23	242 ± 4	19	282 ± 5	23	381 ± 10	84	774 ± 15	122	1285 ± 17	121	1247 ± 42
223	realnetworks-004	176471448	913988	281	2467	237	2056 ± 0	58	330 ± 4	38	333 ± 3	33	402 ± 7	57	585 ± 15	181	1402 ± 51	113	1210 ± 29	119	1202 ± 17
224	regula-000	268743079	29384	114	610	113	2048 ± 0	292	1187 ± 1	229	1126 ± 1	213	1129 ± 0	186	1132 ± 1	151	1159 ± 1	26	491 ± 16	29	500 ± 22
225	remarkai-001	247662347	868314	132	730	226	2052 ± 0	220	831 ± 6	168	849 ± 18	201	1055 ± 25	196	1198 ± 34	191	1519 ± 38	116	1229 ± 20	78	805 ± 56
226	remarkai-002	229537224	808777	64	443	188	2048 ± 0	250	950 ± 6	192	935 ± 4	174	953 ± 3	153	964 ± 4	141	1073 ± 4	108	1115 ± 25	101	1068 ± 54
227	remarkai-003	287249016	58559	301	3896	294	4100 ± 0	261	986 ± 1	201	993 ± 1	185	992 ± 1	161	999 ± 3	128	1019 ± 2	76	787 ± 20	76	793 ± 22
228	rendip-000	0	437653	125	682	130	2048 ± 0	85	464 ± 2	48	458 ± 0	473	481 ± 0	37	483 ± 1	32	556 ± 4	573	576 ± 13	30	573 ± 11
229	rokid-000	264818990	396624	213	1218	241	2056 ± 0	113	546 ± 3	82	542 ± 2	71	545 ± 1	47	522 ± 3	40	563 ± 4	212	3457 ± 62	215	3463 ± 77
230	rokid-001	656613085	413733	197	1071	251	2060 ± 0	241	911 ± 2	186	901 ± 5	157	899 ± 2	142	900 ± 3	108	901 ± 3	210	3345 ± 50	211	3346 ± 149
231	s1-001	445943780	844340	137	772	258	2092 ± 0	137	605 ± 24	102	623 ± 20	161	920 ± 39	234	1567 ± 92	-	-	129	1428 ± 34	128	1415 ± 85
232	s1-002	532647605	95479	228	1374	312	6144 ± 0	302	1257 ± 1	248	1260 ± 1	229	1261 ± 1	206	1262 ± 1	166	1273 ± 1	229	4513 ± 25	227	4479 ± 25
233	saffe-001	88036907	62488	24	168	67	1280 ± 0	47	281 ± 1	-	-	-	-	-	-	-	120	1274 ± 19	123	1277 ± 26	
234	saffe-002	266877685	28285	158	855	212	2048 ± 0	212	817 ± 11	159	805 ± 15	132	809 ± 19	117	815 ± 29	91	813 ± 23	64	717 ± 7	66	714 ± 29
235	samtech-001	294996593	219883	112	605	242	2056 ± 0	51	294 ± 3	-	-	-	-	-	-	-	258	7694 ± 59	258	7678 ± 91	
236	scanovate-001	263253470	328532	110	601	109	2048 ± 0	123	577 ± 24	90	577 ± 21	89	632 ± 27	110	770 ± 28	183	1404 ± 32	267	12054 ± 699	271	13795 ± 305
237	scanovate-002	263153867	457227	157	850	158	2048 ± 0	181	696 ± 32	130	713 ± 33	121	738 ± 28	111	779 ± 32	155	1172 ± 53	201	3021 ± 38	205	3120 ± 163
238	securifai-001	123178989	12456	240	1445	301	4104 ± 0	32	211 ± 1	17	211 ± 1	13	211 ± 1	11	211 ± 1	10	211 ± 1	140	1681 ± 29	143	1701 ± 25
239	securifai-002	203595986	13496	160	863	62	1032 ± 0	19	123 ± 0	11	123 ± 0	7	123 ± 0	5	123 ± 0	4	615 ± 22	42	597 ± 19	49	597 ± 22
240	sensetime-004	977575461	30733	315	7843	60	1028 ± 0	316	1437 ± 15	-	-	-	-	-	-	-	117	1239 ± 31	117	1171 ± 22	
241	sensetime-005	783721534	37673	311	6133	61	1028 ± 0	309	1361 ± 27	255	1304 ± 1	241	1319 ± 1	219	1360 ± 1	190	1514 ± 1	115	1223 ± 28	118	1184 ± 29
242	sertis-000	271945833	68770	58	427	141	2048 ± 0	192	754 ± 0	145	759 ± 0	127	764 ± 0	107	760 ± 0	80	763 ± 0	132	1497 ± 29	136	1582 ± 38
243	sertis-002	471849050	68929	231	1391	169	2048 ± 0	290	1181 ± 1	235	1178 ± 0	219	1183 ± 0	194	1187 ± 0	160	1221 ± 0	103	1086 ± 32	102	1076 ± 31
244	shaman-000	0	120033	84	507	273	4096 ± 0	159	653 ± 16	-	-	-	-	-	-	-	18	380 ± 25	20	379 ± 31	
245	shaman-001	0	174446	89	511	276	4096 ± 0	52	294 ± 2	-	-	-	-	-	-	50	635 ± 19	22	441 ± 25	22	441 ± 25
246	shu-002	748800469	148309	164	890	291	4096 ± 0	191	751 ± 2	147	769 ± 4	164	922 ± 4	228	1431 ± 9	236	3489 ± 47	320	2930763 ± 47355	320	2929759 ± 3949
247	shu-003	439065557	146940	88	511	125	2048 ± 0	215	820 ± 6	163	828 ± 3	169	941 ± 9	213	1308 ± 15	233	3045 ± 44	184	2506 ± 26	186	2512 ± 38
248	siat-002	498527179	7738	279	2434	232	2052 ± 0	124	579 ± 0	-	-	-	-	-	-	-	73	769 ± 13	72	750 ± 13	
249	siat-004	962624717	6984	300	3860	296	4100 ± 0	168	670 ± 0	114	671 ± 7	107	693 ± 10	100	742 ± 10	114	935 ± 17	224	4013 ± 45	221	3782 ± 173
250	sjtu-003	492334366	148243	97	538	123	2048 ± 0	216	821 ± 2	160	820 ± 2	165	923 ± 3	197	1201 ± 3	217	2373 ± 9	134	1560 ± 20	134	1560 ± 14
251	sjtu-004	2000146156	241108	286	2727	307	4608 ± 0	300	1236 ± 2	241	1209 ± 2	235	1294 ± 4	233	1554 ± 5	225	2738 ± 8	203	3057 ± 14	204	3070 ± 20
252	smilart-002	114509977	87805	38	263	50	1024 ± 0	24	176 ± 16	-	-	-	-	-	-	-	280	18784 ± 136	281	18795 ± 51	
253	smilart-003	68956056	91670	30	192	23	512 ± 0	26	180 ± 12	14	181 ± 10	21	313 ± 22	77	665 ± 49	213	2299 ± 196	126	1395 ± 74	97	1027 ± 56
254	sodec-000	856670801	13142	295	3186	284	4096 ± 0	274	1041 ± 2	211	1032 ± 1	196	1035 ± 1	169	1037 ± 2	139	1061 ± 2	150	1794 ± 37	149	1775 ± 23
255	stazu-000	900773557	624676	196	1064	290	4096 ± 0	210	813 ± 25	-	-	-	-	-	-	-	198	2979 ± 31	201	3007 ± 25	
256	starhybrid-001	102921306	289356	155	845	219	2048 ± 0	66	358 ± 82	43	355 ± 49	31	379 ± 58	24	401 ± 79	20	393 ± 67	100	1075 ± 51	103	1078 ± 53
257	suprema-000	252683488	38507	118	625	180	2048 ± 0	198	771 ± 2	150	778 ± 1	146	864 ± 2	180	1109 ± 2	209	2150 ± 4	142	1690 ± 17	142	1688 ± 13
258	supremaid-001	264389887	23479	98	541	193	2048 ± 0	89	479 ± 1	61	481 ± 0	39	490 ± 0	32	522 ± 0	60	704 ± 19	58	652 ± 19	58	652 ± 19
259	synesis-006	749508090	21817	245	1472	302	4104 ± 0	117	549 ± 1	84	546 ± 1	73	552 ± 1	54	558 ± 2	53	639 ± 28	59	697 ± 32	64	688 ± 31
260	synesis-007	1477592536	24145	280	2443	269	3080 ± 0	294	1215 ± 5	249	1268 ± 30	238	1306 ± 67	214	1311 ± 58	185	1423 ± 52	55	684 ± 32	62	686 ± 25
261	synology-000	226326270	25809	67	453	145	2048 ± 0	75	407 ± 14	49	415 ± 14	108	694 ± 31	221	1396 ± 58	241	4568 ± 211	283	19720 ± 203	282	19767 ± 379
262	synology-002	262874215	25943	78	488	161	2048 ± 0	236	886 ± 4	183	892 ± 3	163	920 ± 2	162	1000 ± 5	168	1317 ± 12	130	1466 ± 32	132	1496 ± 45
263	sztu-000	346765308	15871	223	1298	87	2048 ± 0	109	531 ± 0	78	532 ± 0	66	533 ± 0	50	537 ± 0	36	548 ± 0	33	585 ± 11	38	592 ± 13
264	tech5-004	2468118640	118858	287	2733	11	321 ± 0	230	872 ± 2	228	1117 ± 164	208	1114 ± 182	187	1134 ± 179	125	999 ± 44	36	597 ± 13	39	592 ± 16

Notes													
1	The configuration size does not capture static data included in libraries.												
2	The library size is the combined total of all files provided in the submission lib folder. These libraries e.g. OpenCV may or may not be installed on any end user's platform natively and would not need to be installed with the algorithm. Some developers put neural network models in their libraries.												
3	The memory usage is the peak resident set size reported by the ps system call during template generation.												
4	The median template creation times are measured on Intel®Xeon®CPU E5-2630 v4 @ 2.20GHz processors.												
5	The comparison durations, in nanoseconds, are estimated using std::chrono::high_resolution_clock which on the machine in (2) counts 1ns clock ticks. Precision is somewhat worse than that however. The ± value is the median absolute deviation times 1.48 for Normal consistency.												

Table

	ALGORITHM	CONFIG	LIBRARY	TEMPLATE								COMPARISON ⁴			
				NAME		DATA		MEMORY		SIZE		GENERATION TIME (ms) ⁴			
				(KB) ¹	(KB) ²	(MB) ³	(B)	MUGSHOT	480x720	960x1440	1600x2400	3000x4500	GENUINE	IMPOSTOR	
265	tech5-005	1207059515	120517	²³⁷ 1426	¹⁷ 512 ± 0	³⁰³ 1272 ± 109	²¹⁴ 1038 ± 63	¹⁹⁹ 1046 ± 39	¹⁸² 1124 ± 38	¹⁷⁶ 1351 ± 44	¹⁸⁷ 2573 ± 37	¹⁸⁹ 2545 ± 32			
266	tevian-005	943148300	16556	¹⁹⁹ 1083	⁹¹ 2048 ± 0	¹⁵² 633 ± 21	¹¹⁵ 672 ± 25	¹³⁵ 818 ± 37	¹⁸¹ 1117 ± 64	²¹⁶ 2364 ± 121	³¹ 568 ± 22	⁴⁶ 607 ± 35			
267	tevian-006	709112566	19339	¹⁷⁹ 954	²⁰⁹ 2048 ± 0	¹³⁹ 611 ± 1	¹¹¹ 666 ± 41	⁹⁹ 661 ± 32	⁷⁸ 672 ± 37	⁷⁰ 723 ± 31	³⁴ 591 ± 19	³⁷ 573 ± 28			
268	tiger-003	436392290	560292	¹³⁰ 708	²⁴⁰ 2056 ± 0	⁸⁴ 458 ± 21	-	-	-	-	¹⁶⁵ 2031 ± 35	¹⁶⁶ 2029 ± 38			
269	tiger-004	351095179	253683	²²⁴ 1336	²³⁴ 2052 ± 0	²⁰⁶ 798 ± 2	-	-	-	-	³³ 595 ± 5	⁴³ 598 ± 7			
270	tongyi-005	1168078115	138919	²⁷⁴ 2121	²⁵⁷ 2089 ± 0	²² 165 ± 1	-	-	-	-	²⁸¹ 18924 ± 65	²⁸³ 20158 ± 103			
271	toshiba-002	833132802	114260	-	⁷⁵ 1560 ± 0	¹¹⁴ 541 ± 0	-	-	-	-	²¹⁵ 3521 ± 369	¹⁸² 2449 ± 124			
272	toshiba-003	1007744192	114264	²¹⁰ 1197	⁷⁴ 1560 ± 0	¹¹³ 540 ± 0	-	-	-	-	¹⁸¹ 2390 ± 41	¹⁸¹ 2407 ± 81			
273	trueface-001	261246666	186754	¹²⁰ 638	¹³ 500 ± 0	⁷¹ 390 ± 1	-	-	-	-	⁵⁴ 676 ± 26	³⁴ 558 ± 50			
274	trueface-002	260042323	123116	⁷⁷ 486	⁸¹ 2000 ± 0	⁶⁷ 360 ± 0	⁴⁴ 361 ± 0	³⁷ 423 ± 0	⁶⁰ 590 ± 1	-	³ 192 ± 14	³ 186 ± 19			
275	tuputech-000	11752256	17185	² 33	¹³⁴ 2048 ± 0	¹⁸ 122 ± 4	¹⁰ 120 ± 1	⁹ 142 ± 2	¹⁰ 196 ± 5	²¹ 411 ± 14	²⁸⁴ 23893 ± 406	²⁸⁶ 25279 ± 406			
276	twface-000	677617540	11782	²⁸⁴ 2610	¹⁶² 2048 ± 0	²²⁹ 871 ± 1	¹⁷⁷ 873 ± 1	¹⁴⁹ 873 ± 2	¹³⁵ 876 ± 2	¹⁰⁷ 898 ± 1	¹³³ 1504 ± 29	¹³³ 1510 ± 34			
277	ulsee-001	379412284	57261	-	¹⁸⁹ 2048 ± 0	¹⁶¹ 654 ± 2	-	-	-	-	²⁴⁶ 6065 ± 94	²⁴⁷ 6228 ± 77			
278	uluface-002	72	480761	²⁰⁰ 1088	¹⁰⁷ 2048 ± 0	²³² 873 ± 42	¹⁷¹ 855 ± 9	¹⁷⁸ 978 ± 24	²⁰⁸ 1271 ± 40	²¹⁴ 2333 ± 68	²⁸² 19207 ± 1114	²⁷⁹ 18501 ± 274			
279	uluface-003	99694042	529422	²¹⁸ 1264	²⁶⁶ 3072 ± 0	²⁵⁹ 965 ± 11	¹⁹⁷ 968 ± 10	²⁰⁵ 1087 ± 20	²²⁰ 1387 ± 36	²²¹ 2469 ± 86	²⁸⁷ 26057 ± 195	²⁸⁹ 26865 ± 566			
280	upc-001	0	89914	¹⁹⁸ 1077	⁶⁵ 1052 ± 0	¹¹⁸ 551 ± 15	¹²⁴ 703 ± 56	¹¹⁸ 724 ± 51	¹⁰³ 751 ± 49	¹⁰³ 863 ± 33	²⁰⁴ 3114 ± 44	²⁰⁸ 3165 ± 97			
281	vcog-002	3306941103	118946	²⁹⁸ 3666	³²⁰ 61504 ± 5	⁶⁵ 357 ± 25	-	-	-	-	³¹⁵ 296154 ± 3077	³¹⁵ 296436 ± 4883			
282	vd-001	174349133	44058	³⁹ 281	²³¹ 2052 ± 0	⁵⁶ 316 ± 6	-	-	-	-	¹¹⁸ 1258 ± 38	¹¹⁴ 1148 ± 109			
283	vd-002	260606257	34389	¹²⁷ 688	³⁴ 516 ± 0	¹⁷⁷ 684 ± 5	¹¹⁷ 679 ± 4	¹⁰¹ 676 ± 5	⁸⁴ 693 ± 5	⁷⁷ 754 ± 5	¹² 300 ± 14	¹⁴ 319 ± 32			
284	veridas-004	201303428	160684	⁷² 472	¹⁸⁷ 2048 ± 0	¹⁷² 678 ± 22	¹⁴¹ 749 ± 27	²⁵⁶ 1470 ± 52	²⁶¹ 3228 ± 95	²⁵⁷ 10349 ± 273	²³⁶ 5516 ± 42	²⁵⁶ 7425 ± 30			
285	veridas-006	364205776	896424	²⁷¹ 1990	¹³³ 2048 ± 0	²³⁵ 880 ± 8	¹⁸¹ 885 ± 8	²³⁰ 1271 ± 18	²⁵³ 2242 ± 38	²⁵⁰ 6414 ± 156	³⁰² 56940 ± 149	³⁰³ 66077 ± 294			
286	via-000	127408592	11151	¹⁸¹ 964	¹⁷⁹ 2048 ± 0	¹⁸⁴ 707 ± 8	¹³⁸ 740 ± 5	¹⁵⁹ 906 ± 41	¹⁴⁶ 941 ± 40	¹³² 1040 ± 5	⁸⁸ 966 ± 28	⁹⁶ 1021 ± 14			
287	via-001	379141776	11151	²⁵⁵ 1697	¹¹⁷ 2048 ± 0	²⁵⁴ 964 ± 3	²⁰⁴ 1011 ± 3	¹⁹⁰ 1026 ± 4	¹⁷³ 1045 ± 3	¹⁴⁸ 1137 ± 28	⁹⁰ 983 ± 31	⁹² 989 ± 40			
288	videmo-000	142994889	39470	⁵¹ 390	¹⁹¹ 2048 ± 0	²⁰ 142 ± 5	¹² 150 ± 4	¹⁰ 150 ± 6	⁸ 151 ± 4	⁷ 155 ± 8	²⁸ 513 ± 16	³⁰ 523 ± 38			
289	videonetics-001	31616555	5963	⁴ 61	²⁸ 512 ± 0	⁴² 262 ± 3	³⁰ 273 ± 1	⁴² 439 ± 3	¹¹⁸ 820 ± 3	²¹⁸ 2393 ± 43	¹¹¹ 1153 ± 38	¹¹³ 1142 ± 65			
290	videonetics-002	124908941	6289	¹⁷ 115	²²⁴ 2052 ± 0	⁴⁹ 282 ± 5	³⁴ 295 ± 1	⁶² 513 ± 4	¹⁶⁶ 1029 ± 3	²³⁵ 3151 ± 46	¹¹⁴ 1219 ± 57	¹²² 1262 ± 56			
291	vigilantsolutions-009	357169885	49973	¹⁵² 840	⁷² 1548 ± 0	¹⁴⁵ 615 ± 0	¹⁰⁶ 631 ± 0	⁸⁸ 632 ± 1	⁷⁰ 636 ± 0	⁵⁶ 659 ± 0	²⁰ 452 ± 11	²³ 451 ± 11			
292	vigilantsolutions-010	357169886	49973	¹⁵³ 840	⁷³ 1548 ± 0	¹⁴⁴ 615 ± 0	¹⁰⁵ 631 ± 0	⁹⁰ 632 ± 0	⁶⁹ 636 ± 0	⁵⁷ 659 ± 0	²⁵ 490 ± 13	²⁸ 488 ± 11			
293	vinai-000	412049069	866522	¹⁹¹ 1032	¹⁷³ 2048 ± 0	²⁷⁹ 1099 ± 1	²²² 1095 ± 1	²⁰⁷ 1093 ± 1	¹⁷⁹ 1099 ± 1	¹⁴⁶ 1126 ± 1	¹⁹⁹ 2996 ± 20	²⁰⁰ 2993 ± 26			
294	vion-000	233696726	7533	⁸² 498	²²⁸ 2052 ± 0	⁵⁹ 333 ± 1	-	-	-	-	²⁹³ 39839 ± 3561	²⁸⁸ 26830 ± 241			
295	visage-000	50400173	70150	⁶ 73	²⁴ 512 ± 0	³ 27 ± 0	¹ 27 ± 0	¹ 31 ± 0	¹ 38 ± 0	¹ 63 ± 0	¹⁷³ 2220 ± 14	¹⁷⁴ 2218 ± 14			
296	visionbox-001	263034670	190645	¹⁰⁷ 579	¹³² 2048 ± 0	²⁵⁹ 983 ± 7	²²¹ 1093 ± 46	²⁴⁶ 1360 ± 68	²⁵² 2181 ± 105	²⁴⁸ 5955 ± 281	¹¹² 1161 ± 22	¹¹⁵ 1154 ± 20			
297	visionbox-002	265280900	135281	¹¹⁵ 612	²⁵⁰ 2059 ± 0	⁹² 482 ± 1	⁶³ 482 ± 0	⁵² 484 ± 1	⁴² 492 ± 1	²⁹ 517 ± 3	¹⁶⁴ 1969 ± 44	¹⁶² 1931 ± 42			
298	visionlabs-009	723046025	19862	⁶⁵ 444	³¹ 513 ± 0	¹⁰⁴ 515 ± 41	⁵⁹ 472 ± 1	⁴⁹ 474 ± 1	³⁶ 476 ± 1	³¹ 521 ± 1	⁸⁶ 957 ± 28	⁸⁸ 965 ± 32			
299	visionlabs-010	1092895531	19357	¹⁶⁶ 902	³⁰ 513 ± 0	¹⁸⁸ 730 ± 0	¹³¹ 717 ± 1	¹¹⁵ 709 ± 0	⁹² 713 ± 1	⁷⁴ 739 ± 0	³⁸ 600 ± 41	⁵¹ 626 ± 35			
300	visteam-000	33514713	17740	¹² 83	⁷¹ 1536 ± 0	⁹ 96 ± 7	⁷ 102 ± 8	²⁷ 358 ± 19	¹⁶⁵ 1022 ± 50	²³⁸ 3987 ± 211	²⁴⁹ 6361 ± 87	²⁴⁹ 6668 ± 277			
301	visteam-001	190915457	30878	⁵⁵ 410	²⁷⁵ 4096 ± 0	²²⁸ 869 ± 7	¹⁷⁶ 872 ± 6	²¹¹ 1121 ± 15	²⁴⁰ 1719 ± 38	²⁴⁰ 4375 ± 157	²⁵³ 7054 ± 108	²⁵³ 7025 ± 109			
302	vnpt-001	272895047	535529	⁵⁰ 384	¹¹² 2048 ± 0	⁹⁷ 499 ± 2	⁷¹ 499 ± 2	⁵⁶ 494 ± 3	⁴³ 502 ± 3	²⁶ 512 ± 2	¹⁶⁶ 2049 ± 29	¹⁷ 337 ± 121			
303	vnpt-002	278169517	3203296	⁷⁹ 489	²⁰³ 2048 ± 0	¹⁸⁹ 739 ± 2	¹³⁶ 731 ± 2	¹²² 740 ± 1	⁹⁹ 742 ± 2	⁸¹ 763 ± 2	⁷² 766 ± 13	⁷³ 762 ± 13			
304	vocord-008	618359916	345047	²⁴⁸ 1559	²⁶⁵ 2688 ± 0	²⁵³ 962 ± 2	¹⁹⁹ 976 ± 2	²⁰² 1061 ± 3	²⁰² 1236 ± 23	²⁰⁵ 1851 ± 9	²⁰⁰ 3015 ± 50	¹⁹⁹ 2988 ± 62			
305	vocord-009	1413255249	201560	³⁰⁷ 4162	⁷⁸ 1920 ± 0	³¹⁹ 1472 ± 2	²⁶⁵ 1472 ± 1	²⁵⁹ 1549 ± 1	²³⁸ 1667 ± 2	²⁰⁸ 2064 ± 2	¹⁶⁷ 2052 ± 50	¹⁶⁹ 2056 ± 39			
306	vts-000	262747358	169760	²⁵⁶ 1704	²¹⁴ 2048 ± 0	⁹⁴ 486 ± 1	⁶² 481 ± 0	⁵³ 484 ± 0	³⁸ 485 ± 1	³⁰ 517 ± 0	³⁰⁸ 124209 ± 352	³⁰⁸ 123652 ± 358			
307	winsense-001	270774312	32035	¹⁷² 922	⁶⁹ 1280 ± 0	¹⁹⁵ 766 ± 7	²¹⁶ 1058 ± 47	¹⁸¹ 983 ± 97	¹⁷⁴ 1053 ± 119	¹⁶⁹ 1320 ± 84	¹³⁷ 1631 ± 28	¹⁶⁵ 1964 ± 171			
308	winsense-002	288132712	25780	²⁵⁸ 1781	¹⁹⁵ 2048 ± 0	⁹⁶ 494 ± 2	⁷⁰ 498 ± 1	⁶⁴ 519 ± 1	⁴⁹ 537 ± 1	⁵¹ 634 ± 1	¹⁴¹ 1683 ± 8	¹⁴¹ 1683 ± 7			

Notes

- 1 The configuration size does not capture static data included in libraries.
- 2 The library size is the combined total of all files provided in the submission lib folder. These libraries e.g. OpenCV may or may not be installed on any end user's platform natively and would not need to be installed with the algorithm. Some developers put neural network models in their libraries.
- 3 The memory usage is the peak resident set size reported by the ps system call during template generation.
- 4 The median template creation times are measured on Intel®Xeon®CPU E5-2630 v4 @ 2.20GHz processors.
- 5 The comparison durations, in nanoseconds, are estimated using std::chrono::high_resolution_clock which on the machine in (2) counts 1ns clock ticks. Precision is somewhat worse than that however. The ± value is the median absolute deviation times 1.48 for Normal consistency.

Table 12: Summary of algorithms and properties included in this report. The red superscripts give ranking for the quantity in that column.

	ALGORITHM	CONFIG	LIBRARY	TEMPLATE								COMPARISON ⁴									
				NAME	DATA	DATA	MEMORY	SIZE	GENERATION TIME (ms) ⁴				TIME (ns) ⁵								
									(KB) ¹	(KB) ²	(MB) ³	(B)	MUGSHOT	480x720	960x1440	1600x2400	3000x4500	GENUINE	IMPOSTOR		
309	x-laboratory-000	532501437	197310	247	1524	247	2056 ± 0	207	808 ± 7	184	897 ± 113	160	907 ± 103	138	886 ± 103	61	673 ± 39	66	725 ± 19	71	749 ± 34
310	x-laboratory-001	640144084	398792	263	1844	244	2056 ± 0	129	586 ± 2	90	596 ± 5	81	603 ± 6	67	620 ± 7	86	793 ± 14	78	813 ± 28	82	872 ± 32
311	xforwardai-001	348262545	51163	275	2173	185	2048 ± 0	289	1180 ± 2	239	1182 ± 1	221	1194 ± 1	193	1186 ± 2	157	1203 ± 1	75	779 ± 17	77	797 ± 13
312	xforwardai-002	724700382	51163	270	1989	293	4096 ± 0	248	944 ± 1	-	-	-	-	-	-	-	-	128	1406 ± 8	127	1405 ± 13
313	xm-000	591914905	148920	126	688	235	2052 ± 0	234	878 ± 2	179	882 ± 1	183	988 ± 2	205	1258 ± 3	220	2434 ± 7	138	1634 ± 17	137	1632 ± 20
314	yisheng-004	498023846	38653	221	1279	272	3704 ± 0	68	378 ± 12	-	-	-	-	-	-	-	-	58	693 ± 137	31	526 ± 34
315	yitu-003	1562336990	138919	299	3737	255	2082 ± 0	226	860 ± 0	-	-	-	-	-	-	-	-	278	18305 ± 71	278	18286 ± 62
316	yoonik-000	297384719	206059	150	836	127	2048 ± 0	246	941 ± 3	196	965 ± 13	176	964 ± 10	154	964 ± 9	120	974 ± 23	109	1116 ± 34	110	1113 ± 54
317	yoonik-001	354948637	265353	276	2192	114	2048 ± 0	298	1223 ± 3	247	1238 ± 1	227	1238 ± 1	203	1240 ± 1	162	1240 ± 1	61	706 ± 29	65	690 ± 26
318	ytu-000	1512817409	44032	282	2484	183	2048 ± 0	108	530 ± 0	80	533 ± 0	94	640 ± 0	13	861 ± 2	206	1949 ± 8	290	31797 ± 131	291	31794 ± 133
319	yuan-001	379364823	189558	291	2829	92	2048 ± 0	310	1383 ± 3	258	1394 ± 3	251	1408 ± 3	230	1461 ± 4	195	1615 ± 4	180	2344 ± 25	180	2325 ± 42
320	yuan-002	379363758	165662	292	2838	111	2048 ± 0	315	1420 ± 3	261	1429 ± 4	258	1511 ± 4	239	1695 ± 4	219	2408 ± 5	179	2297 ± 23	179	2310 ± 31

Notes

- | | |
|---|---|
| 1 | The configuration size does not capture static data included in libraries. |
| 2 | The library size is the combined total of all files provided in the submission lib folder. These libraries e.g. OpenCV may or may not be installed on any end user's platform natively and would not need to be installed with the algorithm. Some developers put neural network models in their libraries. |
| 3 | The memory usage is the peak resident set size reported by the ps system call during template generation. |
| 4 | The median template creation times are measured on Intel®Xeon®CPU E5-2630 v4 @ 2.20GHz processors. |
| 5 | The comparison durations, in nanoseconds, are estimated using std::chrono::high_resolution_clock which on the machine in (2) counts 1ns clock ticks. Precision is somewhat worse than that however. The ± value is the median absolute deviation times 1.48 for Normal consistency. |

Table 13: Summary of algorithms and properties included in this report. The red superscripts give ranking for the quantity in that column.

Algorithm	FALSE NON-MATCH RATE (FNMR)																		
	CONSTRAINED, COOPERATIVE										LESS CONSTRAINED, NON-COOP.								
	Name	ViSAMC	VISA	MUGSHOT	MUGSHOT12+YRS	VISABORDER	BORDER	BORDER	WILD	CHILDEXP									
	FMR	0.0001	1E-06	1E-05	1E-05	1E-06	1E-06	1E-05	0.0001	0.01									
1	20face-000	0.1268	265	0.1828	264	0.1748	270	0.2768	270	0.1765	259	0.1864	215	0.0927	239	0.0405	178	-	
2	3divi-005	0.0094	139	0.0151	146	0.0078	126	0.0121	126	0.0135	125	0.0231	112	0.0156	130	0.0351	161	-	
3	3divi-006	0.0064	93	0.0094	90	0.0047	67	0.0066	66	0.0091	78	0.0191	90	0.0113	83	0.0289	88	-	
4	acer-000	0.1393	268	0.9075	309	0.9981	311	-		1.0000	308	1.0000	301	0.9998	304	0.9841	308	-	
5	acer-001	0.0294	231	0.0504	236	0.0240	231	0.0463	234	0.0436	226	0.0622	181	0.0360	203	0.0307	121	-	
6	acisw-003	0.9682	316	0.9971	317	0.7892	305	0.8738	303	0.8752	297	0.8275	273	0.6698	290	0.4470	289	-	
7	acisw-006	0.2945	281	0.9788	315	0.6044	293	-		0.9900	301	1.0000	302	0.9999	306	1.0000	314	-	
8	adera-001	0.1021	263	0.1757	262	0.1823	271	0.2967	271	0.1714	258	0.6357	250	0.1127	244	0.1965	264	0.7202	39
9	adera-002	0.0052	60	0.0071	55	0.0047	64	0.0064	61	0.0087	71	0.0159	68	0.0136	104	0.0990	235	-	
10	advance-002	0.0089	129	0.0137	131	0.0073	116	0.0115	122	0.0400	219	0.0722	189	0.0593	224	0.0498	201	-	
11	aifirst-001	0.0119	168	0.0170	161	0.0084	140	0.0127	135	0.0131	122	0.0212	100	0.0138	107	0.0432	186	0.4301	11
12	aigen-001	0.0124	174	0.0219	183	0.0143	202	0.0217	195	0.0236	193	0.8960	276	0.3255	266	0.0681	221	-	
13	aigen-002	0.0192	213	0.0343	214	0.0256	233	0.0402	229	0.0389	218	0.9196	280	0.3876	272	0.1096	242	-	
14	ailabs-001	0.0158	198	0.0276	208	0.0192	220	0.0317	219	0.0352	213	0.0608	177	0.0434	211	0.0338	151	-	
15	aimall-002	0.0119	169	0.0167	159	0.0224	226	0.0411	231	0.0233	188	0.0373	156	0.0235	177	0.0327	144	-	
16	aimall-003	0.0033	32	0.0041	25	0.0033	31	0.0035	19	0.0056	34	0.0109	40	0.0087	51	0.0312	131	-	
17	aiunionface-000	0.0104	151	0.0154	150	0.0082	138	0.0122	127	0.0141	133	0.0243	115	0.0169	138	0.0306	118	-	
18	aize-001	0.0223	220	0.0344	215	0.0199	221	0.0313	217	0.0367	214	0.0522	170	0.0359	202	0.0446	191	-	
19	ajou-001	0.0093	137	0.0147	142	0.0071	114	0.0126	131	0.0173	164	0.0274	126	0.0186	149	0.0348	156	-	
20	alchera-000	0.0165	200	0.0243	196	0.0125	194	0.0186	182	0.0204	178	0.0349	148	0.0243	184	0.0370	169	-	
21	alchera-002	0.0107	156	0.0157	153	0.0104	167	0.0229	197	0.0144	138	0.0246	117	0.0198	161	0.0328	145	-	
22	alice-000	0.0119	171	0.0192	170	0.0106	170	0.0170	172	0.0167	160	0.0265	123	0.0150	124	0.0288	80	-	
23	alleyes-000	0.0058	76	0.0090	85	0.0055	79	0.0087	96	0.0068	52	0.0105	37	0.0076	29	0.0282	54	-	
24	allgovision-000	0.0346	238	0.0527	238	0.0232	228	0.0339	220	0.0372	217	0.0620	180	0.0443	213	0.0607	216	-	
25	alphaface-001	0.0065	97	0.0097	94	0.0039	45	0.0063	60	0.0083	66	-	-	-	-	0.0280	39	-	
26	alphaface-002	0.0052	62	0.0075	62	0.0030	16	0.0044	27	1.0000	311	0.0115	44	0.0084	47	0.0279	35	-	
27	amplifiedgroup-001	0.5034	301	0.5848	296	0.6973	300	0.8316	298	0.7807	289	0.7724	265	0.6354	286	0.4250	287	-	
28	androvideo-000	0.0243	224	0.0438	229	0.0239	230	0.0365	227	0.0483	230	0.1870	216	0.0635	227	0.1163	245	-	
29	anke-004	0.0080	119	0.0154	149	0.0073	115	0.0112	120	0.0102	95	0.0178	82	0.0118	89	0.0288	81	0.3577	6
30	anke-005	0.0070	102	0.0109	110	0.0059	91	0.0094	99	0.0105	98	0.0142	55	0.0102	68	0.0289	86	0.3337	4
31	antheus-000	0.2564	278	0.3776	280	0.7240	301	0.8699	301	0.8899	298	0.9872	284	0.9483	296	0.7668	300	0.9233	56
32	antheus-001	0.1311	266	0.2306	269	0.5113	286	0.6797	286	0.8748	296	0.9908	285	0.9649	299	0.7586	299	-	
33	anyvision-004	0.0267	229	0.0385	224	0.0258	234	0.0487	236	0.0234	191	0.0301	134	0.0191	153	0.0470	195	0.4633	12
34	anyvision-005	0.0023	17	0.0037	17	0.0027	13	0.0035	18	0.0049	22	0.0084	14	0.0069	16	0.0285	67	-	
35	asusaics-000	0.0125	179	0.0209	177	0.0085	141	0.0134	142	0.0143	136	0.7189	259	0.0285	193	0.0295	101	-	
36	asusaics-001	0.0125	177	0.0210	178	0.0085	143	0.0134	143	0.0143	137	0.7437	262	0.0289	194	0.0295	100	-	
37	authenmetric-002	0.0092	135	0.0134	130	0.0095	158	0.0177	175	0.0192	174	0.0463	165	0.0236	178	0.0306	120	-	
38	aware-004	0.0690	255	0.0949	255	0.0837	259	0.1436	258	0.1171	253	0.8137	270	0.1056	243	0.0516	203	-	
39	aware-005	0.0457	246	0.0643	242	0.0603	254	0.1094	253	0.0613	237	0.1075	206	0.0491	215	0.0314	134	-	
40	awiros-001	0.4044	290	0.4622	286	0.5530	288	0.6518	285	0.2008	262	0.1994	219	0.1386	250	0.5584	297	-	
41	awiros-002	0.1990	273	0.2561	271	0.3319	277	0.4411	277	0.3821	276	0.9938	289	0.2634	260	0.0997	236	-	
42	ayftech-001	0.0946	261	0.1941	265	0.2438	273	0.3625	272	0.1558	257	0.1589	211	0.0936	240	0.0785	229	-	
43	ayonix-000	0.4351	294	0.4872	287	0.6150	295	0.7510	293	0.6557	283	0.6361	251	0.4981	279	0.3635	284	0.8434	50
44	bioidtechswiss-001	0.0054	66	0.0072	56	0.0069	109	0.0124	130	0.0060	40	0.0094	22	0.0065	11	0.0313	132	-	

Table 14: FNMR is the proportion of mated comparisons below a threshold set to achieve the FMR given in the header on the fourth row. FMR is the proportion of impostor comparisons at or above that threshold. The light grey values give rank over all algorithms in that column. The pink columns use only same-sex impostors; others are selected regardless of demographics. The exception, in the green column, uses “matched-covariates” i.e. impostors of the same sex, age group, and country of birth. The second pink column includes effects of extended ageing. Missing entries for border, visa, mugshot and wild images generally mean the algorithm did not run to completion. For child exploitation, missing entries arise because NIST executes those runs only infrequently. The VISA columns compare images described in section 2.2. The MUGSHOT columns compare images described in section 2.5. The VISA-BORDER column compare images described in section 2.3 with those of section 2.4. The BORDER column compares images described in section 2.4. The WILD columns compare images described in section 2.6. The CHILD-EXPLOITATION columns compare images described in section 2.1.

	Algorithm	FALSE NON-MATCH RATE (FNMR)										LESS CONSTRAINED, NON-COOP.							
		CONSTRAINED, COOPERATIVE																	
		Name	ViSAMC	VISA	MUGSHOT	MUGSHOT12+YRS	VISABORDER	BORDER	BORDER	WILD	CHILDEXP								
FMR		0.0001	1E-06	1E-05	1E-05	1E-06	1E-06	1E-06	1E-05	0.0001	0.01								
45	bioidechswiss-002	0.0049	53	0.0067	53	0.0064	101	0.0116	123	0.0067	51	0.0117	45	0.0086	49	0.0279	30	-	
46	bm-001	0.7431	308	0.9494	313	0.9586	306	0.9843	304	0.9049	299	0.9021	279	0.8395	293	0.9935	310	0.8845	53
47	boetech-001	0.0662	254	0.0802	251	0.0493	247	0.0791	244	0.0682	242	0.1074	205	0.0758	235	0.1719	257	-	
48	bresee-000	0.8467	311	0.9472	311	0.9819	307	0.9903	305	0.9940	302	0.9919	286	0.9760	300	0.8992	305	-	
49	bresee-001	0.0085	126	0.0143	136	0.0086	147	0.0153	161	0.0108	103	0.0168	76	0.0115	87	0.0355	165	-	
50	camvi-002	0.0125	178	0.0221	186	0.0089	151	0.0145	155	0.0142	134	0.2650	228	0.0166	137	0.0288	78	0.5760	23
51	camvi-004	0.0171	203	0.0316	210	0.0042	51	0.0049	37	0.0097	92	0.6636	254	0.0141	111	0.0284	62	0.5788	24
52	canon-002	0.0034	34	0.0050	36	0.0026	8	0.0033	16	0.0043	12	0.0182	83	0.0065	10	0.0279	33	-	
53	ceiec-003	0.0071	106	0.0107	108	0.0061	97	0.0079	82	0.0160	152	0.0316	136	0.0260	188	0.0308	127	-	
54	ceiec-004	0.0038	38	0.0051	37	0.0045	62	0.0053	43	0.0062	45	0.3939	236	0.0104	73	0.0325	141	-	
55	chosun-001	0.0525	249	0.0936	253	0.0742	258	0.1263	257	0.0978	252	1.0000	307	0.9354	295	0.4446	288	-	
56	chosun-002	0.0390	241	0.0646	243	0.0339	240	0.0576	241	0.0455	228	0.6904	256	0.1746	254	0.0696	224	-	
57	chtface-002	0.0150	193	0.0268	205	0.0096	161	0.0140	148	0.0186	170	0.0320	138	0.0194	156	0.0306	119	-	
58	chtface-003	0.0091	131	0.0146	141	0.0083	139	0.0128	137	0.0132	123	0.0220	107	0.0149	122	0.0301	111	-	
59	canon-001	0.0041	44	0.0061	47	0.0030	21	0.0041	26	0.0048	21	0.0578	173	0.0069	17	0.0279	31	-	
60	cloudwalk-hr-003	0.0026	20	0.0041	26	0.0040	48	0.0058	50	0.0060	43	0.9992	296	0.0094	58	0.7206	298	-	
61	cloudwalk-hr-004	0.0009	1	0.0018	2	0.0034	32	0.0028	7	0.0052	26	0.9992	297	0.0093	57	0.1625	256	-	
62	cloudwalk-mt-002	0.0064	95	0.0085	78	0.0054	78	0.0098	106	0.0070	55	0.0108	39	0.0076	28	0.0283	60	-	
63	cloudwalk-mt-003	0.0013	2	0.0022	3	0.0026	4	0.0027	5	0.0039	6	0.0076	6	0.0067	13	0.0347	154	-	
64	clova-000	0.0099	145	0.0150	143	0.0094	156	0.0147	157	0.0136	127	0.0213	102	0.0152	127	0.0307	122	-	
65	cogent-004	0.0064	96	0.0116	118	0.0096	160	0.0134	144	0.0157	148	0.0325	140	0.0204	163	0.0379	172	0.7177	38
66	cogent-005	0.0060	87	0.0112	113	0.0064	103	0.0070	69	0.0095	88	0.0184	85	0.0135	100	0.0423	183	-	
67	cognitec-000	0.0116	163	0.0177	164	0.0118	189	0.0167	171	0.0285	205	0.9924	287	0.0435	212	0.0953	234	0.8365	49
68	cognitec-002	0.0066	98	0.0101	103	0.0079	129	0.0108	116	0.0181	166	0.0317	137	0.0237	179	0.0372	170	-	
69	cor-001	0.0075	112	0.0113	116	0.0055	81	0.0084	87	0.0091	80	0.0148	60	0.0092	56	0.0277	27	-	
70	corsight-001	0.0040	41	0.0057	42	0.0033	30	0.0047	31	0.0045	13	0.0095	25	0.0063	9	0.0276	17	-	
71	csc-001	0.9158	312	0.9346	310	0.9899	308	-		0.9999	306	0.9959	291	0.9906	302	0.8678	303	-	
72	csc-002	0.0099	146	0.0132	128	0.0077	123	0.0142	152	0.0126	118	0.0195	92	0.0146	118	0.1779	259	-	
73	ctbcbank-000	0.0168	201	0.0250	200	0.0146	204	0.0224	196	0.0211	182	0.8964	278	0.3779	270	1.0000	319	0.8803	52
74	ctbcbank-001	0.0155	196	0.0235	193	0.0148	209	0.0243	202	0.0207	179	0.9279	281	0.3469	267	1.0000	322	-	
75	cubox-001	0.0064	92	0.0080	71	0.0037	40	0.0055	47	0.0060	41	0.0111	41	0.0077	31	0.0300	108	-	
76	cukee-001	0.0036	36	0.0045	31	0.0031	24	0.0046	29	0.0051	25	0.0095	26	0.0079	35	0.1492	253	-	
77	cybercore-000	0.0728	257	0.1110	257	0.1521	268	0.2375	266	0.1874	261	0.1907	217	0.1178	247	0.1191	248	-	
78	cyberextruder-001	0.1972	271	0.2547	270	0.4686	285	0.6387	284	0.3807	275	0.3806	235	0.2582	257	0.1747	258	0.7804	48
79	cyberextruder-002	0.0811	259	0.1336	259	0.1465	267	0.2266	265	0.2086	265	1.0000	316	1.0000	316	0.1000	237	0.6105	26
80	cyberlink-005	0.0060	85	0.0092	88	0.0058	89	0.0067	67	0.0074	58	0.0146	59	0.0105	75	0.0283	59	-	
81	cyberlink-006	0.0042	45	0.0054	39	0.0043	54	0.0049	35	0.0052	28	0.0097	28	0.0077	32	0.0278	28	-	
82	dahua-005	0.0031	29	0.0046	32	0.0035	36	0.0049	38	0.0046	15	0.0076	7	0.0062	8	0.0277	23	-	
83	dahua-006	0.0027	23	0.0039	21	0.0031	23	0.0039	25	0.0039	7	0.0067	5	0.0058	5	0.0280	36	-	
84	decatur-000	0.0714	256	0.1115	258	0.0608	255	0.1106	254	0.0866	247	1.0000	305	0.0714	232	0.0658	219	-	
85	deepglint-002	0.0016	8	0.0027	11	0.0032	25	0.0033	17	0.0043	11	0.0084	15	0.0077	30	0.0280	38	0.3422	5
86	deepglint-003	0.0027	24	0.0038	19	0.0030	19	0.0032	15	0.0043	10	0.0082	13	0.0076	27	0.0279	32	-	
87	deepsea-001	0.0136	184	0.0215	180	0.0142	200	0.0214	194	0.0163	156	0.0250	118	0.0192	154	0.0347	155	0.5606	20
88	depsense-000	0.0145	189	0.0265	204	0.0113	183	0.0196	187	0.0151	141	0.0215	104	0.0129	98	0.0290	89	-	

Table 15: FNMR is the proportion of mated comparisons below a threshold set to achieve the FMR given in the header on the fourth row. FMR is the proportion of impostor comparisons at or above that threshold. The light grey values give rank over all algorithms in that column. The pink columns use only same-sex impostors; others are selected regardless of demographics. The exception, in the green column, uses “matched-covariates” i.e. impostors of the same sex, age group, and country of birth. The second pink column includes effects of extended ageing. Missing entries for border, visa, mugshot and wild images generally mean the algorithm did not run to completion. For child exploitation, missing entries arise because NIST executes those runs only infrequently. The VISA columns compare images described in section 2.2. The MUGSHOT columns compare images described in section 2.5. The VISA-BORDER column compare images described in section 2.3 with those of section 2.4. The BORDER column compares images described in section 2.4. The WILD columns compare images described in section 2.6. The CHILD-EXPLOITATION columns compare images described in section 2.1.

Algorithm	FALSE NON-MATCH RATE (FNMR)																		
	CONSTRAINED, COOPERATIVE								LESS CONSTRAINED, NON-COOP.										
	Name	ViSAMC	VISA	MUGSHOT	MUGSHOT12+YRS	VISABORDER	BORDER	BORDER	WILD	CHILDEXP									
FMR	0.0001	1E-06	1E-05	1E-05	1E-06	1E-06	1E-06	1E-05	0.0001	0.01									
89	dermalog-006	0.0253	227	0.0369	221	0.0171	215	0.0283	213	0.0217	183	0.0358	151	0.0230	173	0.0623	217	0.5852	25
90	dermalog-008	0.0096	143	0.0166	158	0.0086	145	0.0133	141	0.0165	158	0.0586	176	0.0226	172	0.0277	22	-	
91	didiglobalface-001	0.0055	69	0.0092	86	0.0030	17	0.0045	28	0.0088	73	0.0119	48	0.0085	48	0.0282	53	0.4270	9
92	digitalbarriers-002	0.3360	286	0.3690	278	0.0877	261	0.1557	259	0.0971	251	0.0951	199	0.0497	216	0.0436	189	-	
93	dsk-000	0.1526	269	0.2169	267	0.3787	280	0.5426	281	0.3115	268	0.3089	231	0.1994	255	0.2201	268	0.7313	41
94	einetworks-000	0.0099	147	0.0180	166	0.0088	150	0.0140	150	0.0130	121	0.0225	110	0.0147	120	0.0293	97	-	
95	ekin-002	0.1168	264	0.2042	266	0.1530	269	0.2524	268	0.1777	260	0.2773	229	0.1347	249	0.4801	291	-	
96	enface-000	0.0028	26	0.0049	35	0.0043	58	0.0072	70	0.0058	39	0.0150	63	0.0090	54	0.0290	90	-	
97	eocortex-000	0.3485	287	0.6943	302	0.1122	264	0.1574	260	0.2155	266	0.2257	224	0.1606	253	0.2546	276	-	
98	ercacat-001	0.0036	35	0.0044	29	0.0033	28	0.0047	32	0.0106	99	0.0202	96	0.0184	147	0.0258	1	-	
99	expasoft-000	0.0427	243	0.0655	245	0.0239	229	0.0393	228	0.0673	241	0.8963	277	0.3832	271	0.0565	212	-	
100	expasoft-001	0.0328	237	0.0488	234	0.0211	224	0.0342	222	0.0629	239	0.6483	252	0.2816	262	0.0552	210	-	
101	f8-001	0.0249	226	0.0336	212	0.0178	217	0.0232	198	0.0303	209	0.0615	179	0.0408	207	0.0475	197	0.5272	17
102	facesoft-000	0.0085	125	0.0112	114	0.0064	102	0.0107	115	0.0091	79	0.0171	78	0.0107	76	0.0275	14	0.4992	14
103	facetag-000	0.2836	279	0.4081	283	0.2933	275	0.4303	275	0.3448	271	0.6312	249	0.3530	268	0.2087	267	-	
104	facex-001	1.0000	321	1.0000	319	1.0000	315	-	1.0000	316	1.0000	321	1.0000	310	1.0000	313	-		
105	farfaces-001	0.4890	300	0.5860	297	0.5650	289	0.7268	290	0.8015	291	0.7511	263	0.5892	284	0.1976	265	-	
106	fiberhome-nanjing-002	0.0217	219	0.0381	223	0.0874	260	0.1770	262	0.0271	200	0.0351	149	0.0188	150	0.0361	167	-	
107	fiberhome-nanjing-003	0.0090	130	0.0139	134	0.0082	137	0.0144	153	0.0110	107	0.0174	79	0.0107	77	0.0272	6	-	
108	fincore-000	0.0309	234	0.0502	235	0.0281	237	0.0510	238	0.0521	232	0.0815	192	0.0522	218	0.0681	222	-	
109	fujitsulab-001	0.0059	82	0.0082	74	0.0132	196	0.0258	205	0.0140	132	0.0246	116	0.0142	113	0.0271	3	-	
110	fujitsulab-002	0.0091	133	0.0124	122	0.0105	168	0.0156	163	0.0169	162	0.0345	146	0.0146	119	0.0282	49	-	
111	geo-001	0.0180	208	0.0198	172	0.0037	41	0.0055	46	0.0070	53	0.0129	52	0.0094	59	0.0343	153	-	
112	geo-002	0.0171	204	0.0187	169	0.0035	35	0.0051	42	0.0064	47	0.0117	46	0.0083	45	0.0302	113	-	
113	glory-002	0.0241	222	0.0311	209	0.0116	187	0.0151	160	0.0157	149	0.0264	122	0.0188	151	0.1265	249	-	
114	glory-003	0.0076	115	0.0125	124	0.0077	125	0.0103	112	0.0130	120	0.0205	97	0.0143	115	0.0763	226	-	
115	gorilla-005	-	-	-	-	0.0142	201	0.0267	211	0.0228	187	0.0358	150	0.0195	157	0.0307	124	-	
116	gorilla-006	0.0105	155	0.0152	147	0.0106	169	0.0203	190	0.0155	144	0.0218	106	0.0136	101	0.0289	83	-	
117	hertasecurity-000	0.0630	252	0.0780	250	0.0503	249	0.0898	247	0.0738	243	0.0693	188	0.0420	208	0.0575	213	-	
118	hik-001	0.0096	142	0.0125	125	0.0093	155	0.0164	169	0.0108	104	0.0937	197	0.0127	96	0.0271	4	-	
119	hyperverge-001	1.0000	320	1.0000	320	1.0000	322	-	1.0000	319	1.0000	315	1.0000	317	1.0000	317	-		
120	hyperverge-002	0.0050	55	0.0066	52	0.0035	34	0.0051	40	0.0062	44	0.0107	38	0.0074	25	0.0276	20	-	
121	icm-002	0.0143	187	0.0249	199	0.0144	203	0.0256	204	0.0236	194	0.0386	159	0.0263	189	0.0339	152	-	
122	icthtc-000	0.0260	228	0.0396	225	0.0207	223	0.0339	221	0.0291	206	0.0474	166	0.0346	200	0.0459	194	-	
123	id3-006	0.0072	109	0.0103	104	0.0049	70	0.0074	76	0.0095	87	0.0165	73	0.0119	92	0.9938	311	-	
124	id3-007	0.0056	70	0.0078	66	0.0060	95	0.0072	72	0.0275	202	0.1374	210	0.0519	217	0.0487	199	-	
125	idemia-006	0.0046	50	0.0062	50	0.0047	66	0.0066	63	0.0073	57	0.2882	230	0.0094	61	0.0281	43	-	
126	idemia-007	0.0024	18	0.0039	23	0.0032	27	0.0038	23	0.0046	17	0.0092	21	0.0070	19	0.0288	82	-	
127	iit-002	0.0111	161	0.0177	165	0.0085	142	0.0140	149	0.0193	175	0.0332	144	0.0260	187	0.1373	250	-	
128	iit-003	0.0082	124	0.0151	145	0.0053	74	0.0084	88	0.0122	116	0.0199	94	0.0137	106	0.0407	179	-	
129	imagus-002	0.0062	89	0.0086	80	0.0053	76	0.0075	77	0.0121	115	0.0207	98	0.0161	133	0.0735	225	-	
130	imagus-003	0.0059	81	0.0084	76	0.0059	90	0.0081	84	0.0119	111	0.0209	99	0.0162	134	0.1068	240	-	
131	imperial-000	0.0067	101	0.0108	109	0.0080	133	0.0134	145	0.0087	72	0.0581	174	0.0102	69	0.0281	44	-	
132	imperial-002	0.0058	78	0.0081	72	0.0055	80	0.0085	90	0.0083	67	0.0157	67	0.0103	70	0.0273	10	0.5151	15

Table 16: FNMR is the proportion of mated comparisons below a threshold set to achieve the FMR given in the header on the fourth row. FMR is the proportion of impostor comparisons at or above that threshold. The light grey values give rank over all algorithms in that column. The pink columns use only same-sex impostors; others are selected regardless of demographics. The exception, in the green column, uses “matched-covariates” i.e. impostors of the same sex, age group, and country of birth. The second pink column includes effects of extended ageing. Missing entries for border, visa, mugshot and wild images generally mean the algorithm did not run to completion. For child exploitation, missing entries arise because NIST executes those runs only infrequently. The VISA columns compare images described in section 2.2. The MUGSHOT columns compare images described in section 2.5. The VISA-BORDER column compare images described in section 2.3 with those of section 2.4. The BORDER column compares images described in section 2.4. The WILD columns compare images described in section 2.6. The CHILD-EXPLOITATION columns compare images described in section 2.1.

Algorithm	FALSE NON-MATCH RATE (FNMR)												LESS CONSTRAINED, NON-COOP.						
	CONSTRAINED, COOPERATIVE																		
	Name	VISAMC	VISA	MUGSHOT	MUGSHOT12+YRS	VISABORDER	BORDER	BORDER	WILD	CHILDEXP									
FMR	0.0001	1E-06	1E-05	1E-05	1E-06	1E-06	1E-06	1E-05	0.0001	0.01									
133	incode-007	0.0109	158	0.0155	152	0.0056	85	0.0099	107	0.0107	101	0.0168	75	0.0102	67	0.0291	92	-	
134	incode-008	0.0063	90	0.0101	102	0.0046	63	0.0086	95	0.0057	35	0.0104	33	0.0074	23	0.0297	105	-	
135	incode-009	0.0044	47	0.0067	54	0.0034	33	0.0051	39	0.0049	23	0.0091	20	0.0067	14	0.0296	104	-	
136	innefulabs-000	0.0122	172	0.0199	173	0.0112	181	0.0197	188	0.0222	186	0.0372	155	0.0271	190	0.0348	157	-	
137	innovativetechnologyltd-001	0.0578	251	0.0938	254	0.0501	248	0.0981	249	0.0592	236	0.0779	191	0.0422	209	0.0449	193	-	
138	innovativetechnologyltd-002	0.0451	245	0.0716	247	0.0541	251	0.1009	251	0.0506	231	0.0682	185	0.0371	204	0.0804	231	-	
139	innovatrics-006	0.0058	75	0.0089	83	0.0061	98	0.0096	102	0.0096	90	0.0165	74	0.0103	71	0.0281	41	0.3056	3
140	innovatrics-007	0.0040	43	0.0054	40	0.0057	87	0.0078	80	0.0079	63	0.0123	49	0.0088	52	0.0282	55	-	
141	insightface-000	0.0018	13	0.0027	12	0.0029	15	0.0030	14	0.0038	5	0.0077	8	0.0068	15	0.0276	19	-	
142	intellicloudai-001	0.0142	186	0.0234	191	0.0092	154	0.0145	154	0.0162	154	0.0371	154	0.0171	141	0.0409	180	-	
143	intellicloudai-002	0.0059	83	0.0085	77	0.0060	94	0.0069	68	0.0108	102	0.2477	227	0.0171	140	0.0303	114	-	
144	intellifusion-001	0.0072	108	0.0094	91	0.0056	86	0.0085	91	0.0111	109	0.0212	101	0.0143	114	0.0289	84	0.5454	18
145	intellifusion-002	0.0059	79	0.0077	63	0.0040	47	0.0074	75	0.0085	70	0.5352	244	0.0104	74	0.0305	117	-	
146	intellivision-001	0.1335	267	0.2205	268	0.1090	262	0.1670	261	0.1385	255	0.1676	213	0.1170	246	0.2445	271	0.7766	47
147	intellivision-002	0.1000	262	0.1775	263	0.0610	256	0.1009	250	0.0805	246	0.1074	204	0.0682	228	0.0768	227	-	
148	intelresearch-002	0.0058	74	0.0082	75	0.0050	72	0.0086	93	0.0136	126	0.0434	163	0.0216	169	0.0285	71	-	
149	intelresearch-003	0.0046	49	0.0062	49	0.0038	43	0.0060	53	0.0088	75	0.0168	77	0.0136	102	0.0304	116	-	
150	intsysmsu-001	0.9543	315	0.9888	316	0.9923	309	-	-	0.9977	303	0.9955	290	0.9892	301	0.7871	301	-	
151	intsysmsu-002	0.0130	180	0.0254	201	0.0137	198	0.0267	212	0.0160	151	0.0267	125	0.0145	117	0.0289	87	-	
152	iqface-000	0.0091	134	0.0143	135	0.0075	120	0.0110	118	0.0171	163	0.2234	222	0.0359	201	0.0381	173	0.6490	29
153	iqface-003	0.0058	77	0.0079	70	0.0051	73	0.0058	51	0.0104	97	0.0200	95	0.0193	155	0.0402	177	-	
154	irex-000	0.0052	61	0.0099	96	0.0056	84	0.0083	86	0.0137	129	0.0163	72	0.0078	34	0.0285	68	-	
155	isap-001	0.5092	302	0.6588	300	0.6899	299	0.7978	296	0.7200	286	0.7253	260	0.5373	281	0.1931	262	-	
156	isap-002	0.0114	162	0.0186	168	0.0087	148	0.0151	159	0.0156	147	0.5134	243	0.0333	198	0.0354	164	-	
157	isityou-000	0.5682	304	0.7033	303	1.0000	321	-	-	1.0000	312	1.0000	319	1.0000	313	1.0000	321	1.0000	269
158	isystems-001	0.0149	192	0.0245	197	0.0138	199	0.0210	192	0.0209	181	0.0332	143	0.0223	171	0.0524	206	0.5152	16
159	isystems-002	0.0118	166	0.0182	167	0.0111	178	0.0162	167	0.0166	159	0.0284	130	0.0195	158	0.0516	204	0.4876	13
160	itmo-006	0.0125	175	0.0220	185	0.0149	210	0.0266	210	0.0233	189	0.0383	157	0.0285	192	0.0329	146	-	
161	itmo-007	0.0080	120	0.0125	123	0.0107	171	0.0185	180	0.0167	161	0.0222	109	0.0144	116	0.0300	109	-	
162	ivacognitive-001	0.0189	211	0.0351	216	0.0123	191	0.0235	199	0.0198	176	0.0274	127	0.0155	128	0.0296	103	-	
163	iws-000	0.4824	299	0.5801	295	0.6859	298	0.8155	297	0.8251	292	0.7756	266	0.6400	288	0.3251	283	-	
164	kakao-004	0.0078	116	0.0103	105	0.0059	92	0.0102	110	0.0155	145	0.1182	207	0.0230	174	0.0277	24	-	
165	kakao-005	0.0040	40	0.0059	43	0.0036	39	0.0057	48	0.0085	69	0.0239	113	0.0125	94	0.0280	37	-	
166	kedacom-000	0.0055	67	0.0081	73	0.0111	180	0.0120	125	0.0415	221	0.0966	201	0.0686	229	0.2511	274	0.7650	45
167	kiwitech-000	0.0076	114	0.0105	106	0.0081	135	0.0128	138	0.0096	89	0.0163	71	0.0101	66	0.0279	34	-	
168	kneron-003	0.0542	250	0.0902	252	0.0346	241	0.0562	240	0.0919	249	0.1251	209	0.0973	241	0.3053	282	0.6962	34
169	kneron-005	0.0157	197	0.0259	203	0.0126	195	0.0212	193	0.0406	220	0.0693	187	0.0542	221	0.0471	196	-	
170	kookmin-001	0.0462	247	0.0750	248	0.0489	246	0.0842	245	0.0659	240	0.8380	275	0.3212	265	0.0491	200	-	
171	kookmin-002	0.0054	65	0.0077	64	0.0043	55	0.0065	62	0.0123	117	0.7591	264	0.0198	160	0.0285	69	-	
172	lemalabs-001	0.0111	160	0.0175	163	0.0088	149	0.0142	151	0.0143	135	0.0228	111	0.0140	109	0.0281	40	-	
173	line-000	0.0172	205	0.0236	194	0.0109	175	0.0194	185	0.0183	167	0.0291	132	0.0204	164	0.0298	106	-	
174	lookman-002	0.0297	232	0.0547	239	0.0339	239	0.0562	239	0.0614	238	0.0960	200	0.0790	236	0.2640	278	-	
175	lookman-004	0.0074	111	0.0099	97	0.0124	193	0.0149	158	0.0430	225	0.0866	195	0.0694	230	0.2516	275	0.7664	46
176	luxand-000	0.2056	274	0.2814	272	0.4053	282	0.5365	280	0.3497	272	0.3743	233	0.2605	258	0.2222	270	-	

Table 17: FNMR is the proportion of mated comparisons below a threshold set to achieve the FMR given in the header on the fourth row. FMR is the proportion of impostor comparisons at or above that threshold. The light grey values give rank over all algorithms in that column. The pink columns use only same-sex impostors; others are selected regardless of demographics. The exception, in the green column, uses “matched-covariates” i.e. impostors of the same sex, age group, and country of birth. The second pink column includes effects of extended ageing. Missing entries for border, visa, mugshot and wild images generally mean the algorithm did not run to completion. For child exploitation, missing entries arise because NIST executes those runs only infrequently. The VISA columns compare images described in section 2.2. The MUGSHOT columns compare images described in section 2.5. The VISA-BORDER column compare images described in section 2.3 with those of section 2.4. The BORDER column compares images described in section 2.4. The WILD columns compare images described in section 2.6. The CHILD-EXPLOITATION columns compare images described in section 2.1.

Algorithm	FALSE NON-MATCH RATE (FNMR)																		
	CONSTRAINED, COOPERATIVE																		
	Name	VISAMC	VISA	MUGSHOT	MUGSHOT12+YRS	VisABORDER	BORDER	BORDER	WILD	CHILDEXP									
FMR	0.0001	1E-06	1E-05	1E-05	1E-06	1E-06	1E-06	1E-05	0.0001	0.01									
177	megvii-002	0.0104	153	0.0145	138	0.0225	227	0.0345	223	0.0099	94	0.0286	131	0.0240	182	0.0692	223	0.3013	2
178	megvii-003	0.0064	94	0.0094	89	0.0136	197	0.0260	207	0.0050	24	0.0080	10	0.0059	7	0.0288	76	-	
179	meitan-000	0.0197	214	0.0424	228	0.0078	127	0.0074	74	0.0103	96	0.0193	91	0.0164	135	0.1063	239	-	
180	meiya-001	0.0171	202	0.0275	207	0.0159	213	0.0261	209	0.0311	211	0.2250	223	0.0245	185	0.0363	168	-	
181	microfocus-001	0.4482	296	0.5524	294	0.7256	302	0.8416	299	0.7301	287	0.6926	257	0.5180	280	0.2567	277	0.6890	33
182	microfocus-002	0.3605	288	0.5057	289	0.5783	291	0.7223	289	0.5909	279	0.5963	248	0.4160	276	0.1582	255	0.6517	30
183	minivision-000	0.0033	31	0.0048	34	0.0038	44	0.0049	34	0.0055	33	0.0094	24	0.0079	37	0.0273	8	-	
184	mobai-000	0.0360	240	0.0439	231	0.0372	243	0.0700	243	0.0367	215	0.0939	198	0.0795	237	0.2640	279	-	
185	mobai-001	0.0199	216	0.0219	182	0.0047	65	0.0061	56	0.0093	85	0.0174	80	0.0138	108	0.1045	238	-	
186	mobbli-000	0.2938	280	0.3861	281	0.5391	287	0.6888	287	0.6545	282	0.8027	267	0.6207	285	0.5471	295	-	
187	mobbli-001	0.3208	283	0.4375	284	0.5680	290	0.7193	288	0.6282	280	0.5783	246	0.3984	273	0.1866	261	-	
188	moreedian-000	0.3874	289	0.4912	288	0.9988	313	-		0.9990	304	0.9999	299	0.9998	305	0.4788	290	-	
189	mvision-001	0.0191	212	0.0233	189	0.0204	222	0.0356	224	0.0198	177	0.0337	145	0.0242	183	0.0431	185	-	
190	nazhiai-000	0.0040	42	0.0059	44	0.0036	37	0.0048	33	0.0057	36	0.0125	50	0.0083	44	0.0275	15	-	
191	neosystems-001	1.0000	319	1.0000	321	0.2987	276	0.4382	276	0.5173	278	0.6570	253	0.4043	275	0.5091	293	-	
192	netbridge-tech-001	0.4749	298	0.6599	301	0.4438	283	0.5676	282	0.4491	277	1.0000	300	0.9541	297	0.1098	243	-	
193	netbridge-tech-002	0.0101	149	0.0166	157	0.0077	124	0.0127	134	0.0133	124	0.8215	271	0.0523	219	0.0351	162	-	
194	neurotechnology-010	0.0048	52	0.0085	79	0.0056	83	0.0090	98	0.0077	62	1.0000	303	0.0113	82	0.0273	7	-	
195	neurotechnology-011	0.0050	56	0.0087	81	0.0061	99	0.0097	104	0.0077	61	0.0404	162	0.0092	55	0.0293	98	-	
196	rhn-001	0.0066	99	0.0098	95	0.0053	75	0.0079	83	0.0093	83	0.0156	66	0.0109	79	0.0308	129	-	
197	nodeflux-002	0.0186	210	0.0340	213	0.0261	235	0.0451	233	0.0548	233	1.0000	306	1.0000	308	0.0299	107	-	
198	notiontag-000	0.6669	305	0.7885	304	0.3715	279	0.4978	278	0.8571	293	0.8102	269	0.6460	289	0.1807	260	0.6479	28
199	notiontag-001	0.6846	306	0.8006	305	0.3955	281	0.5247	279	0.8669	295	0.8313	274	0.6362	287	0.2221	269	-	
200	nsensecorp-001	0.9909	317	0.9994	318	0.9987	312	-		1.0000	310	1.0000	308	1.0000	309	0.9858	309	-	
201	nsensecorp-002	0.4277	292	0.5375	292	0.6734	297	0.7924	295	0.7194	285	0.6937	258	0.5617	282	0.5530	296	-	
202	ntechlab-009	0.0039	39	0.0054	41	0.0042	53	0.0063	59	0.0275	203	0.0674	184	0.0532	220	0.0537	208	-	
203	ntechlab-010	0.0013	3	0.0017	1	0.0024	3	0.0029	9	0.0031	2	0.0058	2	0.0050	2	0.0292	94	-	
204	omnigarde-000	0.0633	253	0.1002	256	0.1109	263	0.2042	264	0.1288	254	0.5113	242	0.1227	248	0.0357	166	-	
205	openface-001	0.1804	270	0.2921	273	0.2878	274	0.3906	274	0.2054	264	0.2338	226	0.1549	252	0.2445	272	-	
206	oz-001	0.0133	181	0.0215	181	0.0109	176	0.0160	165	0.0235	192	1.0000	322	1.0000	311	0.0417	182	-	
207	oz-002	0.0071	107	0.0099	99	0.0099	163	0.0100	108	0.0139	130	0.0502	168	0.0202	162	0.5084	292	-	
208	papsav1923-001	0.0078	117	0.0130	127	0.0068	107	0.0105	114	0.0119	112	0.0221	108	0.0136	103	0.0293	96	-	
209	paravision-004	0.0030	28	0.0046	33	0.0030	18	0.0036	20	0.0091	82	0.0188	89	0.0173	142	0.0288	79	0.2467	1
210	paravision-006	0.0016	9	0.0025	8	0.0026	6	0.0026	4	0.0075	59	0.9933	288	0.0142	112	0.0277	25	-	
211	pensees-001	0.0087	128	0.0133	129	0.0071	112	0.0122	129	0.0145	139	0.0252	119	0.0195	159	0.0283	58	-	
212	pixelall-005	0.0038	37	0.0052	38	0.0043	56	0.0051	41	0.0077	60	0.0839	194	0.0136	105	0.0279	29	-	
213	pixelall-006	0.0032	30	0.0042	28	0.0032	26	0.0039	24	0.0063	46	0.9960	292	0.0723	233	0.0283	56	-	
214	psl-006	0.0025	19	0.0039	22	0.0028	14	0.0030	13	0.0160	150	0.0482	167	0.0310	196	0.0289	85	-	
215	psl-007	0.0026	22	0.0040	24	0.0027	10	0.0030	11	0.0054	29	0.0101	32	0.0081	40	0.0282	50	-	
216	ptakuratsatu-000	0.0060	84	0.0089	84	0.0070	110	0.0104	113	0.0096	91	0.0152	64	0.0100	64	0.0284	63	-	
217	pxl-001	0.0488	248	0.0752	249	0.0586	253	0.1087	252	0.0946	250	0.1065	203	0.0625	226	0.1088	241	-	
218	pyramid-000	0.0136	183	0.0233	190	0.0117	188	0.0192	184	0.0185	169	0.0322	139	0.0206	166	0.0304	115	-	
219	quantasoft-003	0.0081	123	0.0113	117	0.0056	82	0.0076	79	0.0091	81	0.0161	70	0.0107	78	0.0414	181	-	
220	rankone-009	0.0087	127	0.0119	119	0.0065	104	0.0086	94	0.0088	76	0.0161	69	0.0121	93	0.0323	140	-	

Table 18: FNMR is the proportion of mated comparisons below a threshold set to achieve the FMR given in the header on the fourth row. FMR is the proportion of impostor comparisons at or above that threshold. The light grey values give rank over all algorithms in that column. The pink columns use only same-sex impostors; others are selected regardless of demographics. The exception, in the green column, uses “matched-covariates” i.e. impostors of the same sex, age group, and country of birth. The second pink column includes effects of extended ageing. Missing entries for border, visa, mugshot and wild images generally mean the algorithm did not run to completion. For child exploitation, missing entries arise because NIST executes those runs only infrequently. The VISA columns compare images described in section 2.2. The MUGSHOT columns compare images described in section 2.5. The VISA-BORDER column compare images described in section 2.3 with those of section 2.4. The BORDER column compares images described in section 2.4. The WILD columns compare images described in section 2.6. The CHILD-EXPLOITATION columns compare images described in section 2.1.

		FALSE NON-MATCH RATE (FNMR)																	
	Algorithm	CONSTRAINED, COOPERATIVE								LESS CONSTRAINED, NON-COOP.									
	Name	ViSAMC	VISA	MUGSHOT	MUGSHOT12+YRS	VISABORDER	BORDER	BORDER	WILD	CHILDEXP									
	FMR	0.0001	1E-06	1E-05	1E-05	1E-06	1E-06	1E-05	0.0001	0.01									
221	rankone-010	0.0079	118	0.0112	115	0.0061	96	0.0081	85	0.0088	74	0.0149	61	0.0117	88	0.0320	138	-	
222	realnetworks-002	0.0248	225	0.0358	218	0.0513	250	0.1127	255	0.0371	216	0.0614	178	0.0316	197	0.0334	149	-	
223	realnetworks-004	0.0075	113	0.0101	101	0.0066	105	0.0097	105	0.0108	106	0.0187	87	0.0131	99	0.0285	72	-	
224	regula-000	0.0184	209	0.0376	222	0.0103	165	0.0185	179	0.0120	114	0.9983	295	0.0231	175	0.0273	11	-	
225	remarkai-001	0.0144	188	0.0256	202	0.0102	164	0.0159	164	0.0162	155	0.0582	175	0.0185	148	0.0308	126	-	
226	remarkai-002	0.0151	195	0.0197	171	0.0075	121	0.0108	117	0.0119	113	0.0187	88	0.0127	95	0.0426	184	-	
227	remarkai-003	0.0047	51	0.0063	51	0.0033	29	0.0049	36	0.0054	30	0.0100	31	0.0072	20	0.0275	16	-	
228	rendip-000	0.0055	68	0.0077	65	0.0048	69	0.0060	54	0.0080	64	0.0142	57	0.0110	80	0.0433	187	-	
229	rokid-000	0.0093	138	0.0145	139	0.0073	117	0.0102	111	0.0164	157	0.0280	129	0.0214	168	0.0857	232	-	
230	rokid-001	0.0105	154	0.0162	154	0.0094	157	0.0163	168	0.0181	165	0.0276	128	0.0165	136	0.0325	142	-	
231	s1-001	0.0314	236	0.0651	244	0.0252	232	0.0357	225	0.0444	227	0.0653	183	0.0429	210	0.8493	302	-	
232	s1-002	0.0095	141	0.0144	137	0.0112	182	0.0196	186	0.0234	190	0.0371	153	0.0282	191	0.1167	246	-	
233	saffe-001	0.4339	293	0.5261	290	0.7539	304	0.8736	302	0.7977	290	0.9810	283	0.7435	292	0.3887	285	0.8973	54
234	saffe-002	0.0119	170	0.0206	174	0.0107	174	0.0177	174	0.0244	196	0.9998	298	0.2785	261	0.0308	125	-	
235	samtech-001	0.0197	215	0.0365	219	0.0146	207	0.0241	201	0.0238	195	0.0394	160	0.0251	186	0.0337	150	-	
236	scanovate-001	0.0175	207	0.0331	211	0.0163	214	0.0248	203	0.2476	267	0.3801	234	0.3740	269	0.4060	286	-	
237	scanovate-002	0.0175	206	0.0355	217	0.0146	205	0.0286	214	0.0269	199	0.0301	133	0.0178	144	0.0301	112	-	
238	securifai-001	0.4538	297	0.6142	298	0.5844	292	0.7428	291	0.7051	284	0.9961	293	0.9558	298	0.1963	263	-	
239	securifai-002	0.7557	310	0.8574	306	0.4550	284	0.5953	283	0.9860	300	0.9796	282	0.9158	294	0.2848	280	-	
240	sensetime-004	0.0026	21	0.0038	18	0.0022	2	0.0023	2	0.0042	9	0.0082	12	0.0078	33	0.0293	95	-	
241	sensetime-005	0.0019	14	0.0029	13	0.0022	1	0.0021	1	0.0023	1	0.0044	1	0.0039	1	0.0273	9	-	
242	sertis-000	0.0118	167	0.0208	176	0.0080	131	0.0127	133	0.0110	108	0.0176	81	0.0114	85	0.0285	70	-	
243	sertis-002	0.0049	54	0.0061	45	0.0039	46	0.0061	58	0.0055	32	0.0099	30	0.0070	18	0.0281	42	-	
244	shaman-000	0.9297	314	0.9774	314	0.9990	314	-		0.9999	307	1.0000	304	0.9999	307	0.9575	307	0.9618	58
245	shaman-001	0.3346	285	0.4616	285	0.2368	272	0.3723	273	0.3574	273	0.3527	232	0.2304	256	0.1498	254	0.8990	55
246	shu-002	-		0.0079	69	0.0146	206	0.0308	216	1.0000	309	0.0183	84	0.0115	86	0.0284	64	-	
247	shu-003	0.0028	25	0.0041	27	0.0050	71	0.0088	97	0.0081	65	0.0133	53	0.0094	60	0.0283	61	-	
248	siat-002	0.0091	132	0.0126	126	0.0109	177	0.0190	183	0.0276	204	0.0516	169	0.0464	214	0.0520	205	0.4277	10
249	siat-004	0.0067	100	0.0099	98	0.0152	211	-		0.0275	201	0.4823	240	0.4823	277	1.0000	312	-	
250	sjtu-003	0.0017	11	0.0033	15	0.0030	20	0.0037	21	0.0058	37	0.0104	34	0.0081	41	0.0284	66	-	
251	sjtu-004	0.0014	4	0.0025	6	0.0027	11	0.0028	8	0.0046	16	0.0086	16	0.0073	21	0.0272	5	-	
252	smilart-002	0.2440	276	0.3532	277	-		-		0.3785	274	0.4145	238	0.2611	259	-	0.6999	35	-
253	smilart-003	0.6944	307	0.8836	307	0.0695	257	0.1193	256	0.0894	248	0.1221	208	0.0737	234	0.1190	247	-	
254	sodec-000	0.0033	33	0.0044	30	0.0040	49	0.0053	44	0.0054	31	0.0096	27	0.0080	38	0.0274	12	-	
255	staqu-000	0.0139	185	0.0208	175	0.0104	166	0.0145	156	0.0156	146	0.8063	268	0.1408	251	0.0332	148	-	
256	starhybrid-001	0.0108	157	0.0138	132	0.0081	134	0.0113	121	0.0152	142	0.0265	124	0.0189	152	0.0350	160	0.5584	19
257	suprema-000	0.0064	91	0.0092	87	0.0081	136	0.0096	103	0.0139	131	0.0254	121	0.0220	170	0.1131	244	-	
258	supremaid-001	0.0053	63	0.0073	59	0.0045	60	0.0066	65	0.0099	93	0.0186	86	0.0148	121	0.0352	163	-	
259	synesis-006	0.0070	104	0.0096	93	0.0107	172	0.0166	170	-		0.0128	51	0.0089	53	0.0292	93	-	
260	synesis-007	0.0050	58	0.0073	60	0.0062	100	0.0076	78	-		0.0105	35	0.0080	39	0.0288	77	-	
261	synology-000	0.0149	190	0.0238	195	0.0148	208	0.0261	208	0.0221	185	0.0331	142	0.0209	167	0.0330	147	-	
262	synology-002	0.0104	152	0.0153	148	0.0107	173	0.0184	177	0.0189	172	0.2032	221	0.0180	145	0.0312	130	-	
263	sztu-000	0.0092	136	0.0139	133	0.0091	152	0.0201	189	0.0136	128	0.0685	186	0.0118	90	0.0270	2	-	
264	tech5-004	0.0123	173	0.0234	192	0.0086	146	0.0162	166	0.0065	50	0.0112	42	0.0082	42	0.0281	46	-	

Table 19: FNMR is the proportion of mated comparisons below a threshold set to achieve the FMR given in the header on the fourth row. FMR is the proportion of impostor comparisons at or above that threshold. The light grey values give rank over all algorithms in that column. The pink columns use only same-sex impostors; others are selected regardless of demographics. The exception, in the green column, uses “matched-covariates” i.e. impostors of the same sex, age group, and country of birth. The second pink column includes effects of extended ageing. Missing entries for border, visa, mugshot and wild images generally mean the algorithm did not run to completion. For child exploitation, missing entries arise because NIST executes those runs only infrequently. The VISA columns compare images described in section 2.2. The MUGSHOT columns compare images described in section 2.5. The VISA-BORDER column compare images described in section 2.3 with those of section 2.4. The BORDER column compares images described in section 2.4. The WILD columns compare images described in section 2.6. The CHILD-EXPLOITATION columns compare images described in section 2.1.

Algorithm	FALSE NON-MATCH RATE (FNMR)																		
	CONSTRAINED, COOPERATIVE											LESS CONSTRAINED, NON-COOP.							
	Name	ViSAMC	VISA	MUGSHOT	MUGSHOT12+YRS	ViSABORDER	BORDER	BORDER	WILD	CHILDEXP									
FMR	0.0001	1E-06	1E-05	1E-05	1E-06	1E-06	1E-06	1E-05	0.0001	0.01									
265	tech5-005	0.0054	64	0.0072	57	0.0069	108	0.0122	128	0.0060	42	0.0094	23	0.0066	12	0.0349	159	-	
266	tevian-005	0.0043	46	0.0062	48	0.0057	88	0.0085	92	0.0070	54	0.0135	54	0.0119	91	0.0300	110	0.5625	22
267	tevian-006	0.0045	48	0.0061	46	0.0045	61	0.0066	64	0.0046	19	0.0091	19	0.0075	26	0.0308	128	-	
268	tiger-003	0.0313	235	0.0602	241	0.0188	219	0.0359	226	0.0344	212	-	-	0.0482	198	0.5610	21		
269	tiger-004	0.0779	258	0.1393	260	0.0488	245	0.0905	248	0.0800	244	0.1640	212	0.0617	225	0.0669	220	-	
270	tongyi-005	0.0073	110	0.0146	140	0.0187	218	0.0421	232	0.0161	153	0.0215	103	0.0149	123	0.0399	175	0.6195	27
271	toshiba-002	0.0134	182	0.0222	187	0.0097	162	0.0154	162	-	-	0.0327	141	0.0158	131	0.0434	188	0.7103	36
272	toshiba-003	0.0125	176	0.0214	179	0.0085	144	0.0131	140	-	-	0.0241	114	0.0151	126	0.0282	47	-	
273	trueface-001	0.0204	217	0.0438	230	0.0095	159	0.0138	147	0.0154	143	0.0253	120	0.0169	139	0.0772	228	-	
274	trueface-002	0.0060	86	0.0096	92	0.0048	68	0.0061	57	0.0112	110	0.0198	93	0.0155	129	0.0793	230	-	
275	tuputech-000	0.3218	284	0.3696	279	-	-	-	0.3237	269	0.4304	239	0.2973	264	0.9415	306	-		
276	twface-000	0.0051	59	0.0072	58	0.0041	50	0.0058	49	0.0071	56	0.0153	65	0.0100	63	0.0276	18	-	
277	ulsee-001	0.0151	194	0.0246	198	0.0113	184	0.0185	181	0.0187	171	0.6766	255	0.0181	146	0.0316	135	-	
278	ultinous-000	0.2343	275	0.3484	275	-	-	-	-	-	-	-	-	-	-	0.9447	57		
279	ultinous-001	0.2485	277	0.4003	282	-	-	-	-	-	-	-	-	-	-	0.6847	32		
280	uluface-002	0.0081	121	0.0123	120	0.0071	111	0.0095	101	0.0107	100	1.0000	314	0.0140	110	0.0444	190	0.6729	31
281	uluface-003	0.0100	148	0.0150	144	0.0079	128	0.0128	136	-	-	-	-	-	-	0.0635	218	-	
282	upc-001	0.0234	221	0.0519	237	0.0291	238	0.0490	237	0.0294	207	0.2316	225	0.0389	206	0.0314	133	0.4224	8
283	vcog-002	0.7522	309	0.9033	308	-	-	-	-	-	-	-	-	-	-	0.7523	43		
284	vd-001	0.0243	223	0.0452	232	0.0271	236	0.0402	230	0.0424	224	-	-	-	-	0.1389	251	-	
285	vd-002	0.0429	244	0.0704	246	0.0569	252	0.0844	246	0.0801	245	0.0937	196	0.0577	223	0.0556	211	-	
286	veridas-004	0.0281	230	0.0467	233	0.0353	242	0.0643	242	0.0424	223	0.0644	182	0.0342	199	0.0291	91	-	
287	veridas-006	0.0098	144	0.0167	160	0.0079	130	0.0127	132	0.0127	119	0.0217	105	0.0151	125	0.0286	75	-	
288	via-000	0.0216	218	0.0365	220	0.0177	216	0.0287	215	0.0296	208	0.0572	171	0.0290	195	0.0349	158	0.7638	44
289	via-001	0.0149	191	0.0229	188	0.0114	186	0.0177	176	0.0183	168	0.4056	237	0.0176	143	0.0373	171	-	
290	videmo-000	0.0298	233	0.0423	226	0.0155	212	0.0260	206	0.0246	197	0.0397	161	0.0239	181	0.0541	209	-	
291	videonetics-001	0.5483	303	0.6446	299	0.7517	303	0.8607	300	0.8664	294	0.8255	272	0.6956	291	0.2986	281	0.7297	40
292	videonetics-002	0.4274	291	0.5329	291	0.6081	294	0.7438	292	0.7775	288	0.7297	261	0.5756	283	0.1976	266	0.7435	42
293	vigilantsolutions-009	0.0117	165	0.0165	156	0.0075	122	0.0101	109	0.0219	184	0.0385	158	0.0238	180	0.0277	26	-	
294	vigilantsolutions-010	0.0109	159	0.0164	155	0.0074	119	0.0095	100	0.0209	180	0.0365	152	0.0233	176	0.0277	21	-	
295	vinai-000	0.0081	122	0.0124	121	0.0043	59	0.0072	71	0.0089	77	0.1814	214	0.0112	81	0.0274	13	-	
296	vion-000	0.0419	242	0.0590	240	0.0422	244	0.0478	235	0.0581	235	0.0968	202	0.0847	238	0.2479	273	0.8765	51
297	visage-000	0.0933	260	0.1441	261	0.1316	266	0.2416	267	0.1395	256	0.1920	218	0.1001	242	0.0500	202	-	
298	visionbox-001	0.0159	199	0.0270	206	0.0111	179	0.0173	173	0.0190	173	0.0315	135	0.0205	165	0.0389	174	-	
299	visionbox-002	0.0058	73	0.0079	68	0.0060	93	0.0074	73	0.0084	68	0.0149	62	0.0113	84	0.0447	192	-	
300	visionlabs-009	0.0018	12	0.0025	7	0.0026	5	0.0029	10	0.0035	4	0.0064	4	0.0054	4	0.0283	57	-	
301	visionlabs-010	0.0017	10	0.0024	5	0.0026	7	0.0030	12	0.0033	3	0.0061	3	0.0052	3	0.0282	52	-	
302	visteam-000	0.9200	313	0.9489	312	0.9959	310	-	-	0.9994	305	0.9978	294	0.9914	303	0.8783	304	-	
303	visteam-001	0.4417	295	0.5385	293	0.6410	296	0.7788	294	0.6386	281	0.5904	247	0.4023	274	0.1413	252	-	
304	vnpt-001	0.3117	282	0.3523	276	0.3474	278	0.2747	269	0.3405	270	0.5015	241	0.4827	278	0.5337	294	-	
305	vnpt-002	0.0351	239	0.0424	227	0.0220	225	0.0316	218	0.0471	229	0.0817	193	0.0698	231	0.0400	176	-	
306	vocord-008	0.0029	27	0.0038	20	0.0042	52	0.0055	45	0.0045	14	0.0086	17	0.0073	22	0.0286	73	-	
307	vocord-009	0.0022	16	0.0029	14	0.0036	38	0.0046	30	0.0052	27	0.0098	29	0.0086	50	0.0284	65	-	
308	vts-000	0.0103	150	0.0174	162	0.0080	132	0.0129	139	0.0250	198	0.0450	164	0.0372	205	0.0596	215	-	

Table 20: FNMR is the proportion of mated comparisons below a threshold set to achieve the FMR given in the header on the fourth row. FMR is the proportion of impostor comparisons at or above that threshold. The light grey values give rank over all algorithms in that column. The pink columns use only same-sex impostors; others are selected regardless of demographics. The exception, in the green column, uses “matched-covariates” i.e. impostors of the same sex, age group, and country of birth. The second pink column includes effects of extended ageing. Missing entries for border, visa, mugshot and wild images generally mean the algorithm did not run to completion. For child exploitation, missing entries arise because NIST executes those runs only infrequently. The VISA columns compare images described in section 2.2. The MUGSHOT columns compare images described in section 2.5. The VISA-BORDER column compare images described in section 2.3 with those of section 2.4. The BORDER column compares images described in section 2.4. The WILD columns compare images described in section 2.6. The CHILD-EXPLOITATION columns compare images described in section 2.1.

	Algorithm	FALSE NON-MATCH RATE (FNMR)										LESS CONSTRAINED, NON-COOP.							
		CONSTRAINED, COOPERATIVE																	
		Name	VISAMC	VISA	MUGSHOT	MUGSHOT12+YRS	VISABORDER	BORDER	BORDER	WILD	CHILDEXP								
	FMR	0.0001	1E-06	1E-05	1E-05	1E-06	1E-06	1E-06	1E-05	0.0001	0.01								
309	winsense-001	0.0062	88	0.0099	100	0.0092	153	0.0210	191	0.0093	84	0.0144	58	0.0098	62	0.0320	137	0.4155	7
310	winsense-002	0.0050	57	0.0073	61	0.0038	42	0.0059	52	0.0064	48	0.0118	47	0.0084	46	0.0307	123	-	
311	x-laboratory-000	0.0071	105	0.0106	107	0.0123	192	0.0138	146	0.0419	222	0.5629	245	0.2852	263	0.0295	102	0.9686	59
312	x-laboratory-001	0.0059	80	0.0110	111	0.0054	77	0.0078	81	0.0094	86	0.0142	56	0.0100	65	0.0294	99	-	
313	xforwardai-001	0.0021	15	0.0034	16	0.0027	12	0.0028	6	0.0046	18	0.0088	18	0.0079	36	0.0281	45	-	
314	xforwardai-002	0.0016	7	0.0023	4	0.0026	9	0.0025	3	0.0040	8	0.0081	11	0.0074	24	0.0282	48	-	
315	xm-000	0.0015	5	0.0026	10	0.0031	22	0.0038	22	0.0058	38	0.0105	36	0.0082	43	0.0282	51	-	
316	yisheng-004	0.1988	272	0.3329	274	0.1147	265	0.1849	263	0.2044	263	-	-	-	-	0.0908	233	0.7152	37
317	yitu-003	0.0015	6	0.0026	9	0.0066	106	0.0085	89	0.0064	49	0.0114	43	0.0103	72	0.0325	143	-	
318	yoonik-000	0.0070	103	0.0112	112	0.0074	118	0.0118	124	0.0564	234	0.2013	220	0.1160	245	0.0590	214	-	
319	yoonik-001	0.0057	71	0.0079	67	0.0043	57	0.0061	55	0.0307	210	0.0762	190	0.0556	222	0.0526	207	-	
320	ytu-000	0.0057	72	0.0087	82	0.0121	190	0.0238	200	0.0047	20	0.0078	9	0.0059	6	0.0286	74	-	
321	yuan-001	0.0116	164	0.0220	184	0.0114	185	0.0184	178	0.0149	140	0.0574	172	0.0160	132	0.0321	139	-	
322	yuan-002	0.0094	140	0.0154	151	0.0071	113	0.0110	119	0.0108	105	0.0348	147	0.0127	97	0.0319	136	-	

Table 21: FNMR is the proportion of mated comparisons below a threshold set to achieve the FMR given in the header on the fourth row. FMR is the proportion of impostor comparisons at or above that threshold. The light grey values give rank over all algorithms in that column. The pink columns use only same-sex impostors; others are selected regardless of demographics. The exception, in the green column, uses “matched-covariates” i.e. impostors of the same sex, age group, and country of birth. The second pink column includes effects of extended ageing. Missing entries for border, visa, mugshot and wild images generally mean the algorithm did not run to completion. For child exploitation, missing entries arise because NIST executes those runs only infrequently. The VISA columns compare images described in section 2.2. The MUGSHOT columns compare images described in section 2.5. The VISA-BORDER column compare images described in section 2.3 with those of section 2.4. The BORDER column compares images described in section 2.4. The WILD columns compare images described in section 2.6. The CHILD-EXPLOITATION columns compare images described in section 2.1.

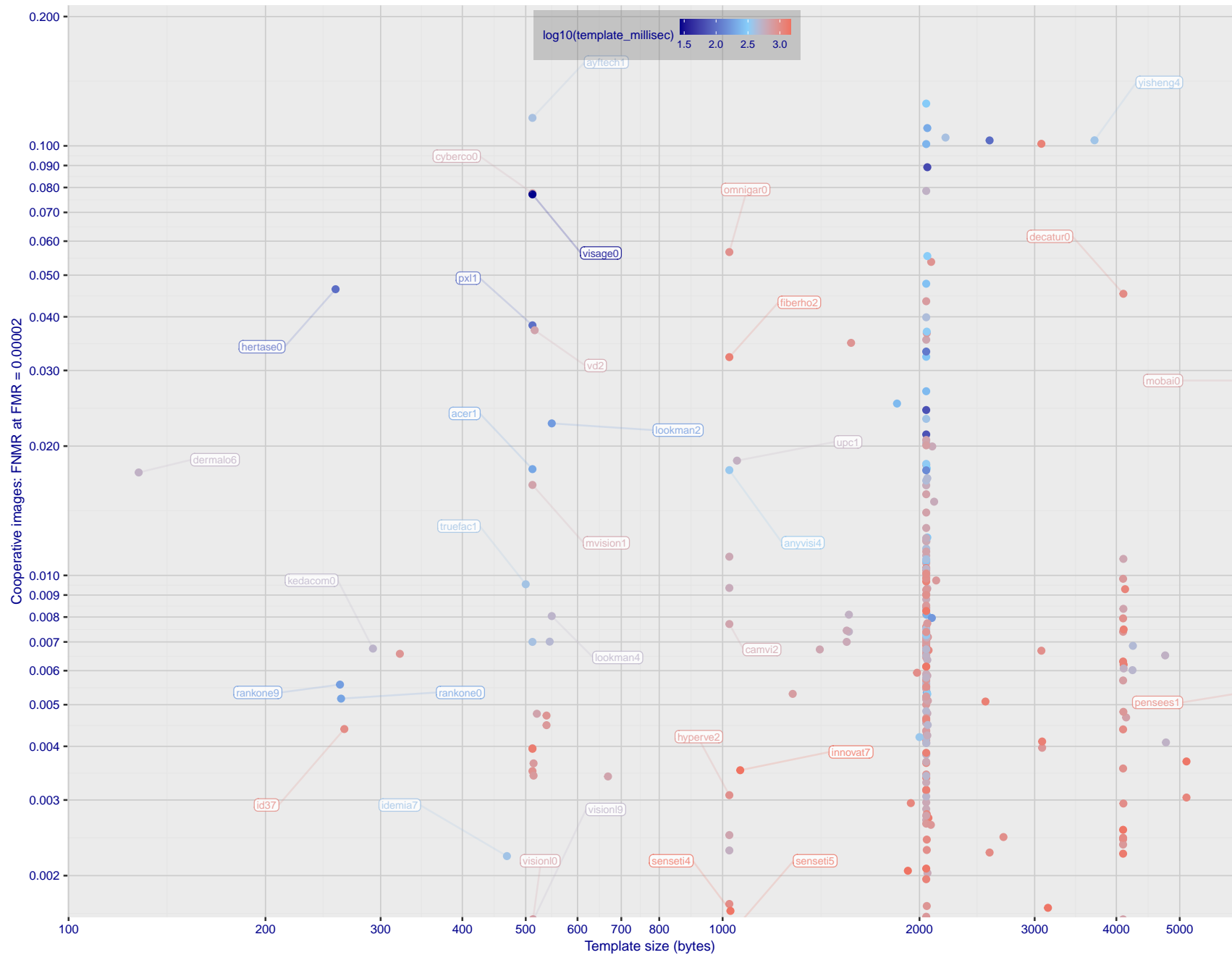


Figure 1: The points show false non-match rates (FNMR) versus the size of the encoded template. FNMR is the geometric mean of FNMR values for visa and mugshot images (from Figs. 50 and 66) at a false match rate (FMR) of 0.0001. The color of the points encodes template generation time - which spans at least one order of magnitude. Durations are measured on a single core of a c. 2016 Intel Xeon CPU E5-2630 v4 running at 2.20GHz. Algorithms with poor FNMR are omitted.

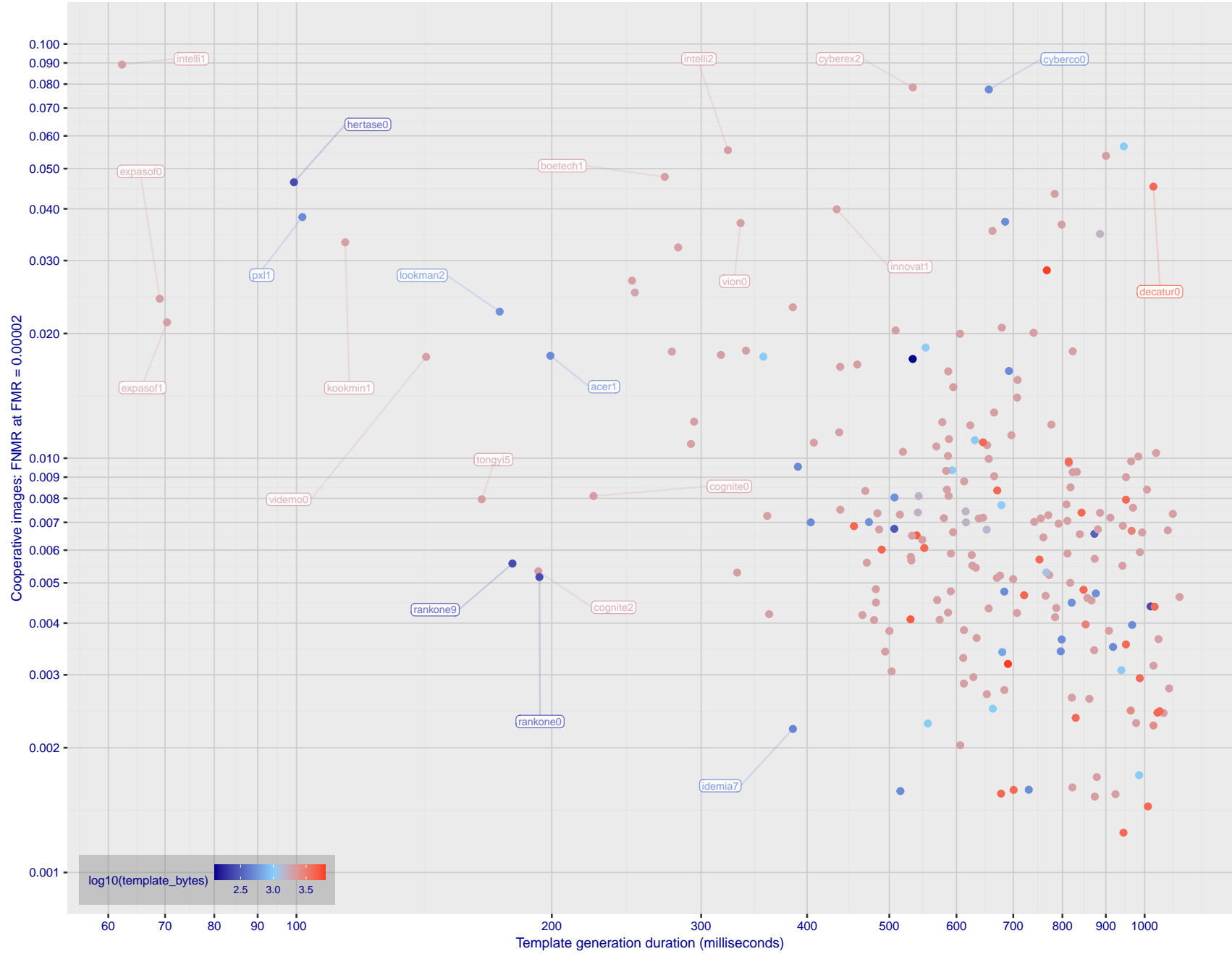


Figure 2: The points show false non-match rates (FNMR) versus the duration of the template generation operation. FNMR is the geometric mean of FNMR values for visa and mugshot images (from Figs. 50 and 66) at a false match rate (FMR) of 0.0001. Template generation time is a median estimated over 640 x 480 pixel portraits. It is measured on a single core of a c. 2016 Intel Xeon CPU E5-2630 v4 running at 2.20GHz. The color of the points encodes template size - which span two orders of magnitude. Algorithms with poor FNMR are omitted.

1 Metrics

1.1 Core accuracy

Given a vector of N genuine scores, u , the false non-match rate (FNMR) is computed as the proportion below some threshold, T:

$$\text{FNMR}(T) = 1 - \frac{1}{N} \sum_{i=1}^N H(u_i - T) \quad (1)$$

where $H(x)$ is the unit step function, and $H(0)$ taken to be 1.

Similarly, given a vector of N impostor scores, v , the false match rate (FMR) is computed as the proportion above T:

$$\text{FMR}(T) = \frac{1}{N} \sum_{i=1}^N H(v_i - T) \quad (2)$$

The threshold, T, can take on any value. We typically generate a set of thresholds from quantiles of the observed impostor scores, v , as follows. Given some interesting false match rate range, $[\text{FMR}_L, \text{FMR}_U]$, we form a vector of K thresholds corresponding to FMR measurements evenly spaced on a logarithmic scale

$$T_k = Q_v(1 - \text{FMR}_k) \quad (3)$$

where Q is the quantile function, and FMR_k comes from

$$\log_{10} \text{FMR}_k = \log_{10} \text{FMR}_L + \frac{k}{K} [\log_{10} \text{FMR}_U - \log_{10} \text{FMR}_L] \quad (4)$$

Error tradeoff characteristics are plots of FNMR(T) vs. FMR(T). These are plotted with $\text{FMR}_U \rightarrow 1$ and FMR_L as low as is sustained by the number of impostor comparisons, N. This is somewhat higher than the “rule of three” limit $3/N$ because samples are not independent, due to re-use of images.

2 Datasets

2.1 Child exploitation images

- ▷ The number of images is on the order of 10^4 .
- ▷ The number of subjects is on the order of 10^3 .
- ▷ The number of subjects with two images on the order of 10^3 .
- ▷ The images are operational. They are taken from ongoing investigations of child exploitation crimes. The images are arbitrarily unconstrained. Pose varies considerably around all three axes, including subject lying down. Resolution varies very widely. Faces can be occluded by other objects, including hair and hands. Lighting varies, although the images are intended for human viewing. Mis-focus is rare. Images are given to the algorithm without any cropping; faces may occupy widely varying areas.
- ▷ The images are usually large from contemporary cameras. The mean interocular distance (IOD) is 70 pixels.
- ▷ The images are of subjects from several countries, due to the global production of this imagery.
- ▷ The images are of children, from infancy to late adolescence.
- ▷ All of the images are live capture, none are scanned. Many have been cropped.
- ▷ When these images are input to the algorithm, they are labelled as being of type "EXPLOITATION" - see Table 4 of the FRVT API.

2.2 Visa images

- ▷ The number of images is on the order of 10^5 .
- ▷ The number of subjects is on the order of 10^5 .
- ▷ The number of subjects with two images is on the order of 10^4 .
- ▷ The images have geometry in reasonable conformance with the ISO/IEC 19794-5 Full Frontal image type. Pose is generally excellent.
- ▷ The images are of size 252x300 pixels. The mean interocular distance (IOD) is 69 pixels.
- ▷ The images are of subjects from greater than 100 countries, with significant imbalance due to visa issuance patterns.
- ▷ The images are of subjects of all ages, including children, again with imbalance due to visa issuance demand.
- ▷ Many of the images are live capture. A substantial number of the images are photographs of paper photographs.
- ▷ When these images are input to the algorithm, they are labelled as being of type "ISO" - see Table 4 of the FRVT API.

2.3 Application images

- ▷ The number of images is on the order of 10^6 .
- ▷ The number of subjects is on the order of 10^6 .
- ▷ The number of subjects with two images is on the order of 10^6 .
- ▷ The images have geometry in good conformance with the ISO/IEC 19794-5 Full Frontal image type. Pose is generally excellent.
- ▷ The images are of size 300x300 pixels. The mean interocular distance (IOD) is 61 pixels.
- ▷ The images are of subjects from greater than 100 countries, with significant imbalance due to population and immigration patterns.

- ▷ The images are of subjects of adults with imbalance due to population and immigration patterns and demand.
- ▷ All of the images are live capture.
- ▷ When these images are input to the algorithm, they are labelled as being of type "ISO" - see Table 4 of the FRVT API.

2.4 Border crossing images

- ▷ The number of images is on the order of 10^6 .
- ▷ The number of subjects is on the order of 10^6 .
- ▷ The number of subjects with two images is on the order of 10^6 .
- ▷ The images are taken with a camera oriented by an attendant toward a cooperating subject. This is done under time constraints so there are roll, pitch and yaw angle variations. Also background illumination is sometimes strong, so the face is under-exposed. There is some perspective distortion due to close range images. Some faces are partially cropped.
- ▷ The images are of subjects from greater than 100 countries, with significant imbalance due to population and immigration patterns.
- ▷ The images are of subjects of adults with imbalance due to population and immigration patterns and demand.
- ▷ The images have mean IOD of 38 pixels.
- ▷ The images are all live capture.
- ▷ When these images are input to the algorithm, they are labelled as being of type "WILD" - see Table 4 of the FRVT API.

2.5 Mugshot images

- ▷ The number of images is on the order of 10^6 .
- ▷ The number of subjects is on the order of 10^6 .
- ▷ The number of subjects with two images is on the order of 10^6 .
- ▷ The images have geometry in reasonable conformance with the ISO/IEC 19794-5 Full Frontal image type.
- ▷ The images are of variable sizes. The median IOD is 105 pixels. The mean IOD is 113 pixels. The 1-st, 5-th, 10-th, 25-th, 75-th, 90-th and 99-th percentiles are 34, 58, 70, 87, 121, 161 and 297 pixels.
- ▷ The images are of subjects from the United States.
- ▷ The images are of adults.
- ▷ The images are all live capture.
- ▷ When these images are input to the algorithm, they are labelled as being of type "mugshot" - see Table 4 of the FRVT API.

2.6 Wild images

- ▷ The number of images is on the order of 10^5 .
- ▷ The number of subjects is on the order of 10^3 .
- ▷ The number of subjects with two images on the order of 10^3 .
- ▷ The images include many photojournalism-style images. Images are given to the algorithm using a variable but generally tight crop of the head. Resolution varies very widely. The images are very unconstrained, with wide yaw and pitch pose variation. Faces can be occluded, including hair and hands.



Figure 3: The figure gives simulated samples of image types used in this report.

- ▷ The images are of adults.
 - ▷ All of the images are live capture, none are scanned.
 - ▷ When these images are input to the algorithm, they are labelled as being of type "WILD" - see Table 4 of the FRVT API.

3 Results

3.1 Test goals

- ▷ To state absolute accuracy for different kinds of images, including those with and without subject cooperation.
 - ▷ To state comparative accuracy, across algorithms.

3.2 Test design

Method: For visa images:

- ▷ The comparisons are of visa photos against visa photos.
 - ▷ The number of genuine comparisons is on the order of 10^4 .
 - ▷ The number of impostor comparisons is on the order of 10^{10} .
 - ▷ The comparisons are fully zero-effort, meaning impostors are paired without attention to sex, age or other covariates. However, later analysis is conducted on subsets.
 - ▷ The number of persons is on the order of 10^5 .
 - ▷ The number of images used to make 1 template is 1.
 - ▷ The number of templates used to make each comparison score is two corresponding to simple one-to-one verification.

Method: For mugshot images:

- ▷ The comparisons are of mugshot photos against mugshot photos.

- ▷ The number of genuine comparisons is on the order of 10^6 .
- ▷ The number of impostor comparisons is on the order of 10^8 .
- ▷ The impostors are paired by sex, but not by age or other covariates.
- ▷ The number of persons is on the order of 10^6 .
- ▷ The number of images used to make 1 template is 1.
- ▷ The number of templates used to make each comparison score is two corresponding to simple one-to-one verification.

Method: For visa-border comparisons:

- ▷ The comparisons are of visa-like frontals against border crossing webcam photos.
- ▷ The number of genuine comparisons is on the order of 10^6 .
- ▷ The number of impostor comparisons is on the order of 10^8 .
- ▷ The impostors are paired by sex, but not by age or other covariates.
- ▷ The number of persons is on the order of 10^6 .
- ▷ The number of images used to make 1 template is 1.
- ▷ The number of templates used to make each comparison score is two corresponding to simple one-to-one verification.

Method: For border-border comparisons:

- ▷ The comparisons are of border crossing webcam photos.
- ▷ The number of genuine comparisons is on the order of 10^6 .
- ▷ The number of impostor comparisons is on the order of 10^8 .
- ▷ The impostors are paired by sex, but not by age or other covariates.
- ▷ The number of persons is on the order of 10^6 .
- ▷ The number of images used to make 1 template is 1.
- ▷ The number of templates used to make each comparison score is two corresponding to simple one-to-one verification.

Method: For wild images:

- ▷ The comparisons are of wild photos against wild photos.
- ▷ The number of genuine comparisons is on the order of 10^6 .
- ▷ The number of impostor comparisons is on the order of 10^7 .
- ▷ The comparisons are fully zero-effort, meaning impostors are paired without attention to sex, age or other covariates.
- ▷ The number of persons is on the order of 10^4 .
- ▷ The number of images used to make 1 template is 1.
- ▷ The number of templates used to make each comparison score is two corresponding to simple one-to-one verification.

Method: For child exploitation images:

- ▷ The comparisons are of unconstrained child exploitation photos against others of the same type.

- ▷ The number of genuine comparisons is on the order of 10^4 .
- ▷ The number of impostor comparisons is on the order of 10^7 .
- ▷ The comparisons are fully zero-effort, meaning impostors are paired without attention to sex, age or other covariates.
- ▷ The number of persons is on the order of 10^3 .
- ▷ The number of images used to make 1 template is 1.
- ▷ The number of templates used to make each comparison score is two corresponding to simple one-to-one verification.
- ▷ We produce two performance statements. First, is a DET as used for visa and mugshot images. The second is a cumulative match characteristic (CMC) summarizing a simulated one-to-many search process. This is done as follows.
 - We regard M enrollment templates as items in a gallery.
 - These M templates come from $M > N$ individuals, because multiple images of a subject are present in the gallery under separate identifiers.
 - We regard the verification templates as search templates.
 - For each search we compute the rank of the highest scoring mate.
 - This process should properly be conducted with a 1:N algorithm, such as those tested in NIST IR 8009. We use the 1:1 algorithms in a simulated 1:N mode here to a) better reflect what a child exploitation analyst does, and b) to show algorithm efficacy is better than that revealed in the verification DETs.

3.3 Failure to enroll

	Algorithm Name	Failure to Enrol Rate ¹											
		APPLICATION	BORDER	CHILD-EXPLOIT	MUGSHOT	VISA	WILD						
	Name	SEC. 2.3	SEC. 2.4	SEC. 2.1	SEC. 2.5	SEC. 2.2	SEC. 2.6						
1	20face-000	0.0000	199	0.0008	152	-	263	0.0000	94	0.0004	176	0.0004	126
2	3divi-005	0.0000	203	0.0008	147	-	99	0.0000	114	0.0002	94	0.0003	105
3	3divi-006	0.0000	175	0.0007	137	-	229	0.0001	160	0.0002	98	0.0005	161
4	acer-000	0.0000	243	0.0024	237	-	166	0.0002	201	0.0004	215	0.0008	191
5	acer-001	0.0000	178	0.0011	186	-	216	0.0001	147	0.0004	186	0.0004	136
6	acisw-003	0.0000	94	0.0000	70	-	206	0.0000	23	0.0000	16	0.0001	89
7	acisw-006	0.0000	33	0.0000	23	-	74	0.0000	63	0.0000	61	0.0001	85
8	adera-001	0.0000	242	0.0034	253	0.1928	43	0.0003	223	0.0005	256	0.0505	291
9	adera-002	0.0000	244	0.0034	254	-	191	0.0003	222	0.0005	254	0.0505	290
10	advance-002	0.0000	157	0.0013	205	-	156	0.0000	133	0.0004	189	0.0009	197
11	aifirst-001	0.0000	14	0.0000	36	0.0000	5	0.0000	75	0.0000	51	0.0000	72
12	aigen-001	0.0000	123	0.0000	55	-	291	0.0000	9	0.0000	29	0.0000	5
13	aigen-002	0.0000	99	0.0000	65	-	197	0.0000	18	0.0000	18	0.0000	15
14	ailabs-001	0.0000	168	0.0090	292	-	142	0.0007	270	0.0005	233	0.0016	217
15	aimall-002	0.0000	247	0.0043	267	-	168	0.0012	282	0.0005	251	0.0005	168
16	aimall-003	0.0000	223	0.0012	200	-	100	0.0004	236	0.0005	225	0.0004	146
17	aiunionface-000	0.0000	126	0.0000	48	-	262	0.0000	1	0.0000	38	0.0000	75
18	aize-001	0.0001	281	0.0040	262	-	162	0.0026	299	0.0022	298	0.0058	242
19	ajou-001	0.0000	187	0.0020	228	-	320	0.0001	162	0.0004	217	0.0045	234
20	alchera-000	0.0000	274	0.0041	266	-	214	0.0004	240	0.0014	292	0.0038	231
21	alchera-002	0.0000	189	0.0008	156	-	311	0.0001	182	0.0004	149	0.0003	120
22	alice-000	0.0000	122	0.0006	118	-	289	0.0000	102	0.0004	150	0.0004	144
23	alleyes-000	0.0000	197	0.0010	172	-	284	0.0002	188	0.0004	198	0.0004	151
24	allgovision-000	0.0007	302	0.0062	283	-	295	0.0026	298	0.0052	310	0.0131	260
25	alphaface-001	0.0000	188	0.0012	193	-	316	0.0000	135	0.0004	197	0.0004	131
26	alphaface-002	0.0000	183	0.0012	194	-	199	0.0000	136	0.0004	196	0.0004	132
27	amplifiedgroup-001	0.0114	313	0.1023	315	-	213	0.0189	316	0.0279	319	0.1390	313
28	androvideo-000	0.0000	31	0.0000	21	-	62	0.0000	60	0.0000	65	0.0002	91
29	anke-004	0.0000	179	0.0011	183	0.0944	36	0.0001	168	0.0004	201	0.0006	177
30	anke-005	0.0000	177	0.0012	195	0.1228	38	0.0001	179	0.0004	212	0.0007	182
31	antheus-000	0.0000	119	0.0000	52	0.0000	20	0.0000	6	0.0000	34	0.0242	272
32	antheus-001	0.0000	77	0.0000	79	-	247	0.0000	33	0.0000	2	0.0242	273
33	anyvision-004	0.0000	230	0.0017	218	0.1660	41	0.0001	180	0.0004	183	0.0080	247
34	anyvision-005	0.0000	142	0.0013	202	-	88	0.0000	116	0.0004	153	0.0004	147
35	asusaics-000	0.0000	87	0.0000	72	-	222	0.0000	26	0.0000	14	0.0000	20
36	asusaics-001	0.0000	88	0.0000	73	-	231	0.0000	27	0.0000	12	0.0000	21
37	authenmetric-002	0.0000	2	0.0000	42	-	108	0.0000	81	0.0000	45	0.0000	67
38	aware-004	0.0000	209	0.0023	234	-	221	0.0002	193	0.0005	224	0.0014	214
39	aware-005	0.0000	212	0.0020	226	-	210	0.0001	187	0.0004	200	0.0011	201
40	awirots-001	0.0039	306	0.0369	308	-	174	0.0386	317	0.0872	320	0.3415	317
41	awirots-002	0.0000	257	0.0038	259	-	224	0.0007	268	0.0012	288	0.0208	268
42	ayftech-001	0.0002	293	0.0046	273	-	298	0.0043	306	0.0111	280	0.0091	252
43	ayonix-000	0.0053	309	0.0341	306	0.0000	15	0.0113	313	0.0137	316	0.1194	308
44	biodtechswiss-001	0.0000	201	0.0007	132	-	255	0.0000	104	0.0004	193	0.0025	228
45	biodtechswiss-002	0.0000	154	0.0007	135	-	177	0.0000	110	0.0004	191	0.0005	169
46	bm-001	0.0000	111	0.0000	57	0.0000	23	0.0000	87	0.0000	27	0.0000	7
47	bootech-001	0.0087	311	0.0272	300	-	186	0.0032	304	0.0160	317	0.0946	304
48	bresee-000	0.0000	133	0.0010	175	-	111	0.0002	195	0.0003	124	0.0003	99
49	bresee-001	0.0000	170	0.0010	176	-	253	0.0002	194	0.0003	122	0.0003	98
50	camvi-002	0.0000	60	0.0000	7	0.0000	10	0.0000	45	0.0000	79	0.0000	34
51	camvi-004	0.0000	116	0.0000	91	0.0000	21	0.0000	4	0.0000	31	0.0000	3
52	canon-002	0.0000	1	0.0000	40	-	115	0.0000	79	0.0000	43	0.0000	64
53	ceiec-003	0.0000	93	0.0013	206	-	215	0.0001	150	0.0004	192	0.0004	127
54	ceiec-004	0.0000	26	0.0008	150	-	85	0.0000	112	0.0004	155	0.0004	152
55	chosun-001	0.0000	86	0.0000	71	-	223	0.0000	25	0.0000	13	0.0000	19
56	chosun-002	0.0000	27	0.0000	33	-	84	0.0000	73	0.0000	56	0.0000	58
57	chtface-002	0.0000	255	0.0021	230	-	73	0.0002	215	0.0007	267	0.0014	213
58	chtface-003	0.0000	237	0.0018	221	-	69	0.0001	154	0.0006	259	0.0010	199

Table 22: FTE is the proportion of failed template generation attempts. Failures can occur because the software throws an exception, or because the software electively refuses to process the input image. This would typically occur if a face is not detected. FTE is measured as the number of function calls that give EITHER a non-zero error code OR that give a “small” template. This is defined as one whose size is less than 0.3 times the median template size for that algorithm. This second rule is needed because some algorithms incorrectly fail to return a non-zero error code when template generation fails.

¹The effects of FTE are included in the accuracy results of this report by regarding any template comparison involving a failed template to produce a low similarity score. Thus higher FTE results in higher FNMR and lower FMR.

	Algorithm	Failure to Enrol Rate ¹						
		APPLICATION	BORDER	CHILD-EXPLOIT	MUGSHOT	VISA	WILD	
Name	SEC. 2.3	SEC. 2.4	SEC. 2.1	SEC. 2.5	SEC. 2.2	SEC. 2.6		
59	cib-001	0.0000	28	0.0000	34	-	83	0.0000
60	cloudwalk-hr-003	0.0000	181	0.0008	153	-	185	0.0001
61	cloudwalk-hr-004	0.0000	161	0.0011	191	-	161	0.0004
62	cloudwalk-mt-002	0.0000	172	0.0003	102	-	226	0.0001
63	cloudwalk-mt-003	0.0000	184	0.0007	128	-	200	0.0002
64	clova-000	0.0000	252	0.0022	233	-	281	0.0006
65	cogent-004	0.0000	79	0.0000	80	0.0000	18	0.0000
66	cogent-005	0.0000	74	0.0000	77	-	238	0.0000
67	cognitec-000	0.0005	299	0.0112	295	0.6342	59	0.0007
68	cognitec-002	0.0001	279	0.0069	284	-	155	0.0003
69	cor-001	0.0000	151	0.0006	120	-	175	0.0002
70	corsight-001	0.0000	130	0.0006	123	-	116	0.0001
71	csc-001	0.0000	264	0.0030	244	-	280	0.0002
72	csc-002	0.0015	304	0.0033	250	-	209	0.0006
73	ctcbank-000	0.0001	280	0.0051	277	0.3285	50	0.0011
74	ctcbank-001	0.0000	258	0.0036	258	-	264	0.0005
75	cubox-001	0.0000	59	0.0000	8	-	151	0.0000
76	cuhkee-001	0.0000	144	0.0011	189	-	87	0.0000
77	cybercore-000	0.0000	174	0.0073	287	-	230	0.0001
78	cyberextruder-001	0.0029	305	0.0293	301	0.5338	57	0.0024
79	cyberextruder-002	0.0013	303	0.0840	314	0.2672	49	0.0027
80	cyberlink-005	0.0000	186	0.0009	163	-	189	0.0003
81	cyberlink-006	0.0000	112	0.0005	112	-	302	0.0000
82	dahua-005	0.0000	47	0.0000	86	-	158	0.0000
83	dahua-006	0.0000	12	0.0000	88	-	96	0.0000
84	decatur-000	0.0000	206	0.0020	225	-	176	0.0004
85	deepglint-002	0.0000	163	0.0004	108	0.0669	33	0.0002
86	deepglint-003	0.0000	167	0.0004	109	-	141	0.0002
87	deepsea-001	0.0000	128	0.0000	49	0.0000	19	0.0000
88	deeppense-000	0.0000	23	0.0006	124	-	77	0.0000
89	dermalog-006	0.0005	300	0.0031	247	0.1797	42	0.0013
90	dermalog-008	0.0000	253	0.0031	246	-	314	0.0006
91	didiglobalface-001	0.0000	160	0.0012	192	0.2175	45	0.0000
92	digitalbarriers-002	0.0001	284	0.0045	270	-	245	0.0028
93	dsk-000	0.0000	9	0.0000	46	0.0000	8	0.0000
94	einetworks-000	0.0000	259	0.0017	217	-	257	0.0002
95	ekin-002	0.0000	13	0.0000	89	-	97	0.0000
96	enface-000	0.0000	109	0.0012	199	-	297	0.0000
97	eocortex-000	0.0095	312	0.0602	311	-	114	0.0094
98	ercacat-001	0.0000	127	0.0005	113	-	254	0.0000
99	expasoft-000	0.0000	115	0.0000	58	-	308	0.0000
100	expasoft-001	0.0000	42	0.0000	17	-	183	0.0000
101	f8-001	0.0003	296	0.0059	282	0.2026	44	0.0035
102	facesoft-000	0.0000	19	0.0000	39	0.0000	7	0.0000
103	facetag-000	0.0000	85	0.0000	83	-	243	0.0000
104	facex-001	0.0001	291	0.0360	307	-	304	0.0047
105	farfaces-001	0.0000	256	0.0007	134	-	218	0.0003
106	fiberhome-nanjing-002	0.0000	213	0.0006	125	-	194	0.0001
107	fiberhome-nanjing-003	0.0000	110	0.0004	107	-	296	0.0000
108	fincore-000	0.0000	165	0.0008	154	-	132	0.0001
109	fujitsulab-001	0.0000	53	0.0014	208	-	163	0.0002
110	fujitsulab-002	0.0000	78	0.0009	161	-	246	0.0001
111	geo-001	0.0000	198	0.0011	182	-	287	0.0000
112	geo-002	0.0000	138	0.0015	210	-	105	0.0001
113	glory-002	0.0003	294	0.0045	269	-	279	0.0015
114	glory-003	0.0000	222	0.0027	240	-	122	0.0004
115	gorilla-005	0.0000	3	0.0008	151	-	110	0.0000
116	gorilla-006	0.0000	68	0.0006	126	-	130	0.0000

Table 23: FTE is the proportion of failed template generation attempts. Failures can occur because the software throws an exception, or because the software electively refuses to process the input image. This would typically occur if a face is not detected. FTE is measured as the number of function calls that give EITHER a non-zero error code OR that give a “small” template. This is defined as one whose size is less than 0.3 times the median template size for that algorithm. This second rule is needed because some algorithms incorrectly fail to return a non-zero error code when template generation fails.

¹ The effects of FTE are included in the accuracy results of this report by regarding any template comparison involving a failed template to produce a low similarity score. Thus higher FTE results in higher FNMR and lower FMR.

	Algorithm	Failure to Enrol Rate ¹						
		APPLICATION	BORDER	CHILD-EXPLOIT	MUGSHOT	VISA	WILD	
Name	SEC. 2.3	SEC. 2.4	SEC. 2.1	SEC. 2.5	SEC. 2.2	SEC. 2.6		
117 gorilla-007	- 320	- 325	- 212	- 325	- 323	- 325		
118 hertasecurity-000	0.0133 315	0.0077 290	- 70	0.0025 297	0.0243 318	0.0171 265		
119 hik-001	0.0000 129	0.0000 92	- 268	0.0000 3	0.0000 37	0.0000 1		
120 hyperverge-001	0.0000 273	0.0072 285	- 219	0.0015 291	0.0014 291	0.0042 232		
121 hyperverge-002	0.0000 102	0.0008 148	- 192	0.0002 214	0.0004 165	0.0004 153		
122 icm-002	0.0000 95	0.0001 93	- 207	0.0000 24	0.0000 88	0.0000 76		
123 icthtc-000	0.0001 290	0.0047 275	- 310	0.0028 303	0.0029 305	0.0086 249		
124 id3-006	0.0000 221	0.0009 170	- 113	0.0004 241	0.0005 248	0.0008 194		
125 id3-007	0.0000 194	0.0041 264	- 274	0.0001 167	0.0004 180	0.0052 240		
126 idemria-006	0.0000 75	0.0004 111	- 237	0.0000 96	0.0003 128	0.0003 107		
127 idemria-007	0.0000 38	0.0004 110	- 173	0.0000 98	0.0003 130	0.0003 108		
128 iit-002	0.0000 262	0.0021 229	- 272	0.0009 277	0.0005 255	0.0443 289		
129 iit-003	0.0000 182	0.0008 155	- 195	0.0000 111	0.0004 142	0.0069 245		
130 imagus-002	0.0000 229	0.0018 219	- 265	0.0000 121	0.0004 187	0.0296 279		
131 imagus-003	0.0000 69	0.0000 4	- 139	0.0000 43	0.0000 84	0.0000 32		
132 imperial-000	0.0000 10	0.0000 47	- 119	0.0000 86	0.0000 42	0.0000 69		
133 imperial-002	0.0000 37	0.0000 27	0.0000	- 2	0.0000 67	0.0000 64	0.0000 51	
134 incode-007	0.0000 218	0.0009 166	- 259	0.0002 196	0.0004 160	0.0007 188		
135 incode-008	0.0000 217	0.0009 167	- 283	0.0002 197	0.0004 159	0.0007 189		
136 incode-009	0.0000 207	0.0009 165	- 144	0.0002 199	0.0004 161	0.0007 190		
137 innefulabs-000	0.0000 134	0.0024 236	- 123	0.0003 226	0.0005 244	0.0004 141		
138 innovativetechnologyltd-001	0.0001 288	0.0050 276	- 290	0.0024 296	0.0025 301	0.0055 241		
139 innovativetechnologyltd-002	0.0000 228	0.0046 272	- 261	0.0057 311	0.0005 247	0.0247 276		
140 innovatrics-006	0.0000 145	0.0009 169	0.0350	28	0.0000 118	0.0004 145	0.0003 123	
141 innovatrics-007	0.0000 137	0.0007 142	- 102	0.0001 140	0.0003 115	0.0003 113		
142 insightface-000	0.0000 39	0.0000 15	- 171	0.0000 53	0.0000 72	0.0000 43		
143 intelliloudai-001	0.0000 121	0.0000 54	- 285	0.0000 8	0.0000 28	0.0001 83		
144 intelliloudai-002	0.0000 15	0.0008 149	- 91	0.0000 113	0.0004 140	0.0012 206		
145 intellifusion-001	0.0000 147	0.0005 115	0.0949	37	0.0001 152	0.0003 132	0.0005 165	
146 intellifusion-002	0.0000 18	0.0000 90	- 103	0.0000 91	0.0000 48	0.0001 84		
147 intellivision-001	0.0042 307	0.0296 302	0.5495	58	0.0048 309	0.0042 309	0.1358 311	
148 intellivision-002	0.0000 275	0.0046 271	- 95	0.0012 281	0.0005 258	0.0146 262		
149 intelresearch-002	0.0000 146	0.0022 231	- 86	0.0000 126	0.0004 138	0.0003 121		
150 intelresearch-003	0.0000 164	0.0006 119	- 125	0.0000 103	0.0004 156	0.0003 125		
151 intsysmsu-001	0.0000 22	0.0010 173	- 82	0.0001 164	0.0004 182	0.0004 150		
152 intsysmsu-002	0.0000 89	0.0010 174	- 228	0.0001 163	0.0004 177	0.0004 149		
153 iqface-000	0.0000 32	0.0000 22	0.0000	1	0.0000 62	0.0000 68	0.0000 49	
154 iqface-003	0.0000 260	0.0076 289	- 145	0.0006 261	0.0005 257	0.0069 244		
155 irexx-000	0.0000 233	0.0009 168	- 149	0.0000 125	0.0005 227	0.0003 122		
156 isap-001	0.0000 96	0.0000 69	- 208	0.0000 22	0.0000 15	0.0000 18		
157 isap-002	0.0000 21	0.0000 28	- 81	0.0000 68	0.0000 59	0.0000 52		
158 isityou-000	0.0068 310	0.0316 305	0.4714	54	0.0023 292	0.0010 276	0.0663 299	
159 isystems-001	0.0000 265	0.0035 255	0.1421	39	0.0010 279	0.0007 269	0.0128 258	
160 isystems-002	0.0000 266	0.0035 256	0.1421	40	0.0010 278	0.0007 268	0.0128 257	
161 itmo-006	0.0000 114	0.0015 211	- 307	0.0004 247	0.0004 178	0.0006 176		
162 itmo-007	0.0000 7	0.0009 160	- 124	0.0003 234	0.0000 39	0.0004 139		
163 ivacognitive-001	0.0000 211	0.0011 185	- 234	0.0001 148	0.0004 211	0.0011 202		
164 iws-000	0.0005 301	0.0650 312	- 71	0.0024 295	0.0012 284	0.0936 303		
165 kakao-004	0.0000 106	0.0000 61	- 309	0.0000 15	0.0000 24	0.0000 11		
166 kakao-005	0.0000 41	0.0000 87	- 182	0.0000 55	0.0000 90	0.0000 45		
167 kedacom-000	0.0000 8	0.0000 45	0.0000	9	0.0000 84	0.0000 40	0.0000 68	
168 kiwitech-000	0.0000 152	0.0009 157	- 172	0.0004 245	0.0005 231	0.0004 157		
169 kneron-003	0.0239 317	0.0306 303	0.4883	56	0.0044 307	0.0016 295	0.1823 315	
170 kneron-005	0.0000 268	0.0226 298	- 241	0.0006 259	0.0005 239	0.0097 253		
171 kookmin-001	0.0000 25	0.0000 32	- 90	0.0000 72	0.0000 55	0.0000 56		
172 kookmin-002	0.0000 65	0.0000 2	- 127	0.0000 41	0.0000 86	0.0000 31		
173 lemalabs-001	0.0000 104	0.0005 116	- 318	0.0002 202	0.0004 144	0.0004 130		
174 line-000	0.0000 36	0.0000 26	- 68	0.0000 66	0.0000 63	0.0000 77		

Table 24: FTE is the proportion of failed template generation attempts. Failures can occur because the software throws an exception, or because the software electively refuses to process the input image. This would typically occur if a face is not detected. FTE is measured as the number of function calls that give EITHER a non-zero error code OR that give a “small” template. This is defined as one whose size is less than 0.3 times the median template size for that algorithm. This second rule is needed because some algorithms incorrectly fail to return a non-zero error code when template generation fails.

¹The effects of FTE are included in the accuracy results of this report by regarding any template comparison involving a failed template to produce a low similarity score. Thus higher FTE results in higher FNMR and lower FMR.

	Algorithm	Failure to Enrol Rate ¹											
		APPLICATION	BORDER	CHILD-EXPLOIT	MUGSHOT	VISA	WILD	SEC. 2.3	SEC. 2.4	SEC. 2.1	SEC. 2.5	SEC. 2.2	SEC. 2.6
175	lookman-002	0.0000	30	0.0000	20	-	63	0.0000	59	0.0000	66	0.0000	48
176	lookman-004	0.0000	124	0.0000	56	0.0000	22	0.0000	10	0.0000	30	0.0000	6
177	luxand-000	0.0000	108	0.0000	64	-	324	0.0000	17	0.0000	21	0.0000	13
178	megvii-002	0.0000	125	0.0006	121	0.0274	27	0.0054	310	0.0004	151	0.0126	256
179	megvii-003	0.0000	140	0.0010	180	-	79	0.0002	211	0.0004	206	0.0011	204
180	meituan-000	0.0000	50	0.0001	96	-	170	0.0000	97	0.0002	96	0.0001	87
181	meiya-001	0.0000	263	0.0028	243	-	220	0.0004	248	0.0010	277	0.0025	227
182	microfocus-001	0.0001	286	0.0053	280	0.0791	34	0.0008	273	0.0016	293	0.0220	270
183	microfocus-002	0.0001	287	0.0053	279	0.0791	35	0.0008	272	0.0016	294	0.0220	269
184	minivision-000	0.0000	100	0.0000	66	-	196	0.0000	19	0.0000	19	0.0000	14
185	mobai-000	0.0000	241	0.0114	296	-	256	0.0003	228	0.0012	286	0.1242	309
186	mobai-001	0.0000	205	0.0040	261	-	67	0.0001	169	0.0012	285	0.0523	292
187	mobbl-000	0.0116	314	0.0720	313	-	312	0.0119	314	0.0063	312	0.1136	307
188	mobbl-001	0.0000	261	0.0052	278	-	288	0.0002	190	0.0005	249	0.0181	267
189	moreidian-000	0.0000	185	0.0009	158	-	201	0.0004	243	0.0005	230	0.0004	155
190	mvision-001	0.0000	105	0.0000	60	-	322	0.0000	14	0.0000	23	0.0000	10
191	nazhiai-000	0.0000	5	0.0000	43	-	107	0.0000	82	0.0000	46	0.0000	65
192	neosystems-001	0.0000	62	0.0000	85	-	134	0.0013	285	0.9994	322	0.0002	97
193	netbridge-tech-001	0.0000	91	0.0000	68	-	202	0.0000	21	0.0000	17	0.0000	17
194	netbridge-tech-002	0.0000	120	0.0000	53	-	273	0.0000	7	0.0000	35	0.0000	4
195	neurotechnology-010	0.0000	173	0.0001	94	-	217	0.0000	124	0.0002	93	0.0003	114
196	neurotechnology-011	0.0000	215	0.0013	201	-	305	0.0002	192	0.0003	131	0.0020	224
197	nhn-001	0.0000	200	0.0019	222	-	260	0.0001	155	0.0004	219	0.0020	225
198	nodeflux-002	0.0000	176	0.0261	299	-	204	0.0008	271	0.0005	246	0.0008	196
199	notiontag-000	0.0000	16	0.0000	37	0.0000	6	0.0000	76	0.0000	52	0.0000	62
200	notiontag-001	0.0000	118	0.0000	50	-	276	0.0027	301	0.0000	32	0.0132	261
201	nsensecorp-001	0.0000	272	0.0024	235	-	140	0.0014	288	0.0101	315	0.0375	285
202	nsensecorp-002	0.0000	148	0.0009	159	-	65	0.0003	217	0.0011	278	0.0178	266
203	ntechlab-009	0.0000	235	0.0009	164	-	198	0.0001	178	0.0004	137	0.0005	159
204	ntechlab-010	0.0000	156	0.0005	114	-	153	0.0001	166	0.0004	146	0.0006	170
205	null-000	-	324	-	323	-	299	-	322	-	325	-	322
206	null-082	-	326	-	320	-	282	-	321	-	326	-	321
207	omnigarde-000	0.0000	202	0.0008	145	-	269	0.0000	105	0.0004	181	0.0003	124
208	openface-001	0.0000	248	0.0104	294	-	233	0.0004	239	0.0006	263	0.0856	301
209	oz-001	0.0000	234	0.0011	190	-	225	0.0006	265	0.0004	164	0.0014	212
210	oz-002	0.0000	58	0.0003	101	-	152	0.0000	100	0.0003	121	0.0002	95
211	papsav1923-001	0.0000	139	0.0007	136	-	104	0.0001	161	0.0002	99	0.0005	162
212	paravision-004	0.0000	231	0.0007	143	0.0570	30	0.0002	204	0.0004	173	0.0008	192
213	paravision-006	0.0000	4	0.0000	41	-	109	0.0000	80	0.0000	44	0.0000	66
214	pensees-001	0.0000	141	0.0000	30	-	76	0.0000	70	0.0000	60	0.0000	54
215	pixelall-005	0.0000	49	0.0000	12	-	167	0.0000	50	0.0000	74	0.0000	40
216	pixelall-006	0.0000	103	0.0000	59	-	321	0.0000	13	0.0000	22	0.0000	9
217	psl-006	0.0000	166	0.0002	98	-	143	0.0000	42	0.0003	101	0.0001	86
218	psl-007	0.0000	136	0.0007	127	-	92	0.0000	130	0.0003	125	0.0003	115
219	ptakuratsatu-000	0.0000	153	0.0007	141	-	181	0.0001	139	0.0003	116	0.0003	112
220	pxl-001	0.0000	278	0.0044	268	-	300	0.0005	252	0.0022	299	0.0323	281
221	pyramid-000	0.0001	283	0.0041	265	-	251	0.0005	251	0.0007	270	0.0015	215
222	quantasoft-003	0.0000	239	0.0015	213	-	252	0.0005	250	0.0006	261	0.0088	251
223	rankone-009	0.0000	6	0.0000	44	-	112	0.0000	83	0.0000	47	0.0000	73
224	rankone-010	0.0000	57	0.0000	6	-	148	0.0000	44	0.0000	83	0.0000	33
225	realnetworks-002	0.0000	227	0.0003	104	-	319	0.0004	235	0.0003	110	0.0004	148
226	realnetworks-004	0.0000	190	0.0003	100	-	313	0.0000	88	0.0002	100	0.0003	106
227	regula-000	0.0000	70	0.0000	74	-	240	0.0000	28	0.0000	8	0.0000	23
228	remarkai-001	0.0000	45	0.0000	19	-	180	0.0000	58	0.0000	71	0.0000	78
229	remarkai-002	0.0000	107	0.0000	62	-	315	0.0000	16	0.0000	25	0.0000	74
230	remarkai-003	0.0000	132	0.0007	133	-	106	0.0000	123	0.0004	152	0.0004	143
231	rendip-000	0.0000	226	0.0016	214	-	205	0.0002	198	0.0004	222	0.0013	211
232	rokid-000	0.0000	81	0.0072	286	-	250	0.0001	159	0.0005	238	0.0354	284

Table 25: FTE is the proportion of failed template generation attempts. Failures can occur because the software throws an exception, or because the software electively refuses to process the input image. This would typically occur if a face is not detected. FTE is measured as the number of function calls that give EITHER a non-zero error code OR that give a “small” template. This is defined as one whose size is less than 0.3 times the median template size for that algorithm. This second rule is needed because some algorithms incorrectly fail to return a non-zero error code when template generation fails.

¹ The effects of FTE are included in the accuracy results of this report by regarding any template comparison involving a failed template to produce a low similarity score. Thus higher FTE results in higher FNMR and lower FMR.

	Algorithm	Failure to Enrol Rate ¹							
		Name	APPLICATION	BORDER	CHILD-EXPLOIT	MUGSHOT	VISA	WILD	
	Name	SEC. 2.3	SEC. 2.4	SEC. 2.1	SEC. 2.5	SEC. 2.2	SEC. 2.6		
233	rokid-001	0.0000	29	0.0013	204	-	61	0.0000	61
234	s1-001	0.0000	277	0.0073	288	-	301	0.0013	283
235	s1-002	0.0000	219	0.0089	291	-	267	0.0001	175
236	saffe-001	0.0000	46	0.0000	10	0.0000	12	0.0000	48
237	saffe-002	0.0000	63	0.0000	1	-	133	0.0000	39
238	samtech-001	0.0001	282	0.0032	249	-	159	0.0004	244
239	scanovate-001	0.0208	316	0.2388	316	-	211	0.0024	293
240	scanovate-002	0.0000	220	0.0018	220	-	266	0.0000	134
241	securifai-001	0.0000	56	0.0000	5	-	147	0.0000	90
242	securifai-002	0.0000	66	0.0000	3	-	126	0.0000	40
243	sensetime-004	0.0000	180	0.0011	188	-	188	0.0000	89
244	sensetime-005	0.0000	55	0.0004	106	-	160	0.0000	109
245	sertis-000	0.0000	90	0.0007	138	-	227	0.0000	138
246	sertis-002	0.0000	80	0.0007	131	-	249	0.0000	132
247	shaman-000	0.0000	84	0.0000	84	0.0000	16	0.0000	38
248	shaman-001	0.0000	35	0.0000	25	0.0000	3	0.0000	65
249	shu-002	0.0000	208	0.0010	177	-	244	0.0005	249
250	shu-003	0.0000	97	0.0007	129	-	187	0.0001	145
251	siat-002	0.0000	171	0.0012	198	0.0616	31	0.0000	119
252	siat-004	0.0000	193	0.0011	187	-	306	0.0000	108
253	sjtu-003	0.0000	67	0.0005	117	-	131	0.0000	128
254	sjtu-004	0.0000	34	0.0000	24	-	75	0.0000	64
255	smilart-002	0.0000	269	0.0036	257	0.2422	48	0.0003	232
256	smilart-003	0.0003	295	0.0100	293	-	326	0.0014	287
257	sodec-000	0.0000	44	0.0000	18	-	178	0.0000	57
258	ssai-000	-	323	-	324	-	317	-	323
259	stachu-000	0.0000	61	0.0000	9	-	150	0.0000	47
260	starhybrid-001	0.0001	285	0.0033	252	0.2340	47	0.0009	276
261	suprema-000	0.0000	204	0.0017	216	-	78	0.0002	206
262	supremaid-001	0.0000	135	0.0020	227	-	120	0.0001	165
263	synesis-006	0.0000	113	0.0003	105	-	303	0.0000	127
264	synesis-007	0.0000	159	0.0013	203	-	169	0.0002	210
265	synology-000	0.0000	101	0.0000	67	-	193	0.0000	20
266	synology-002	0.0000	54	0.0000	14	-	165	0.0000	52
267	sztu-000	0.0000	71	0.0000	75	-	239	0.0000	29
268	tech5-004	0.0000	169	0.0008	146	-	137	0.0003	219
269	tech5-005	0.0000	150	0.0007	144	-	72	0.0000	106
270	tevian-005	0.0001	289	0.0041	263	0.3606	51	0.0006	262
271	tevian-006	0.0000	43	0.0012	196	-	179	0.0003	224
272	tiger-003	0.0000	192	-	322	0.0619	32	0.0001	172
273	tiger-004	0.0000	276	0.0022	232	-	93	0.0001	174
274	tongyi-005	0.0000	40	0.0000	16	0.0000	14	0.0000	54
275	toshiba-002	0.0000	24	0.0000	31	0.0000	4	0.0000	71
276	toshiba-003	0.0000	52	0.0001	95	-	164	0.0001	173
277	trueface-001	0.0000	214	0.0038	260	-	294	0.0007	269
278	trueface-002	0.0000	216	0.0046	274	-	292	0.0003	216
279	tuputech-000	0.0003	297	0.0116	297	-	286	0.0632	318
280	twface-000	0.0000	20	0.0000	29	-	80	0.0000	69
281	ulsee-001	0.0000	117	0.0000	51	-	275	0.0000	5
282	ultinous-000	-	321	-	326	0.0007	25	-	326
283	ultinous-001	-	325	-	319	0.0007	26	-	320
284	uluface-002	0.0000	51	0.0000	13	0.0000	13	0.0000	51
285	uluface-003	0.0000	92	0.0001	97	-	203	0.0002	189
286	upc-001	0.0000	251	0.0003	103	0.0450	29	0.0003	218
287	vcog-002	-	322	0.3719	318	0.2209	46	-	324
288	vd-001	0.0000	267	0.0030	245	-	121	0.0004	242
289	vd-002	0.0000	72	0.0000	76	-	236	0.0000	30
290	veridas-004	0.0000	249	0.0026	239	-	293	0.0001	171

Table 26: FTE is the proportion of failed template generation attempts. Failures can occur because the software throws an exception, or because the software electively refuses to process the input image. This would typically occur if a face is not detected. FTE is measured as the number of function calls that give EITHER a non-zero error code OR that give a “small” template. This is defined as one whose size is less than 0.3 times the median template size for that algorithm. This second rule is needed because some algorithms incorrectly fail to return a non-zero error code when template generation fails.

¹ The effects of FTE are included in the accuracy results of this report by regarding any template comparison involving a failed template to produce a low similarity score. Thus higher FTE results in higher FNMR and lower FMR.

	Algorithm	Failure to Enrol Rate ¹												
		Name	APPLICATION		BORDER		CHILD-EXPLOIT		MUGSHOT		VISA		WILD	
			SEC. 2.3	SEC. 2.4	SEC. 2.1	SEC. 2.5	SEC. 2.2	SEC. 2.6						
291	veridas-006	0.0000	250	0.0026	238	-	258	0.0001	170	0.0005	237	0.0006	173	
292	via-000	0.0000	83	0.0000	82	0.0000	17	0.0000	36	0.0000	5	0.0001	82	
293	via-001	0.0000	76	0.0000	78	-	248	0.0000	32	0.0000	1	0.0001	81	
294	videmo-000	0.0000	210	0.0019	223	-	232	0.0003	227	0.0012	287	0.0158	263	
295	videonetics-001	0.0004	298	0.0309	304	0.4799	55	0.0015	290	0.0010	275	0.0112	254	
296	videonetics-002	0.0000	225	0.0459	310	0.4598	53	0.0006	263	0.0005	253	0.0013	208	
297	vigilantsolutions-009	0.0000	240	0.0028	242	-	190	0.0001	149	0.0004	143	0.0005	163	
298	vigilantsolutions-010	0.0000	238	0.0028	241	-	129	0.0001	151	0.0004	147	0.0005	164	
299	vinali-000	0.0000	17	0.0000	38	-	94	0.0000	77	0.0000	53	0.0000	61	
300	vion-000	0.0050	308	0.0392	309	0.6388	60	0.0130	315	0.0078	313	0.1389	312	
301	visage-000	0.0000	254	0.0054	281	-	278	0.0009	274	0.0006	260	0.0064	243	
302	visionbox-001	0.0000	271	0.0033	251	-	323	0.0005	258	0.0011	282	0.0028	230	
303	visionbox-002	0.0000	64	0.0017	215	-	128	0.0000	117	0.0004	223	0.0046	236	
304	visionlabs-009	0.0000	158	0.0010	171	-	154	0.0001	144	0.0004	185	0.0006	179	
305	visionlabs-010	0.0000	236	0.0009	162	-	277	0.0001	181	0.0004	179	0.0006	175	
306	visteam-000	0.0000	270	0.0031	248	-	136	0.0005	253	0.0011	279	0.0026	229	
307	visteam-001	0.0000	232	0.0014	207	-	66	0.0002	200	0.0004	188	0.0011	203	
308	vnpt-001	0.0652	319	0.2829	317	-	146	0.2116	319	0.1598	321	0.3544	318	
309	vnpt-002	0.0000	195	0.0002	99	-	270	0.0003	229	0.0003	105	0.0001	88	
310	vocord-008	0.0000	162	0.0015	212	-	135	0.0003	230	0.0001	91	0.0007	184	
311	vocord-009	0.0000	191	0.0006	122	-	325	0.0001	185	0.0003	102	0.0003	101	
312	vts-000	0.0000	224	0.0011	184	-	138	0.0001	186	0.0004	221	0.0013	209	
313	winsense-001	0.0000	48	0.0000	11	0.0000	11	0.0000	49	0.0000	78	0.0000	39	
314	winsense-002	0.0000	82	0.0000	81	-	242	0.0000	35	0.0000	4	0.0000	27	
315	x-laboratory-000	0.0247	318	0.0000	63	0.0000	24	0.0005	257	0.0002	97	0.0000	12	
316	x-laboratory-001	0.0000	149	0.0012	197	-	64	0.0001	176	0.0004	210	0.0007	180	
317	xforwardai-001	0.0000	143	0.0007	140	-	89	0.0003	221	0.0004	205	0.0004	129	
318	xforwardai-002	0.0000	155	0.0007	139	-	157	0.0003	220	0.0004	207	0.0004	128	
319	xm-000	0.0000	73	0.0007	130	-	235	0.0001	146	0.0003	111	0.0004	156	
320	yisheng-004	0.0002	292	-	321	0.4279	52	0.0013	284	0.0006	262	0.0321	280	
321	yitu-003	0.0000	11	0.0000	35	-	98	0.0009	275	0.0000	50	0.0000	60	
322	yoonik-000	0.0000	196	0.0019	224	-	271	0.0001	157	0.0004	209	0.0009	198	
323	yoonik-001	0.0000	98	0.0014	209	-	184	0.0001	183	0.0004	203	0.0017	220	
324	ytu-000	0.0000	131	0.0010	181	-	117	0.0002	212	0.0004	204	0.0011	205	
325	yuan-001	0.0000	246	0.0010	178	-	101	0.0005	255	0.0005	241	0.0005	166	
326	yuan-002	0.0000	245	0.0010	179	-	118	0.0005	256	0.0005	240	0.0005	167	

Table 27: FTE is the proportion of failed template generation attempts. Failures can occur because the software throws an exception, or because the software electively refuses to process the input image. This would typically occur if a face is not detected. FTE is measured as the number of function calls that give EITHER a non-zero error code OR that give a “small” template. This is defined as one whose size is less than 0.3 times the median template size for that algorithm. This second rule is needed because some algorithms incorrectly fail to return a non-zero error code when template generation fails.

¹ The effects of FTE are included in the accuracy results of this report by regarding any template comparison involving a failed template to produce a low similarity score. Thus higher FTE results in higher FNMR and lower FMR.

3.4 Recognition accuracy

Core algorithm accuracy is stated via:

▷ **Cooperative subjects**

- The summary table of Figure 21;
- The visa image DETs of Figure 50;
- The mugshot DETs of Figure 66;
- The mugshot ageing profiles of Figure 243;
- The human-difficult pairs of Figure 17

▷ **Non-cooperative subjects**

- The photojournalism DET of Figure 80
- The child-exploitation DET of Figure 83;
- The child-exploitation CMC of Figure 87.

Figure 196 shows dependence of false match rate on algorithm score threshold. This allows a deployer to set a threshold to target a particular false match rate appropriate to the security objectives of the application.

Figure 163 likewise shows FMR(T) but for mugshots, and specially four subsets of the population.

Note that in both the mugshot and visa sets false match rates vary with the ethnicity, age, and sex, of the enrollee and impostor. For example figure 104 summarizes FMR for impostors paired from four groups black females, black males, white females, white males.

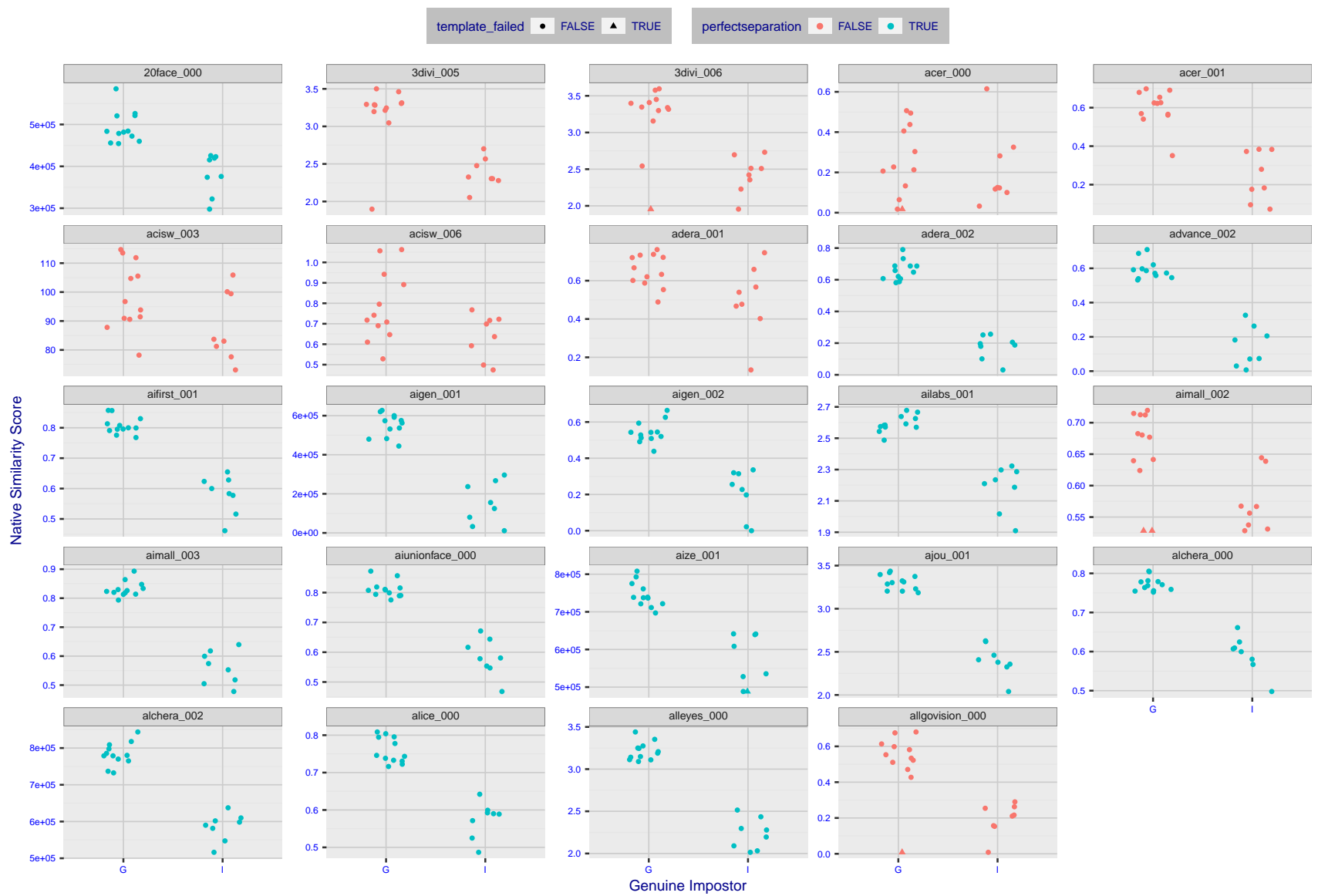


Figure 4: The Figure shows, in blue, algorithms that correctly separate the 12 genuine and 8 impostor pairs used in the May 2018 paper Face recognition accuracy of forensic examiners, superrecognizers, and face recognition algorithms (Phillips et al. [1]). In red are algorithms that are imperfect. Some algorithms fail only because they failed to make a template e.g. due to face detection failure (shown as a triangle). Others fail because the pairs were selected for that study because they had been difficult for three leading algorithms used in FRVT 2006. Caution: Given the small sample size ($n=20$) the figure may change substantially if larger or different sets were used. The images can be downloaded from the [Supplemental Information](#) page provided with that publication.

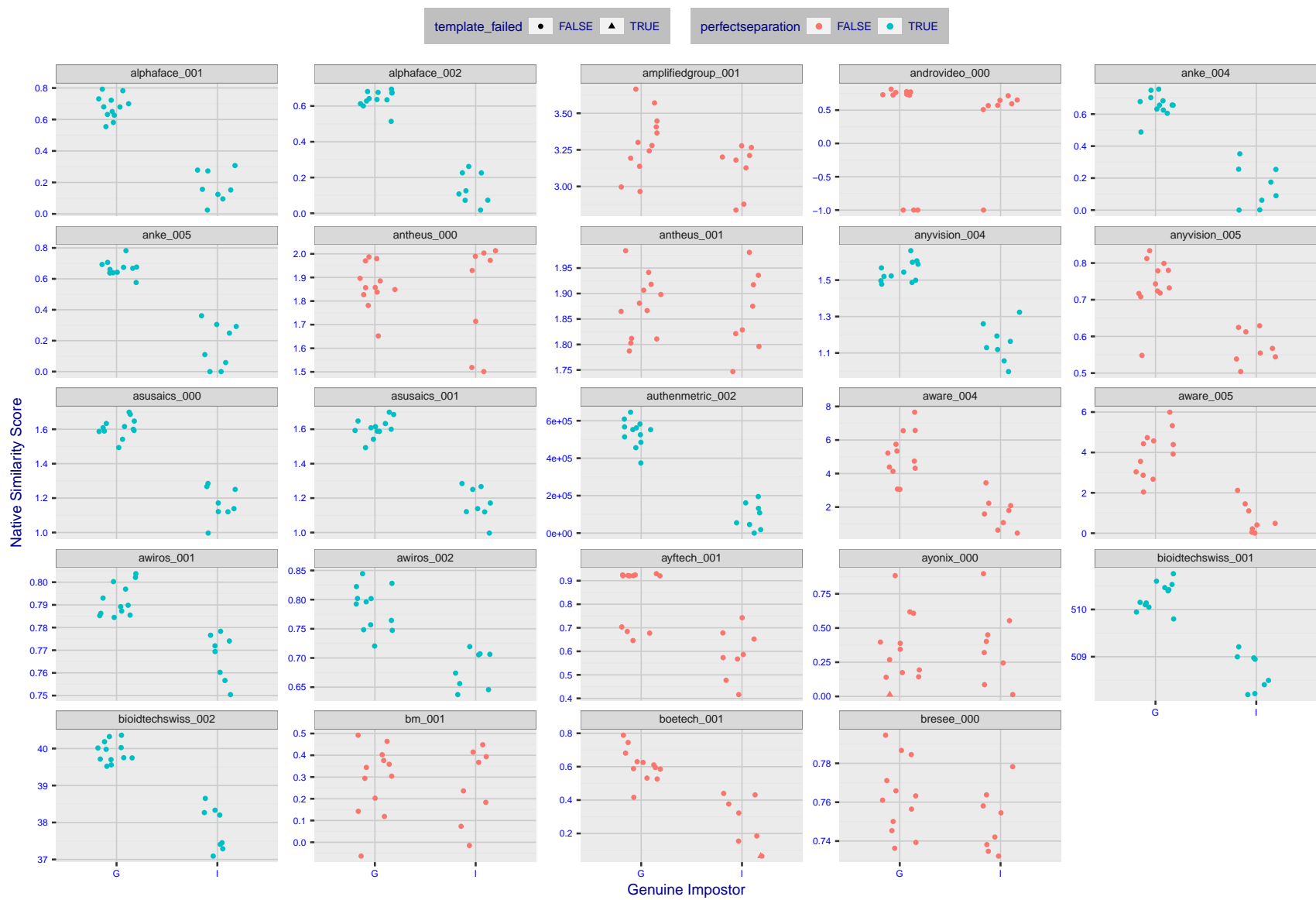


Figure 5: The Figure shows, in blue, algorithms that correctly separate the 12 genuine and 8 impostor pairs used in the May 2018 paper [Face recognition accuracy of forensic examiners, superrecognizers, and face recognition algorithms](#) (Phillips et al. [1]). In red are algorithms that are imperfect. Some algorithms fail only because they failed to make a template e.g. due to face detection failure (shown as a triangle). Others fail because the pairs were selected for that study because they had been difficult for three leading algorithms used in FRVT 2006. Caution: Given the small sample size ($n=20$) the figure may change substantially if larger or different sets were used. The images can be downloaded from the [Supplemental Information](#) page provided with that publication.



Figure 6: The Figure shows, in blue, algorithms that correctly separate the 12 genuine and 8 impostor pairs used in the May 2018 paper [Face recognition accuracy of forensic examiners, superrecognizers, and face recognition algorithms](#) (Phillips et al. [1]). In red are algorithms that imperfect. Some algorithms fail only because they failed to make a template e.g. due to face detection failure (shown as a triangle). Others fail because the pairs were selected for that study because they had been difficult for three leading algorithms used in FRVT 2006. Caution: Given the small sample size ($n=20$) the figure may change substantially if larger or different sets were used. The images can be downloaded from the [Supplemental Information](#) page provided with that publication.

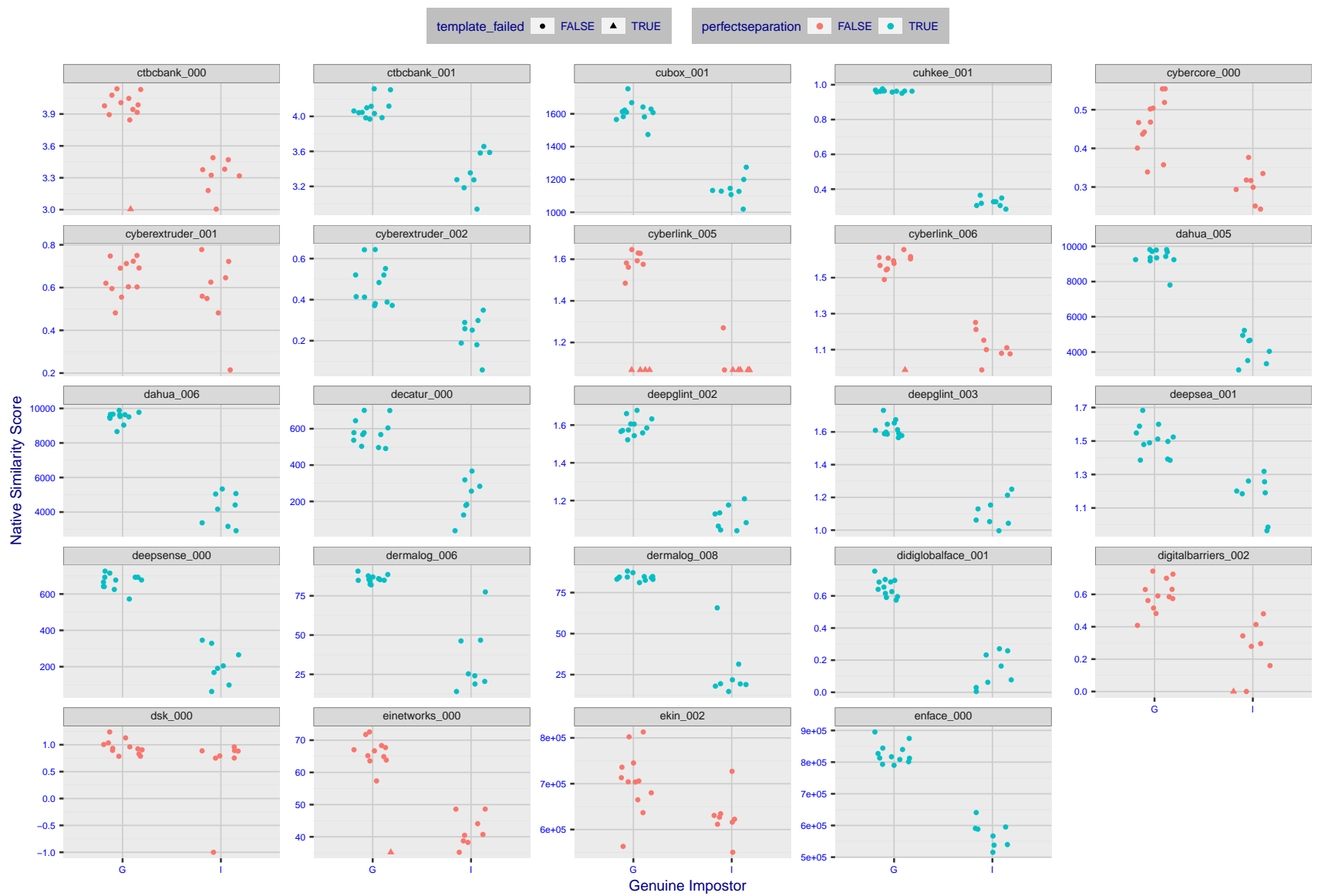


Figure 7: The Figure shows, in blue, algorithms that correctly separate the 12 genuine and 8 impostor pairs used in the May 2018 paper Face recognition accuracy of forensic examiners, superrecognizers, and face recognition algorithms (Phillips et al. [1]). In red are algorithms that are imperfect. Some algorithms fail only because they failed to make a template e.g. due to face detection failure (shown as a triangle). Others fail because the pairs were selected for that study because they had been difficult for three leading algorithms used in FRVT 2006. Caution: Given the small sample size ($n=20$) the figure may change substantially if larger or different sets were used. The images can be downloaded from the [Supplemental Information](#) page provided with that publication.

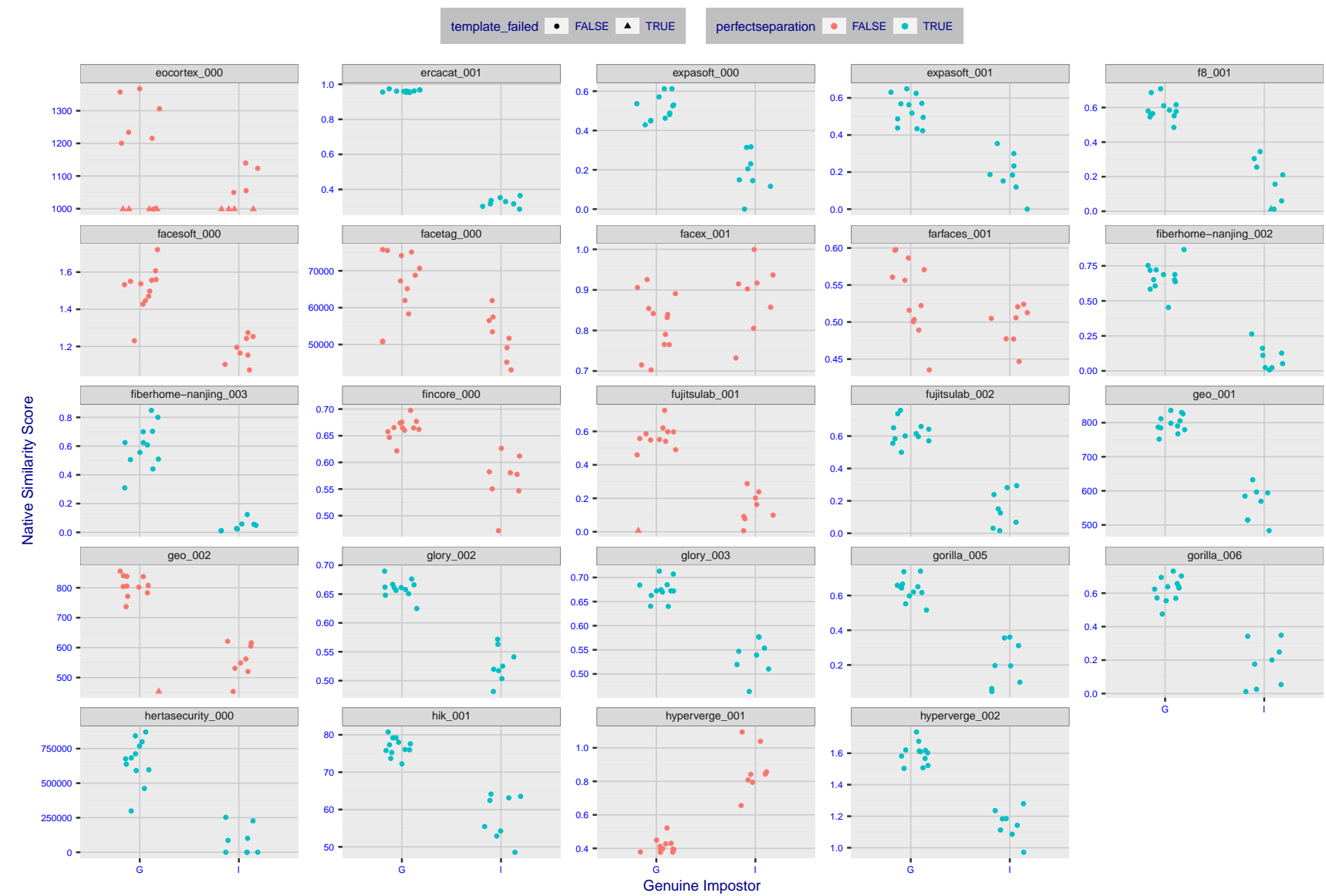


Figure 8: The Figure shows, in blue, algorithms that correctly separate the 12 genuine and 8 impostor pairs used in the May 2018 paper [Face recognition accuracy of forensic examiners, superrecognizers, and face recognition algorithms](#) (Phillips et al. [1]). In red are algorithms that are imperfect. Some algorithms fail only because they failed to make a template e.g. due to face detection failure (shown as a triangle). Others fail because the pairs were selected for that study because they had been difficult for three leading algorithms used in FRVT 2006. Caution: Given the small sample size ($n=20$) the figure may change substantially if larger or different sets were used. The images can be downloaded from the [Supplemental Information](#) page provided with that publication.

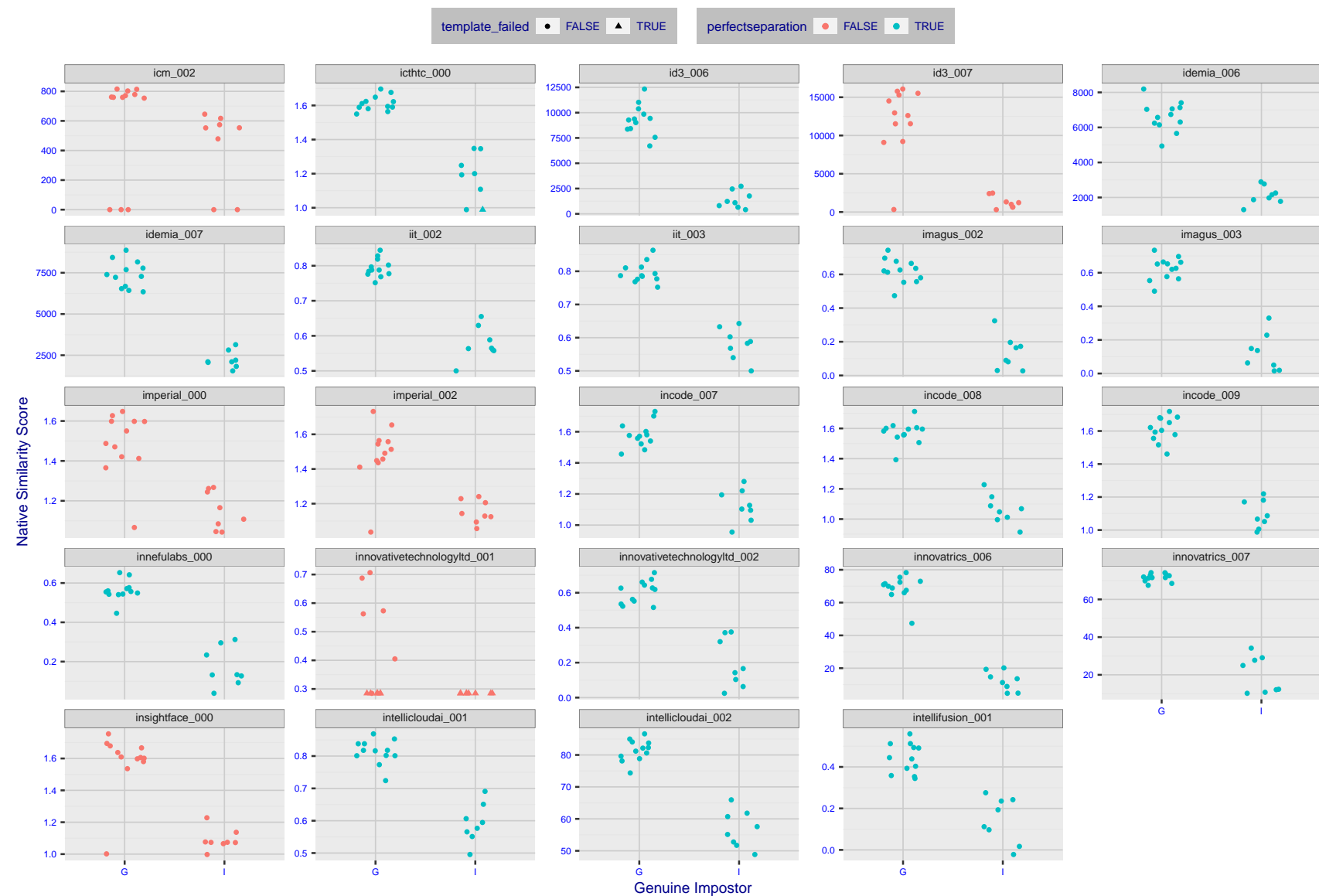


Figure 9: The Figure shows, in blue, algorithms that correctly separate the 12 genuine and 8 impostor pairs used in the May 2018 paper Face recognition accuracy of forensic examiners, superrecognizers, and face recognition algorithms (Phillips et al. [1]). In red are algorithms that are imperfect. Some algorithms fail only because they failed to make a template e.g. due to face detection failure (shown as a triangle). Others fail because the pairs were selected for that study because they had been difficult for three leading algorithms used in FRVT 2006. Caution: Given the small sample size ($n=20$) the figure may change substantially if larger or different sets were used. The images can be downloaded from the [Supplemental Information](#) page provided with that publication.

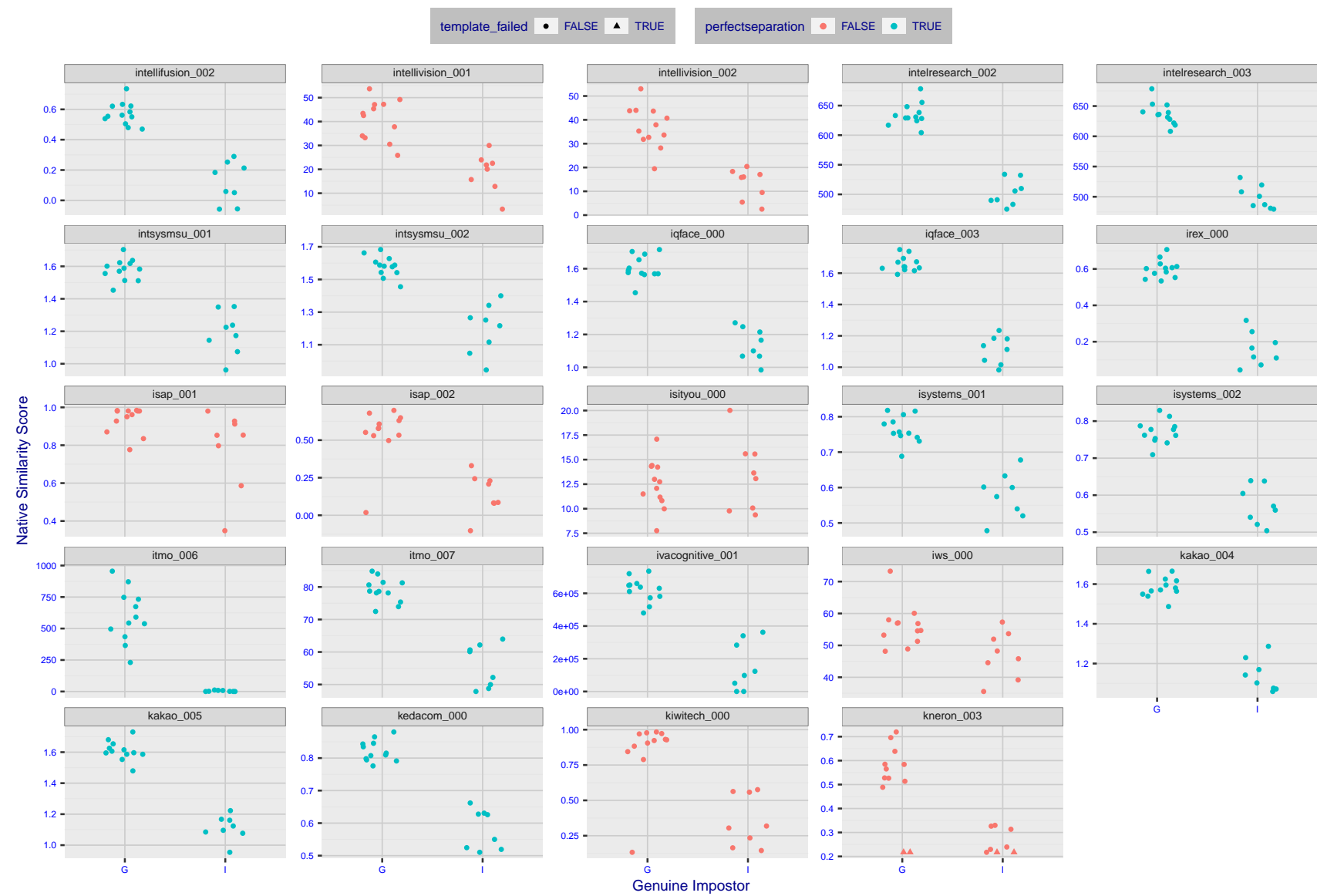


Figure 10: The Figure shows, in blue, algorithms that correctly separate the 12 genuine and 8 impostor pairs used in the May 2018 paper Face recognition accuracy of forensic examiners, superrecognizers, and face recognition algorithms (Phillips et al. [1]). In red are algorithms that are imperfect. Some algorithms fail only because they failed to make a template e.g. due to face detection failure (shown as a triangle). Others fail because the pairs were selected for that study because they had been difficult for three leading algorithms used in FRVT 2006. Caution: Given the small sample size ($n=20$) the figure may change substantially if larger or different sets were used. The images can be downloaded from the [Supplemental Information](#) page provided with that publication.



Figure 11: The Figure shows, in blue, algorithms that correctly separate the 12 genuine and 8 impostor pairs used in the May 2018 paper [Face recognition accuracy of forensic examiners, superrecognizers, and face recognition algorithms](#) (Phillips et al. [1]). In red are algorithms that are imperfect. Some algorithms fail only because they failed to make a template e.g. due to face detection failure (shown as a triangle). Others fail because the pairs were selected for that study because they had been difficult for three leading algorithms used in FRVT 2006. Caution: Given the small sample size ($n=20$) the figure may change substantially if larger or different sets were used. The images can be downloaded from the [Supplemental Information](#) page provided with that publication.

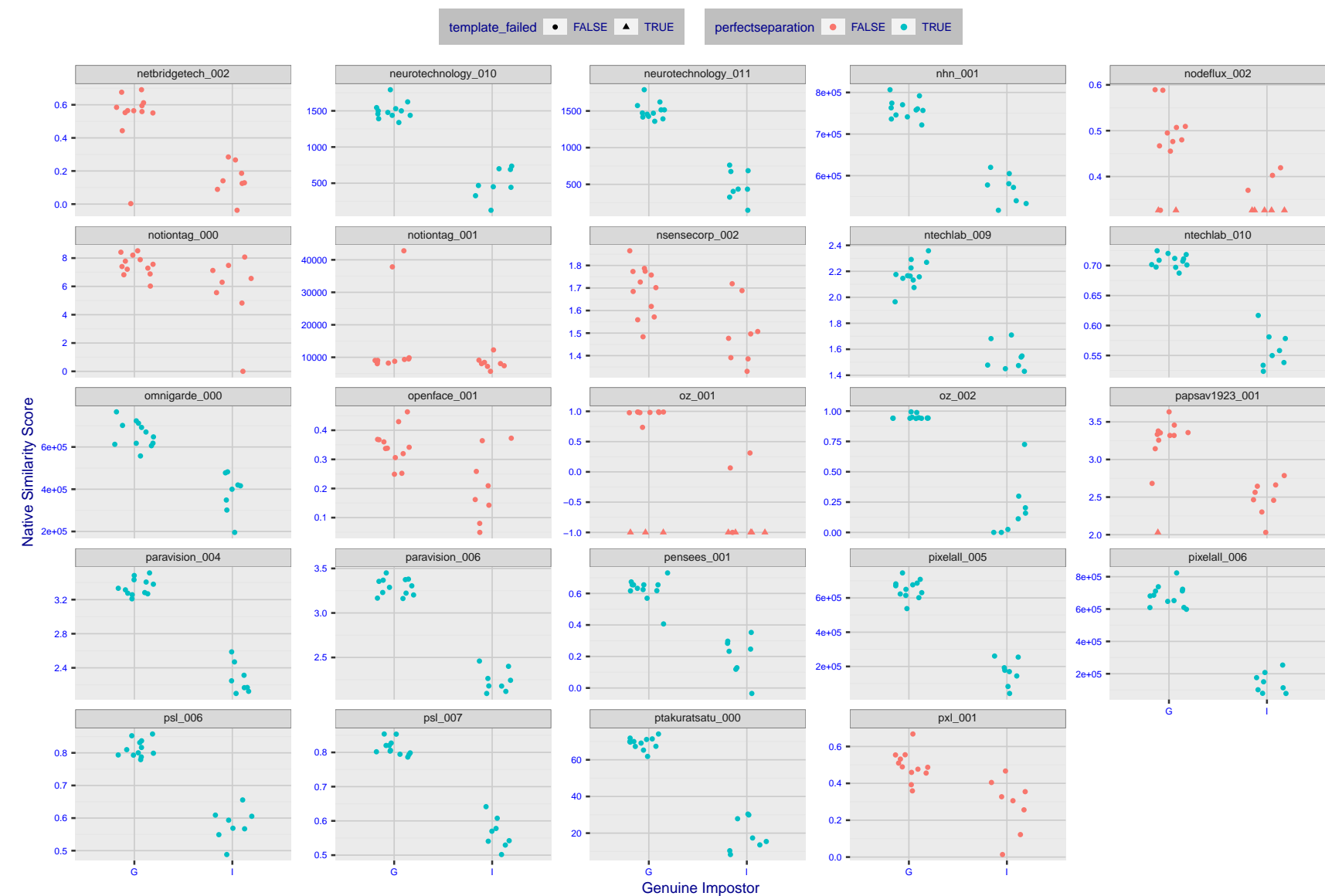


Figure 12: The Figure shows, in blue, algorithms that correctly separate the 12 genuine and 8 impostor pairs used in the May 2018 paper [Face recognition accuracy of forensic examiners, superrecognizers, and face recognition algorithms](#) (Phillips et al. [1]). In red are algorithms that are imperfect. Some algorithms fail only because they failed to make a template e.g. due to face detection failure (shown as a triangle). Others fail because the pairs were selected for that study because they had been difficult for three leading algorithms used in FRVT 2006. Caution: Given the small sample size ($n=20$) the figure may change substantially if larger or different sets were used. The images can be downloaded from the [Supplemental Information](#) page provided with that publication.

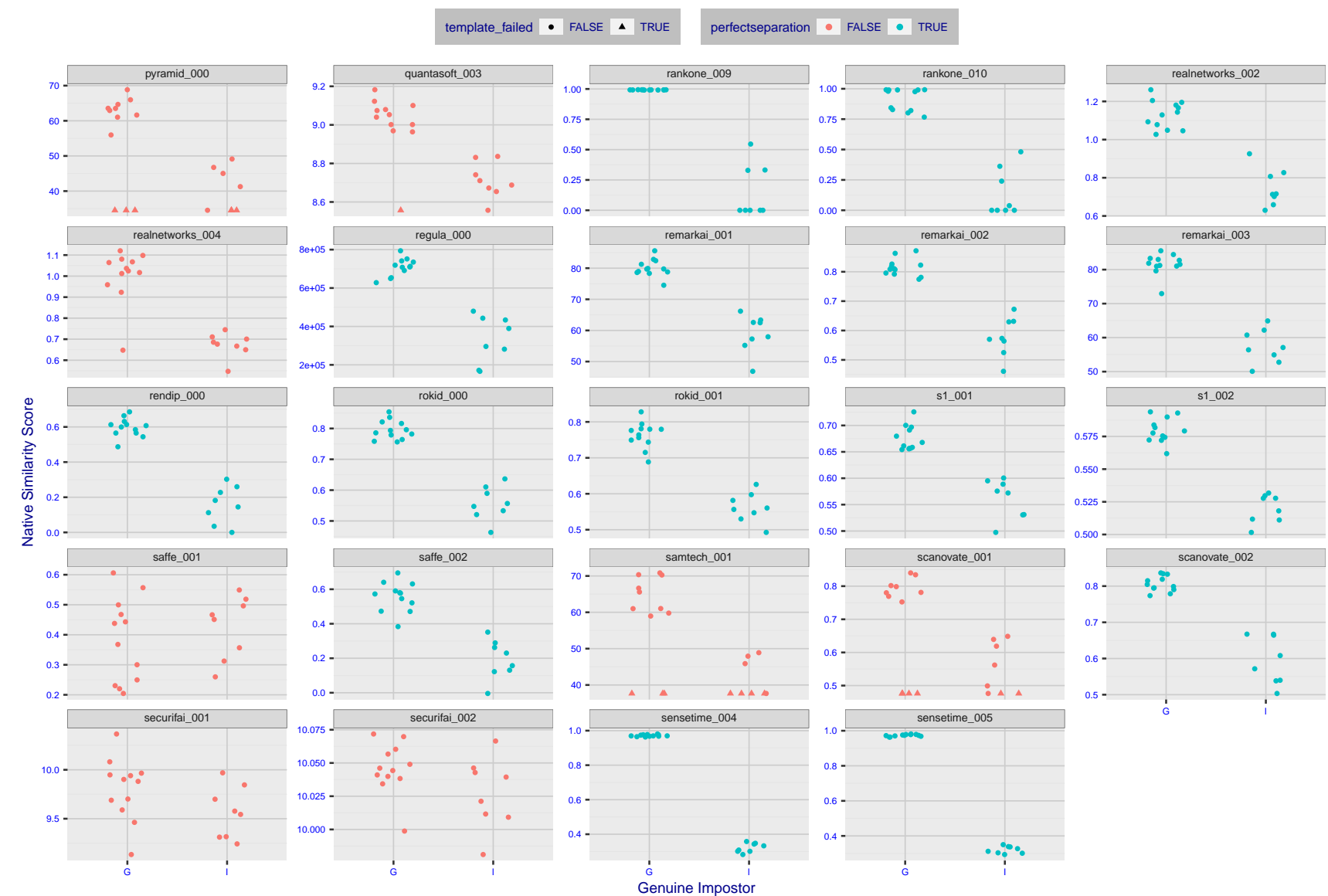


Figure 13: The Figure shows, in blue, algorithms that correctly separate the 12 genuine and 8 impostor pairs used in the May 2018 paper [Face recognition accuracy of forensic examiners, superrecognizers, and face recognition algorithms](#) (Phillips et al. [1]). In red are algorithms that are imperfect. Some algorithms fail only because they failed to make a template e.g. due to face detection failure (shown as a triangle). Others fail because the pairs were selected for that study because they had been difficult for three leading algorithms used in FRVT 2006. Caution: Given the small sample size ($n=20$) the figure may change substantially if larger or different sets were used. The images can be downloaded from the [Supplemental Information](#) page provided with that publication.

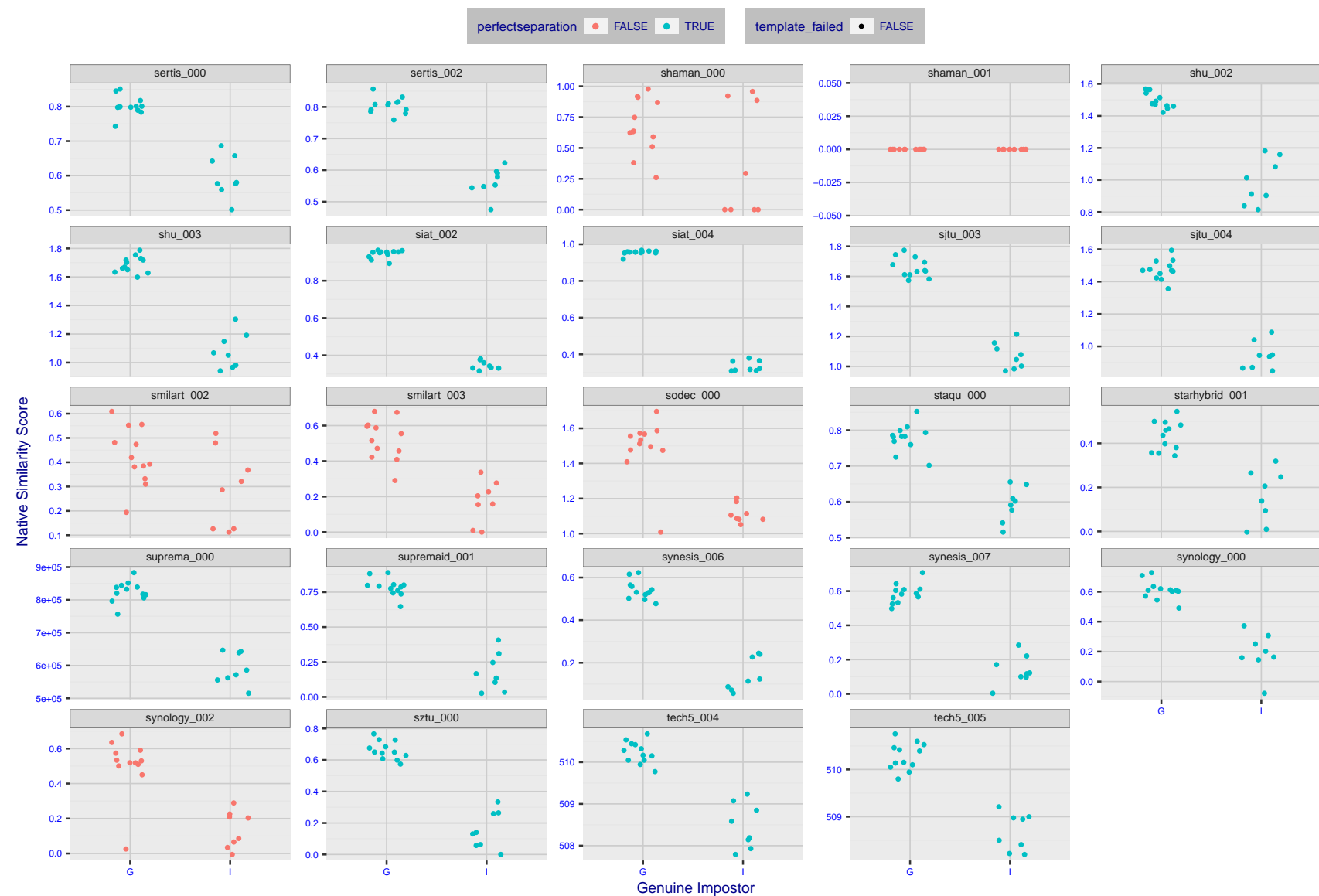


Figure 14: The Figure shows, in blue, algorithms that correctly separate the 12 genuine and 8 impostor pairs used in the May 2018 paper Face recognition accuracy of forensic examiners, superrecognizers, and face recognition algorithms (Phillips et al. [1]). In red are algorithms that are imperfect. Some algorithms fail only because they failed to make a template e.g. due to face detection failure (shown as a triangle). Others fail because the pairs were selected for that study because they had been difficult for three leading algorithms used in FRVT 2006. Caution: Given the small sample size ($n=20$) the figure may change substantially if larger or different sets were used. The images can be downloaded from the [Supplemental Information](#) page provided with that publication.

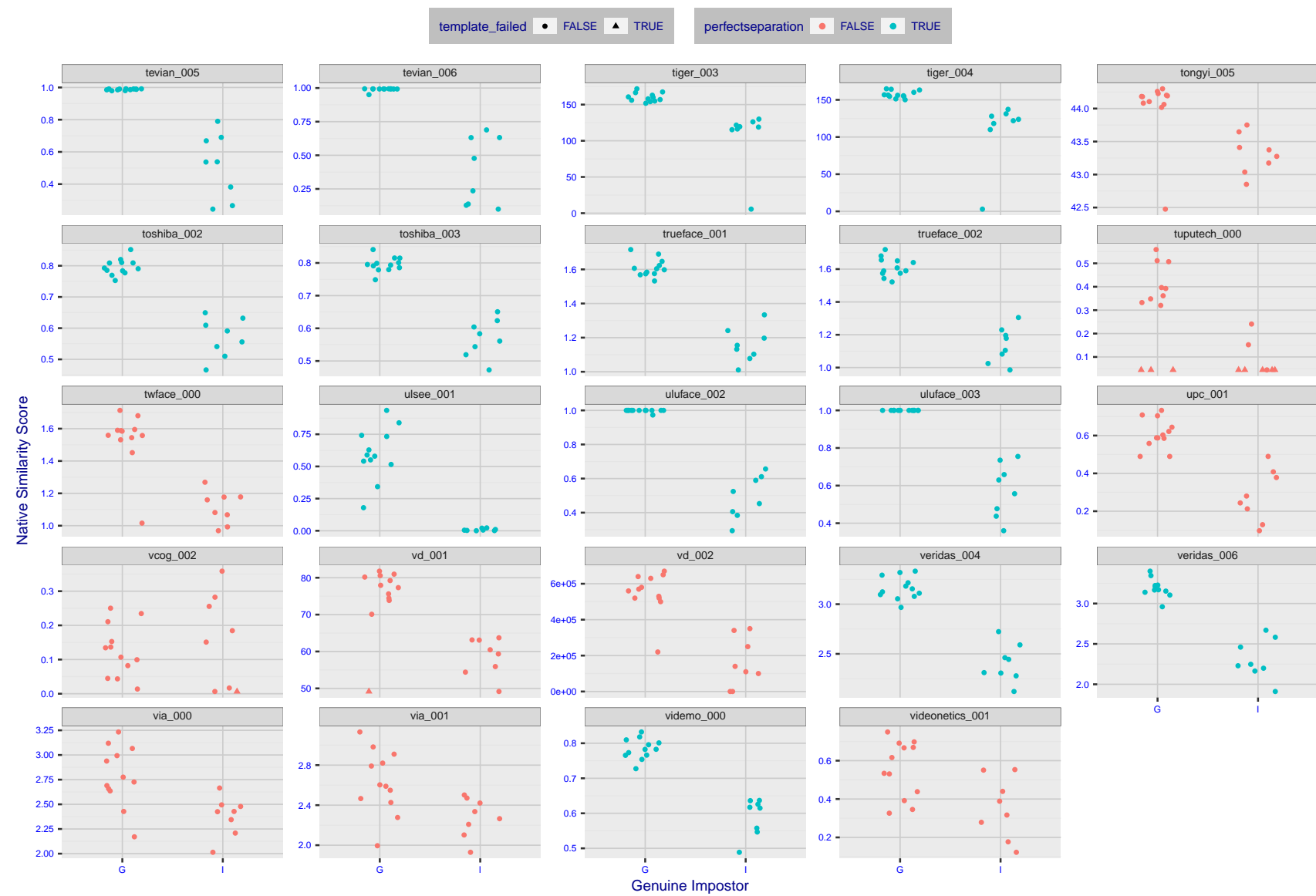


Figure 15: The Figure shows, in blue, algorithms that correctly separate the 12 genuine and 8 impostor pairs used in the May 2018 paper [Face recognition accuracy of forensic examiners, superrecognizers, and face recognition algorithms](#) (Phillips et al. [1]). In red are algorithms that are imperfect. Some algorithms fail only because they failed to make a template e.g. due to face detection failure (shown as a triangle). Others fail because the pairs were selected for that study because they had been difficult for three leading algorithms used in FRVT 2006. Caution: Given the small sample size ($n=20$) the figure may change substantially if larger or different sets were used. The images can be downloaded from the [Supplemental Information](#) page provided with that publication.

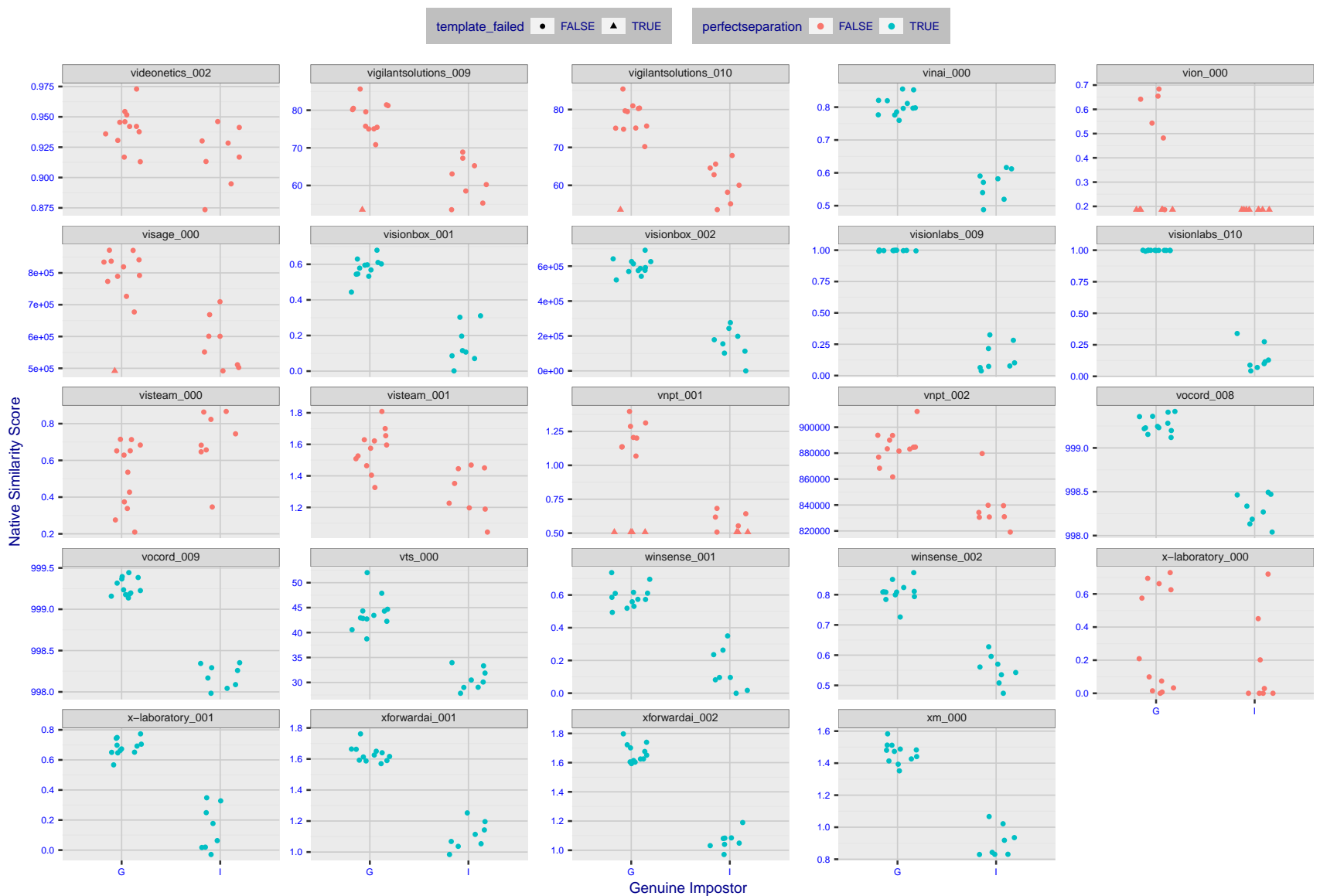


Figure 16: The Figure shows, in blue, algorithms that correctly separate the 12 genuine and 8 impostor pairs used in the May 2018 paper Face recognition accuracy of forensic examiners, superrecognizers, and face recognition algorithms (Phillips et al. [1]). In red are algorithms that are imperfect. Some algorithms fail only because they failed to make a template e.g. due to face detection failure (shown as a triangle). Others fail because the pairs were selected for that study because they had been difficult for three leading algorithms used in FRVT 2006. Caution: Given the small sample size ($n=20$) the figure may change substantially if larger or different sets were used. The images can be downloaded from the [Supplemental Information](#) page provided with that publication.

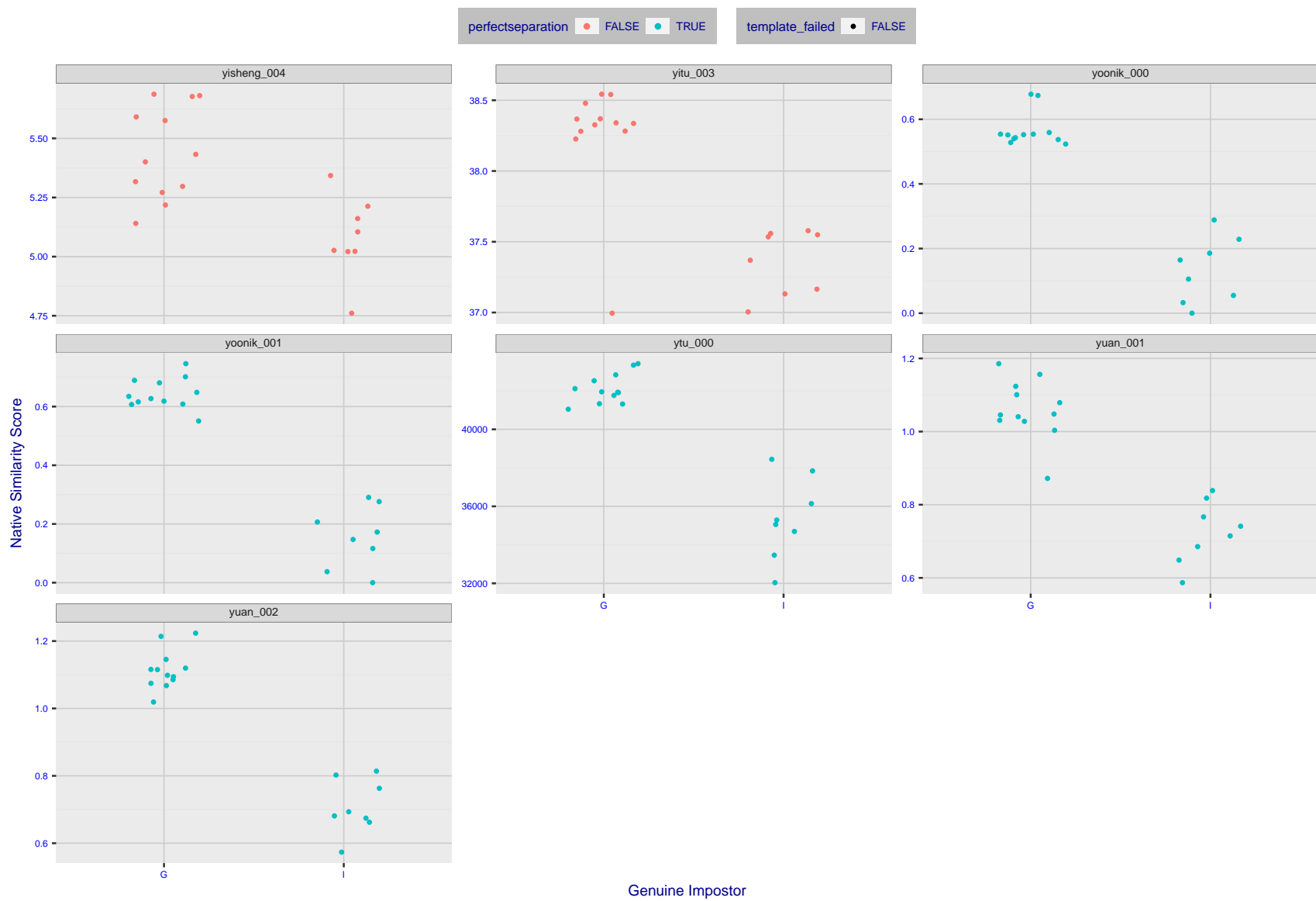


Figure 17: The Figure shows, in blue, algorithms that correctly separate the 12 genuine and 8 impostor pairs used in the May 2018 paper [Face recognition accuracy of forensic examiners, superrecognizers, and face recognition algorithms](#) (Phillips et al. [1]). In red are algorithms that are imperfect. Some algorithms fail only because they failed to make a template e.g. due to face detection failure (shown as a triangle). Others fail because the pairs were selected for that study because they had been difficult for three leading algorithms used in FRVT 2006. Caution: Given the small sample size ($n=20$) the figure may change substantially if larger or different sets were used. The images can be downloaded from the [Supplemental Information](#) page provided with that publication.

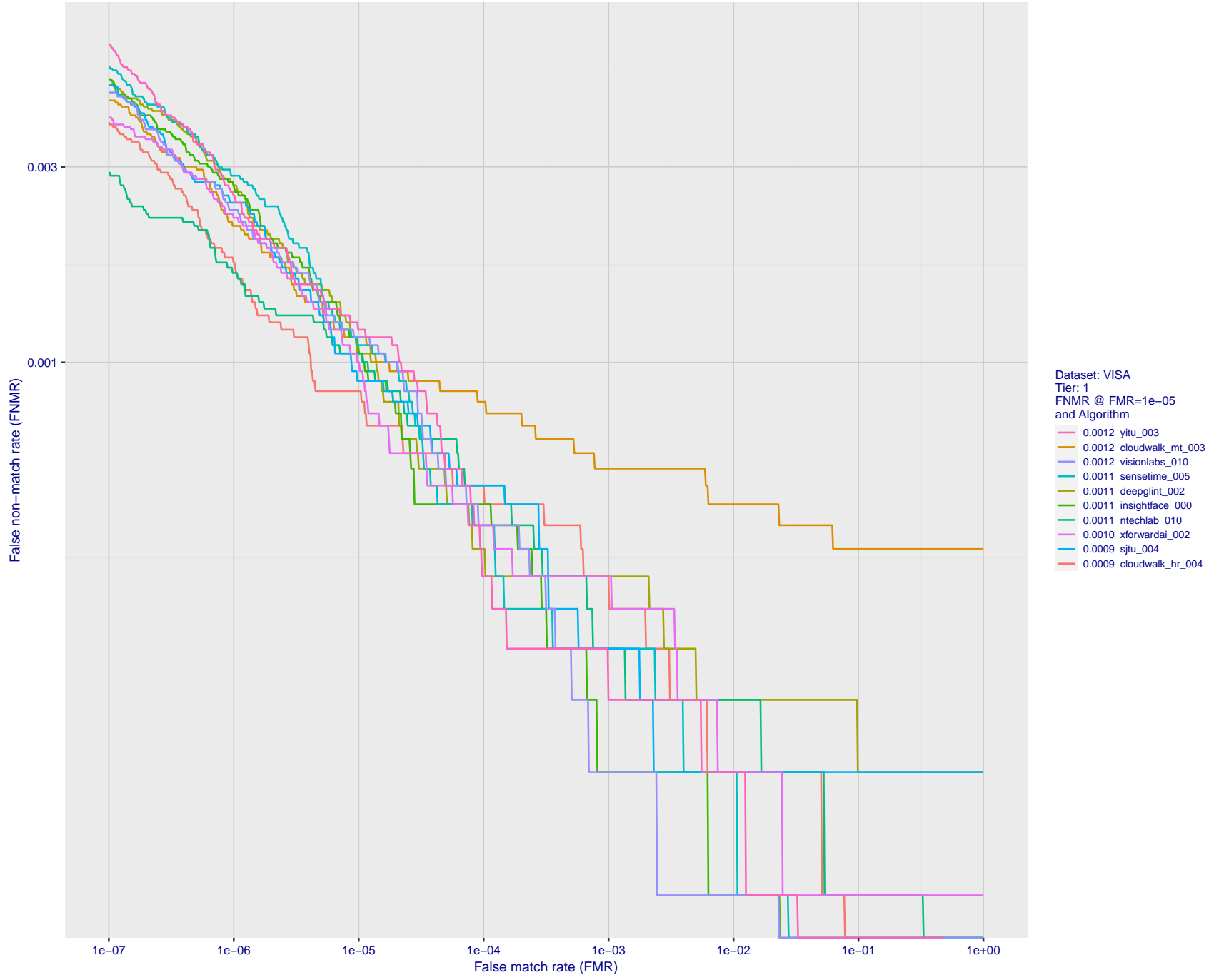


Figure 18: For the visa images, detection error tradeoff (DET) characteristics showing false non-match rate vs. false match rate plotted parametrically on threshold, T . The scales are logarithmic in order to show many decades of FMR.

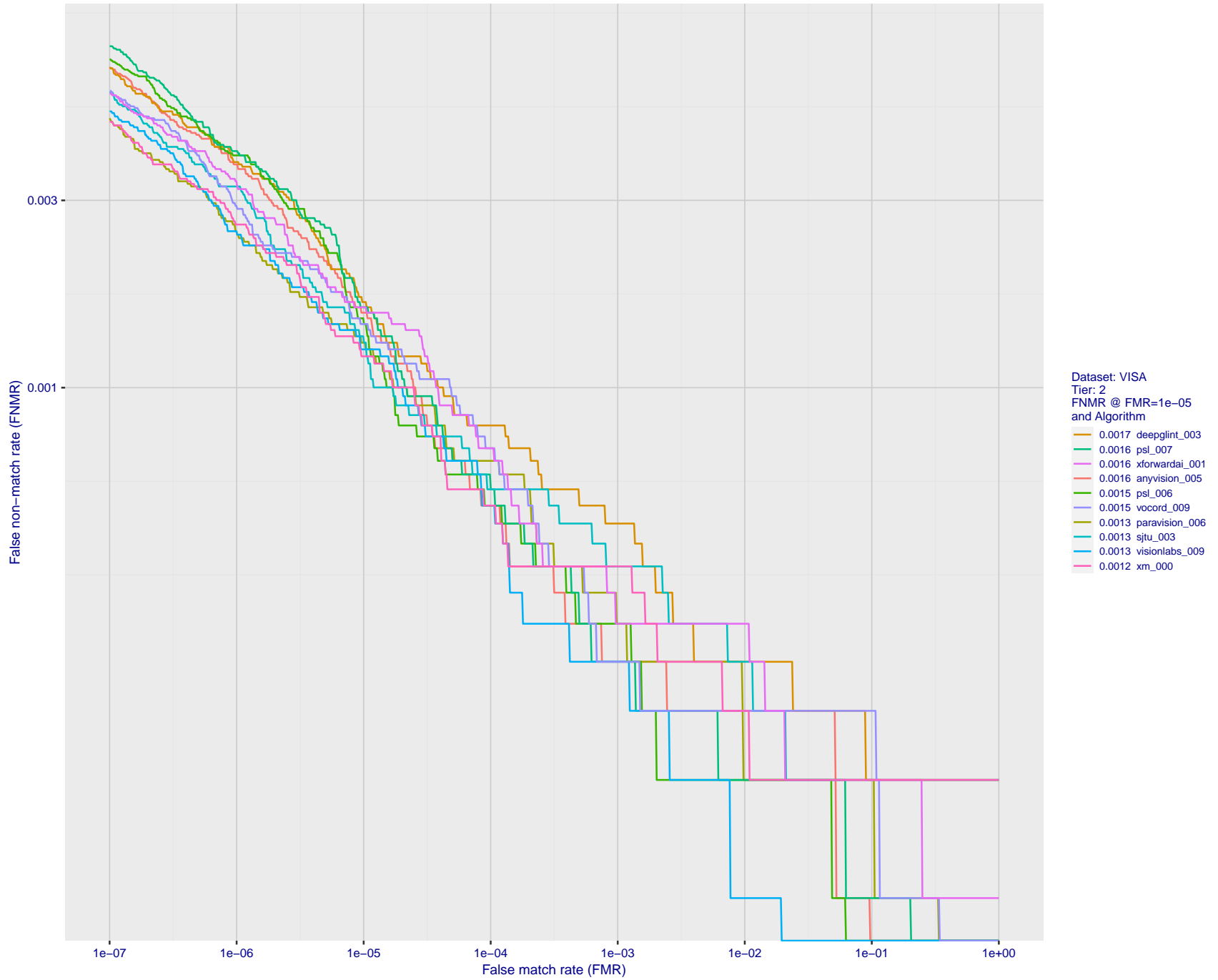


Figure 19: For the visa images, detection error tradeoff (DET) characteristics showing false non-match rate vs. false match rate plotted parametrically on threshold, T . The scales are logarithmic in order to show many decades of FMR.

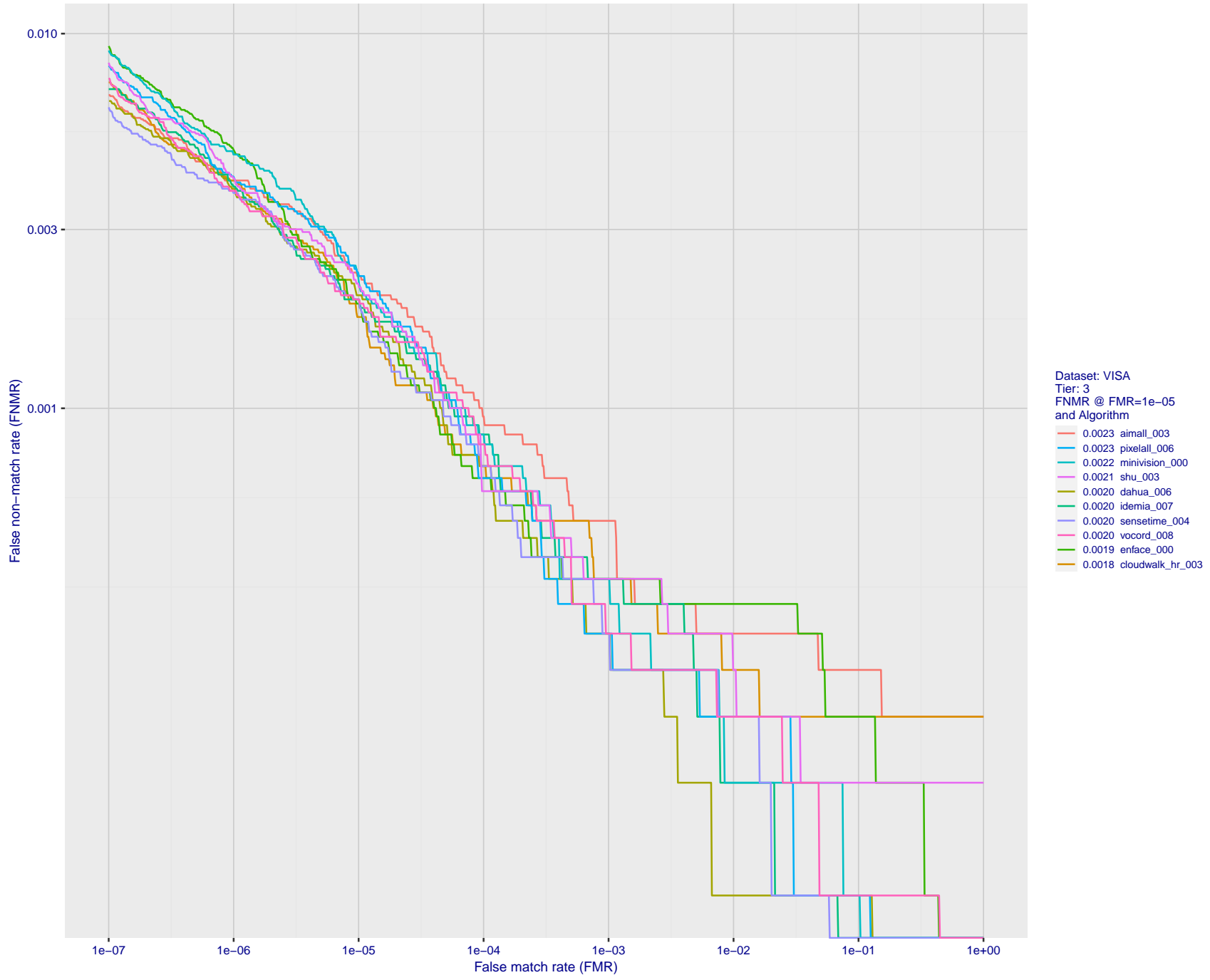


Figure 20: For the visa images, detection error tradeoff (DET) characteristics showing false non-match rate vs. false match rate plotted parametrically on threshold, T . The scales are logarithmic in order to show many decades of FMR.

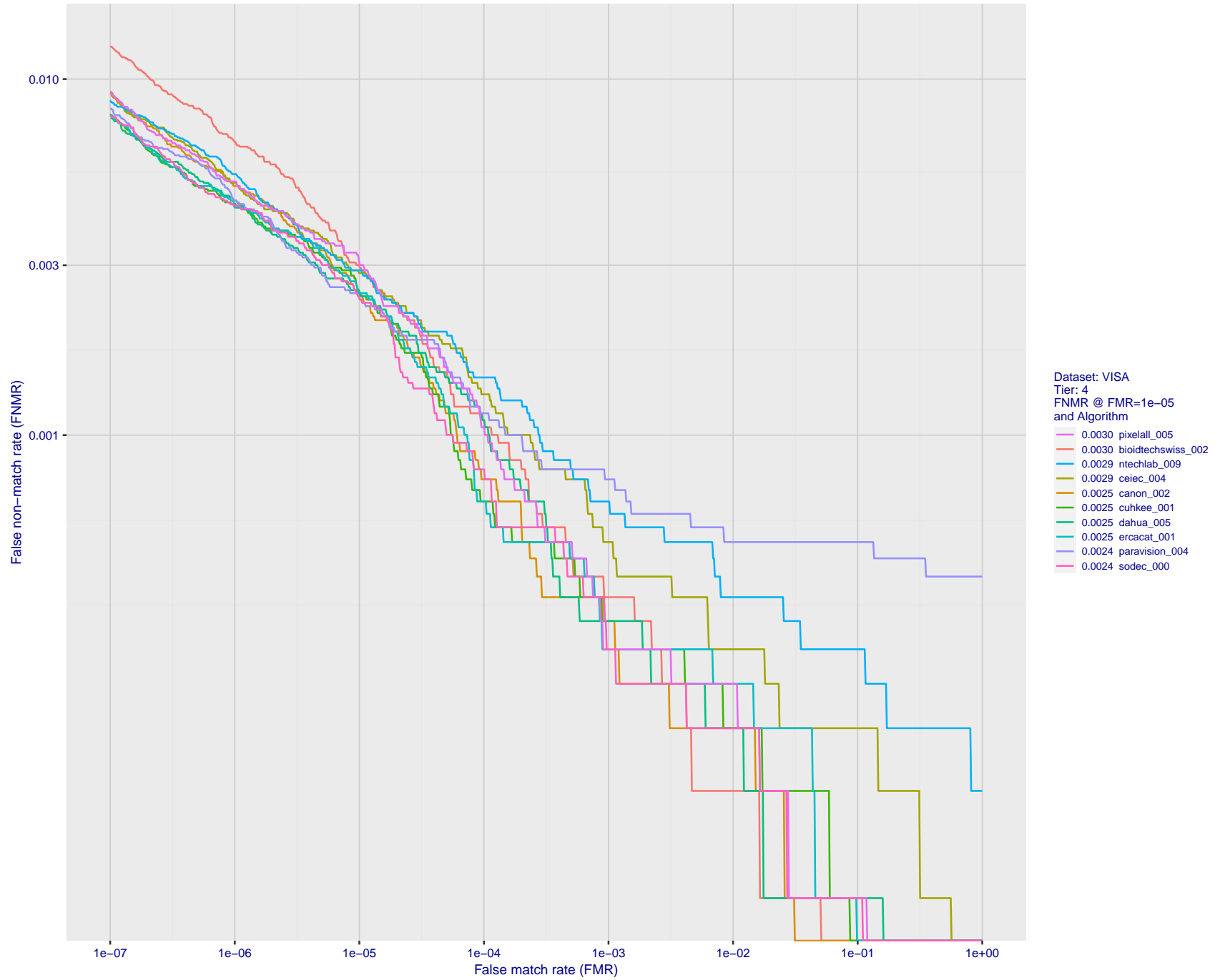


Figure 21: For the visa images, detection error tradeoff (DET) characteristics showing false non-match rate vs. false match rate plotted parametrically on threshold, T . The scales are logarithmic in order to show many decades of FMR.

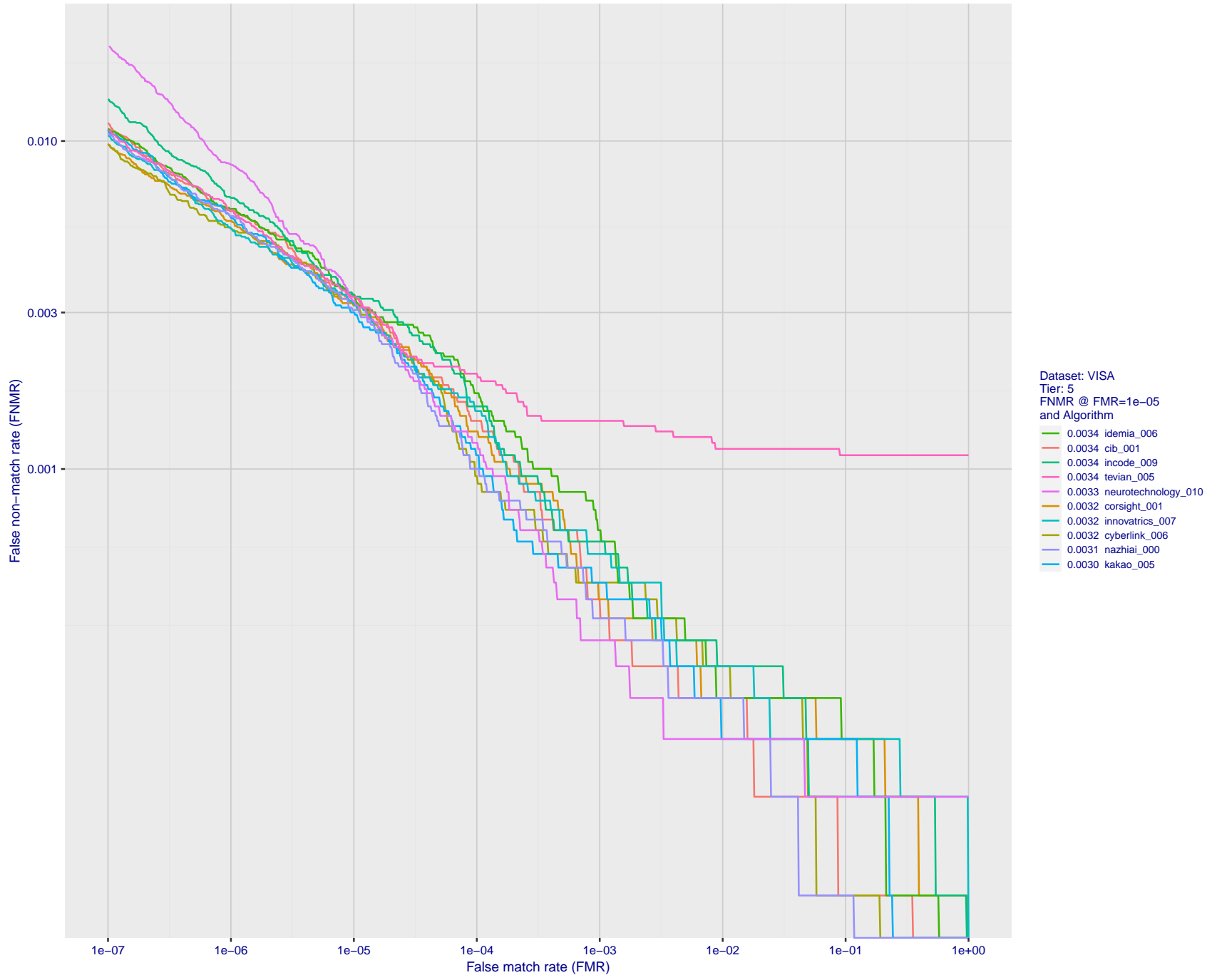


Figure 22: For the visa images, detection error tradeoff (DET) characteristics showing false non-match rate vs. false match rate plotted parametrically on threshold, T . The scales are logarithmic in order to show many decades of FMR.

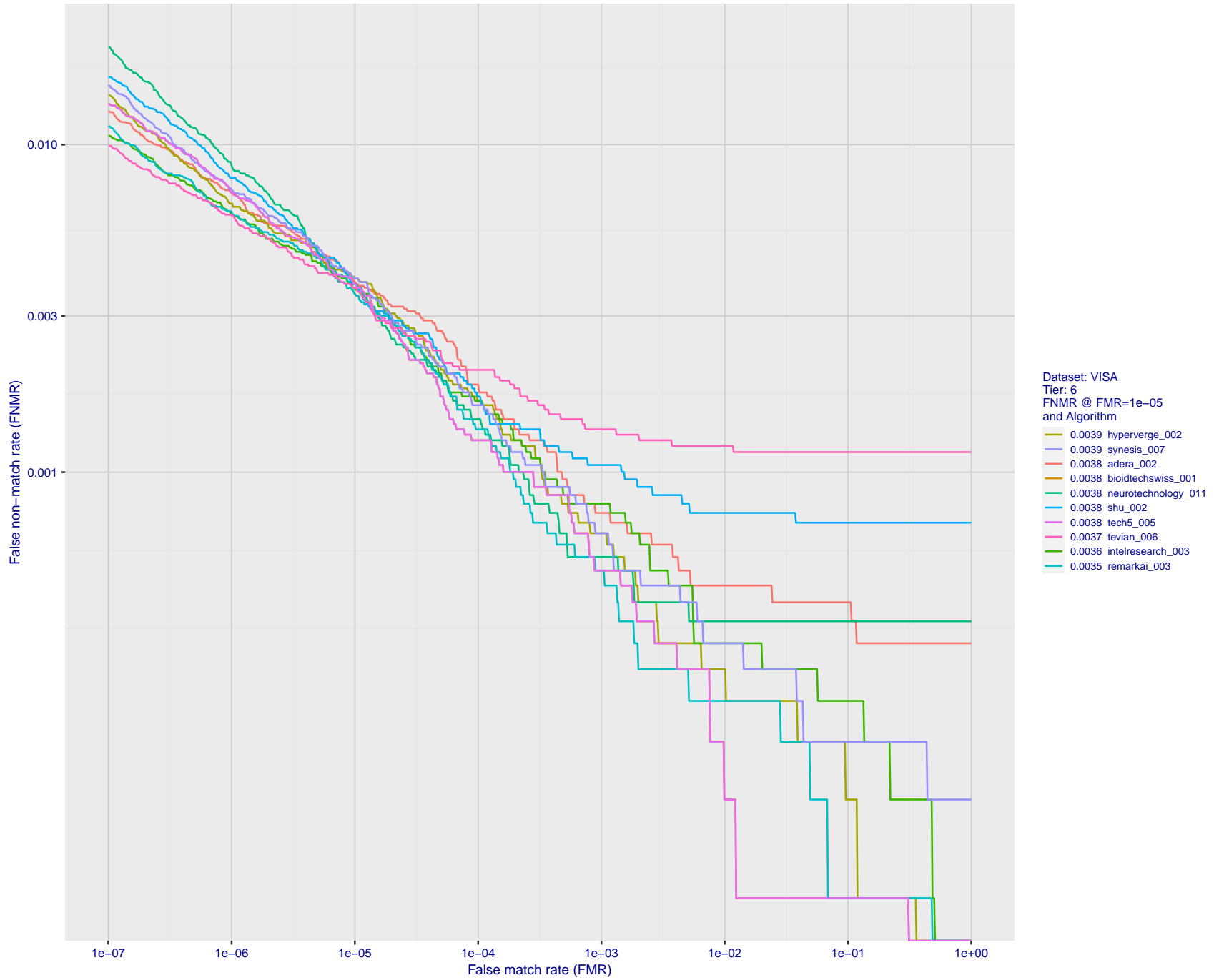


Figure 23: For the visa images, detection error tradeoff (DET) characteristics showing false non-match rate vs. false match rate plotted parametrically on threshold, T . The scales are logarithmic in order to show many decades of FMR.

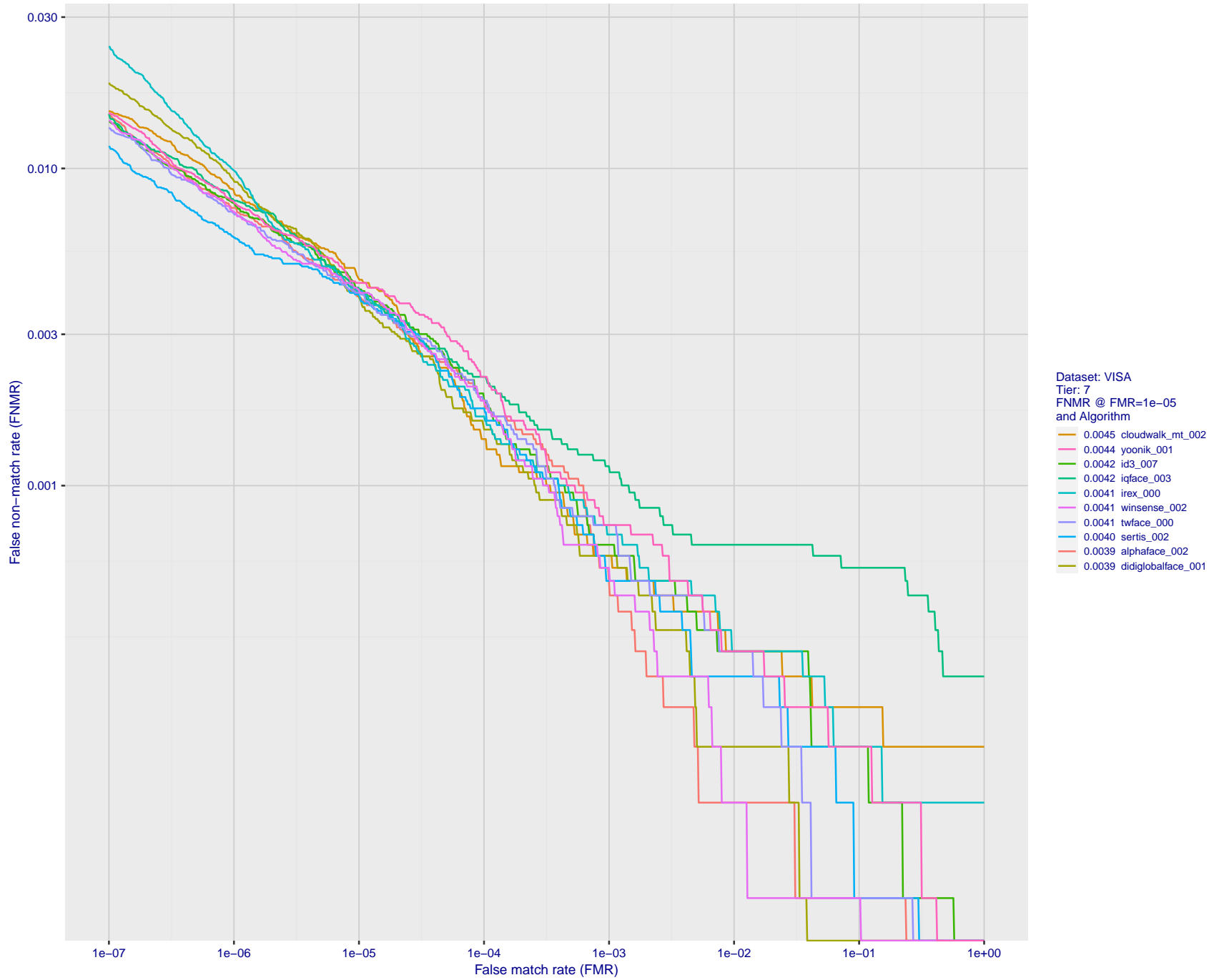


Figure 24: For the visa images, detection error tradeoff (DET) characteristics showing false non-match rate vs. false match rate plotted parametrically on threshold, T . The scales are logarithmic in order to show many decades of FMR.

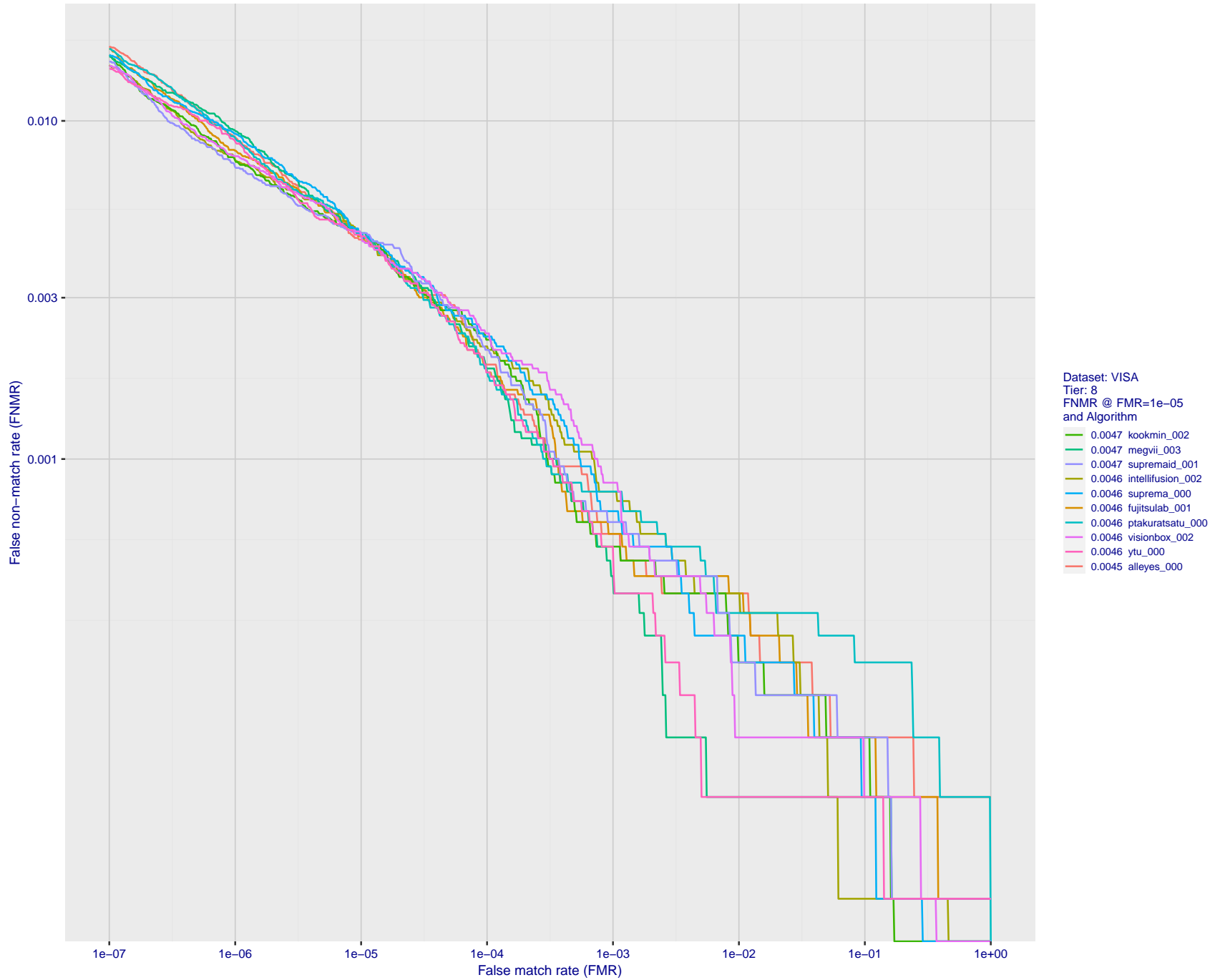


Figure 25: For the visa images, detection error tradeoff (DET) characteristics showing false non-match rate vs. false match rate plotted parametrically on threshold, T . The scales are logarithmic in order to show many decades of FMR.

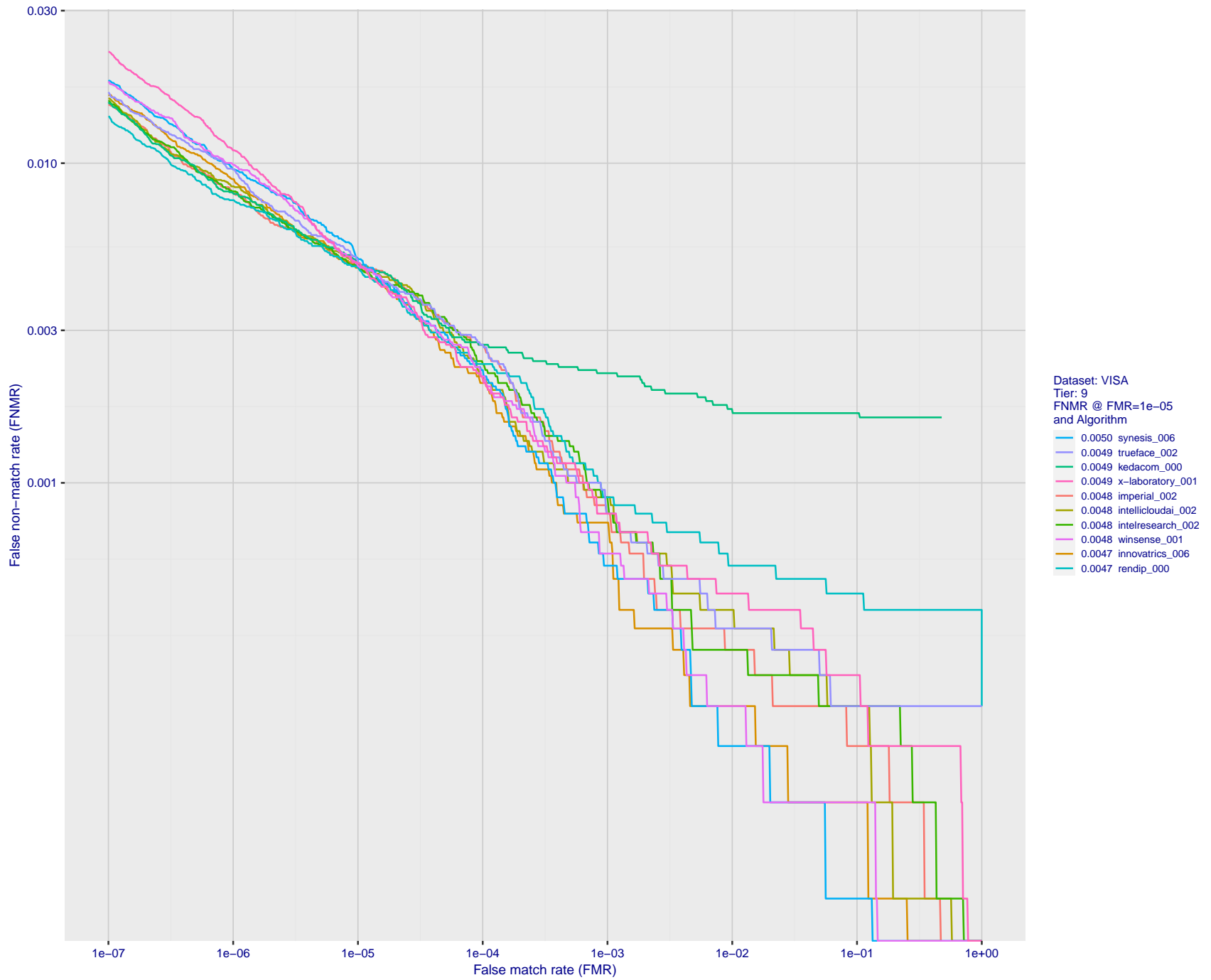


Figure 26: For the visa images, detection error tradeoff (DET) characteristics showing false non-match rate vs. false match rate plotted parametrically on threshold, T . The scales are logarithmic in order to show many decades of FMR.

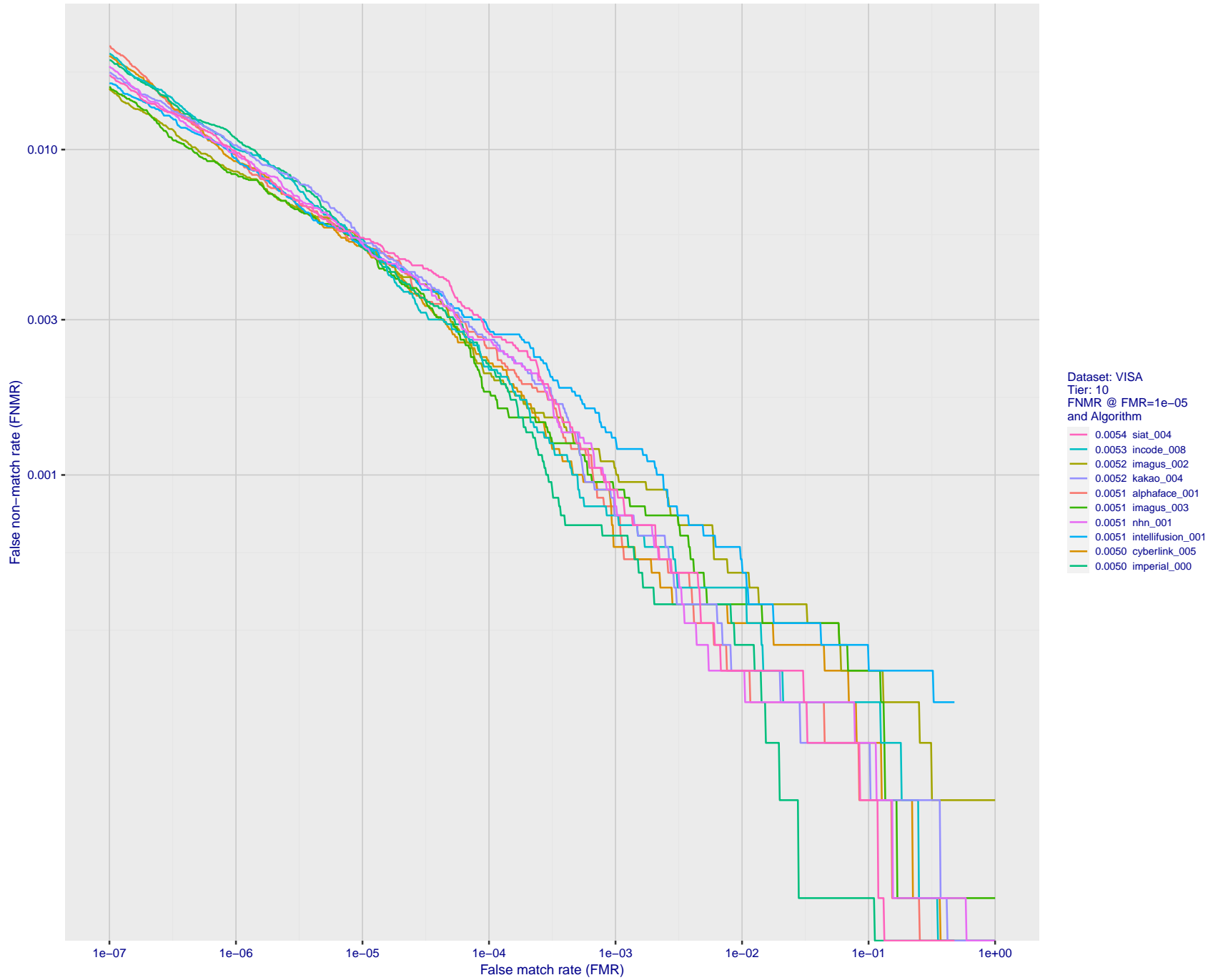


Figure 27: For the visa images, detection error tradeoff (DET) characteristics showing false non-match rate vs. false match rate plotted parametrically on threshold, T . The scales are logarithmic in order to show many decades of FMR.

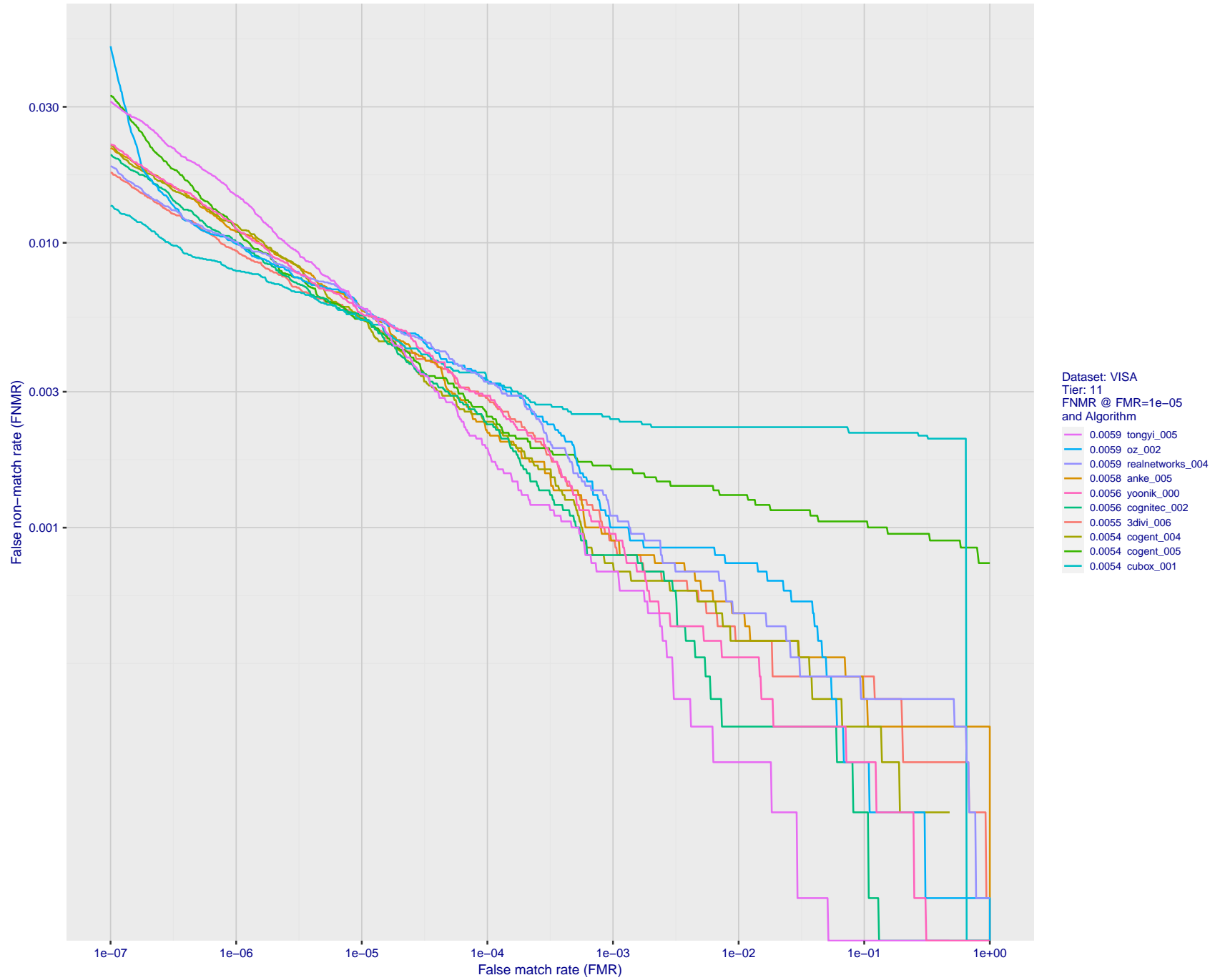


Figure 28: For the visa images, detection error tradeoff (DET) characteristics showing false non-match rate vs. false match rate plotted parametrically on threshold, T . The scales are logarithmic in order to show many decades of FMR.

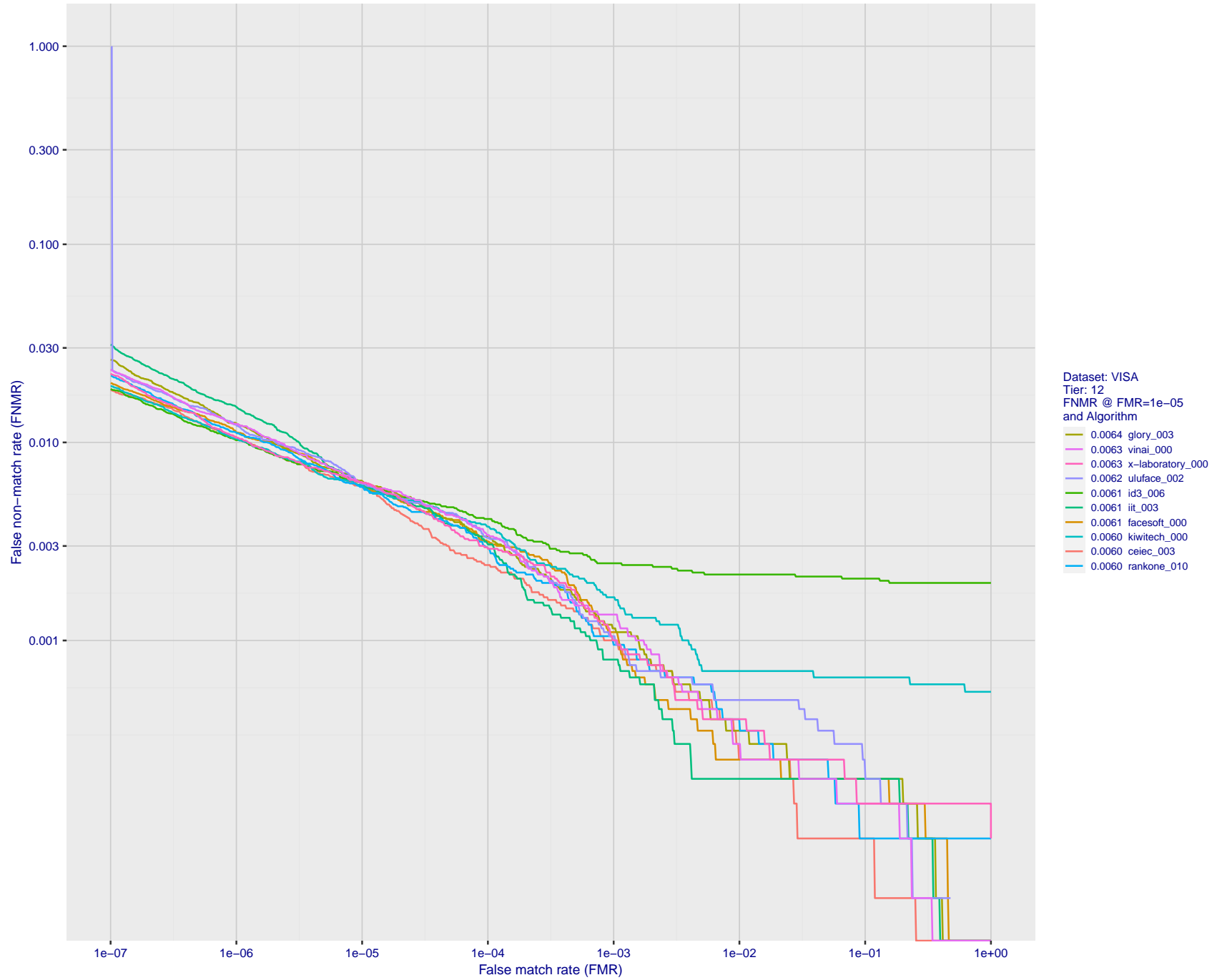


Figure 29: For the visa images, detection error tradeoff (DET) characteristics showing false non-match rate vs. false match rate plotted parametrically on threshold, T . The scales are logarithmic in order to show many decades of FMR.

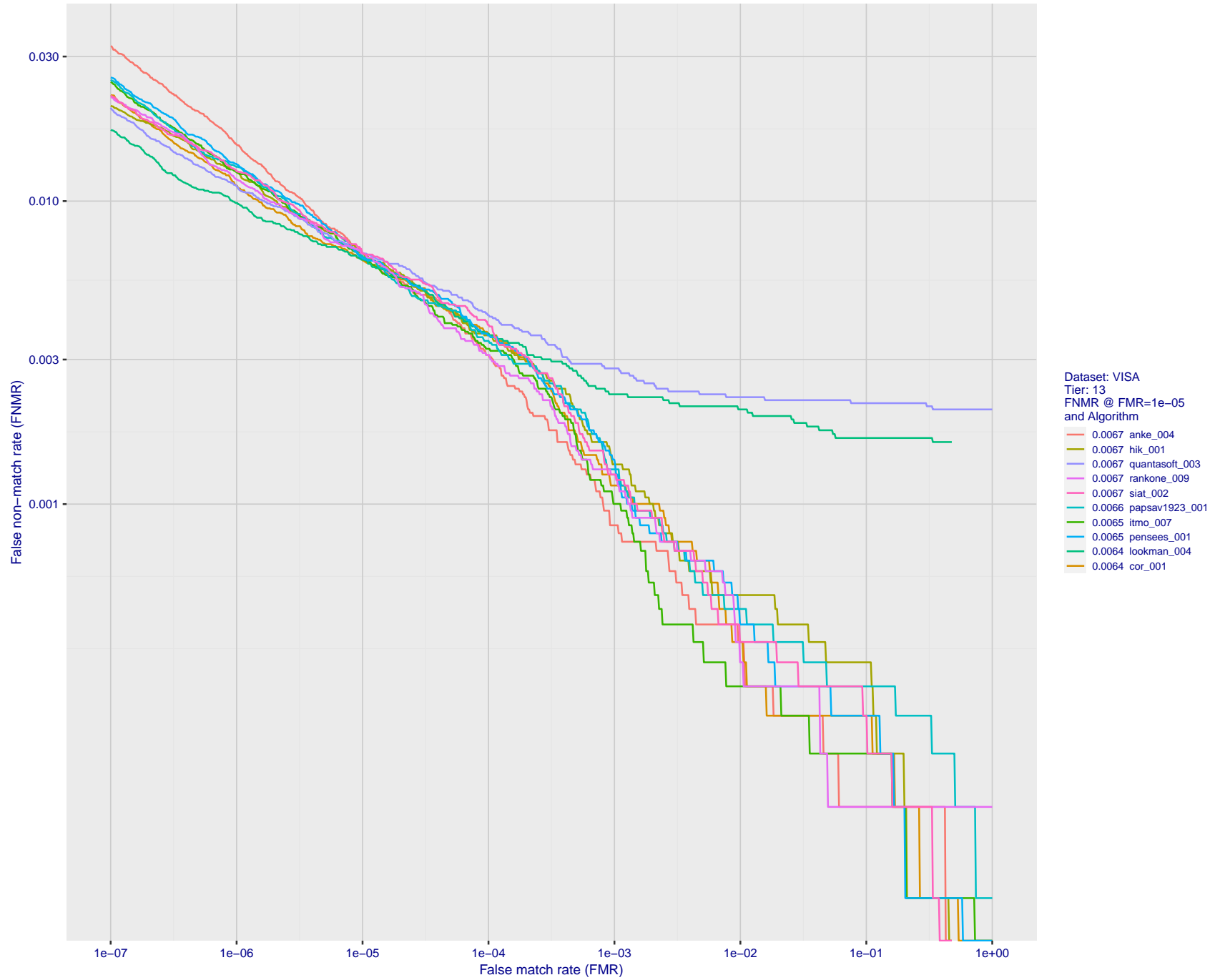


Figure 30: For the visa images, detection error tradeoff (DET) characteristics showing false non-match rate vs. false match rate plotted parametrically on threshold, T . The scales are logarithmic in order to show many decades of FMR.

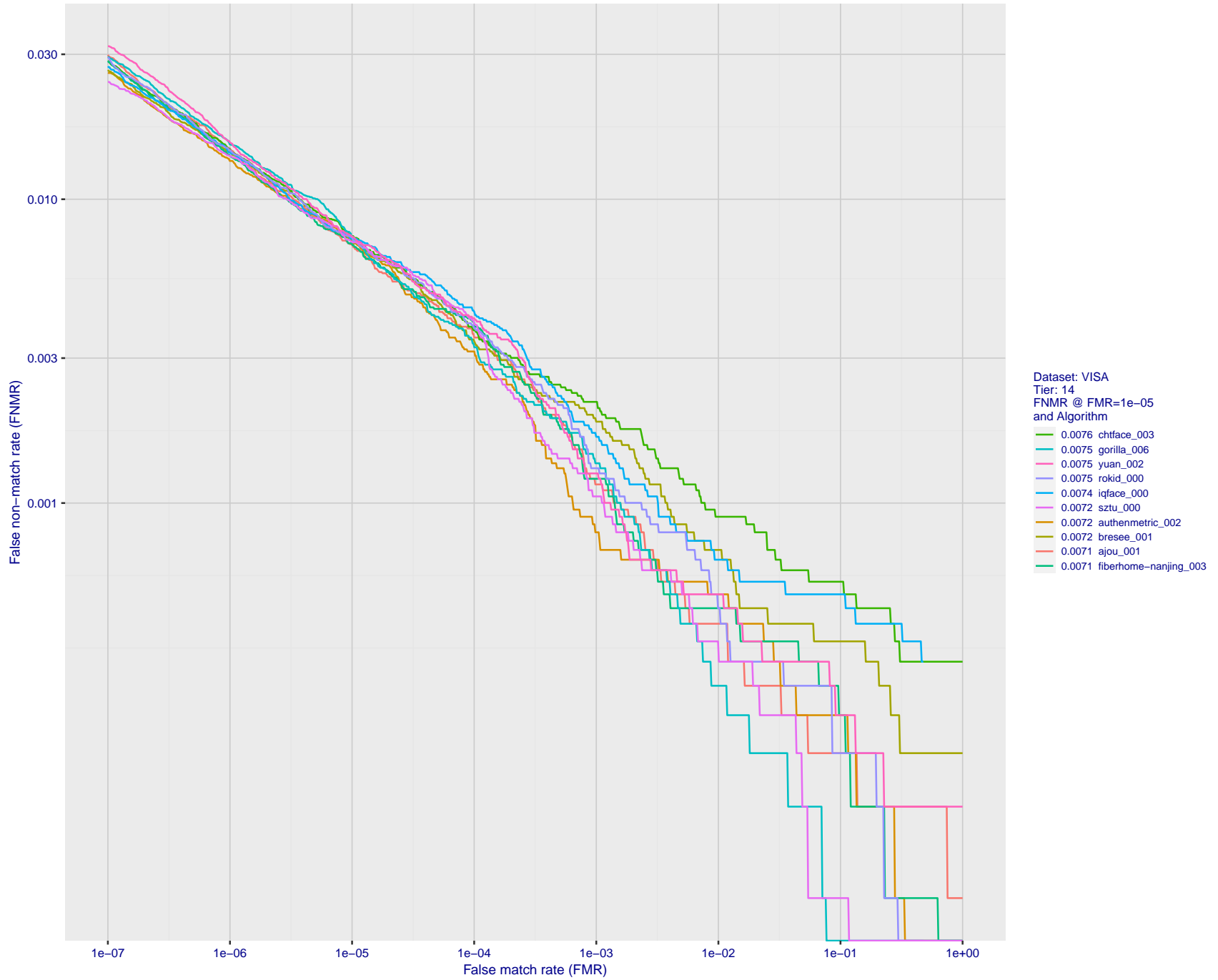


Figure 31: For the visa images, detection error tradeoff (DET) characteristics showing false non-match rate vs. false match rate plotted parametrically on threshold, T . The scales are logarithmic in order to show many decades of FMR.

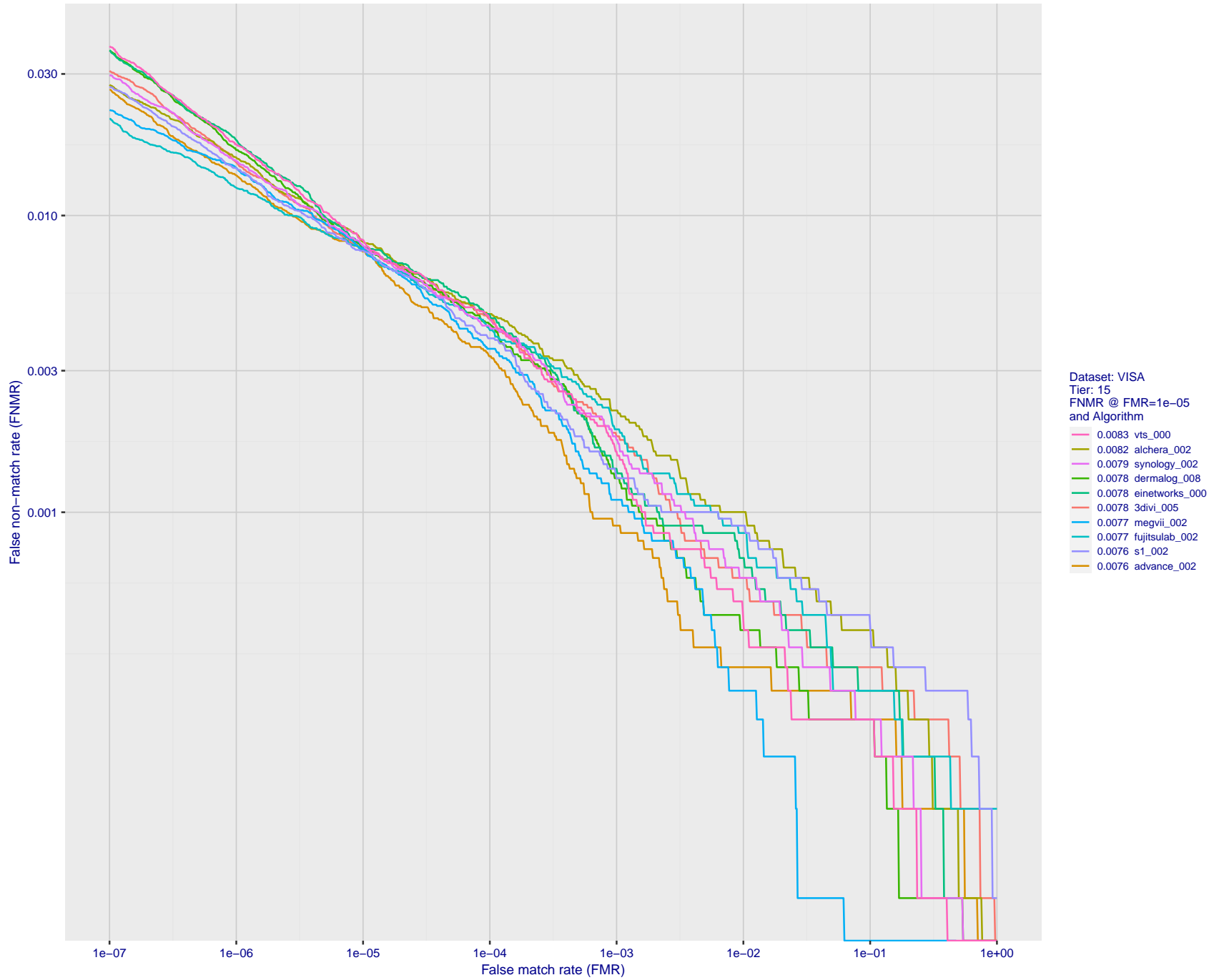


Figure 32: For the visa images, detection error tradeoff (DET) characteristics showing false non-match rate vs. false match rate plotted parametrically on threshold, T . The scales are logarithmic in order to show many decades of FMR.

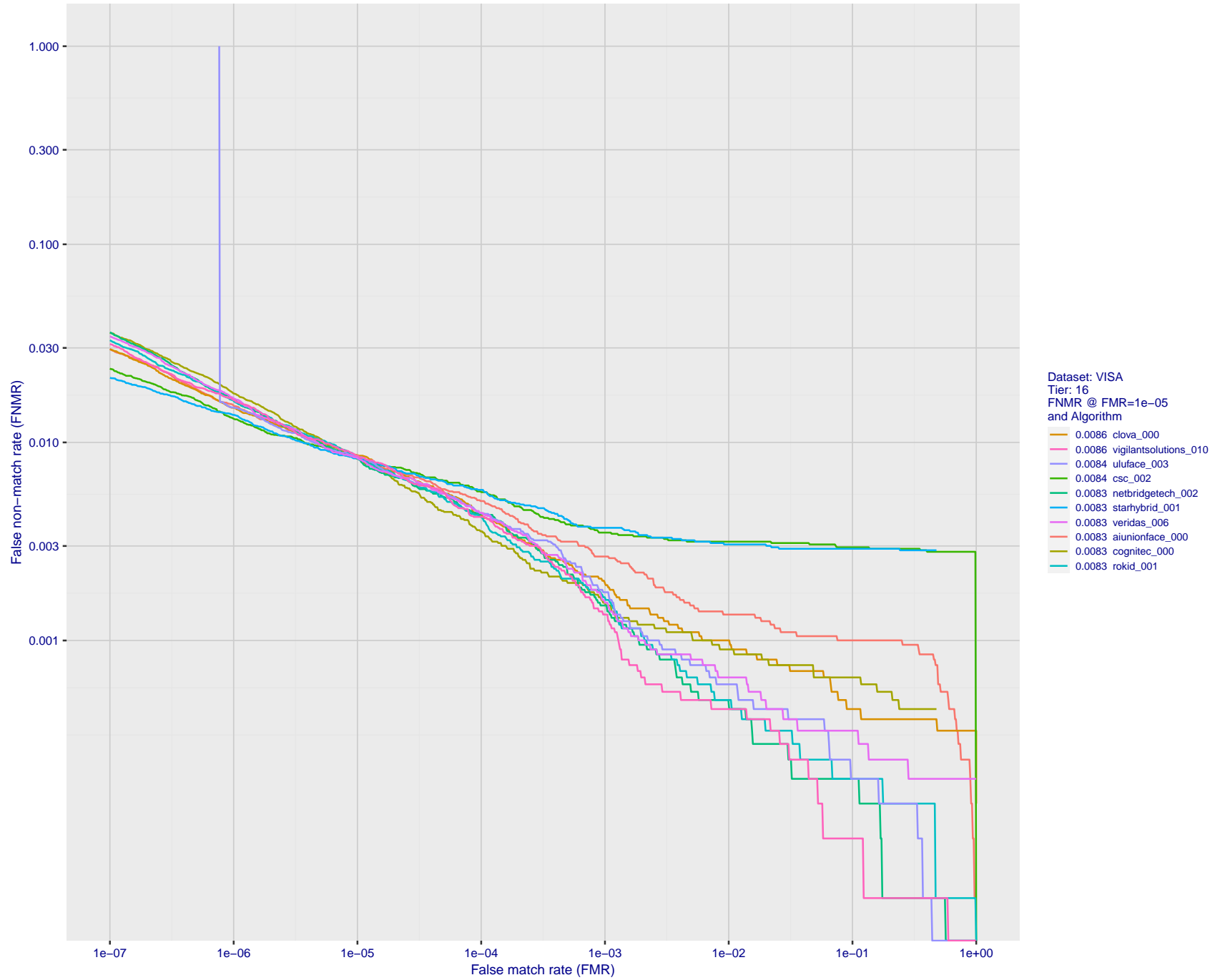


Figure 33: For the visa images, detection error tradeoff (DET) characteristics showing false non-match rate vs. false match rate plotted parametrically on threshold, T . The scales are logarithmic in order to show many decades of FMR.

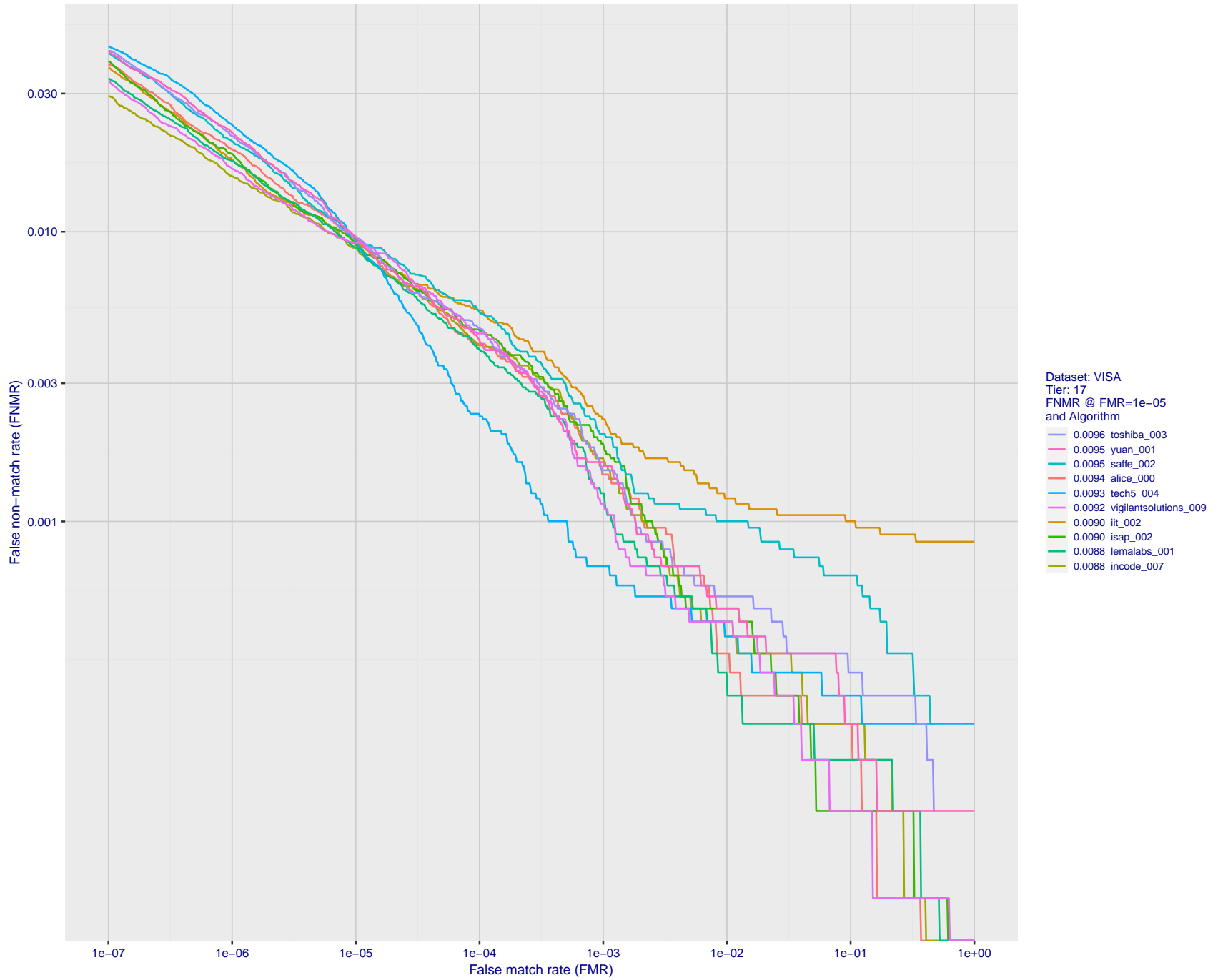


Figure 34: For the visa images, detection error tradeoff (DET) characteristics showing false non-match rate vs. false match rate plotted parametrically on threshold, T . The scales are logarithmic in order to show many decades of FMR.

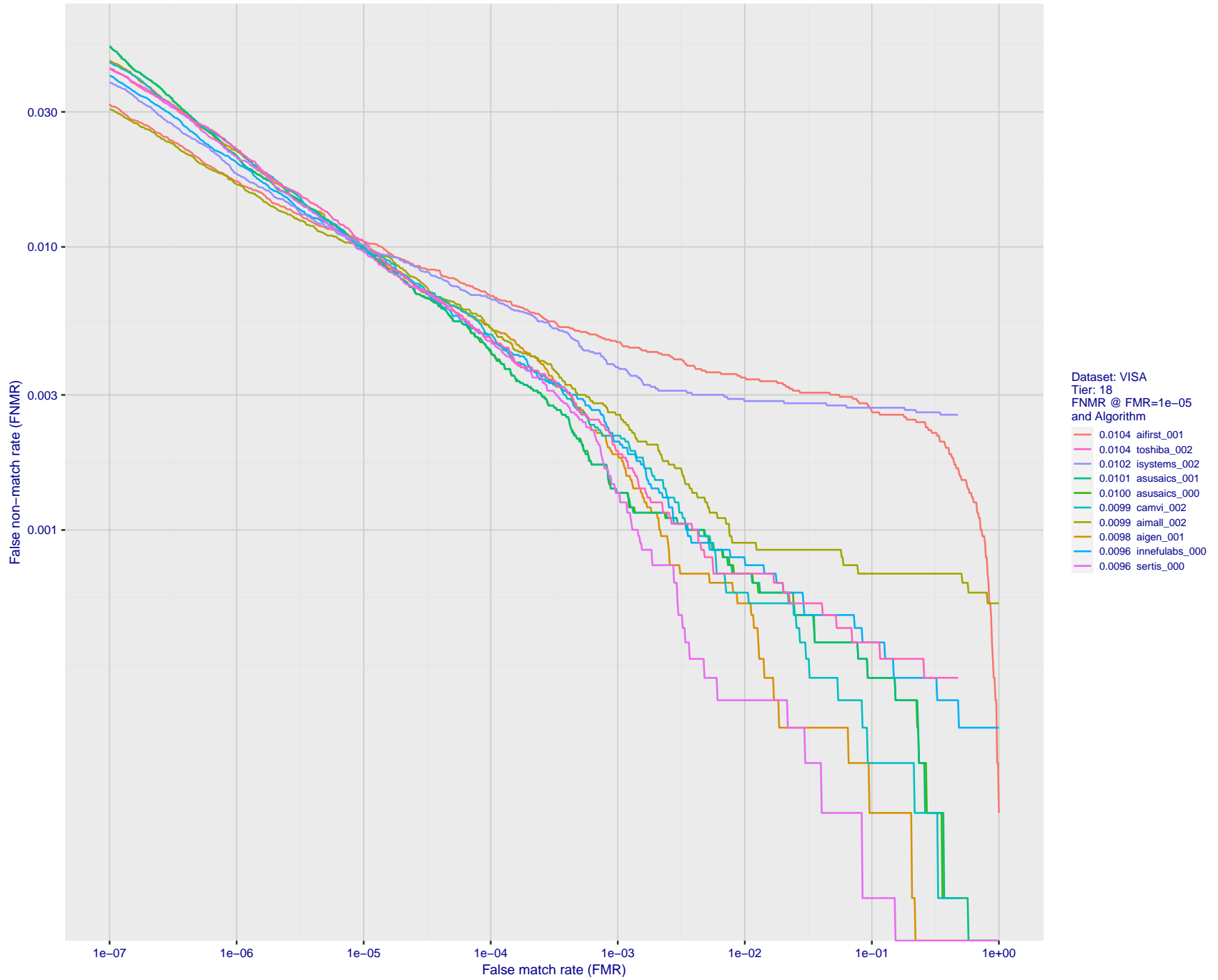


Figure 35: For the visa images, detection error tradeoff (DET) characteristics showing false non-match rate vs. false match rate plotted parametrically on threshold, T . The scales are logarithmic in order to show many decades of FMR.

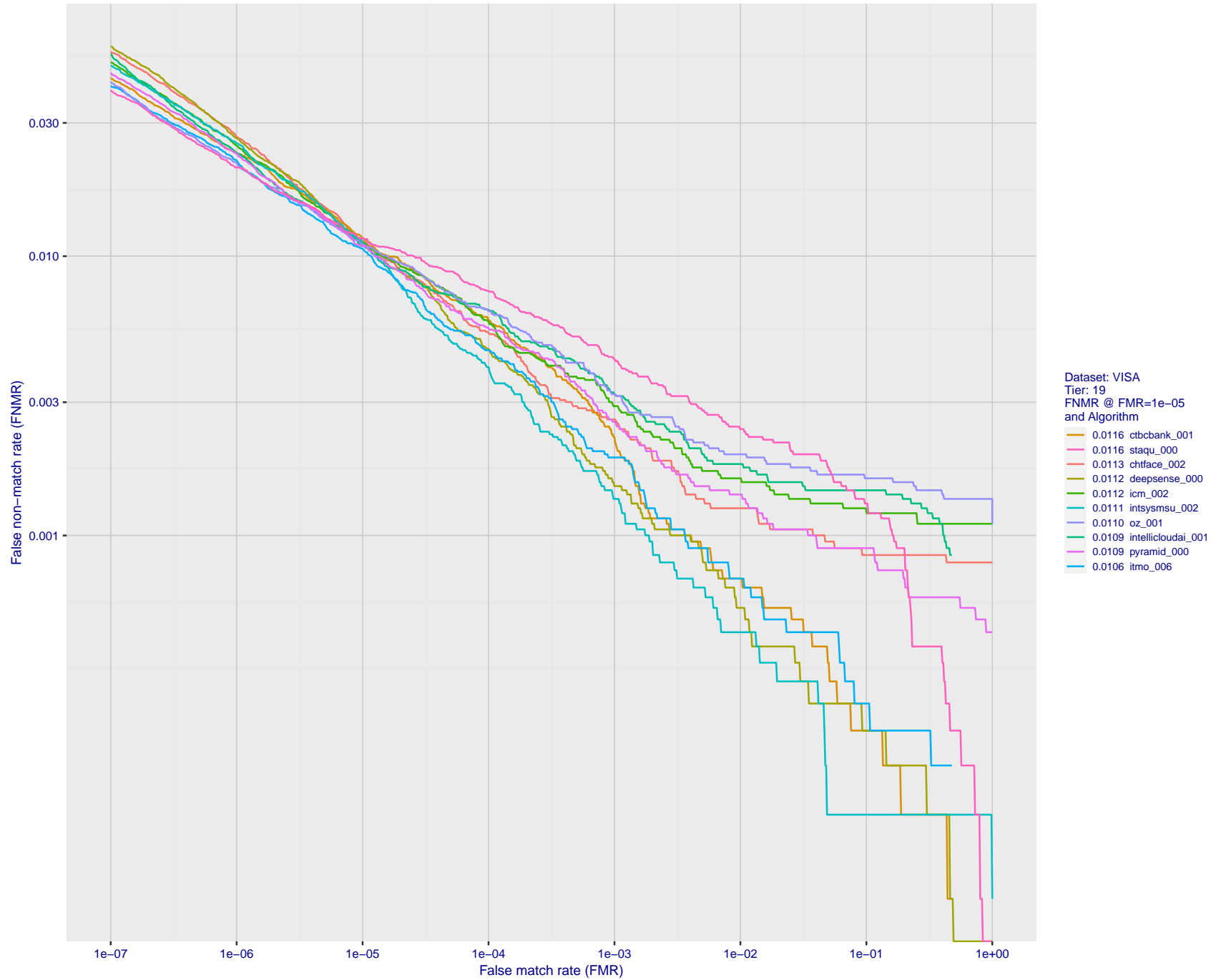


Figure 36: For the visa images, detection error tradeoff (DET) characteristics showing false non-match rate vs. false match rate plotted parametrically on threshold, T . The scales are logarithmic in order to show many decades of FMR.

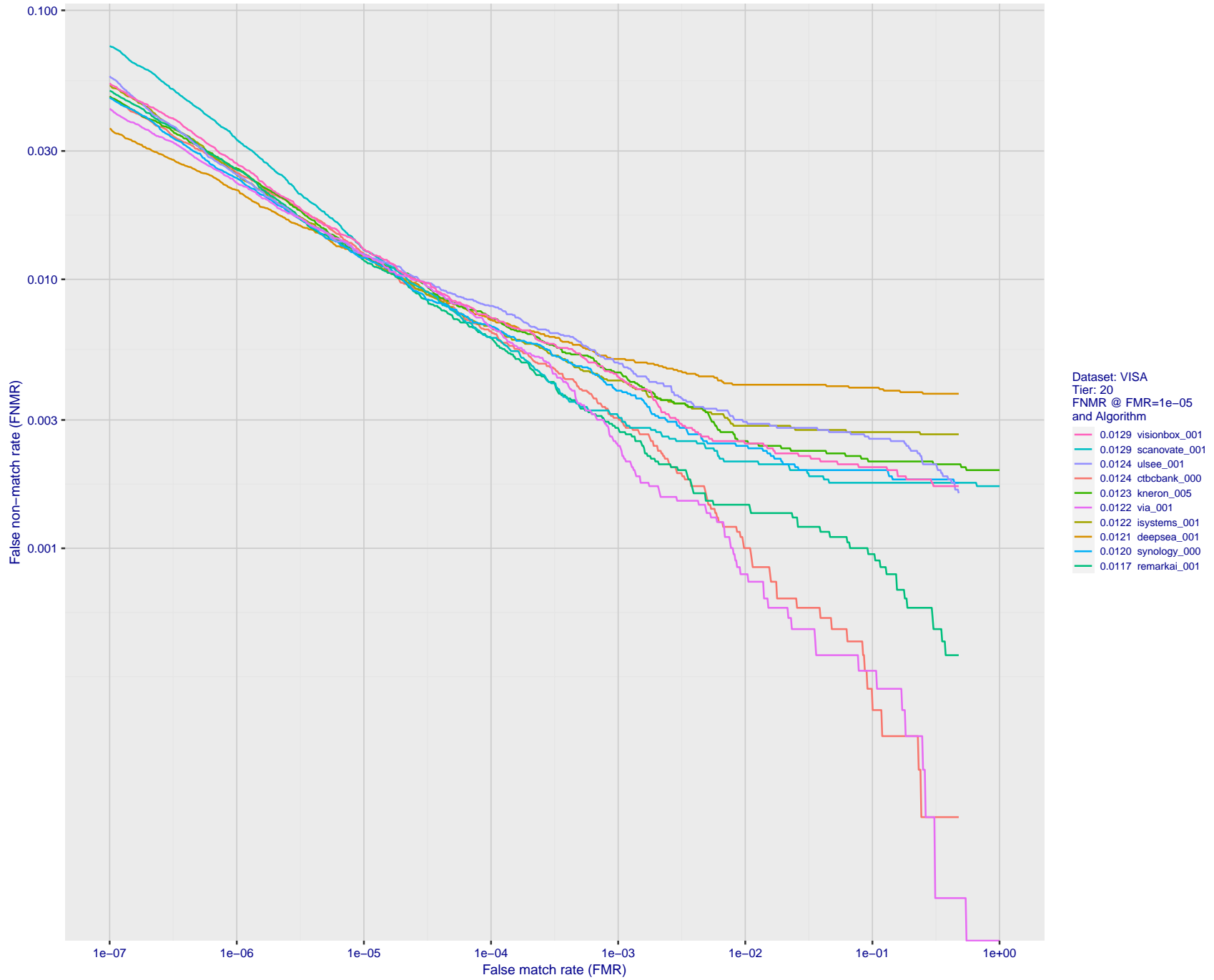


Figure 37: For the visa images, detection error tradeoff (DET) characteristics showing false non-match rate vs. false match rate plotted parametrically on threshold, T . The scales are logarithmic in order to show many decades of FMR.

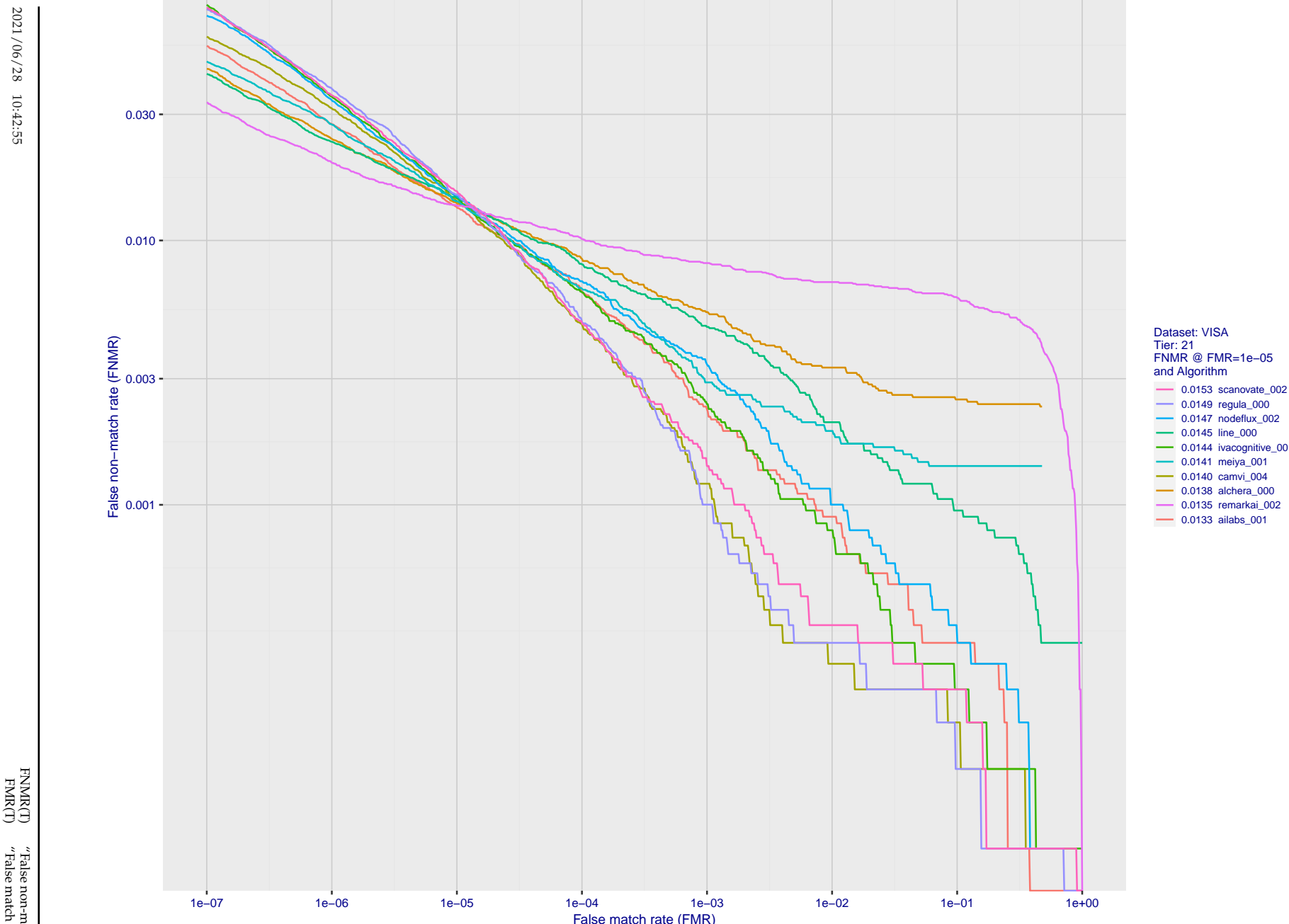


Figure 38: For the visa images, detection error tradeoff (DET) characteristics showing false non-match rate vs. false match rate plotted parametrically on threshold, T . The scales are logarithmic in order to show many decades of FMR.

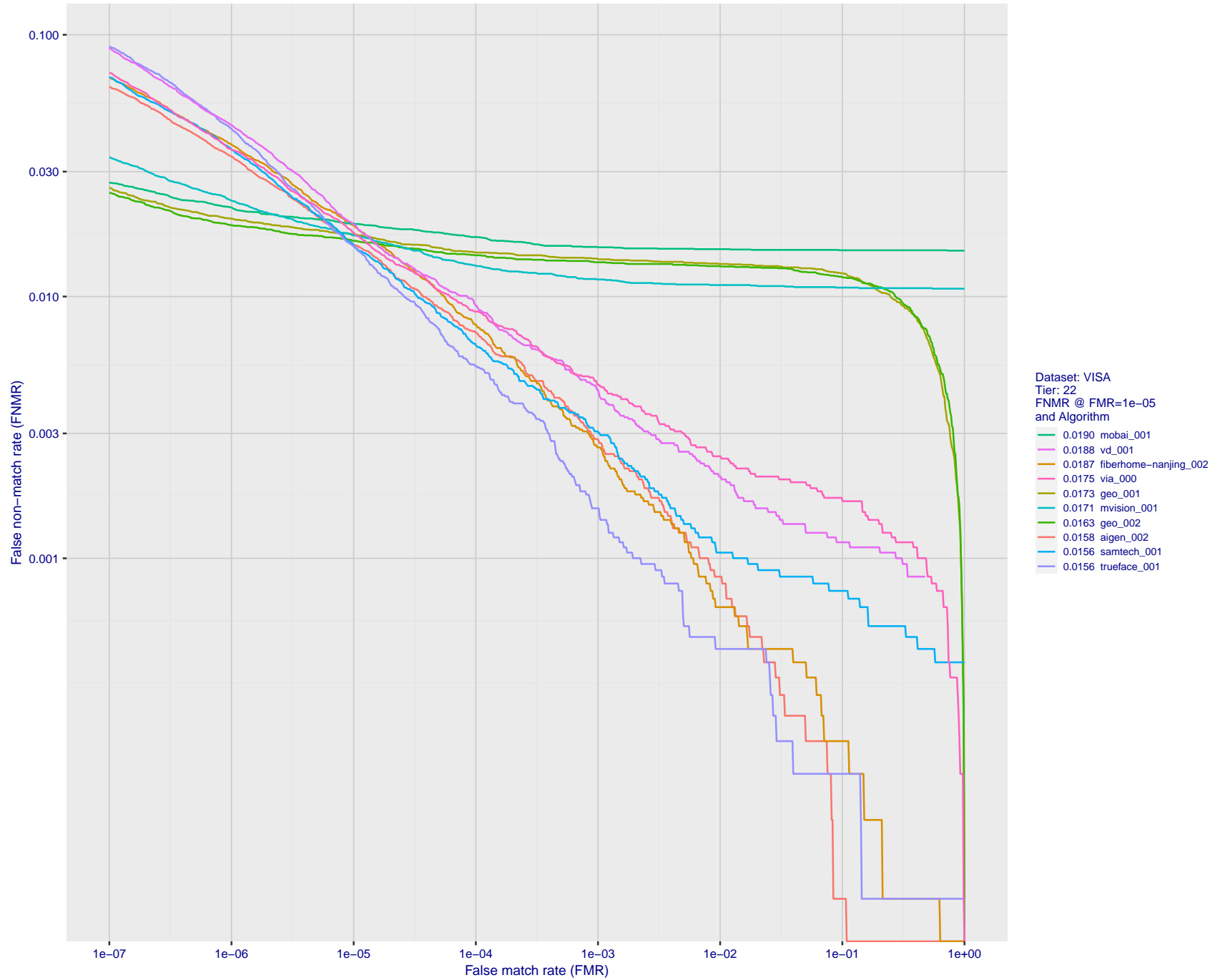


Figure 39: For the visa images, detection error tradeoff (DET) characteristics showing false non-match rate vs. false match rate plotted parametrically on threshold, T . The scales are logarithmic in order to show many decades of FMR.

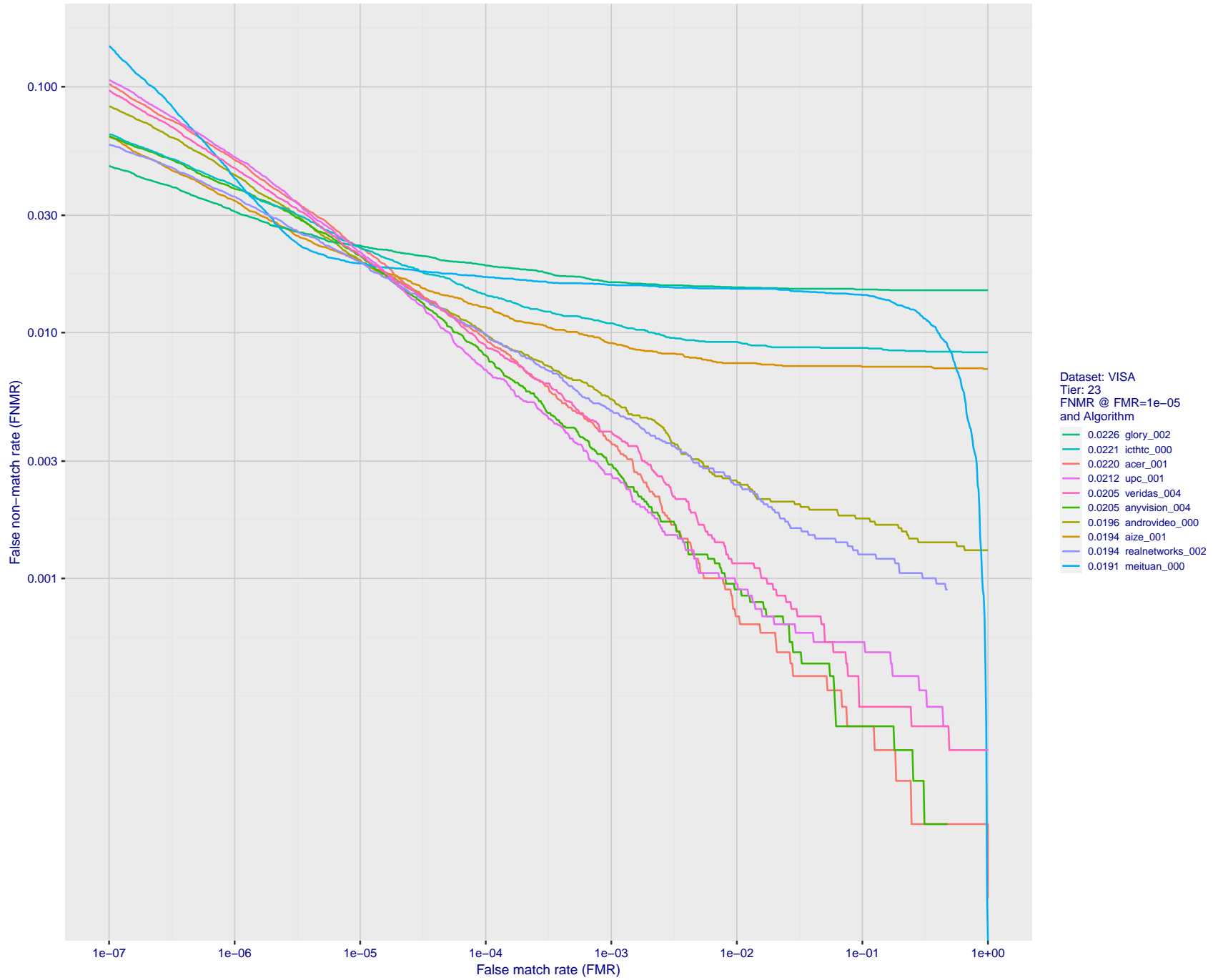


Figure 40: For the visa images, detection error tradeoff (DET) characteristics showing false non-match rate vs. false match rate plotted parametrically on threshold, T . The scales are logarithmic in order to show many decades of FMR.

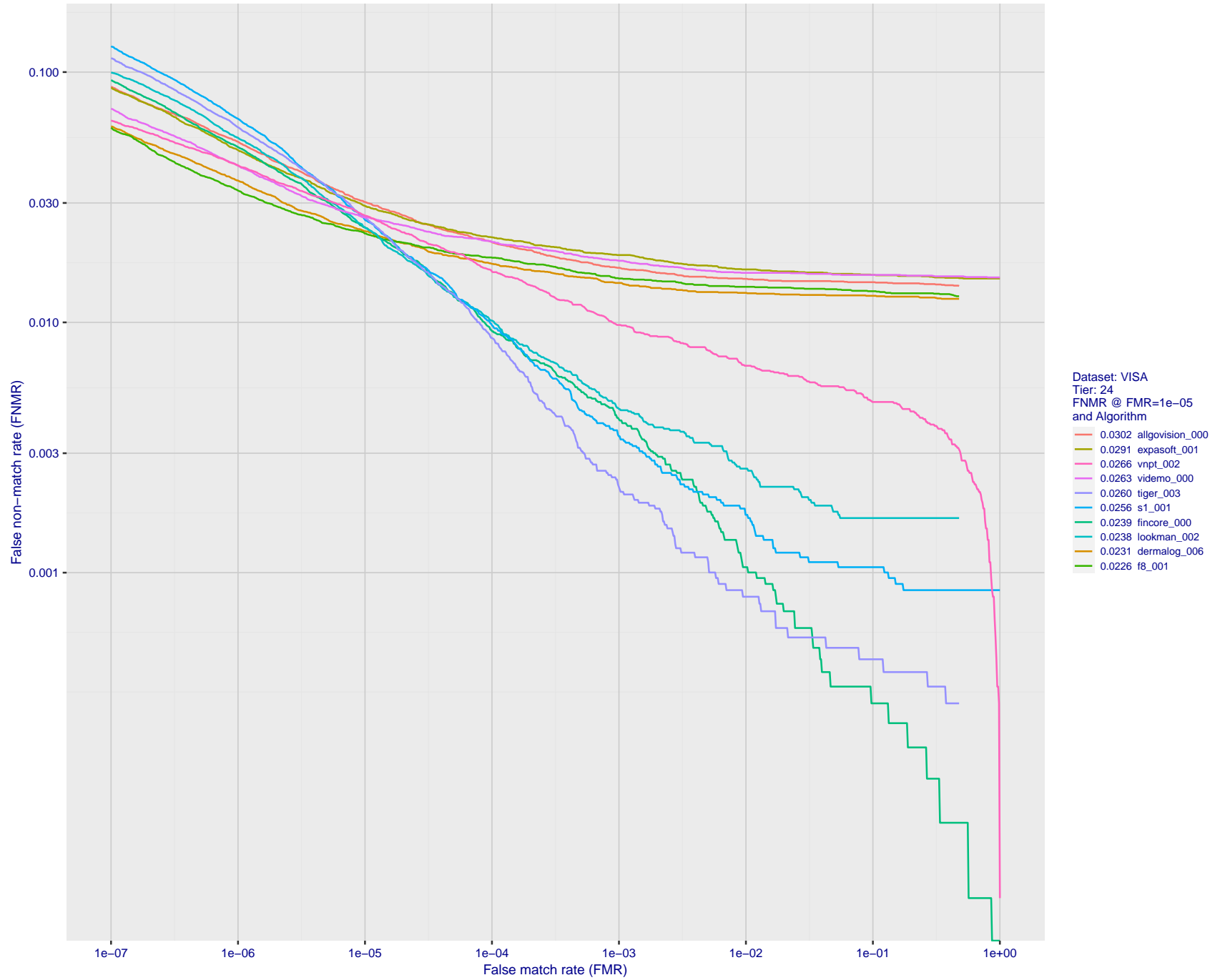


Figure 41: For the visa images, detection error tradeoff (DET) characteristics showing false non-match rate vs. false match rate plotted parametrically on threshold, T . The scales are logarithmic in order to show many decades of FMR.

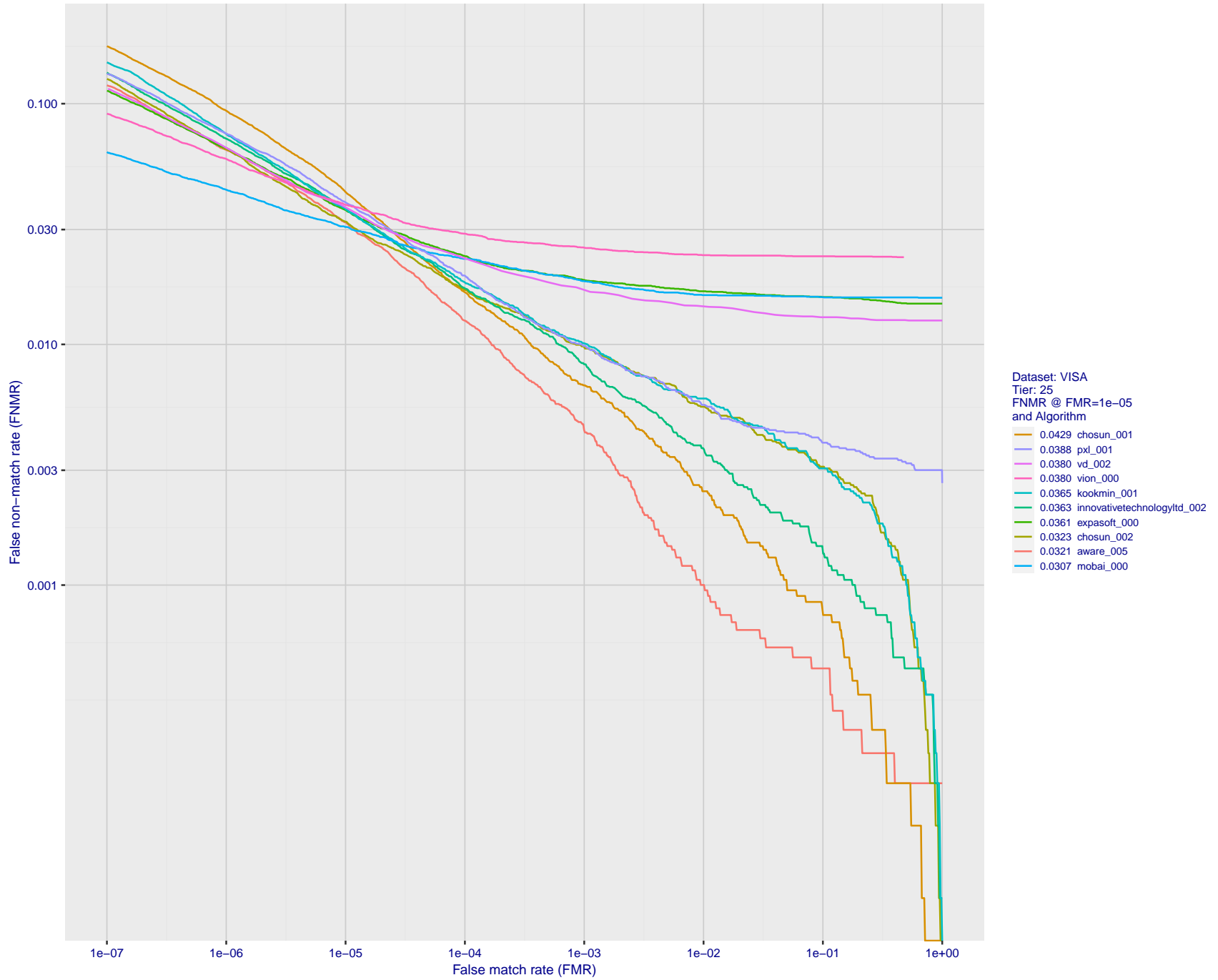


Figure 42: For the visa images, detection error tradeoff (DET) characteristics showing false non-match rate vs. false match rate plotted parametrically on threshold, T . The scales are logarithmic in order to show many decades of FMR.

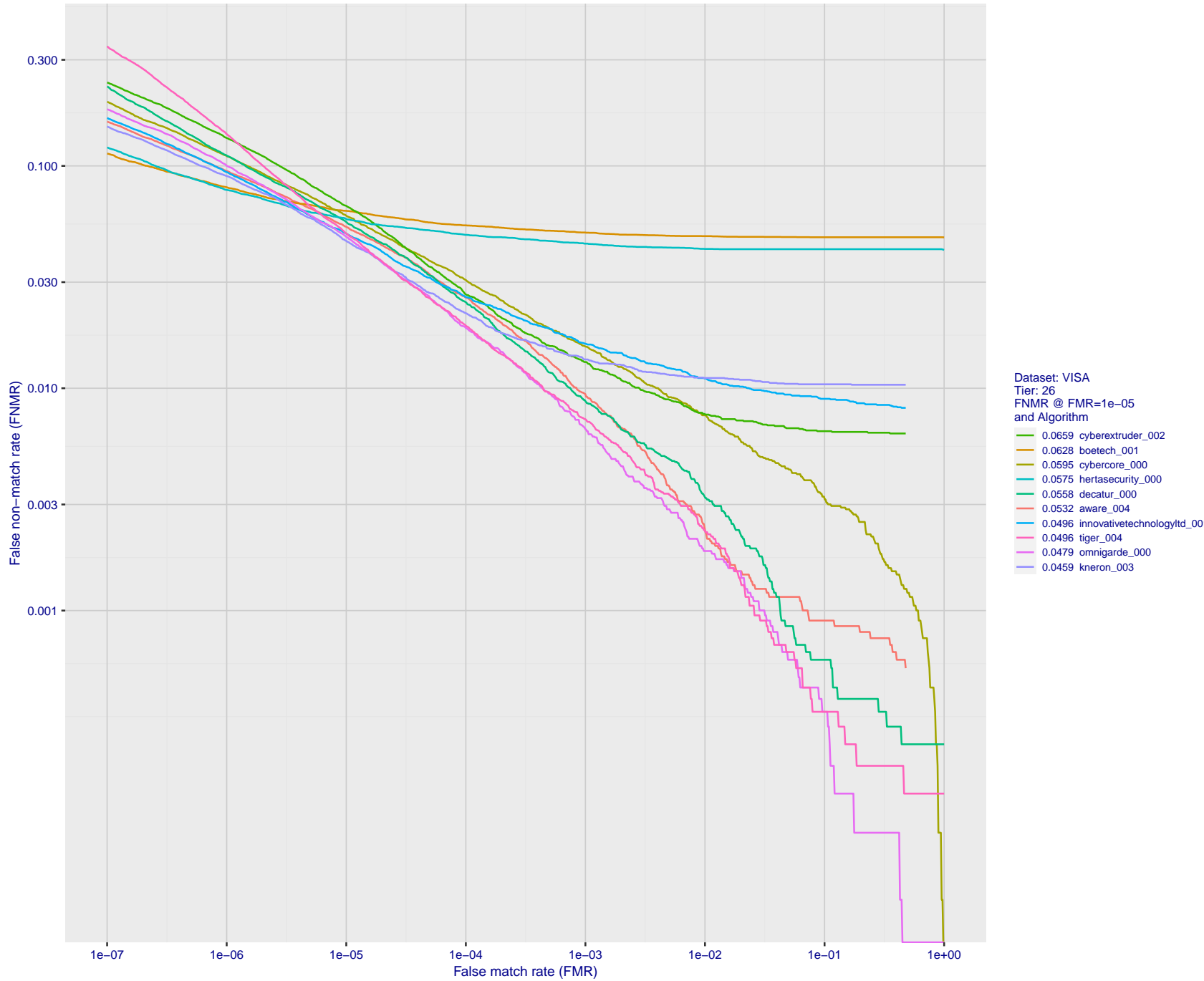


Figure 43: For the visa images, detection error tradeoff (DET) characteristics showing false non-match rate vs. false match rate plotted parametrically on threshold, T . The scales are logarithmic in order to show many decades of FMR.

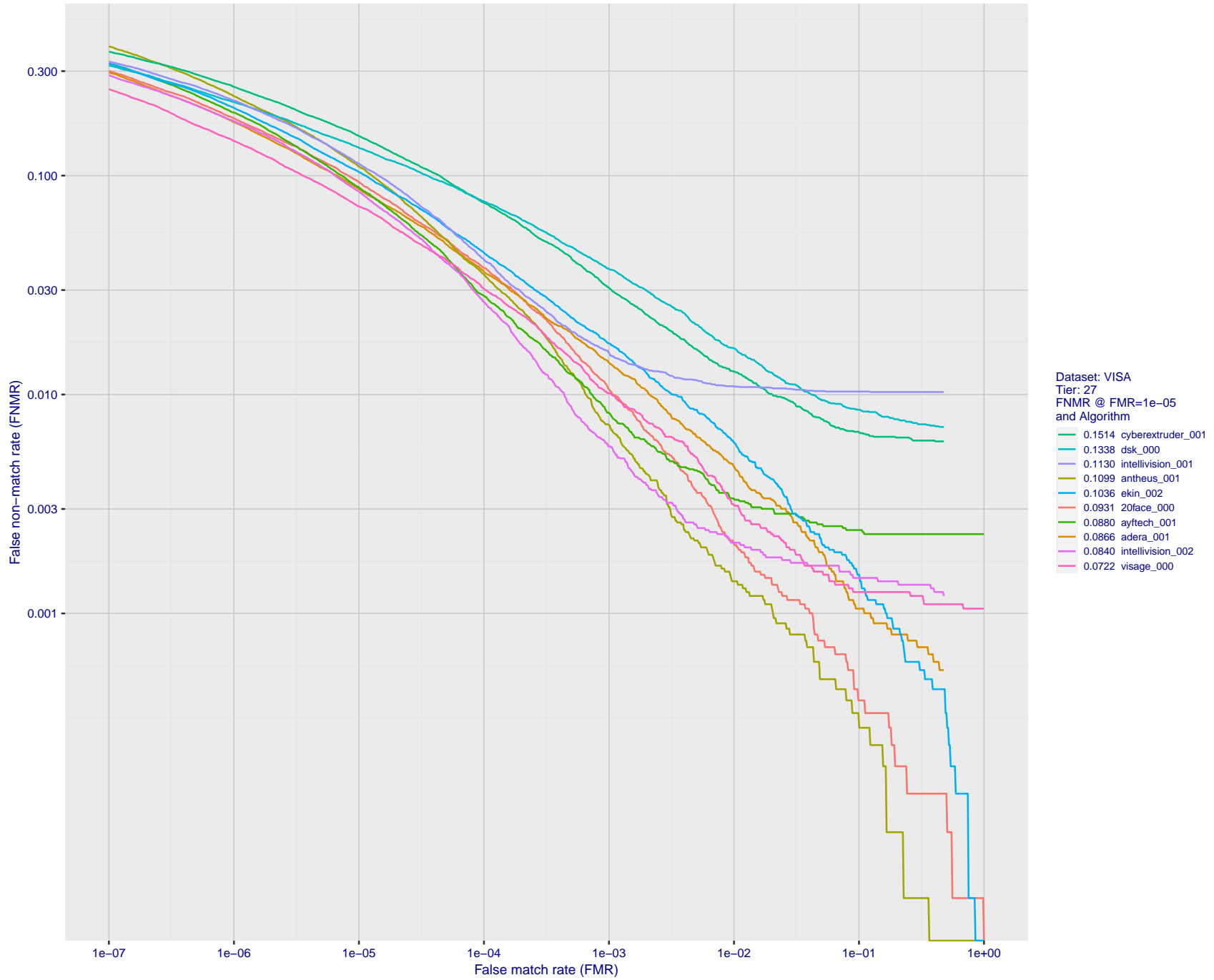


Figure 44: For the visa images, detection error tradeoff (DET) characteristics showing false non-match rate vs. false match rate plotted parametrically on threshold, T . The scales are logarithmic in order to show many decades of FMR.

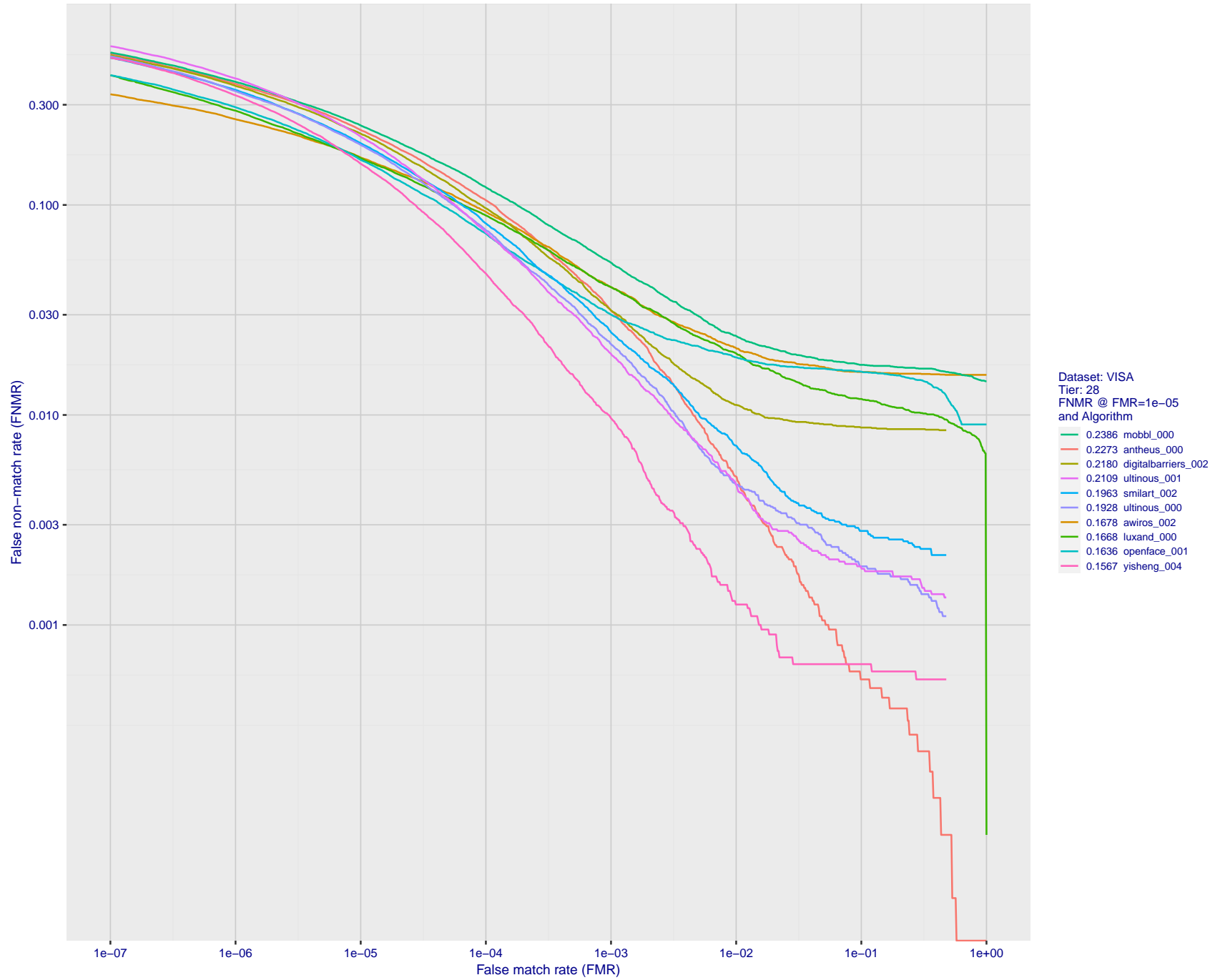


Figure 45: For the visa images, detection error tradeoff (DET) characteristics showing false non-match rate vs. false match rate plotted parametrically on threshold, T . The scales are logarithmic in order to show many decades of FMR.

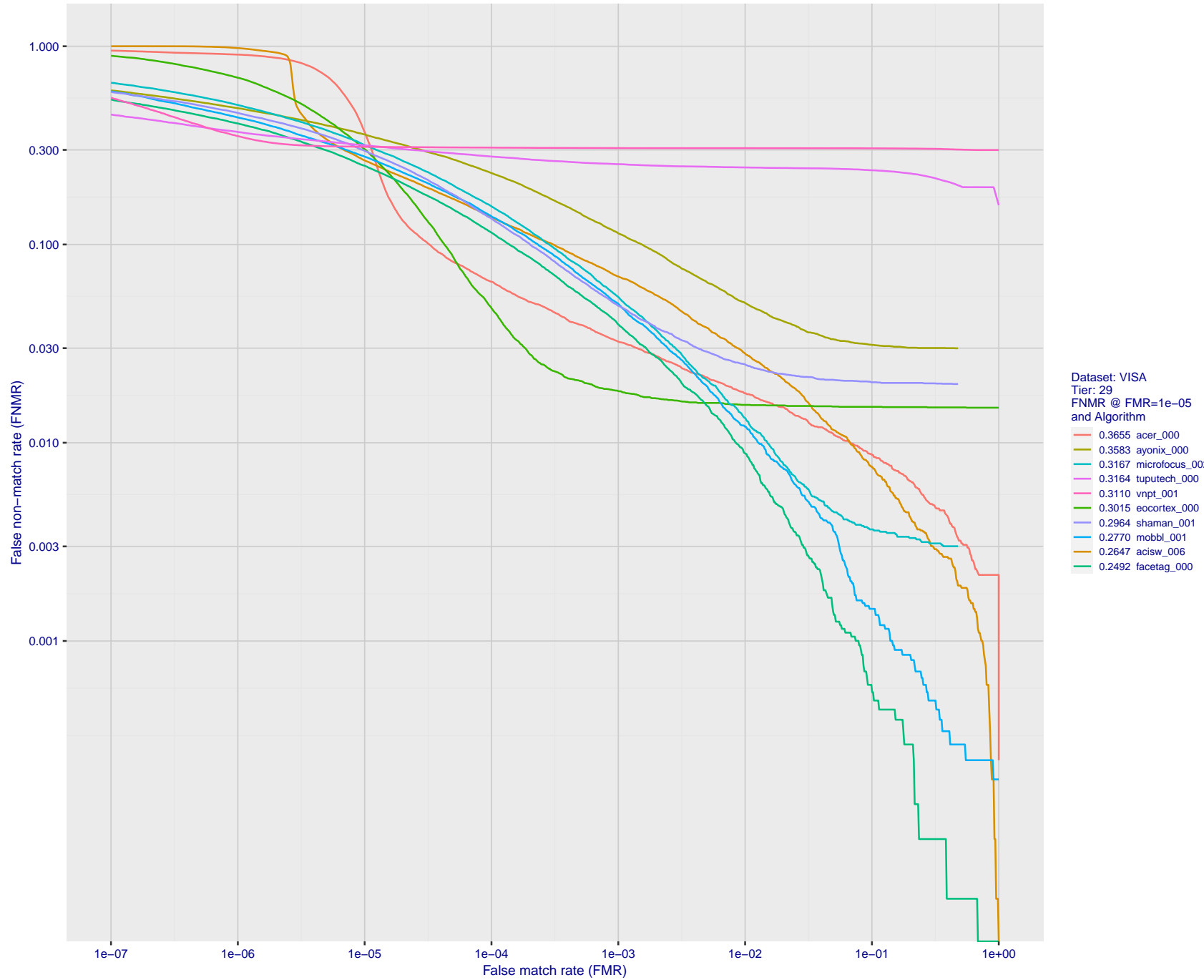


Figure 46: For the visa images, detection error tradeoff (DET) characteristics showing false non-match rate vs. false match rate plotted parametrically on threshold, T . The scales are logarithmic in order to show many decades of FMR.

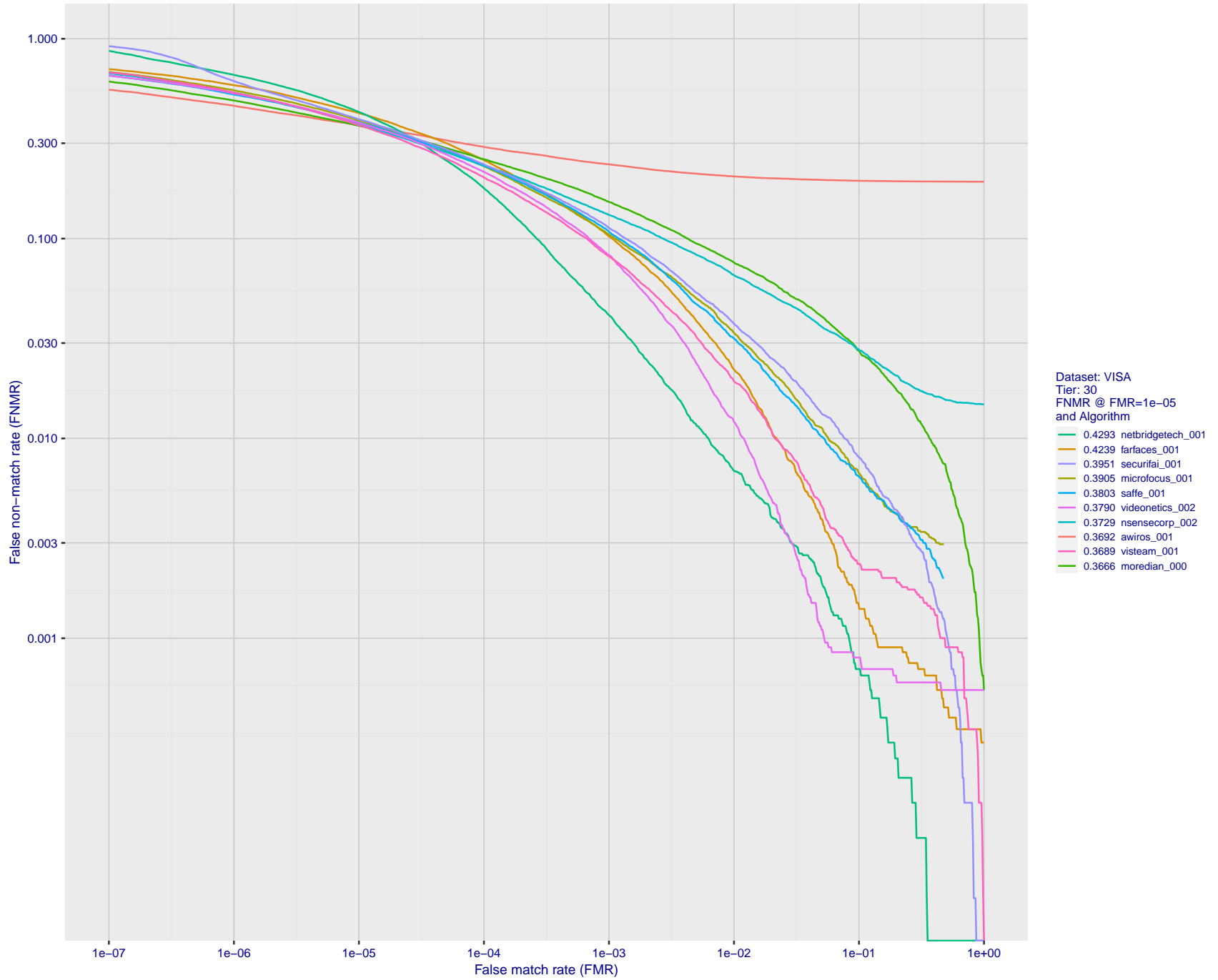


Figure 47: For the visa images, detection error tradeoff (DET) characteristics showing false non-match rate vs. false match rate plotted parametrically on threshold, T . The scales are logarithmic in order to show many decades of FMR.

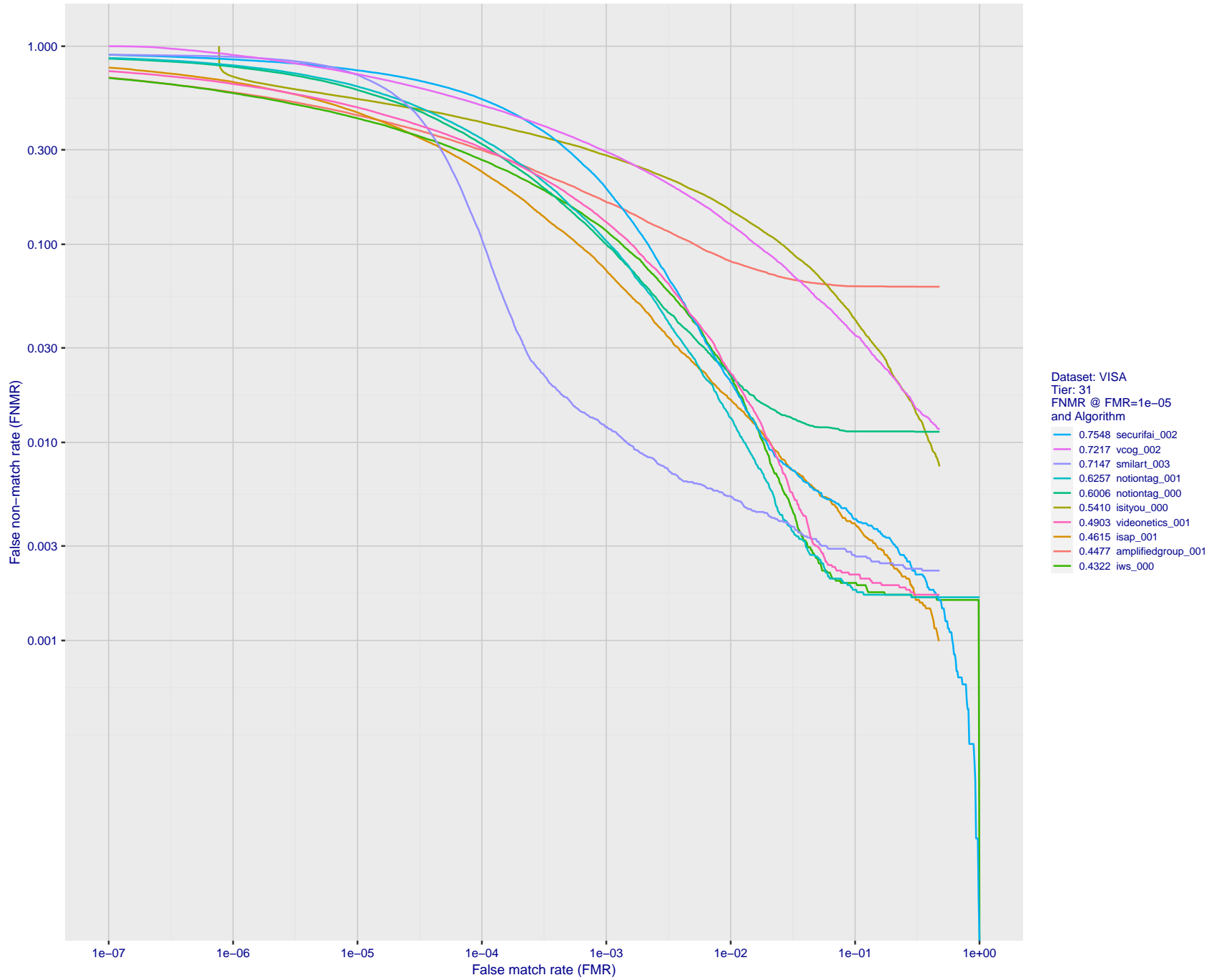


Figure 48: For the visa images, detection error tradeoff (DET) characteristics showing false non-match rate vs. false match rate plotted parametrically on threshold, T . The scales are logarithmic in order to show many decades of FMR.

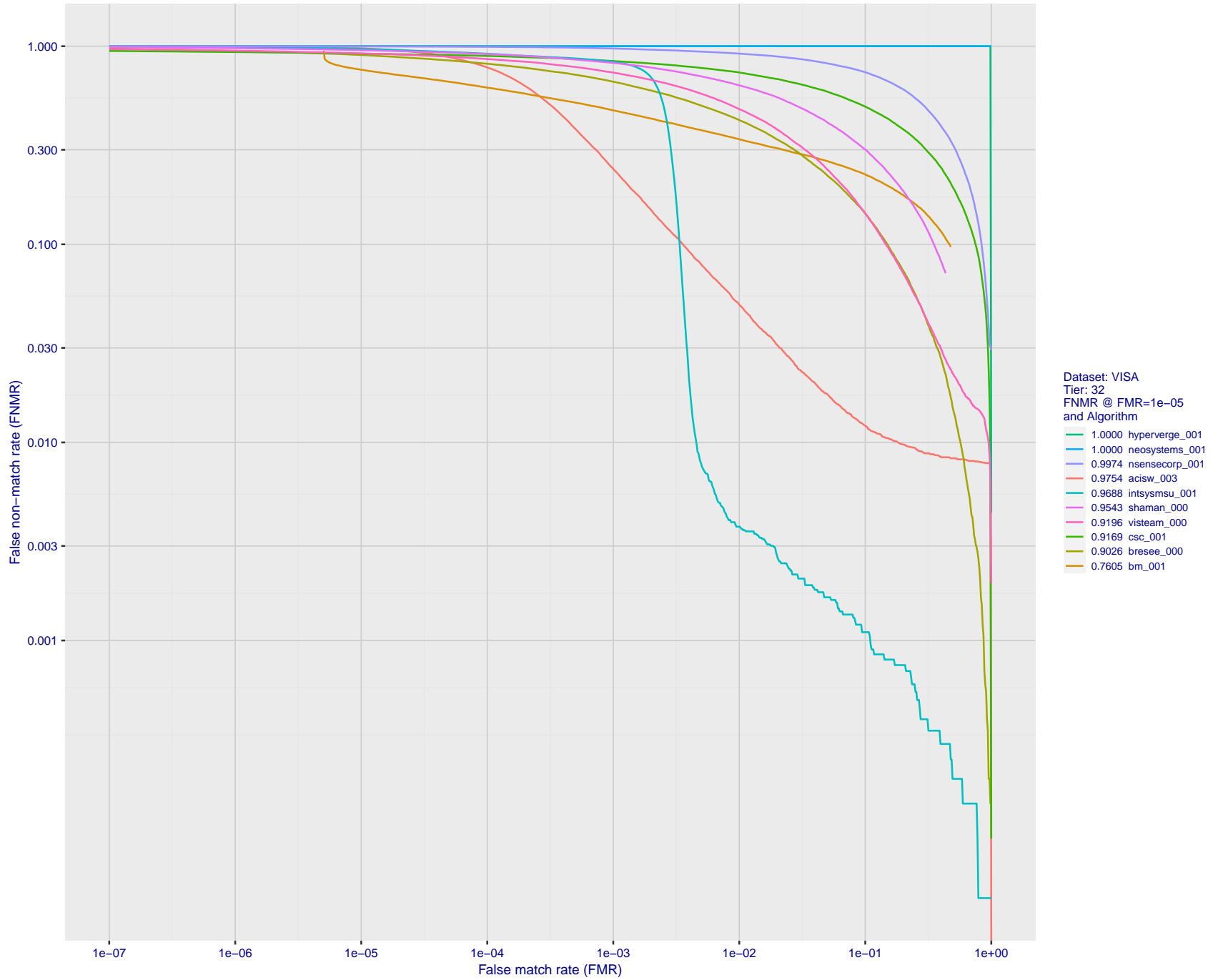


Figure 49: For the visa images, detection error tradeoff (DET) characteristics showing false non-match rate vs. false match rate plotted parametrically on threshold, T . The scales are logarithmic in order to show many decades of FMR.

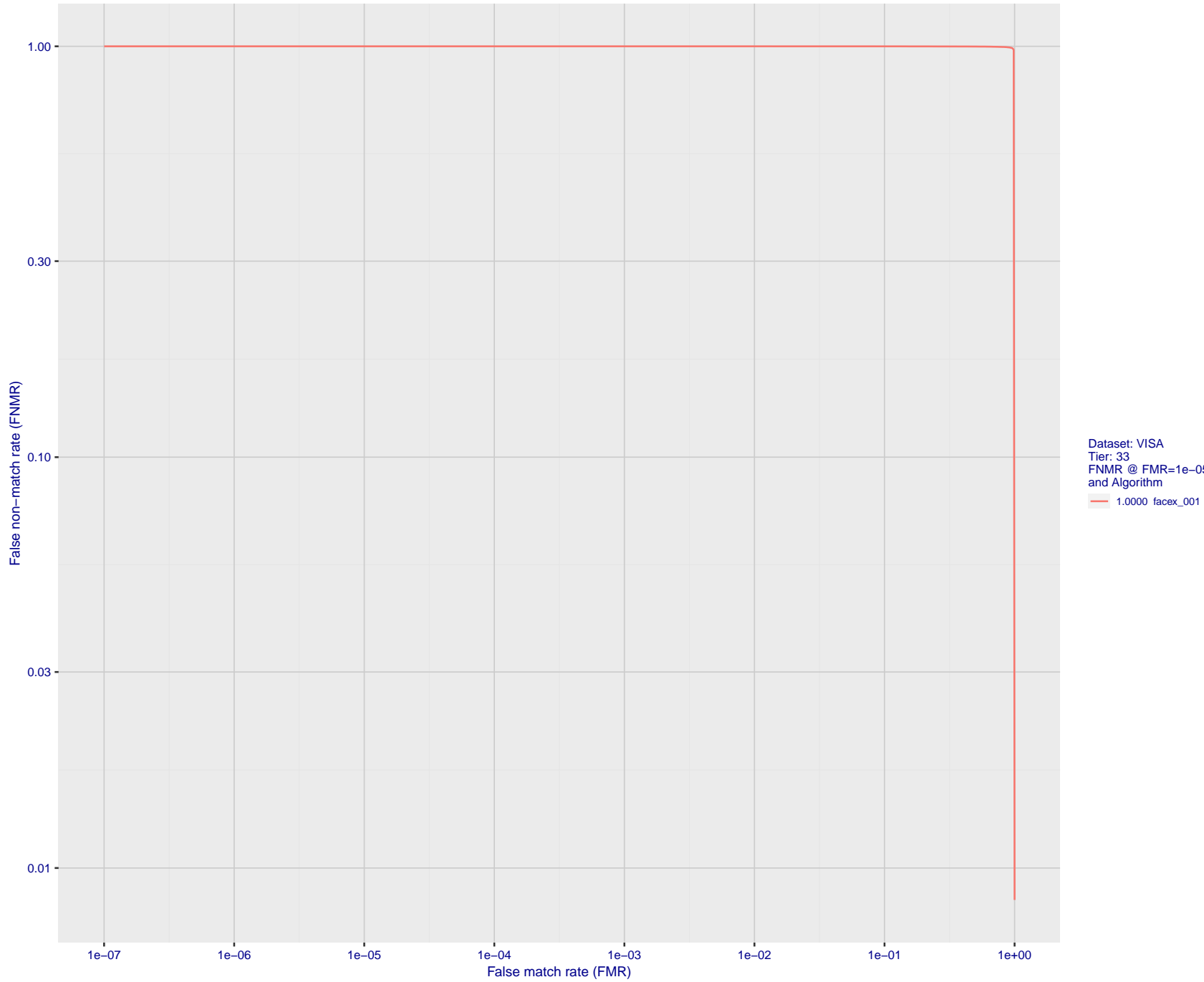


Figure 50: For the visa images, detection error tradeoff (DET) characteristics showing false non-match rate vs. false match rate plotted parametrically on threshold, T . The scales are logarithmic in order to show many decades of FMR.

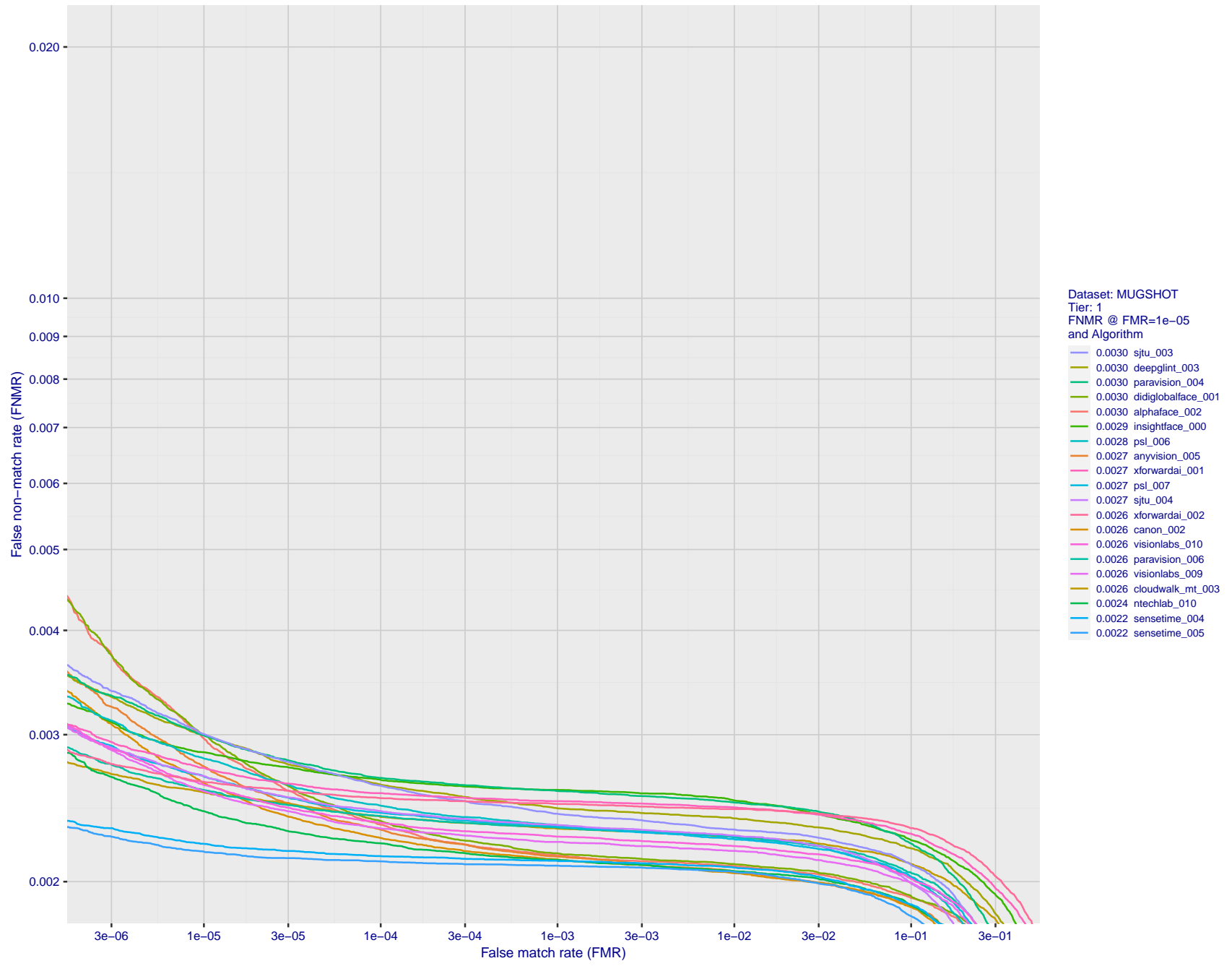


Figure 51: For the mugshot images, detection error tradeoff (DET) characteristics showing false non-match rate vs. false match rate plotted parametrically on threshold, T . The scales are logarithmic in order to show decades of FMR.

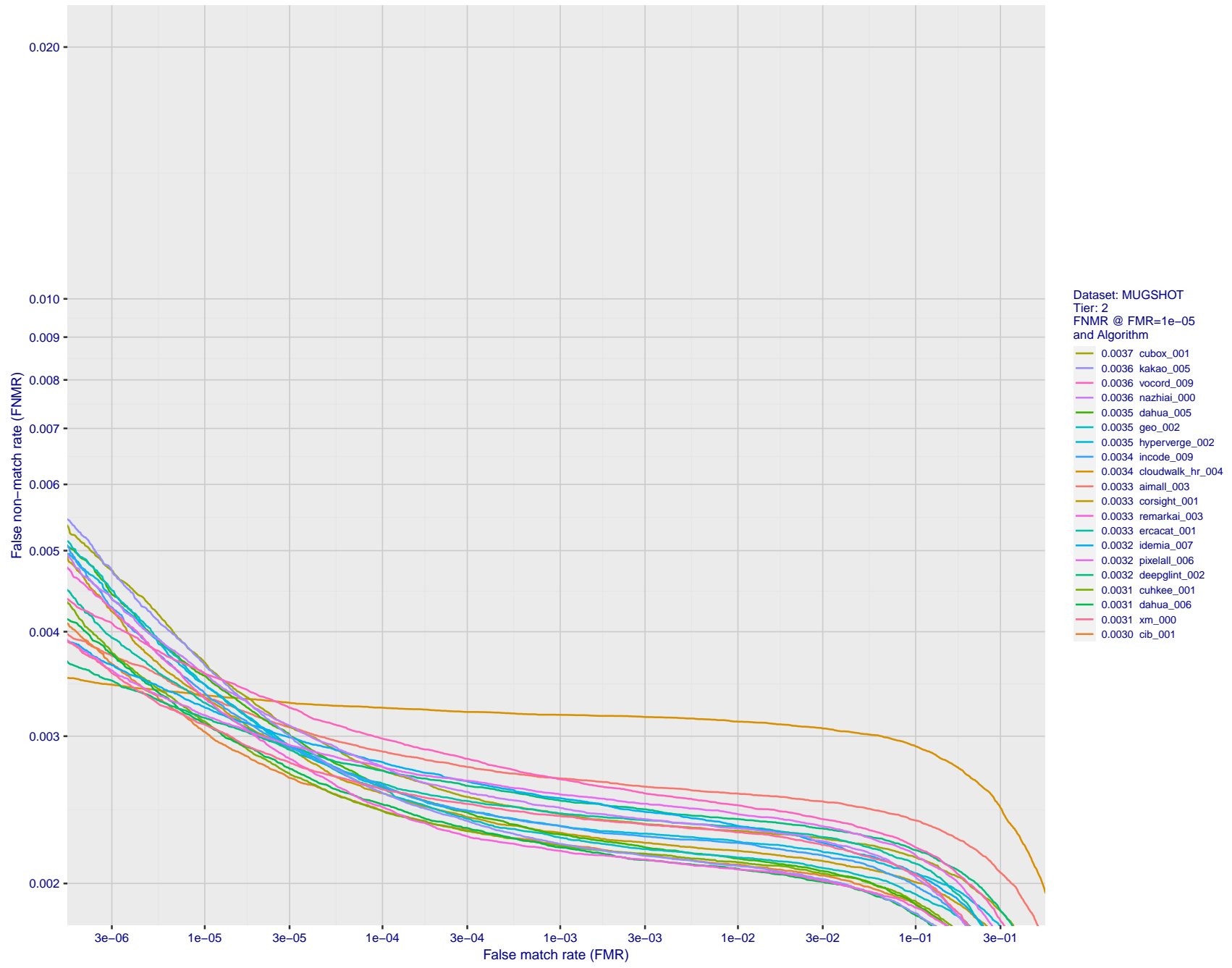


Figure 52: For the mugshot images, detection error tradeoff (DET) characteristics showing false non-match rate vs. false match rate plotted parametrically on threshold, T . The scales are logarithmic in order to show decades of FMR.

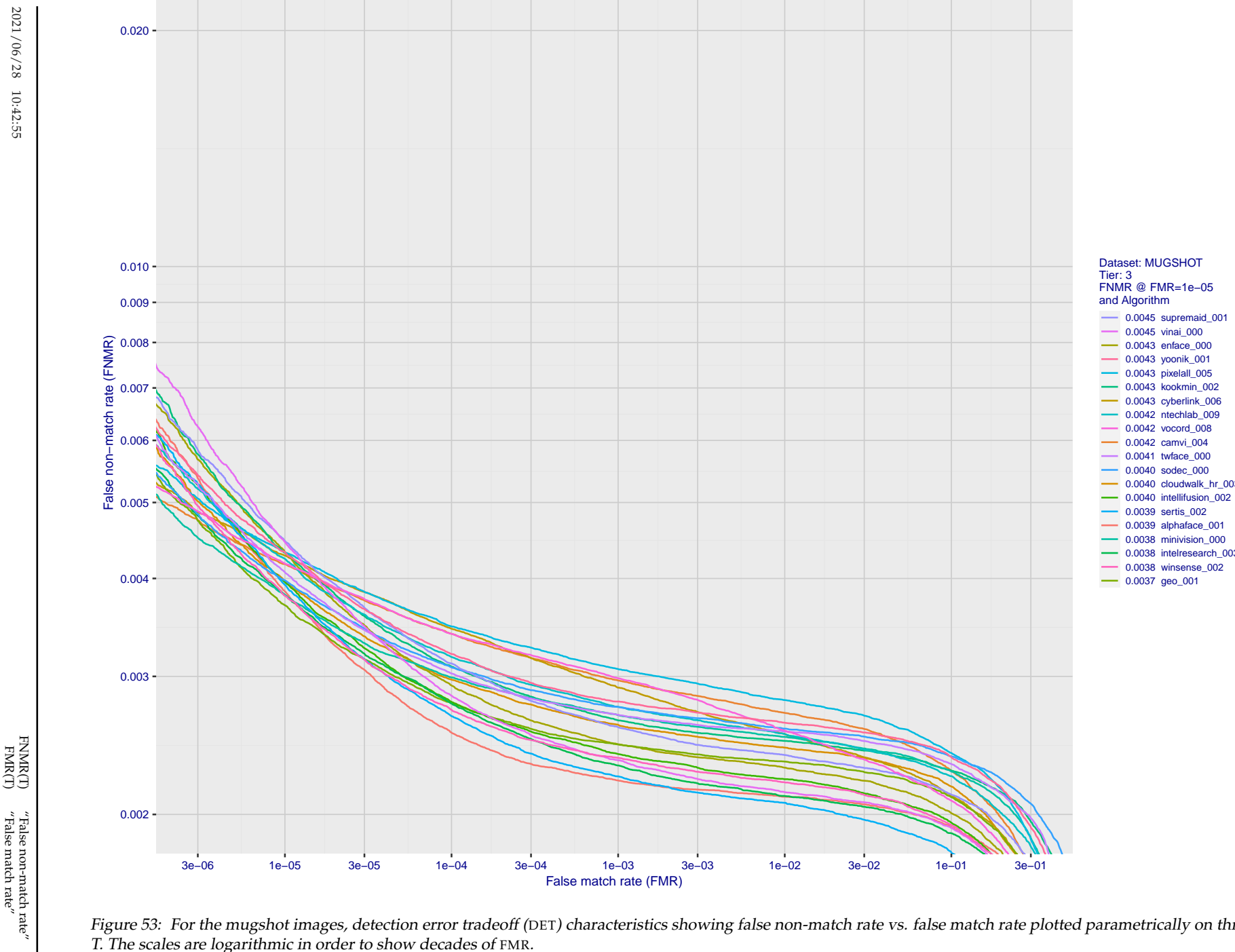


Figure 53: For the mugshot images, detection error tradeoff (DET) characteristics showing false non-match rate vs. false match rate plotted parametrically on threshold, T . The scales are logarithmic in order to show decades of FMR.

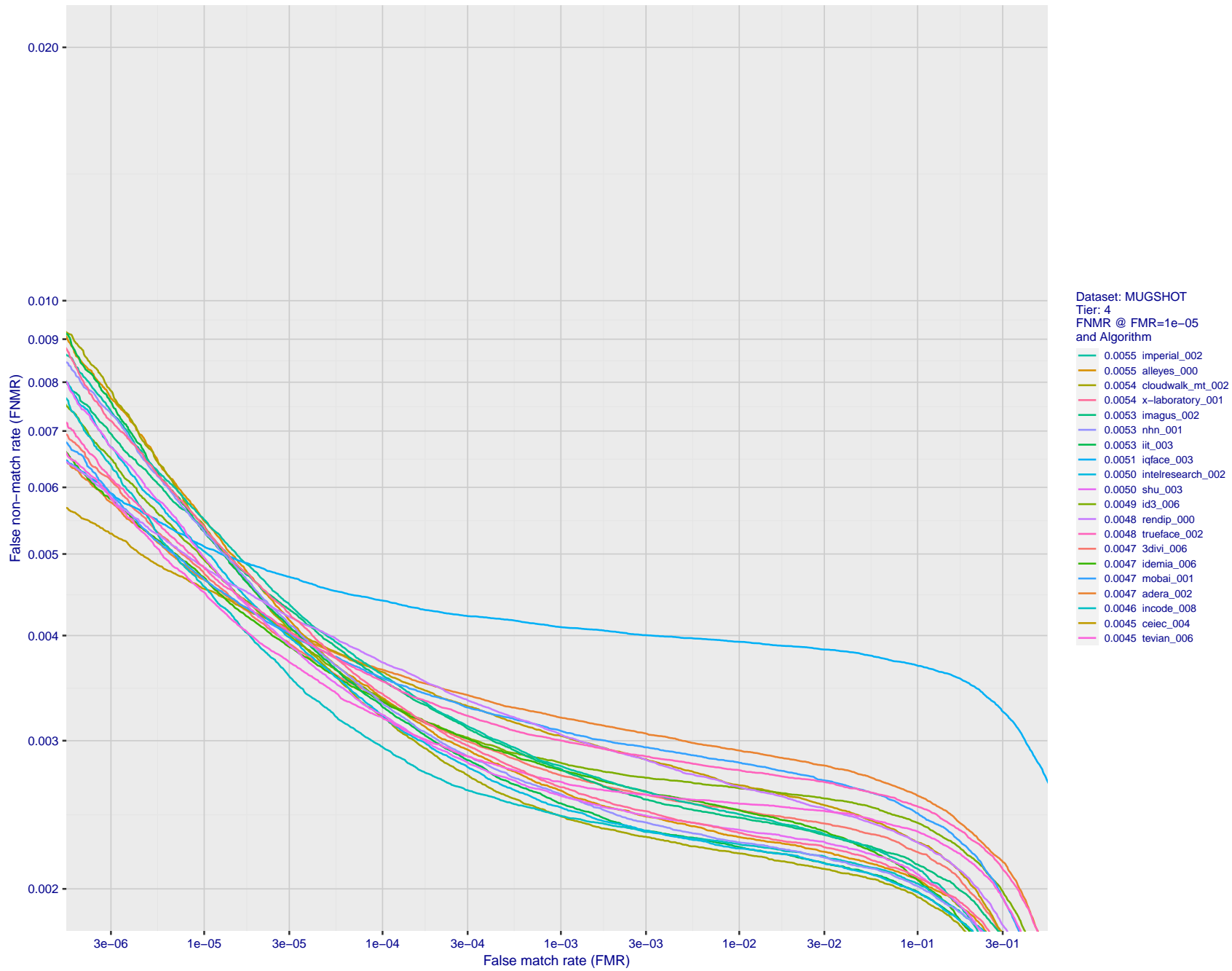


Figure 54: For the mugshot images, detection error tradeoff (DET) characteristics showing false non-match rate vs. false match rate plotted parametrically on threshold, T . The scales are logarithmic in order to show decades of FMR.

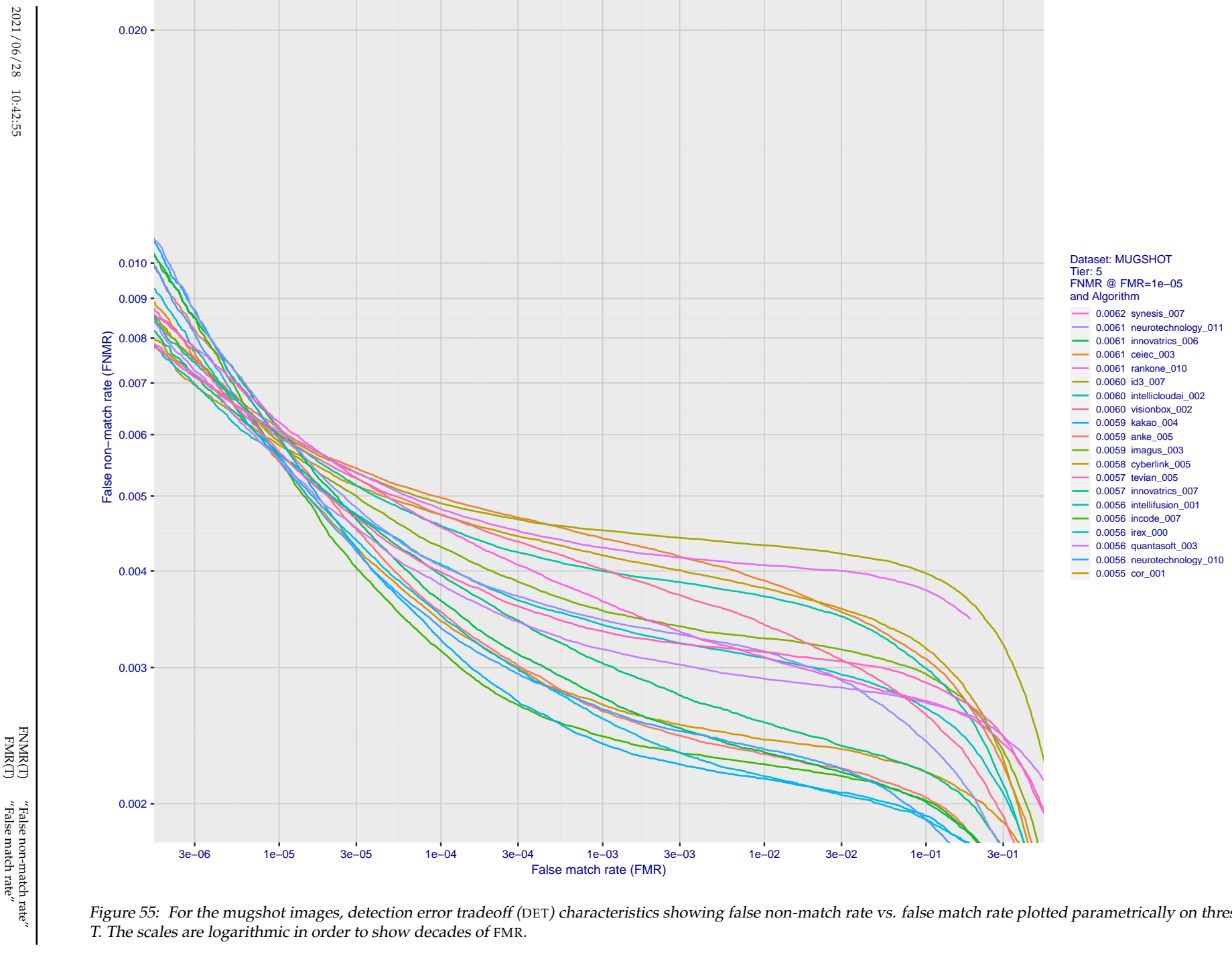


Figure 55: For the mugshot images, detection error tradeoff (DET) characteristics showing false non-match rate vs. false match rate plotted parametrically on threshold, T . The scales are logarithmic in order to show decades of FMR.

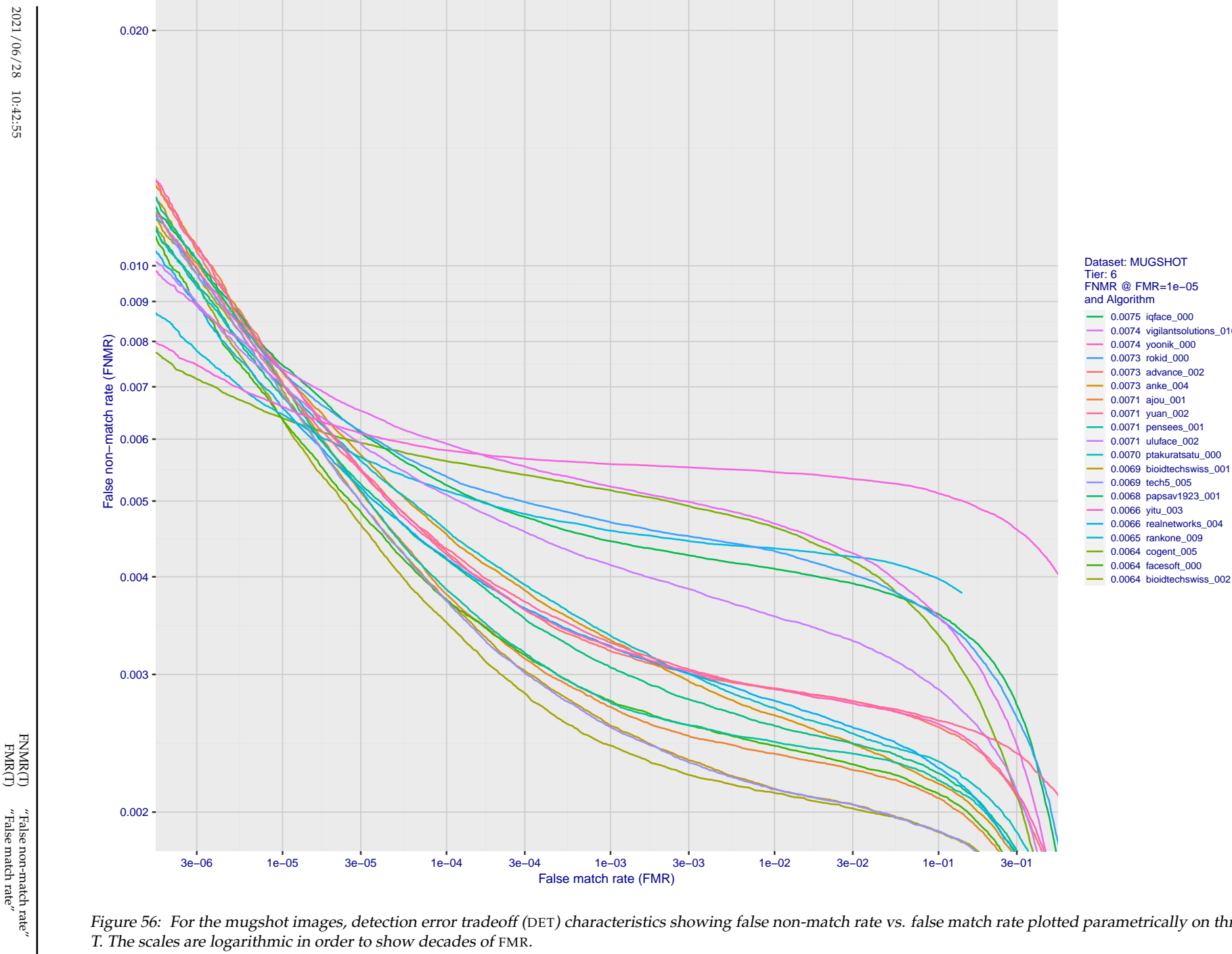


Figure 56: For the mugshot images, detection error tradeoff (DET) characteristics showing false non-match rate vs. false match rate plotted parametrically on threshold, T . The scales are logarithmic in order to show decades of FMR.

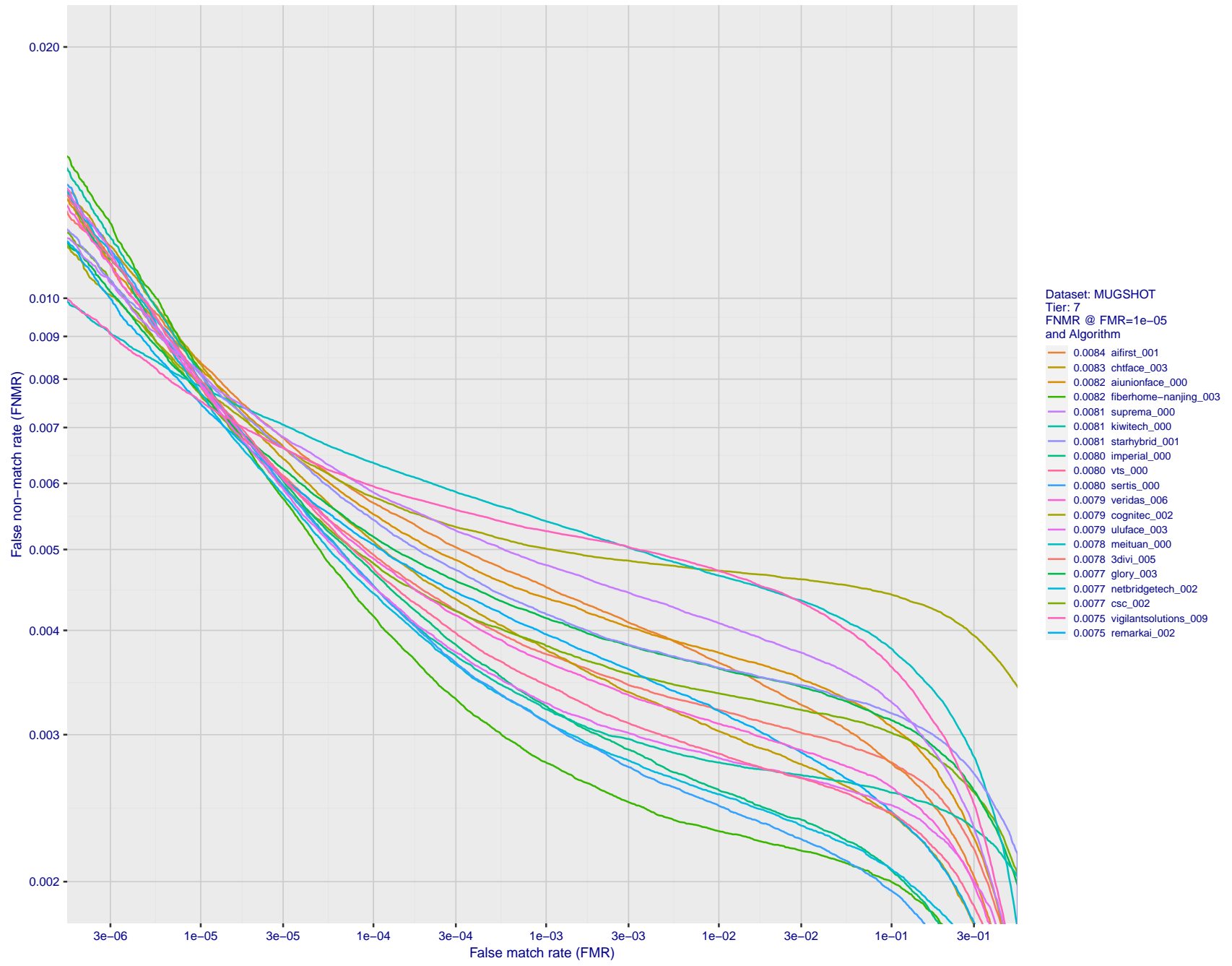
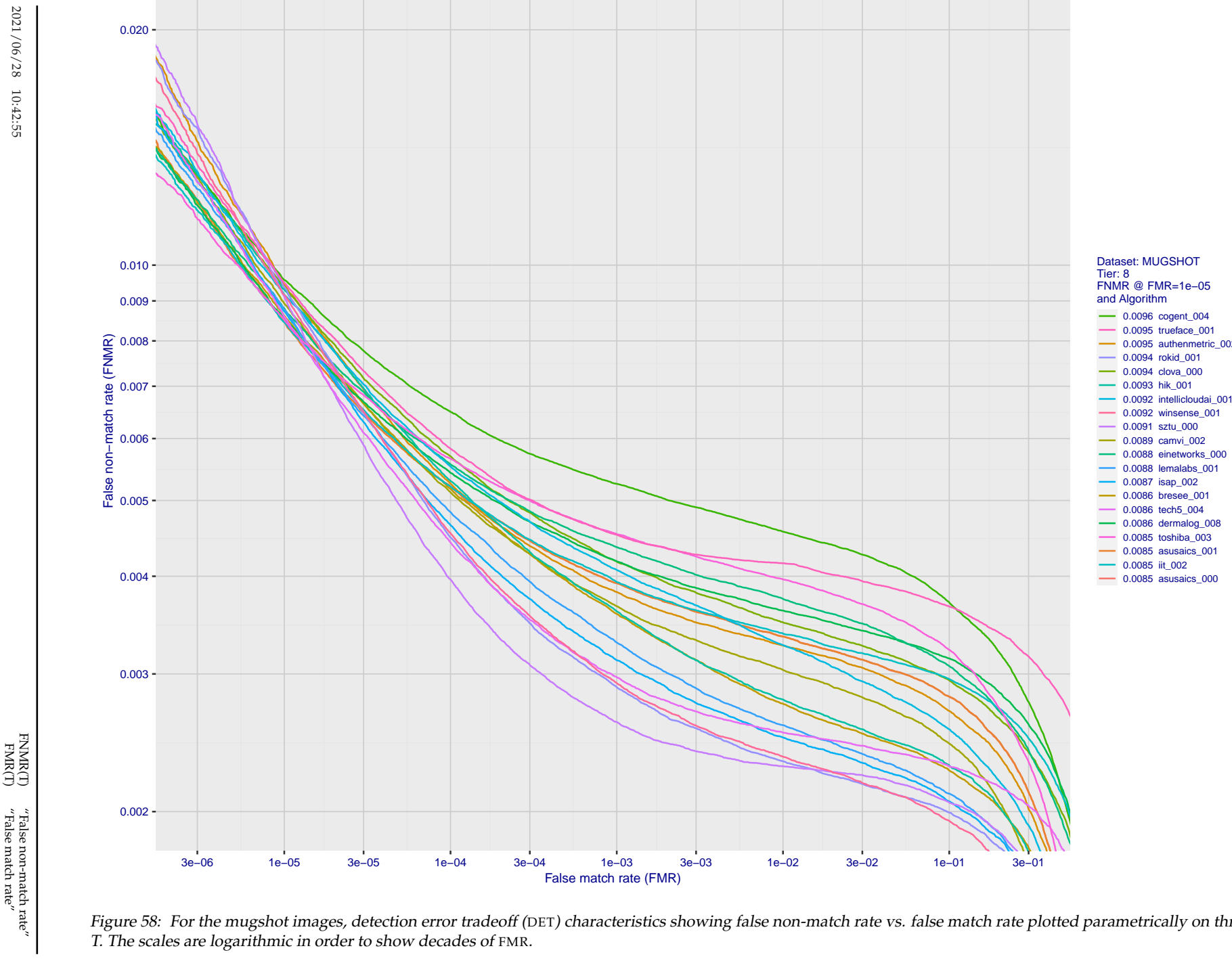


Figure 57: For the mugshot images, detection error tradeoff (DET) characteristics showing false non-match rate vs. false match rate plotted parametrically on threshold, T . The scales are logarithmic in order to show decades of FMR.



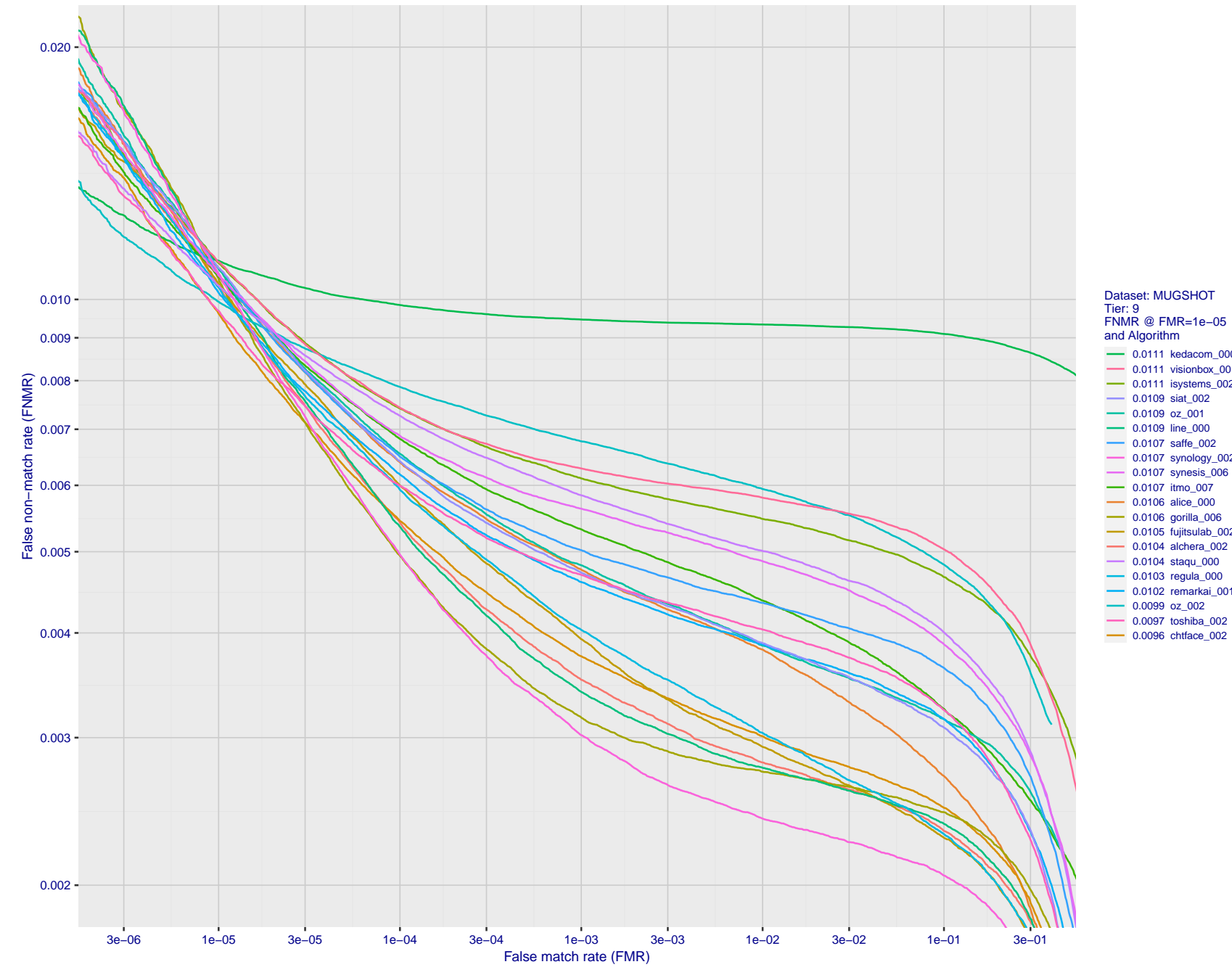


Figure 59: For the mugshot images, detection error tradeoff (DET) characteristics showing false non-match rate vs. false match rate plotted parametrically on threshold, T . The scales are logarithmic in order to show decades of FMR.

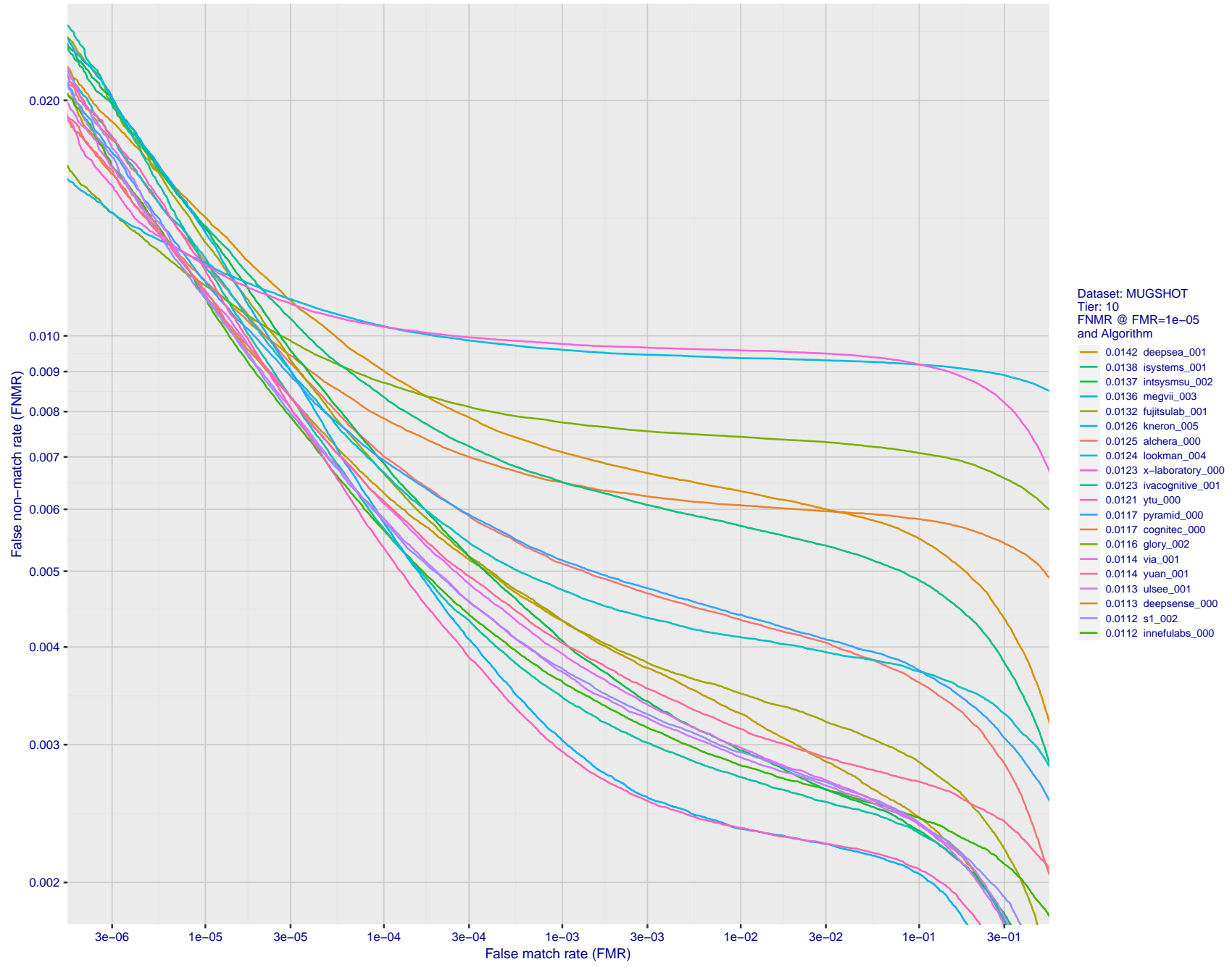


Figure 60: For the mugshot images, detection error tradeoff (DET) characteristics showing false non-match rate vs. false match rate plotted parametrically on threshold, T . The scales are logarithmic in order to show decades of FMR.

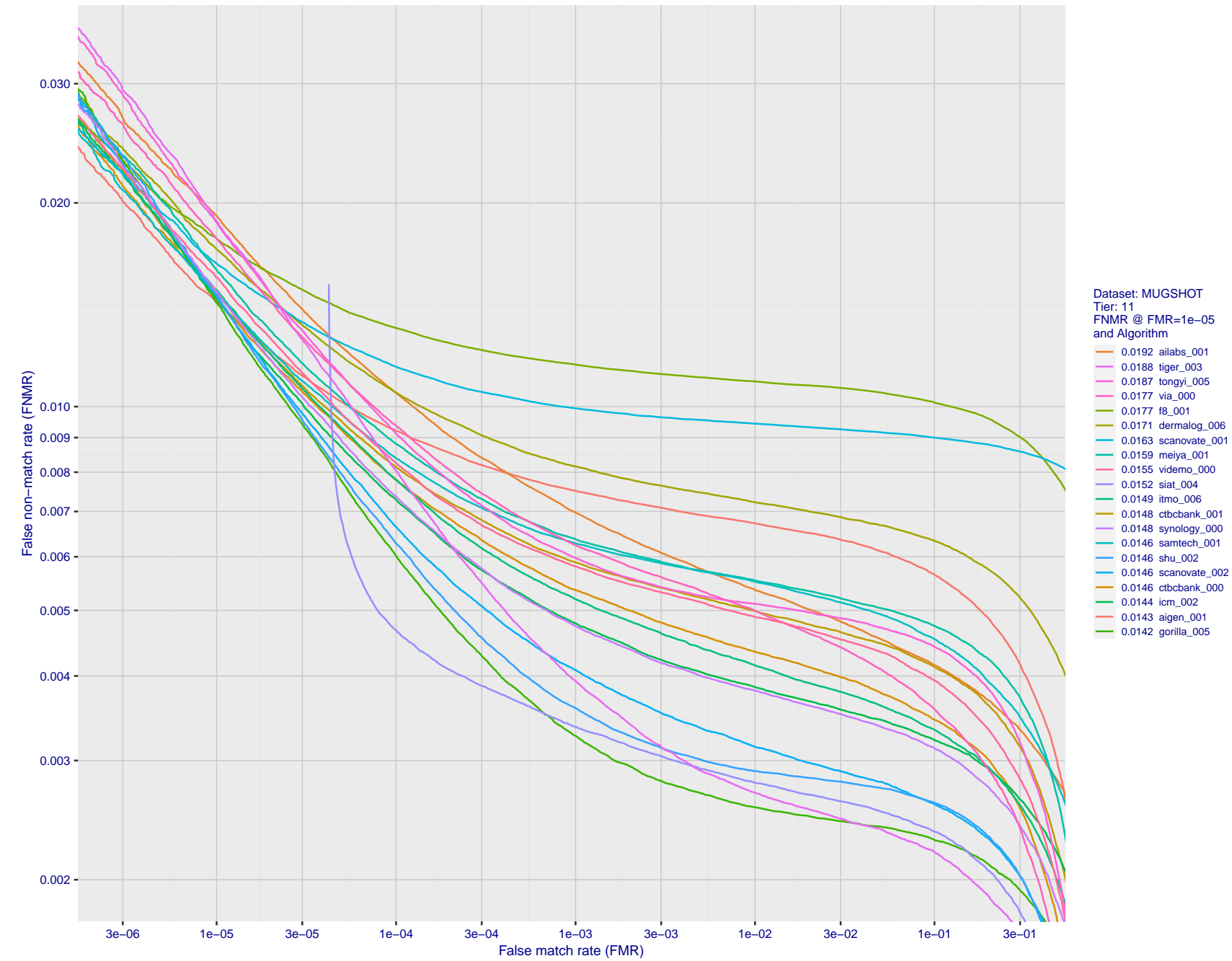


Figure 61: For the mugshot images, detection error tradeoff (DET) characteristics showing false non-match rate vs. false match rate plotted parametrically on threshold, T . The scales are logarithmic in order to show decades of FMR.

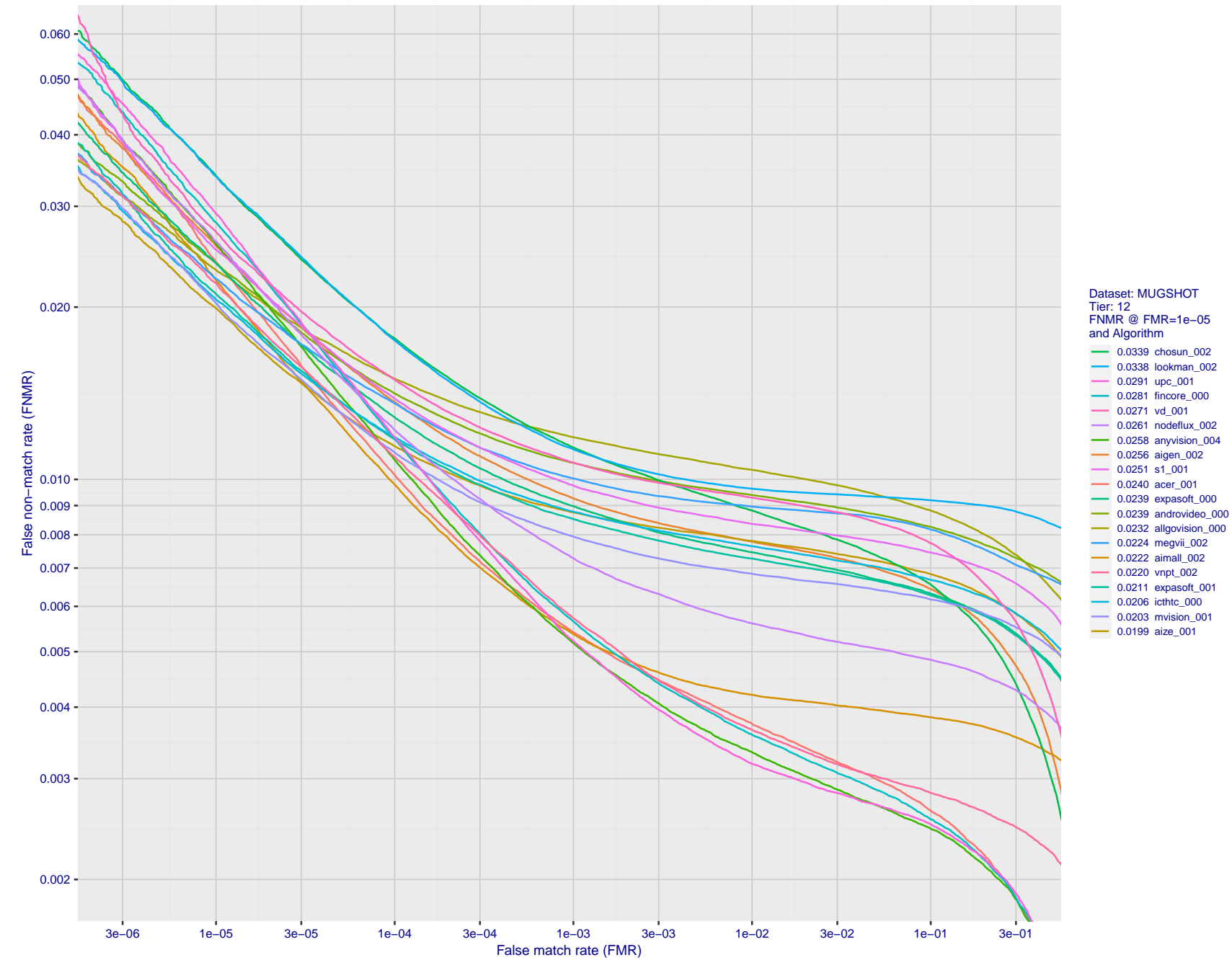


Figure 62: For the mugshot images, detection error tradeoff (DET) characteristics showing false non-match rate vs. false match rate plotted parametrically on threshold, T . The scales are logarithmic in order to show decades of FMR.

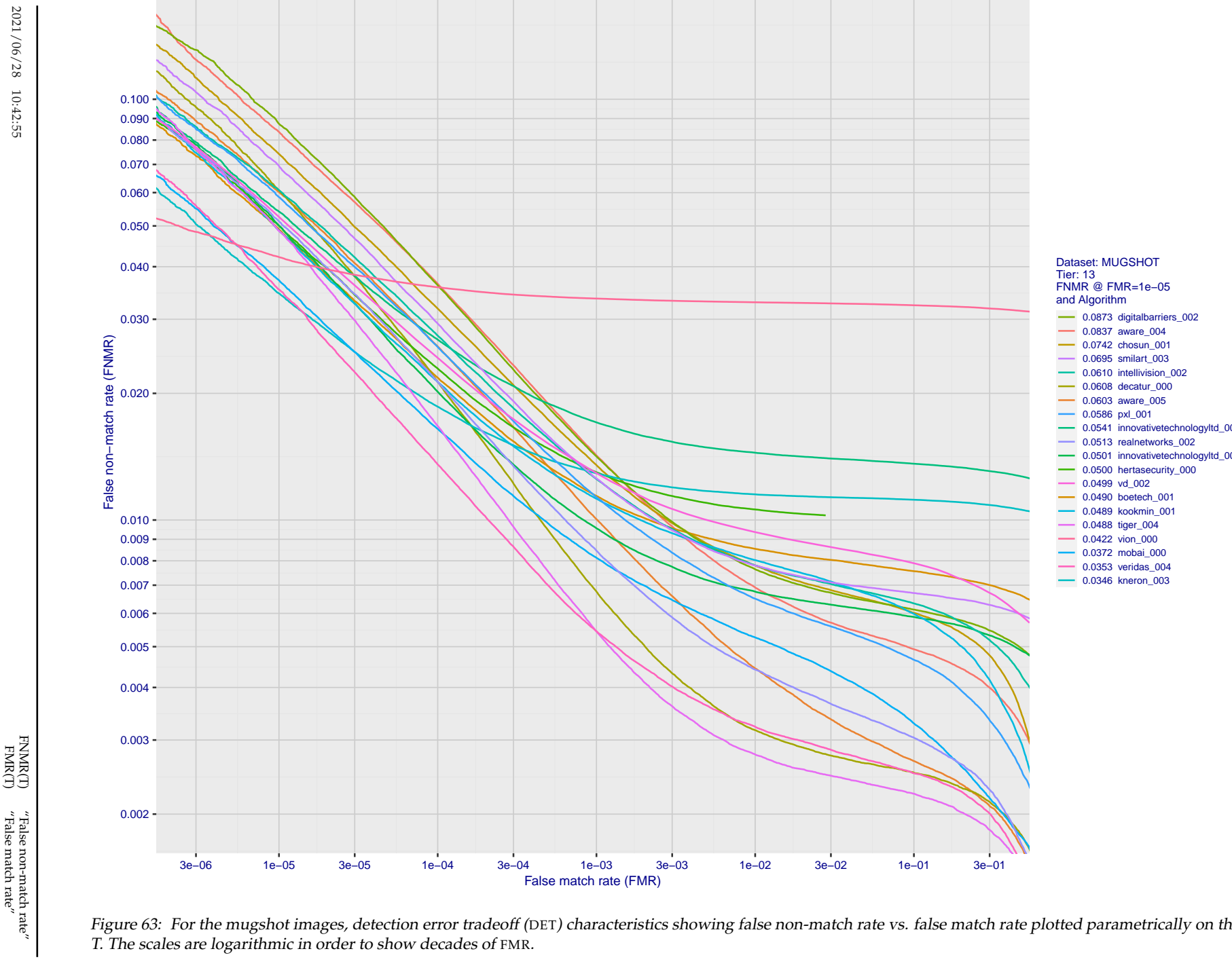


Figure 63: For the mugshot images, detection error tradeoff (DET) characteristics showing false non-match rate vs. false match rate plotted parametrically on threshold, T . The scales are logarithmic in order to show decades of FMR.

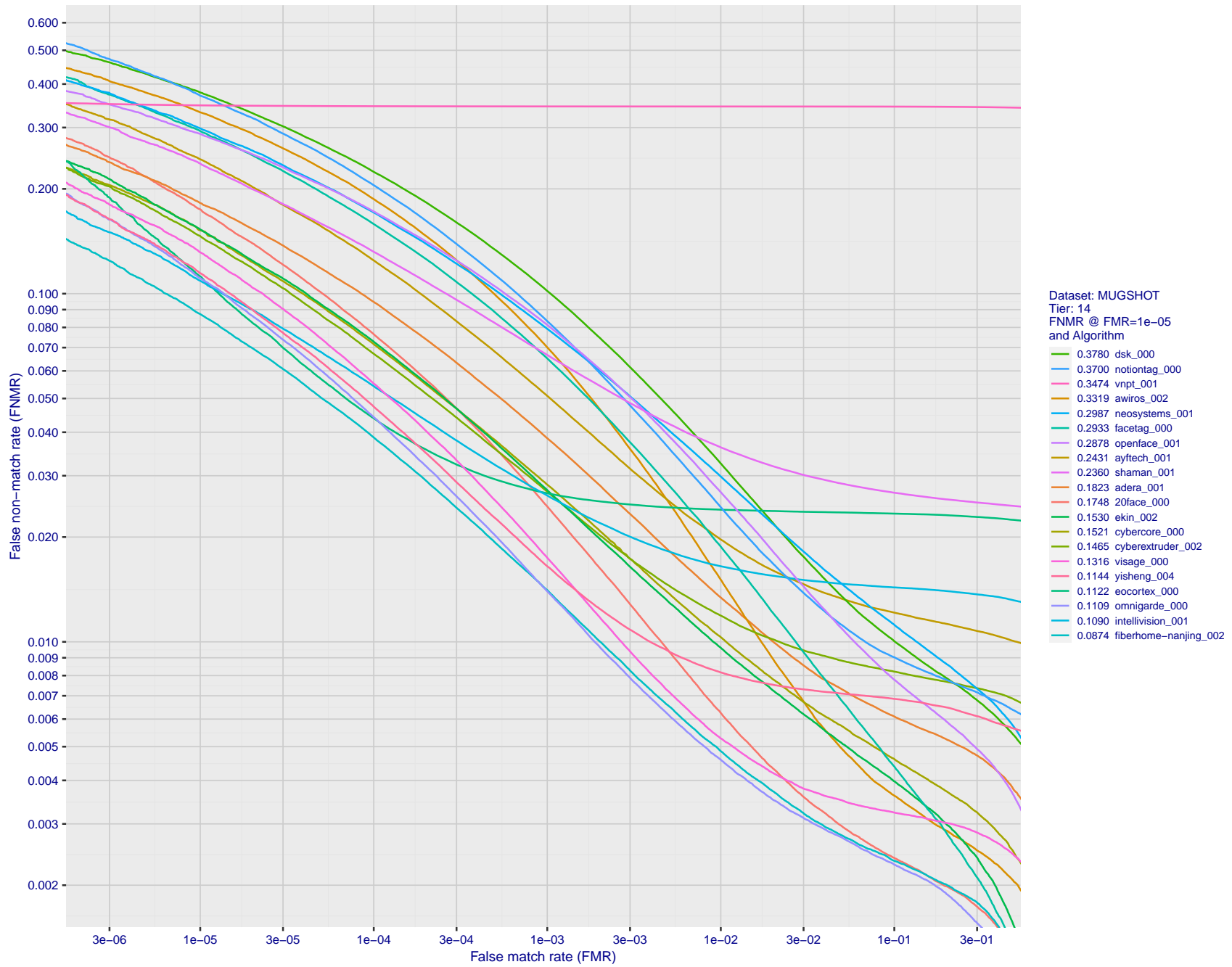


Figure 64: For the mugshot images, detection error tradeoff (DET) characteristics showing false non-match rate vs. false match rate plotted parametrically on threshold, T . The scales are logarithmic in order to show decades of FMR.

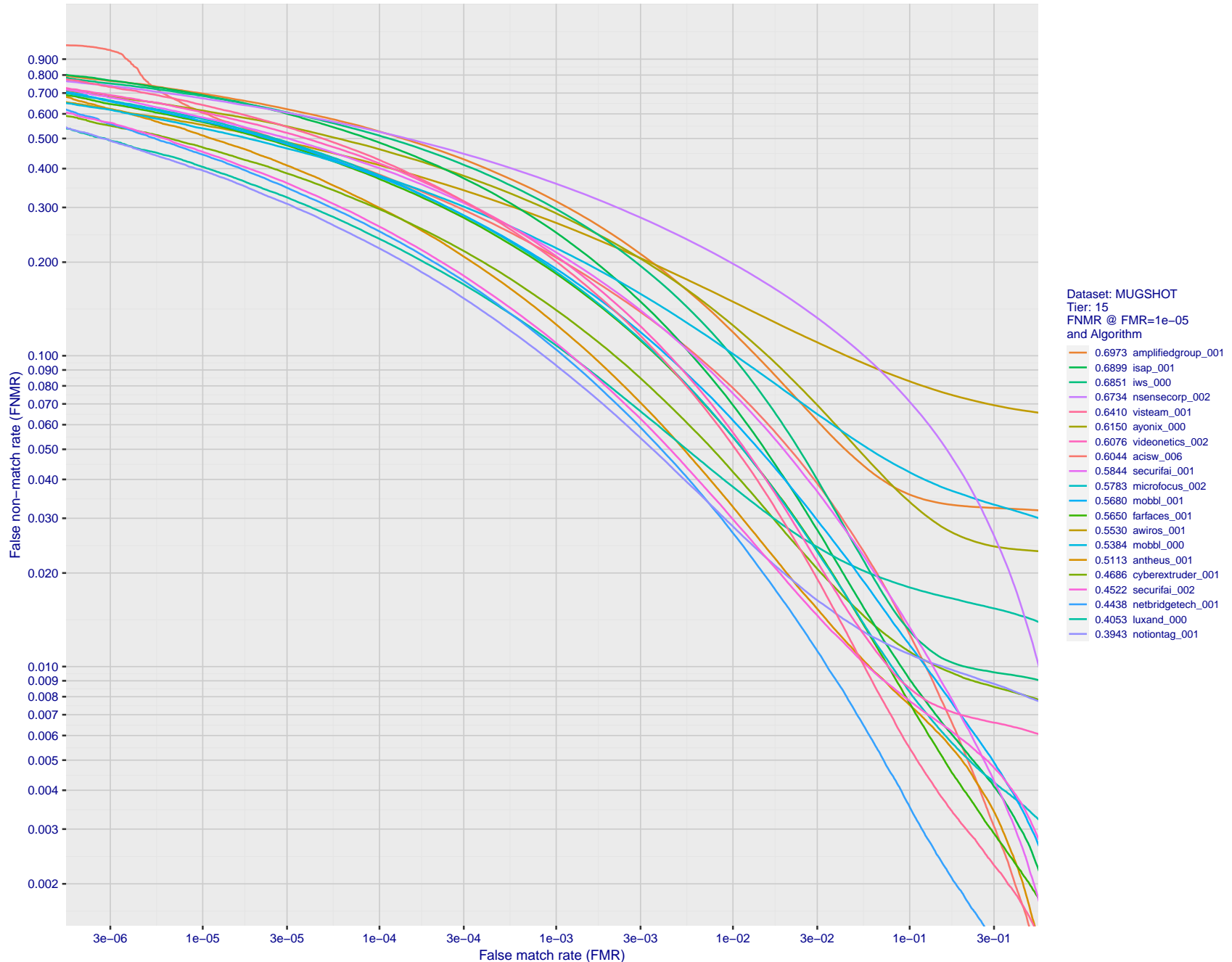


Figure 65: For the mugshot images, detection error tradeoff (DET) characteristics showing false non-match rate vs. false match rate plotted parametrically on threshold, T . The scales are logarithmic in order to show decades of FMR.

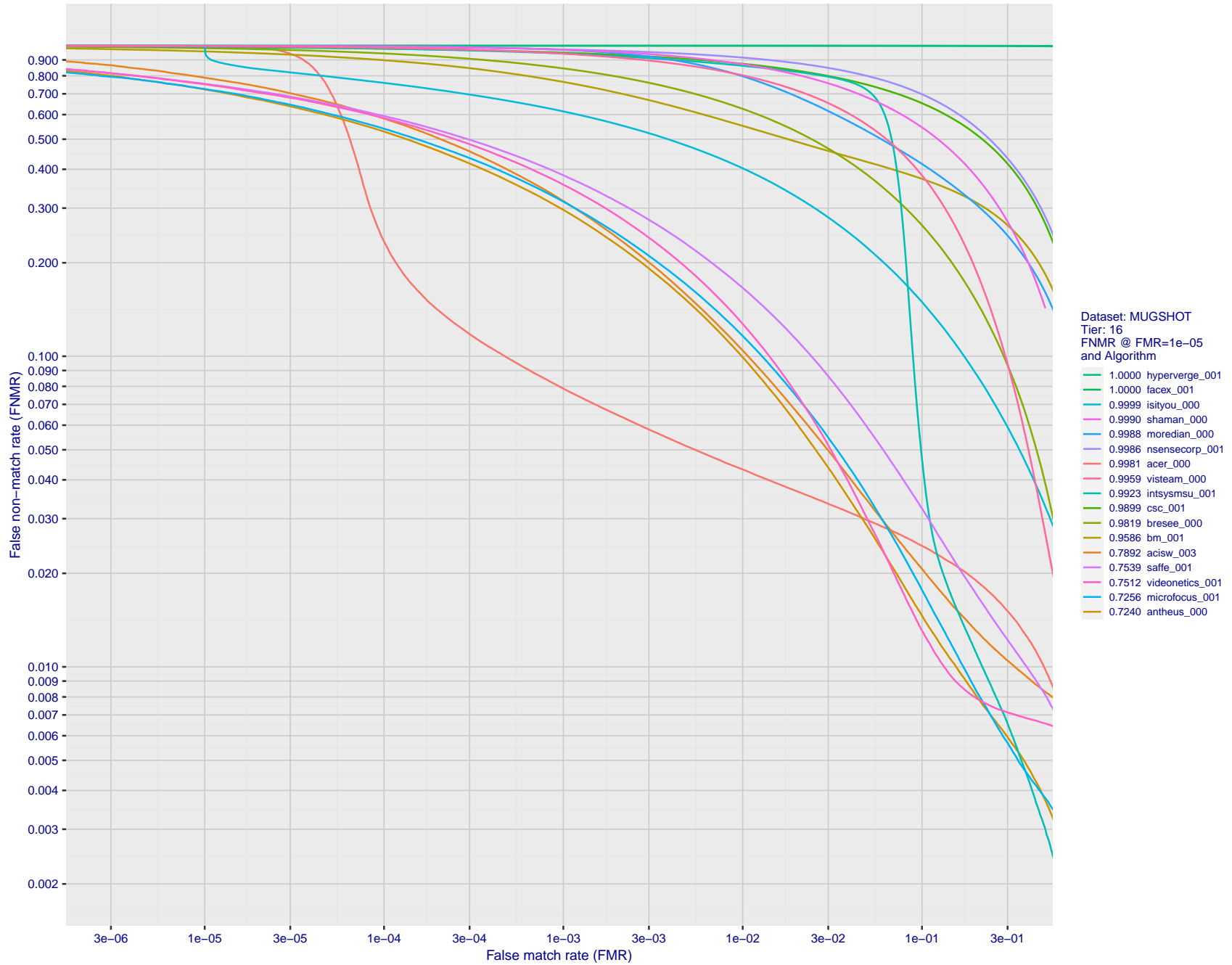


Figure 66: For the mugshot images, detection error tradeoff (DET) characteristics showing false non-match rate vs. false match rate plotted parametrically on threshold, T . The scales are logarithmic in order to show decades of FMR.

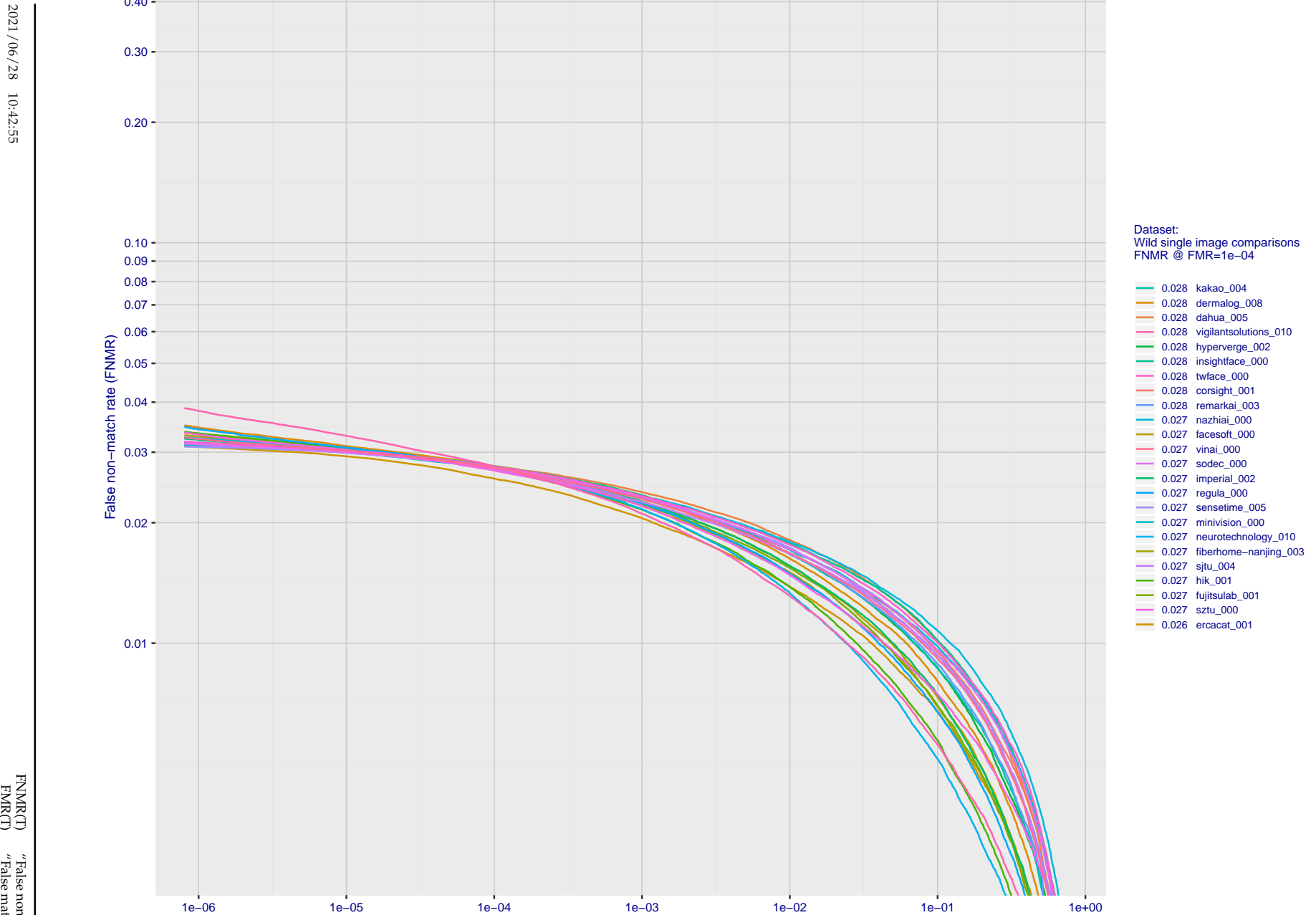


Figure 67: For the 2018 wild image comparisons, detection error tradeoff (DET) characteristics showing false non-match rate vs. false match rate plotted parametrically on threshold, T. The scales are logarithmic in order to show several decades of FMR.

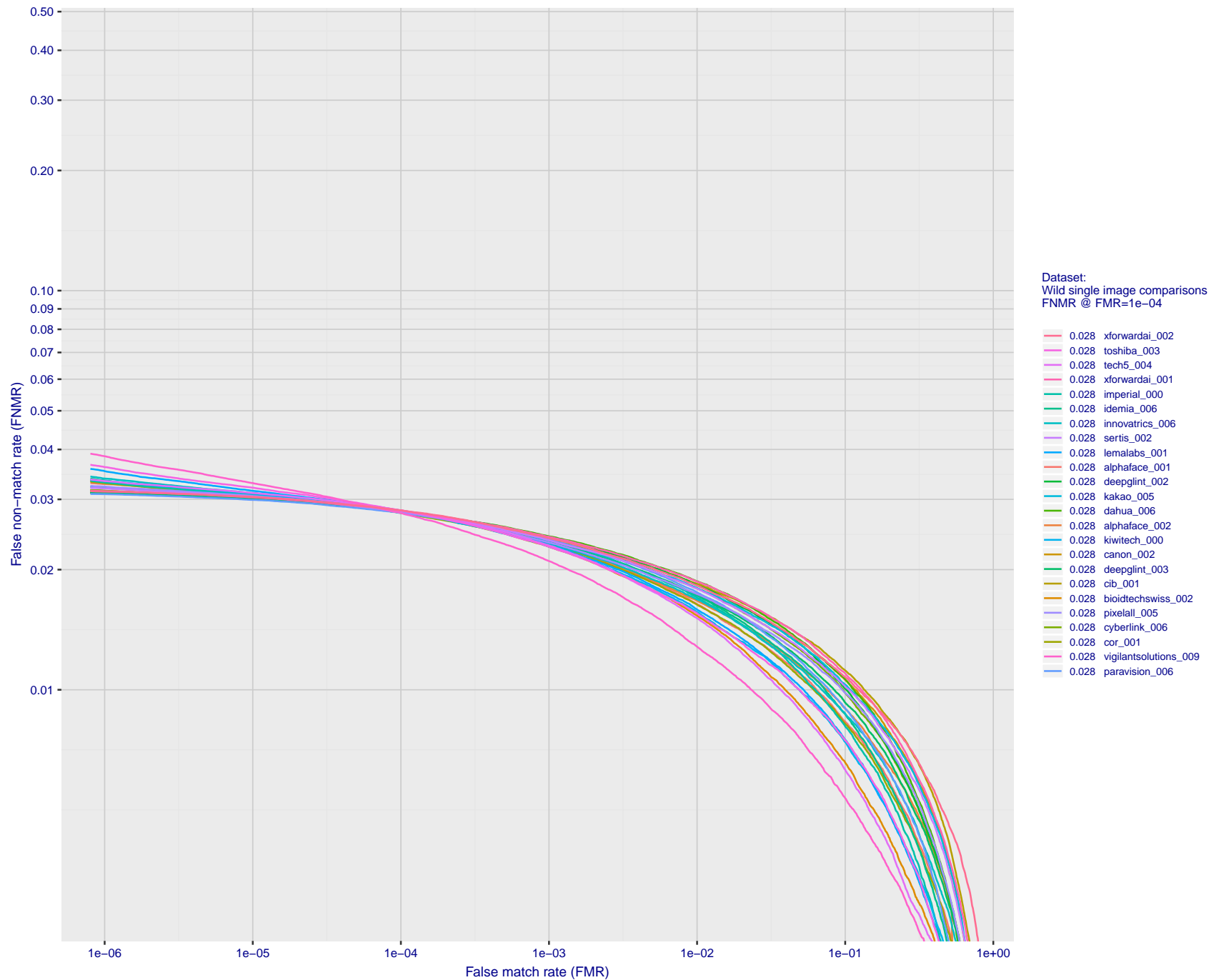


Figure 68: For the 2018 wild image comparisons, detection error tradeoff (DET) characteristics showing false non-match rate vs. false match rate plotted parametrically on threshold, T . The scales are logarithmic in order to show several decades of FMR.

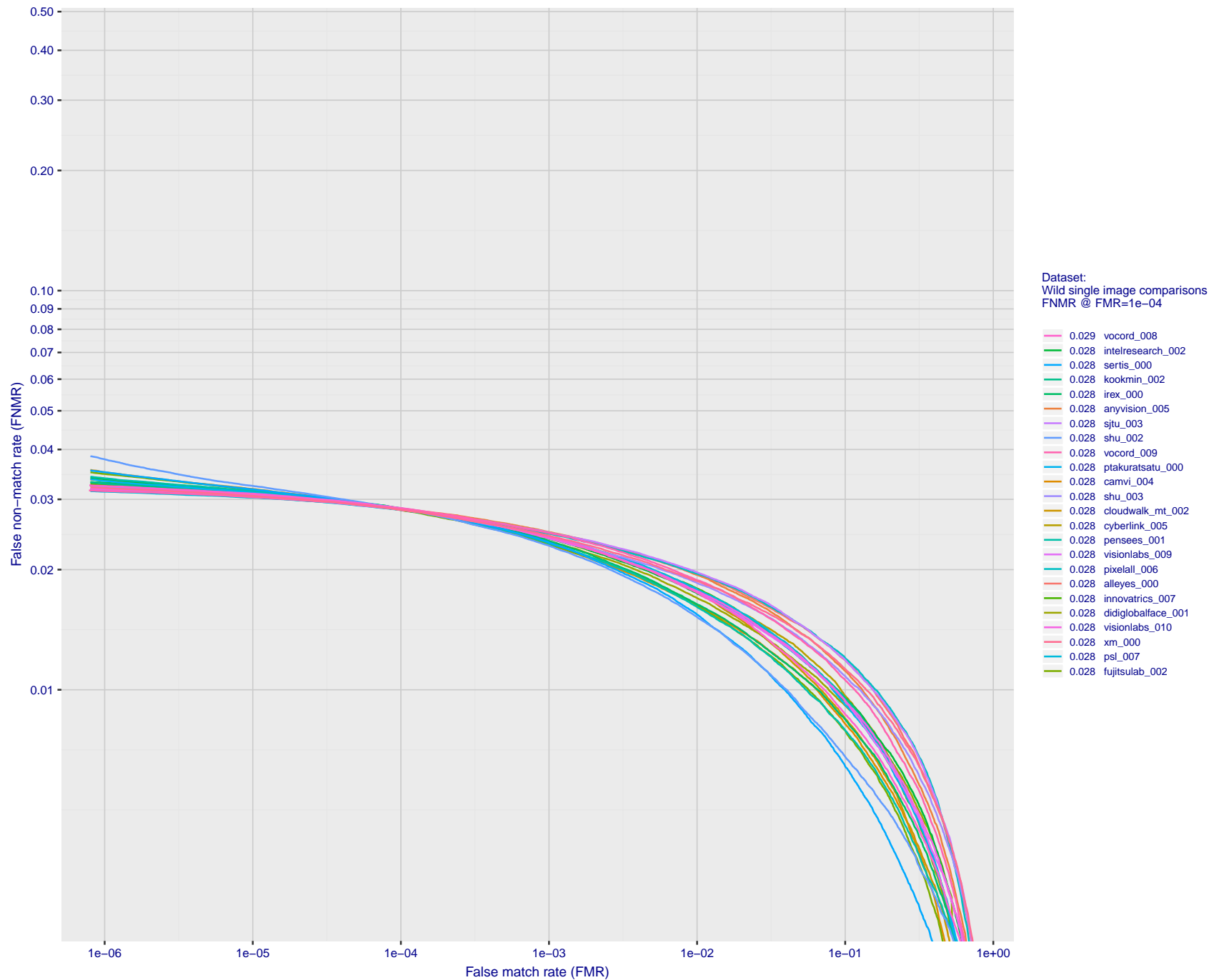


Figure 69: For the 2018 wild image comparisons, detection error tradeoff (DET) characteristics showing false non-match rate vs. false match rate plotted parametrically on threshold, T. The scales are logarithmic in order to show several decades of FMR.

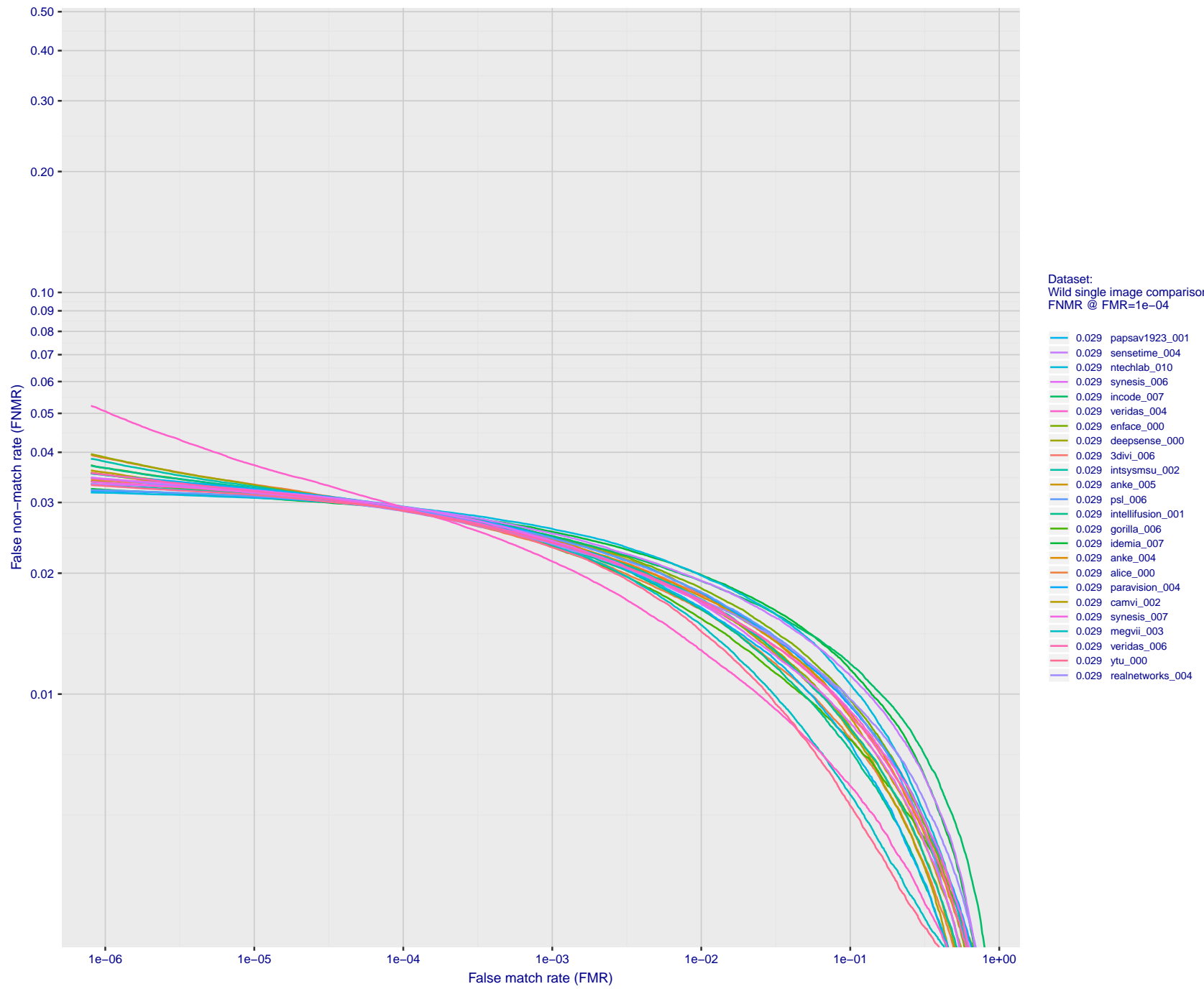


Figure 70: For the 2018 wild image comparisons, detection error tradeoff (DET) characteristics showing false non-match rate vs. false match rate plotted parametrically on threshold, T. The scales are logarithmic in order to show several decades of FMR.

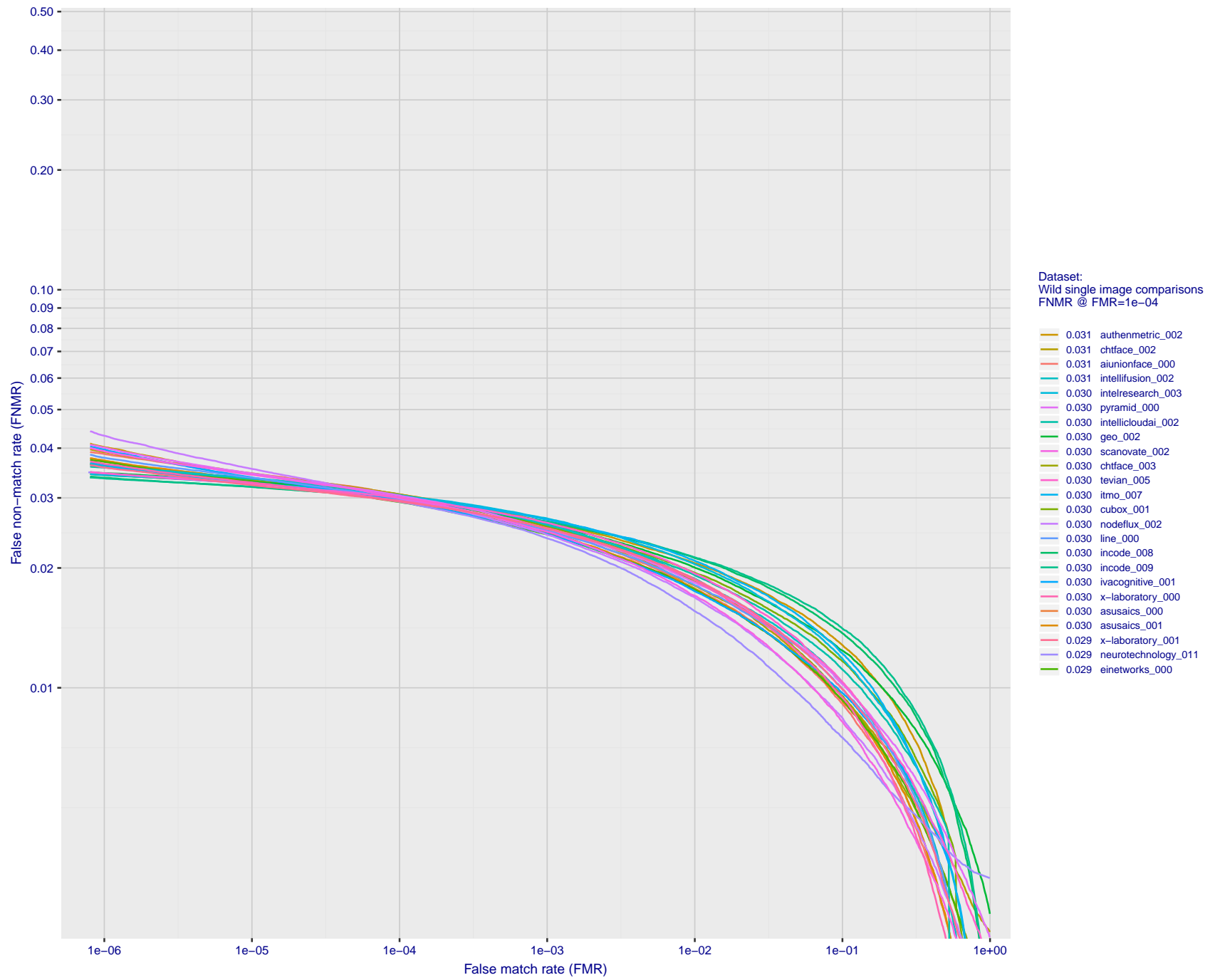


Figure 71: For the 2018 wild image comparisons, detection error tradeoff (DET) characteristics showing false non-match rate vs. false match rate plotted parametrically on threshold, T . The scales are logarithmic in order to show several decades of FMR.

2021/06/28 10:42:55

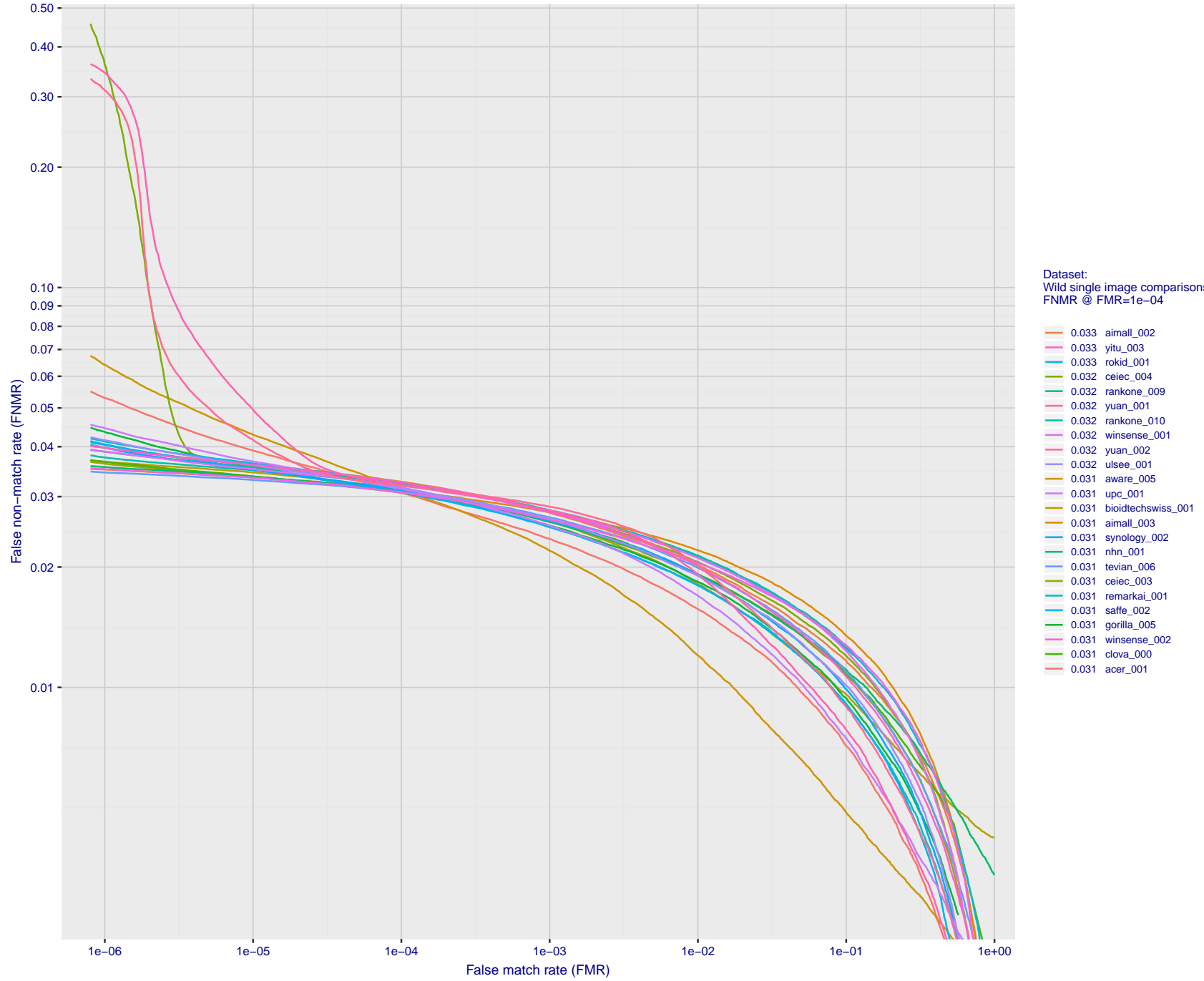


Figure 72: For the 2018 wild image comparisons, detection error tradeoff (DET) characteristics showing false non-match rate vs. false match rate plotted parametrically on threshold, T . The scales are logarithmic in order to show several decades of FMR.

2021/06/28 10:42:55

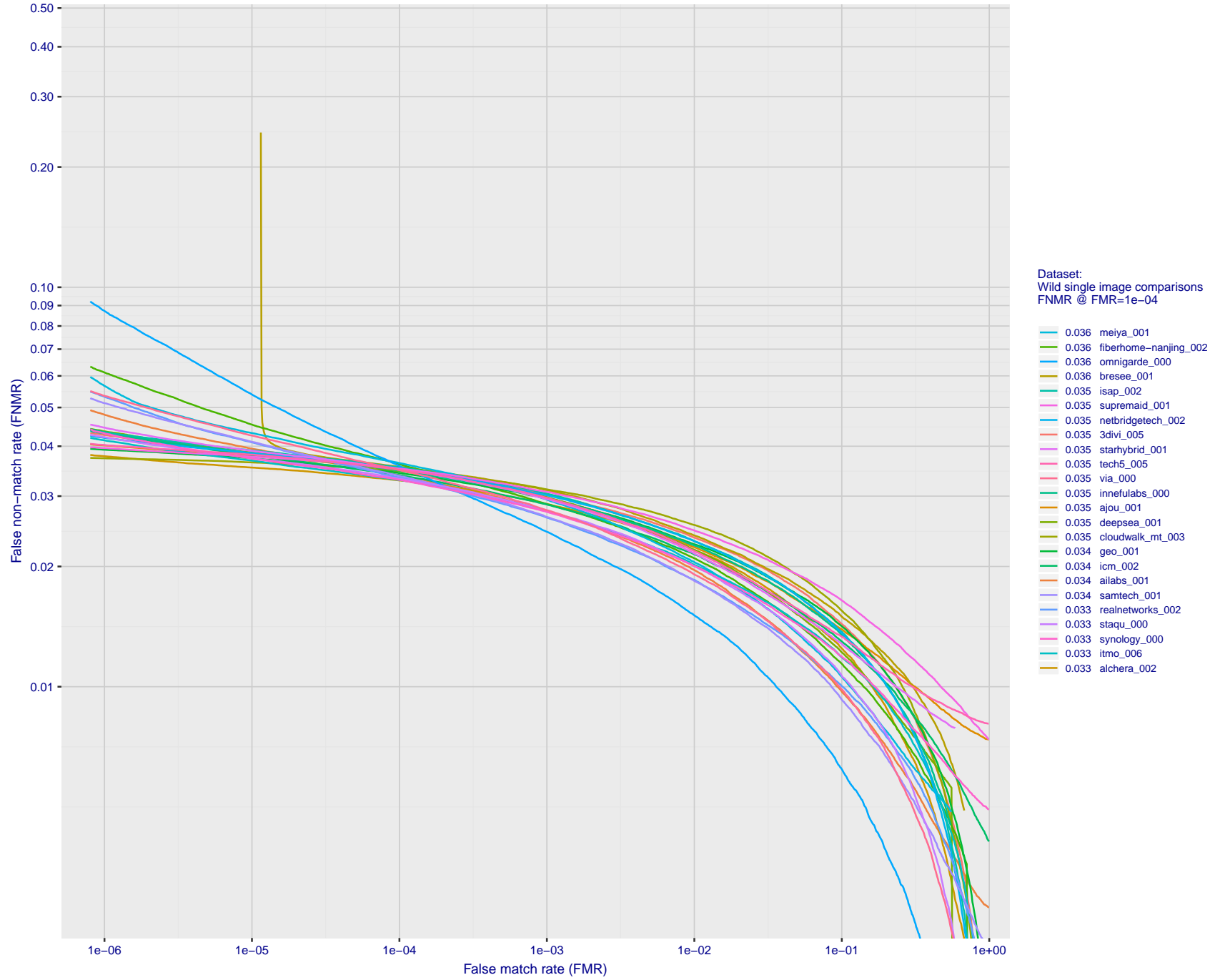


Figure 73: For the 2018 wild image comparisons, detection error tradeoff (DET) characteristics showing false non-match rate vs. false match rate plotted parametrically on threshold, T . The scales are logarithmic in order to show several decades of FMR.

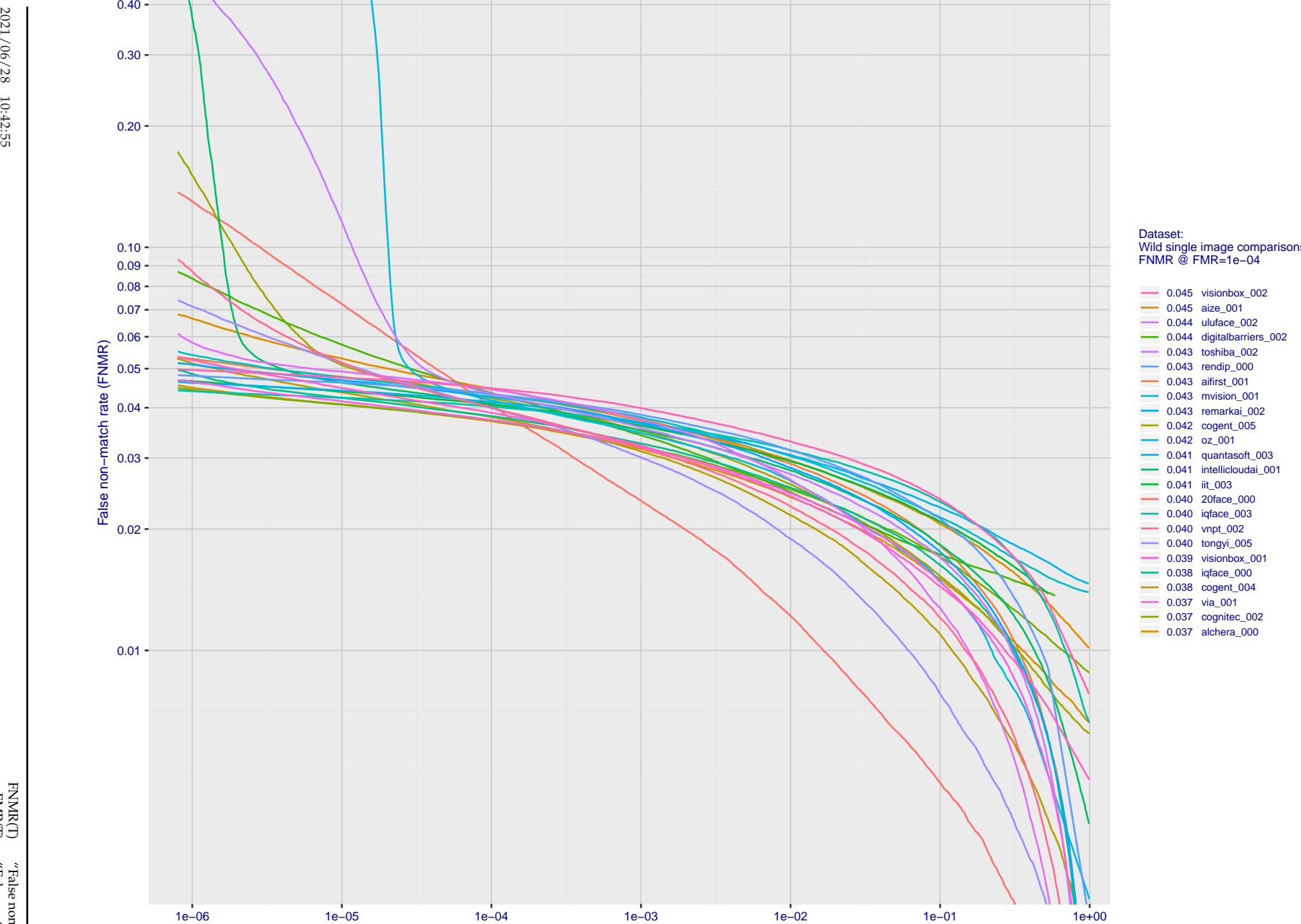


Figure 74: For the 2018 wild image comparisons, detection error tradeoff (DET) characteristics showing false non-match rate vs. false match rate plotted parametrically on threshold, T . The scales are logarithmic in order to show several decades of FMR.

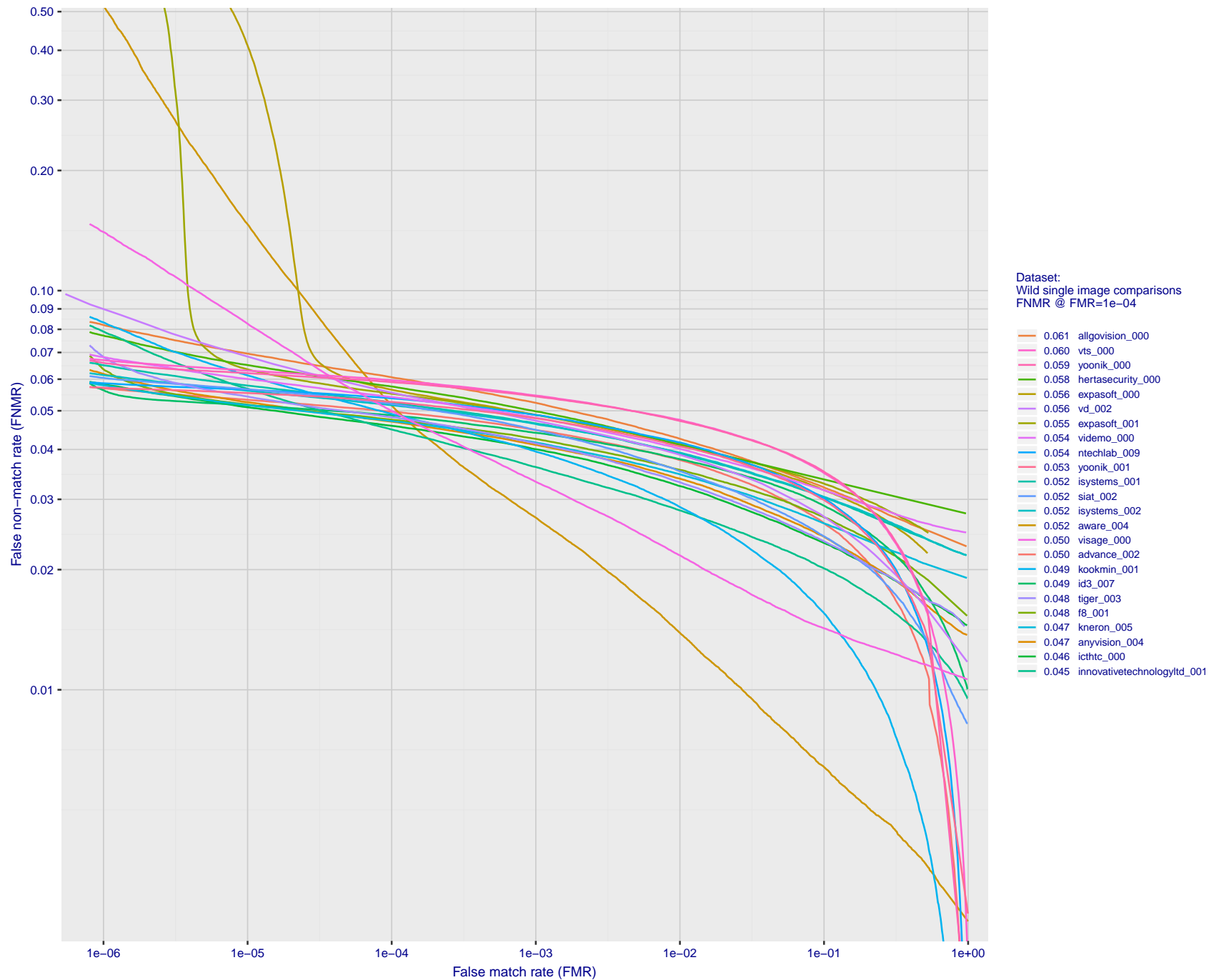


Figure 75: For the 2018 wild image comparisons, detection error tradeoff (DET) characteristics showing false non-match rate vs. false match rate plotted parametrically on threshold, T . The scales are logarithmic in order to show several decades of FMR.

2021/06/28 10:42:55

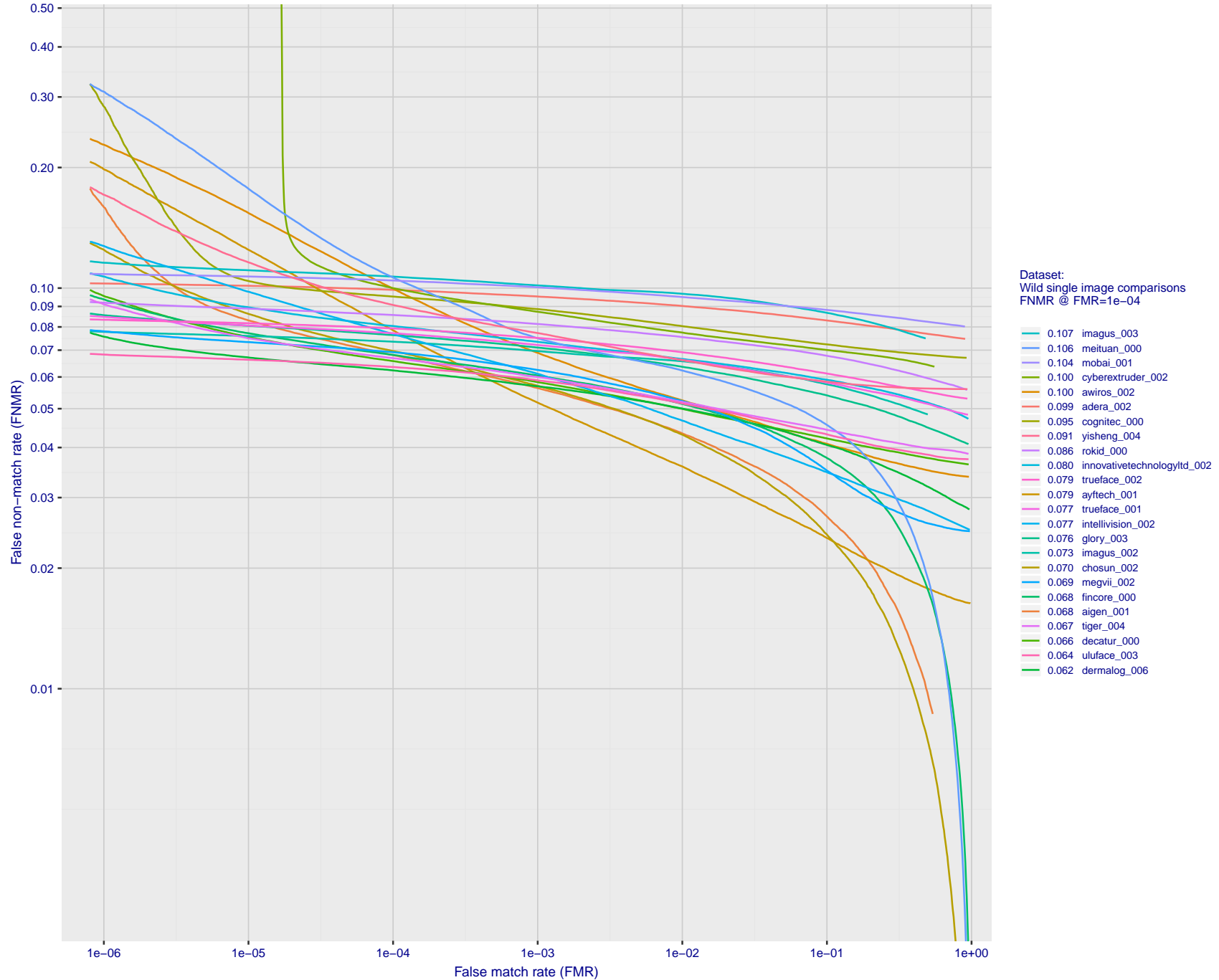


Figure 76: For the 2018 wild image comparisons, detection error tradeoff (DET) characteristics showing false non-match rate vs. false match rate plotted parametrically on threshold, T . The scales are logarithmic in order to show several decades of FMR.

2021/06/28 10:42:55

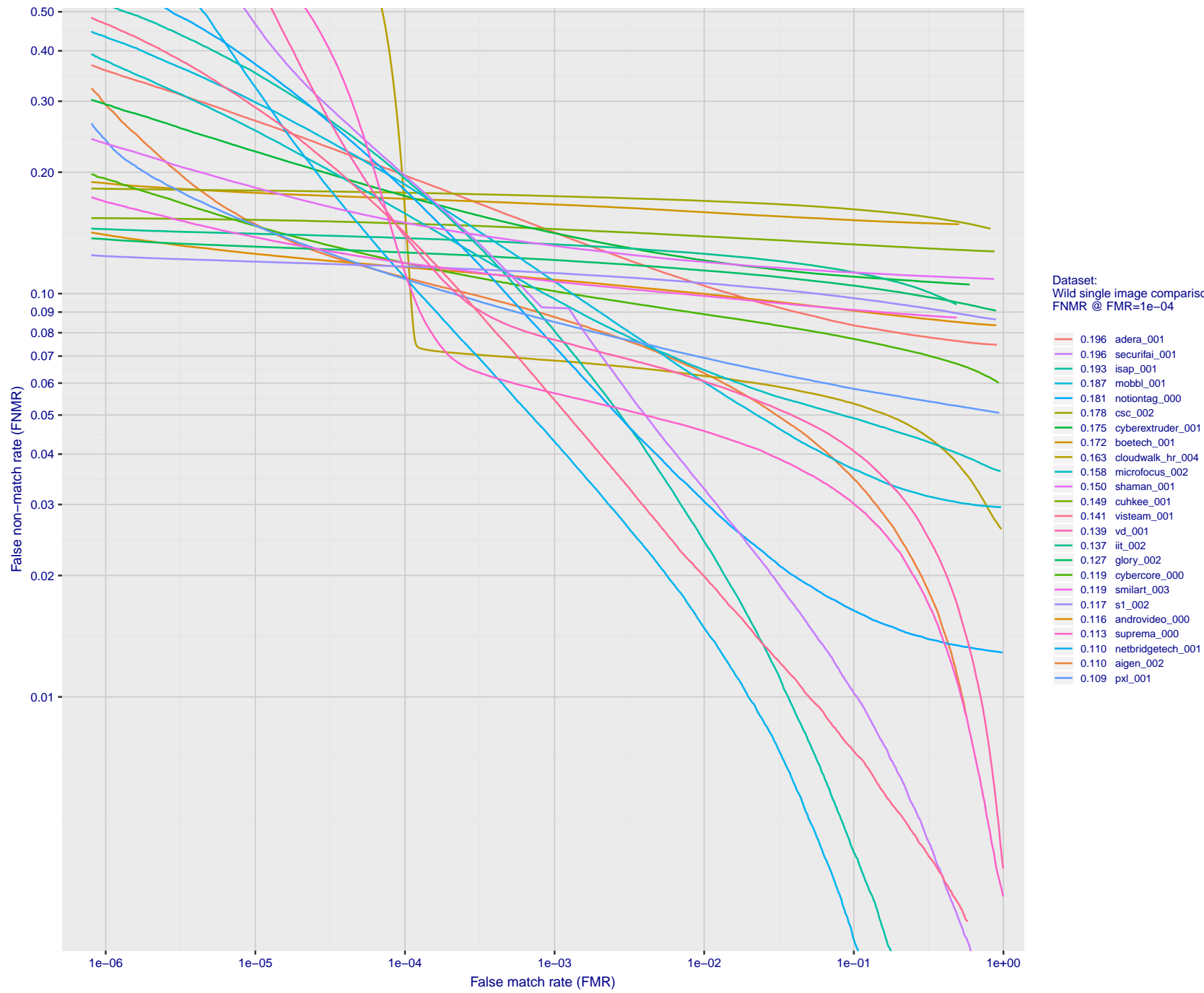


Figure 77: For the 2018 wild image comparisons, detection error tradeoff (DET) characteristics showing false non-match rate vs. false match rate plotted parametrically on threshold, T . The scales are logarithmic in order to show several decades of FMR.

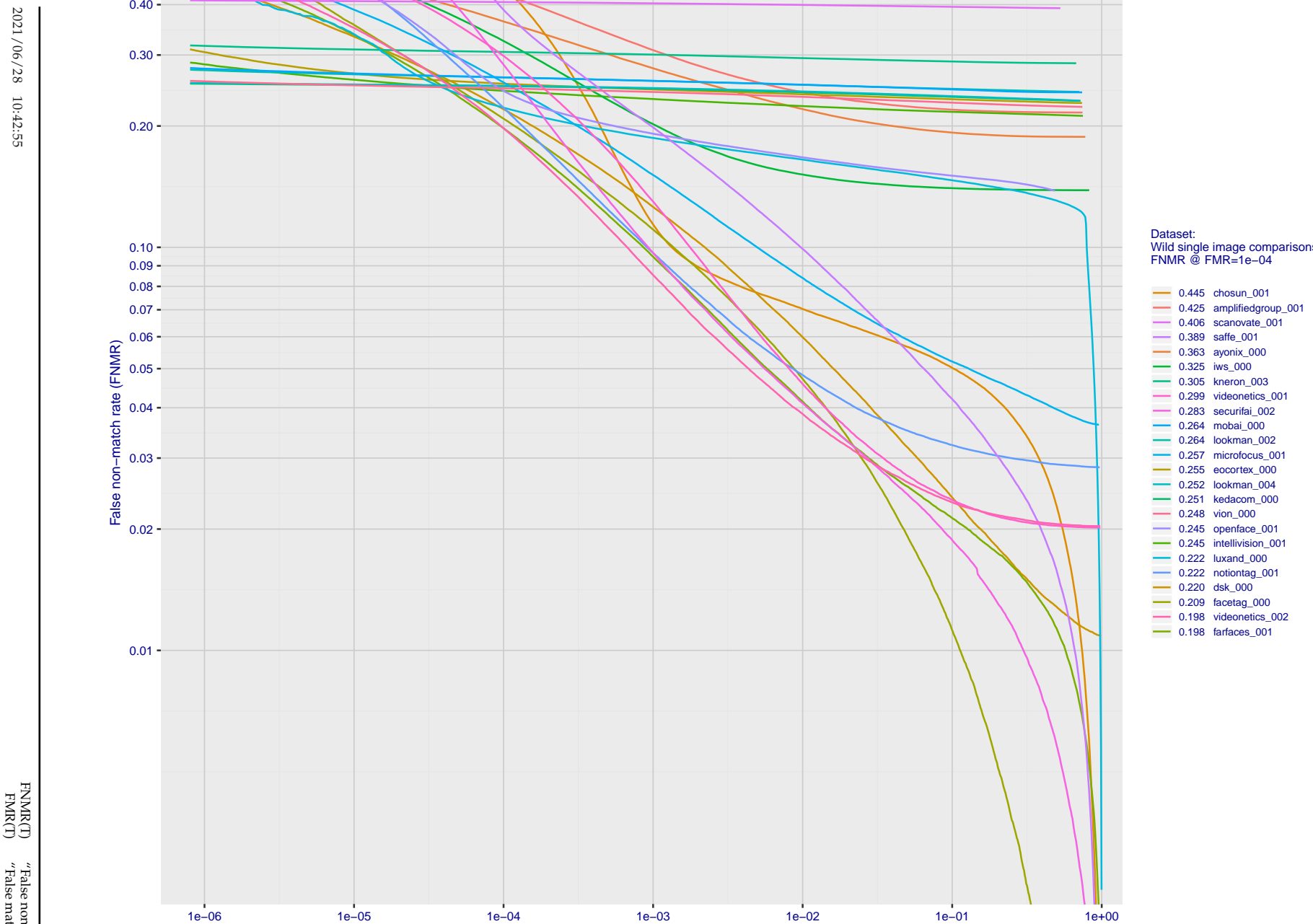


Figure 78: For the 2018 wild image comparisons, detection error tradeoff (DET) characteristics showing false non-match rate vs. false match rate plotted parametrically on threshold, T . The scales are logarithmic in order to show several decades of FMR.

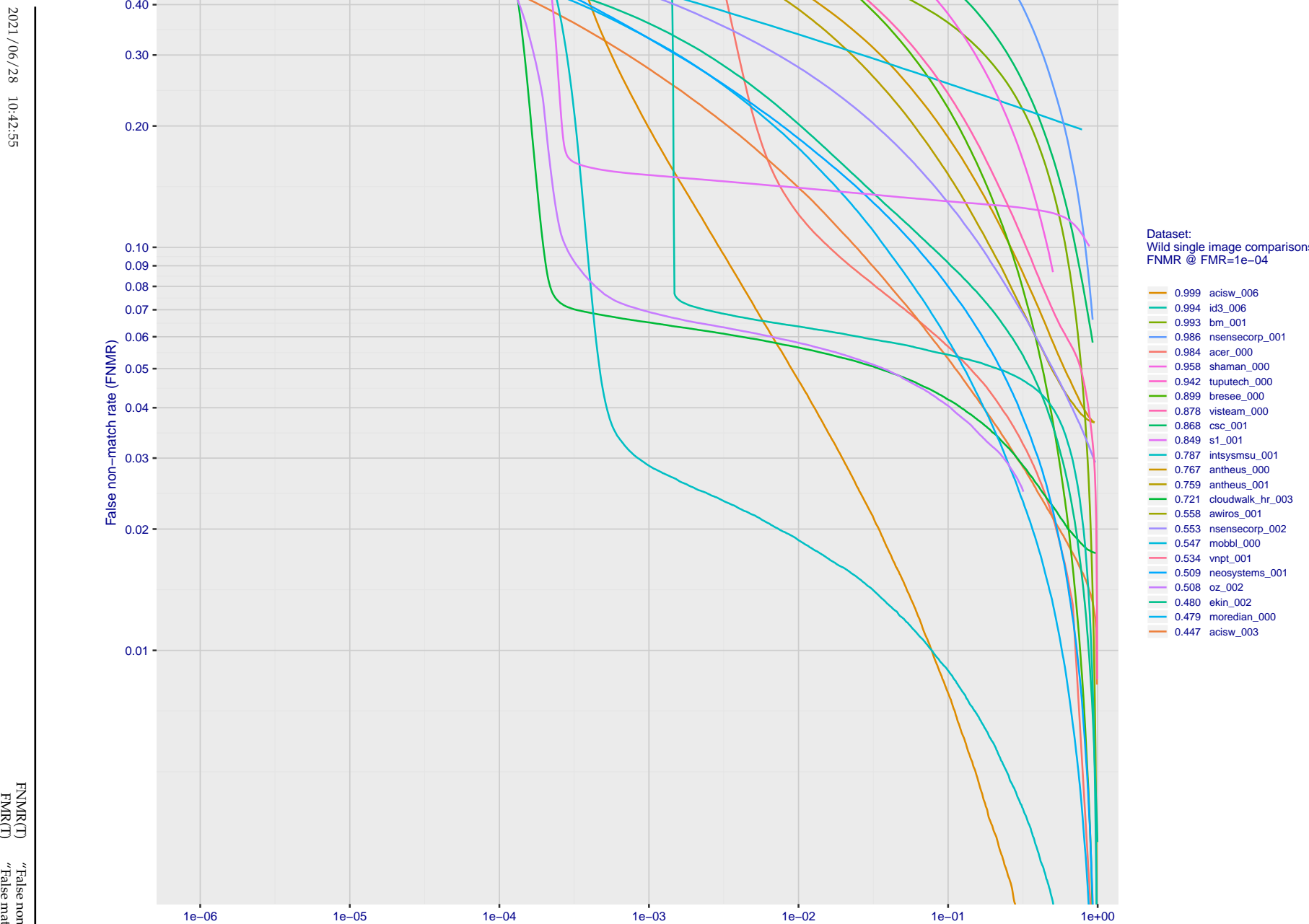


Figure 79: For the 2018 wild image comparisons, detection error tradeoff (DET) characteristics showing false non-match rate vs. false match rate plotted parametrically on threshold, T. The scales are logarithmic in order to show several decades of FMR.

2021/06/28 10:42:55

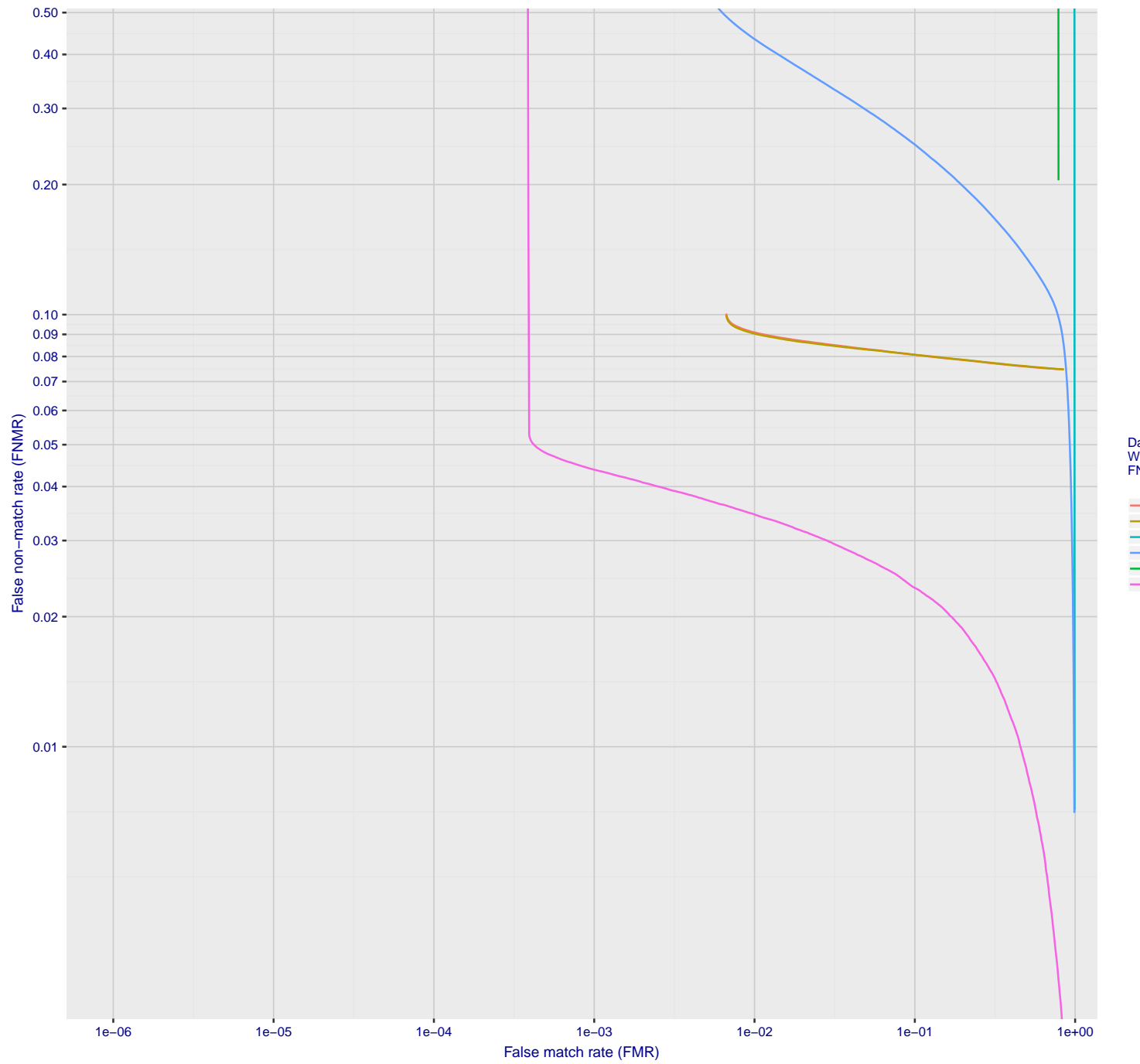


Figure 80: For the 2018 wild image comparisons, detection error tradeoff (DET) characteristics showing false non-match rate vs. false match rate plotted parametrically on threshold, T . The scales are logarithmic in order to show several decades of FMR.

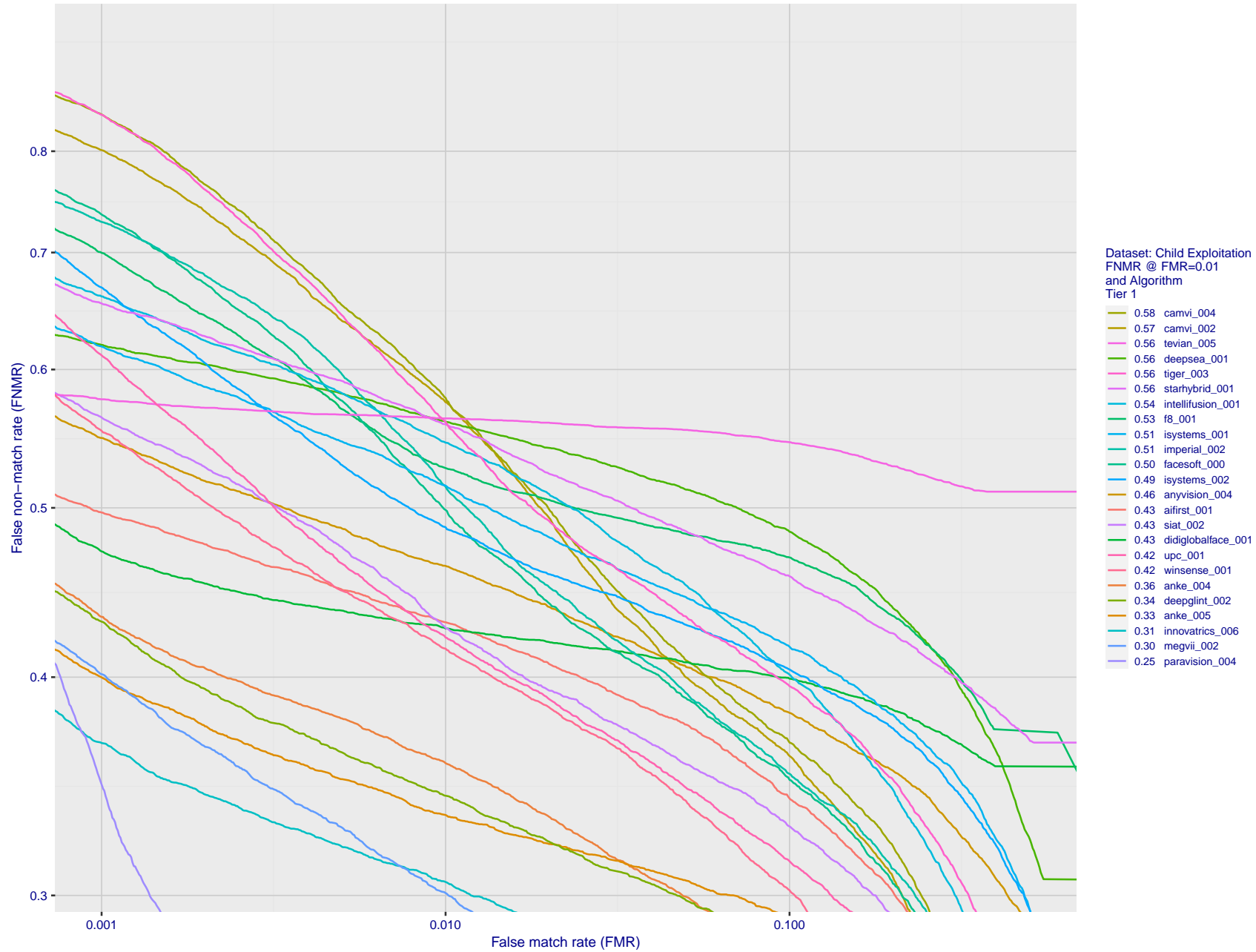


Figure 81: For child exploitation images, detection error tradeoff (DET) characteristics showing false non-match rate vs. false match rate plotted parametrically on threshold, T. The scales are logarithmic in order to show many decades of FMR. Accuracy is poor because many images have adverse quality characteristics, and because detection and enrollment fails.

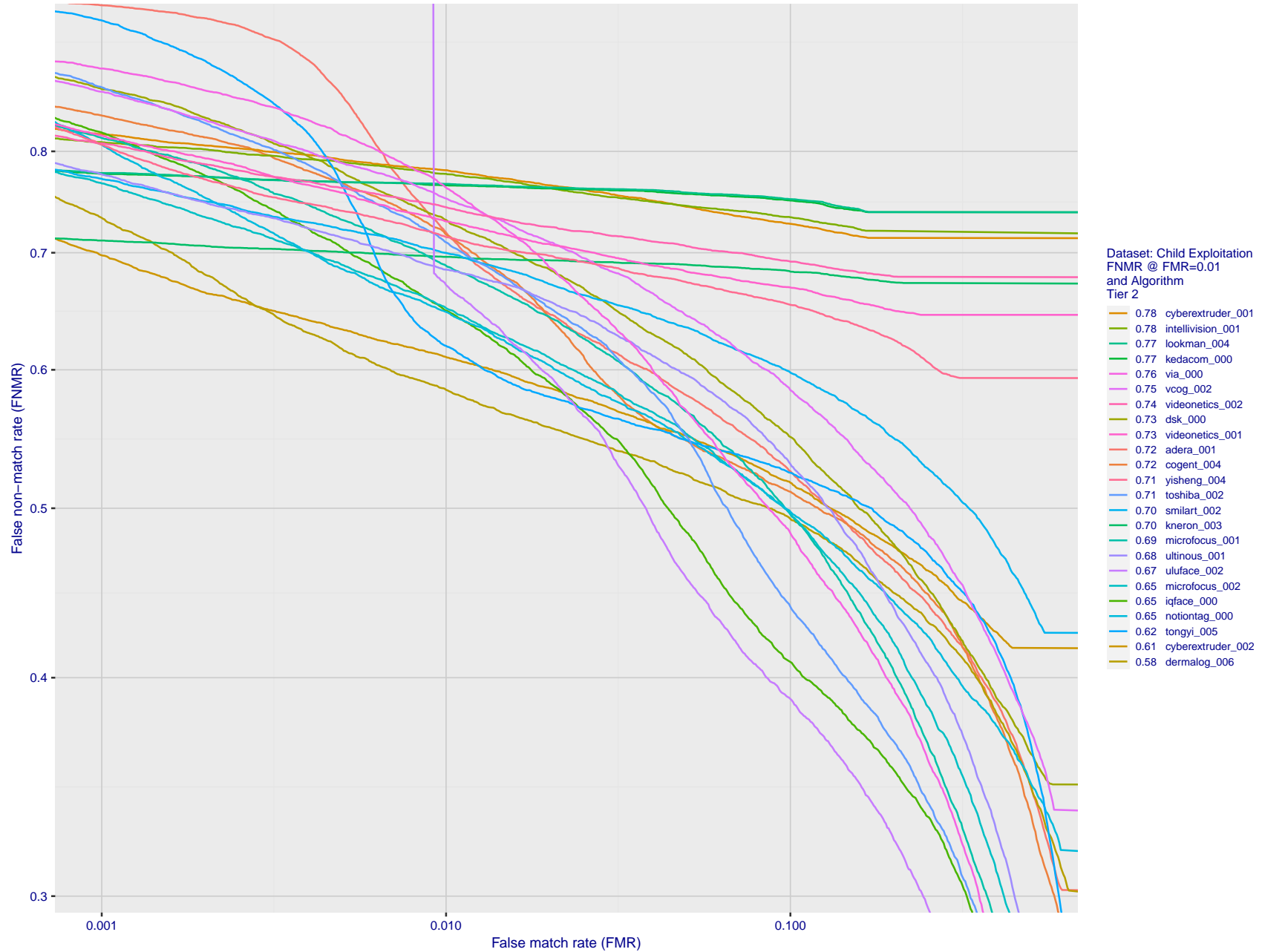


Figure 82: For child exploitation images, detection error tradeoff (DET) characteristics showing false non-match rate vs. false match rate plotted parametrically on threshold, T . The scales are logarithmic in order to show many decades of FMR. Accuracy is poor because many images have adverse quality characteristics, and because detection and enrollment fails.

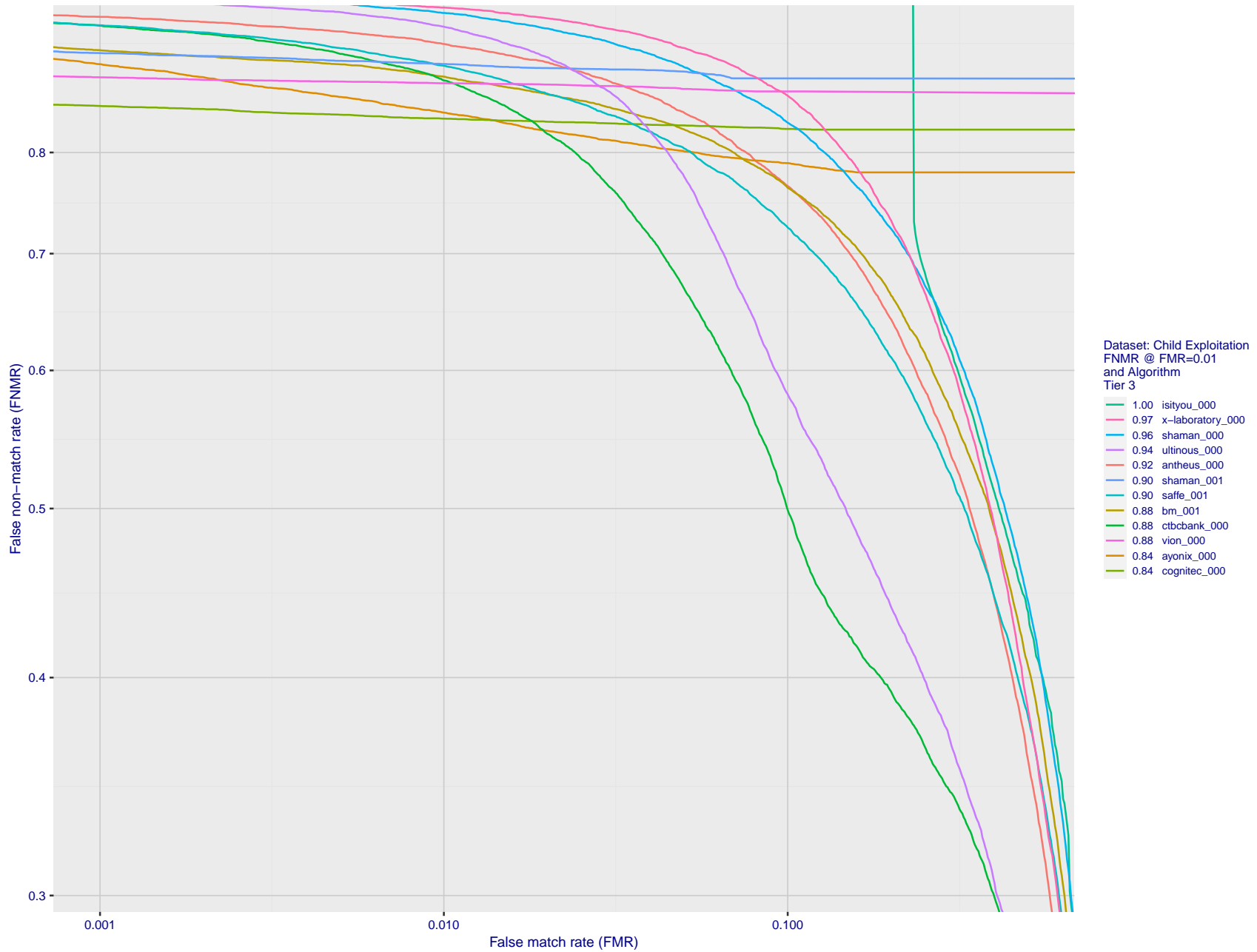


Figure 83: For child exploitation images, detection error tradeoff (DET) characteristics showing false non-match rate vs. false match rate plotted parametrically on threshold, T . The scales are logarithmic in order to show many decades of FMR. Accuracy is poor because many images have adverse quality characteristics, and because detection and enrollment fails.

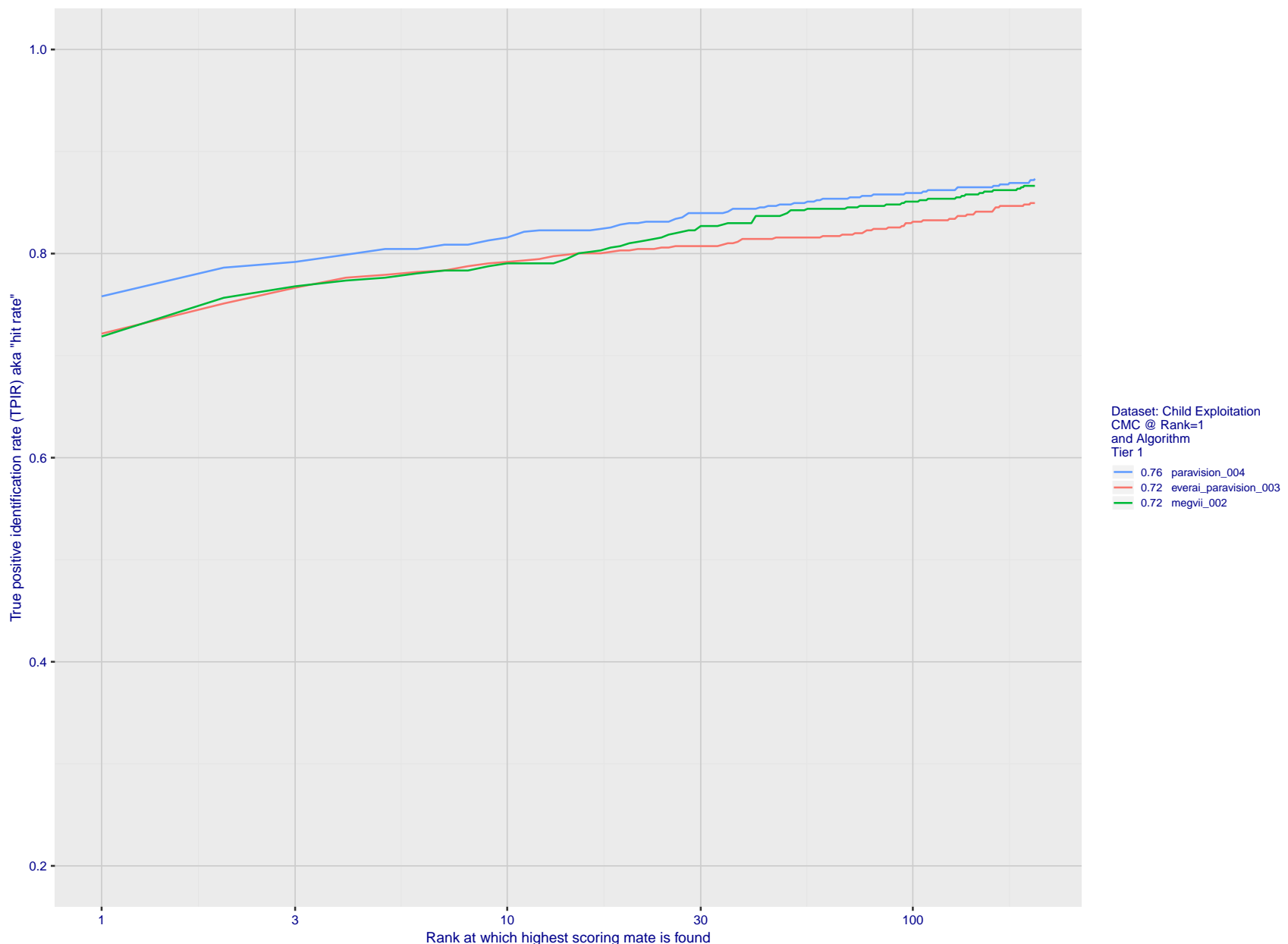


Figure 84: For child exploitation images, cumulative match characteristics (CMC) showing true positive identification rate vs. rank. This is simulation of a one-to-many search experiment - see discussion in section 3.2. The scales are logarithmic in order to show the effect of long candidate lists. Accuracy is poor but much improved relative to the 1:1 DETs of Fig. 83 because a search can succeed if any of a subject's several enrolled images matches the search image with a high score.

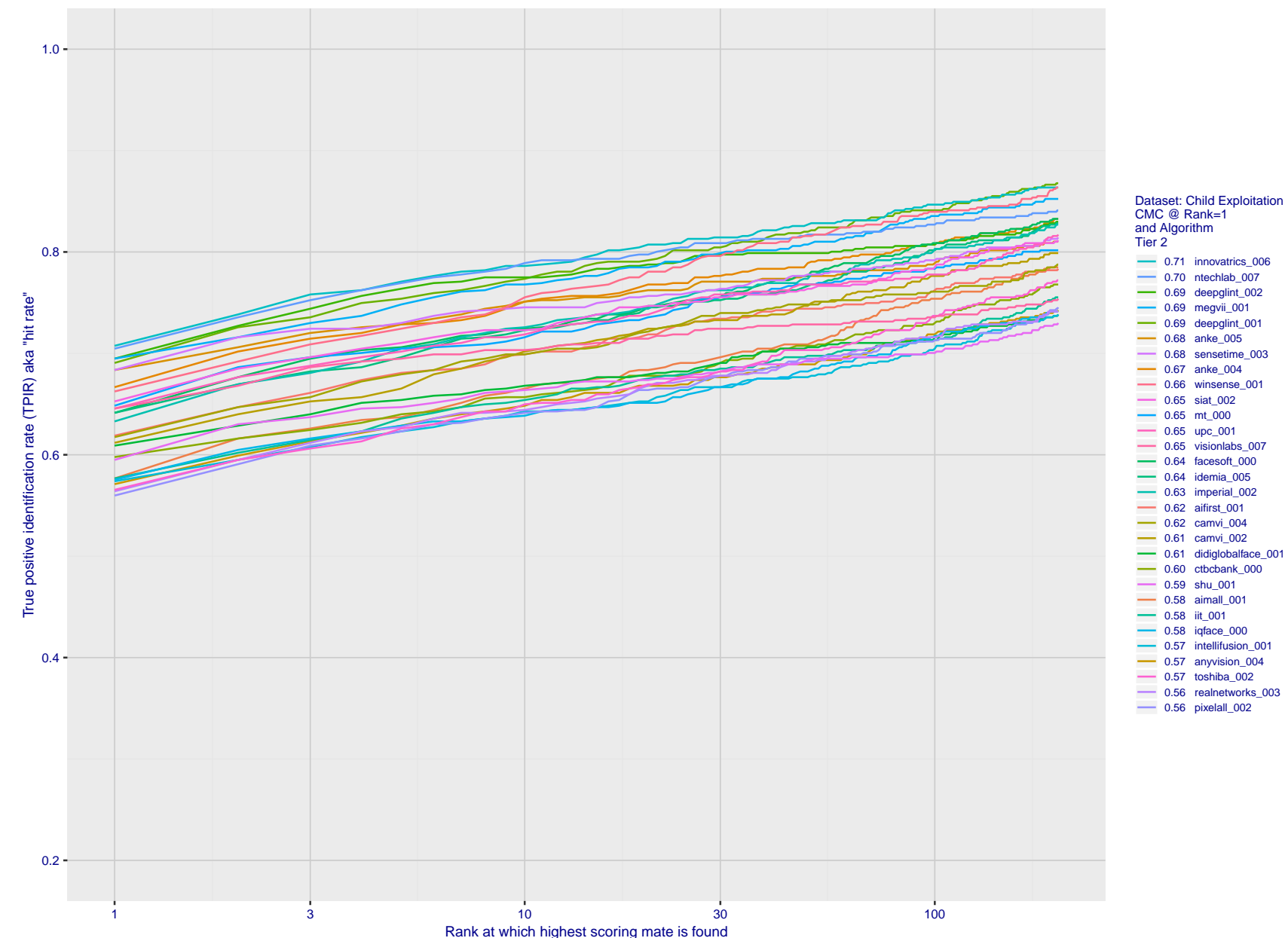


Figure 85: For child exploitation images, cumulative match characteristics (CMC) showing true positive identification rate vs. rank. This is simulation of a one-to-many search experiment - see discussion in section 3.2. The scales are logarithmic in order to show the effect of long candidate lists. Accuracy is poor but much improved relative to the 1:1 DETs of Fig. 83 because a search can succeed if any of a subject's several enrolled images matches the search image with a high score.

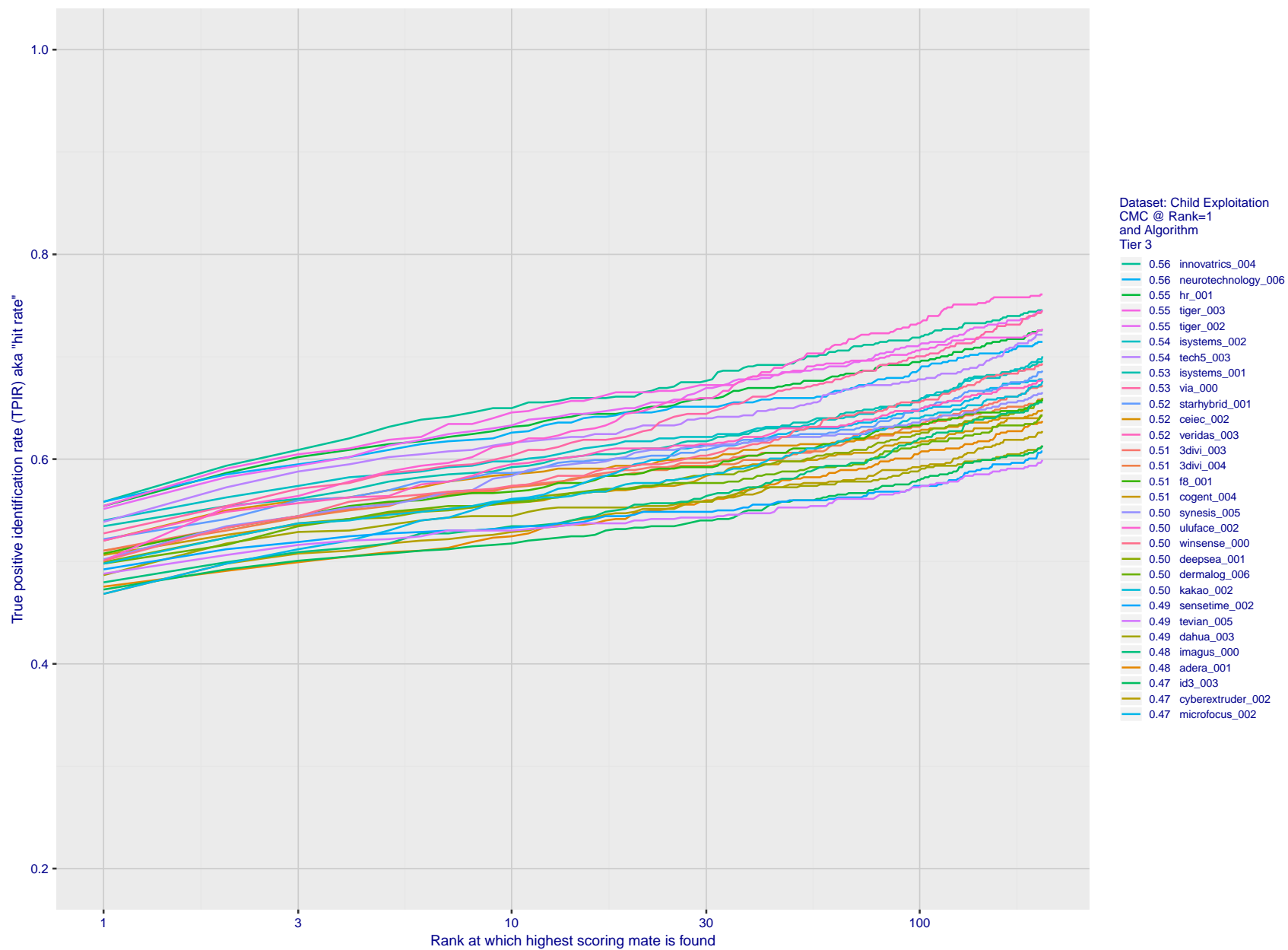


Figure 86: For child exploitation images, cumulative match characteristics (CMC) showing true positive identification rate vs. rank. This is simulation of a one-to-many search experiment - see discussion in section 3.2. The scales are logarithmic in order to show the effect of long candidate lists. Accuracy is poor but much improved relative to the 1:1 DETs of Fig. 83 because a search can succeed if any of a subject's several enrolled images matches the search image with a high score.

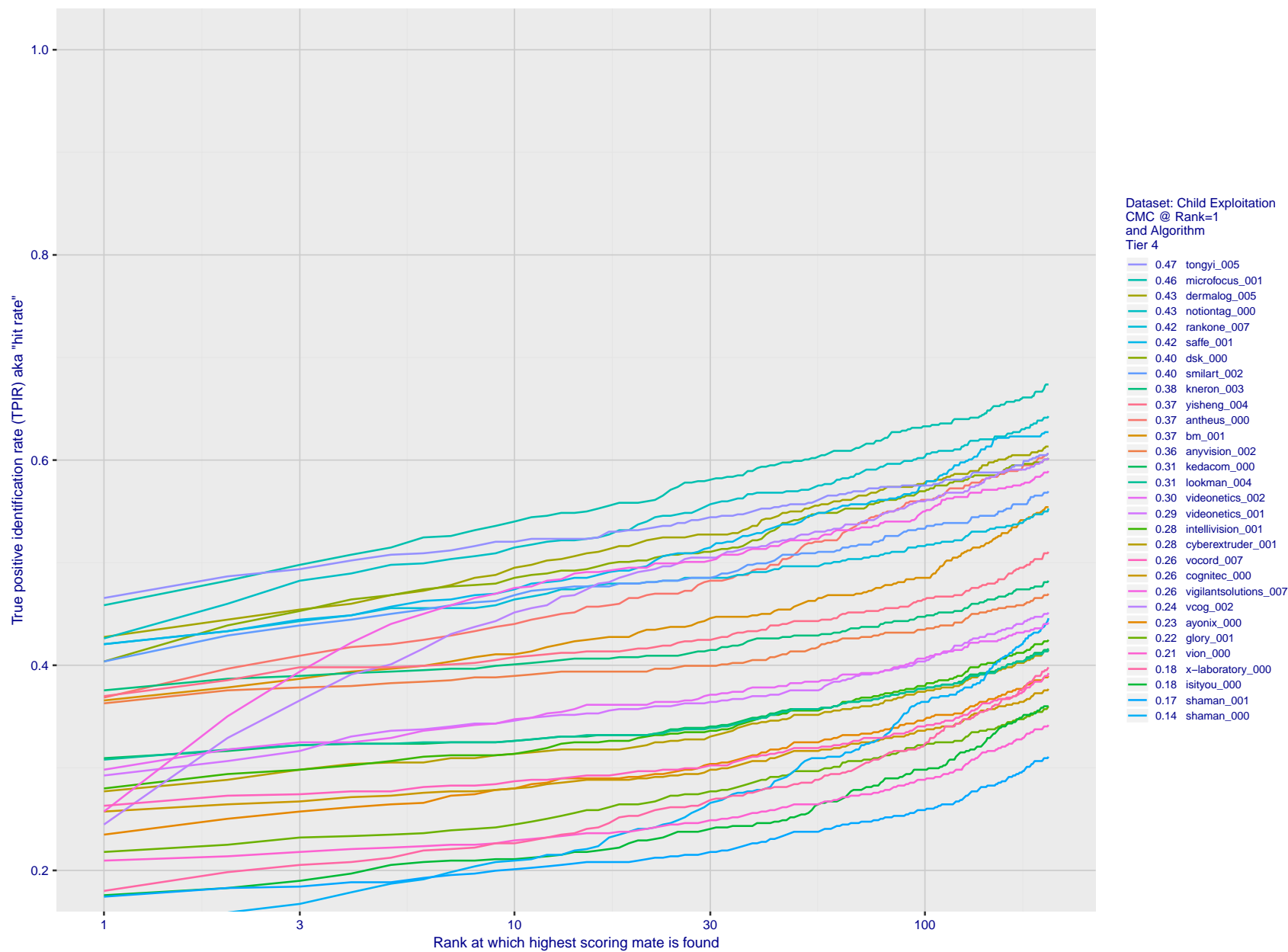


Figure 87: For child exploitation images, cumulative match characteristics (CMC) showing true positive identification rate vs. rank. This is simulation of a one-to-many search experiment - see discussion in section 3.2. The scales are logarithmic in order to show the effect of long candidate lists. Accuracy is poor but much improved relative to the 1:1 DETs of Fig. 83 because a search can succeed if any of a subject's several enrolled images matches the search image with a high score.

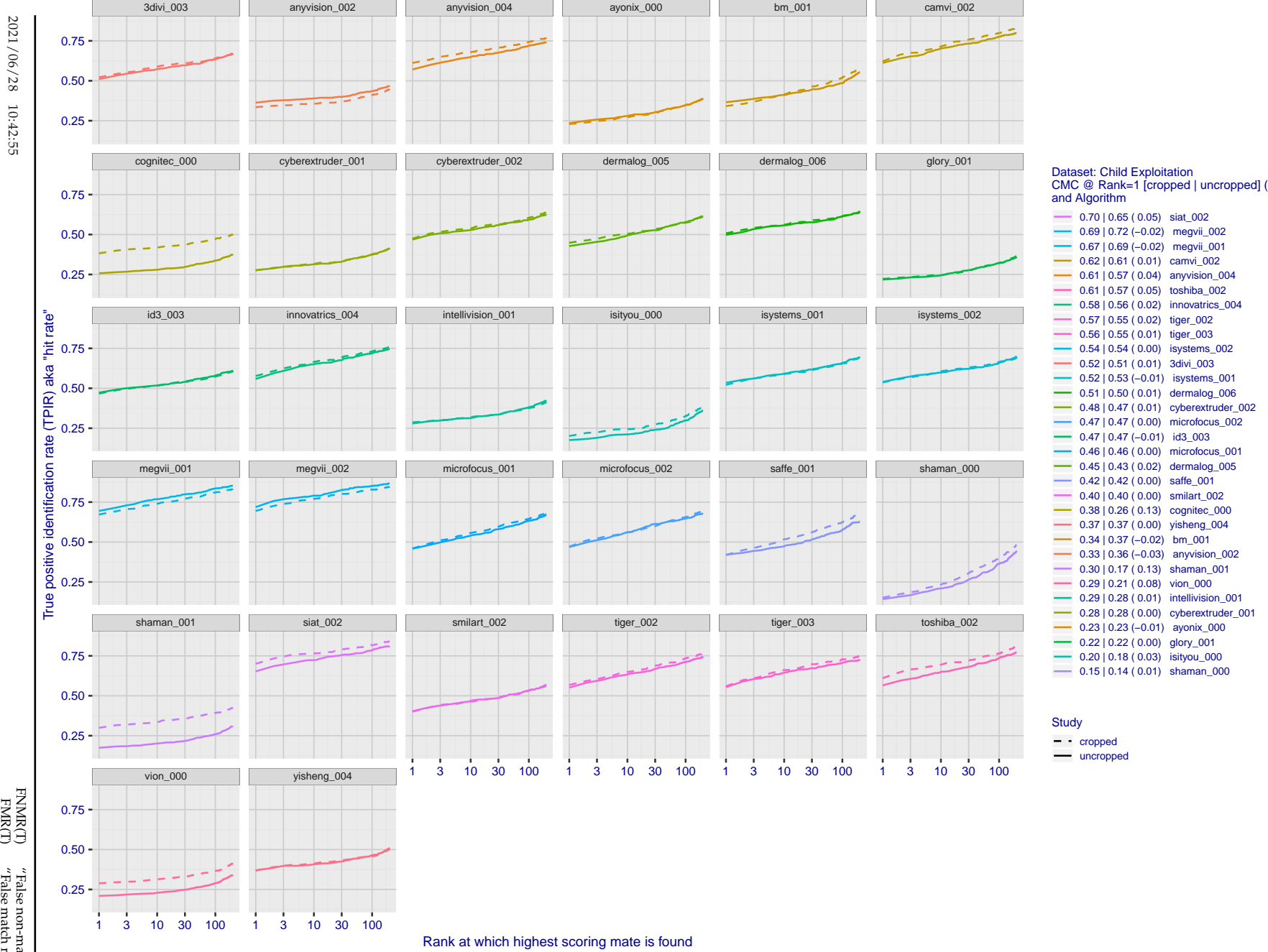


Figure 88: For child exploitation images, cumulative match characteristics (CMC) showing true positive identification rate vs. rank for two cases: 1. Whole image provided to the algorithm; 2. Human annotated rectangular region, cropped and provided to the algorithm. The difference between the traces is associated with detection of difficult faces, and fine localization.



Figure 89: For the mugshot images, FMR for same-sex impostor pairs of images annotated with codes for black female, black male, white female, white male. The threshold is set for each algorithm to give FMR = 0.001 for white males which is the demographic that usually gives the lowest FMR. This means the top right box is the same color in all panels. The panels are sorted over multiple pages in order of FMR on black females, which is the demographic that usually gives the highest FMR.

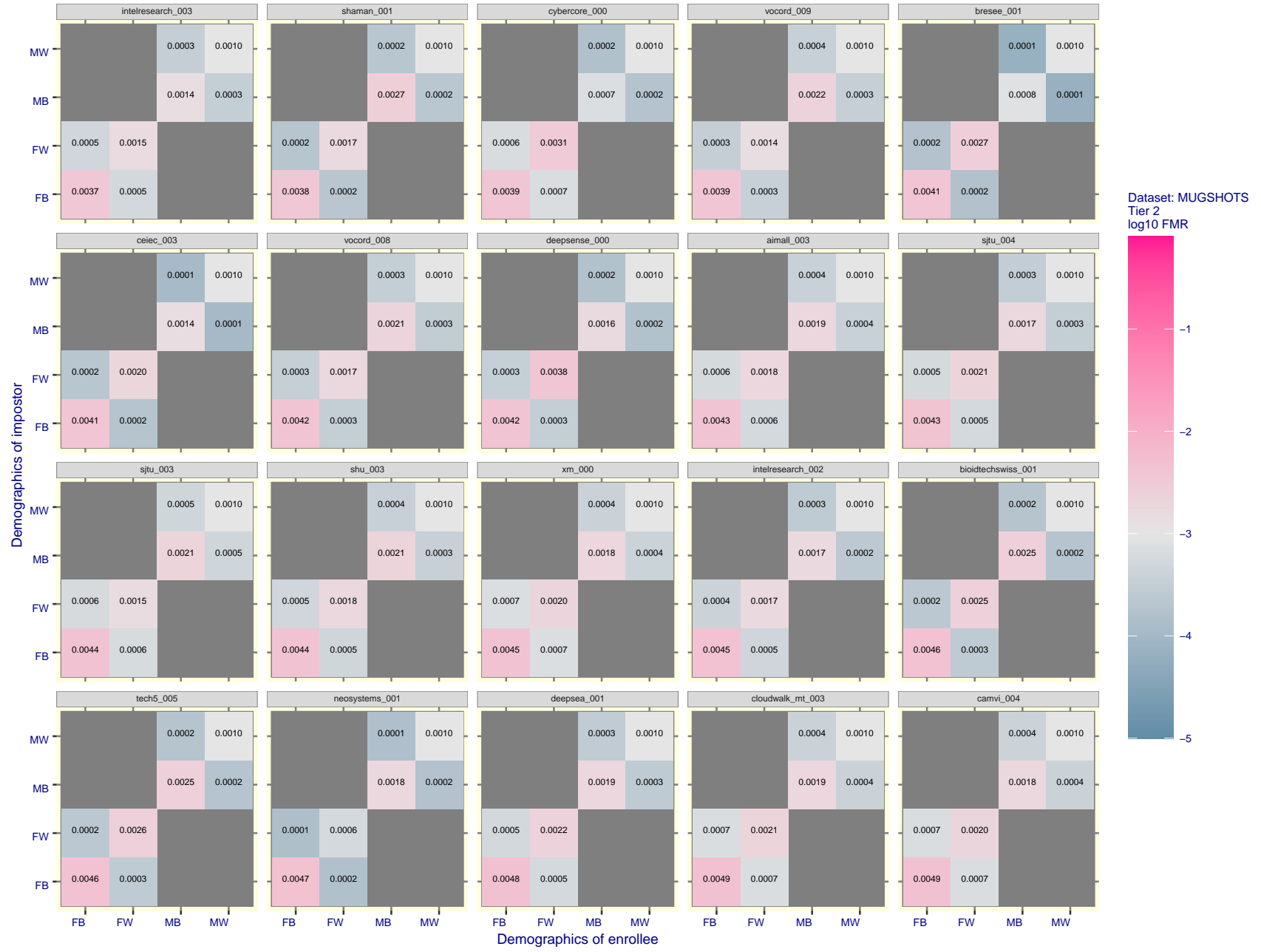


Figure 90: For the mugshot images, FMR for same-sex impostor pairs of images annotated with codes for black female, black male, white female, white male. The threshold is set for each algorithm to give FMR = 0.001 for white males which is the demographic that usually gives the lowest FMR. This means the top right box is the same color in all panels. The panels are sorted over multiple pages in order of FMR on black females, which is the demographic that usually gives the highest FMR.

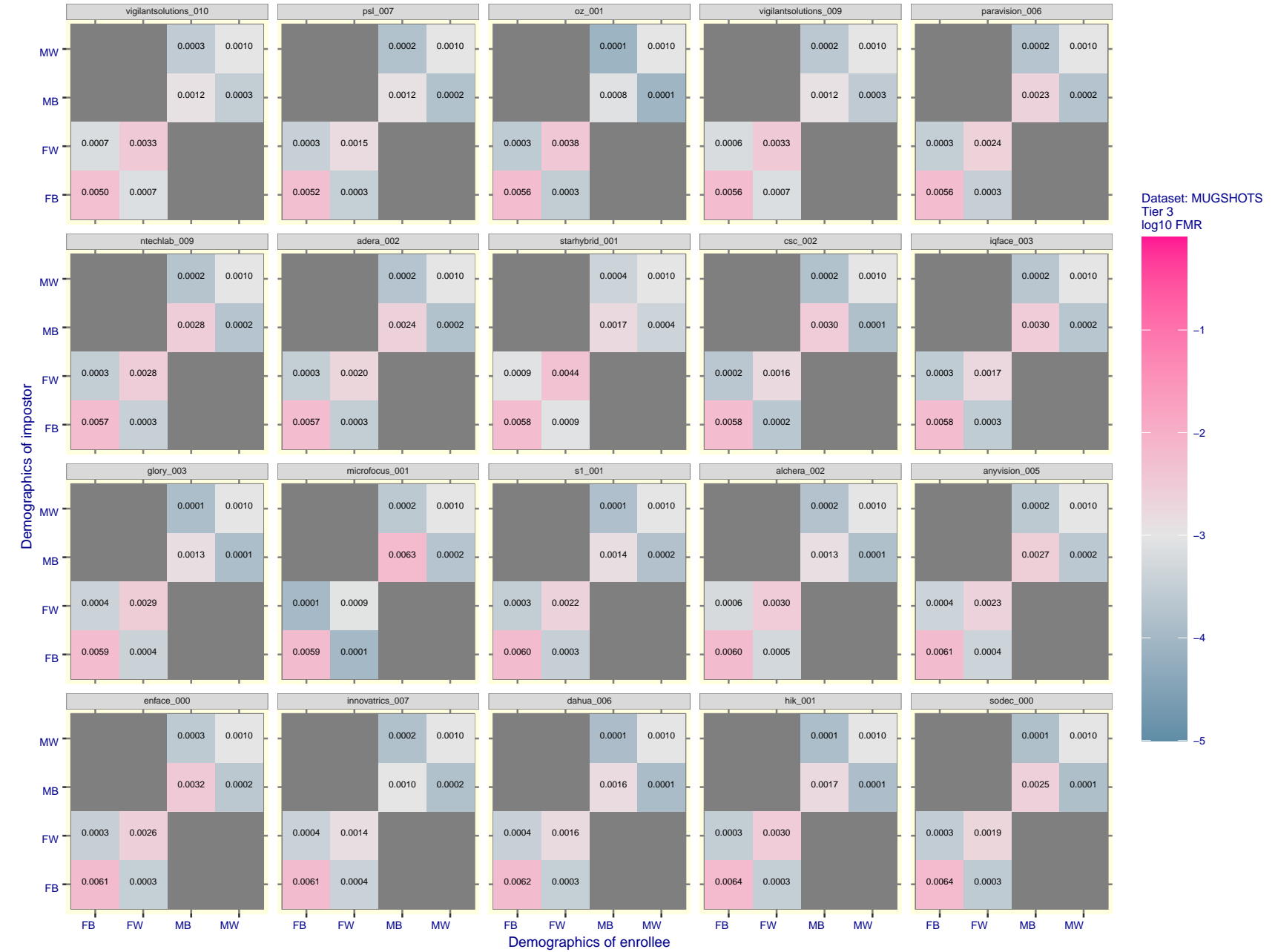


Figure 91: For the mugshot images, FMR for same-sex impostor pairs of images annotated with codes for black female, black male, white female, white male. The threshold is set for each algorithm to give $\text{FMR} = 0.001$ for white males which is the demographic that usually gives the lowest FMR. This means the top right box is the same color in all panels. The panels are sorted over multiple pages in order of FMR on black females, which is the demographic that usually gives the highest FMR.

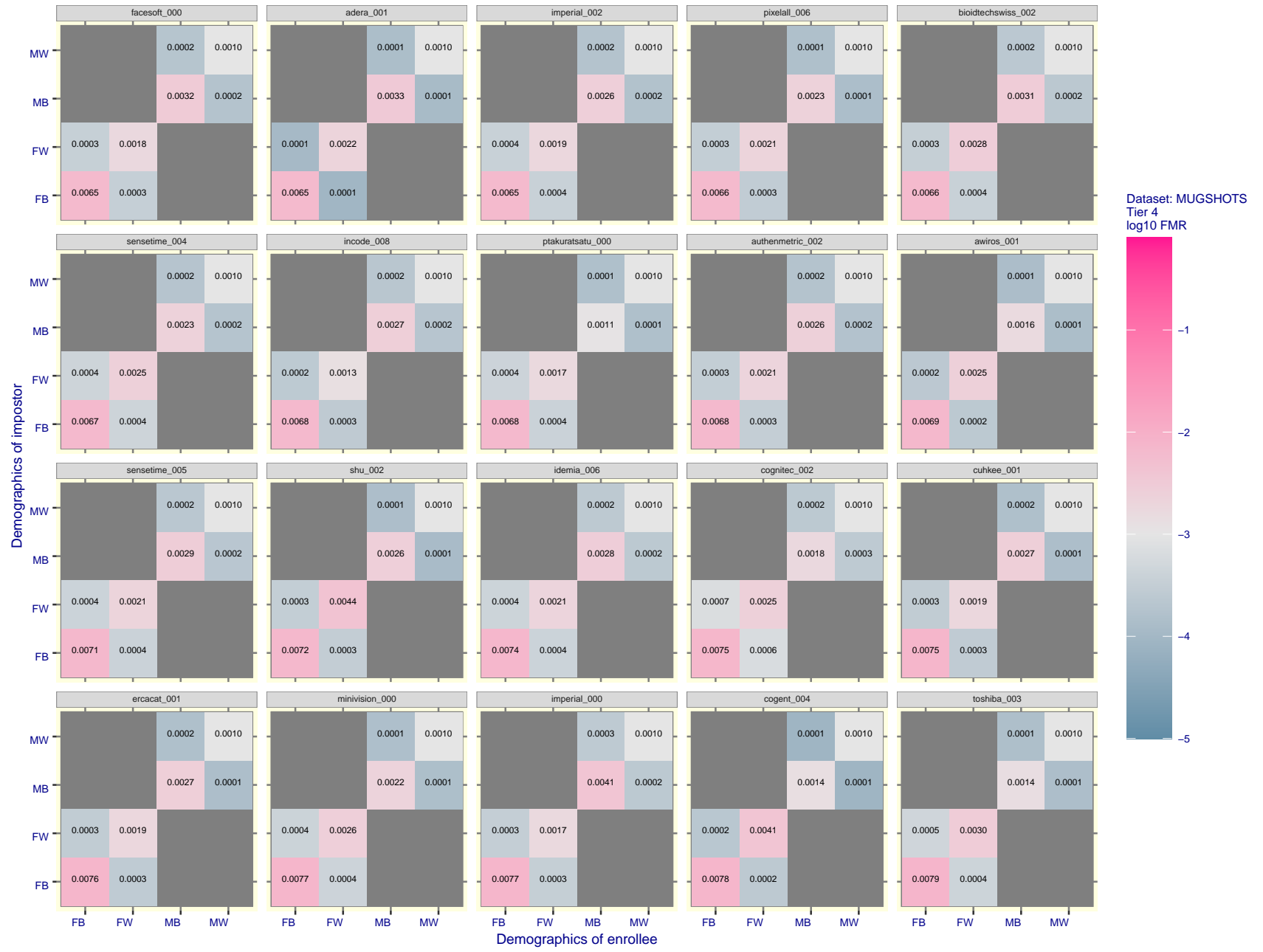


Figure 92: For the mugshot images, FMR for same-sex impostor pairs of images annotated with codes for black female, black male, white female, white male. The threshold is set for each algorithm to give FMR = 0.001 for white males which is the demographic that usually gives the lowest FMR. This means the top right box is the same color in all panels. The panels are sorted over multiple pages in order of FMR on black females, which is the demographic that usually gives the highest FMR.

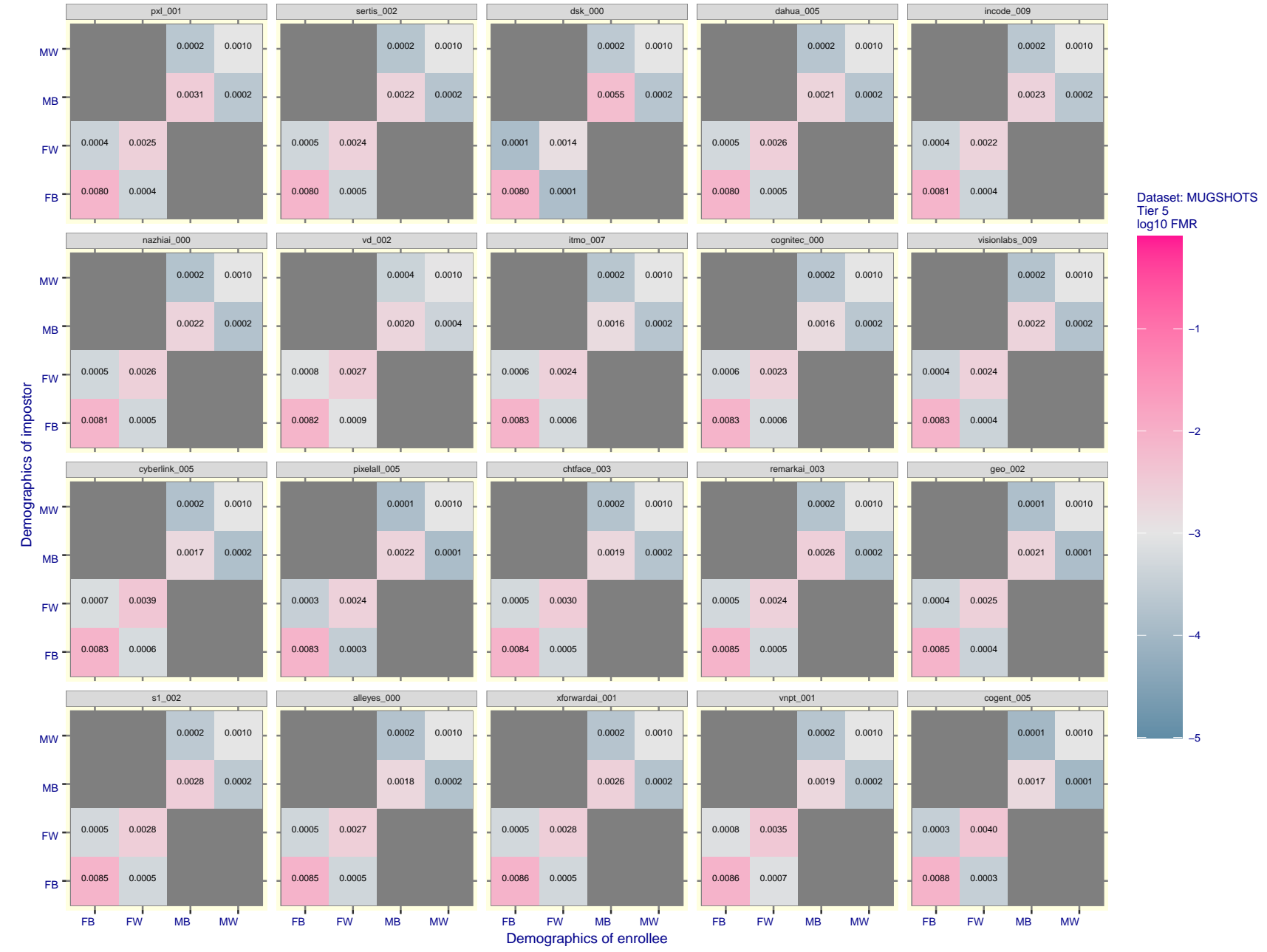


Figure 93: For the mugshot images, FMR for same-sex impostor pairs of images annotated with codes for black female, black male, white female, white male. The threshold is set for each algorithm to give $\text{FMR} = 0.001$ for white males which is the demographic that usually gives the lowest FMR. This means the top right box is the same color in all panels. The panels are sorted over multiple pages in order of FMR on black females, which is the demographic that usually gives the highest FMR.

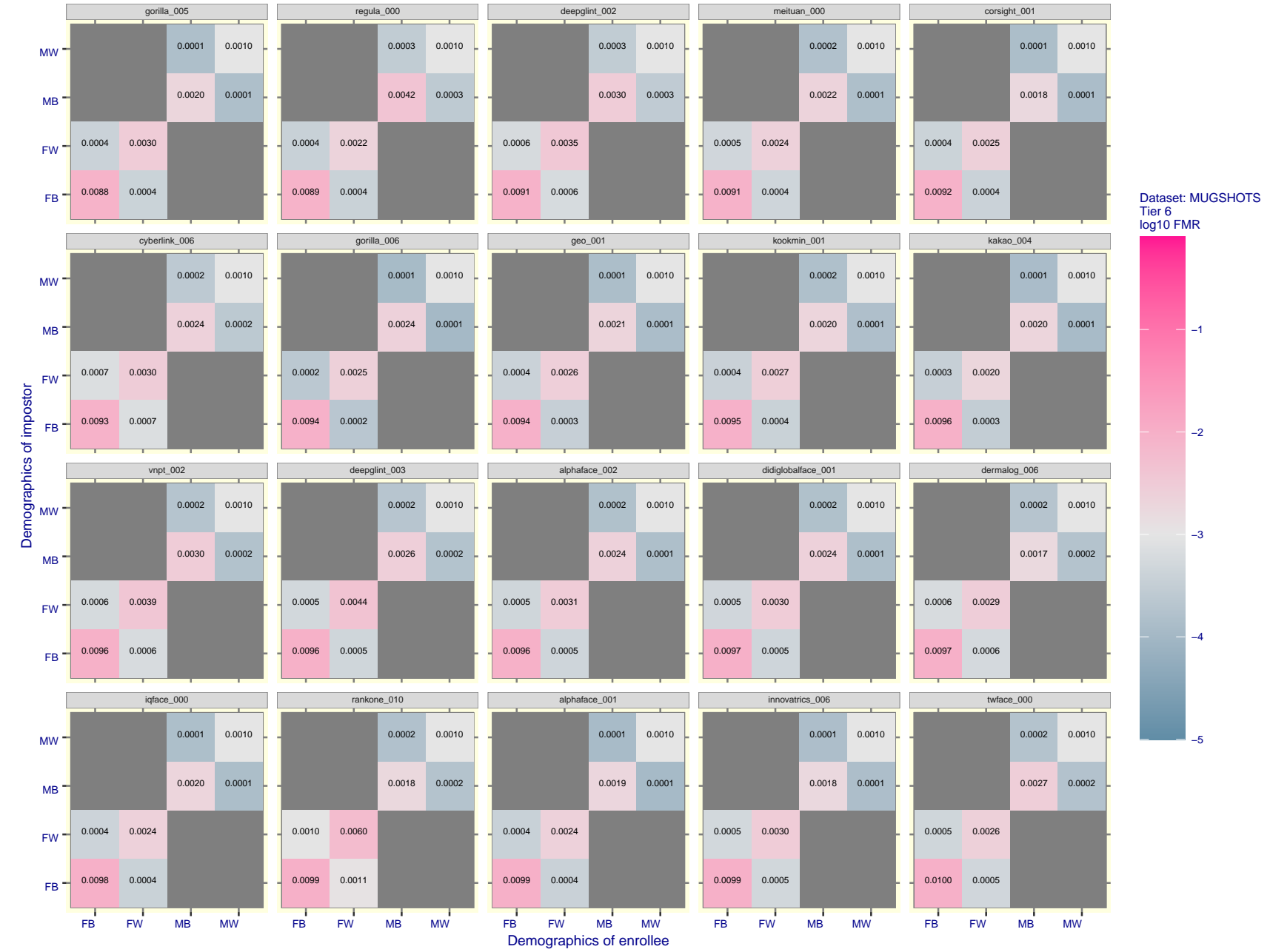


Figure 94: For the mugshot images, FMR for same-sex impostor pairs of images annotated with codes for black female, black male, white female, white male. The threshold is set for each algorithm to give $\text{FMR} = 0.001$ for white males which is the demographic that usually gives the lowest FMR. This means the top right box is the same color in all panels. The panels are sorted over multiple pages in order of FMR on black females, which is the demographic that usually gives the highest FMR.

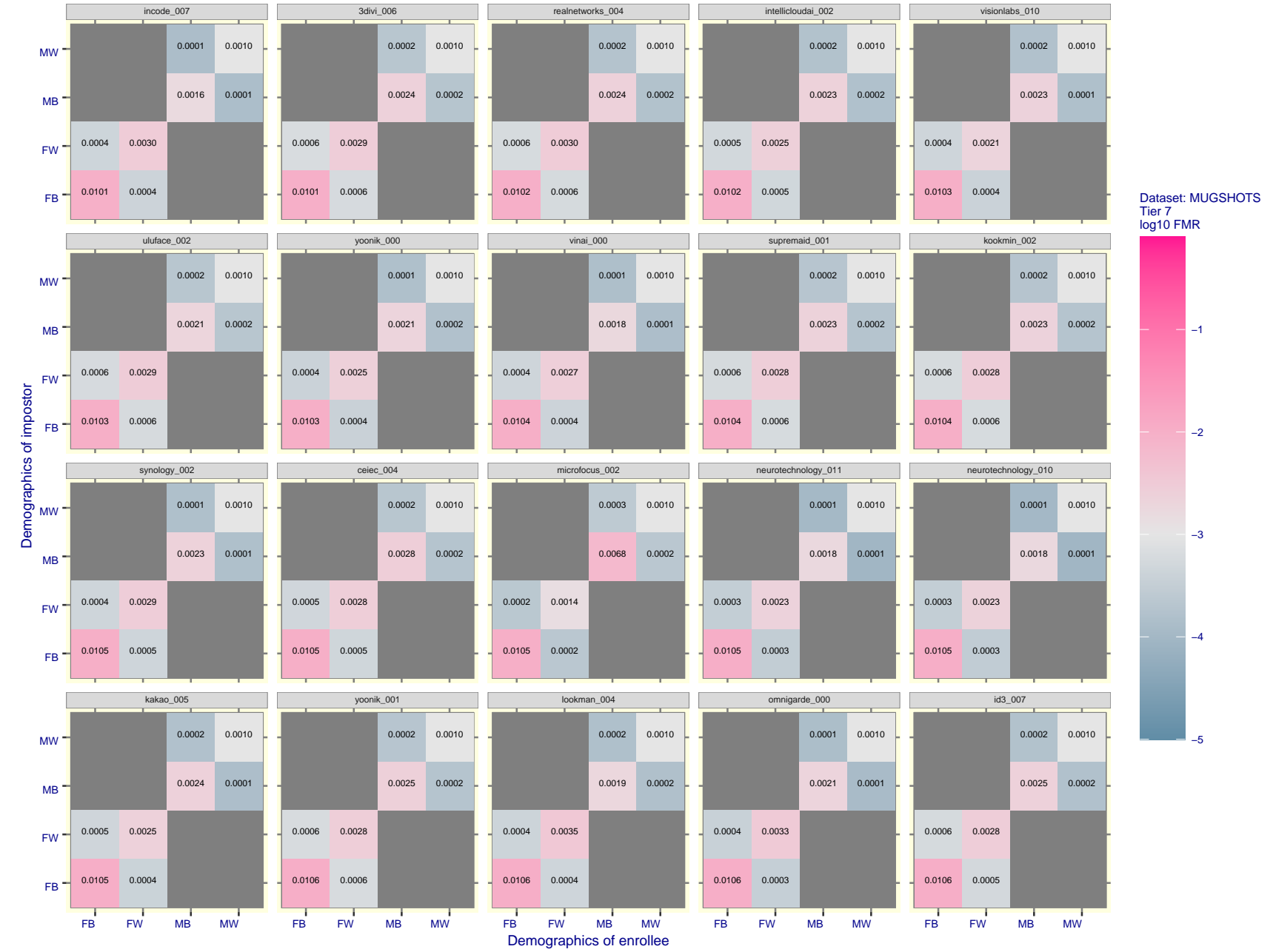


Figure 95: For the mugshot images, FMR for same-sex impostor pairs of images annotated with codes for black female, black male, white female, white male. The threshold is set for each algorithm to give $FMR = 0.001$ for white males which is the demographic that usually gives the lowest FMR. This means the top right box is the same color in all panels. The panels are sorted over multiple pages in order of FMR on black females, which is the demographic that usually gives the highest FMR.

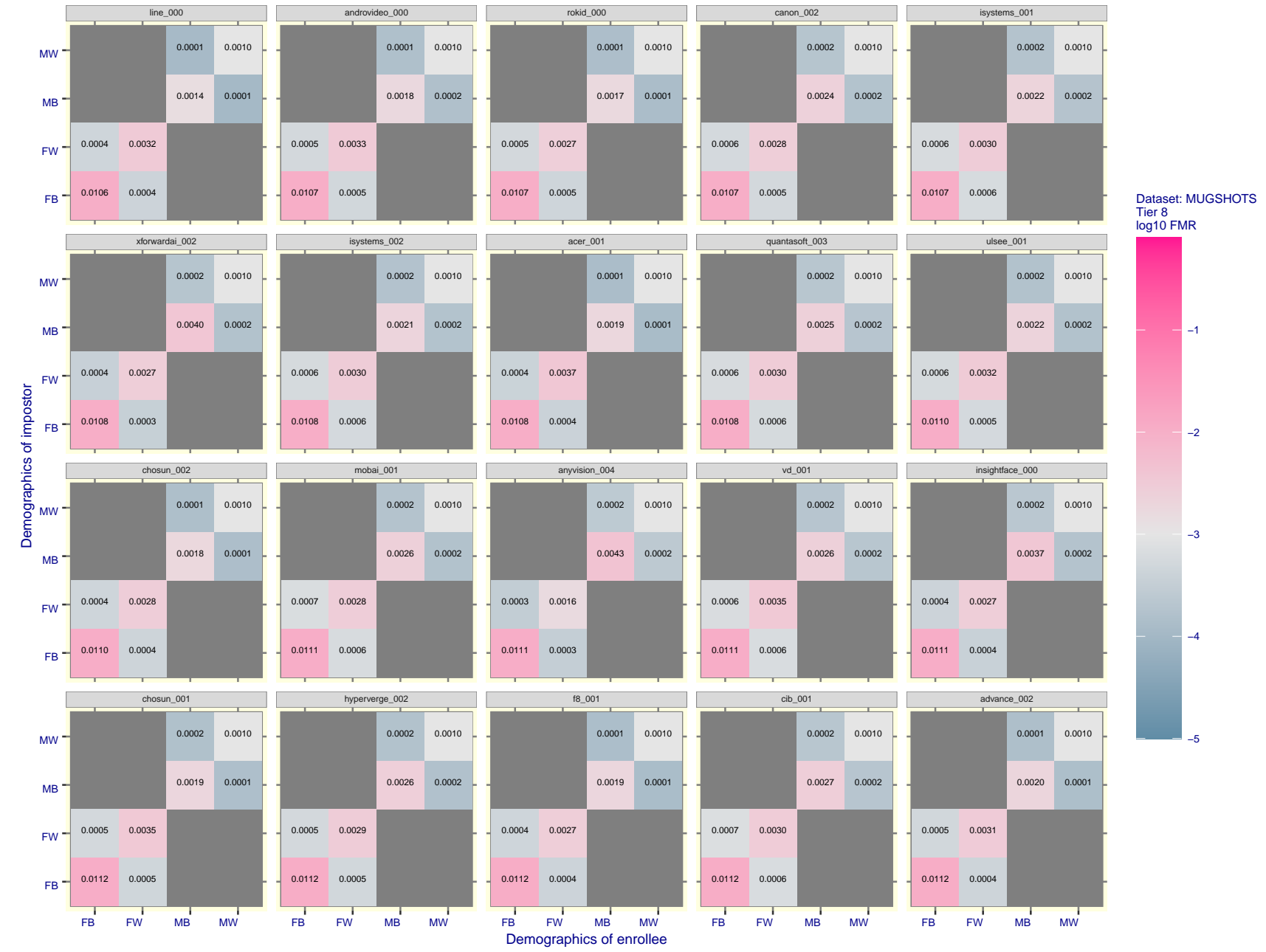


Figure 96: For the mugshot images, FMR for same-sex impostor pairs of images annotated with codes for black female, black male, white female, white male. The threshold is set for each algorithm to give FMR = 0.001 for white males which is the demographic that usually gives the lowest FMR. This means the top right box is the same color in all panels. The panels are sorted over multiple pages in order of FMR on black females, which is the demographic that usually gives the highest FMR.

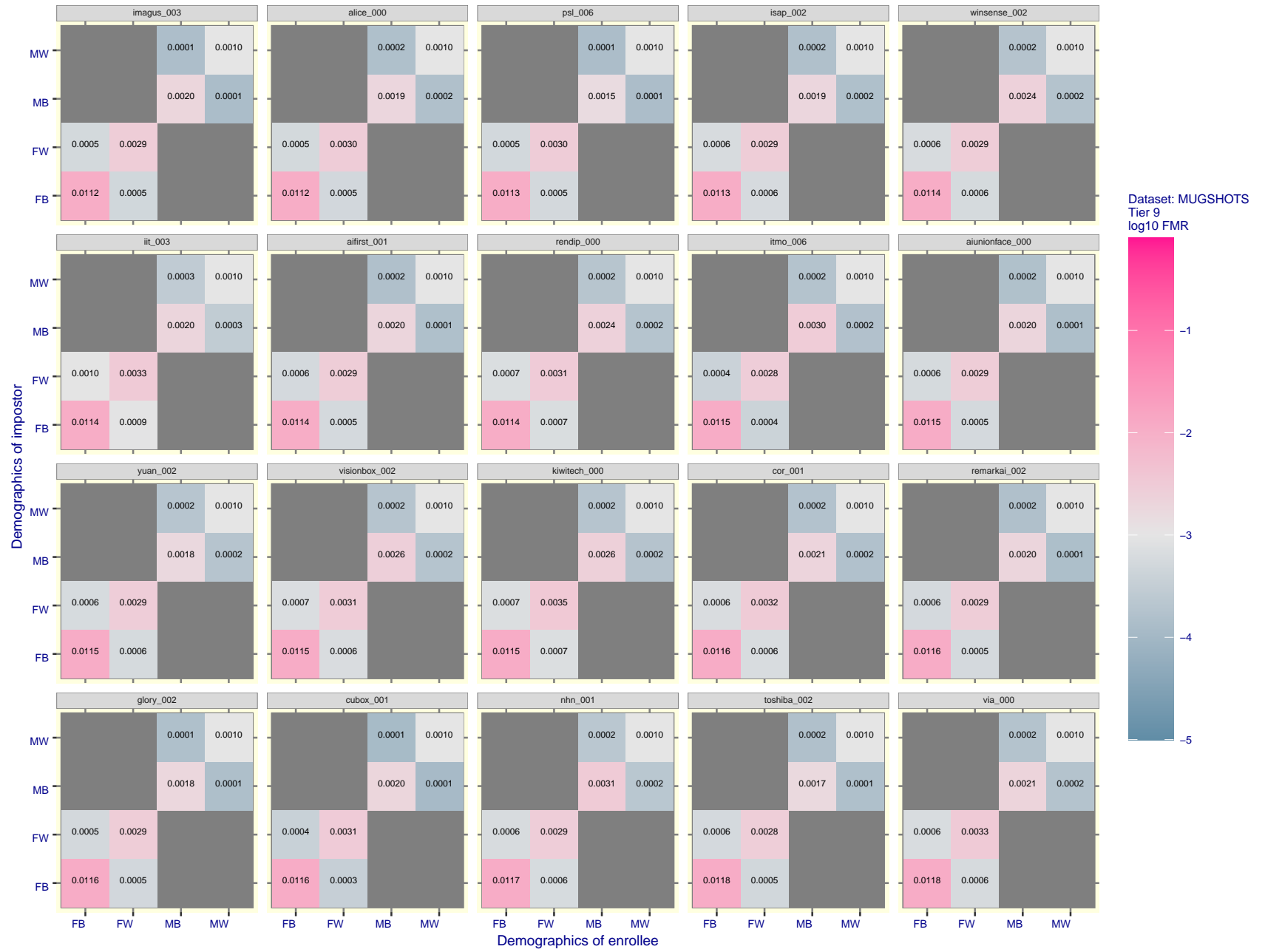


Figure 97: For the mugshot images, FMR for same-sex impostor pairs of images annotated with codes for black female, black male, white female, white male. The threshold is set for each algorithm to give $FMR = 0.001$ for white males which is the demographic that usually gives the lowest FMR. This means the top right box is the same color in all panels. The panels are sorted over multiple pages in order of FMR on black females, which is the demographic that usually gives the highest FMR.

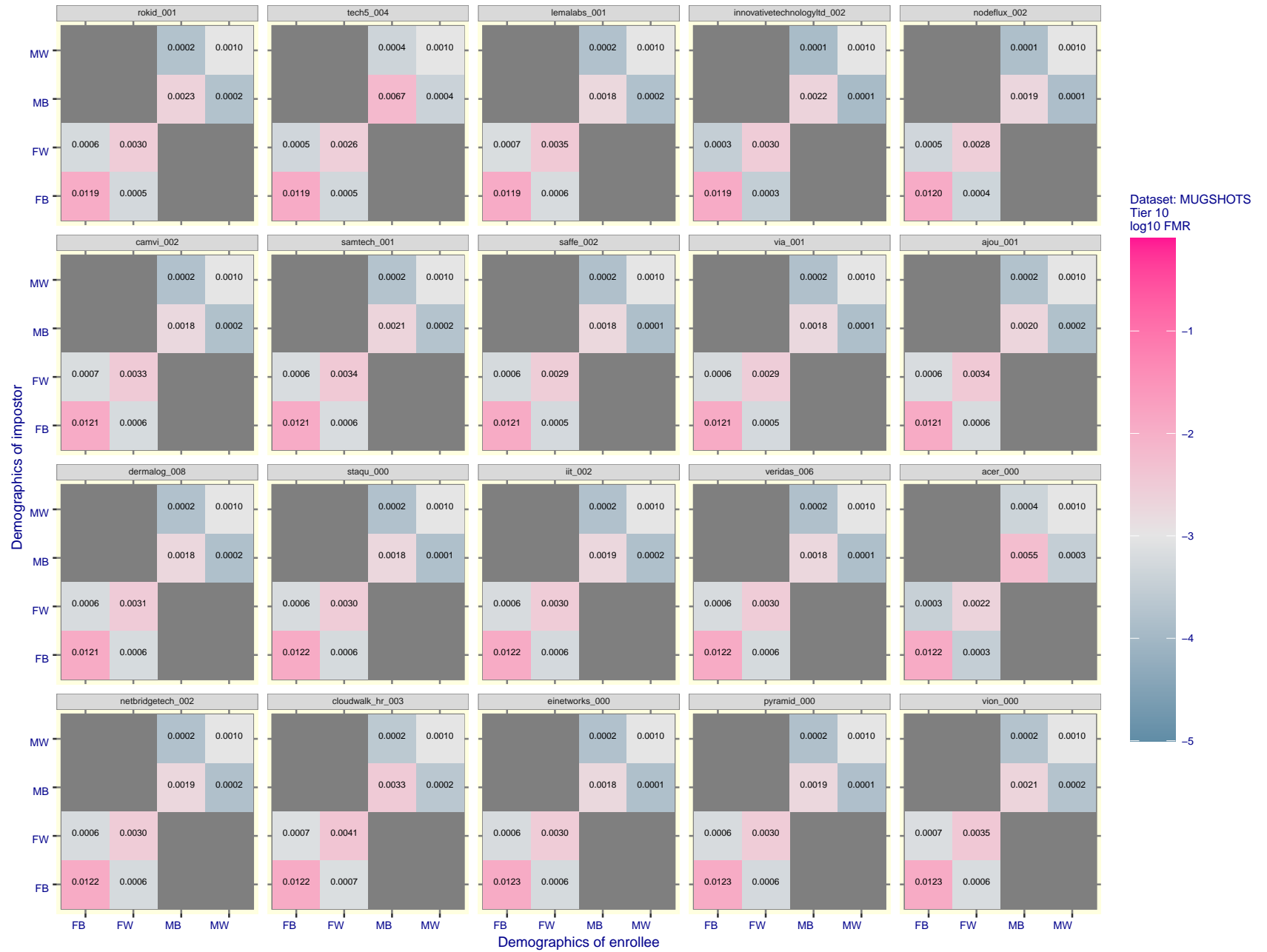


Figure 98: For the mugshot images, FMR for same-sex impostor pairs of images annotated with codes for black female, black male, white female, white male. The threshold is set for each algorithm to give $FMR = 0.001$ for white males which is the demographic that usually gives the lowest FMR. This means the top right box is the same color in all panels. The panels are sorted over multiple pages in order of FMR on black females, which is the demographic that usually gives the highest FMR.



Figure 99: For the mugshot images, FMR for same-sex impostor pairs of images annotated with codes for black female, black male, white female, white male. The threshold is set for each algorithm to give $FMR = 0.001$ for white males which is the demographic that usually gives the lowest FMR. This means the top right box is the same color in all panels. The panels are sorted over multiple pages in order of FMR on black females, which is the demographic that usually gives the highest FMR.

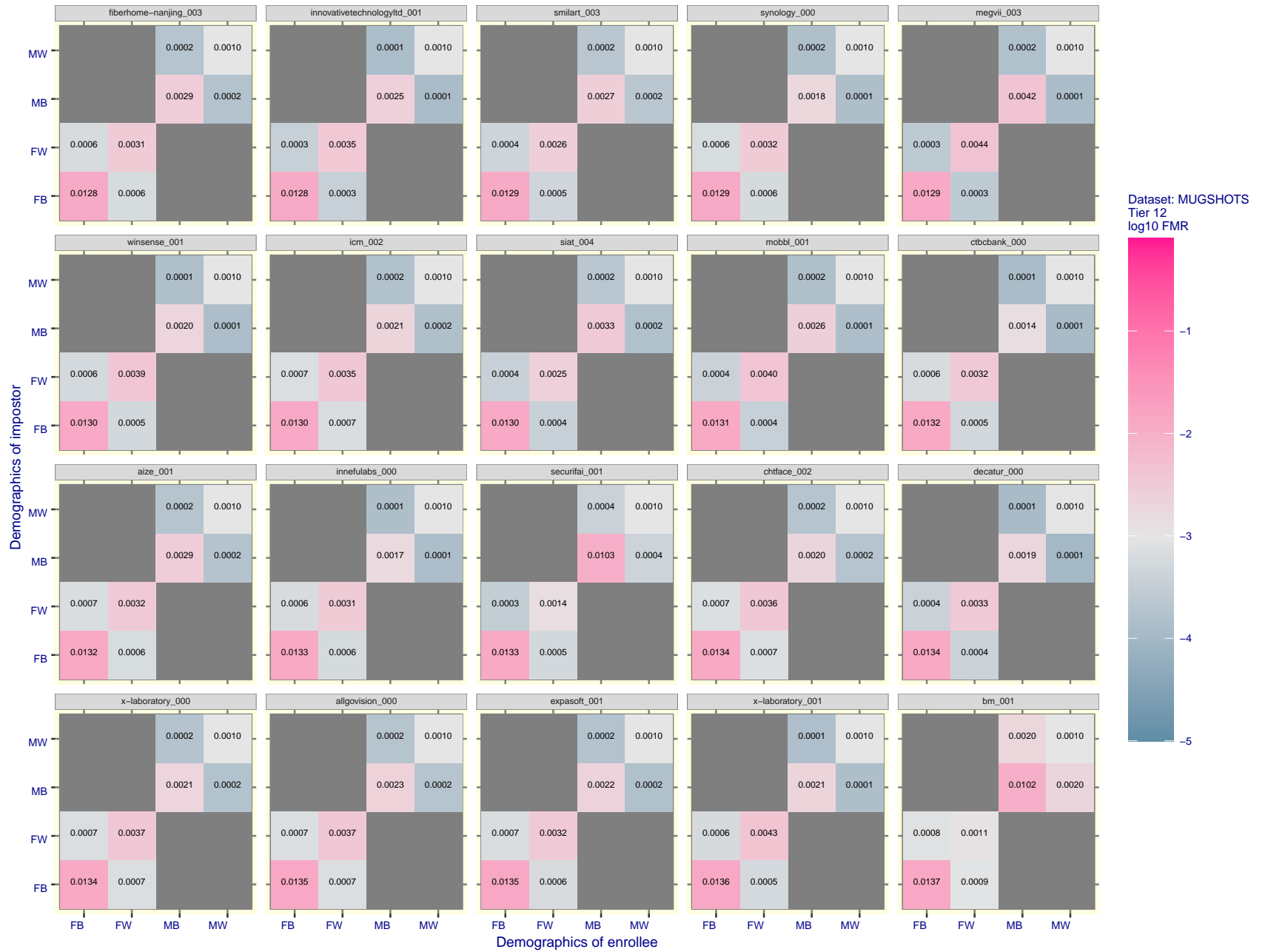


Figure 100: For the mugshot images, FMR for same-sex impostor pairs of images annotated with codes for black female, black male, white female, white male. The threshold is set for each algorithm to give FMR = 0.001 for white males which is the demographic that usually gives the lowest FMR. This means the top right box is the same color in all panels. The panels are sorted over multiple pages in order of FMR on black females, which is the demographic that usually gives the highest FMR.

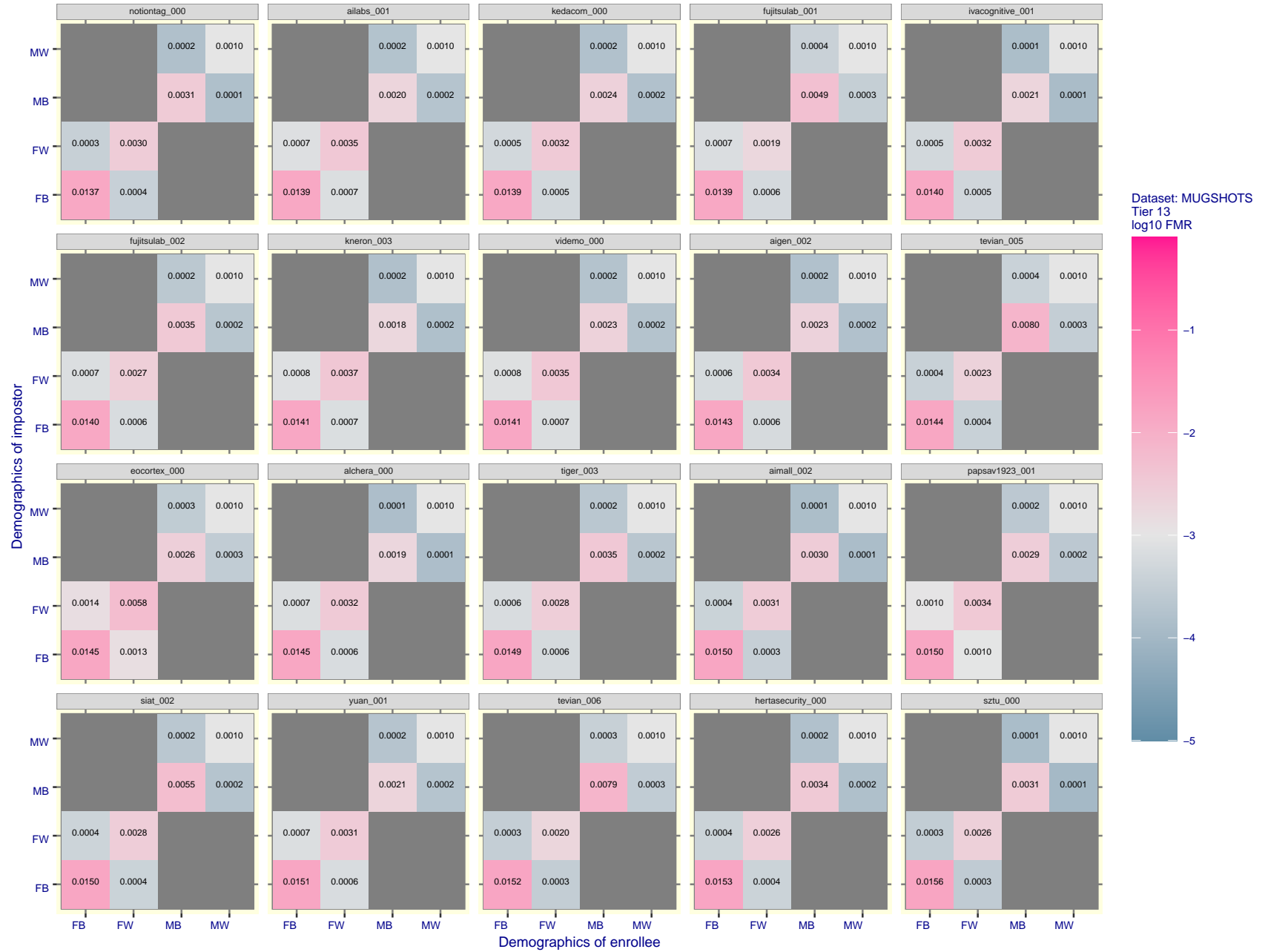


Figure 101: For the mugshot images, FMR for same-sex impostor pairs of images annotated with codes for black female, black male, white female, white male. The threshold is set for each algorithm to give $FMR = 0.001$ for white males which is the demographic that usually gives the lowest FMR. This means the top right box is the same color in all panels. The panels are sorted over multiple pages in order of FMR on black females, which is the demographic that usually gives the highest FMR.

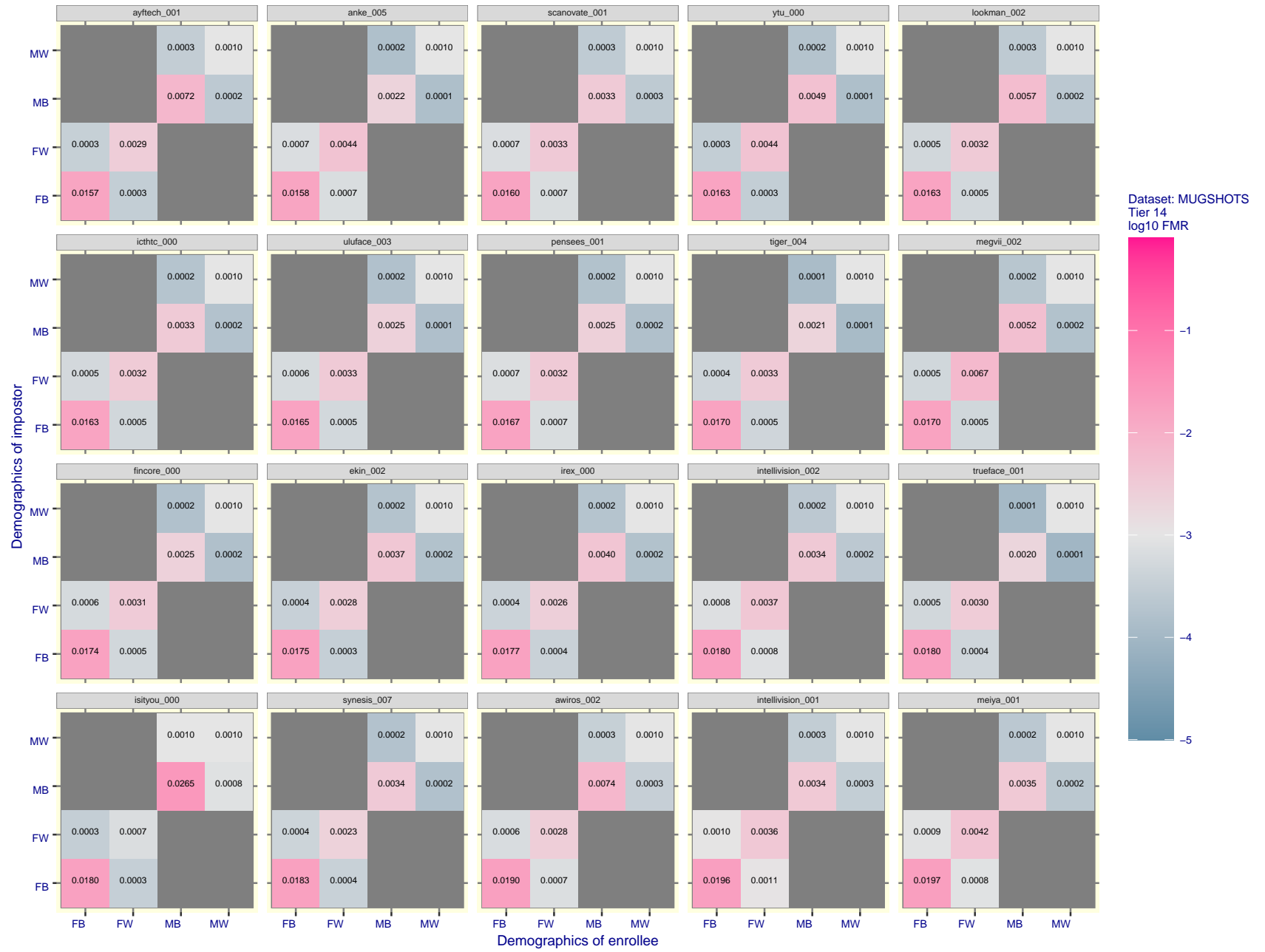


Figure 102: For the mugshot images, FMR for same-sex impostor pairs of images annotated with codes for black female, black male, white female, white male. The threshold is set for each algorithm to give FMR = 0.001 for white males which is the demographic that usually gives the lowest FMR. This means the top right box is the same color in all panels. The panels are sorted over multiple pages in order of FMR on black females, which is the demographic that usually gives the highest FMR.



Figure 103: For the mugshot images, FMR for same-sex impostor pairs of images annotated with codes for black female, black male, white female, white male. The threshold is set for each algorithm to give $FMR = 0.001$ for white males which is the demographic that usually gives the lowest FMR. This means the top right box is the same color in all panels. The panels are sorted over multiple pages in order of FMR on black females, which is the demographic that usually gives the highest FMR.

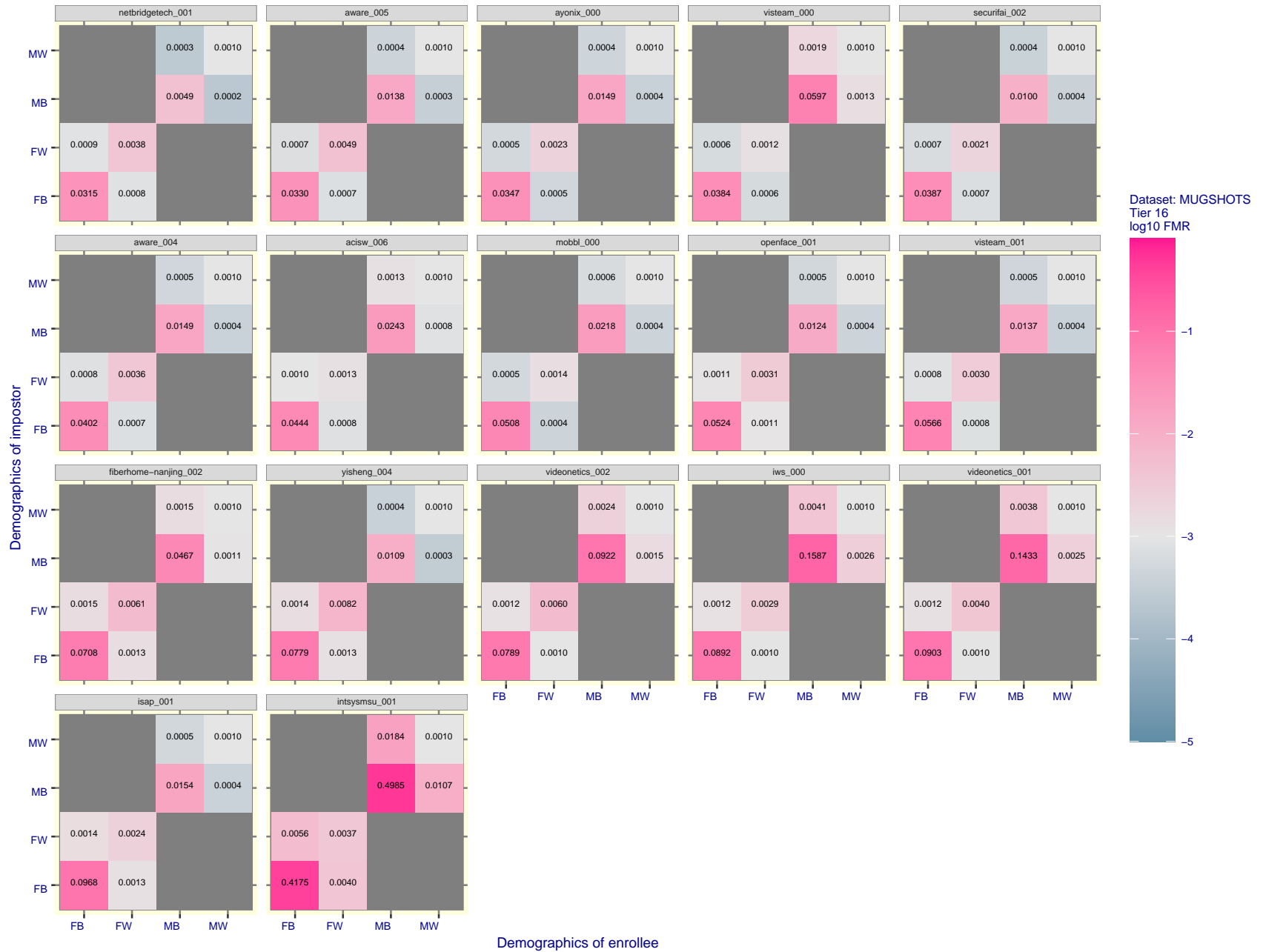


Figure 104: For the mugshot images, FMR for same-sex impostor pairs of images annotated with codes for black female, black male, white female, white male. The threshold is set for each algorithm to give $\text{FMR} = 0.001$ for white males which is the demographic that usually gives the lowest FMR. This means the top right box is the same color in all panels. The panels are sorted over multiple pages in order of FMR on black females, which is the demographic that usually gives the highest FMR.

2021/06/28 10:42:55

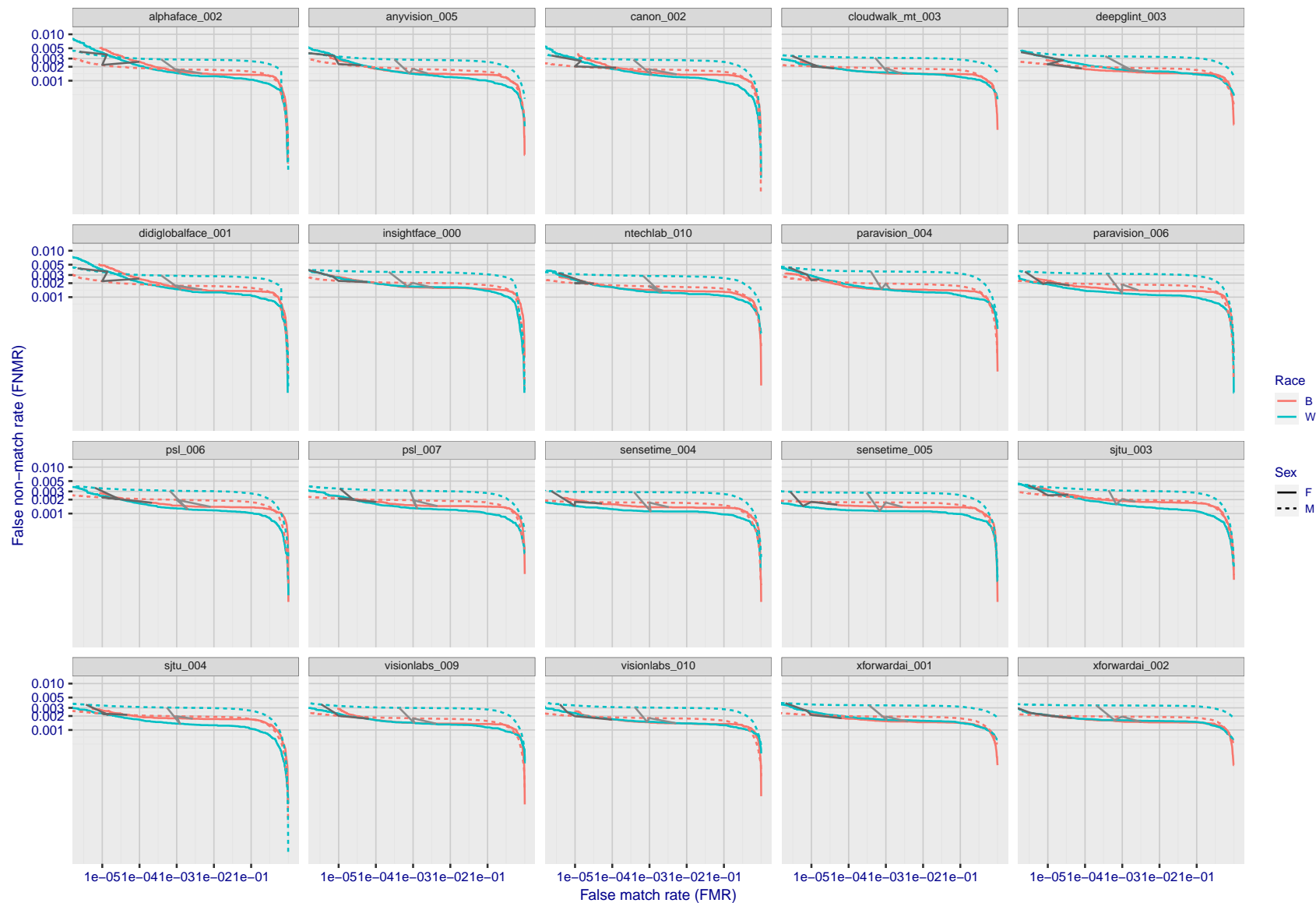


Figure 105: For the mugshot images, error tradeoff characteristics for white females, black females, black males and white males. The Z-shaped grey lines correspond to fixed thresholds, showing both FNMR and FMR vary at one T value. Note: Many of the plots will naively be read as saying women gives worse error rates than men because the solid traces lie above the dotted ones. However, this is misleading and incomplete: The grey lines show the traces reveal horizontal shifts. Thus for the cogent-003 algorithm FNMR for men is higher than for women at a fixed threshold but, at the same time, FMR is higher for women - see Figure 163. As access control systems almost always operate at a fixed threshold, the naive interpretation is incorrect.

FNMR(T)"False non-match rate"
"False match rate"

2021/06/28 10:42:55

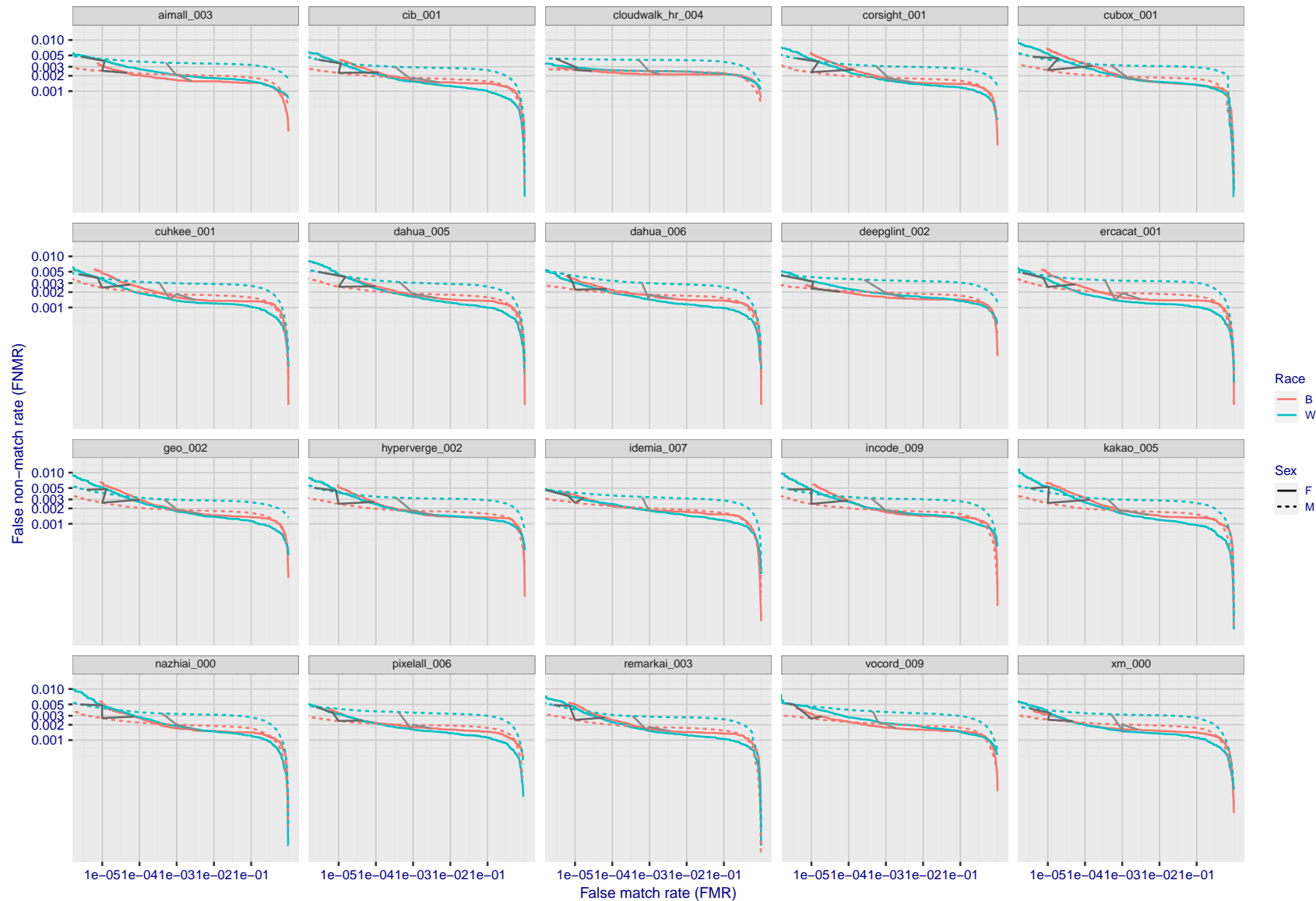


Figure 106: For the mugshot images, error tradeoff characteristics for white females, black females, black males and white males. The Z-shaped grey lines correspond to fixed thresholds, showing both FNMR and FMR vary at one T value. Note: Many of the plots will naively be read as saying women gives worse error rates than men because the solid traces lie above the dotted ones. However, this is misleading and incomplete: The grey lines show the traces reveal horizontal shifts. Thus for the cogent-003 algorithm FNMR for men is higher than for women at a fixed threshold but, at the same time, FMR is higher for women - see Figure 163. As access control systems almost always operate at a fixed threshold, the naive interpretation is incorrect.

FNMR(T)"False non-match rate"
"False match rate"

2021/06/28 10:42:55

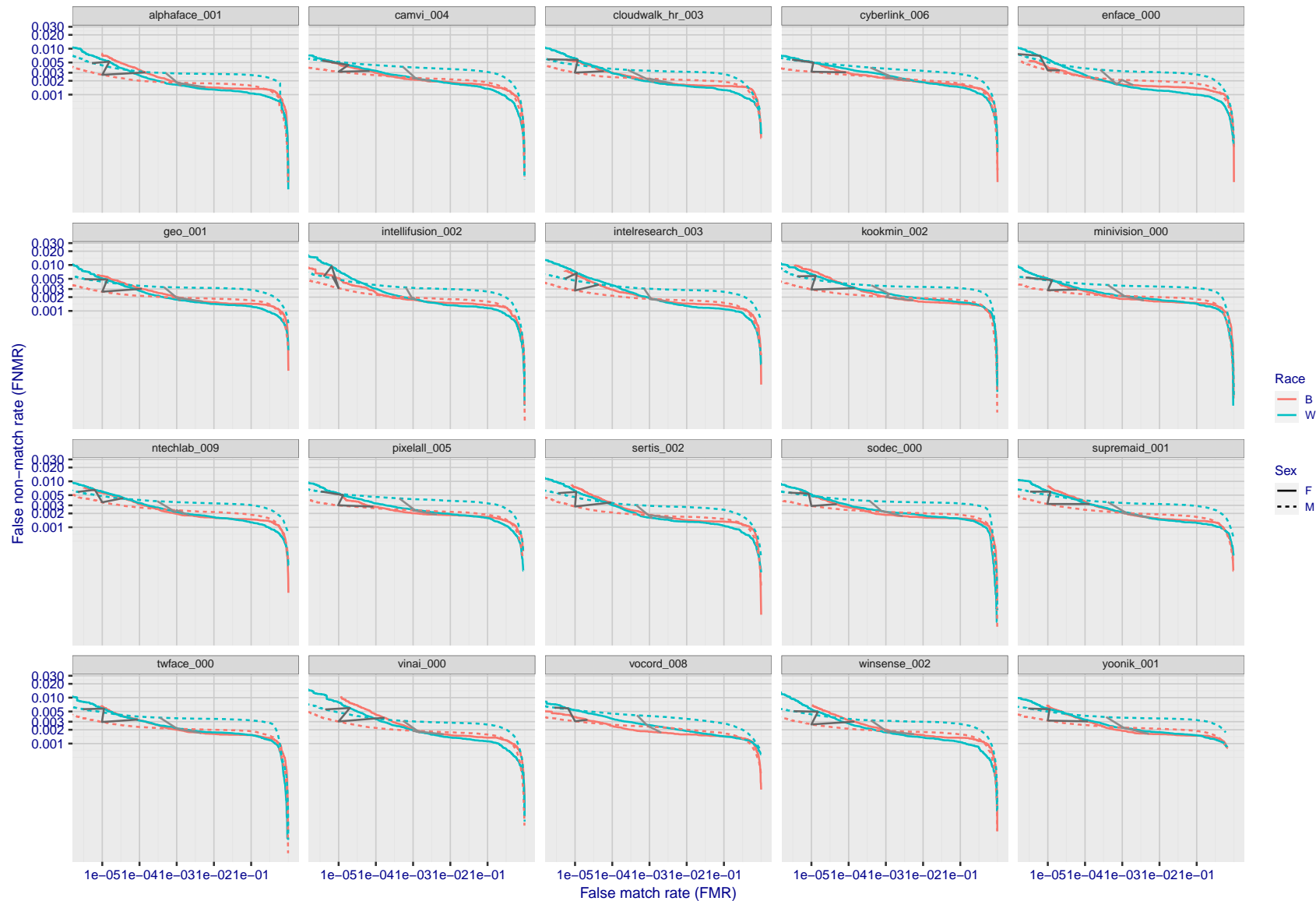


Figure 107: For the mugshot images, error tradeoff characteristics for white females, black females, black males and white males. The Z-shaped grey lines correspond to fixed thresholds, showing both FNMR and FMR vary at one T value. Note: Many of the plots will naively be read as saying women gives worse error rates than men because the solid traces lie above the dotted ones. However, this is misleading and incomplete: The grey lines show the traces reveal horizontal shifts. Thus for the cogent-003 algorithm FNMR for men is higher than for women at a fixed threshold but, at the same time, FMR is higher for women - see Figure 163. As access control systems almost always operate at a fixed threshold, the naive interpretation is incorrect.

FNMR(T)"False non-match rate"
"False match rate"

2021/06/28 10:42:55

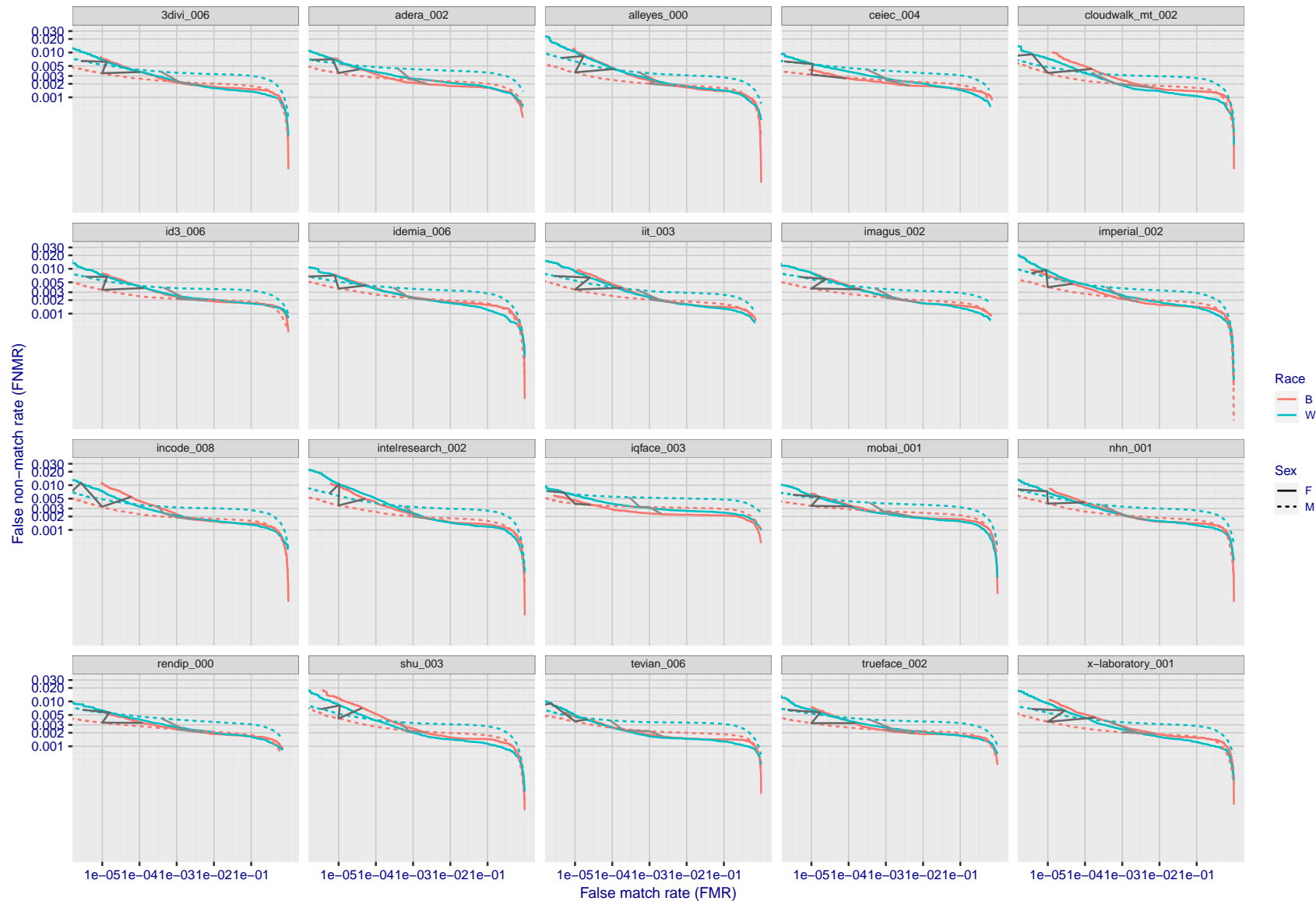


Figure 108: For the mugshot images, error tradeoff characteristics for white females, black females, black males and white males. The Z-shaped grey lines correspond to fixed thresholds, showing both FNMR and FMR vary at one T value. Note: Many of the plots will naively be read as saying women gives worse error rates than men because the solid traces lie above the dotted ones. However, this is misleading and incomplete: The grey lines show the traces reveal horizontal shifts. Thus for the cogent-003 algorithm FNMR for men is higher than for women at a fixed threshold but, at the same time, FMR is higher for women - see Figure 163. As access control systems almost always operate at a fixed threshold, the naive interpretation is incorrect.

FNMR(T)"False non-match rate"
"False match rate"

2021/06/28 10:42:55

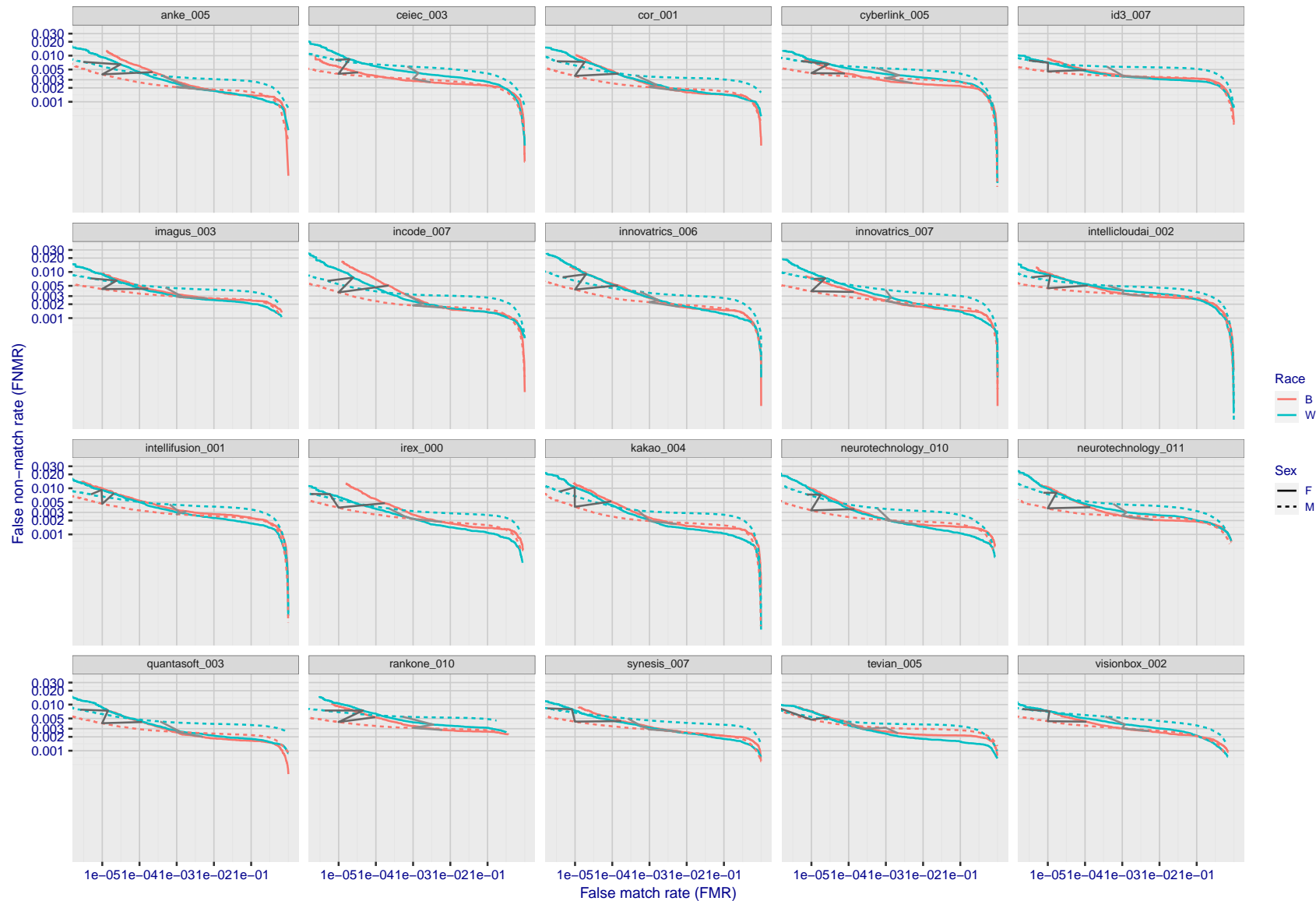


Figure 109: For the mugshot images, error tradeoff characteristics for white females, black females, black males and white males. The Z-shaped grey lines correspond to fixed thresholds, showing both FNMR and FMR vary at one T value. Note: Many of the plots will naively be read as saying women gives worse error rates than men because the solid traces lie above the dotted ones. However, this is misleading and incomplete: The grey lines show the traces reveal horizontal shifts. Thus for the cogent-003 algorithm FNMR for men is higher than for women at a fixed threshold but, at the same time, FMR is higher for women - see Figure 163. As access control systems almost always operate at a fixed threshold, the naive interpretation is incorrect.

FNMR(T)

"False non-match rate"

FMR(T)

"False match rate"

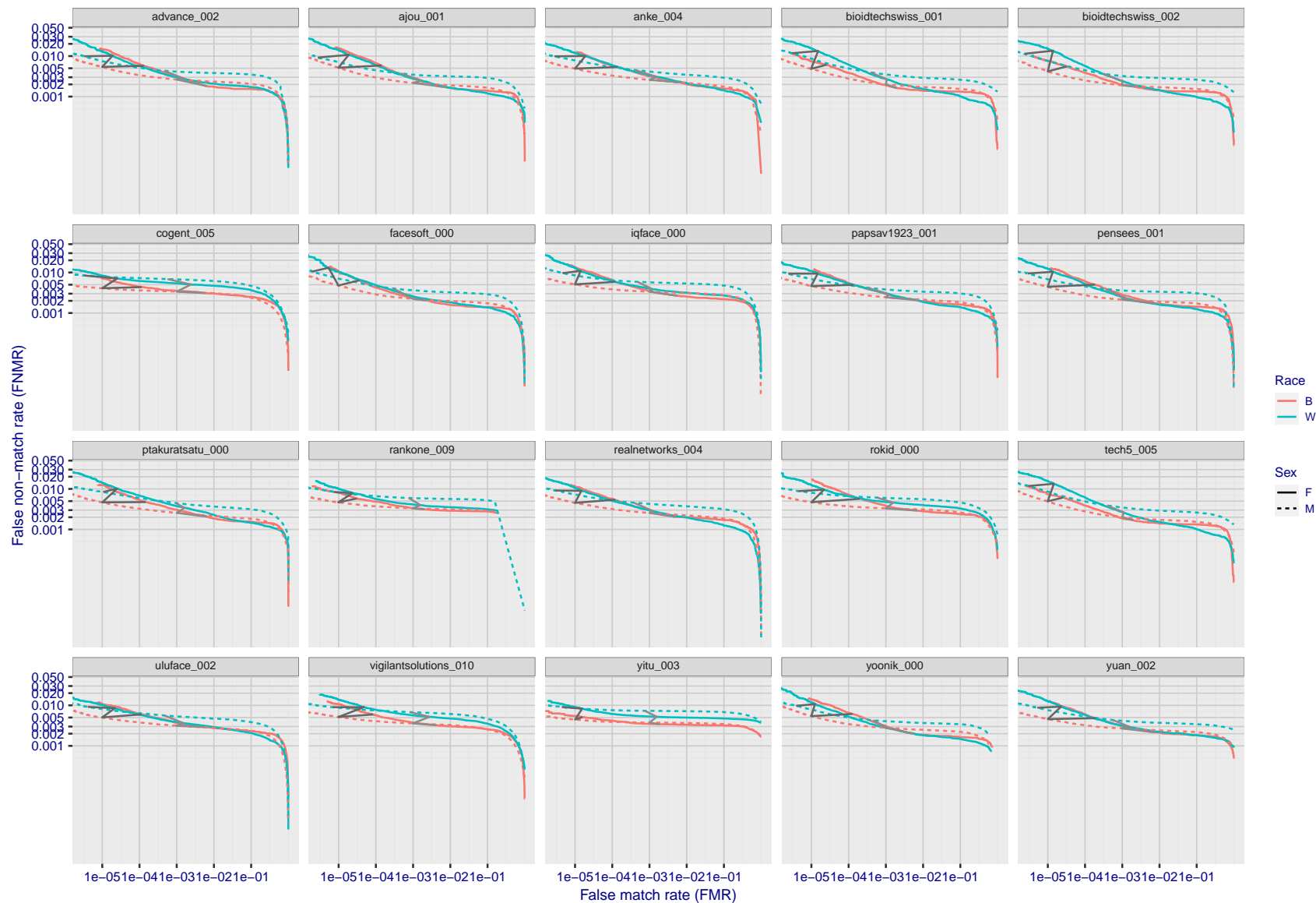


Figure 110: For the mugshot images, error tradeoff characteristics for white females, black females, black males and white males. The Z-shaped grey lines correspond to fixed thresholds, showing both FNMR and FMR vary at one T value. Note: Many of the plots will naively be read as saying women gives worse error rates than men because the solid traces lie above the dotted ones. However, this is misleading and incomplete: The grey lines show the traces reveal horizontal shifts. Thus for the cogent-003 algorithm FNMR for men is higher than for women at a fixed threshold but, at the same time, FMR is higher for women - see Figure 163. As access control systems almost always operate at a fixed threshold, the naive interpretation is incorrect.

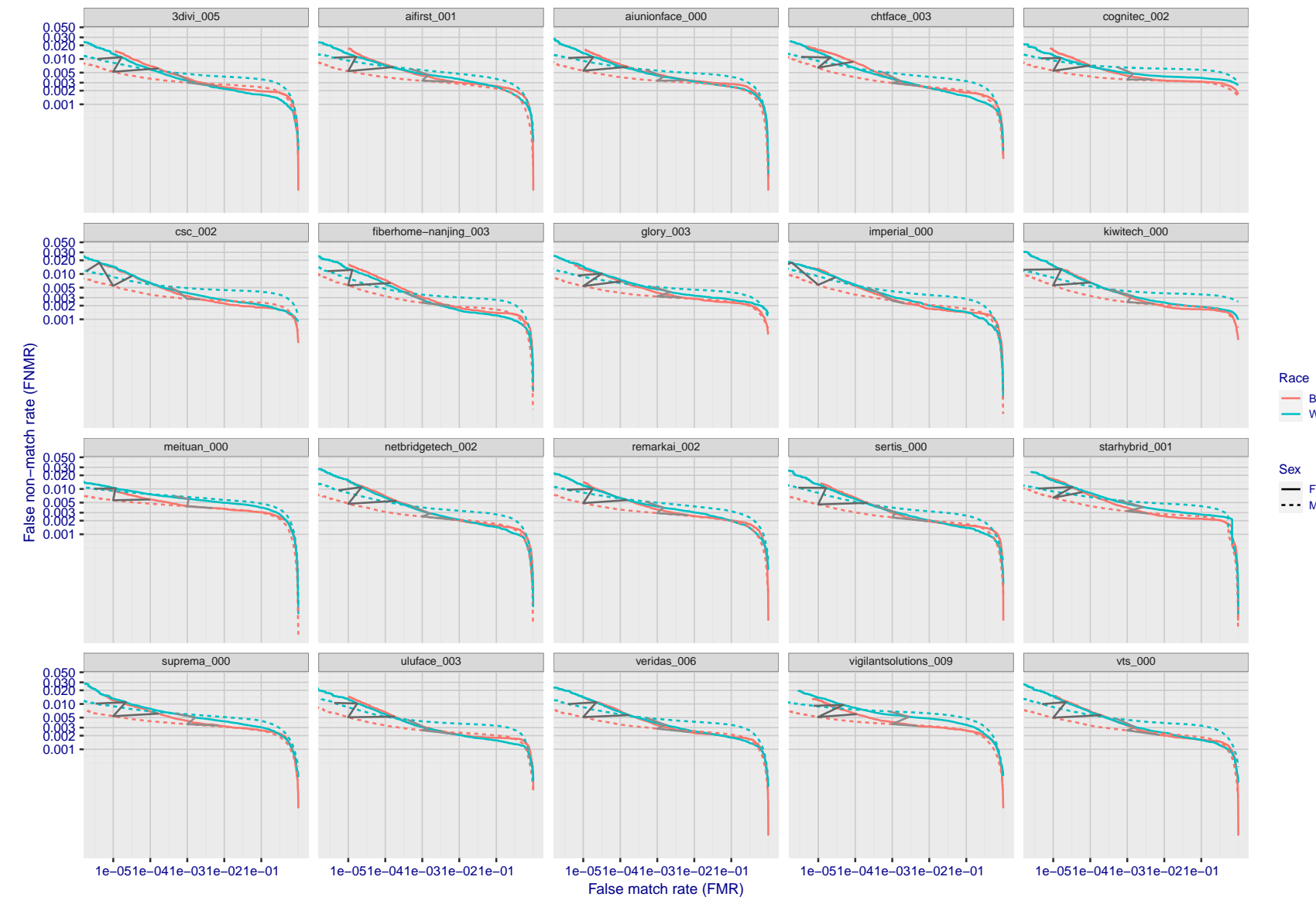


Figure 111: For the mugshot images, error tradeoff characteristics for white females, black females, black males and white males. The Z-shaped grey lines correspond to fixed thresholds, showing both FNMR and FMR vary at one T value. Note: Many of the plots will naively be read as saying women gives worse error rates than men because the solid traces lie above the dotted ones. However, this is misleading and incomplete: The grey lines show the traces reveal horizontal shifts. Thus for the cogent-003 algorithm FNMR for men is higher than for women at a fixed threshold but, at the same time, FMR is higher for women - see Figure 163. As access control systems almost always operate at a fixed threshold, the naive interpretation is incorrect.

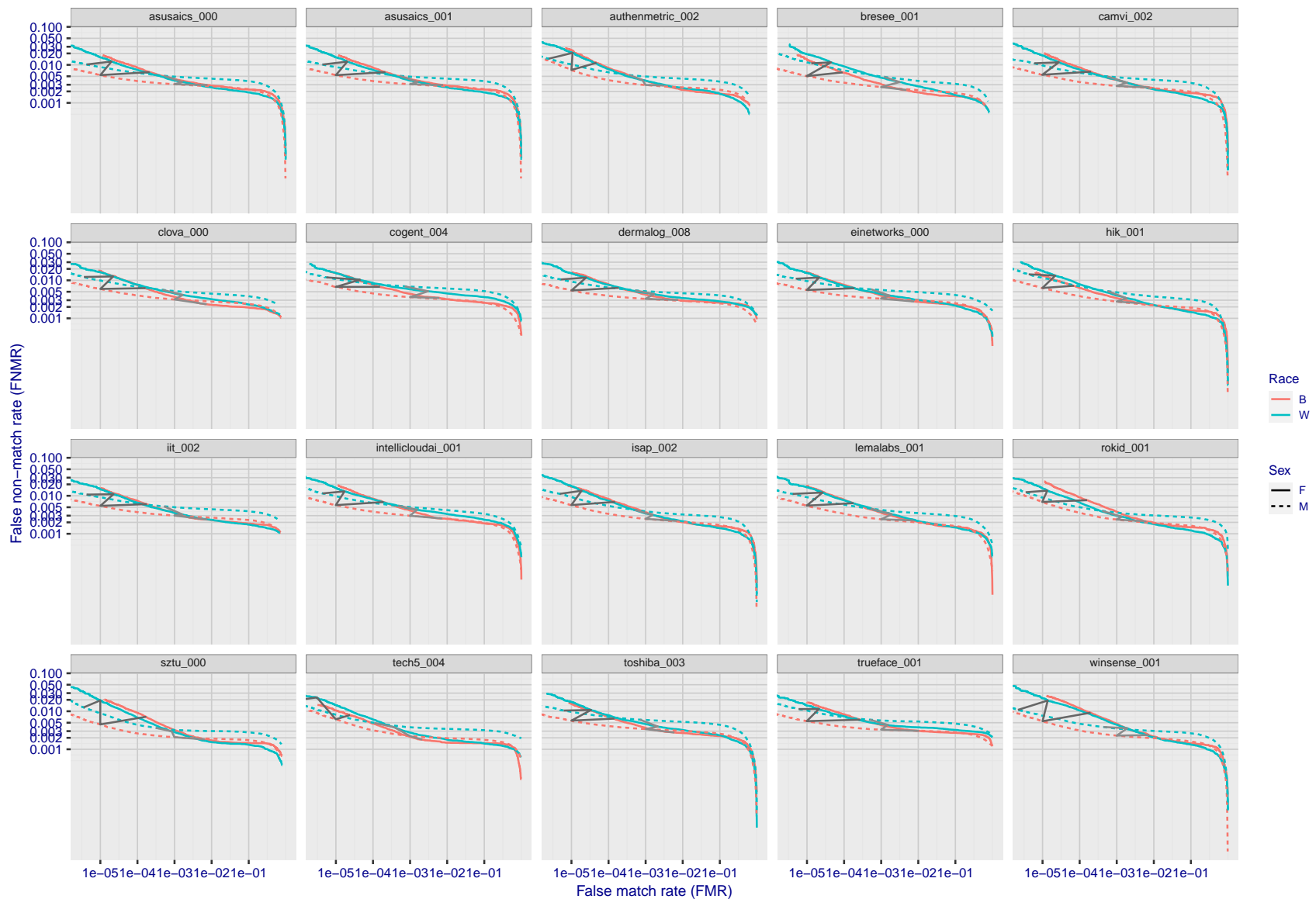


Figure 112: For the mugshot images, error tradeoff characteristics for white females, black females, black males and white males. The Z-shaped grey lines correspond to fixed thresholds, showing both FNMR and FMR vary at one T value. Note: Many of the plots will naively be read as saying women gives worse error rates than men because the solid traces lie above the dotted ones. However, this is misleading and incomplete: The grey lines show the traces reveal horizontal shifts. Thus for the cogent-003 algorithm FNMR for men is higher than for women at a fixed threshold but, at the same time, FMR is higher for women - see Figure 163. As access control systems almost always operate at a fixed threshold, the naive interpretation is incorrect.

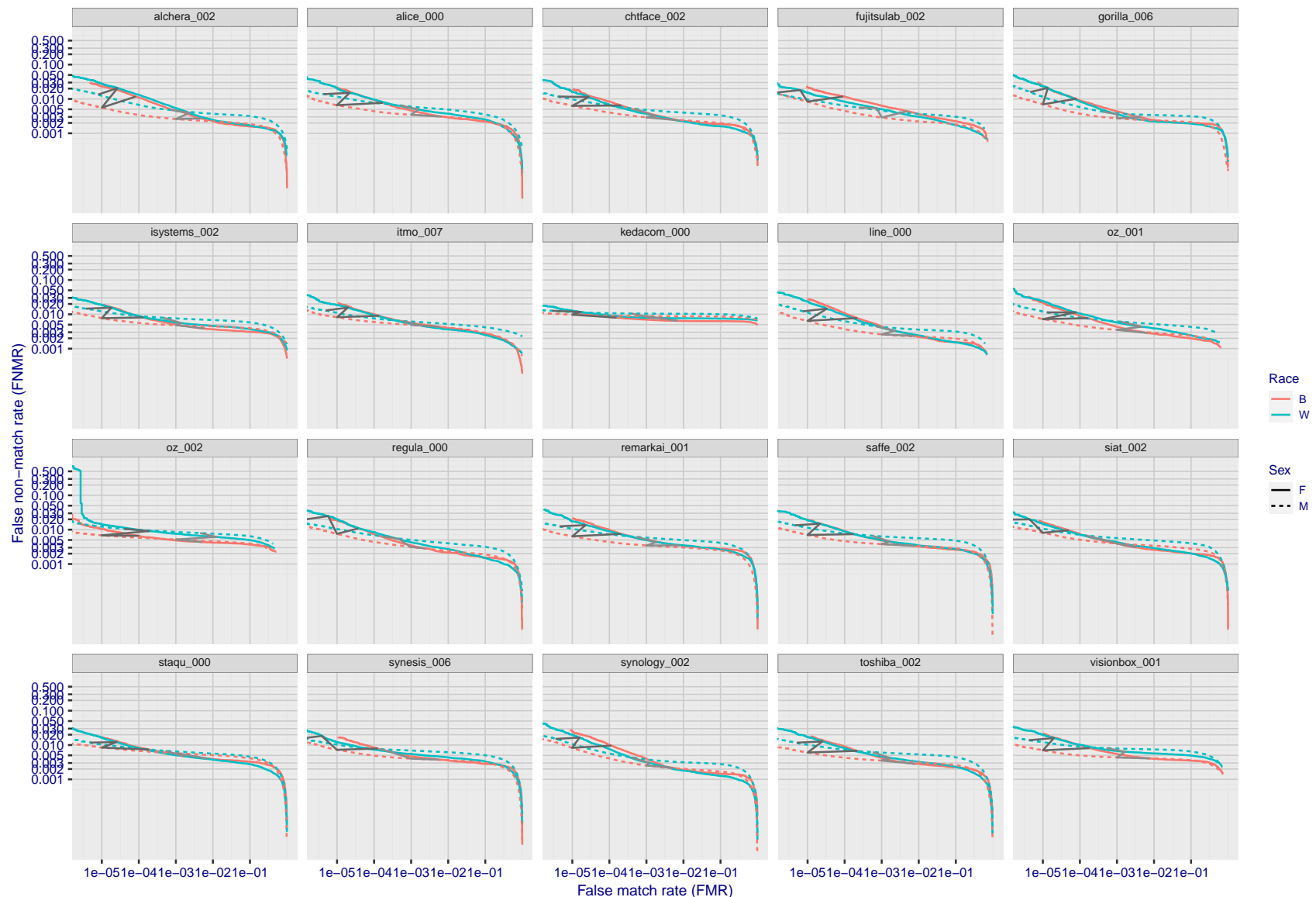


Figure 113: For the mugshot images, error tradeoff characteristics for white females, black females, black males and white males. The Z-shaped grey lines correspond to fixed thresholds, showing both FNMR and FMR vary at one T value. Note: Many of the plots will naively be read as saying women gives worse error rates than men because the solid traces lie above the dotted ones. However, this is misleading and incomplete: The grey lines show the traces reveal horizontal shifts. Thus for the cogent-003 algorithm FNMR for men is higher than for women at a fixed threshold but, at the same time, FMR is higher for women - see Figure 163. As access control systems almost always operate at a fixed threshold, the naive interpretation is incorrect.

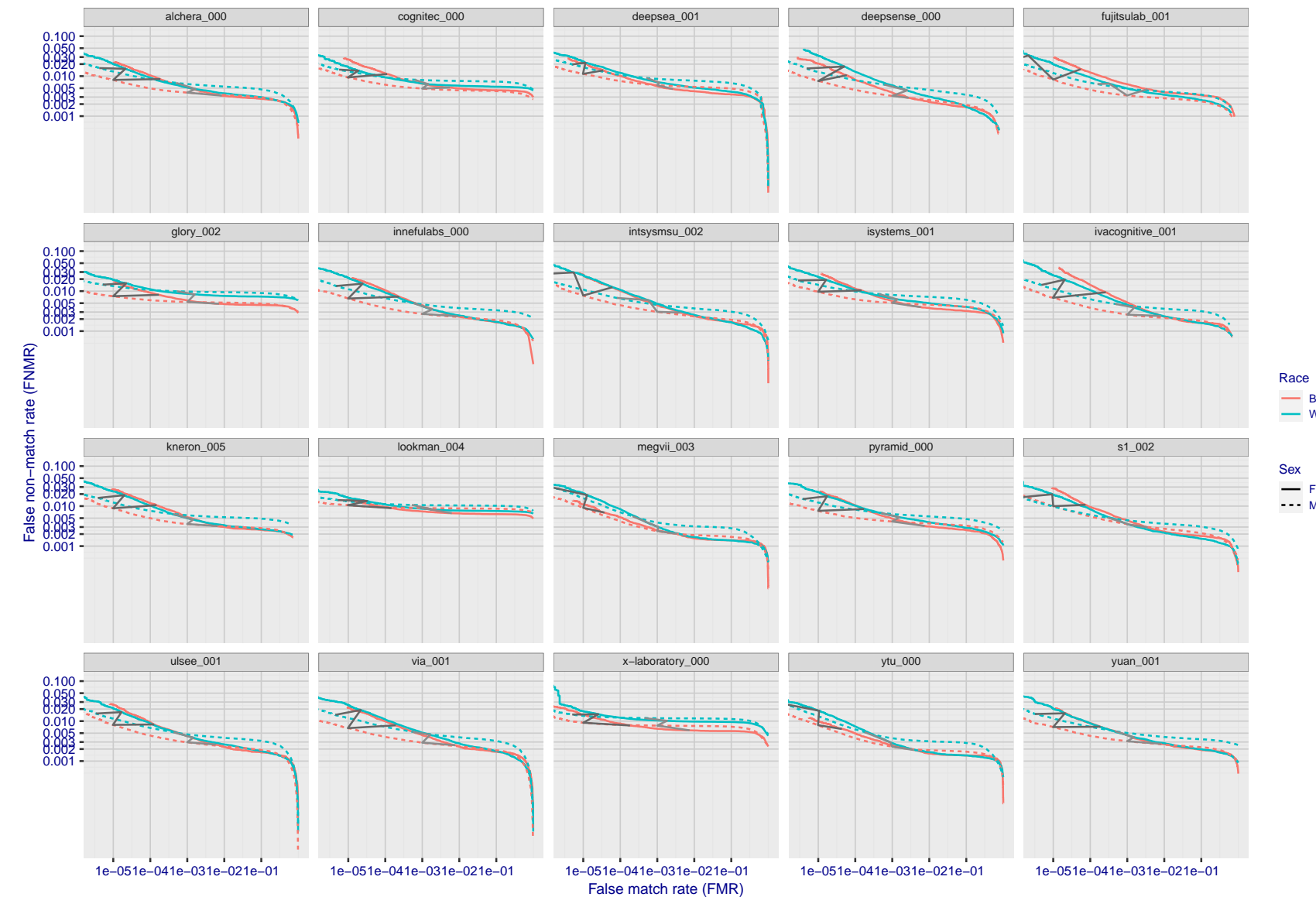


Figure 114: For the mugshot images, error tradeoff characteristics for white females, black females, black males and white males. The Z-shaped grey lines correspond to fixed thresholds, showing both FNMR and FMR vary at one T value. Note: Many of the plots will naively be read as saying women gives worse error rates than men because the solid traces lie above the dotted ones. However, this is misleading and incomplete: The grey lines show the traces reveal horizontal shifts. Thus for the cogent-003 algorithm FNMR for men is higher than for women at a fixed threshold but, at the same time, FMR is higher for women - see Figure 163. As access control systems almost always operate at a fixed threshold, the naive interpretation is incorrect.

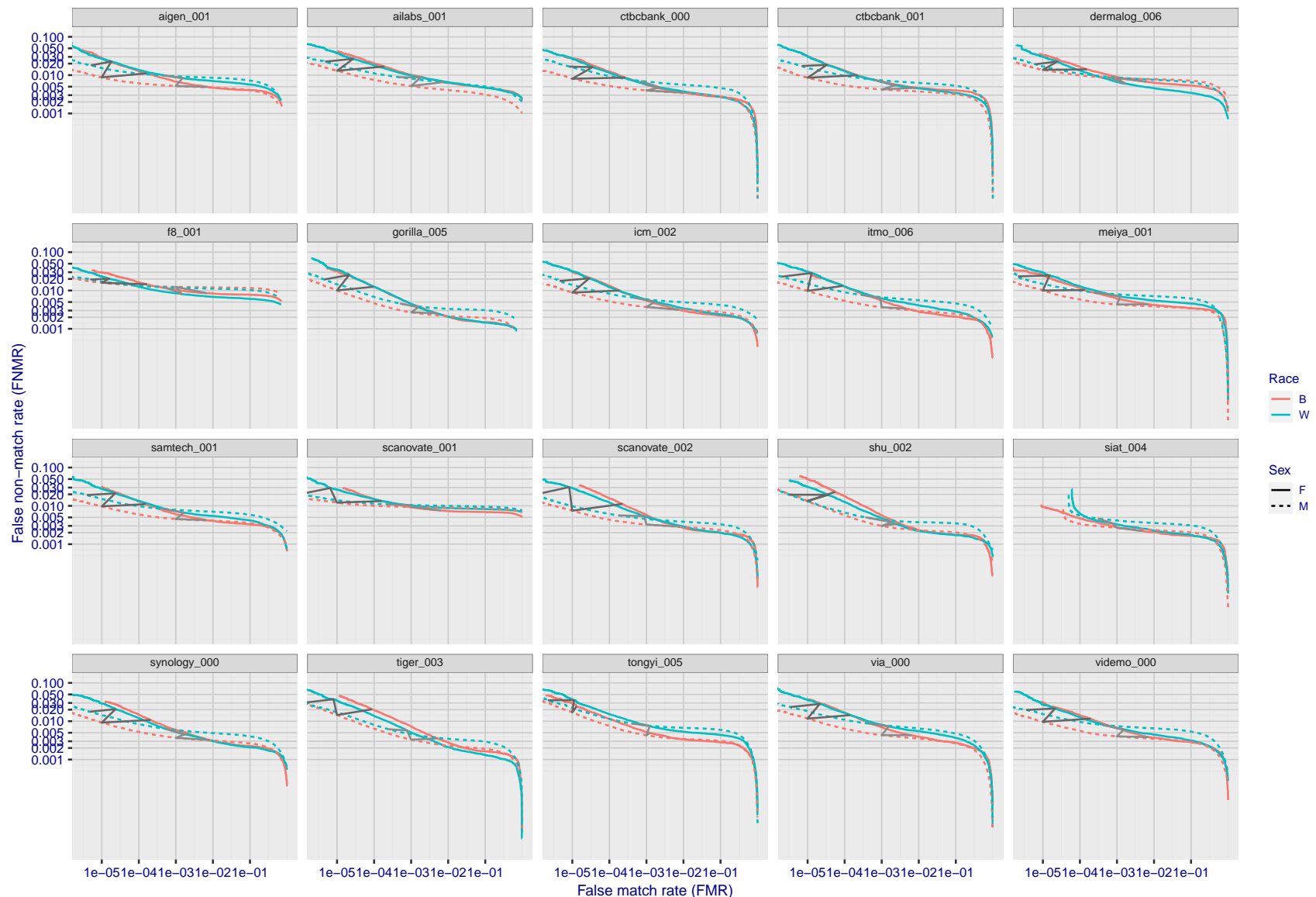


Figure 115: For the mugshot images, error tradeoff characteristics for white females, black females, black males and white males. The Z-shaped grey lines correspond to fixed thresholds, showing both FNMR and FMR vary at one T value. Note: Many of the plots will naively be read as saying women gives worse error rates than men because the solid traces lie above the dotted ones. However, this is misleading and incomplete: The grey lines show the traces reveal horizontal shifts. Thus for the cogent-003 algorithm FNMR for men is higher than for women at a fixed threshold but, at the same time, FMR is higher for women - see Figure 163. As access control systems almost always operate at a fixed threshold, the naive interpretation is incorrect.

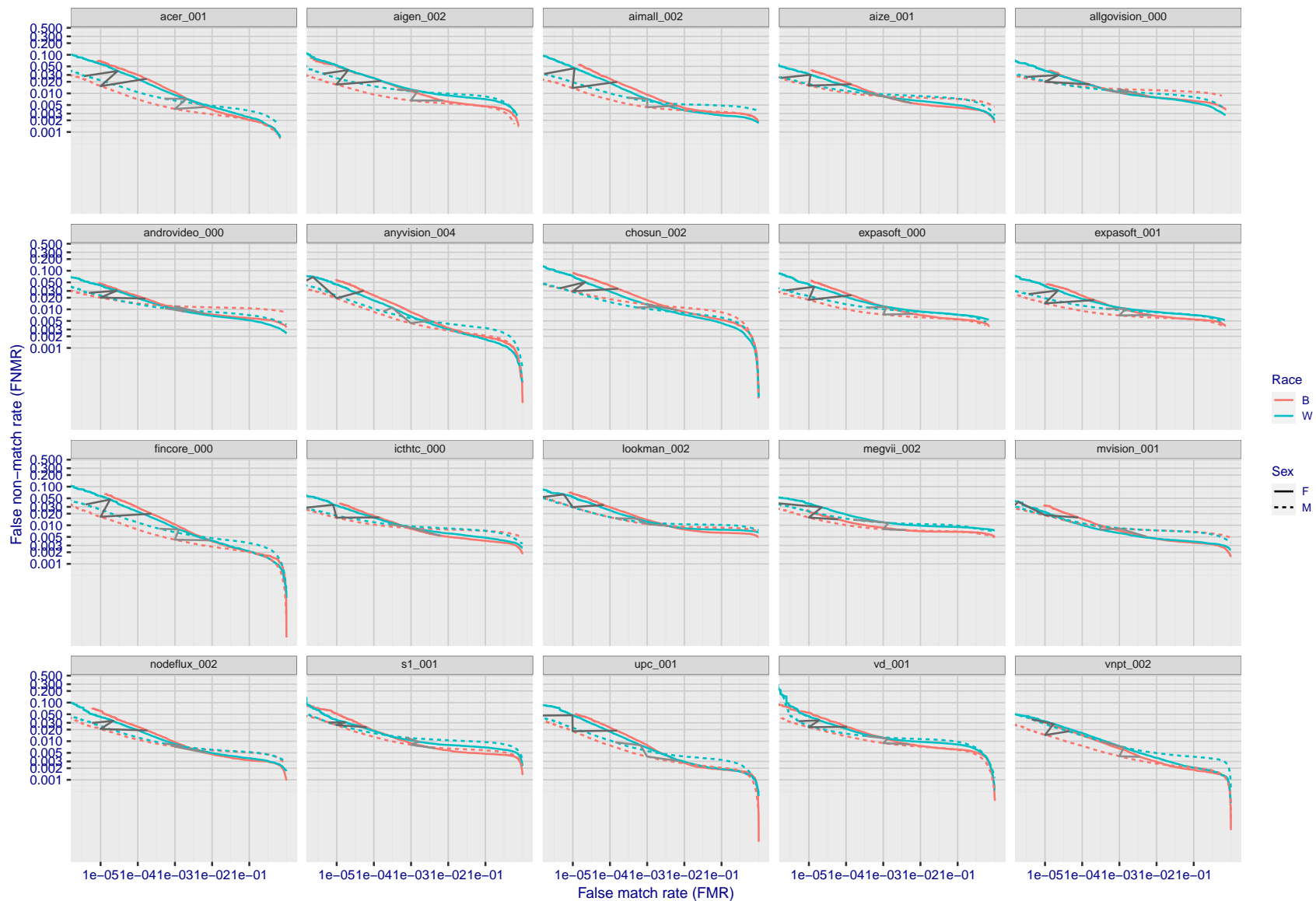


Figure 116: For the mugshot images, error tradeoff characteristics for white females, black females, black males and white males. The Z-shaped grey lines correspond to fixed thresholds, showing both FNMR and FMR vary at one T value. Note: Many of the plots will naively be read as saying women gives worse error rates than men because the solid traces lie above the dotted ones. However, this is misleading and incomplete: The grey lines show the traces reveal horizontal shifts. Thus for the cogent-003 algorithm FNMR for men is higher than for women at a fixed threshold but, at the same time, FMR is higher for women - see Figure 163. As access control systems almost always operate at a fixed threshold, the naive interpretation is incorrect.

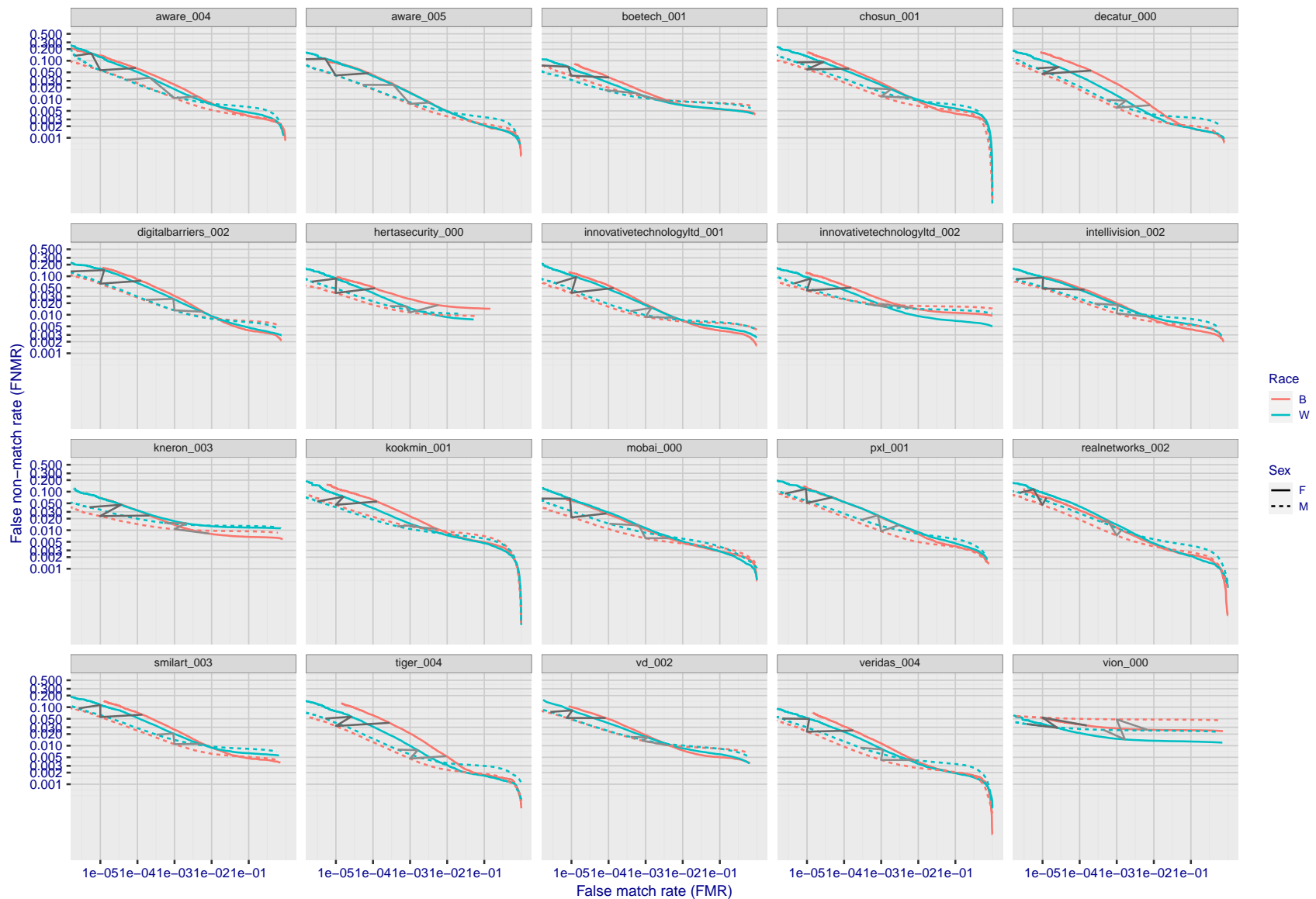


Figure 117: For the mugshot images, error tradeoff characteristics for white females, black females, black males and white males. The Z-shaped grey lines correspond to fixed thresholds, showing both FNMR and FMR vary at one T value. Note: Many of the plots will naively be read as saying women gives worse error rates than men because the solid traces lie above the dotted ones. However, this is misleading and incomplete: The grey lines show the traces reveal horizontal shifts. Thus for the cogent-003 algorithm FNMR for men is higher than for women at a fixed threshold but, at the same time, FMR is higher for women - see Figure 163. As access control systems almost always operate at a fixed threshold, the naive interpretation is incorrect.

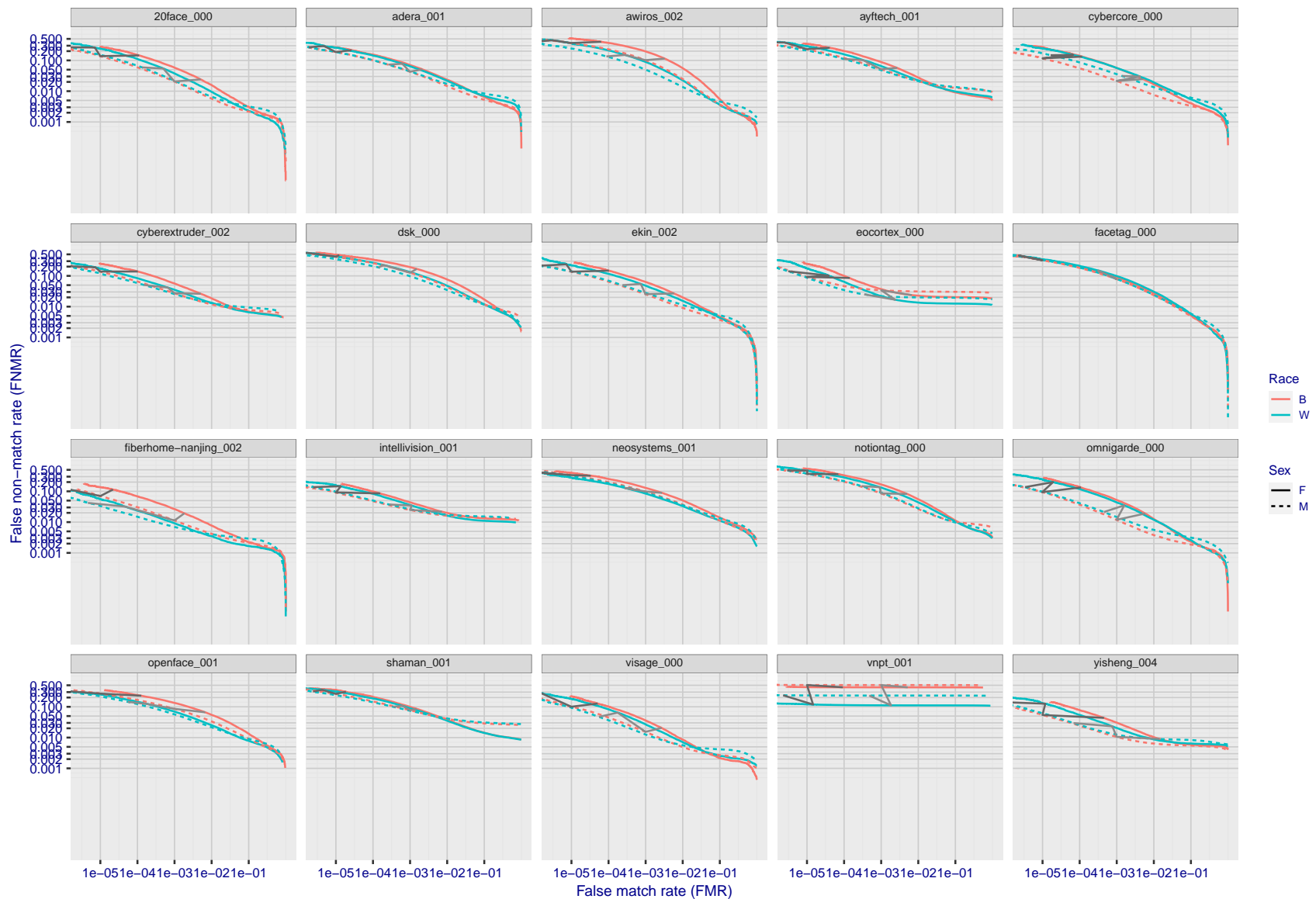


Figure 118: For the mugshot images, error tradeoff characteristics for white females, black females, black males and white males. The Z-shaped grey lines correspond to fixed thresholds, showing both FNMR and FMR vary at one T value. Note: Many of the plots will naively be read as saying women gives worse error rates than men because the solid traces lie above the dotted ones. However, this is misleading and incomplete: The grey lines show the traces reveal horizontal shifts. Thus for the cogent-003 algorithm FNMR for men is higher than for women at a fixed threshold but, at the same time, FMR is higher for women - see Figure 163. As access control systems almost always operate at a fixed threshold, the naive interpretation is incorrect.

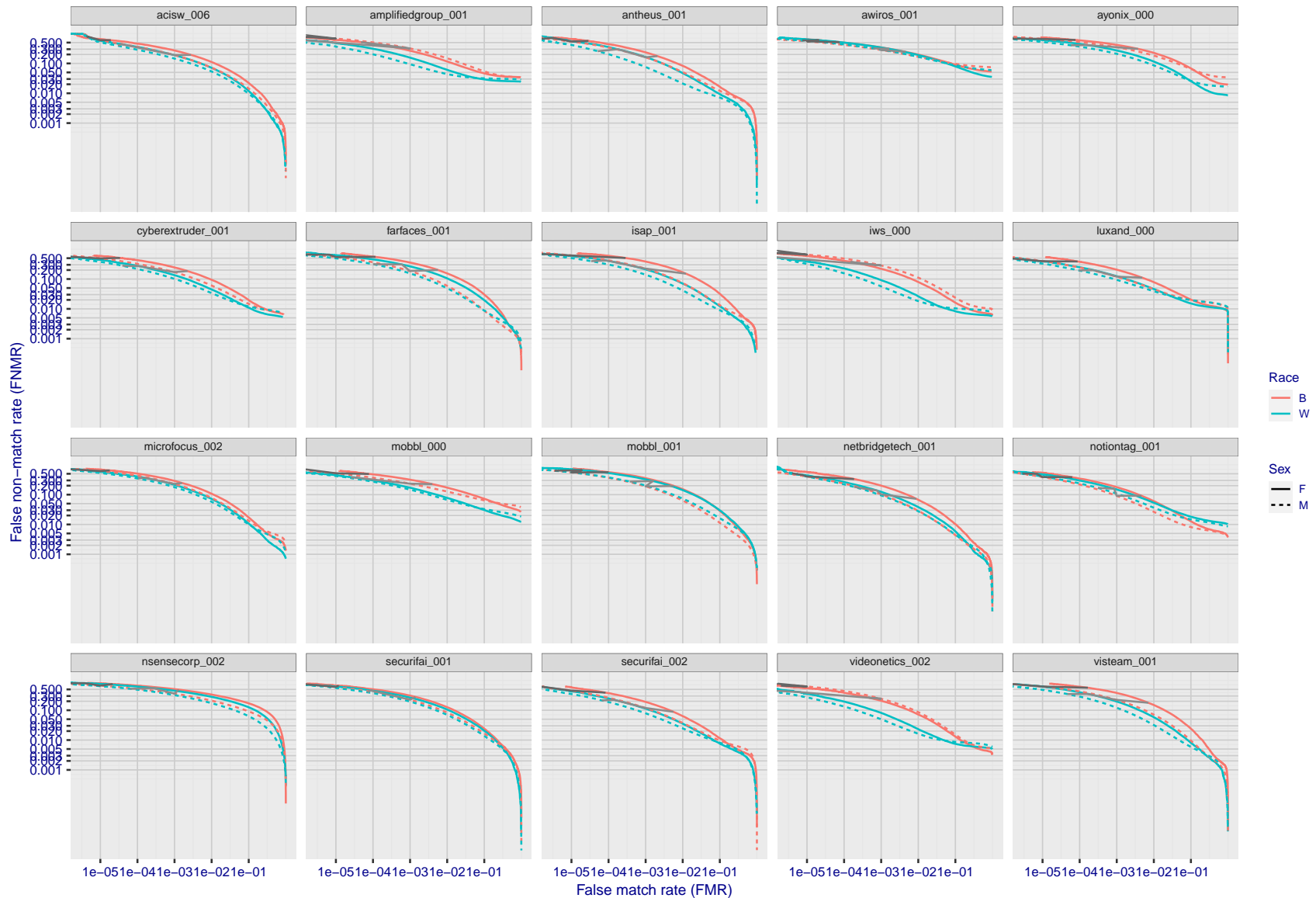


Figure 119: For the mugshot images, error tradeoff characteristics for white females, black females, black males and white males. The Z-shaped grey lines correspond to fixed thresholds, showing both FNMR and FMR vary at one T value. Note: Many of the plots will naively be read as saying women gives worse error rates than men because the solid traces lie above the dotted ones. However, this is misleading and incomplete: The grey lines show the traces reveal horizontal shifts. Thus for the cogent-003 algorithm FNMR for men is higher than for women at a fixed threshold but, at the same time, FMR is higher for women - see Figure 163. As access control systems almost always operate at a fixed threshold, the naive interpretation is incorrect.

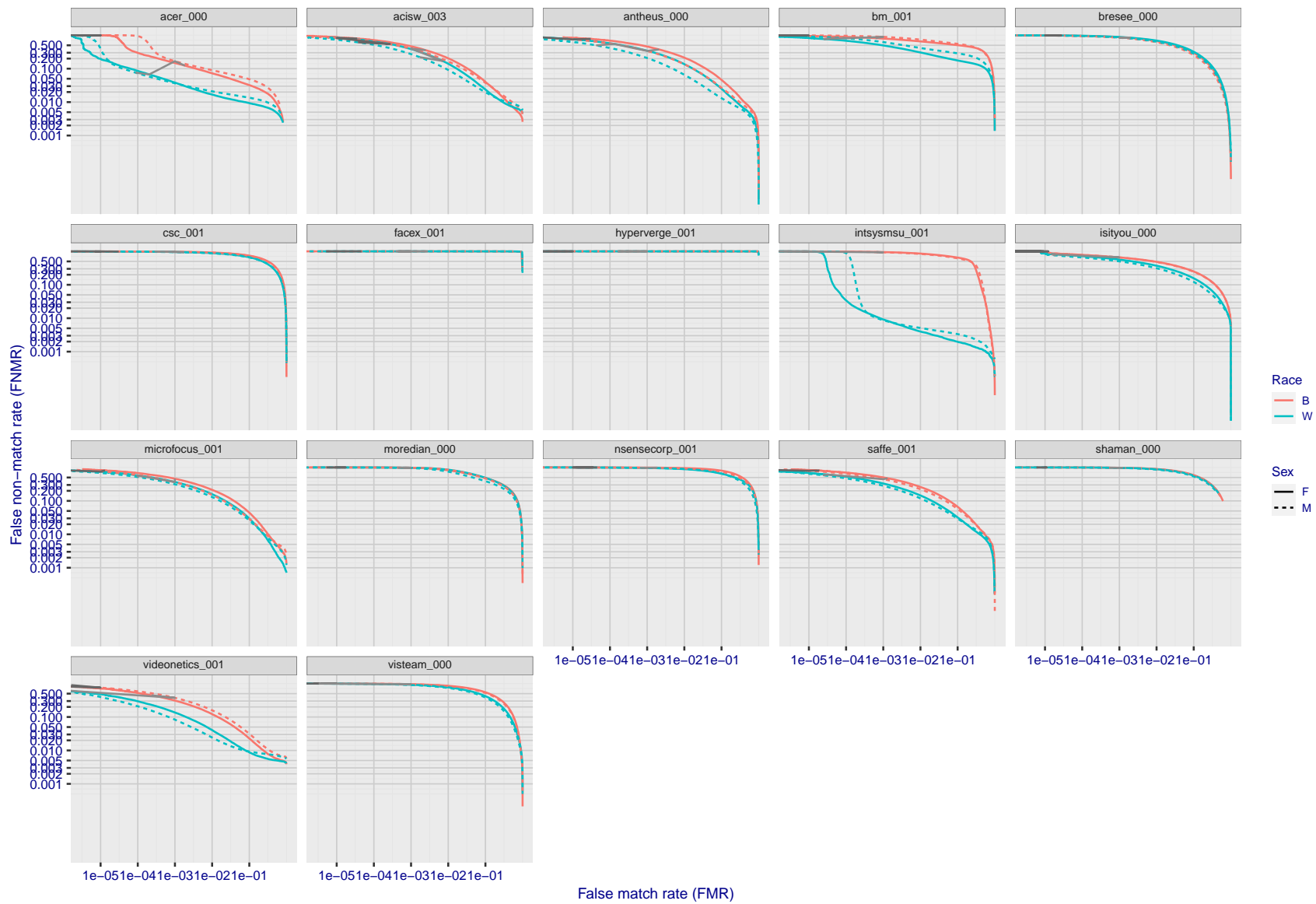


Figure 120: For the mugshot images, error tradeoff characteristics for white females, black females, black males and white males. The Z-shaped grey lines correspond to fixed thresholds, showing both FNMR and FMR vary at one T value. Note: Many of the plots will naively be read as saying women gives worse error rates than men because the solid traces lie above the dotted ones. However, this is misleading and incomplete: The grey lines show the traces reveal horizontal shifts. Thus for the cogent-003 algorithm FNMR for men is higher than for women at a fixed threshold but, at the same time, FMR is higher for women - see Figure 163. As access control systems almost always operate at a fixed threshold, the naive interpretation is incorrect.

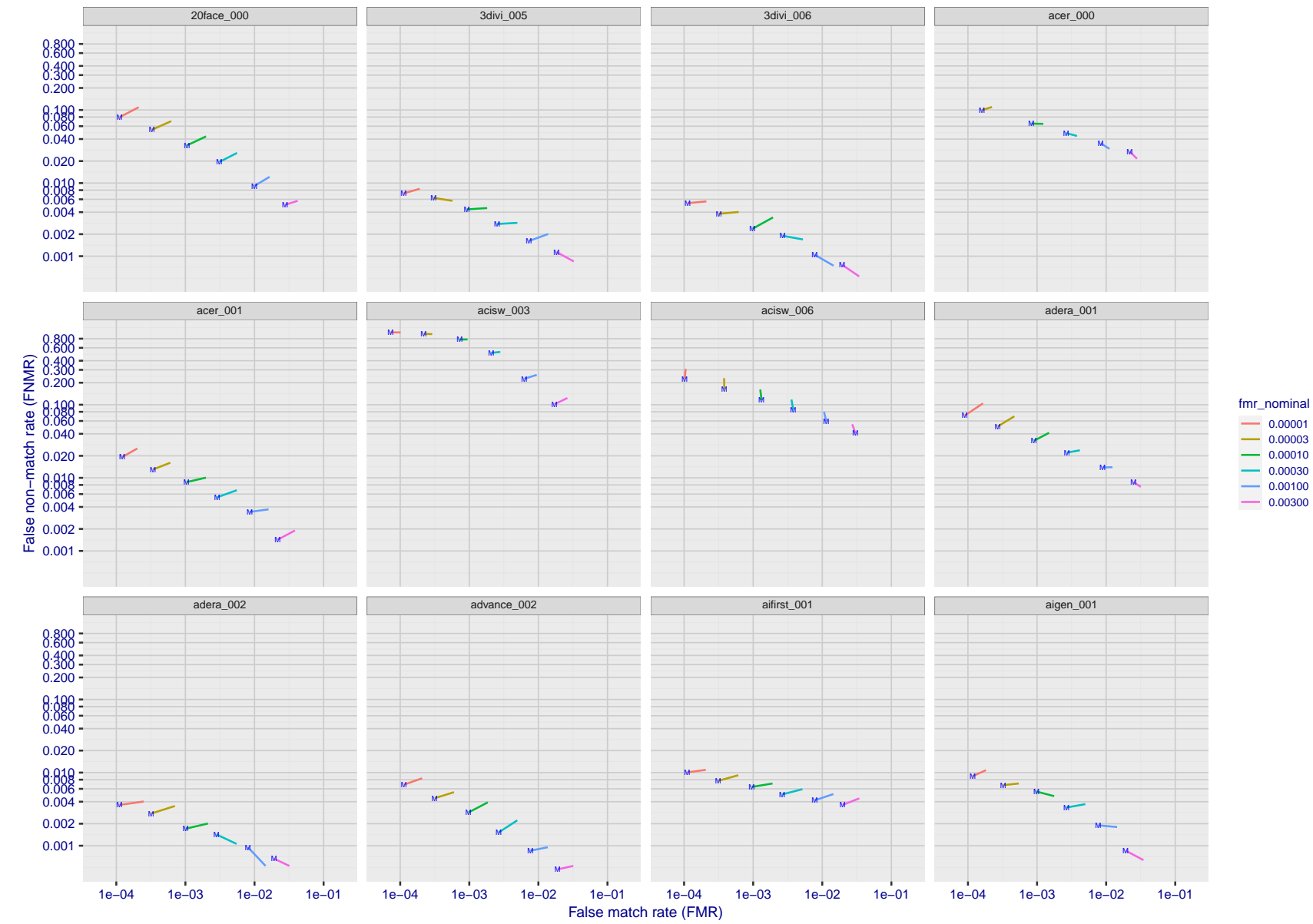


Figure 121: For the visa images, FNMR and FMR at six operating points along the DET characteristic. At each point a line is drawn between $(FMR, FNMR)_{MALE}$ and $(FMR, FNMR)_{FEMALE}$ showing how which sex has lower FMR and/or FNMR. The "M" label denotes male, the other end of the line corresponds to female. The six operating thresholds are selected to give the nominal false match rates given in the legend, and are computed over all impostor pairs regardless of age, sex, and place of birth. The plotted FMR values are broadly an order of magnitude larger than the nominal rates because FMR is computed over demographically-matched impostor pairs i.e individuals of the same sex, from the same geographic region (see section 3.6.1), and the same age group (see section 3.6.2).

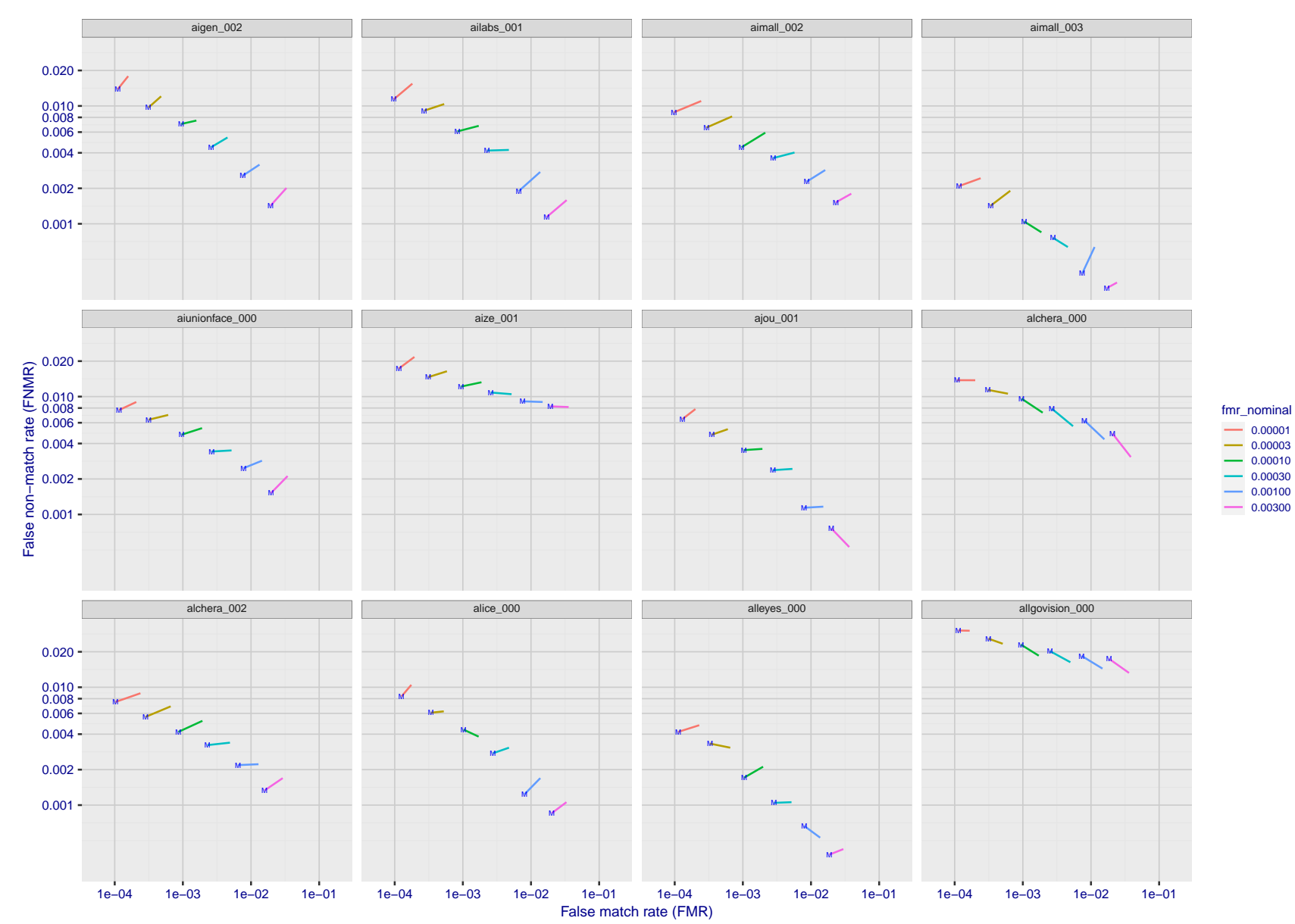


Figure 122: For the visa images, FNMR and FMR at six operating points along the DET characteristic. At each point a line is drawn between $(FMR, FNMR)_{MALE}$ and $(FMR, FNMR)_{FEMALE}$ showing how which sex has lower FMR and/or FNMR. The "M" label denotes male, the other end of the line corresponds to female. The six operating thresholds are selected to give the nominal false match rates given in the legend, and are computed over all impostor pairs regardless of age, sex, and place of birth. The plotted FMR values are broadly an order of magnitude larger than the nominal rates because FMR is computed over demographically-matched impostor pairs i.e individuals of the same sex, from the same geographic region (see section 3.6.1), and the same age group (see section 3.6.2).

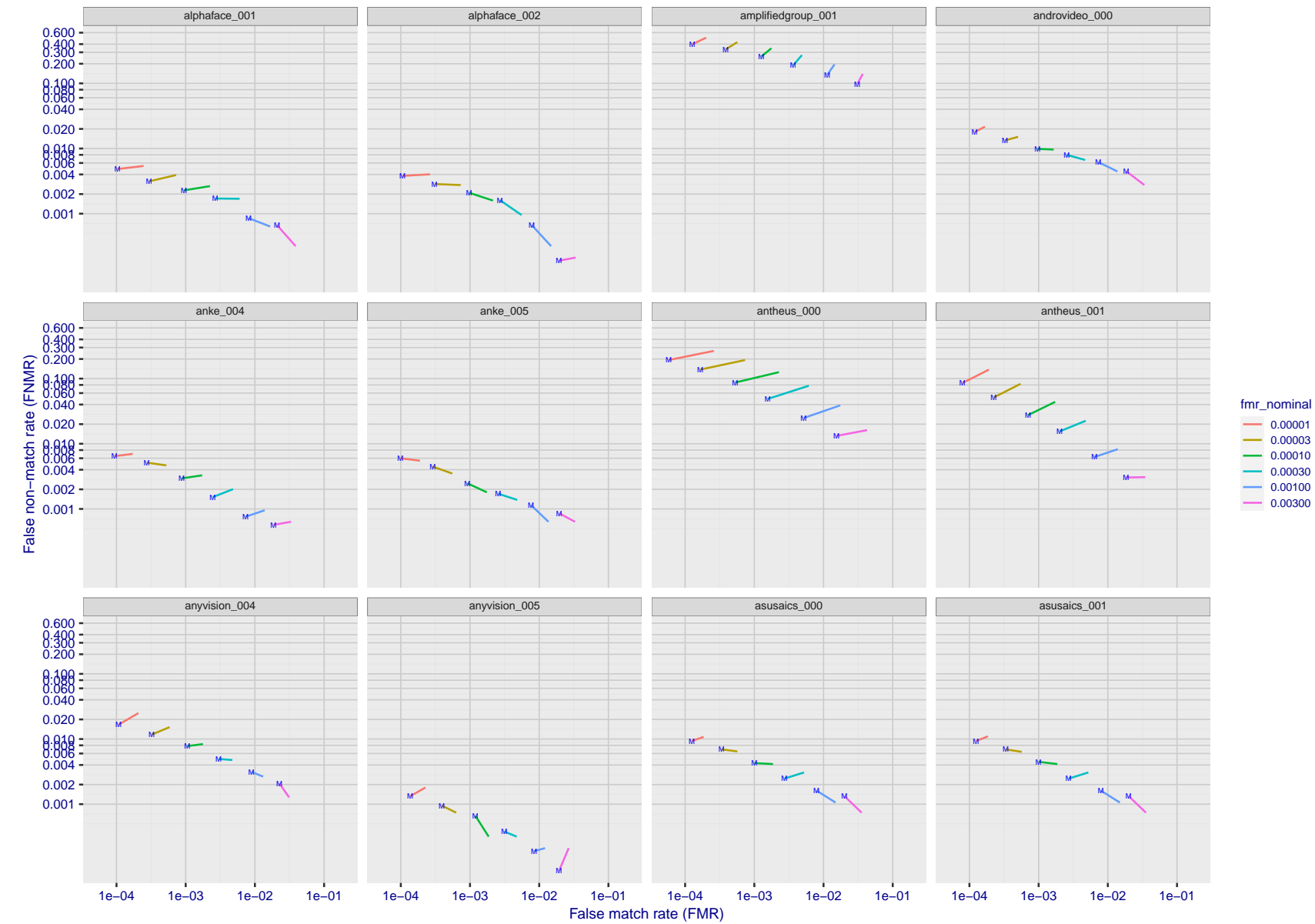


Figure 123: For the visa images, FNMR and FMR at six operating points along the DET characteristic. At each point a line is drawn between $(FMR, FNMR)_{MALE}$ and $(FMR, FNMR)_{FEMALE}$ showing how which sex has lower FMR and/or FNMR. The "M" label denotes male, the other end of the line corresponds to female. The six operating thresholds are selected to give the nominal false match rates given in the legend, and are computed over all impostor pairs regardless of age, sex, and place of birth. The plotted FMR values are broadly an order of magnitude larger than the nominal rates because FMR is computed over demographically-matched impostor pairs i.e individuals of the same sex, from the same geographic region (see section 3.6.1), and the same age group (see section 3.6.2).

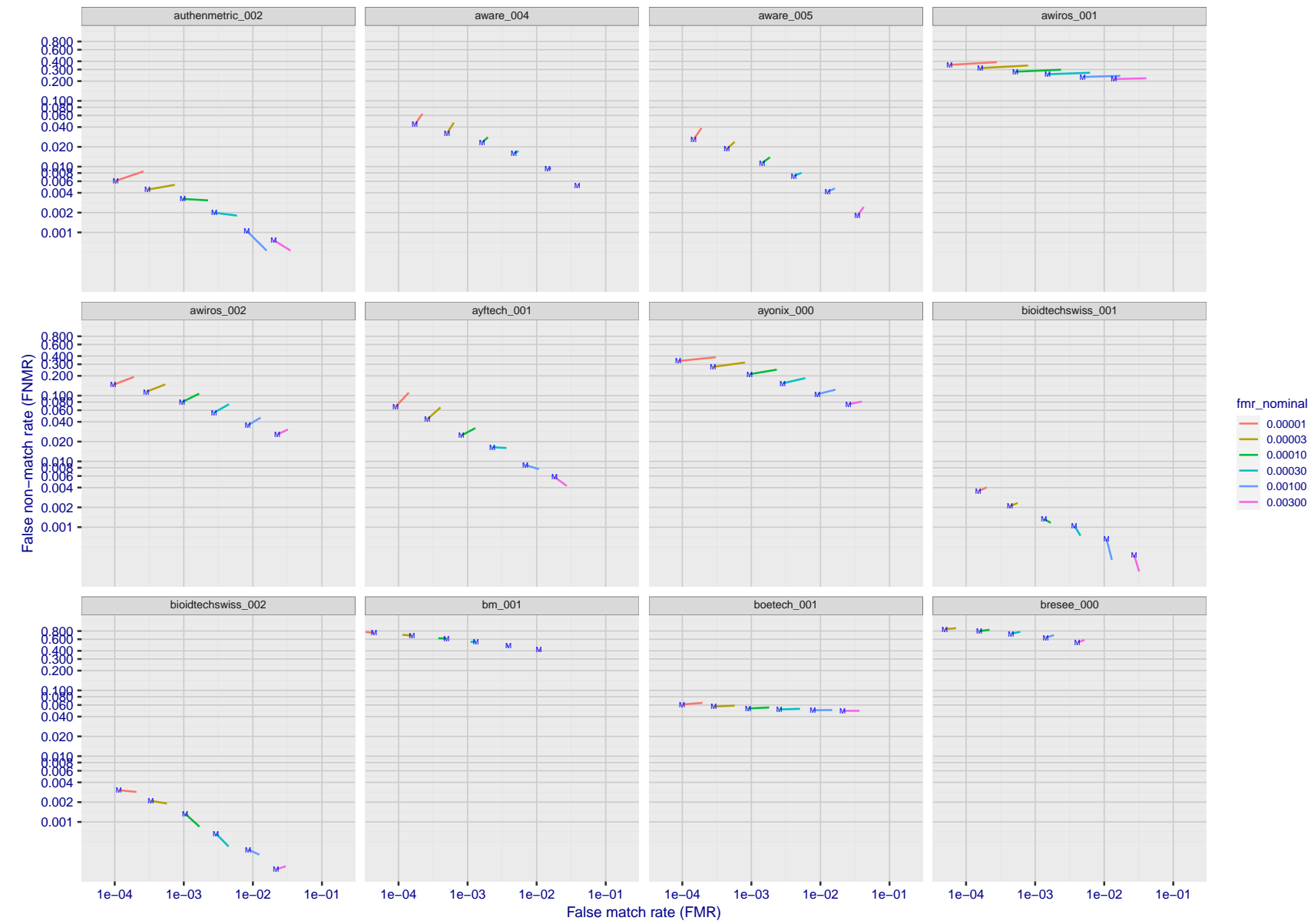


Figure 124: For the visa images, FNMR and FMR at six operating points along the DET characteristic. At each point a line is drawn between $(FMR, FNMR)_{MALE}$ and $(FMR, FNMR)_{FEMALE}$ showing how which sex has lower FMR and/or FNMR. The "M" label denotes male, the other end of the line corresponds to female. The six operating thresholds are selected to give the nominal false match rates given in the legend, and are computed over all impostor pairs regardless of age, sex, and place of birth. The plotted FMR values are broadly an order of magnitude larger than the nominal rates because FMR is computed over demographically-matched impostor pairs i.e individuals of the same sex, from the same geographic region (see section 3.6.1), and the same age group (see section 3.6.2).

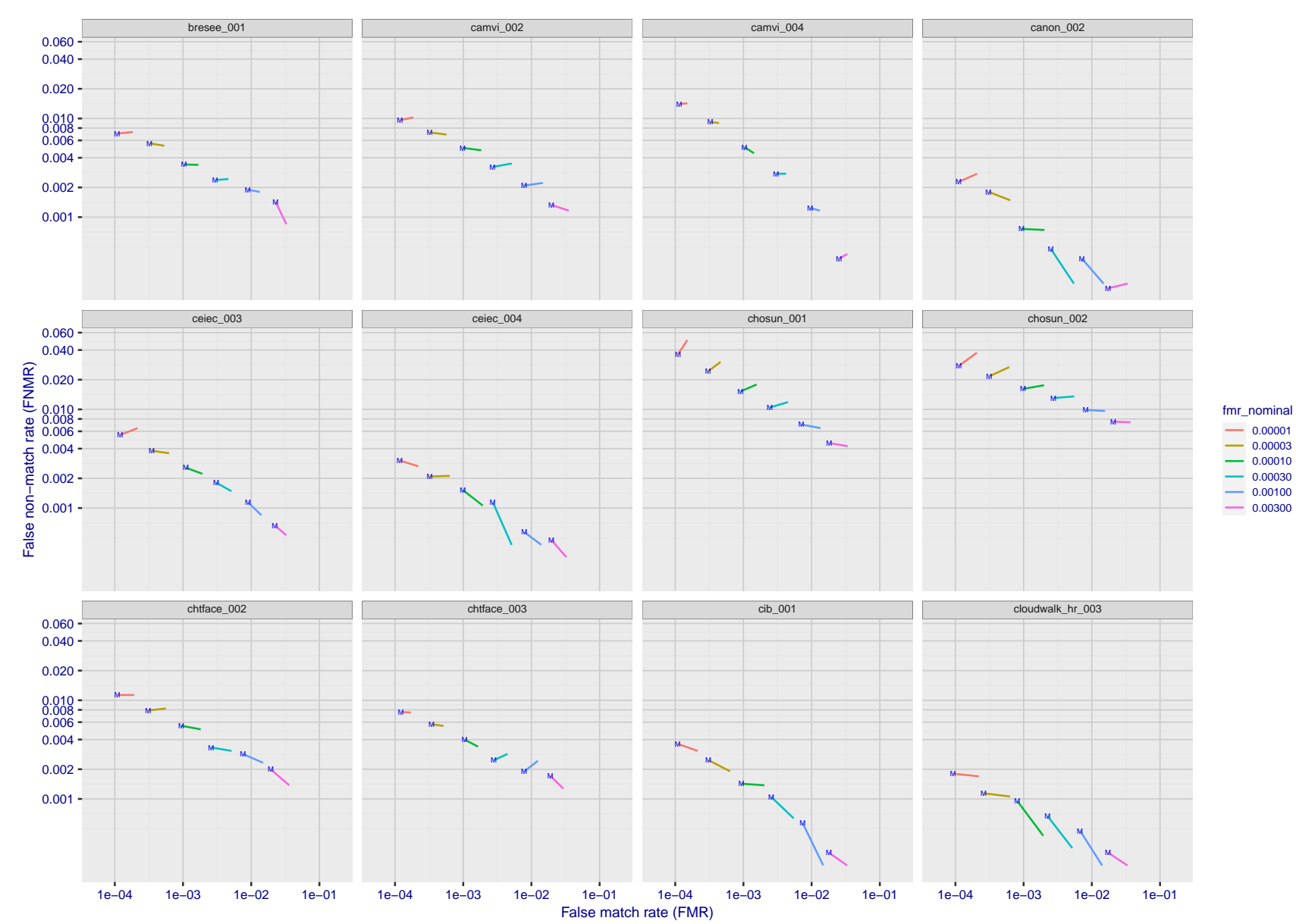


Figure 125: For the visa images, FNMR and FMR at six operating points along the DET characteristic. At each point a line is drawn between $(FMR, FNMR)_{MALE}$ and $(FMR, FNMR)_{FEMALE}$ showing how which sex has lower FMR and/or FNMR. The "M" label denotes male, the other end of the line corresponds to female. The six operating thresholds are selected to give the nominal false match rates given in the legend, and are computed over all impostor pairs regardless of age, sex, and place of birth. The plotted FMR values are broadly an order of magnitude larger than the nominal rates because FMR is computed over demographically-matched impostor pairs i.e individuals of the same sex, from the same geographic region (see section 3.6.1), and the same age group (see section 3.6.2).

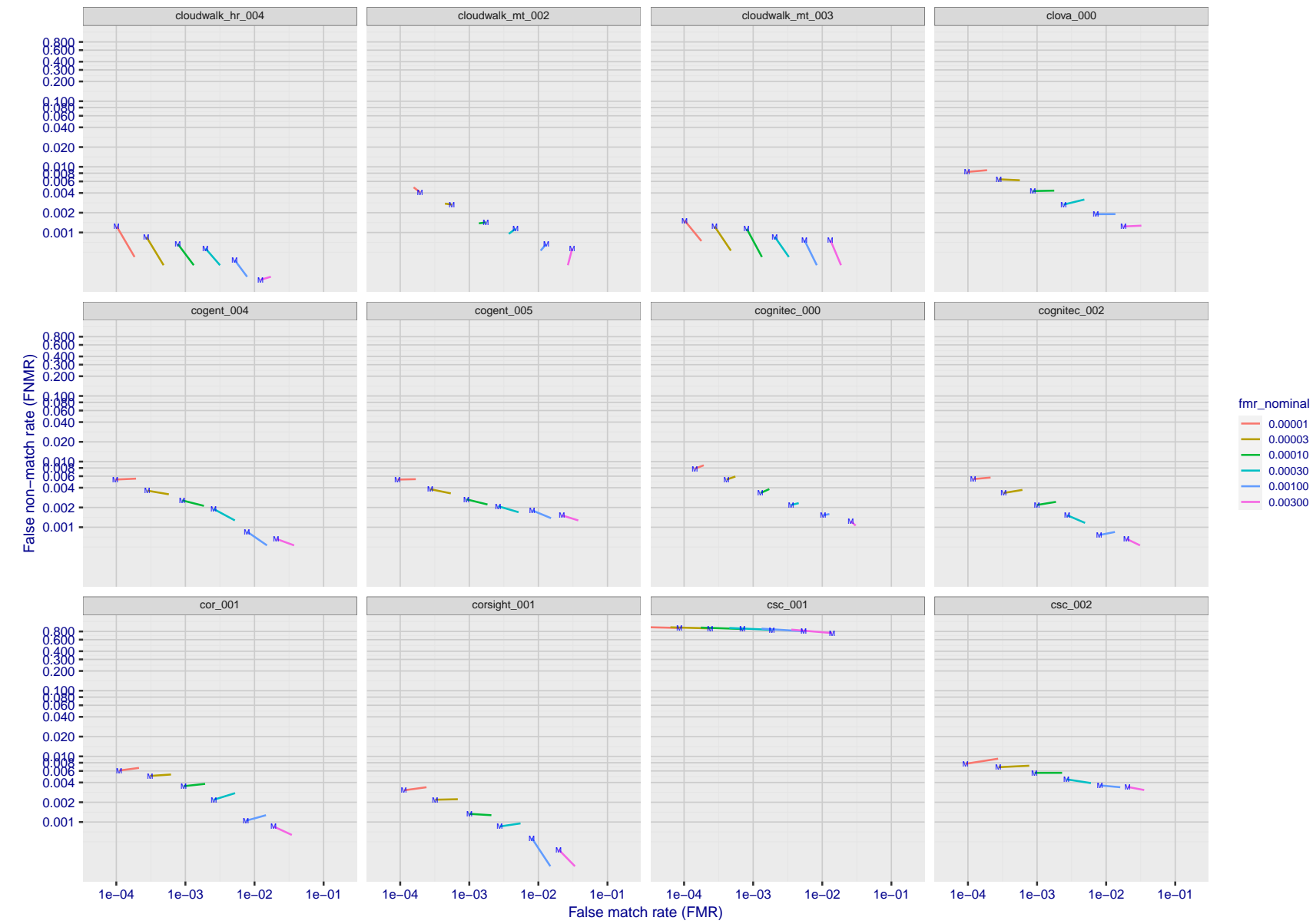


Figure 126: For the visa images, FNMR and FMR at six operating points along the DET characteristic. At each point a line is drawn between $(FMR, FNMR)_{MALE}$ and $(FMR, FNMR)_{FEMALE}$ showing how which sex has lower FMR and/or FNMR. The "M" label denotes male, the other end of the line corresponds to female. The six operating thresholds are selected to give the nominal false match rates given in the legend, and are computed over all impostor pairs regardless of age, sex, and place of birth. The plotted FMR values are broadly an order of magnitude larger than the nominal rates because FMR is computed over demographically-matched impostor pairs i.e individuals of the same sex, from the same geographic region (see section 3.6.1), and the same age group (see section 3.6.2).

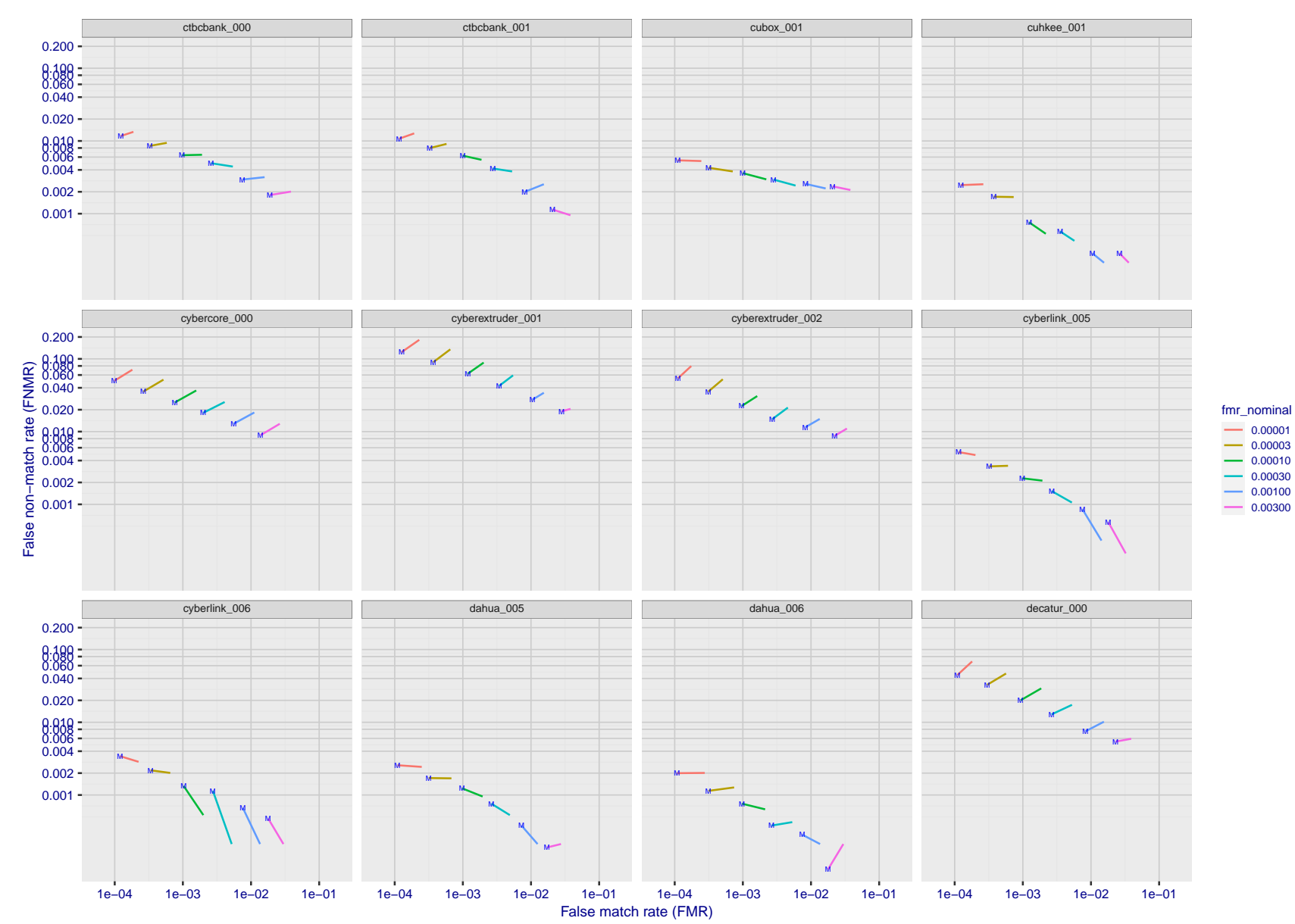


Figure 127: For the visa images, FNMR and FMR at six operating points along the DET characteristic. At each point a line is drawn between $(FMR, FNMR)_{MALE}$ and $(FMR, FNMR)_{FEMALE}$ showing how which sex has lower FMR and/or FNMR. The "M" label denotes male, the other end of the line corresponds to female. The six operating thresholds are selected to give the nominal false match rates given in the legend, and are computed over all impostor pairs regardless of age, sex, and place of birth. The plotted FMR values are broadly an order of magnitude larger than the nominal rates because FMR is computed over demographically-matched impostor pairs i.e individuals of the same sex, from the same geographic region (see section 3.6.1), and the same age group (see section 3.6.2).

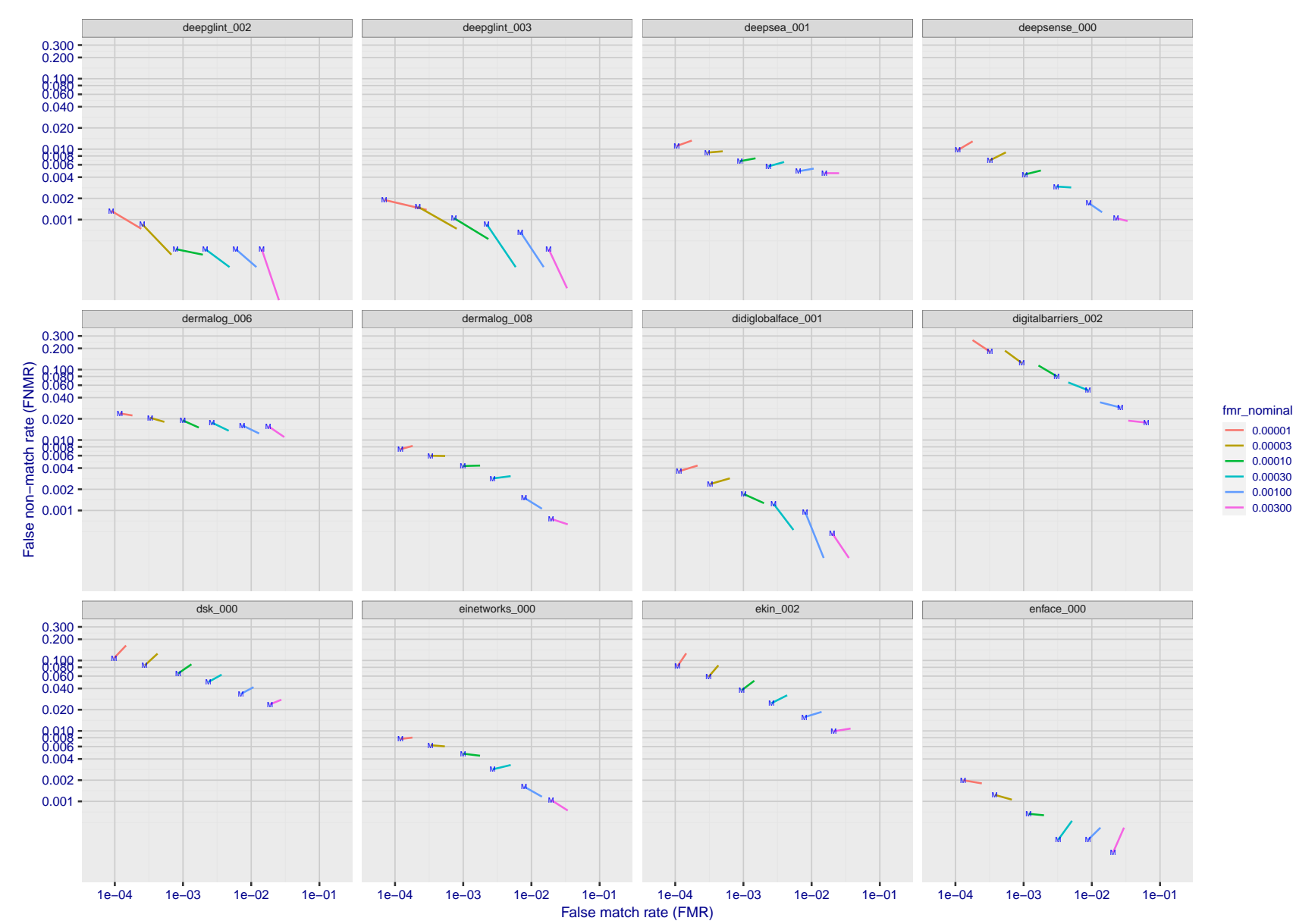


Figure 128: For the visa images, FNMR and FMR at six operating points along the DET characteristic. At each point a line is drawn between $(FMR, FNMR)_{MALE}$ and $(FMR, FNMR)_{FEMALE}$ showing how which sex has lower FMR and/or FNMR. The "M" label denotes male, the other end of the line corresponds to female. The six operating thresholds are selected to give the nominal false match rates given in the legend, and are computed over all impostor pairs regardless of age, sex, and place of birth. The plotted FMR values are broadly an order of magnitude larger than the nominal rates because FMR is computed over demographically-matched impostor pairs i.e individuals of the same sex, from the same geographic region (see section 3.6.1), and the same age group (see section 3.6.2).

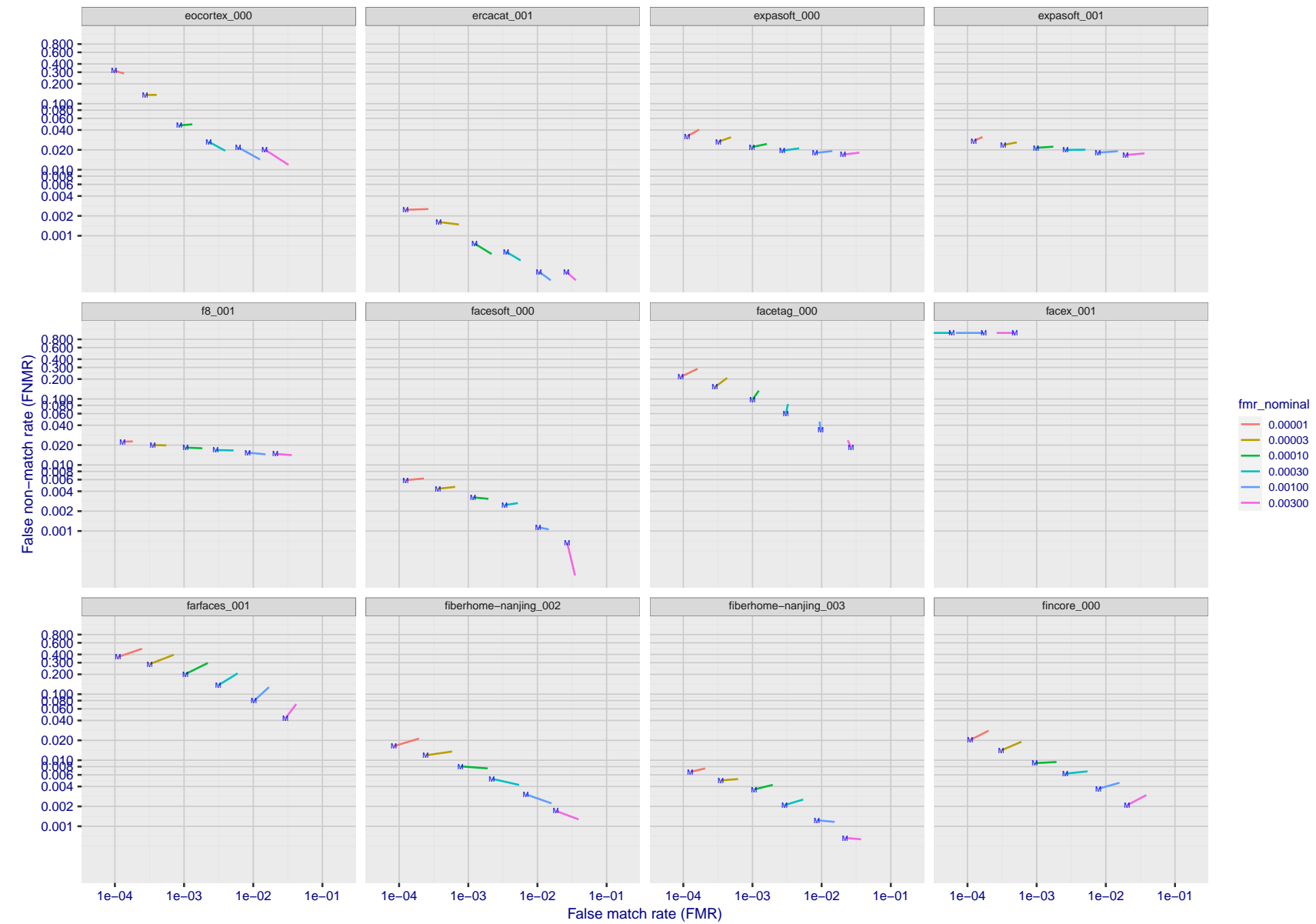


Figure 129: For the visa images, FNMR and FMR at six operating points along the DET characteristic. At each point a line is drawn between $(FMR, FNMR)_{MALE}$ and $(FMR, FNMR)_{FEMALE}$ showing how which sex has lower FMR and/or FNMR. The "M" label denotes male, the other end of the line corresponds to female. The six operating thresholds are selected to give the nominal false match rates given in the legend, and are computed over all impostor pairs regardless of age, sex, and place of birth. The plotted FMR values are broadly an order of magnitude larger than the nominal rates because FMR is computed over demographically-matched impostor pairs i.e individuals of the same sex, from the same geographic region (see section 3.6.1), and the same age group (see section 3.6.2).

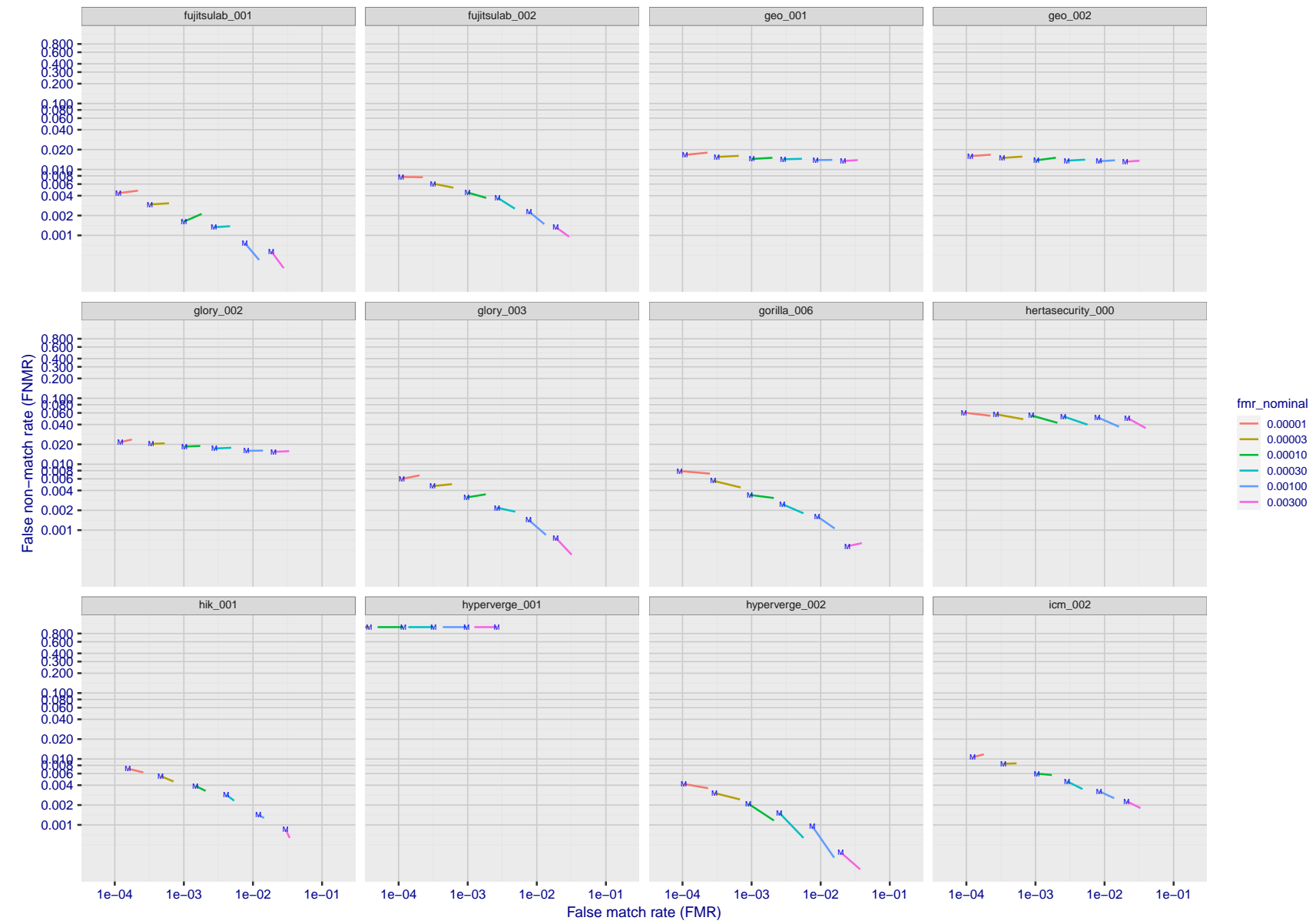


Figure 130: For the visa images, FNMR and FMR at six operating points along the DET characteristic. At each point a line is drawn between $(FMR, FNMR)_{MALE}$ and $(FMR, FNMR)_{FEMALE}$ showing how which sex has lower FMR and/or FNMR. The "M" label denotes male, the other end of the line corresponds to female. The six operating thresholds are selected to give the nominal false match rates given in the legend, and are computed over all impostor pairs regardless of age, sex, and place of birth. The plotted FMR values are broadly an order of magnitude larger than the nominal rates because FMR is computed over demographically-matched impostor pairs i.e individuals of the same sex, from the same geographic region (see section 3.6.1), and the same age group (see section 3.6.2).

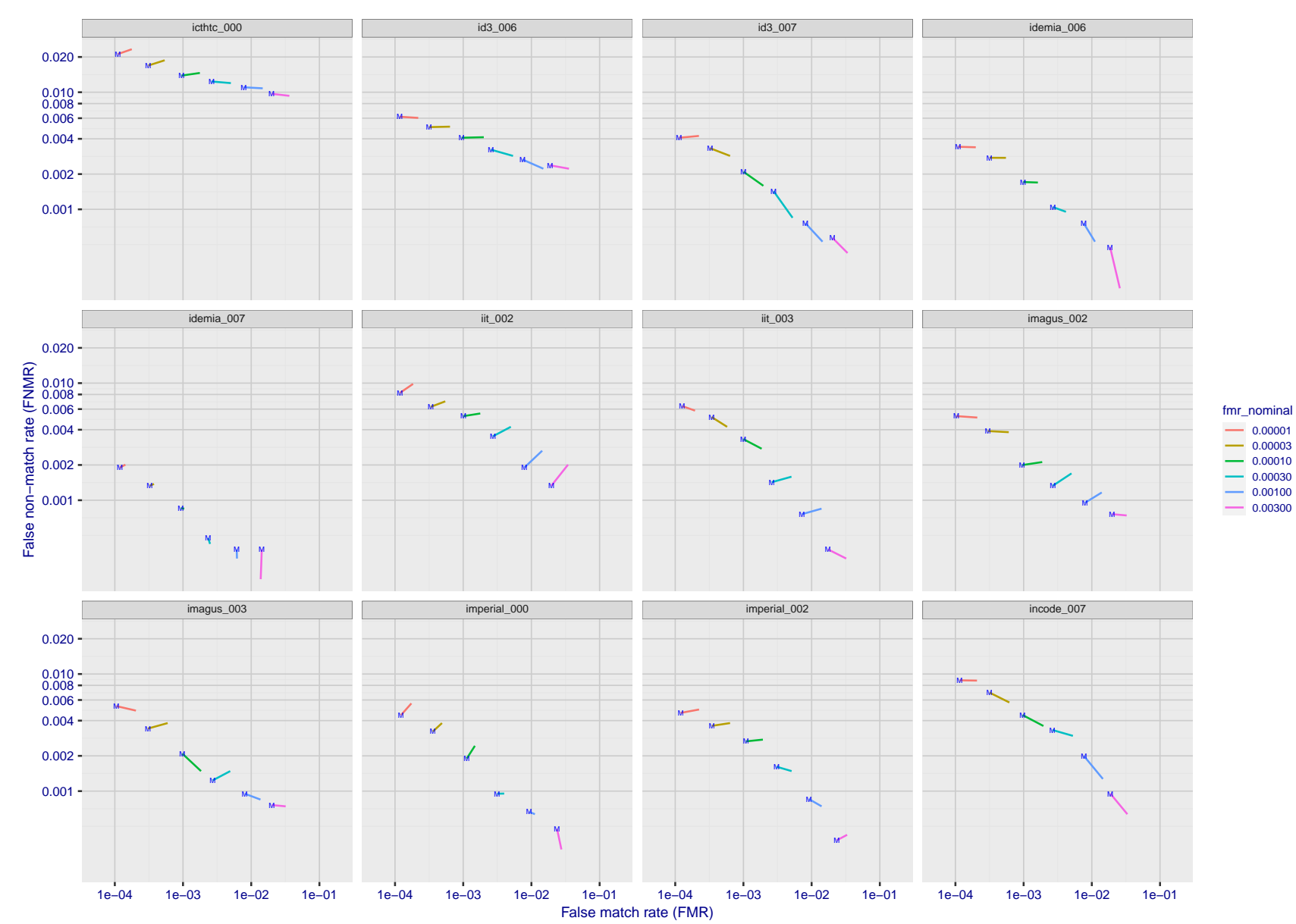


Figure 131: For the visa images, FNMR and FMR at six operating points along the DET characteristic. At each point a line is drawn between $(FMR, FNMR)_{MALE}$ and $(FMR, FNMR)_{FEMALE}$ showing how which sex has lower FMR and/or FNMR. The "M" label denotes male, the other end of the line corresponds to female. The six operating thresholds are selected to give the nominal false match rates given in the legend, and are computed over all impostor pairs regardless of age, sex, and place of birth. The plotted FMR values are broadly an order of magnitude larger than the nominal rates because FMR is computed over demographically-matched impostor pairs i.e individuals of the same sex, from the same geographic region (see section 3.6.1), and the same age group (see section 3.6.2).

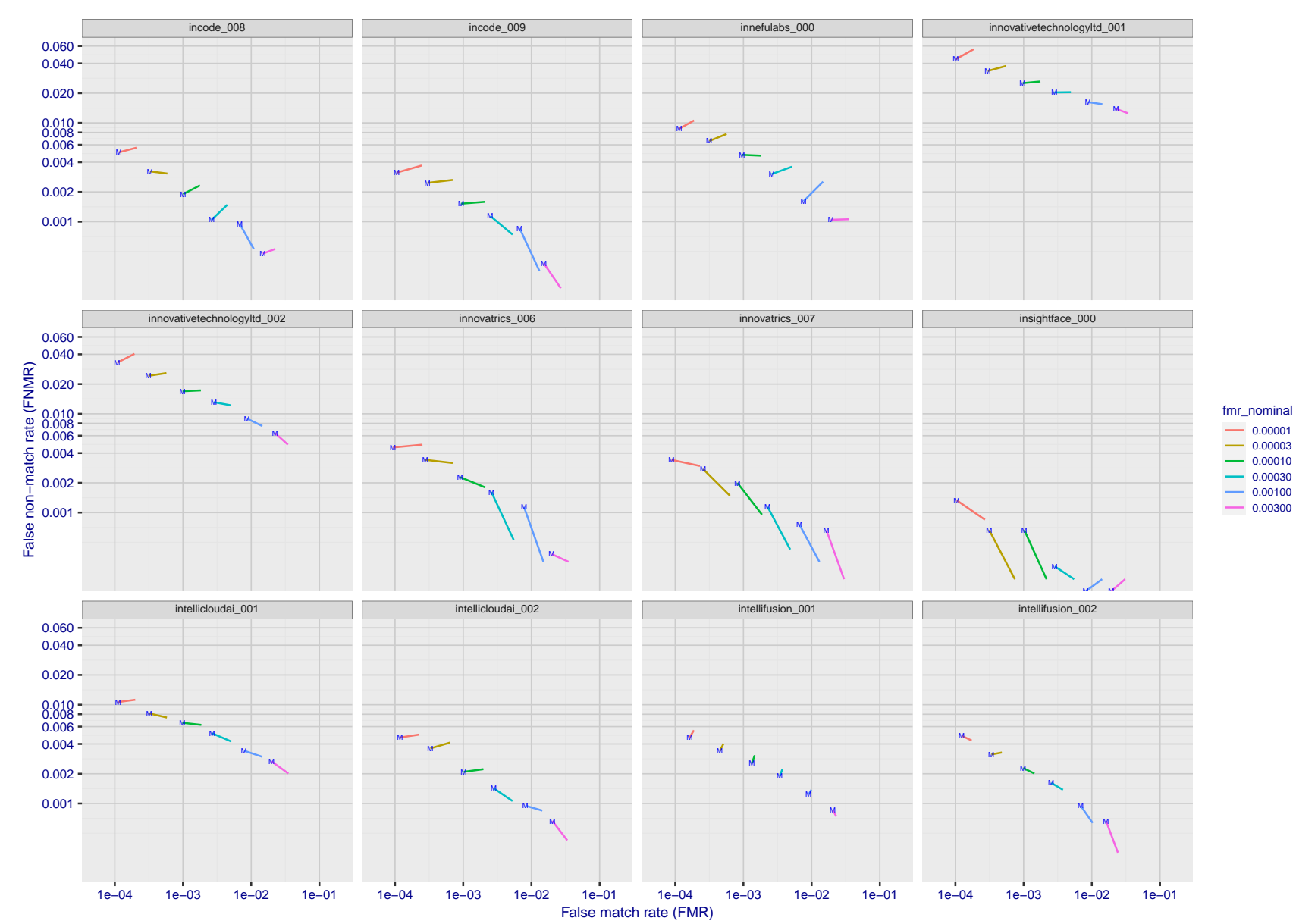


Figure 132: For the visa images, FNMR and FMR at six operating points along the DET characteristic. At each point a line is drawn between $(FMR, FNMR)_{MALE}$ and $(FMR, FNMR)_{FEMALE}$ showing how which sex has lower FMR and/or FNMR. The "M" label denotes male, the other end of the line corresponds to female. The six operating thresholds are selected to give the nominal false match rates given in the legend, and are computed over all impostor pairs regardless of age, sex, and place of birth. The plotted FMR values are broadly an order of magnitude larger than the nominal rates because FMR is computed over demographically-matched impostor pairs i.e individuals of the same sex, from the same geographic region (see section 3.6.1), and the same age group (see section 3.6.2).

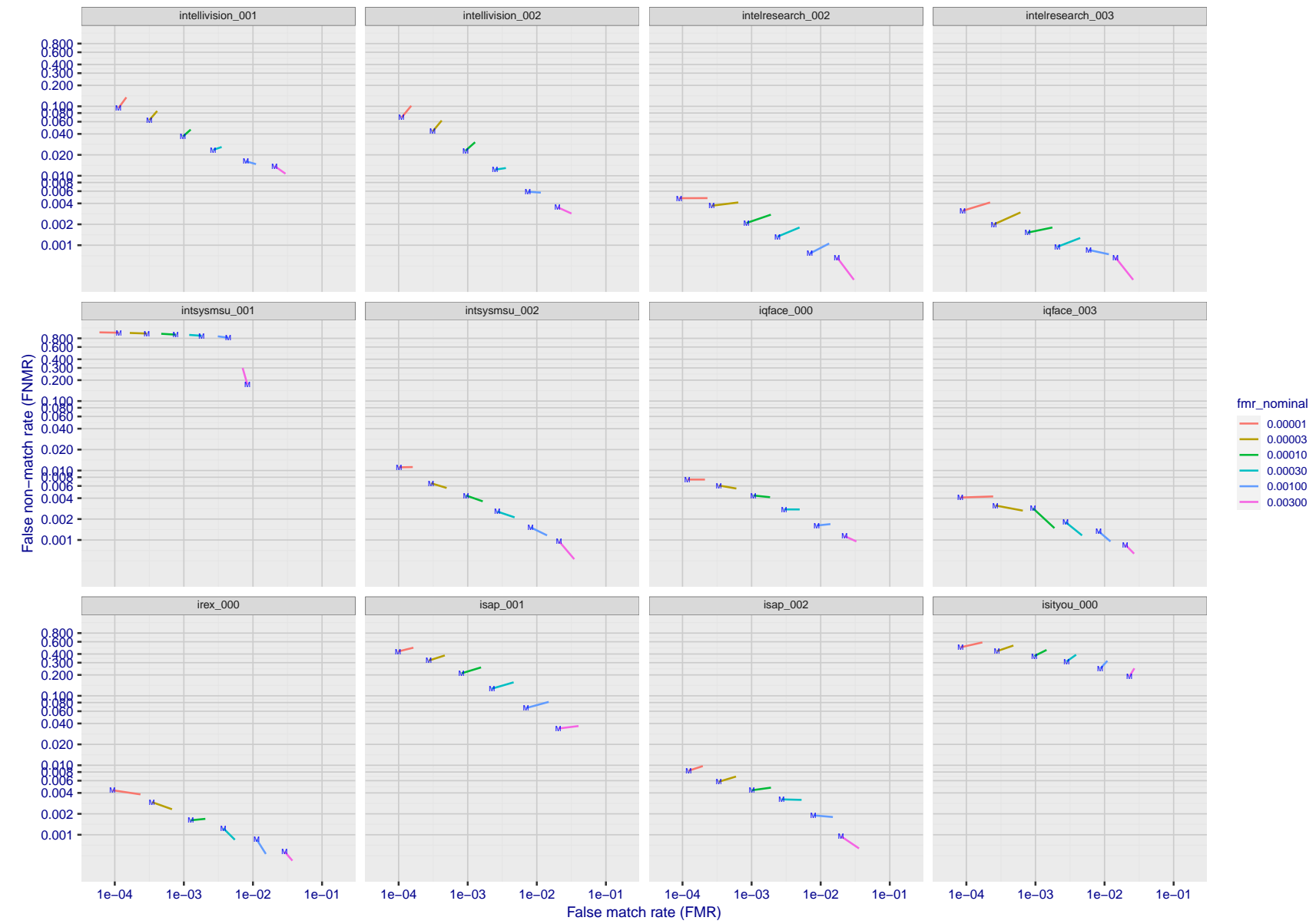


Figure 133: For the visa images, FNMR and FMR at six operating points along the DET characteristic. At each point a line is drawn between $(FMR, FNMR)_{MALE}$ and $(FMR, FNMR)_{FEMALE}$ showing how which sex has lower FMR and/or FNMR. The "M" label denotes male, the other end of the line corresponds to female. The six operating thresholds are selected to give the nominal false match rates given in the legend, and are computed over all impostor pairs regardless of age, sex, and place of birth. The plotted FMR values are broadly an order of magnitude larger than the nominal rates because FMR is computed over demographically-matched impostor pairs i.e individuals of the same sex, from the same geographic region (see section 3.6.1), and the same age group (see section 3.6.2).

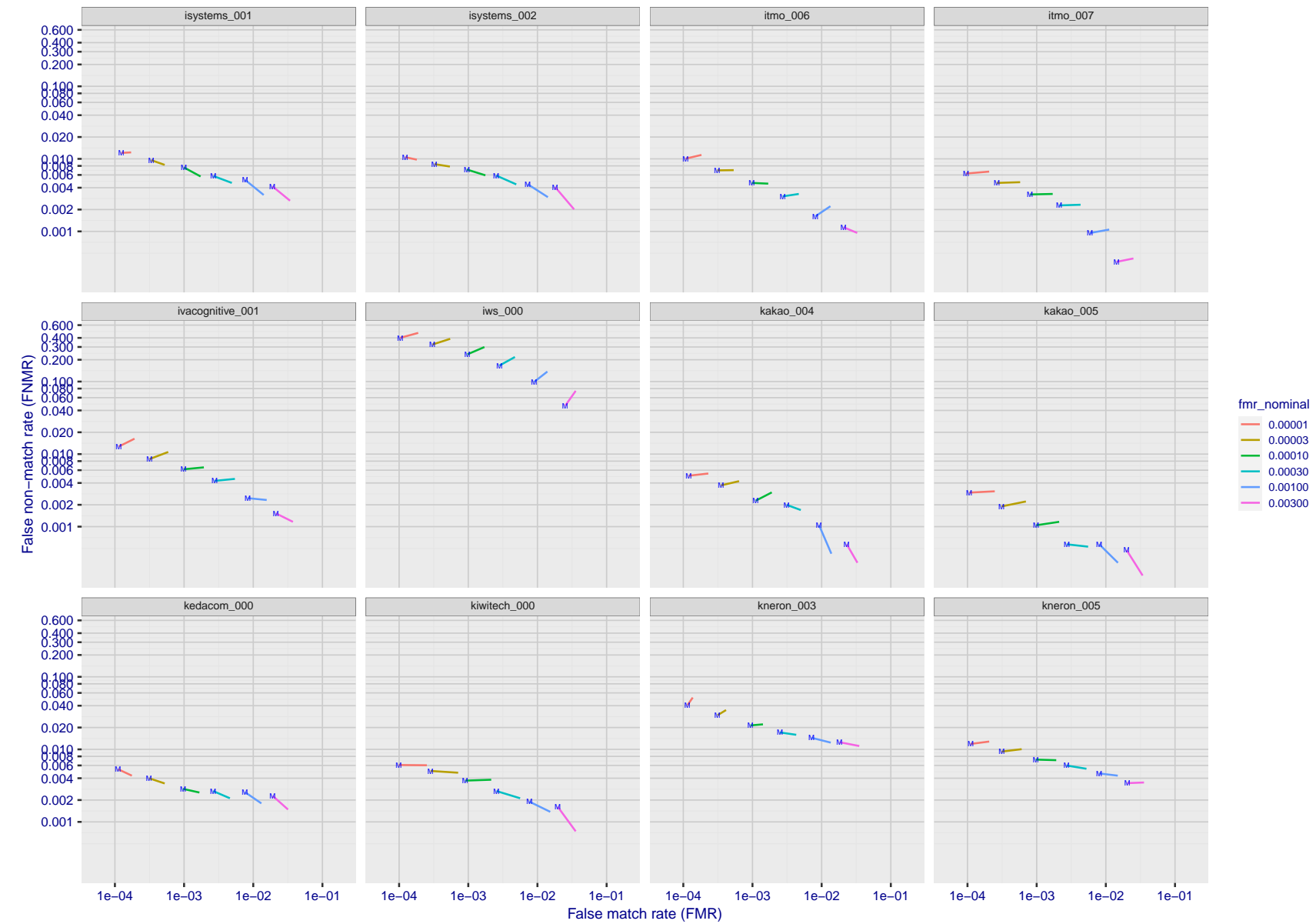


Figure 134: For the visa images, FNMR and FMR at six operating points along the DET characteristic. At each point a line is drawn between $(FMR, FNMR)_{MALE}$ and $(FMR, FNMR)_{FEMALE}$ showing how which sex has lower FMR and/or FNMR. The "M" label denotes male, the other end of the line corresponds to female. The six operating thresholds are selected to give the nominal false match rates given in the legend, and are computed over all impostor pairs regardless of age, sex, and place of birth. The plotted FMR values are broadly an order of magnitude larger than the nominal rates because FMR is computed over demographically-matched impostor pairs i.e individuals of the same sex, from the same geographic region (see section 3.6.1), and the same age group (see section 3.6.2).

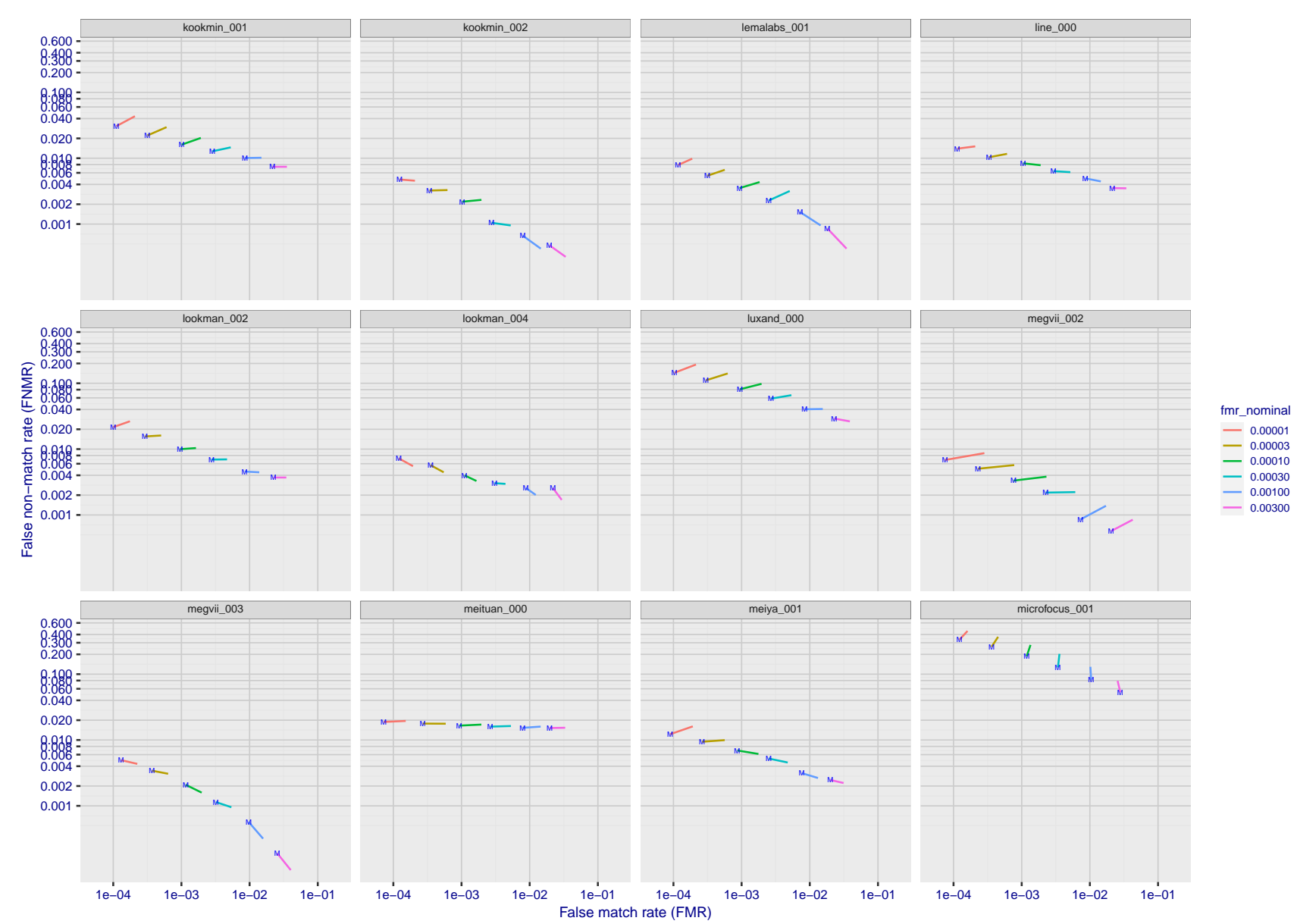


Figure 135: For the visa images, FNMR and FMR at six operating points along the DET characteristic. At each point a line is drawn between $(FMR, FNMR)_{MALE}$ and $(FMR, FNMR)_{FEMALE}$ showing how which sex has lower FMR and/or FNMR. The "M" label denotes male, the other end of the line corresponds to female. The six operating thresholds are selected to give the nominal false match rates given in the legend, and are computed over all impostor pairs regardless of age, sex, and place of birth. The plotted FMR values are broadly an order of magnitude larger than the nominal rates because FMR is computed over demographically-matched impostor pairs i.e individuals of the same sex, from the same geographic region (see section 3.6.1), and the same age group (see section 3.6.2).

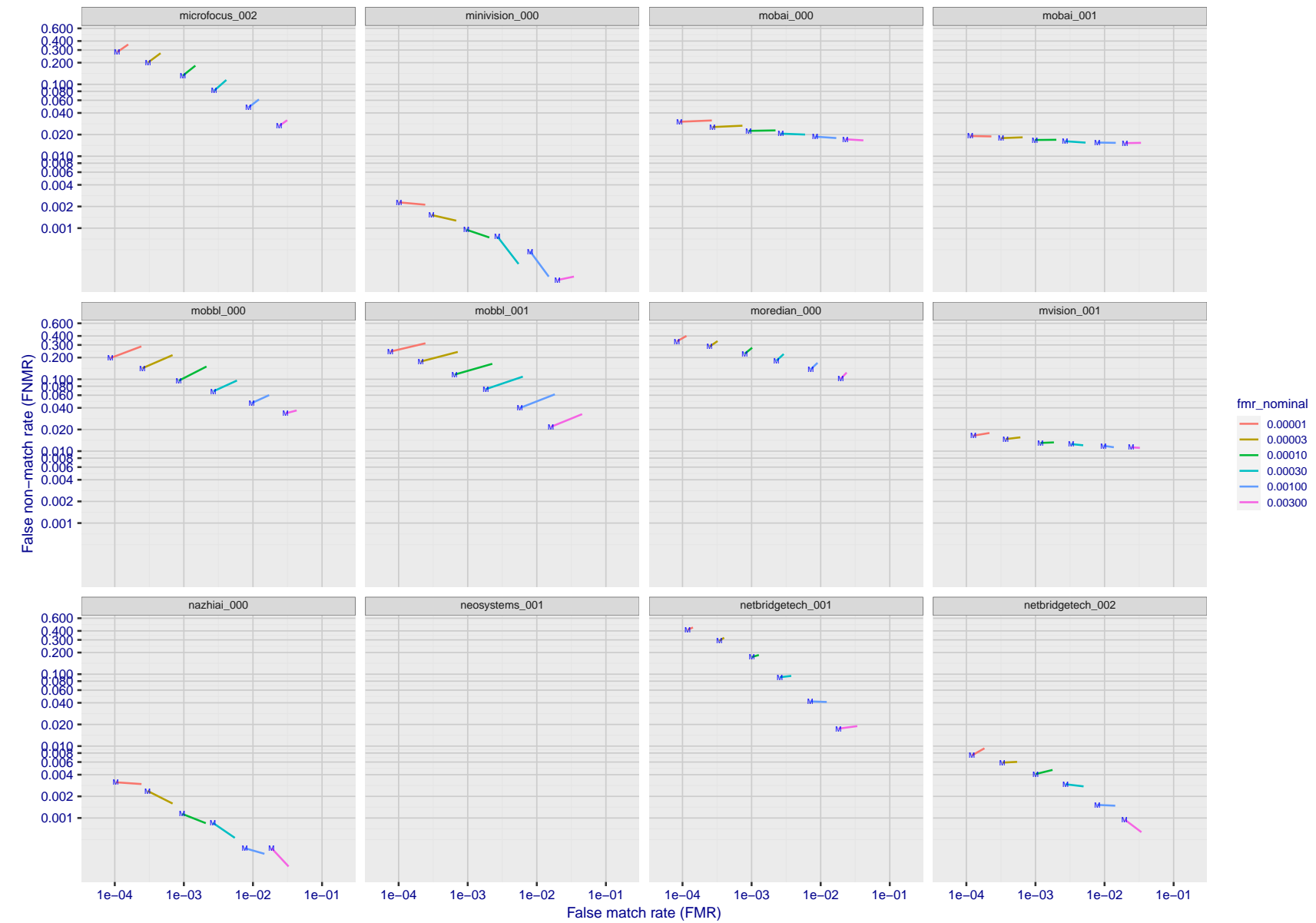


Figure 136: For the visa images, FNMR and FMR at six operating points along the DET characteristic. At each point a line is drawn between $(FMR, FNMR)_{MALE}$ and $(FMR, FNMR)_{FEMALE}$ showing how which sex has lower FMR and/or FNMR. The "M" label denotes male, the other end of the line corresponds to female. The six operating thresholds are selected to give the nominal false match rates given in the legend, and are computed over all impostor pairs regardless of age, sex, and place of birth. The plotted FMR values are broadly an order of magnitude larger than the nominal rates because FMR is computed over demographically-matched impostor pairs i.e individuals of the same sex, from the same geographic region (see section 3.6.1), and the same age group (see section 3.6.2).

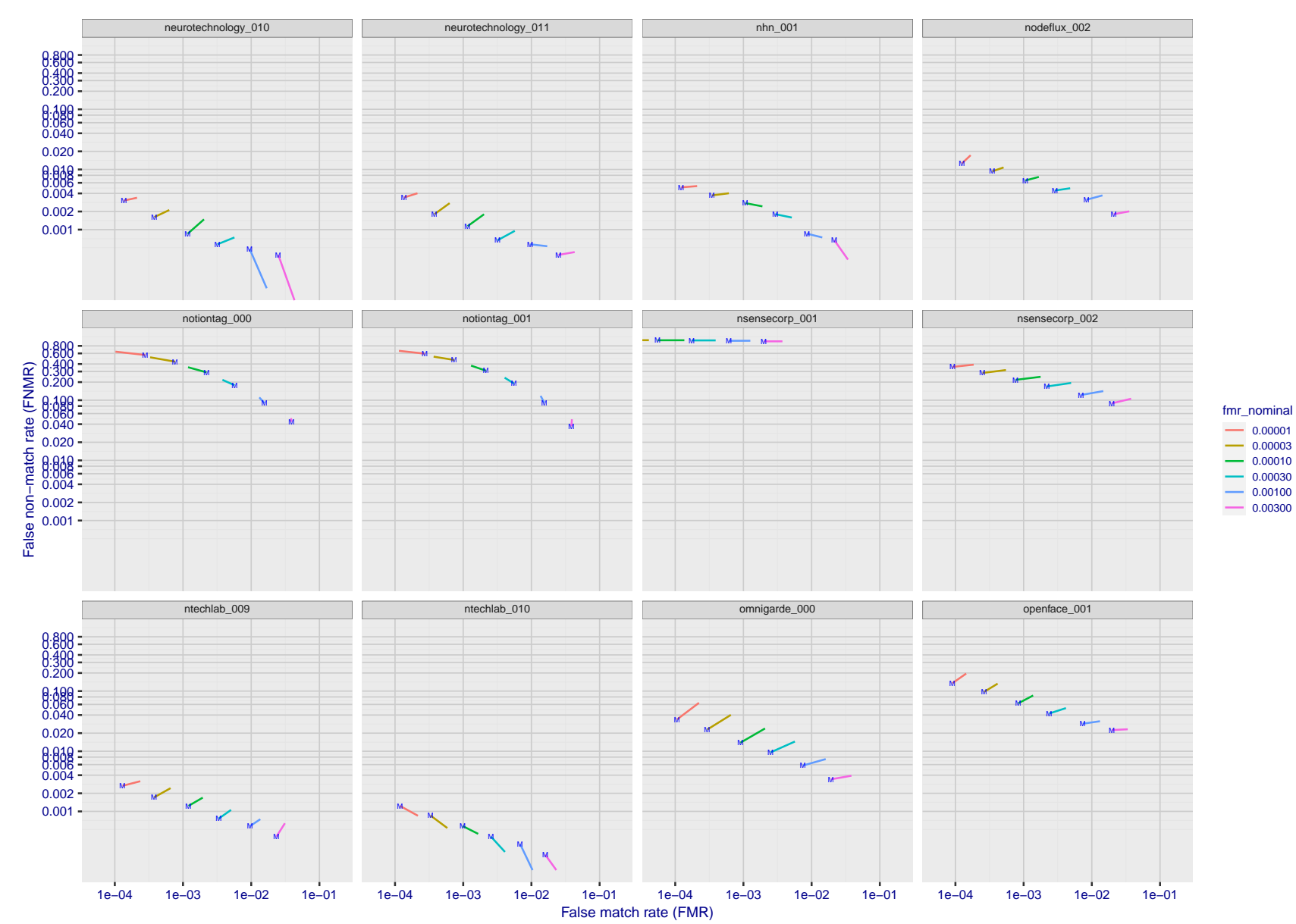


Figure 137: For the visa images, FNMR and FMR at six operating points along the DET characteristic. At each point a line is drawn between $(FMR, FNMR)_{MALE}$ and $(FMR, FNMR)_{FEMALE}$ showing how which sex has lower FMR and/or FNMR. The "M" label denotes male, the other end of the line corresponds to female. The six operating thresholds are selected to give the nominal false match rates given in the legend, and are computed over all impostor pairs regardless of age, sex, and place of birth. The plotted FMR values are broadly an order of magnitude larger than the nominal rates because FMR is computed over demographically-matched impostor pairs i.e individuals of the same sex, from the same geographic region (see section 3.6.1), and the same age group (see section 3.6.2).

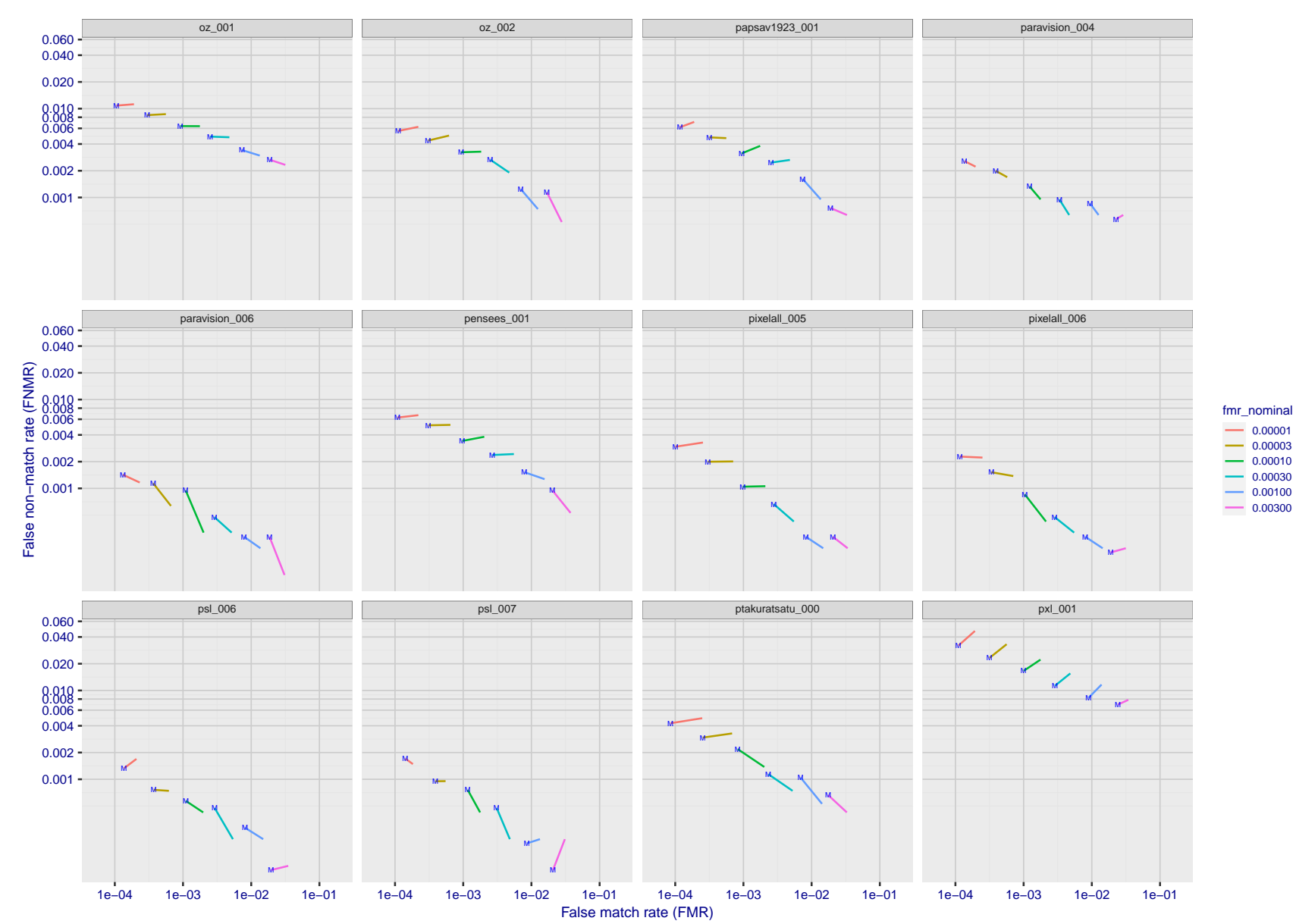


Figure 138: For the visa images, FNMR and FMR at six operating points along the DET characteristic. At each point a line is drawn between $(FMR, FNMR)_{MALE}$ and $(FMR, FNMR)_{FEMALE}$ showing how which sex has lower FMR and/or FNMR. The "M" label denotes male, the other end of the line corresponds to female. The six operating thresholds are selected to give the nominal false match rates given in the legend, and are computed over all impostor pairs regardless of age, sex, and place of birth. The plotted FMR values are broadly an order of magnitude larger than the nominal rates because FMR is computed over demographically-matched impostor pairs i.e individuals of the same sex, from the same geographic region (see section 3.6.1), and the same age group (see section 3.6.2).

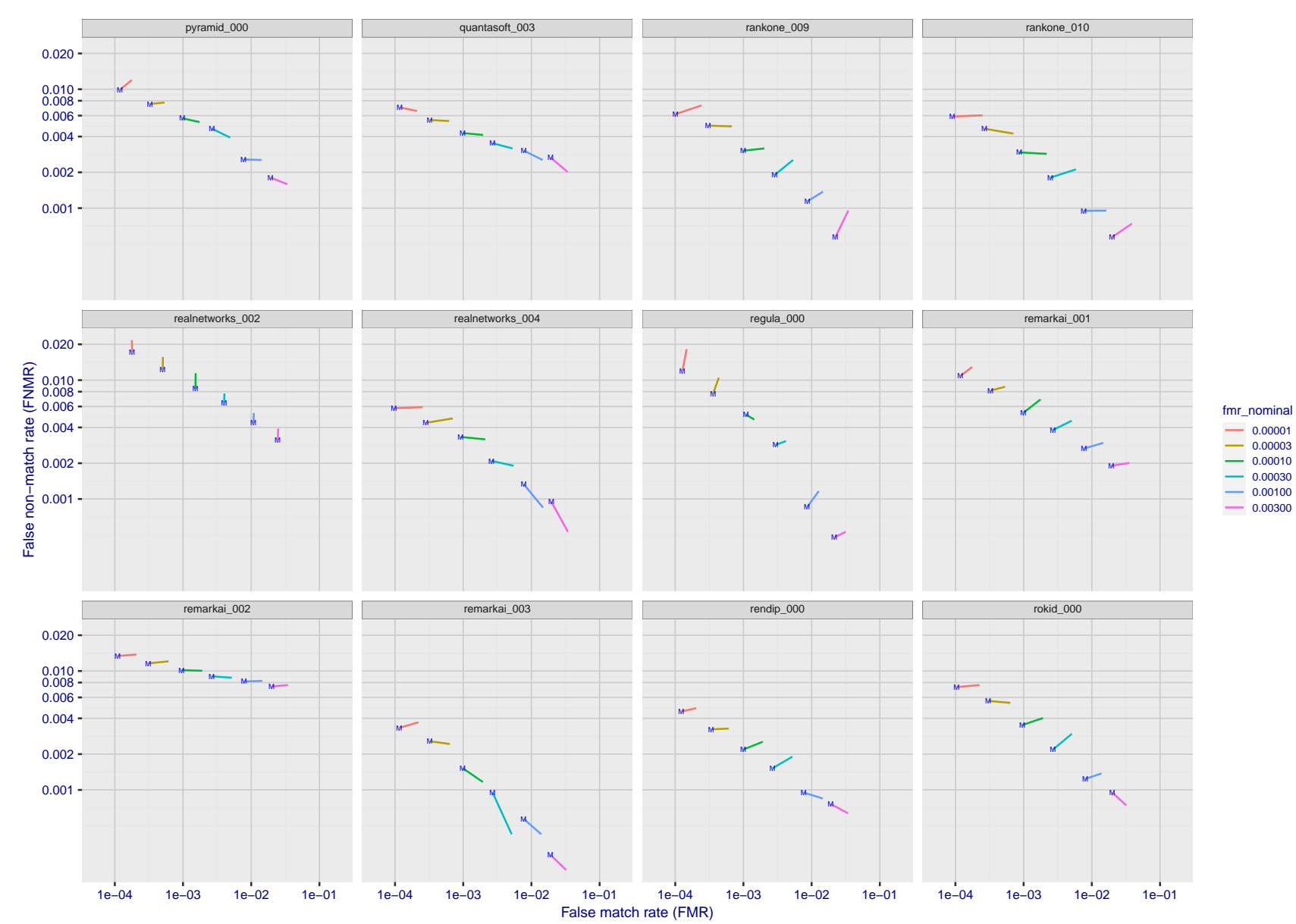


Figure 139: For the visa images, FNMR and FMR at six operating points along the DET characteristic. At each point a line is drawn between $(FMR, FNMR)_{MALE}$ and $(FMR, FNMR)_{FEMALE}$ showing how which sex has lower FMR and/or FNMR. The "M" label denotes male, the other end of the line corresponds to female. The six operating thresholds are selected to give the nominal false match rates given in the legend, and are computed over all impostor pairs regardless of age, sex, and place of birth. The plotted FMR values are broadly an order of magnitude larger than the nominal rates because FMR is computed over demographically-matched impostor pairs i.e individuals of the same sex, from the same geographic region (see section 3.6.1), and the same age group (see section 3.6.2).

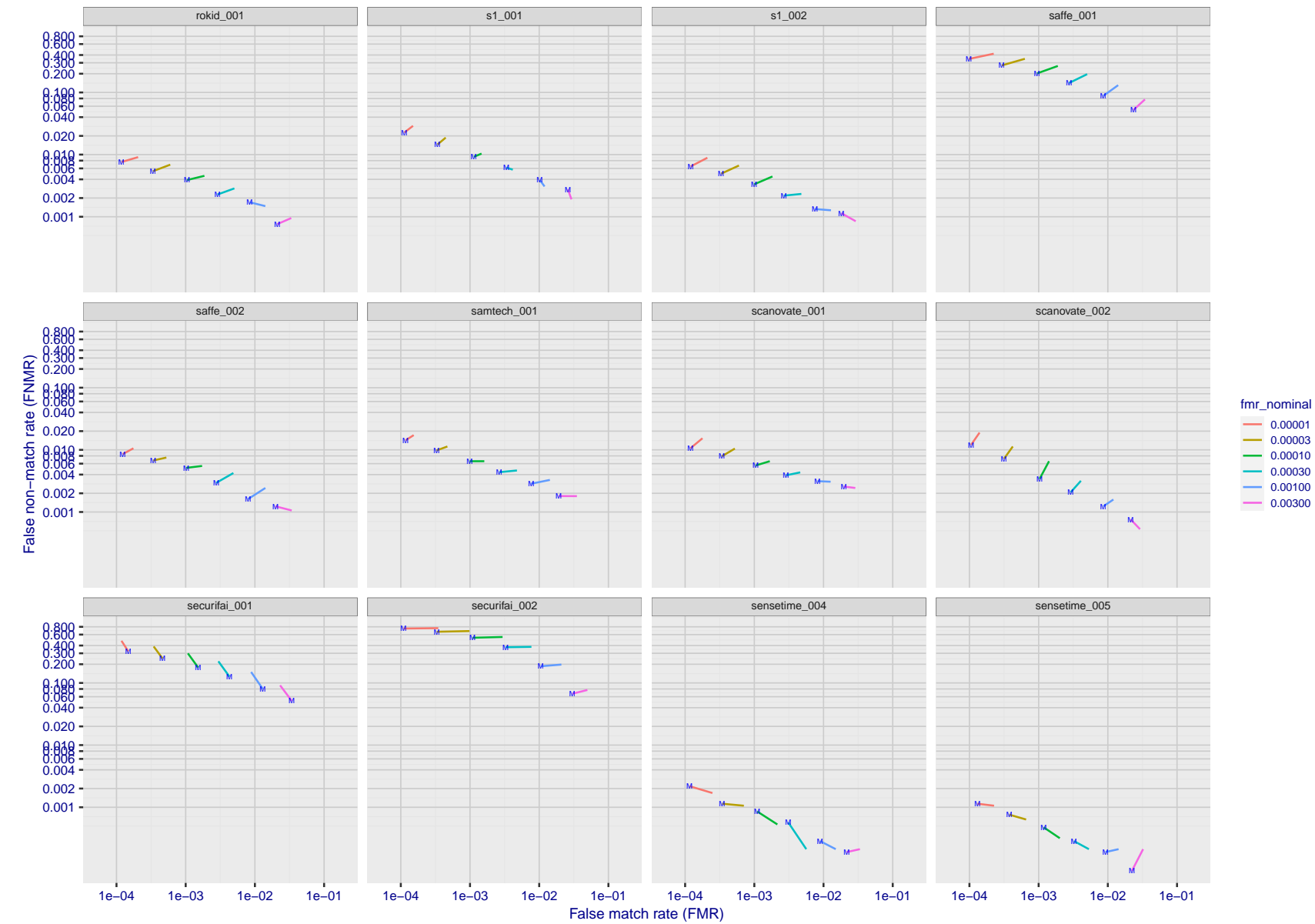


Figure 140: For the visa images, FNMR and FMR at six operating points along the DET characteristic. At each point a line is drawn between $(FMR, FNMR)_{MALE}$ and $(FMR, FNMR)_{FEMALE}$ showing how which sex has lower FMR and/or FNMR. The "M" label denotes male, the other end of the line corresponds to female. The six operating thresholds are selected to give the nominal false match rates given in the legend, and are computed over all impostor pairs regardless of age, sex, and place of birth. The plotted FMR values are broadly an order of magnitude larger than the nominal rates because FMR is computed over demographically-matched impostor pairs i.e individuals of the same sex, from the same geographic region (see section 3.6.1), and the same age group (see section 3.6.2).

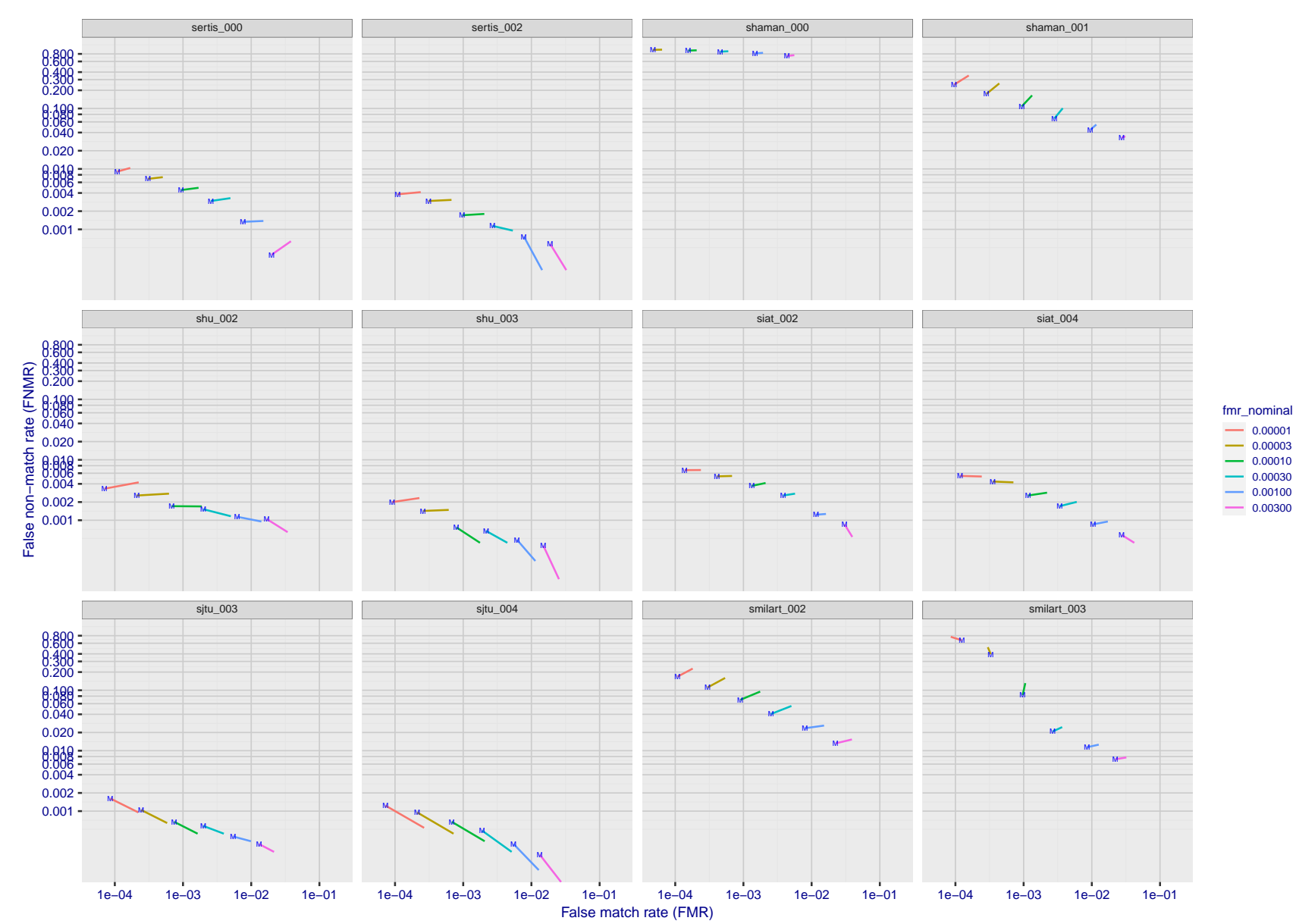


Figure 141: For the visa images, FNMR and FMR at six operating points along the DET characteristic. At each point a line is drawn between $(FMR, FNMR)_{MALE}$ and $(FMR, FNMR)_{FEMALE}$ showing how which sex has lower FMR and/or FNMR. The "M" label denotes male, the other end of the line corresponds to female. The six operating thresholds are selected to give the nominal false match rates given in the legend, and are computed over all impostor pairs regardless of age, sex, and place of birth. The plotted FMR values are broadly an order of magnitude larger than the nominal rates because FMR is computed over demographically-matched impostor pairs i.e individuals of the same sex, from the same geographic region (see section 3.6.1), and the same age group (see section 3.6.2).

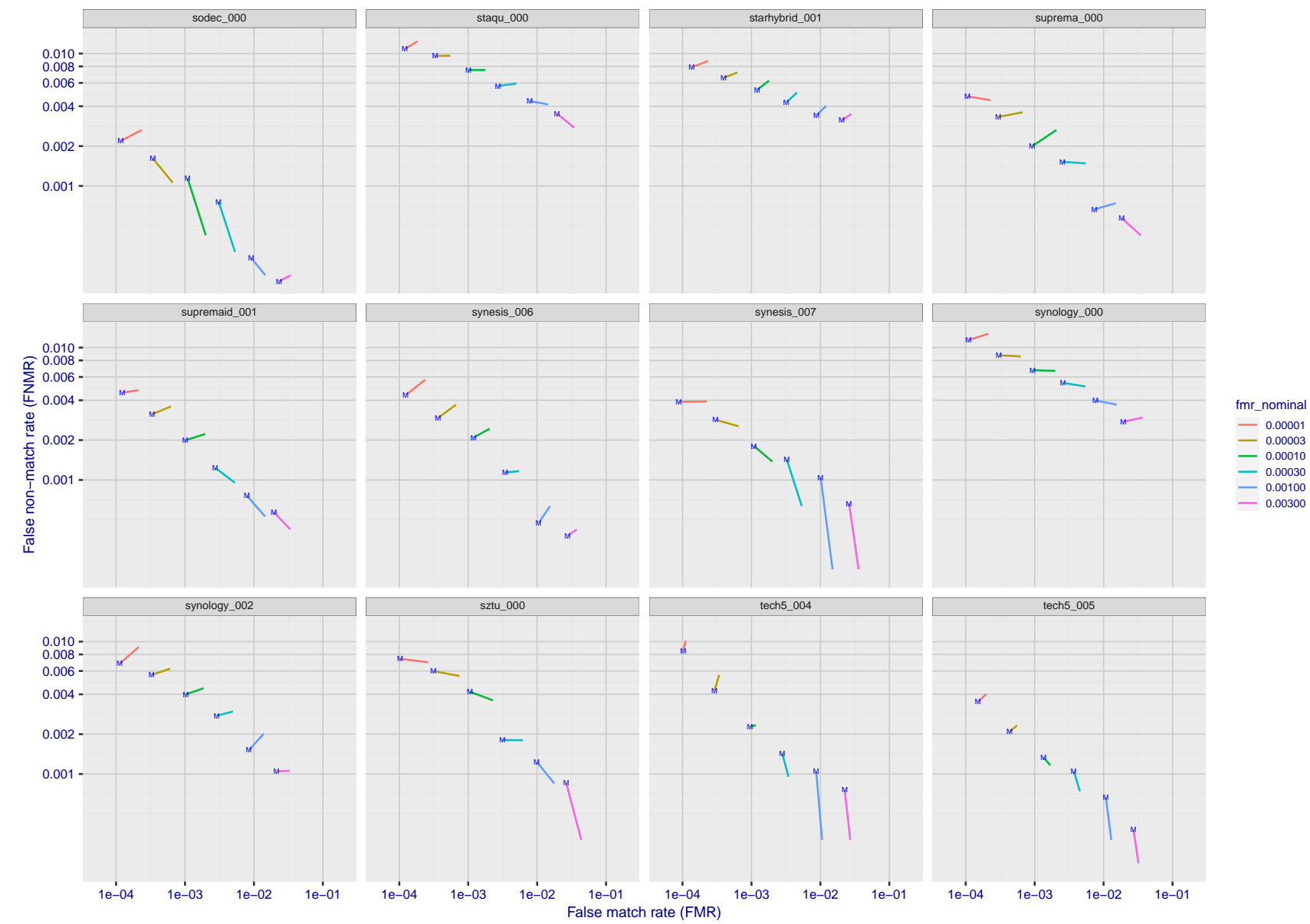


Figure 142: For the visa images, FNMR and FMR at six operating points along the DET characteristic. At each point a line is drawn between $(FMR, FNMR)_{MALE}$ and $(FMR, FNMR)_{FEMALE}$ showing how which sex has lower FMR and/or FNMR. The "M" label denotes male, the other end of the line corresponds to female. The six operating thresholds are selected to give the nominal false match rates given in the legend, and are computed over all impostor pairs regardless of age, sex, and place of birth. The plotted FMR values are broadly an order of magnitude larger than the nominal rates because FMR is computed over demographically-matched impostor pairs i.e individuals of the same sex, from the same geographic region (see section 3.6.1), and the same age group (see section 3.6.2).

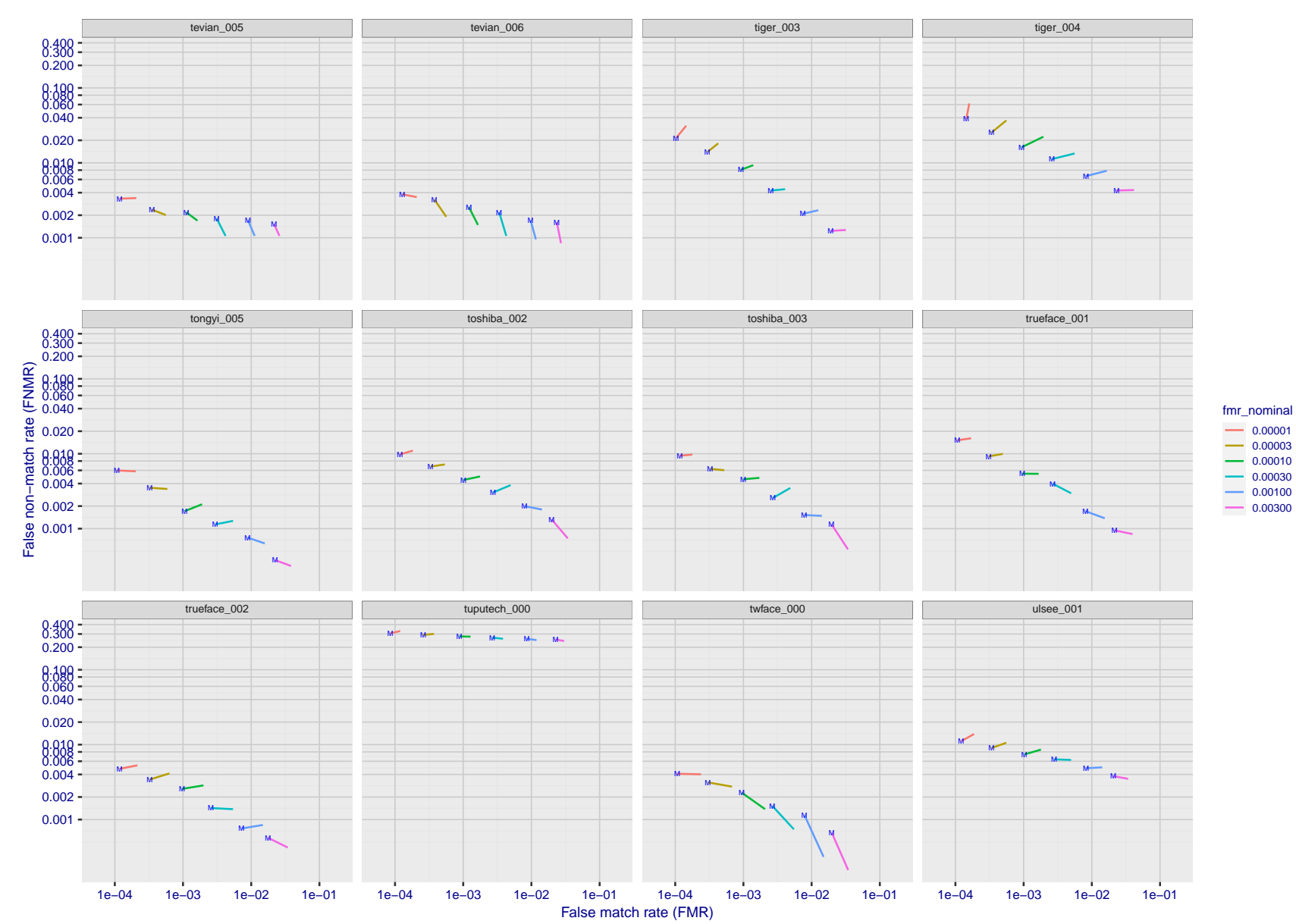


Figure 143: For the visa images, FNMR and FMR at six operating points along the DET characteristic. At each point a line is drawn between $(FMR, FNMR)_{MALE}$ and $(FMR, FNMR)_{FEMALE}$ showing how which sex has lower FMR and/or FNMR. The "M" label denotes male, the other end of the line corresponds to female. The six operating thresholds are selected to give the nominal false match rates given in the legend, and are computed over all impostor pairs regardless of age, sex, and place of birth. The plotted FMR values are broadly an order of magnitude larger than the nominal rates because FMR is computed over demographically-matched impostor pairs i.e individuals of the same sex, from the same geographic region (see section 3.6.1), and the same age group (see section 3.6.2).

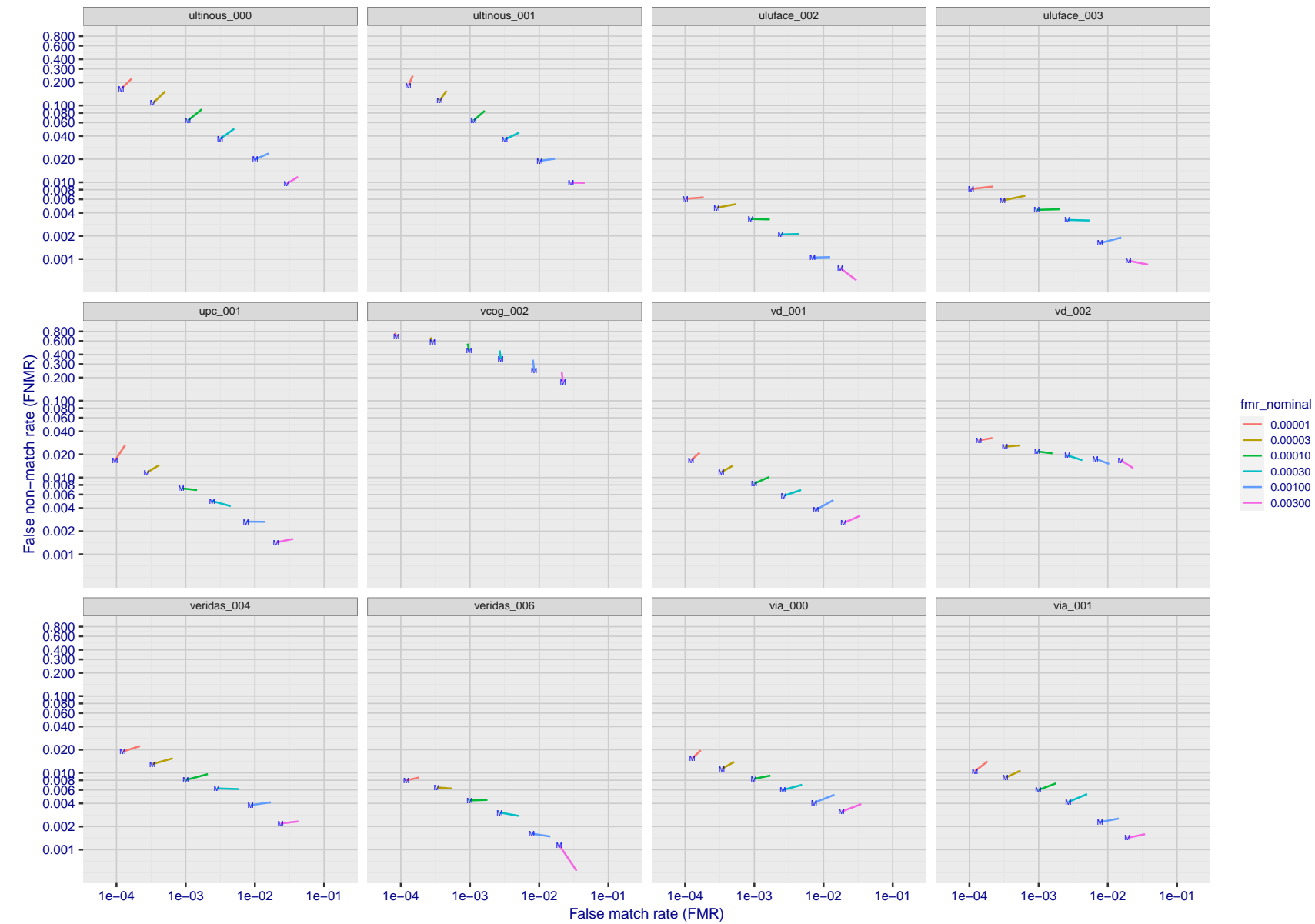


Figure 144: For the visa images, FNMR and FMR at six operating points along the DET characteristic. At each point a line is drawn between $(FMR, FNMR)_{MALE}$ and $(FMR, FNMR)_{FEMALE}$ showing how which sex has lower FMR and/or FNMR. The "M" label denotes male, the other end of the line corresponds to female. The six operating thresholds are selected to give the nominal false match rates given in the legend, and are computed over all impostor pairs regardless of age, sex, and place of birth. The plotted FMR values are broadly an order of magnitude larger than the nominal rates because FMR is computed over demographically-matched impostor pairs i.e individuals of the same sex, from the same geographic region (see section 3.6.1), and the same age group (see section 3.6.2).

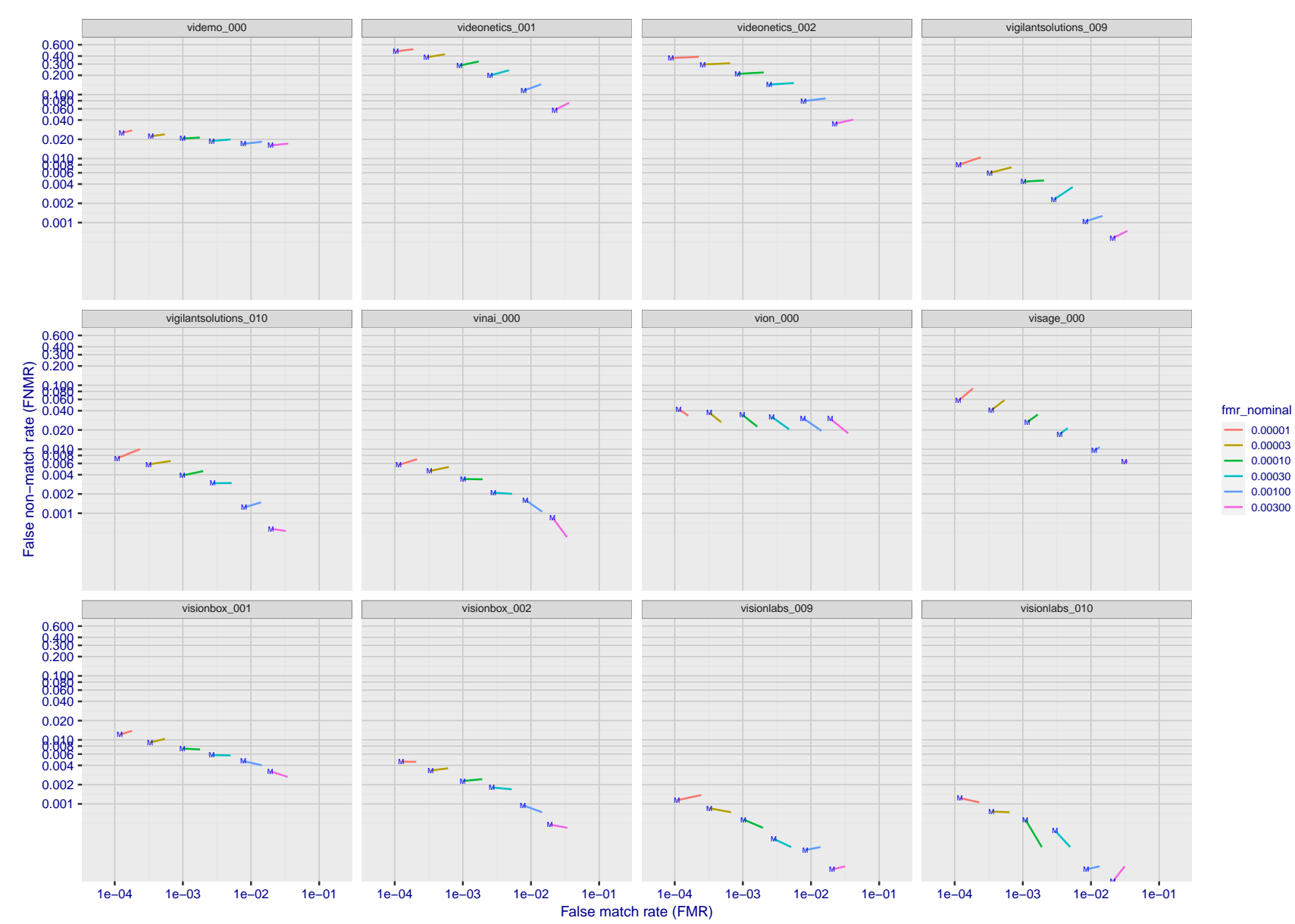


Figure 145: For the visa images, FNMR and FMR at six operating points along the DET characteristic. At each point a line is drawn between $(FMR, FNMR)_{MALE}$ and $(FMR, FNMR)_{FEMALE}$ showing how which sex has lower FMR and/or FNMR. The "M" label denotes male, the other end of the line corresponds to female. The six operating thresholds are selected to give the nominal false match rates given in the legend, and are computed over all impostor pairs regardless of age, sex, and place of birth. The plotted FMR values are broadly an order of magnitude larger than the nominal rates because FMR is computed over demographically-matched impostor pairs i.e individuals of the same sex, from the same geographic region (see section 3.6.1), and the same age group (see section 3.6.2).

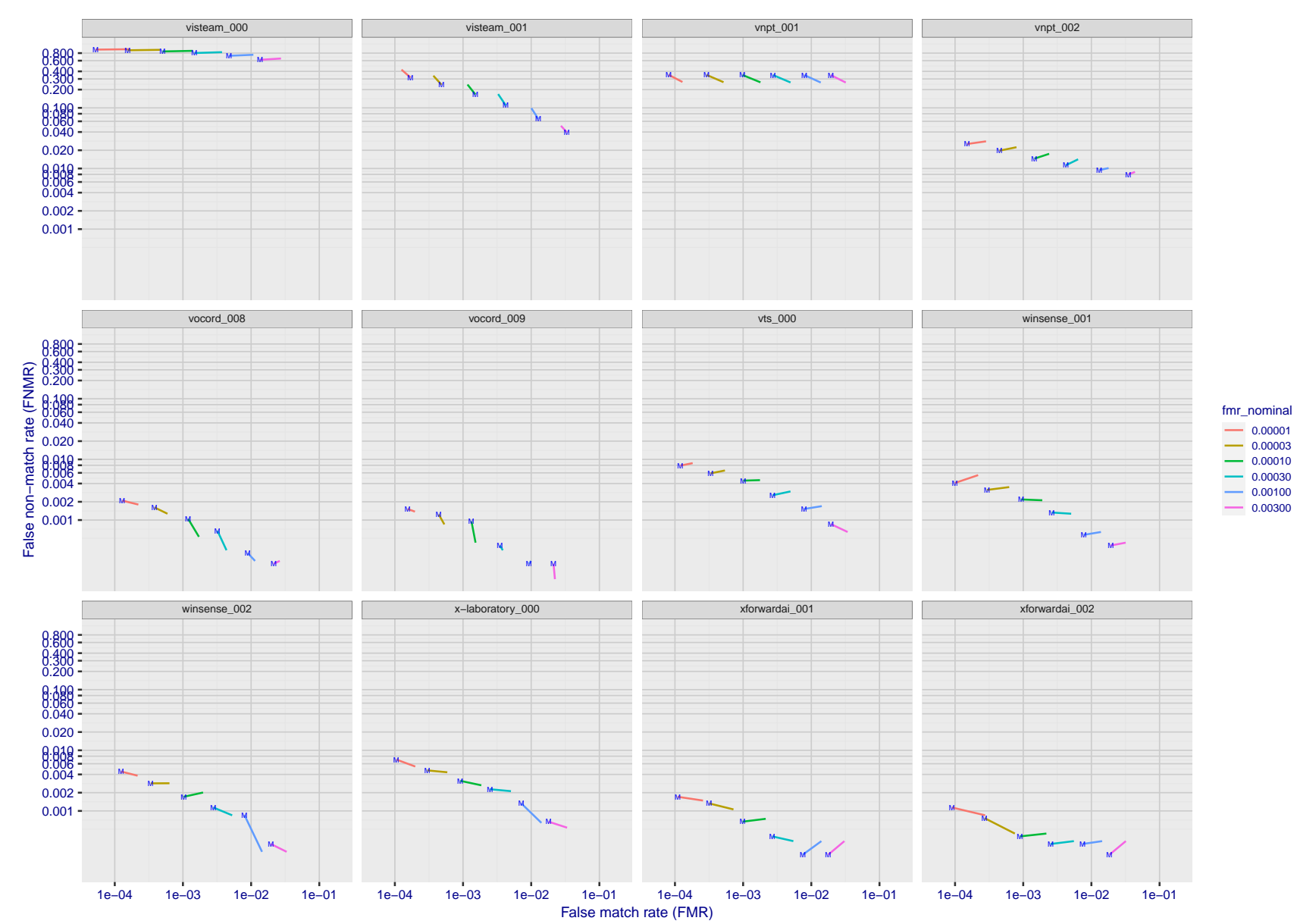


Figure 146: For the visa images, FNMR and FMR at six operating points along the DET characteristic. At each point a line is drawn between $(FMR, FNMR)_{MALE}$ and $(FMR, FNMR)_{FEMALE}$ showing how which sex has lower FMR and/or FNMR. The "M" label denotes male, the other end of the line corresponds to female. The six operating thresholds are selected to give the nominal false match rates given in the legend, and are computed over all impostor pairs regardless of age, sex, and place of birth. The plotted FMR values are broadly an order of magnitude larger than the nominal rates because FMR is computed over demographically-matched impostor pairs i.e individuals of the same sex, from the same geographic region (see section 3.6.1), and the same age group (see section 3.6.2).

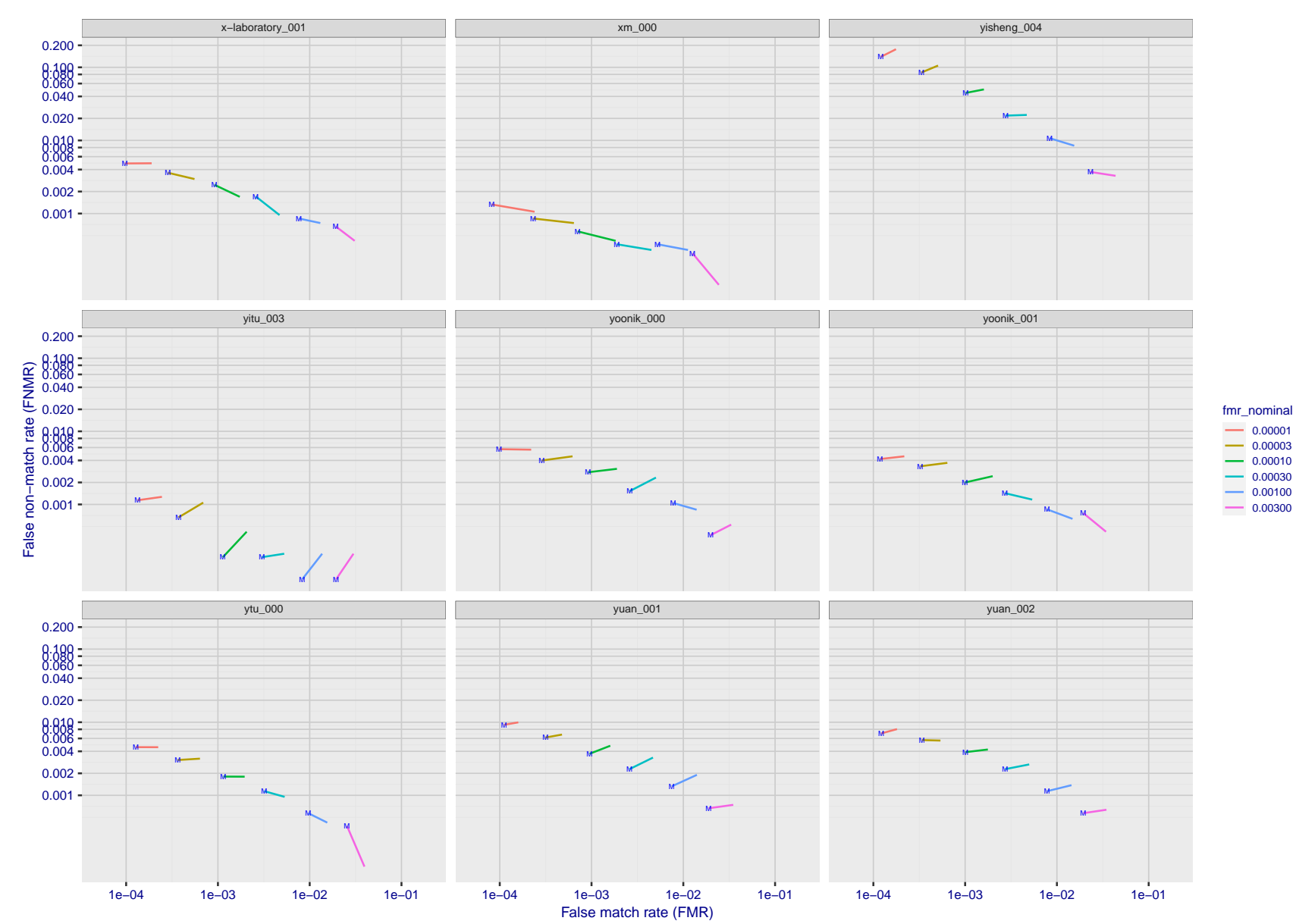


Figure 147: For the visa images, FNMR and FMR at six operating points along the DET characteristic. At each point a line is drawn between $(FMR, FNMR)_{MALE}$ and $(FMR, FNMR)_{FEMALE}$ showing how which sex has lower FMR and/or FNMR. The "M" label denotes male, the other end of the line corresponds to female. The six operating thresholds are selected to give the nominal false match rates given in the legend, and are computed over all impostor pairs regardless of age, sex, and place of birth. The plotted FMR values are broadly an order of magnitude larger than the nominal rates because FMR is computed over demographically-matched impostor pairs i.e individuals of the same sex, from the same geographic region (see section 3.6.1), and the same age group (see section 3.6.2).

2021/06/28 10:42:55

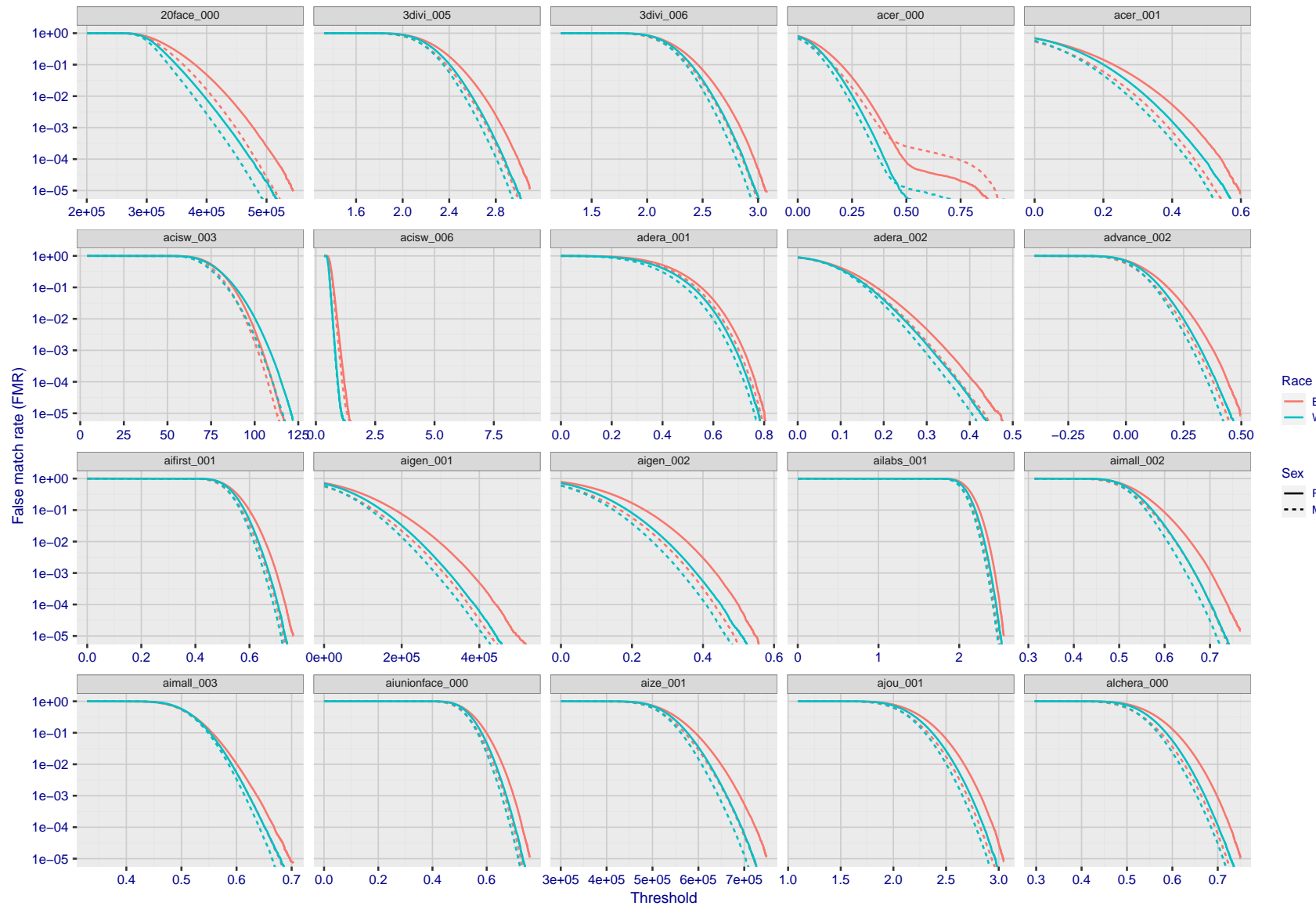


Figure 148: For the mugshot images, the false match calibration curves show false match rate vs. threshold. Separate curves appear for white females, black females, black males and white males.

2021/06/28 10:42:55

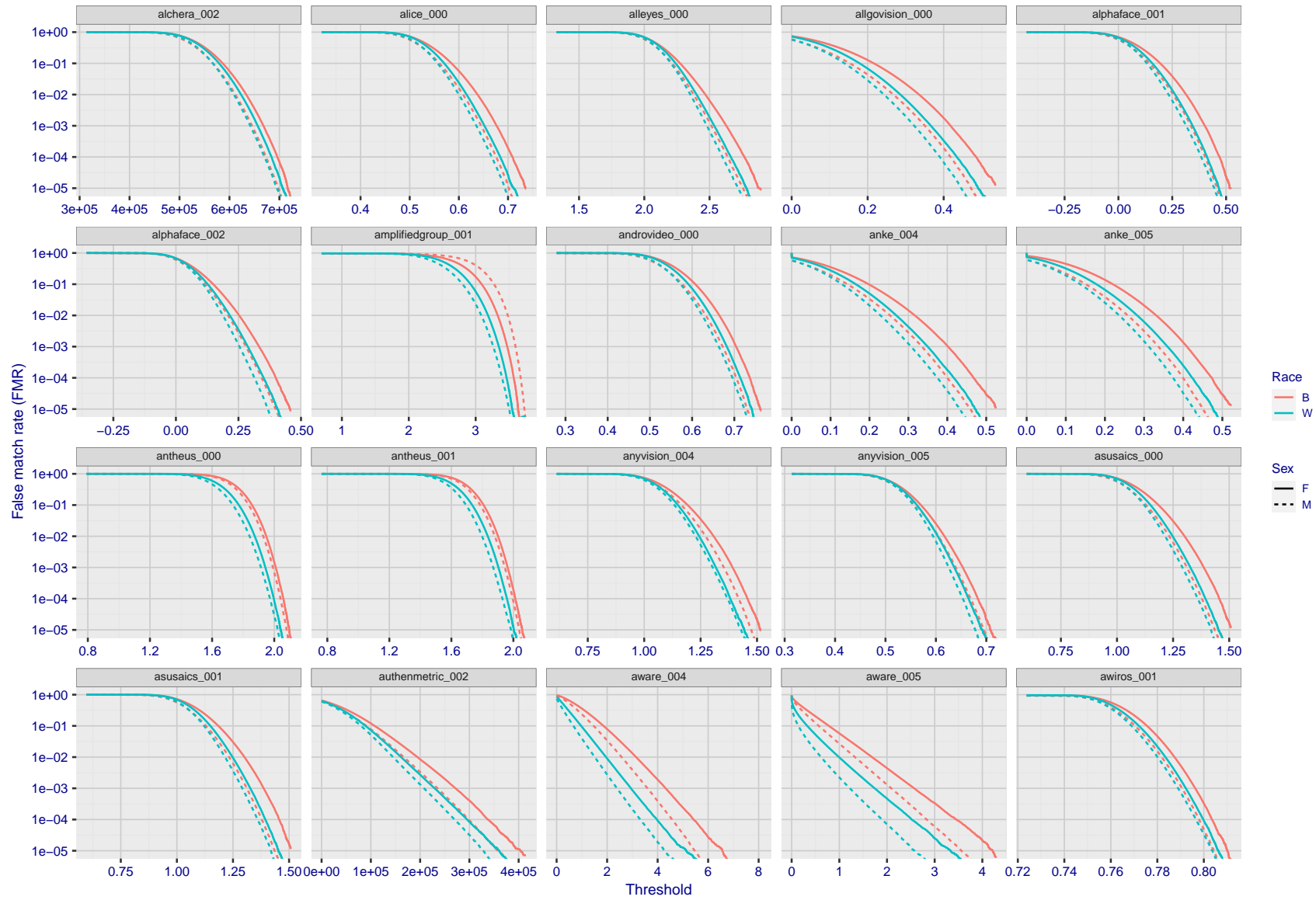


Figure 149: For the mugshot images, the false match calibration curves show false match rate vs. threshold. Separate curves appear for white females, black females, black males and white males.

2021/06/28 10:42:55

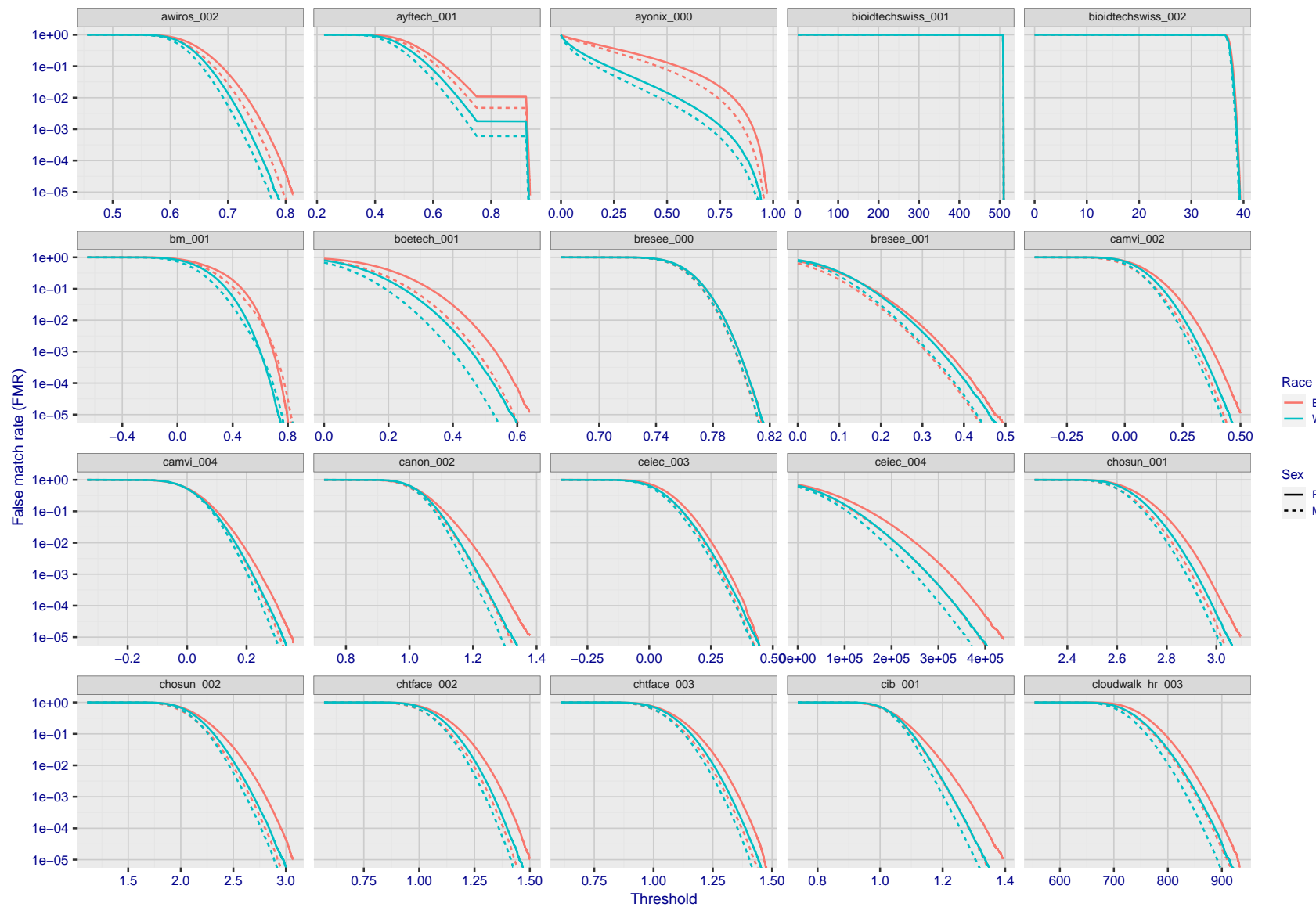


Figure 150: For the mugshot images, the false match calibration curves show false match rate vs. threshold. Separate curves appear for white females, black females, black males and white males.

FNMR(T)
"False non-match rate"
"False match rate"

2021/06/28 10:42:55

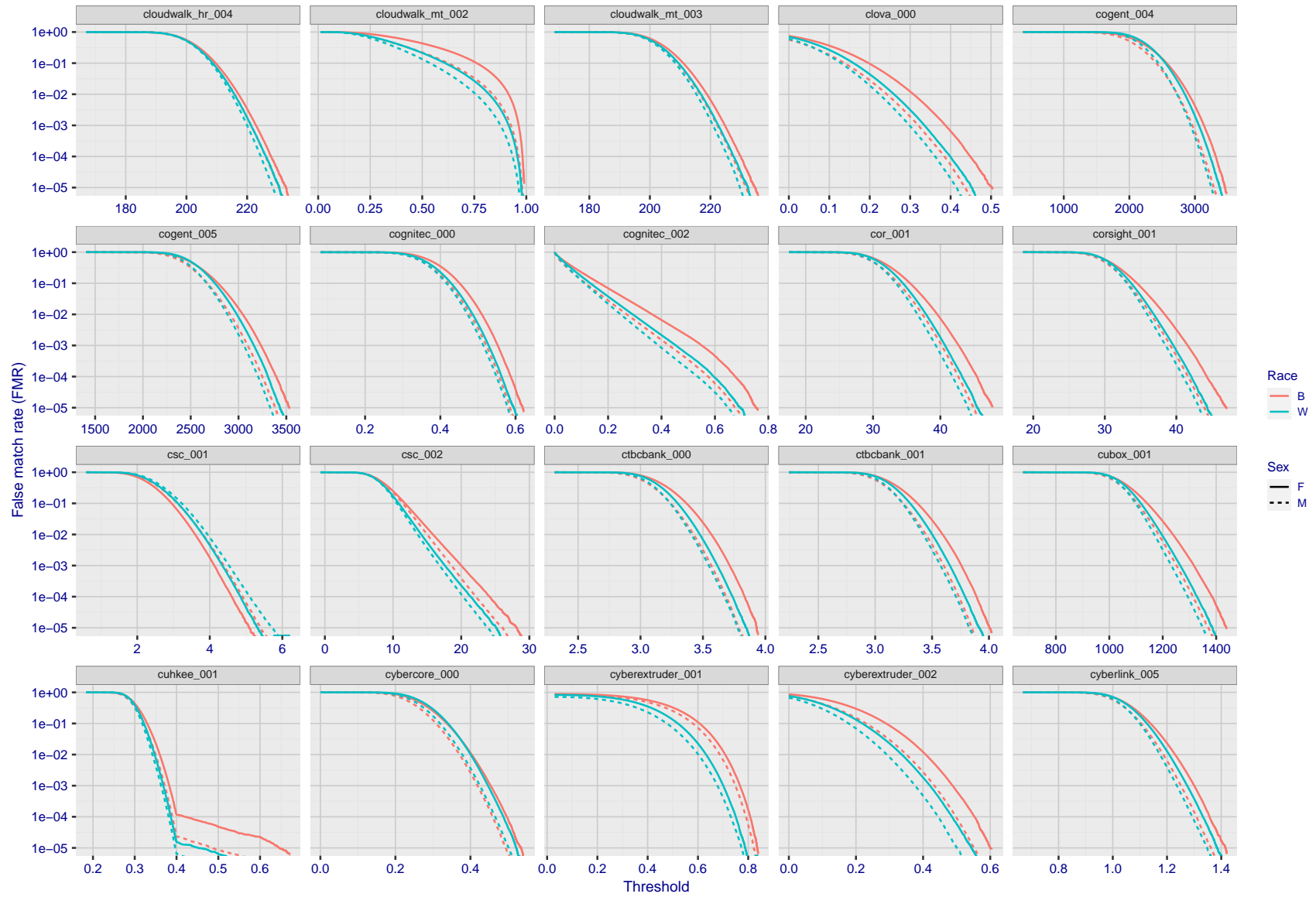


Figure 151: For the mugshot images, the false match calibration curves show false match rate vs. threshold. Separate curves appear for white females, black females, black males and white males.

2021/06/28 10:42:55

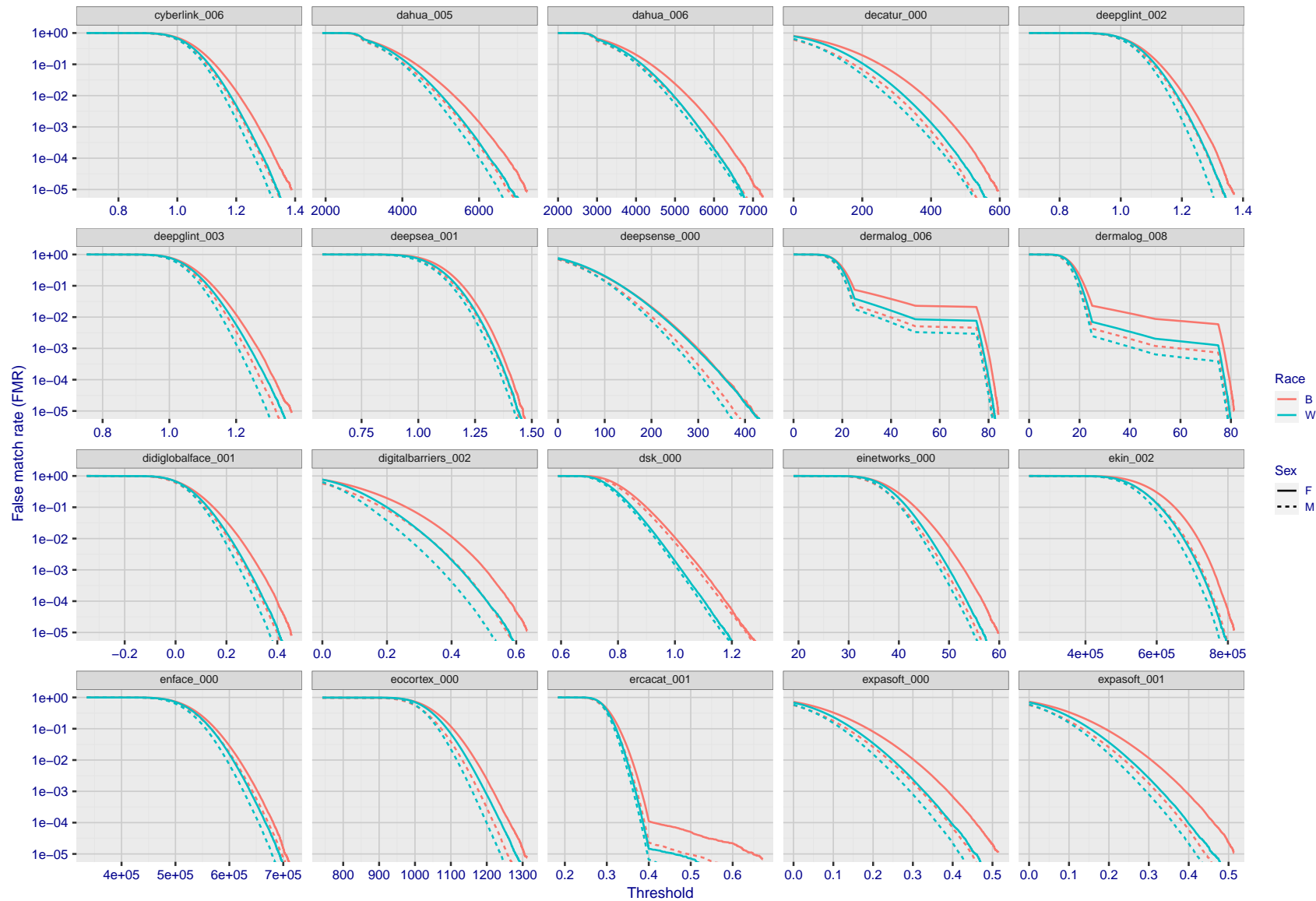


Figure 152: For the mugshot images, the false match calibration curves show false match rate vs. threshold. Separate curves appear for white females, black females, black males and white males.

FNMR(T)
"False non-match rate"
"False match rate"

2021/06/28 10:42:55

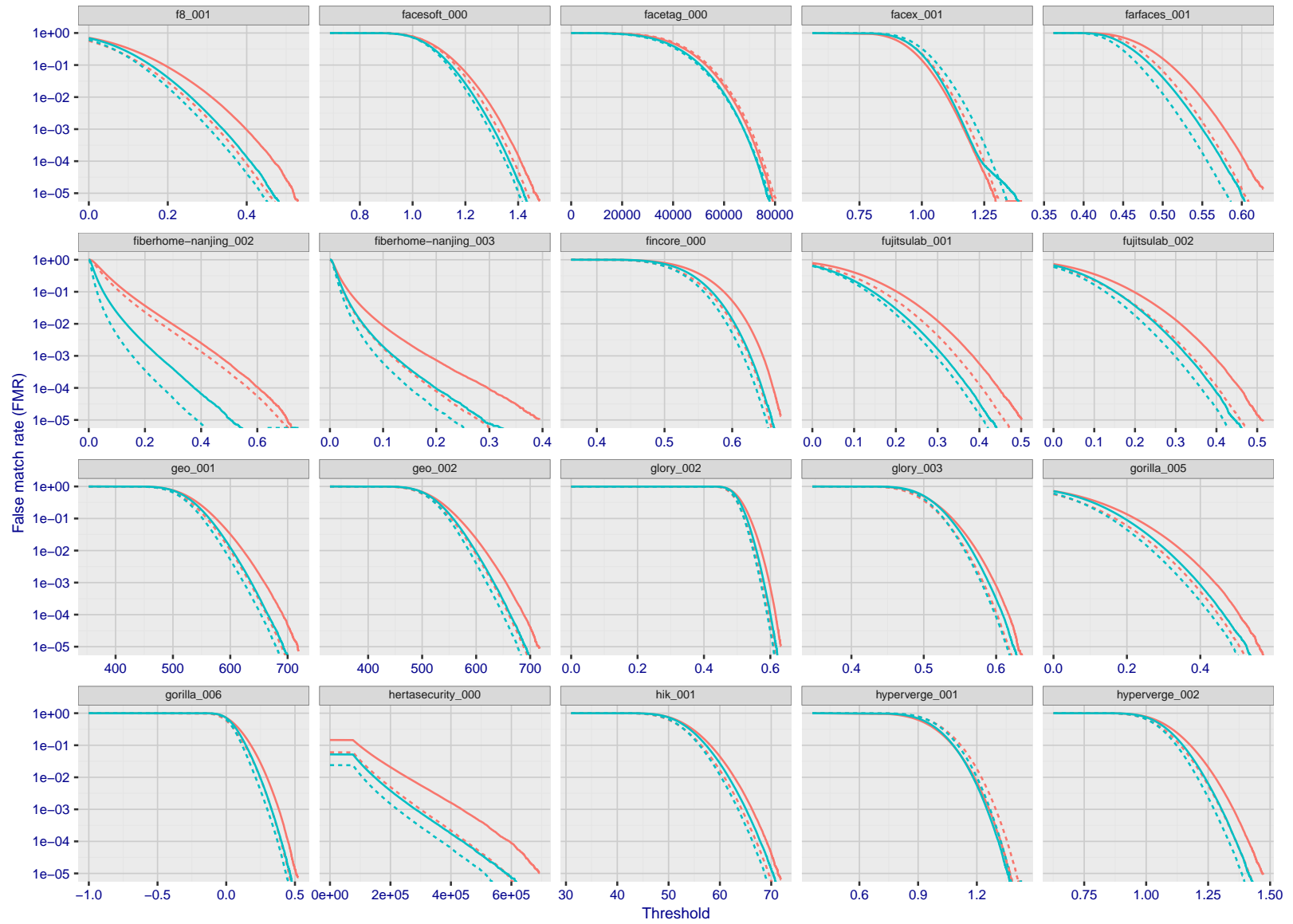


Figure 153: For the mugshot images, the false match calibration curves show false match rate vs. threshold. Separate curves appear for white females, black females, black males and white males.

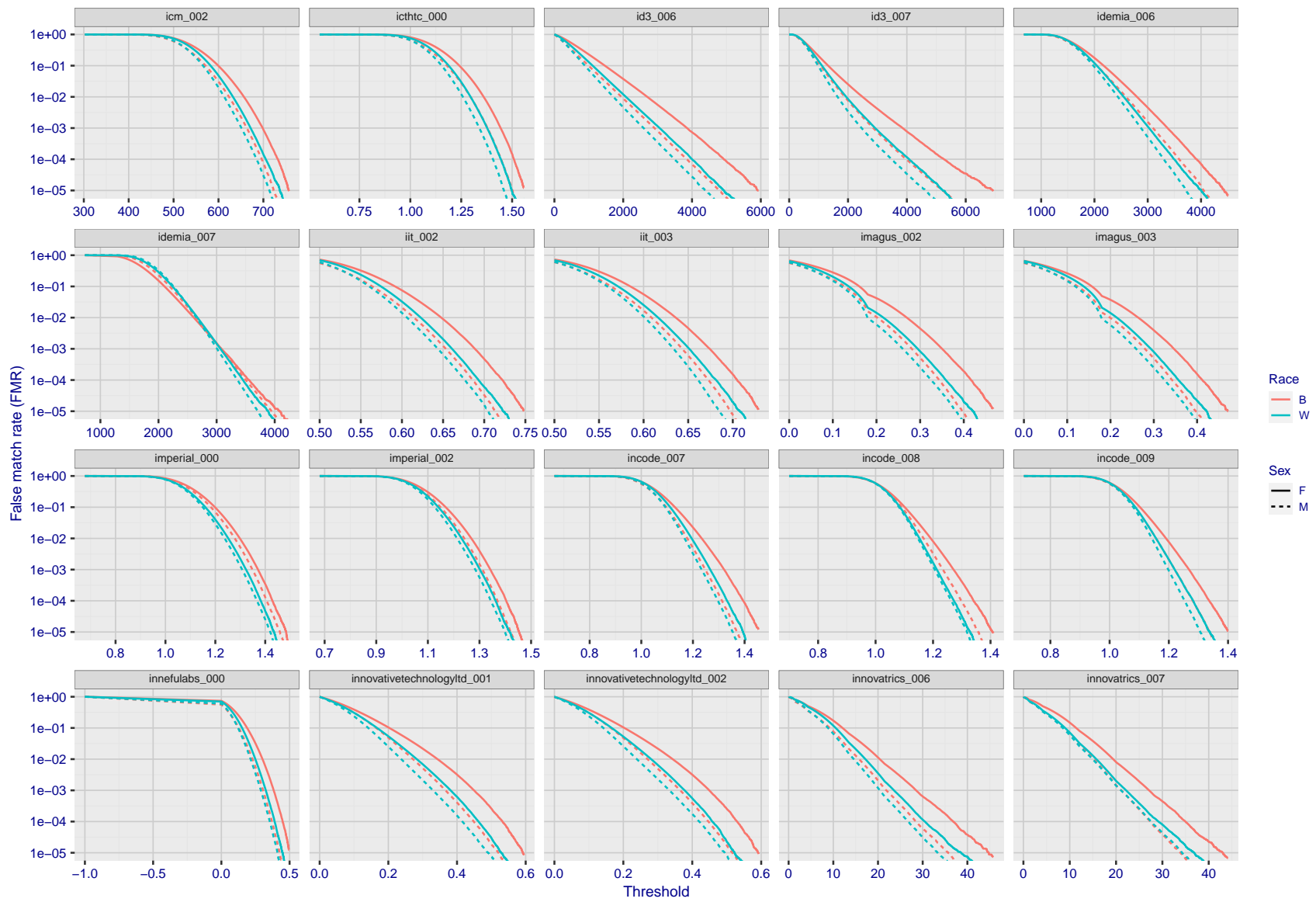


Figure 154: For the mugshot images, the false match calibration curves show false match rate vs. threshold. Separate curves appear for white females, black females, black males and white males.

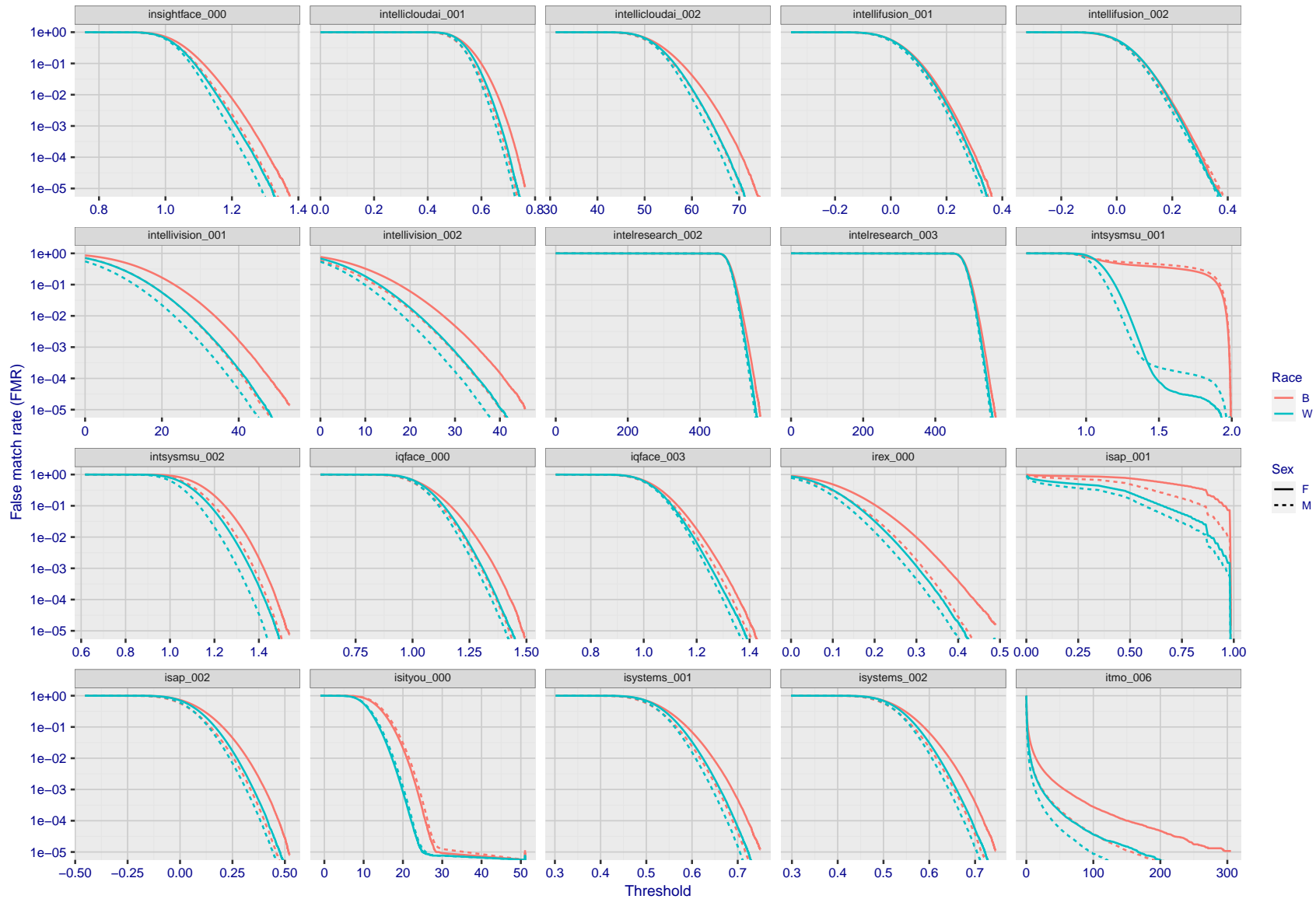


Figure 155: For the mugshot images, the false match calibration curves show false match rate vs. threshold. Separate curves appear for white females, black females, black males and white males.

2021/06/28 10:42:55

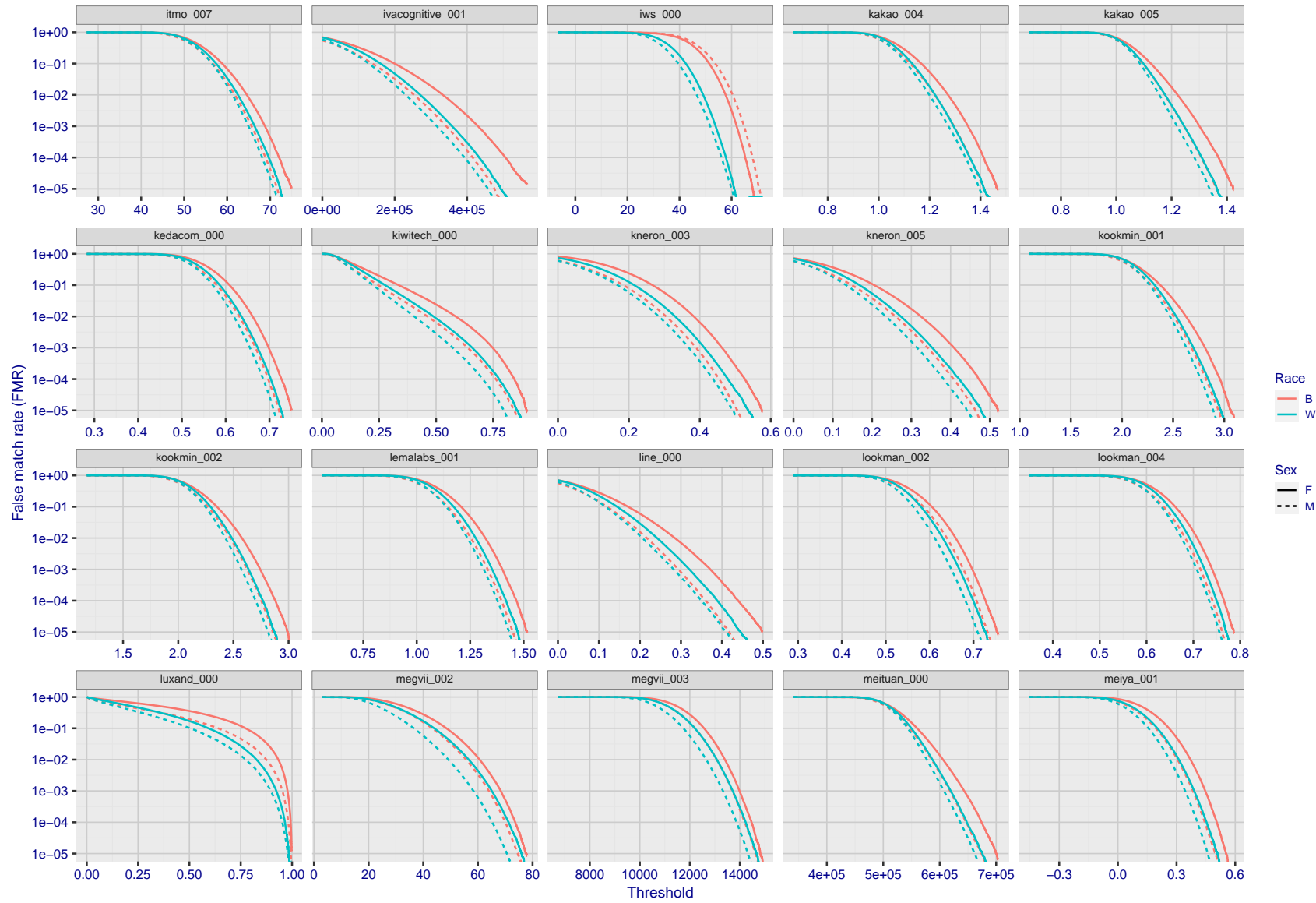


Figure 156: For the mugshot images, the false match calibration curves show false match rate vs. threshold. Separate curves appear for white females, black females, black males and white males.

2021/06/28 10:42:55

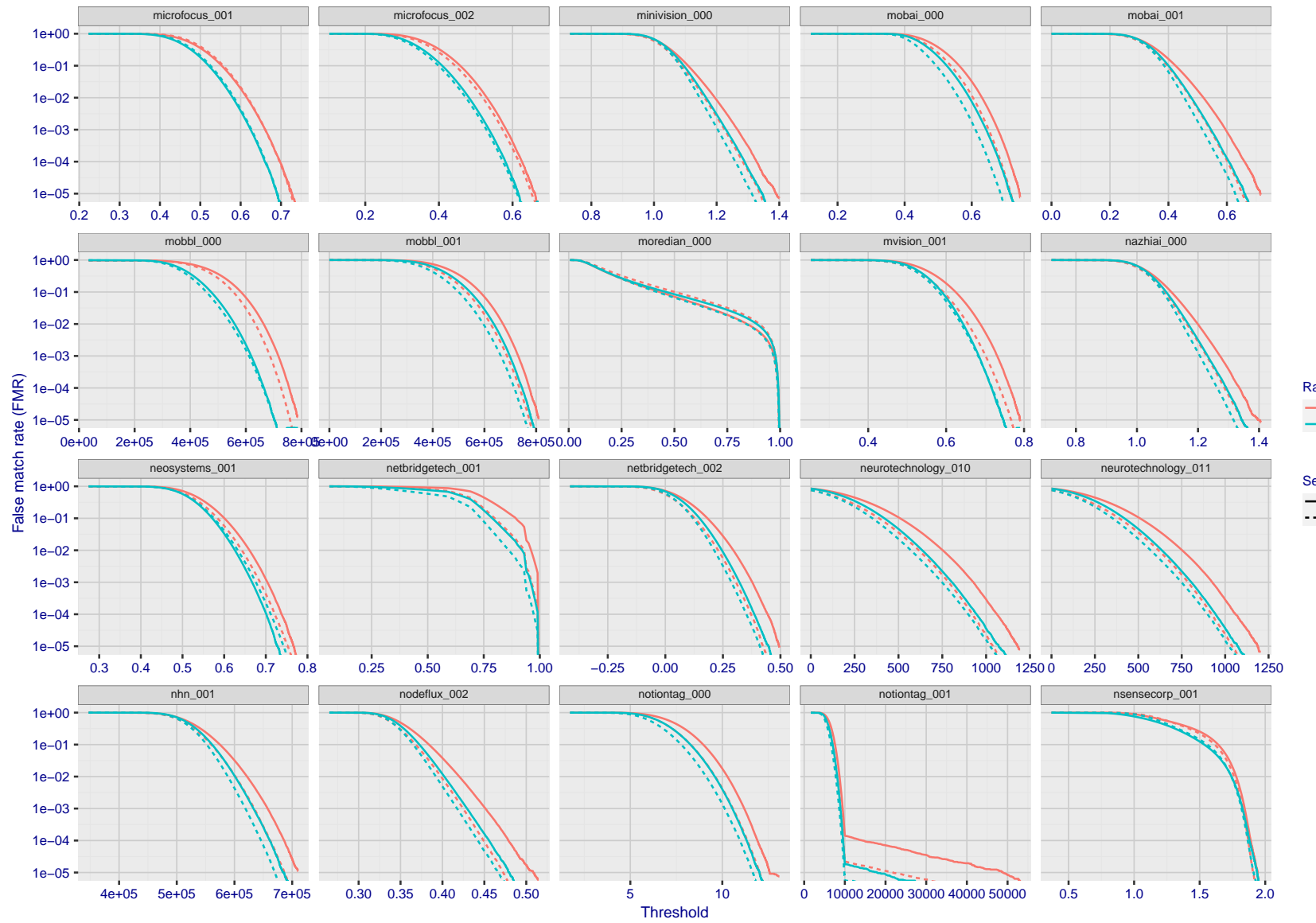


Figure 157: For the mugshot images, the false match calibration curves show false match rate vs. threshold. Separate curves appear for white females, black females, black males and white males.

2021/06/28 10:42:55

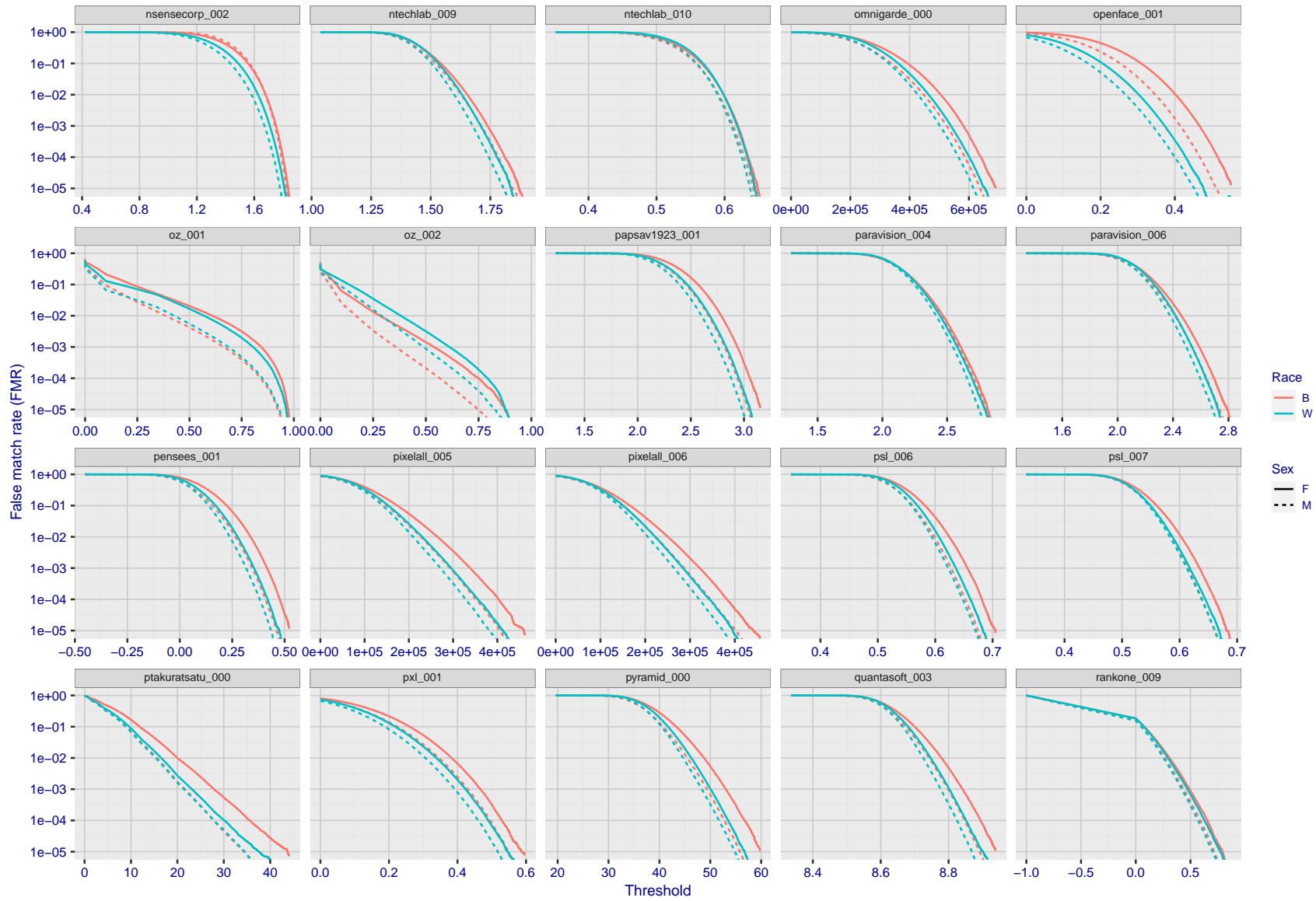


Figure 158: For the mugshot images, the false match calibration curves show false match rate vs. threshold. Separate curves appear for white females, black females, black males and white males.

FNMR(T)
"False non-match rate"
"False match rate"

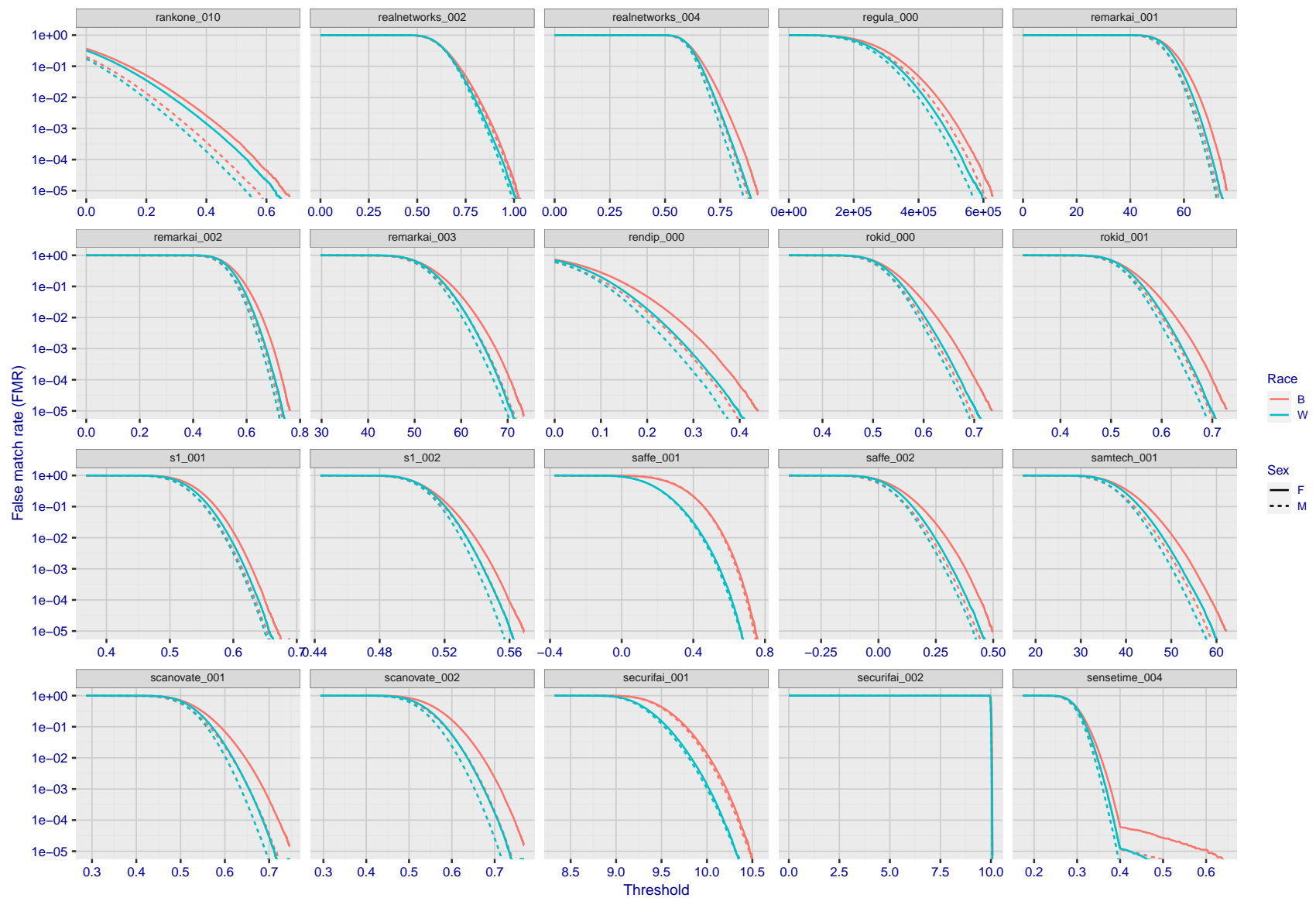


Figure 159: For the mugshot images, the false match calibration curves show false match rate vs. threshold. Separate curves appear for white females, black females, black males and white males.

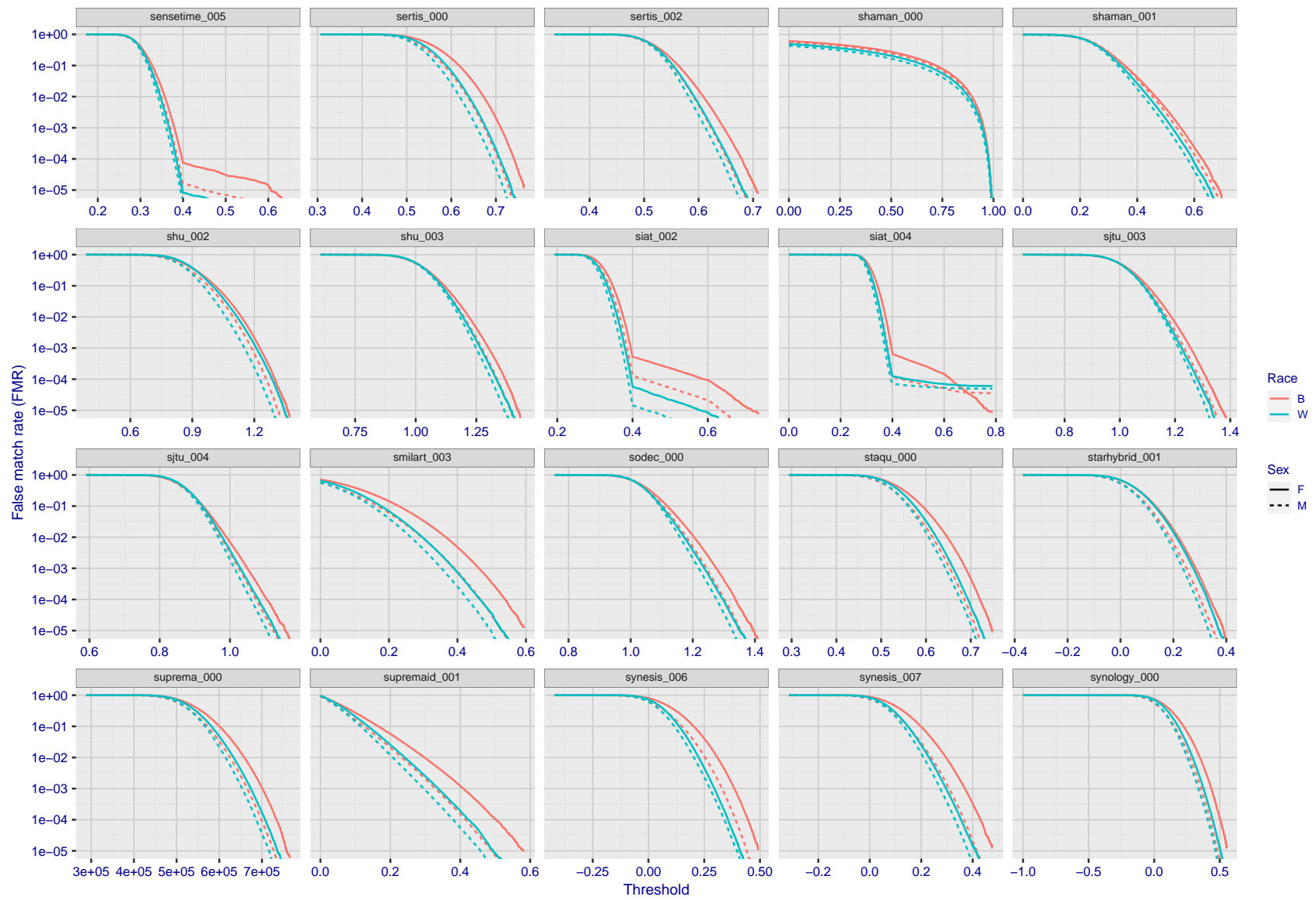


Figure 160: For the mugshot images, the false match calibration curves show false match rate vs. threshold. Separate curves appear for white females, black females, black males and white males.

2021/06/28 10:42:55

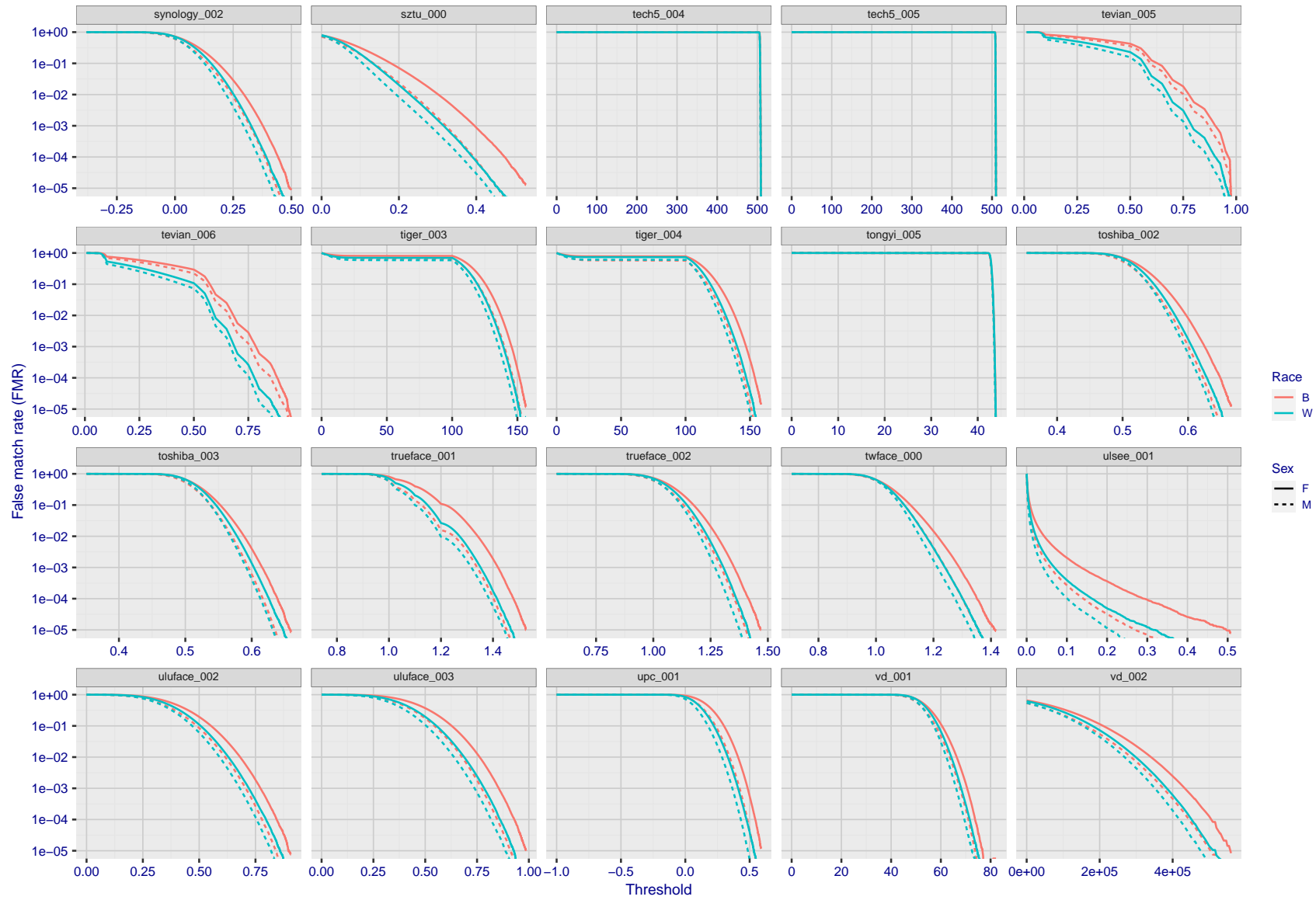


Figure 161: For the mugshot images, the false match calibration curves show false match rate vs. threshold. Separate curves appear for white females, black females, black males and white males.

2021/06/28 10:42:55

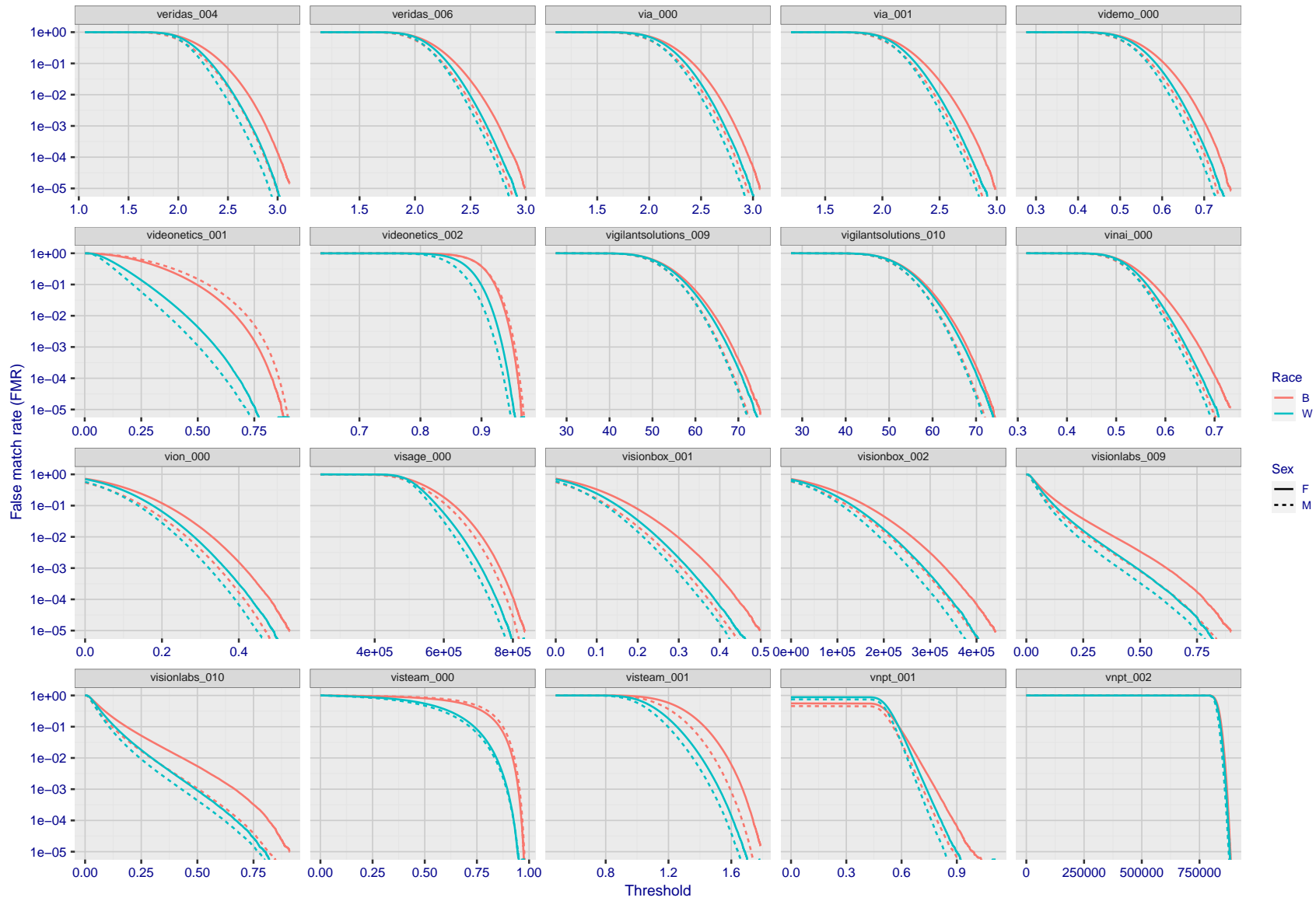


Figure 162: For the mugshot images, the false match calibration curves show false match rate vs. threshold. Separate curves appear for white females, black females, black males and white males.

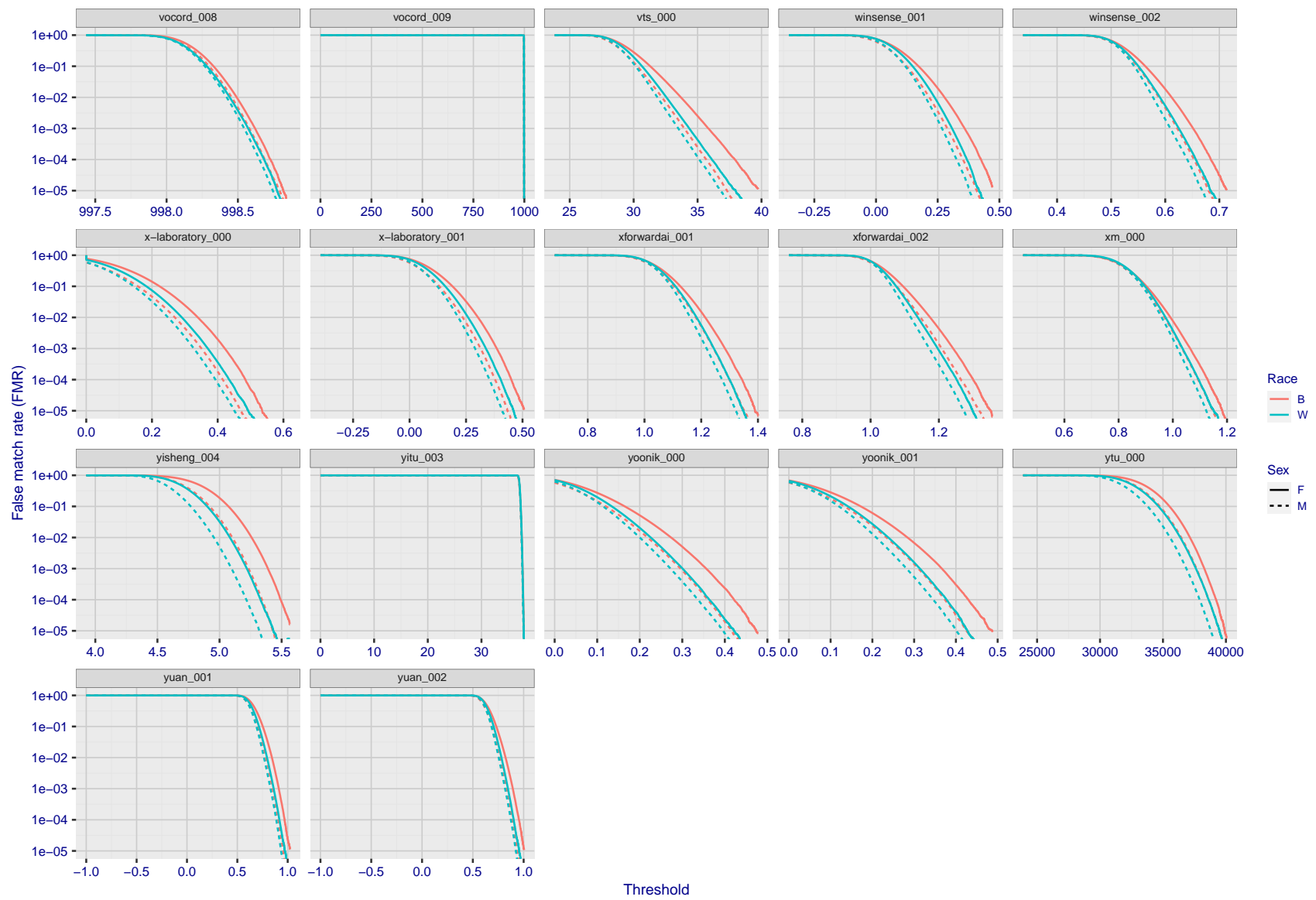


Figure 163: For the mugshot images, the false match calibration curves show false match rate vs. threshold. Separate curves appear for white females, black females, black males and white males.

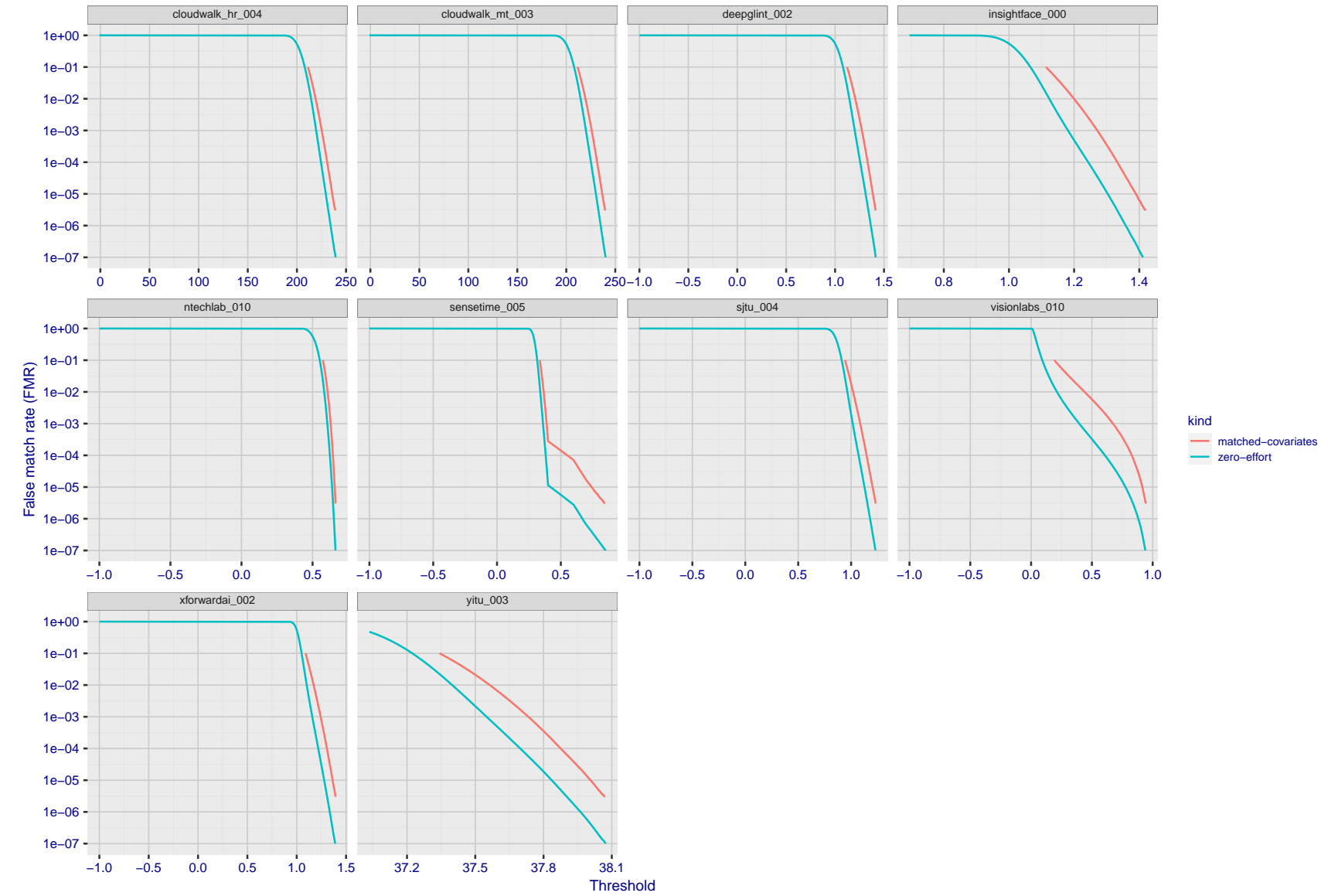


Figure 164: For the visa images, the false match calibration curves show FMR vs. threshold, T . The blue (lower) curves are for zero-effort impostors (i.e. comparing all images against all). The red (upper) curves are for persons of the same-sex, same-age, and same national-origin. This shows that FMR is underestimated (by a factor of 10 or more) by using a zero-effort impostor calculation to calibrate T . As shown later (sec. 3.6), FMR is higher for demographic-matched impostors.

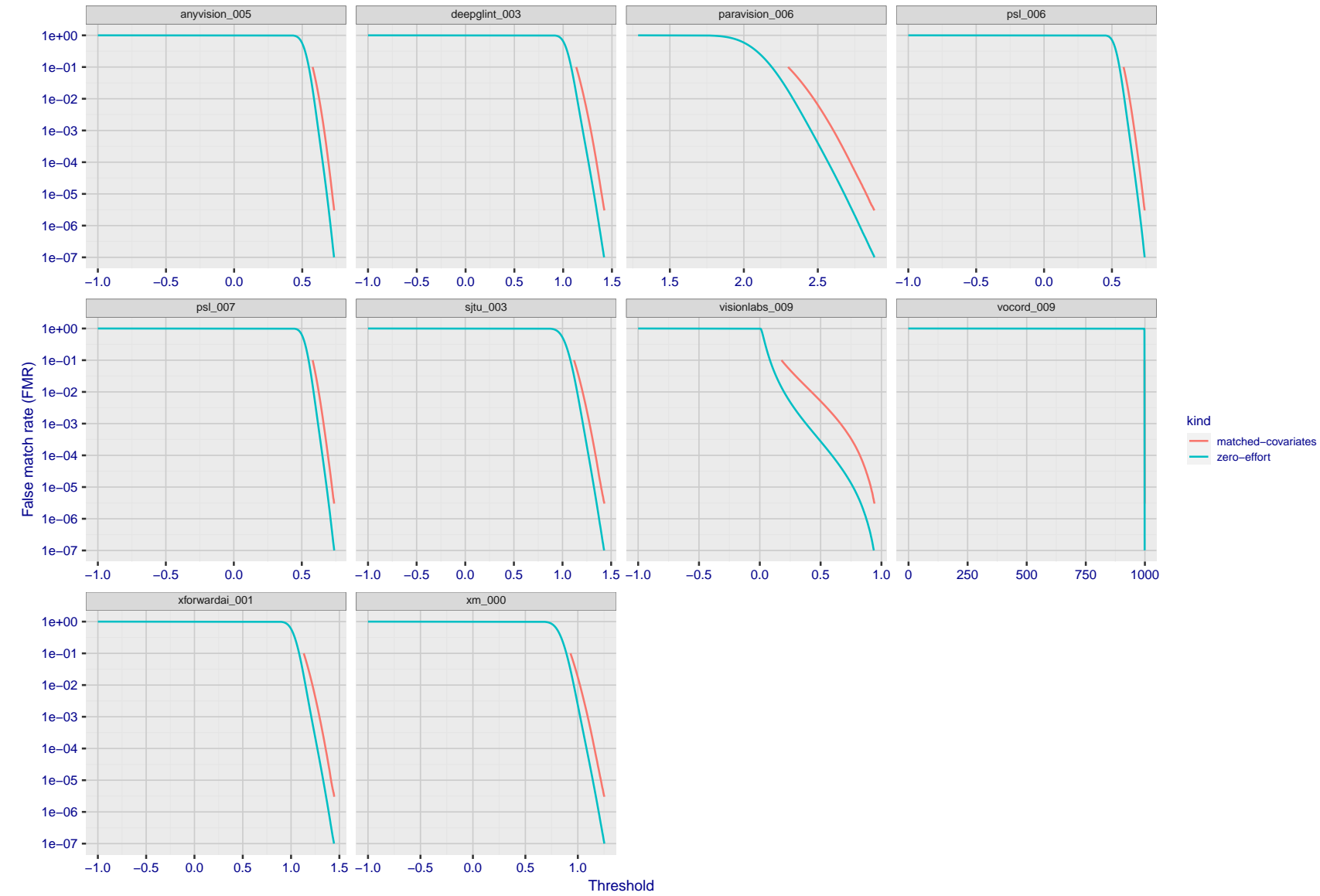


Figure 165: For the visa images, the false match calibration curves show FMR vs. threshold, T . The blue (lower) curves are for zero-effort impostors (i.e. comparing all images against all). The red (upper) curves are for persons of the same-sex, same-age, and same national-origin. This shows that FMR is underestimated (by a factor of 10 or more) by using a zero-effort impostor calculation to calibrate T . As shown later (sec. 3.6), FMR is higher for demographic-matched impostors.

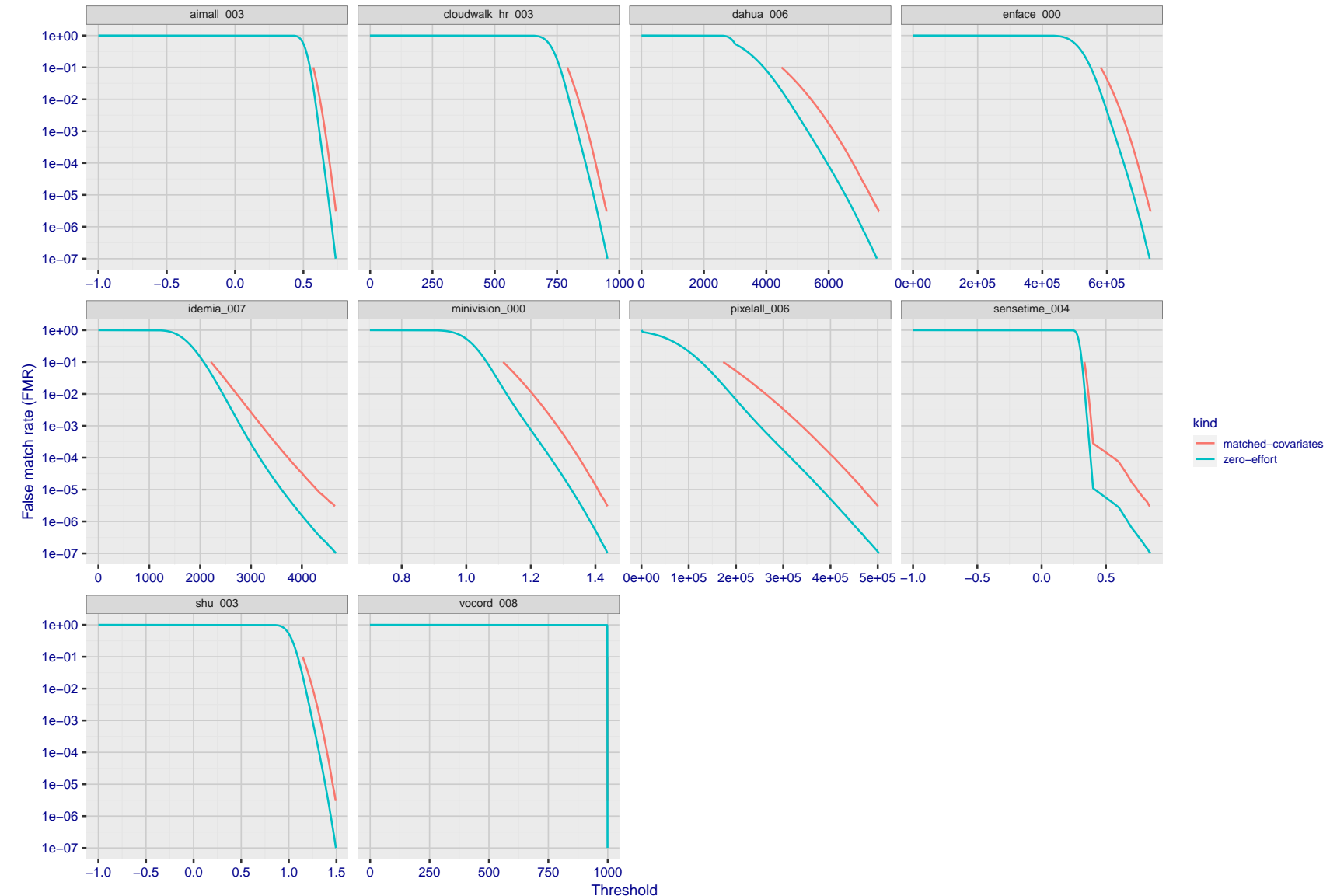


Figure 166: For the visa images, the false match calibration curves show FMR vs. threshold, T . The blue (lower) curves are for zero-effort impostors (i.e. comparing all images against all). The red (upper) curves are for persons of the same-sex, same-age, and same national-origin. This shows that FMR is underestimated (by a factor of 10 or more) by using a zero-effort impostor calculation to calibrate T . As shown later (sec. 3.6), FMR is higher for demographic-matched impostors.

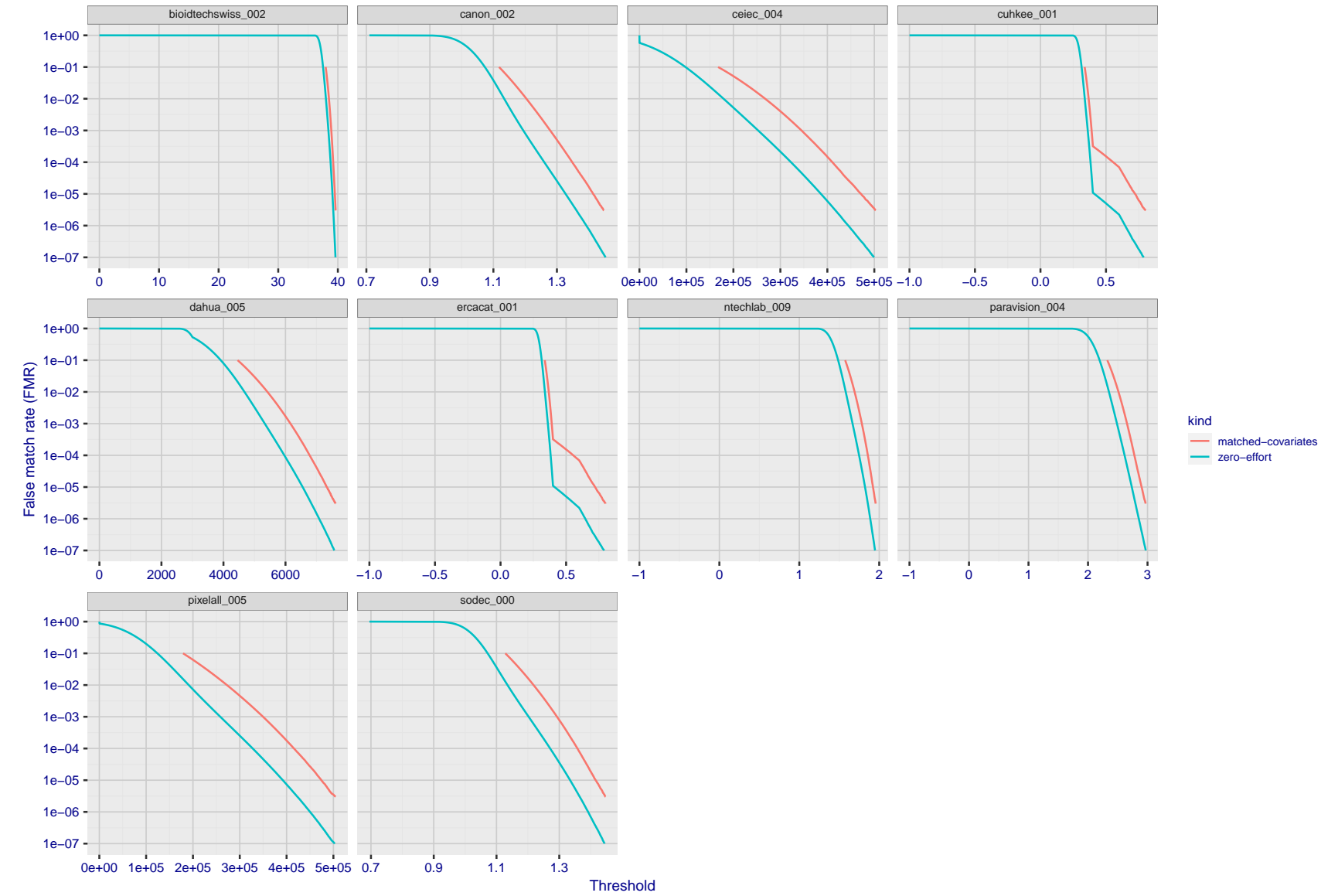


Figure 167: For the visa images, the false match calibration curves show FMR vs. threshold, T . The blue (lower) curves are for zero-effort impostors (i.e. comparing all images against all). The red (upper) curves are for persons of the same-sex, same-age, and same national-origin. This shows that FMR is underestimated (by a factor of 10 or more) by using a zero-effort impostor calculation to calibrate T . As shown later (sec. 3.6), FMR is higher for demographic-matched impostors.

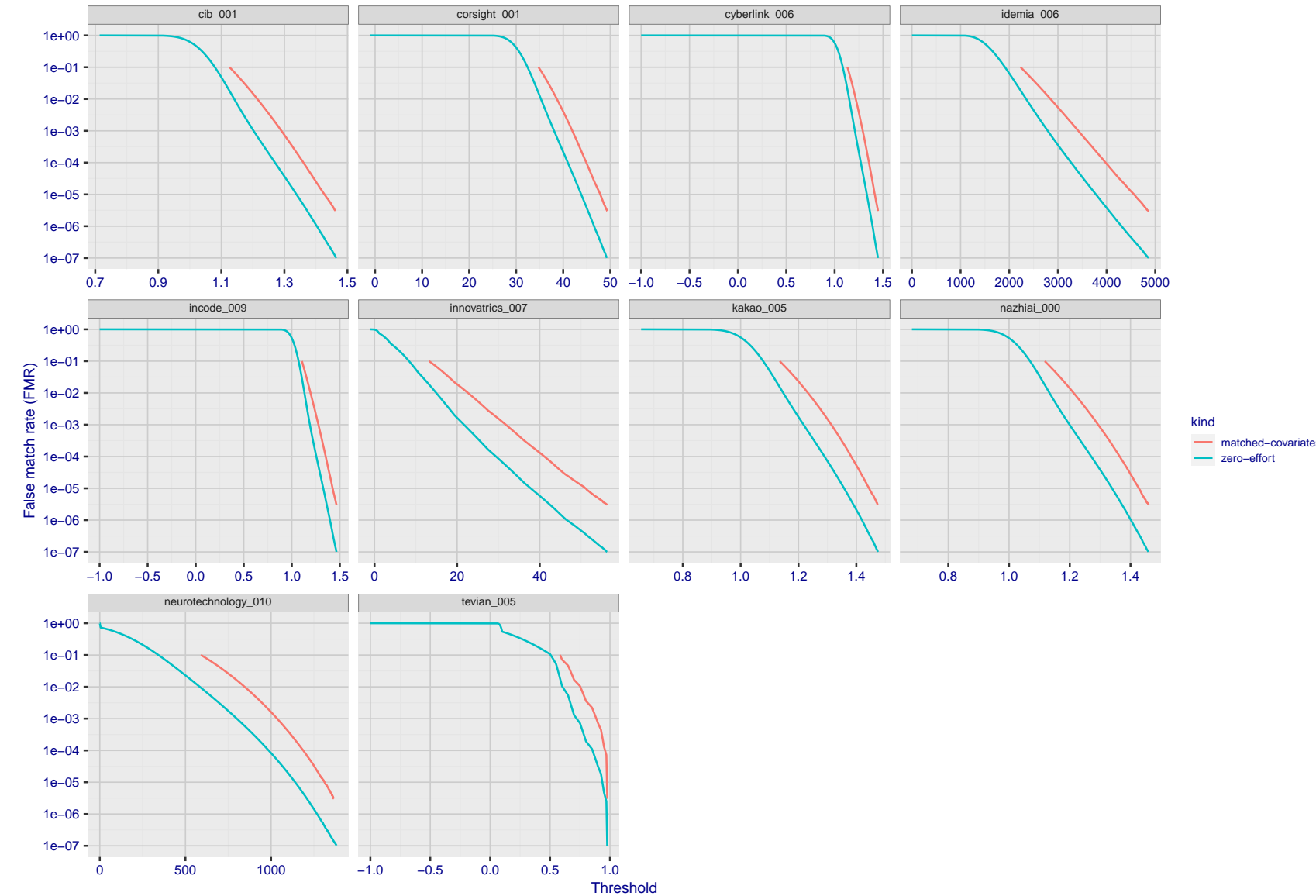


Figure 168: For the visa images, the false match calibration curves show FMR vs. threshold, T . The blue (lower) curves are for zero-effort impostors (i.e. comparing all images against all). The red (upper) curves are for persons of the same-sex, same-age, and same national-origin. This shows that FMR is underestimated (by a factor of 10 or more) by using a zero-effort impostor calculation to calibrate T . As shown later (sec. 3.6), FMR is higher for demographic-matched impostors.

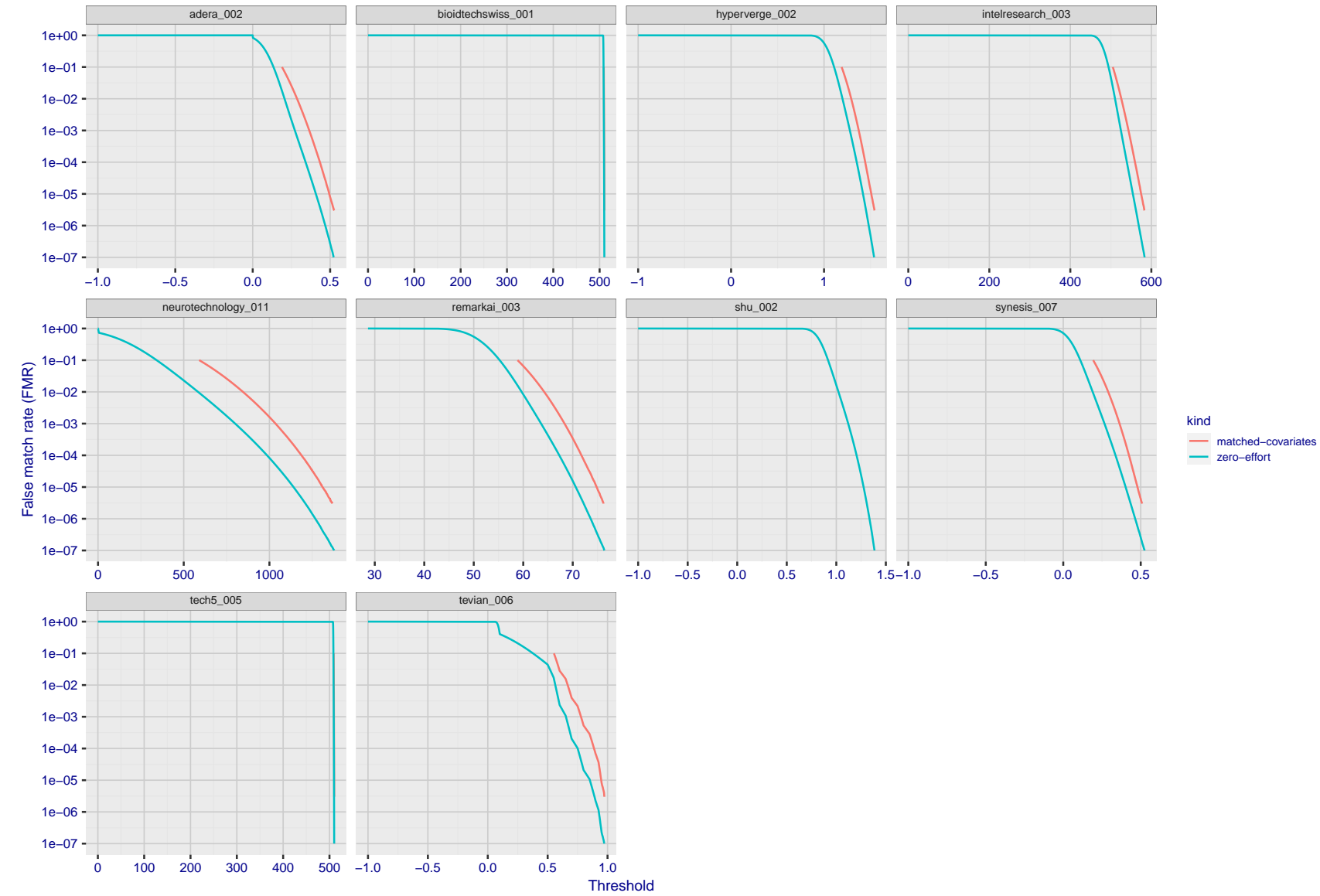


Figure 169: For the visa images, the false match calibration curves show FMR vs. threshold, T . The blue (lower) curves are for zero-effort impostors (i.e. comparing all images against all). The red (upper) curves are for persons of the same-sex, same-age, and same national-origin. This shows that FMR is underestimated (by a factor of 10 or more) by using a zero-effort impostor calculation to calibrate T . As shown later (sec. 3.6), FMR is higher for demographic-matched impostors.

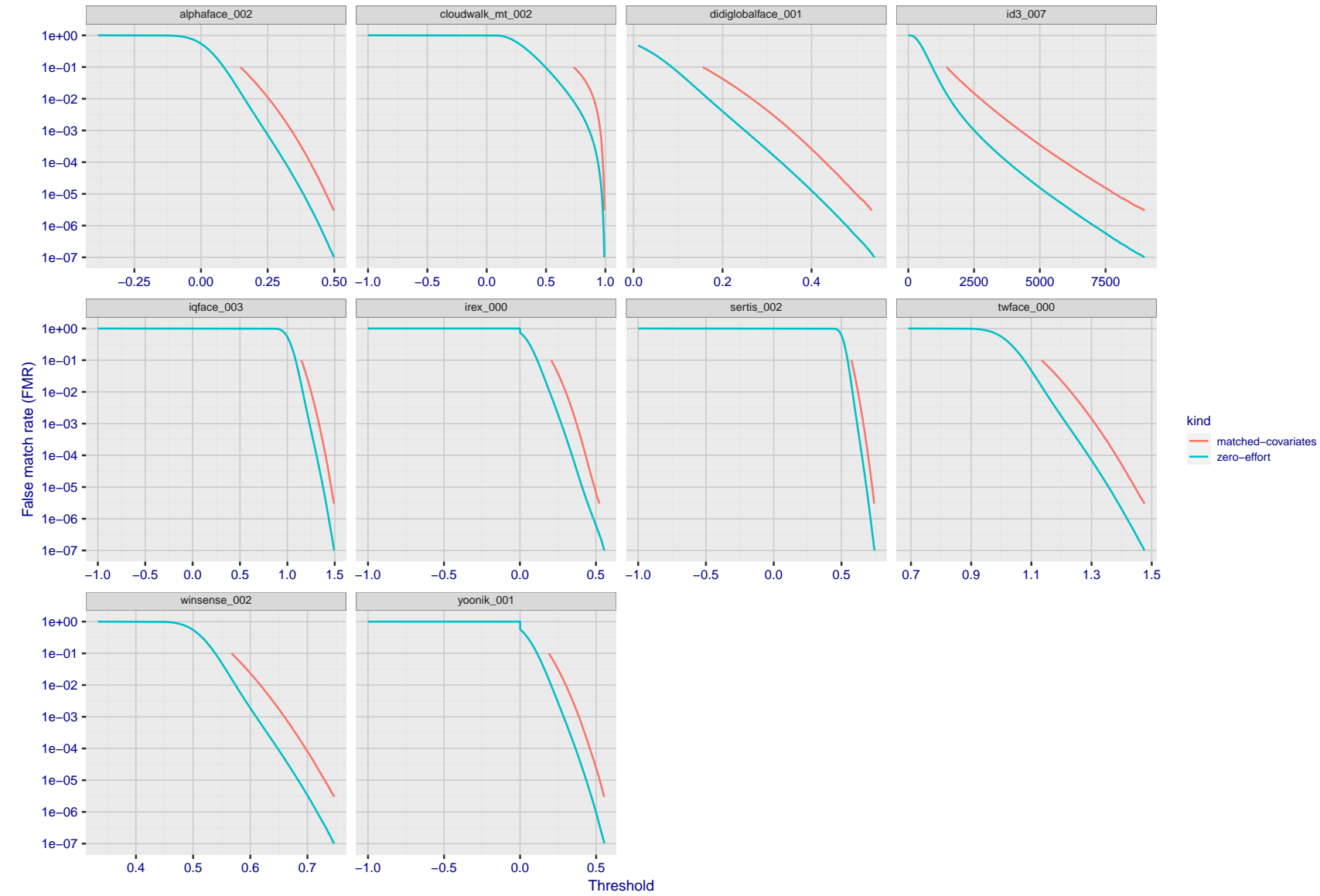


Figure 170: For the visa images, the false match calibration curves show FMR vs. threshold, T . The blue (lower) curves are for zero-effort impostors (i.e. comparing all images against all). The red (upper) curves are for persons of the same-sex, same-age, and same national-origin. This shows that FMR is underestimated (by a factor of 10 or more) by using a zero-effort impostor calculation to calibrate T . As shown later (sec. 3.6), FMR is higher for demographic-matched impostors.

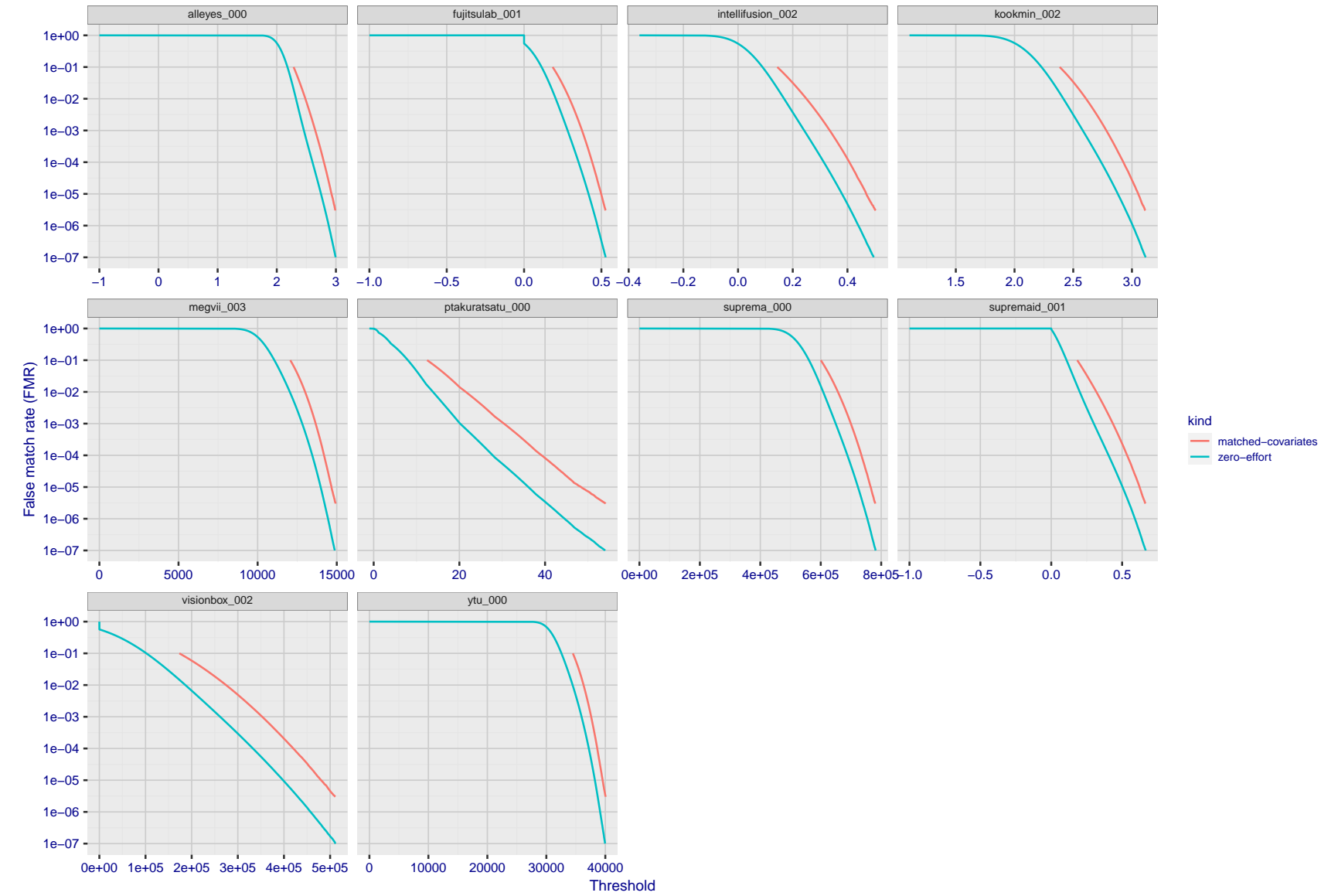


Figure 171: For the visa images, the false match calibration curves show FMR vs. threshold, T . The blue (lower) curves are for zero-effort impostors (i.e. comparing all images against all). The red (upper) curves are for persons of the same-sex, same-age, and same national-origin. This shows that FMR is underestimated (by a factor of 10 or more) by using a zero-effort impostor calculation to calibrate T . As shown later (sec. 3.6), FMR is higher for demographic-matched impostors.

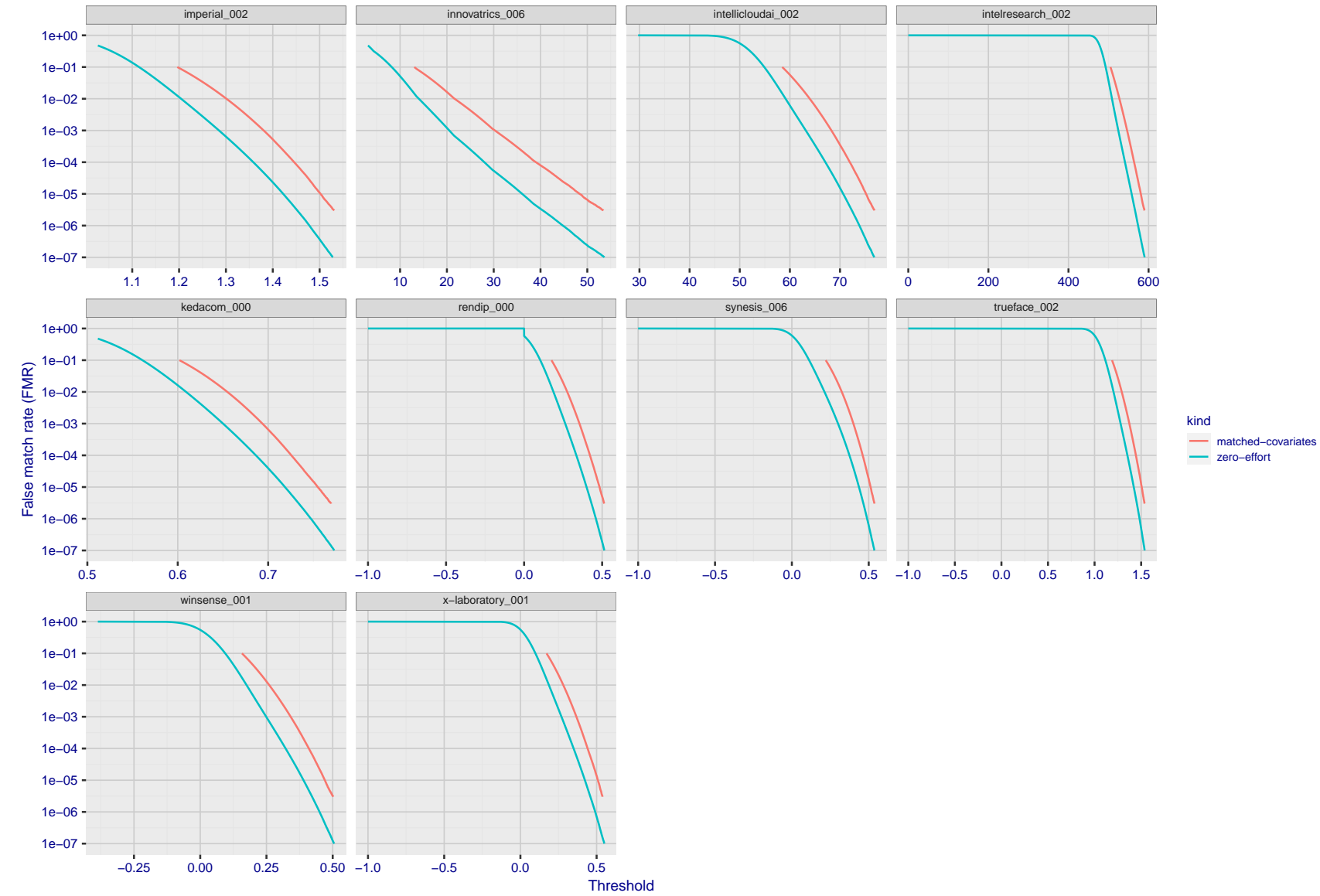


Figure 172: For the visa images, the false match calibration curves show FMR vs. threshold, T . The blue (lower) curves are for zero-effort impostors (i.e. comparing all images against all). The red (upper) curves are for persons of the same-sex, same-age, and same national-origin. This shows that FMR is underestimated (by a factor of 10 or more) by using a zero-effort impostor calculation to calibrate T . As shown later (sec. 3.6), FMR is higher for demographic-matched impostors.

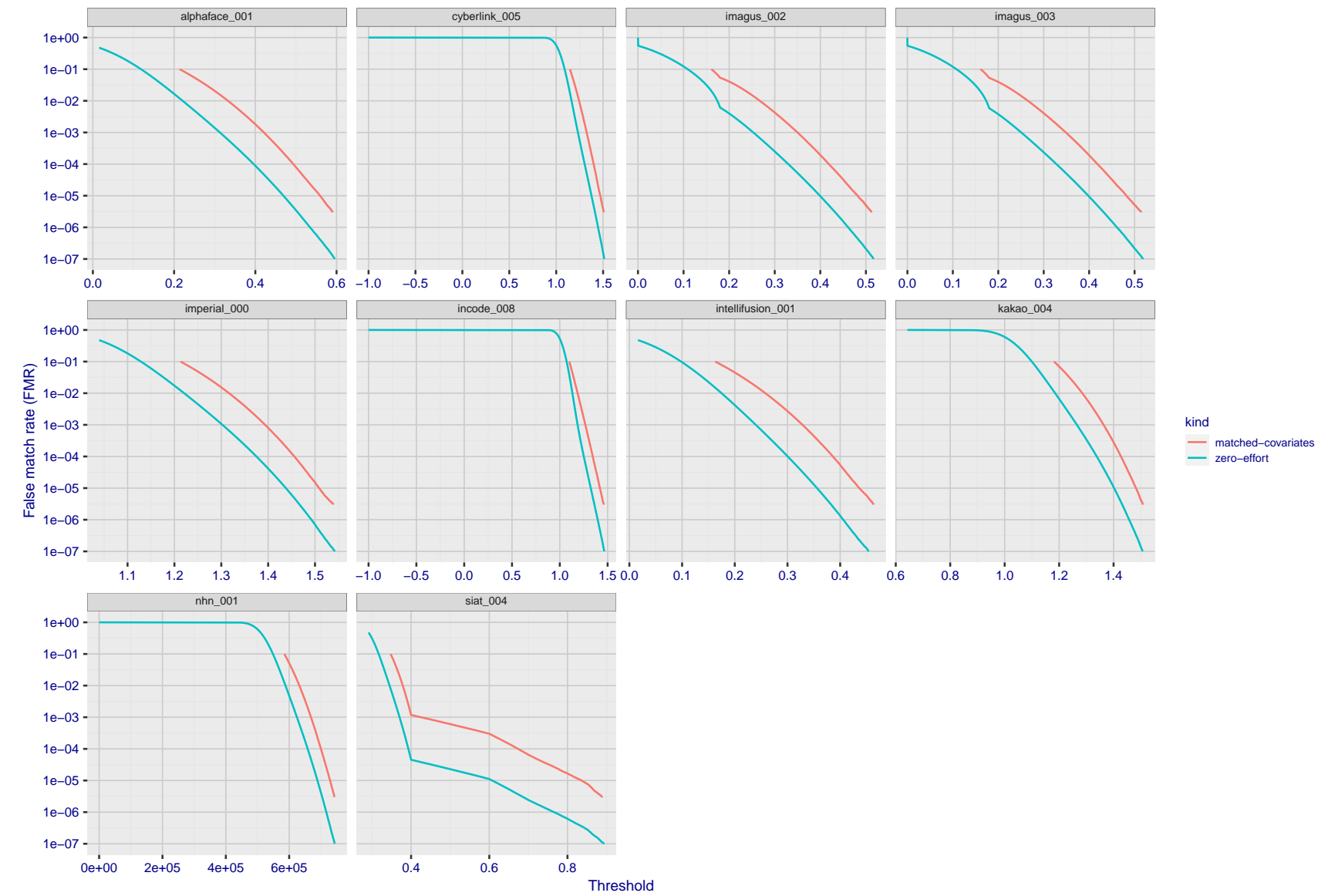


Figure 173: For the visa images, the false match calibration curves show FMR vs. threshold, T . The blue (lower) curves are for zero-effort impostors (i.e. comparing all images against all). The red (upper) curves are for persons of the same-sex, same-age, and same national-origin. This shows that FMR is underestimated (by a factor of 10 or more) by using a zero-effort impostor calculation to calibrate T . As shown later (sec. 3.6), FMR is higher for demographic-matched impostors.

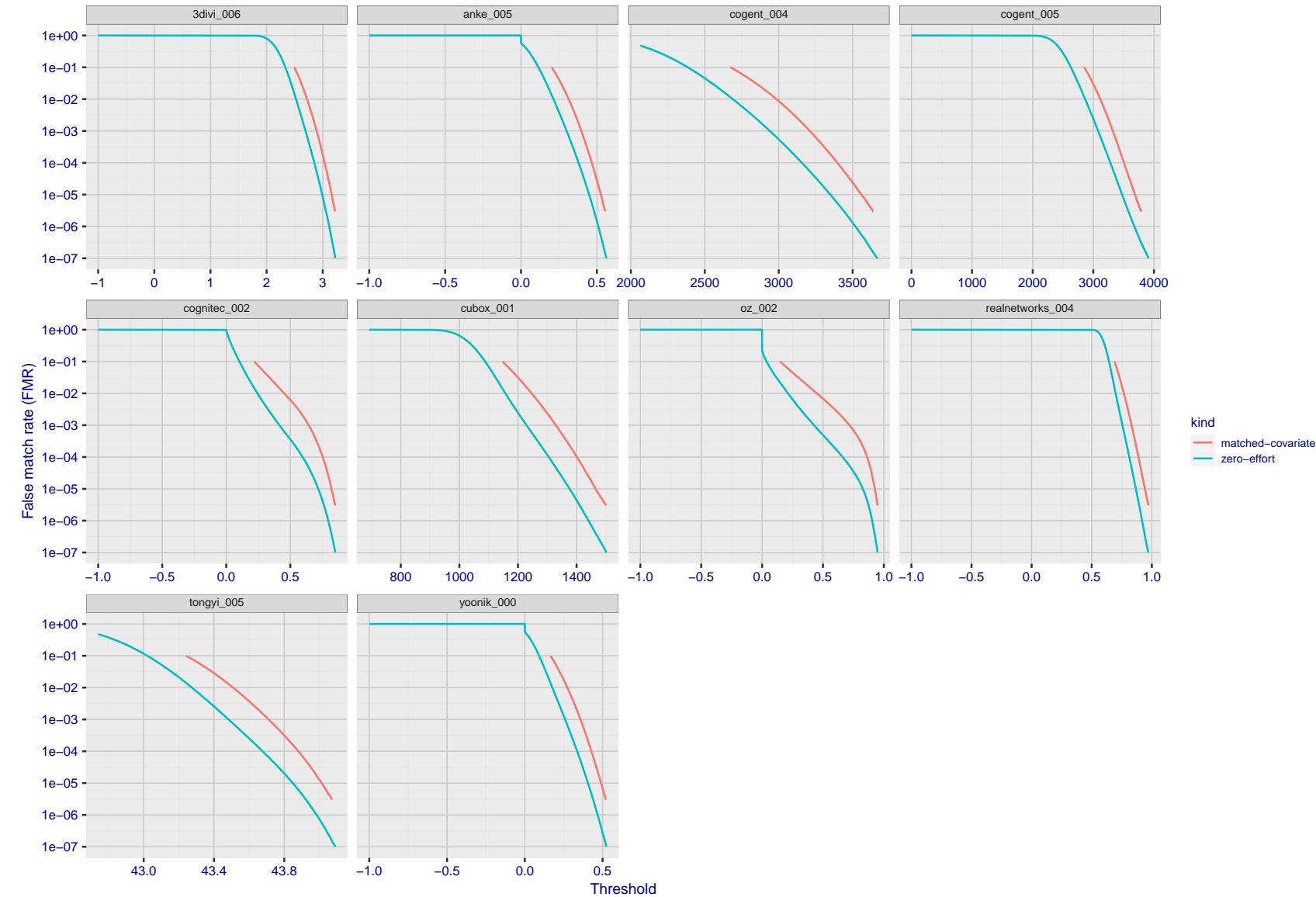


Figure 174: For the visa images, the false match calibration curves show FMR vs. threshold, T . The blue (lower) curves are for zero-effort impostors (i.e. comparing all images against all). The red (upper) curves are for persons of the same-sex, same-age, and same national-origin. This shows that FMR is underestimated (by a factor of 10 or more) by using a zero-effort impostor calculation to calibrate T . As shown later (sec. 3.6), FMR is higher for demographic-matched impostors.

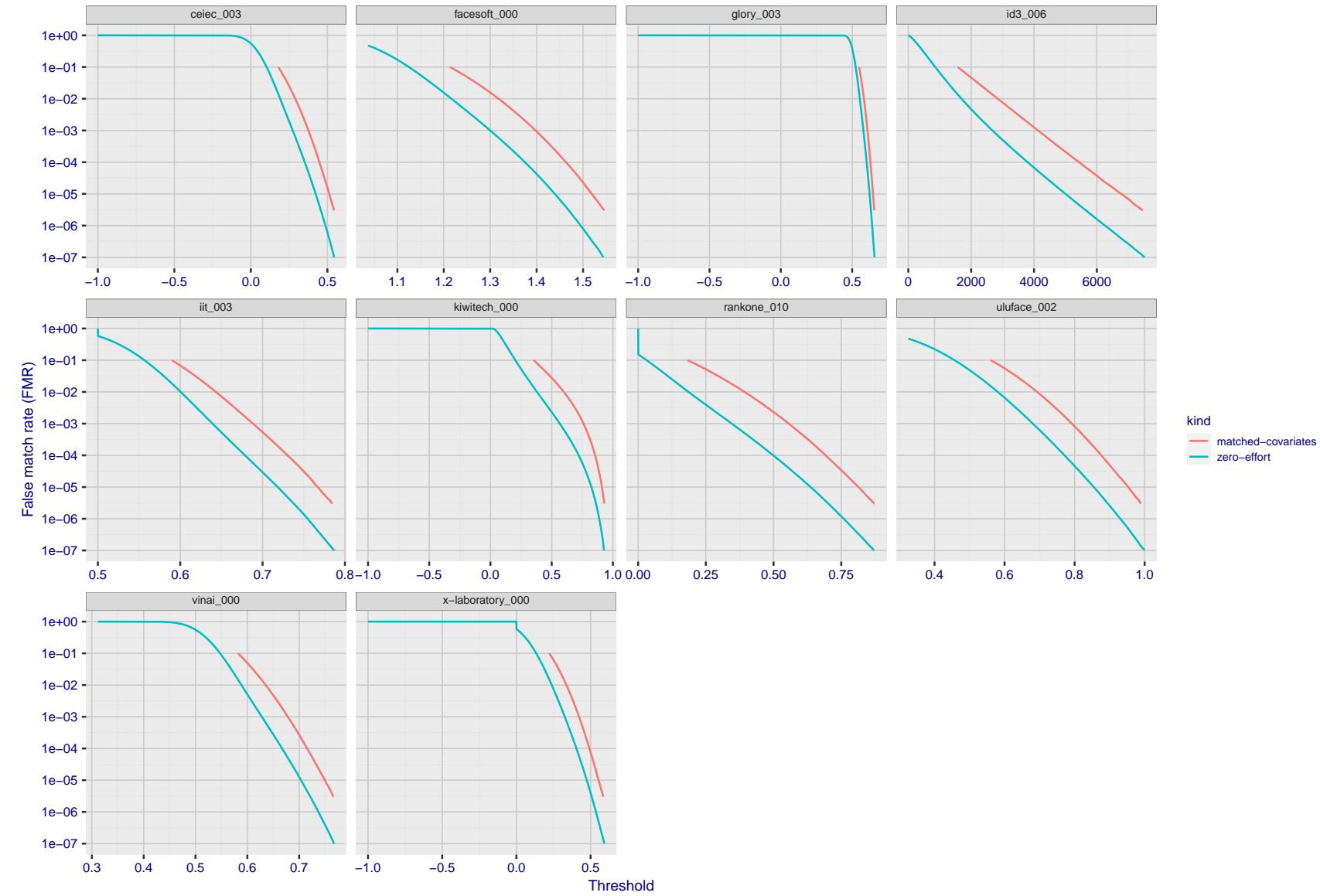


Figure 175: For the visa images, the false match calibration curves show FMR vs. threshold, T . The blue (lower) curves are for zero-effort impostors (i.e. comparing all images against all). The red (upper) curves are for persons of the same-sex, same-age, and same national-origin. This shows that FMR is underestimated (by a factor of 10 or more) by using a zero-effort impostor calculation to calibrate T . As shown later (sec. 3.6), FMR is higher for demographic-matched impostors.

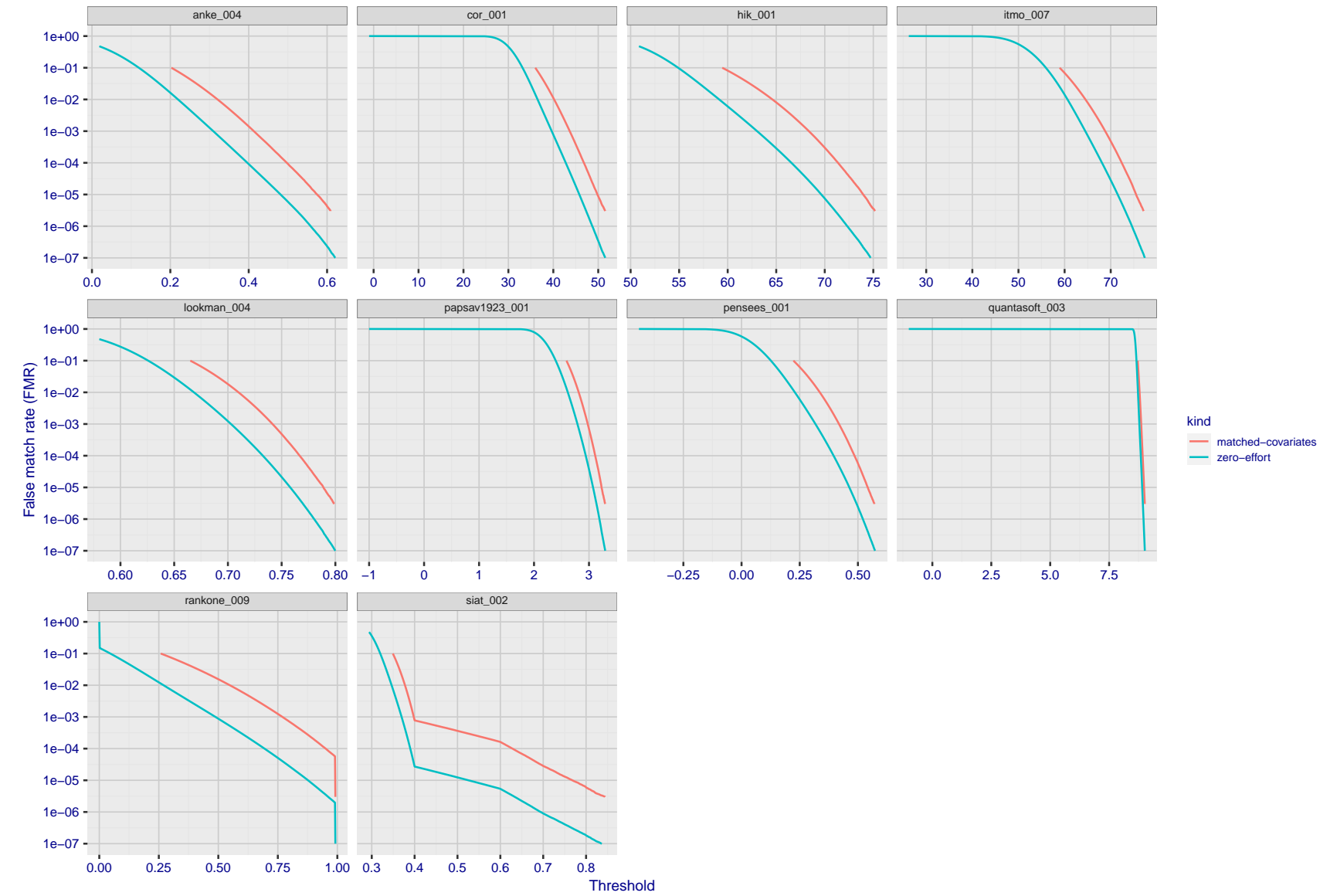


Figure 176: For the visa images, the false match calibration curves show FMR vs. threshold, T . The blue (lower) curves are for zero-effort impostors (i.e. comparing all images against all). The red (upper) curves are for persons of the same-sex, same-age, and same national-origin. This shows that FMR is underestimated (by a factor of 10 or more) by using a zero-effort impostor calculation to calibrate T . As shown later (sec. 3.6), FMR is higher for demographic-matched impostors.

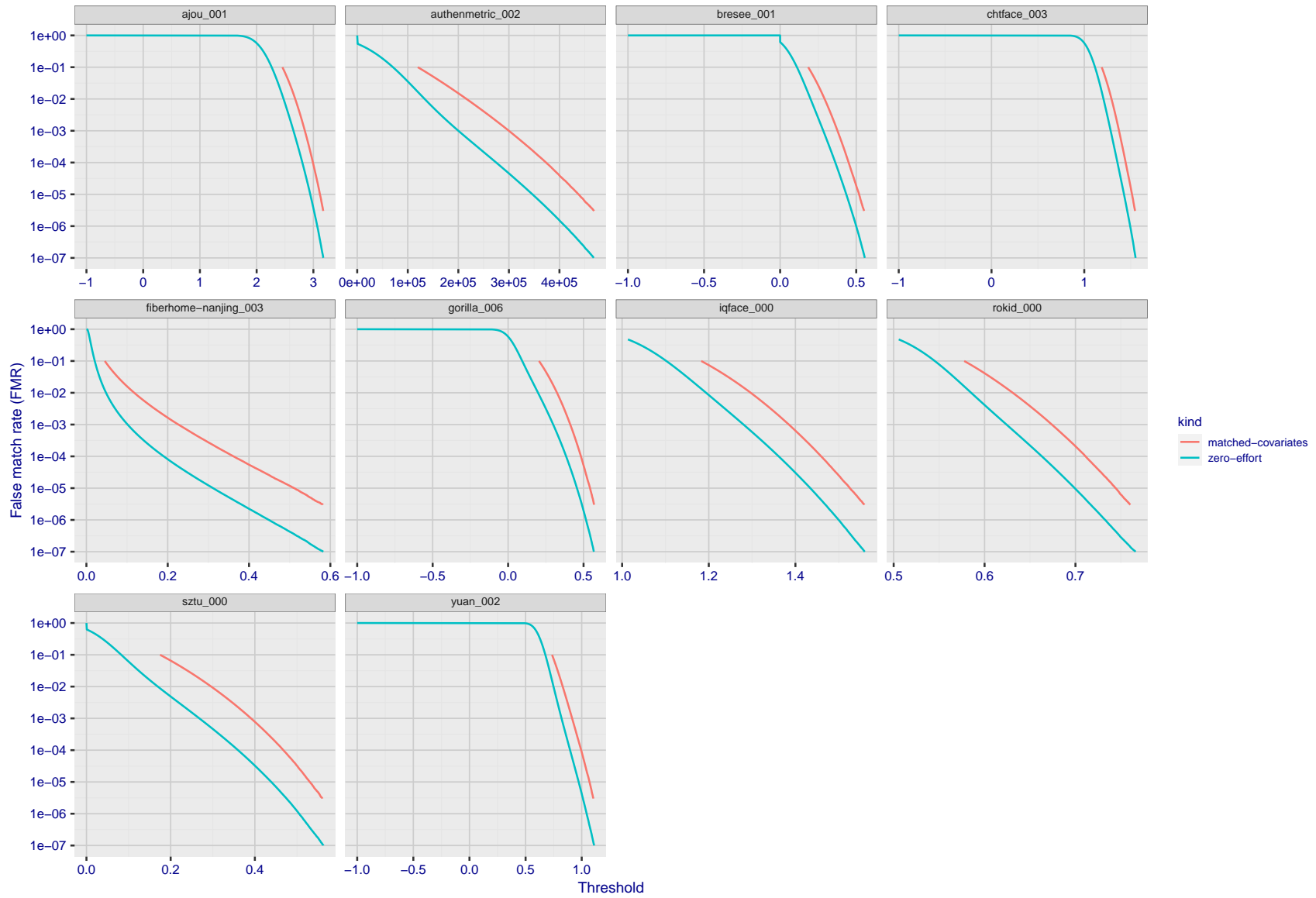


Figure 177: For the visa images, the false match calibration curves show FMR vs. threshold, T . The blue (lower) curves are for zero-effort impostors (i.e. comparing all images against all). The red (upper) curves are for persons of the same-sex, same-age, and same national-origin. This shows that FMR is underestimated (by a factor of 10 or more) by using a zero-effort impostor calculation to calibrate T . As shown later (sec. 3.6), FMR is higher for demographic-matched impostors.

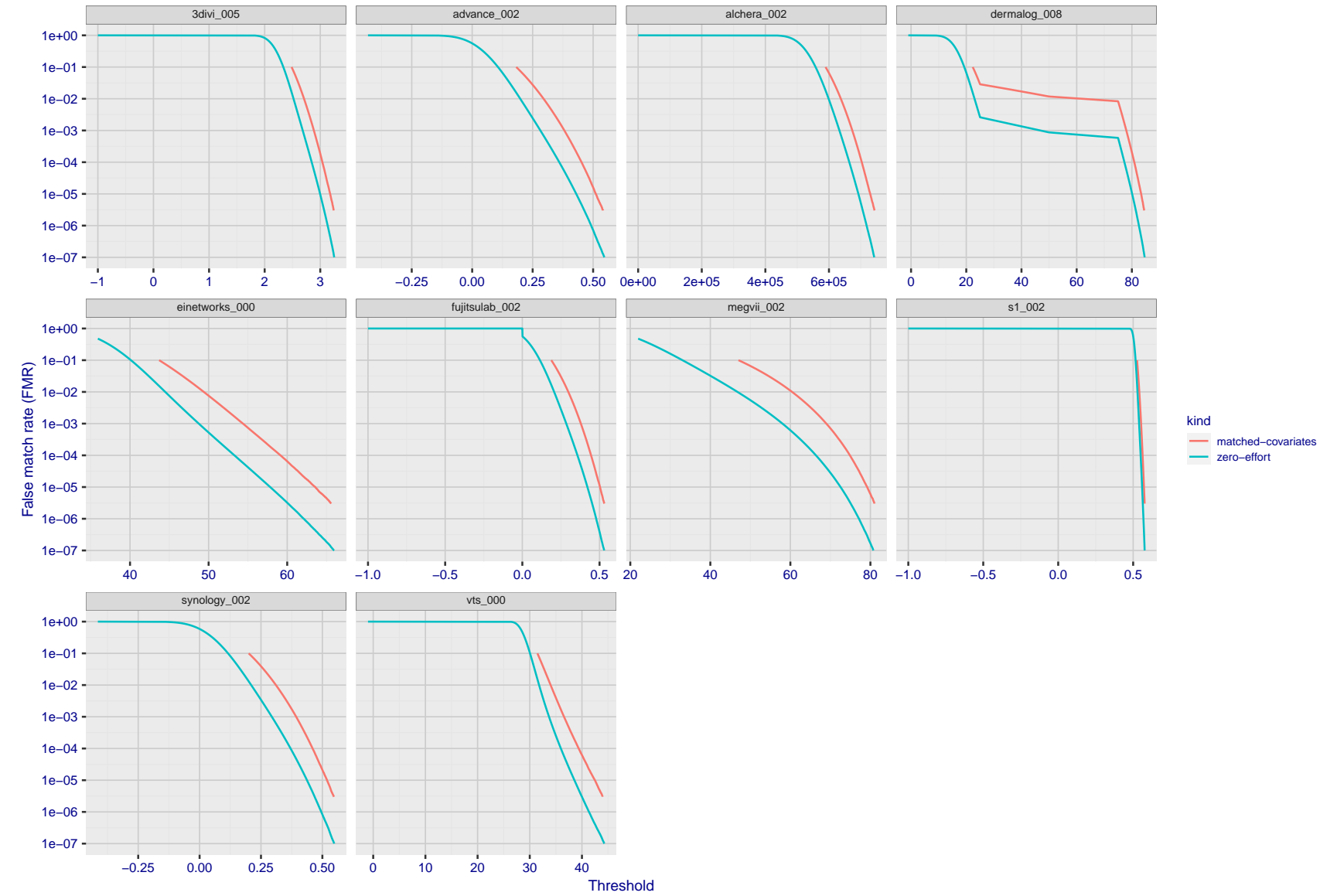


Figure 178: For the visa images, the false match calibration curves show FMR vs. threshold, T . The blue (lower) curves are for zero-effort impostors (i.e. comparing all images against all). The red (upper) curves are for persons of the same-sex, same-age, and same national-origin. This shows that FMR is underestimated (by a factor of 10 or more) by using a zero-effort impostor calculation to calibrate T . As shown later (sec. 3.6), FMR is higher for demographic-matched impostors.

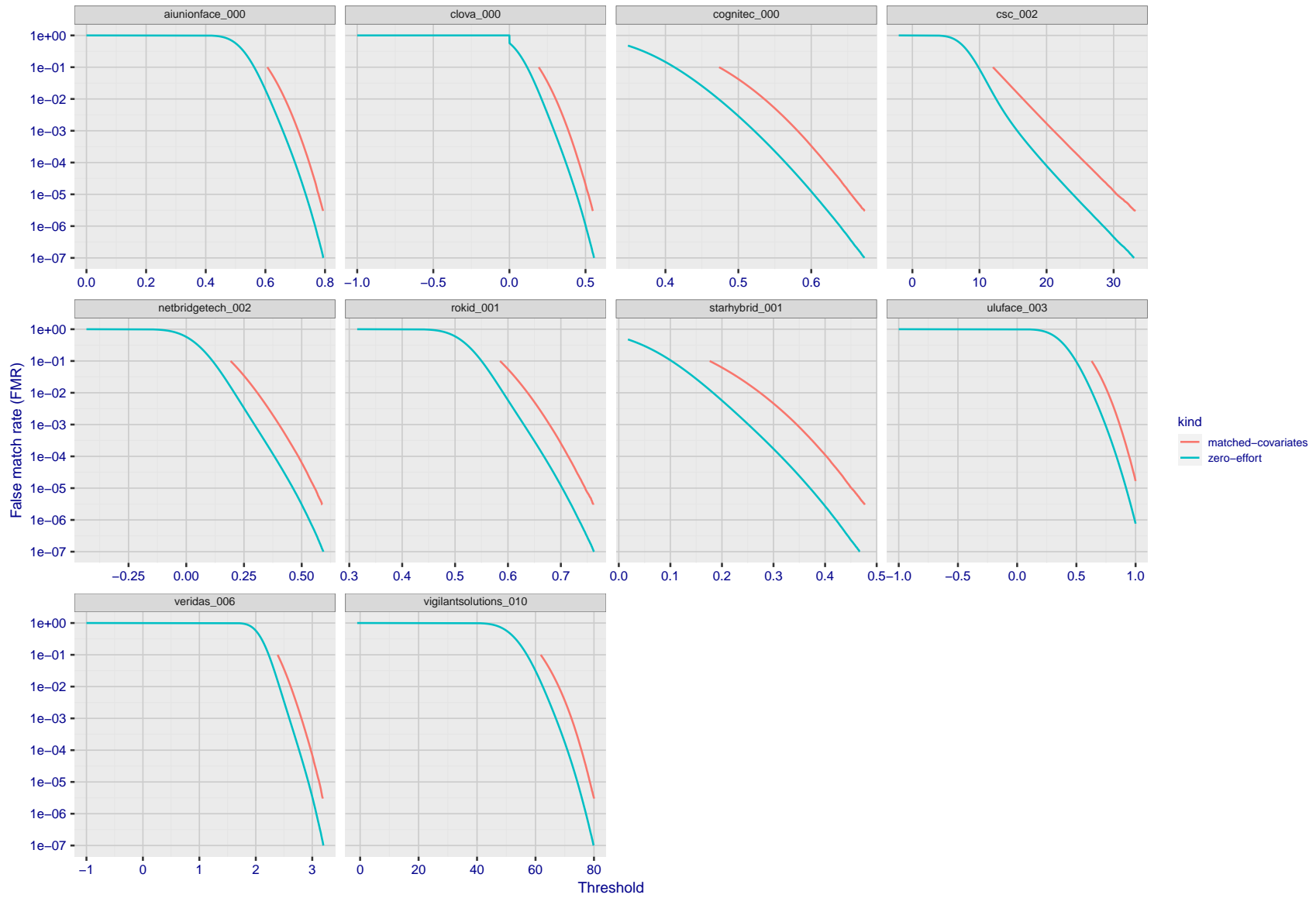


Figure 179: For the visa images, the false match calibration curves show FMR vs. threshold, T . The blue (lower) curves are for zero-effort impostors (i.e. comparing all images against all). The red (upper) curves are for persons of the same-sex, same-age, and same national-origin. This shows that FMR is underestimated (by a factor of 10 or more) by using a zero-effort impostor calculation to calibrate T . As shown later (sec. 3.6), FMR is higher for demographic-matched impostors.

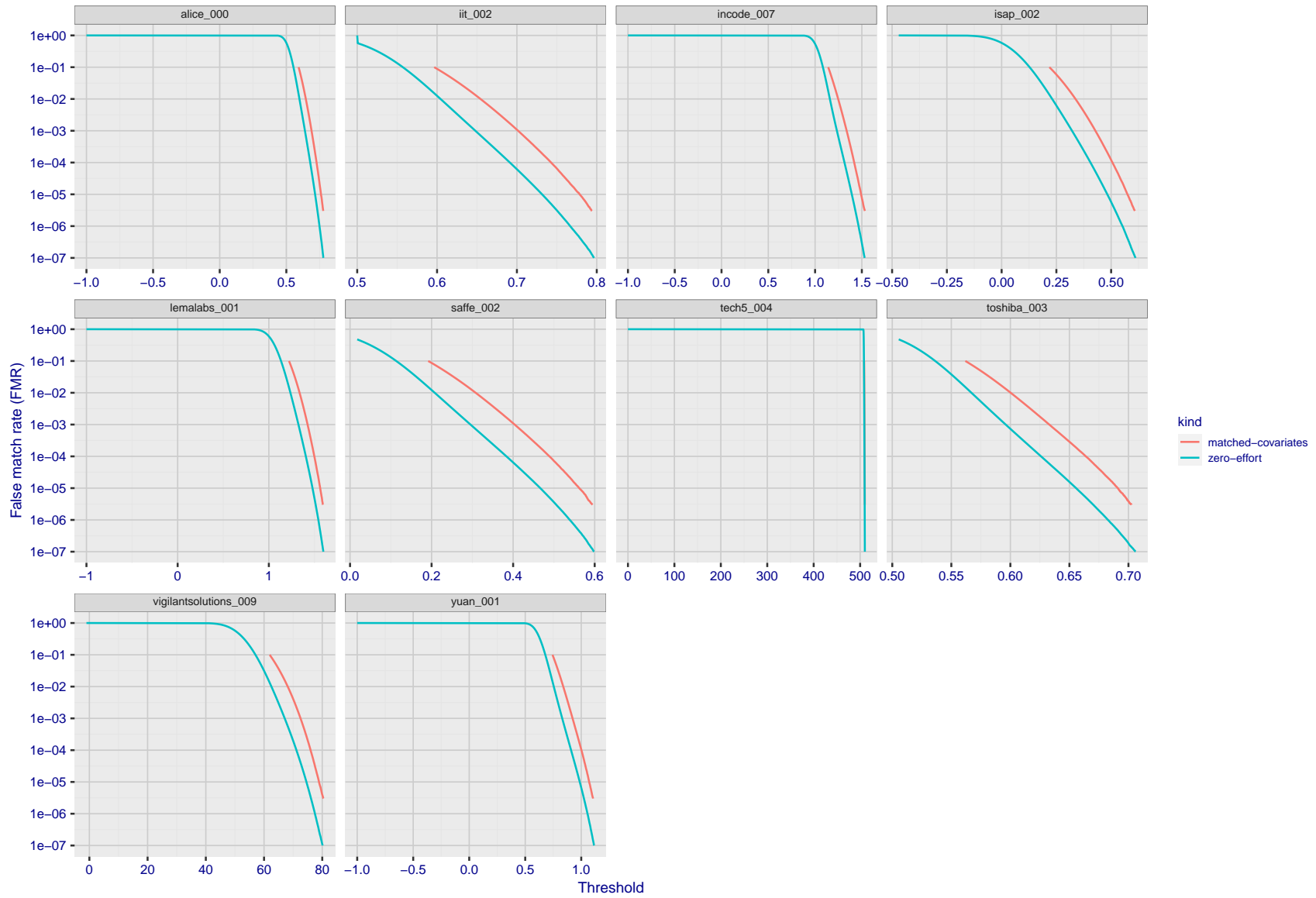


Figure 180: For the visa images, the false match calibration curves show FMR vs. threshold, T . The blue (lower) curves are for zero-effort impostors (i.e. comparing all images against all). The red (upper) curves are for persons of the same-sex, same-age, and same national-origin. This shows that FMR is underestimated (by a factor of 10 or more) by using a zero-effort impostor calculation to calibrate T . As shown later (sec. 3.6), FMR is higher for demographic-matched impostors.

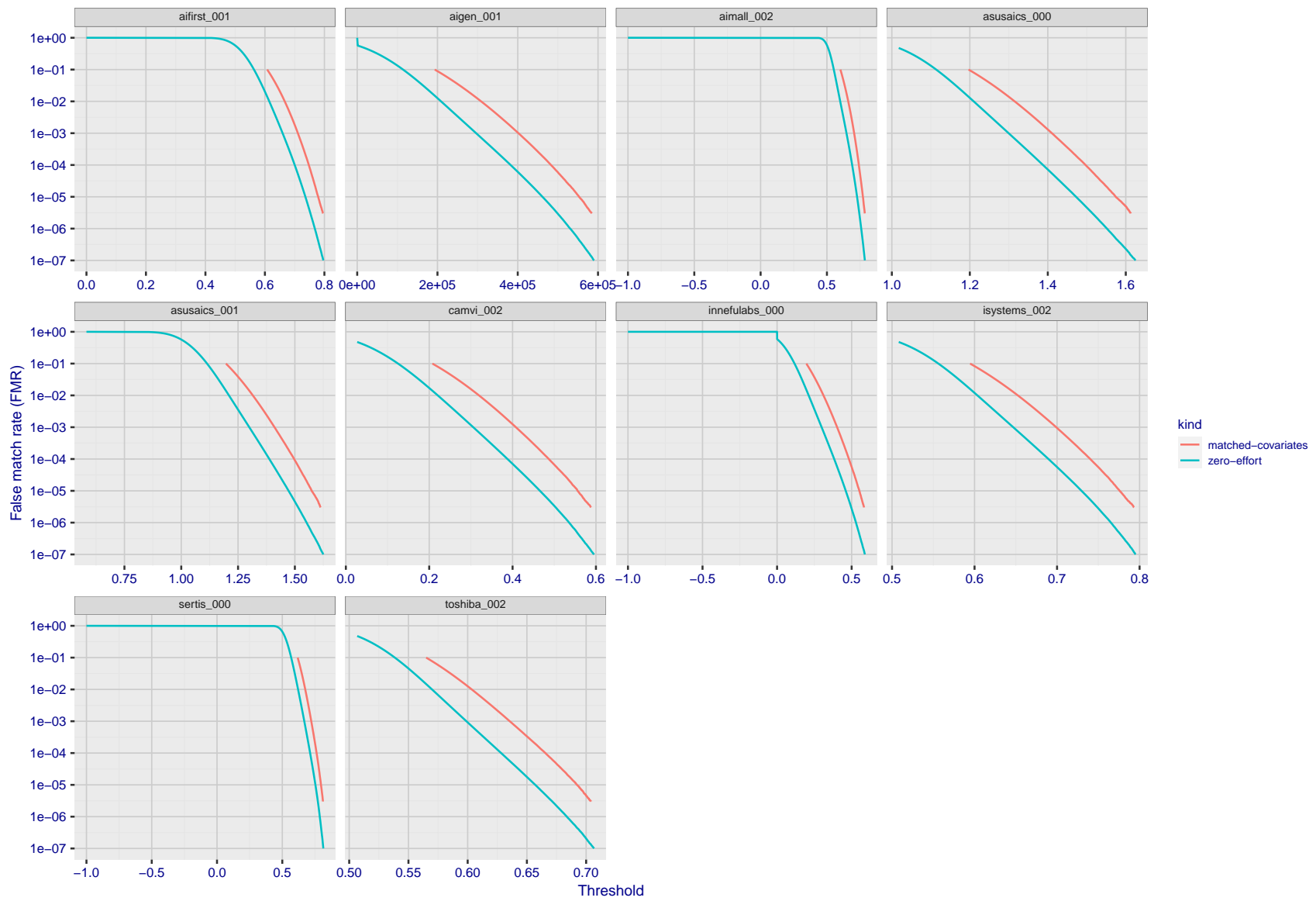


Figure 181: For the visa images, the false match calibration curves show FMR vs. threshold, T . The blue (lower) curves are for zero-effort impostors (i.e. comparing all images against all). The red (upper) curves are for persons of the same-sex, same-age, and same national-origin. This shows that FMR is underestimated (by a factor of 10 or more) by using a zero-effort impostor calculation to calibrate T . As shown later (sec. 3.6), FMR is higher for demographic-matched impostors.

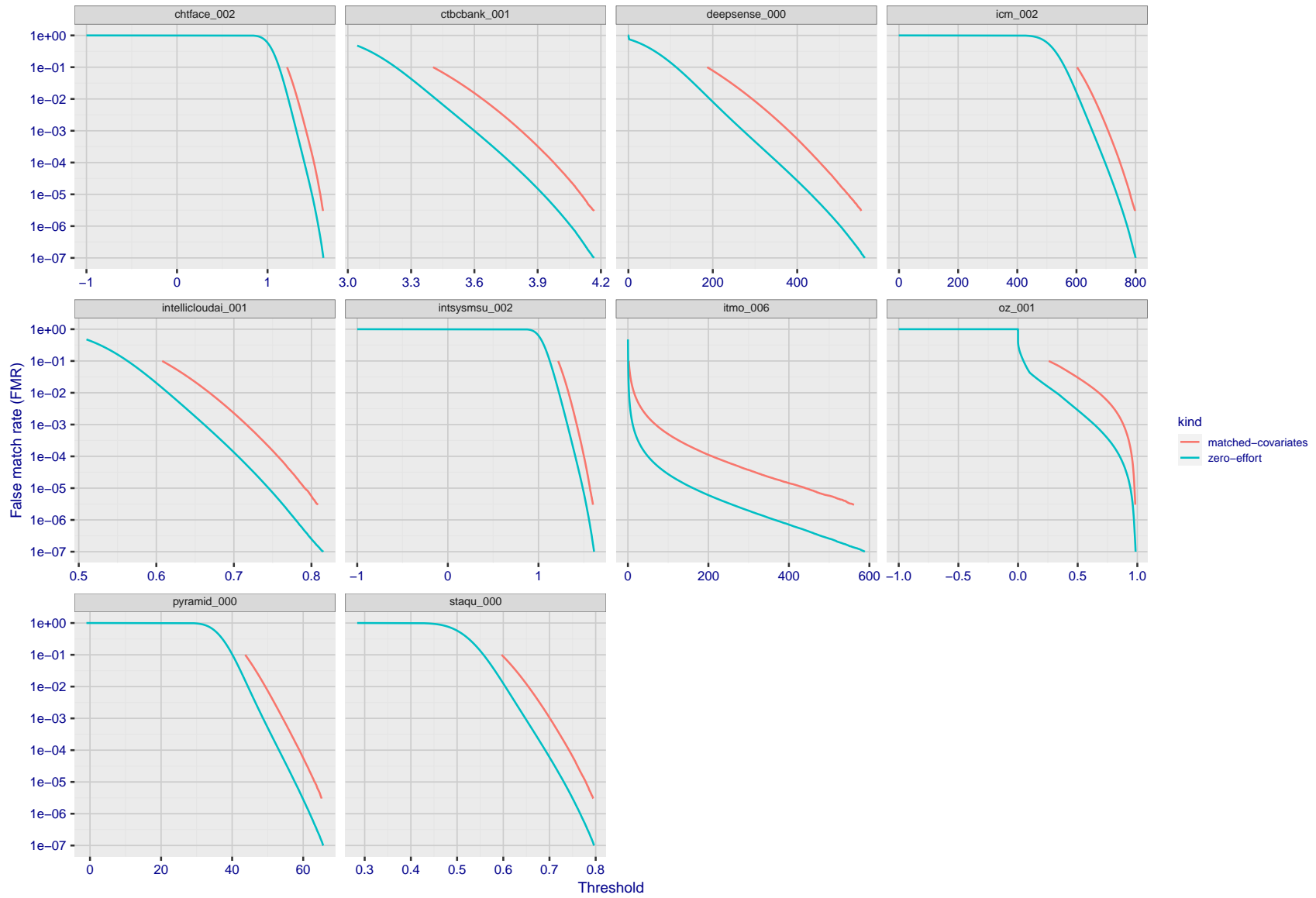


Figure 182: For the visa images, the false match calibration curves show FMR vs. threshold, T . The blue (lower) curves are for zero-effort impostors (i.e. comparing all images against all). The red (upper) curves are for persons of the same-sex, same-age, and same national-origin. This shows that FMR is underestimated (by a factor of 10 or more) by using a zero-effort impostor calculation to calibrate T . As shown later (sec. 3.6), FMR is higher for demographic-matched impostors.

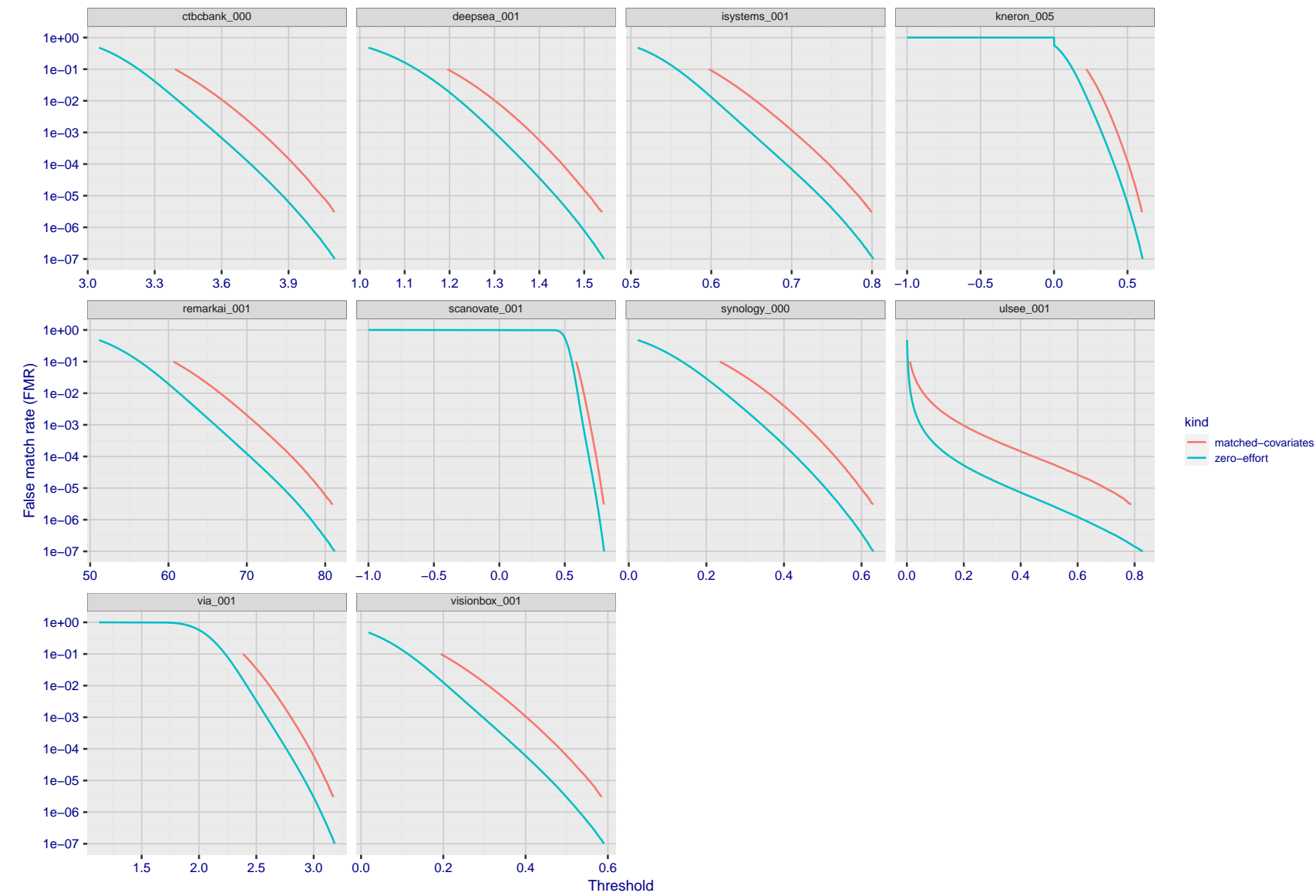


Figure 183: For the visa images, the false match calibration curves show FMR vs. threshold, T . The blue (lower) curves are for zero-effort impostors (i.e. comparing all images against all). The red (upper) curves are for persons of the same-sex, same-age, and same national-origin. This shows that FMR is underestimated (by a factor of 10 or more) by using a zero-effort impostor calculation to calibrate T . As shown later (sec. 3.6), FMR is higher for demographic-matched impostors.

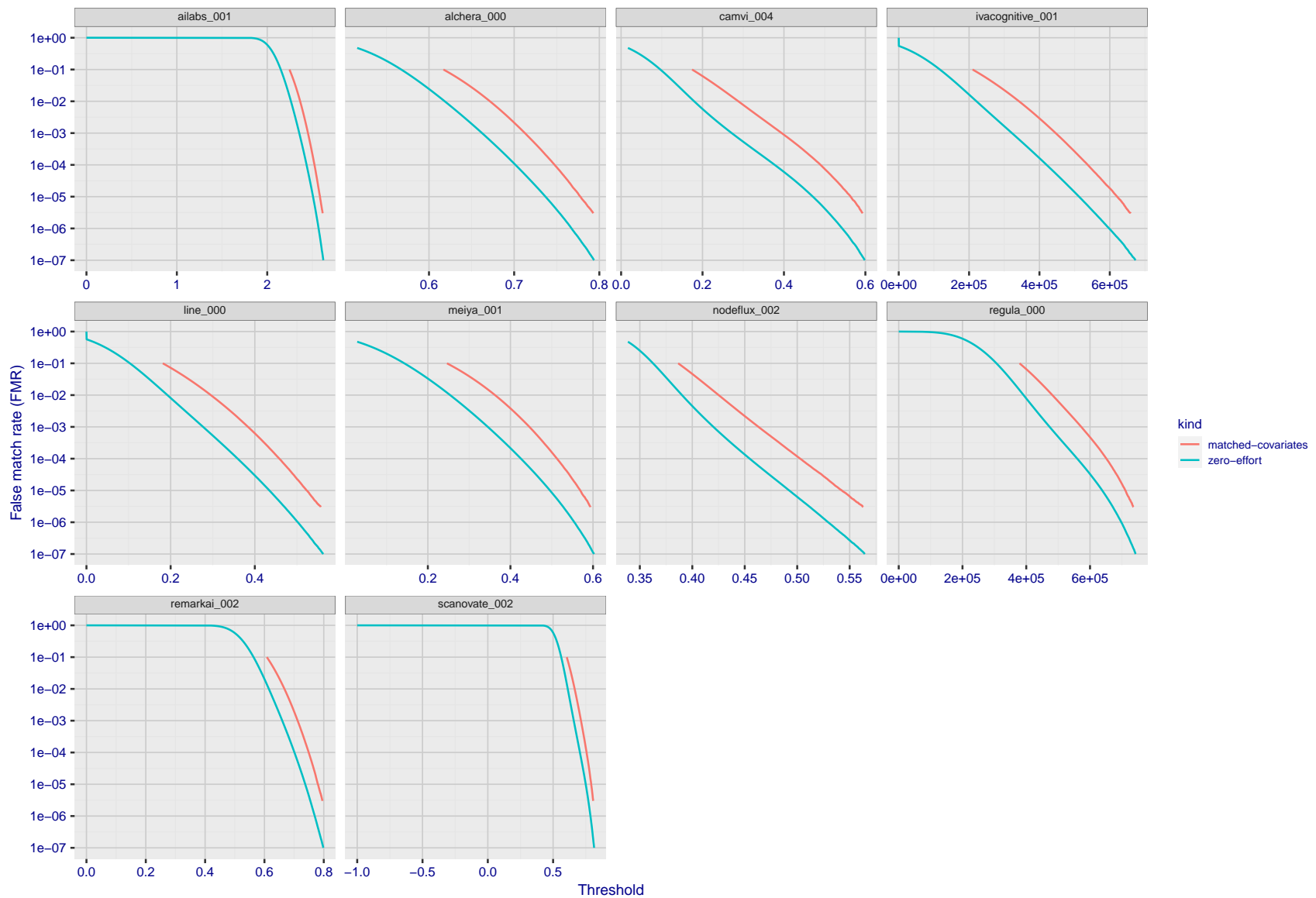


Figure 184: For the visa images, the false match calibration curves show FMR vs. threshold, T . The blue (lower) curves are for zero-effort impostors (i.e. comparing all images against all). The red (upper) curves are for persons of the same-sex, same-age, and same national-origin. This shows that FMR is underestimated (by a factor of 10 or more) by using a zero-effort impostor calculation to calibrate T . As shown later (sec. 3.6), FMR is higher for demographic-matched impostors.

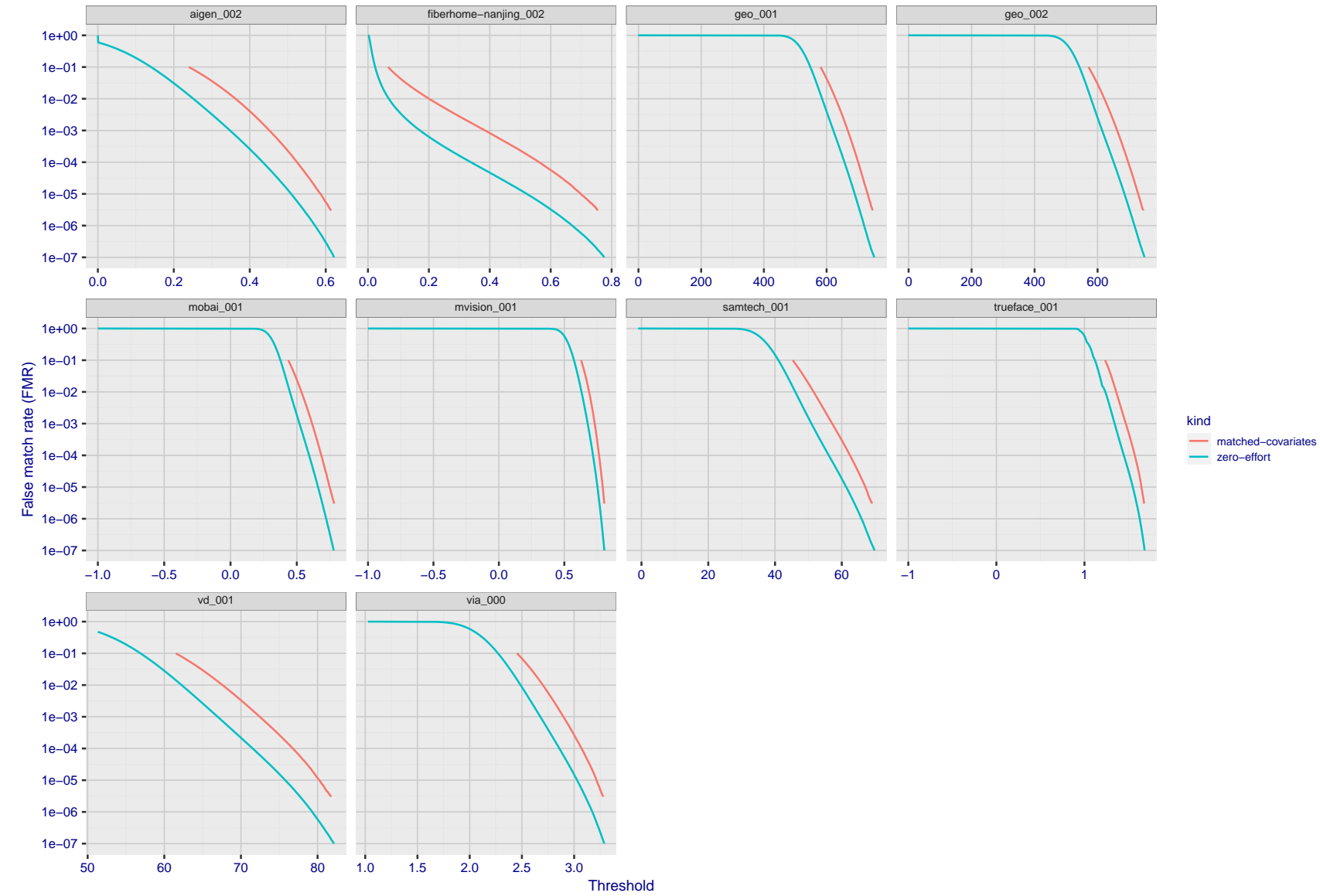


Figure 185: For the visa images, the false match calibration curves show FMR vs. threshold, T . The blue (lower) curves are for zero-effort impostors (i.e. comparing all images against all). The red (upper) curves are for persons of the same-sex, same-age, and same national-origin. This shows that FMR is underestimated (by a factor of 10 or more) by using a zero-effort impostor calculation to calibrate T . As shown later (sec. 3.6), FMR is higher for demographic-matched impostors.

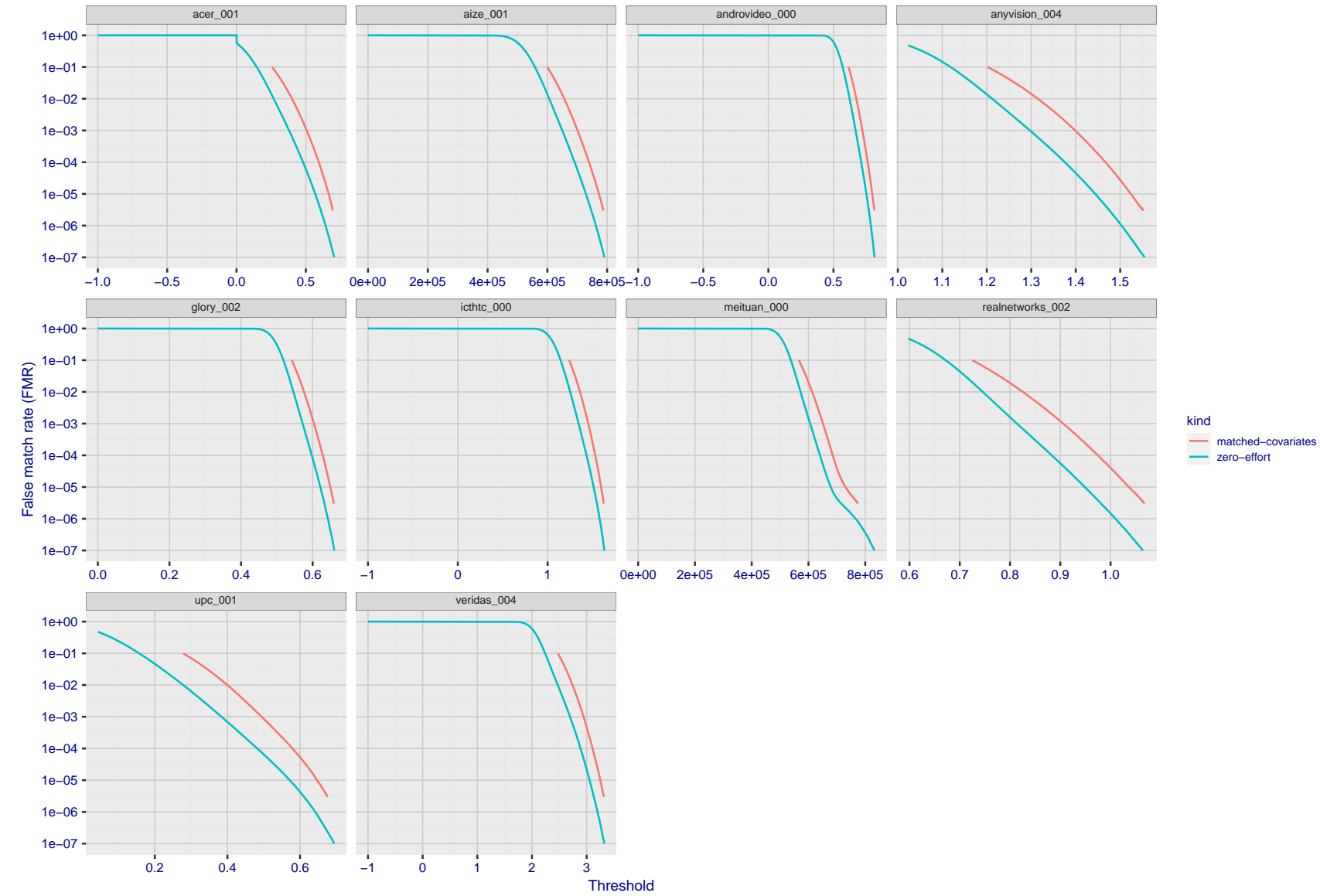


Figure 186: For the visa images, the false match calibration curves show FMR vs. threshold, T . The blue (lower) curves are for zero-effort impostors (i.e. comparing all images against all). The red (upper) curves are for persons of the same-sex, same-age, and same national-origin. This shows that FMR is underestimated (by a factor of 10 or more) by using a zero-effort impostor calculation to calibrate T . As shown later (sec. 3.6), FMR is higher for demographic-matched impostors.

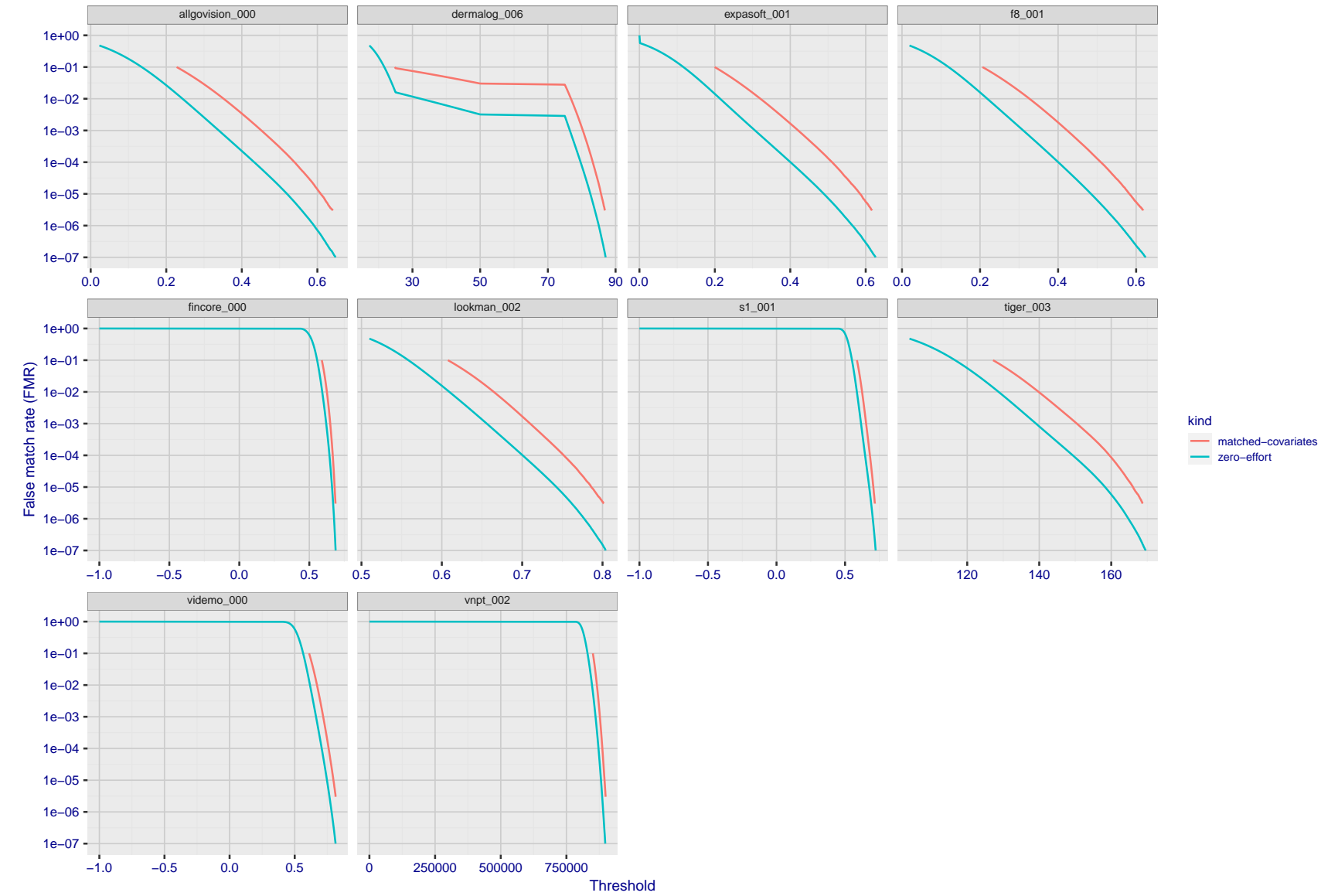


Figure 187: For the visa images, the false match calibration curves show FMR vs. threshold, T . The blue (lower) curves are for zero-effort impostors (i.e. comparing all images against all). The red (upper) curves are for persons of the same-sex, same-age, and same national-origin. This shows that FMR is underestimated (by a factor of 10 or more) by using a zero-effort impostor calculation to calibrate T . As shown later (sec. 3.6), FMR is higher for demographic-matched impostors.

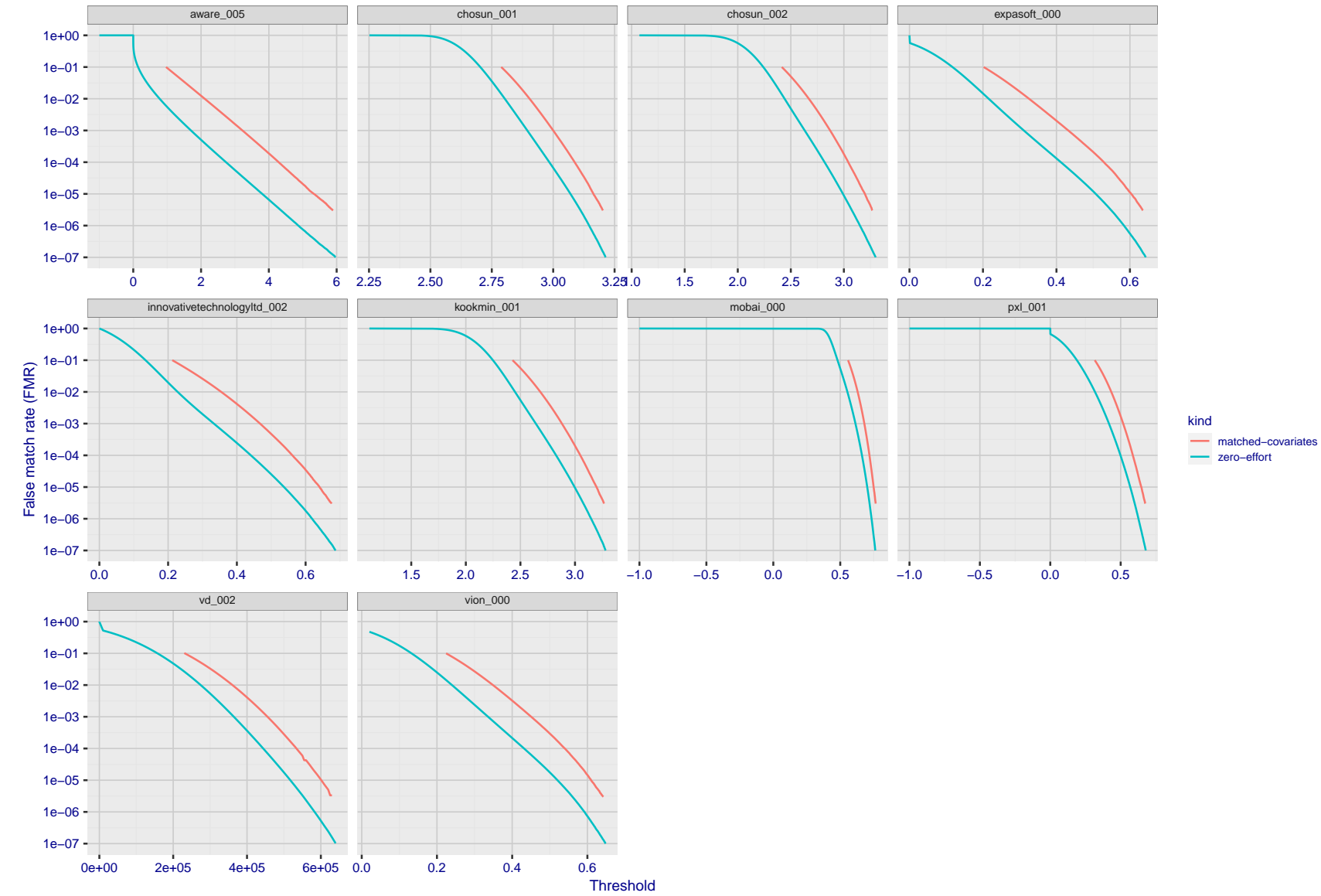


Figure 188: For the visa images, the false match calibration curves show FMR vs. threshold, T . The blue (lower) curves are for zero-effort impostors (i.e. comparing all images against all). The red (upper) curves are for persons of the same-sex, same-age, and same national-origin. This shows that FMR is underestimated (by a factor of 10 or more) by using a zero-effort impostor calculation to calibrate T . As shown later (sec. 3.6), FMR is higher for demographic-matched impostors.

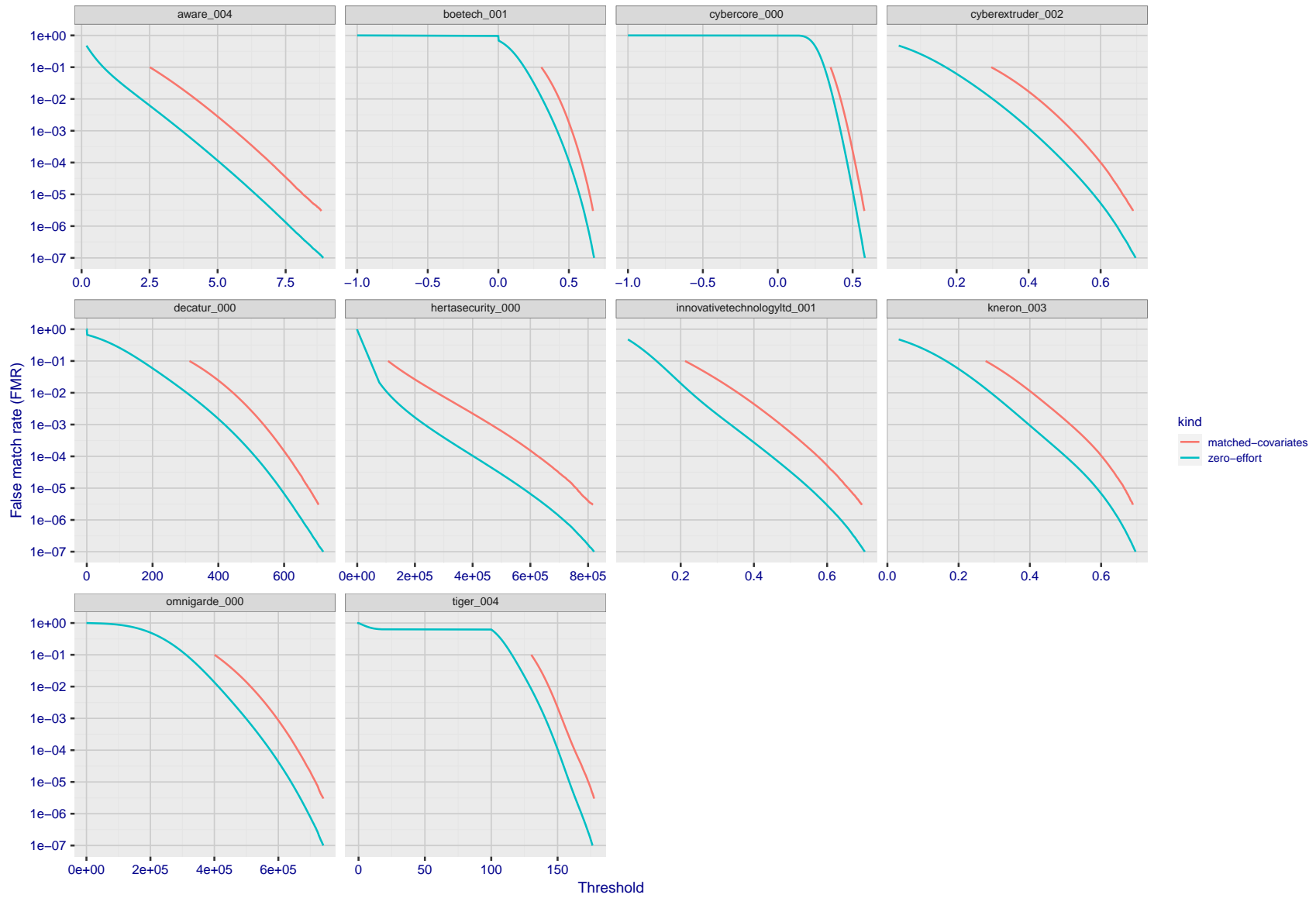


Figure 189: For the visa images, the false match calibration curves show FMR vs. threshold, T . The blue (lower) curves are for zero-effort impostors (i.e. comparing all images against all). The red (upper) curves are for persons of the same-sex, same-age, and same national-origin. This shows that FMR is underestimated (by a factor of 10 or more) by using a zero-effort impostor calculation to calibrate T . As shown later (sec. 3.6), FMR is higher for demographic-matched impostors.

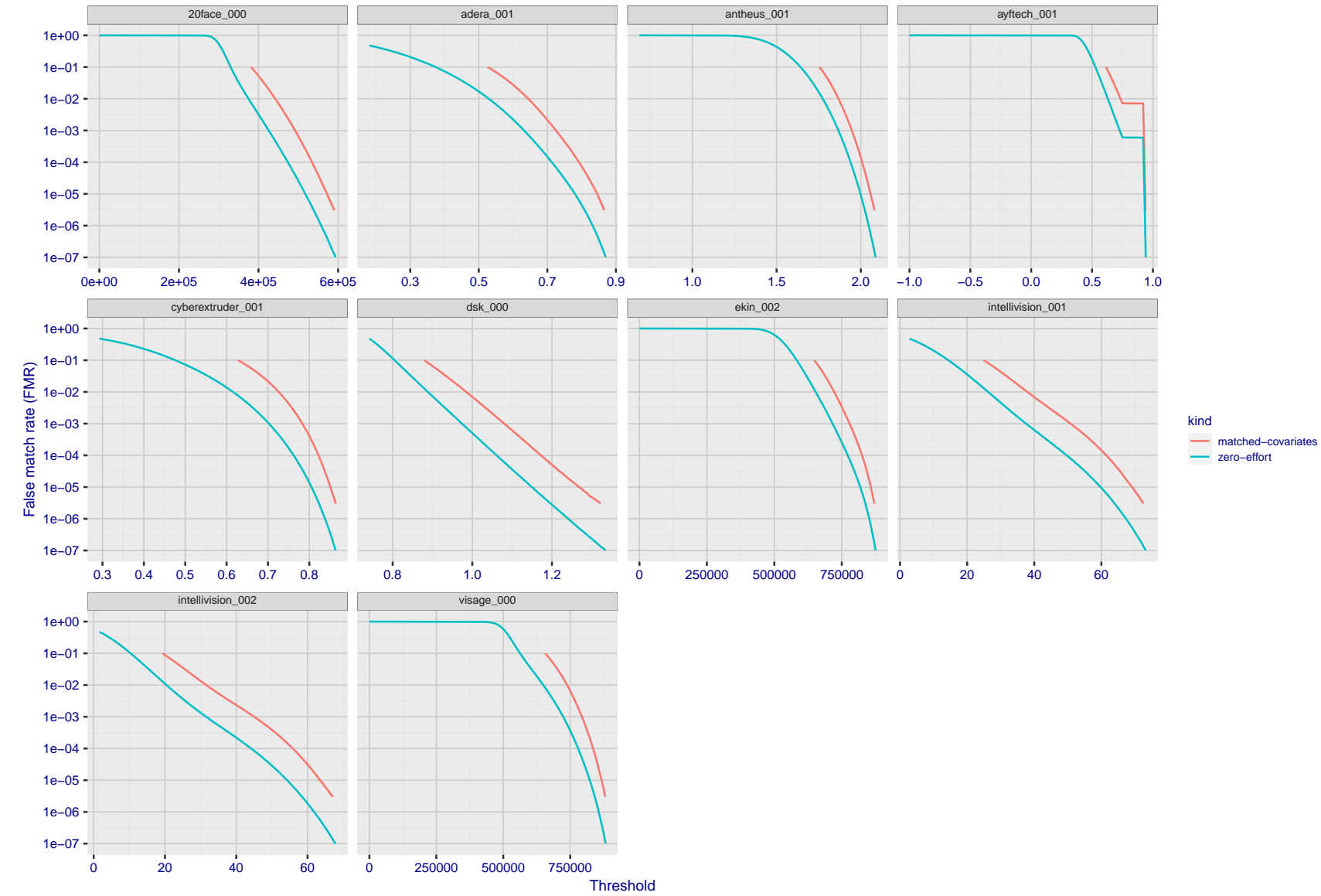


Figure 190: For the visa images, the false match calibration curves show FMR vs. threshold, T . The blue (lower) curves are for zero-effort impostors (i.e. comparing all images against all). The red (upper) curves are for persons of the same-sex, same-age, and same national-origin. This shows that FMR is underestimated (by a factor of 10 or more) by using a zero-effort impostor calculation to calibrate T . As shown later (sec. 3.6), FMR is higher for demographic-matched impostors.

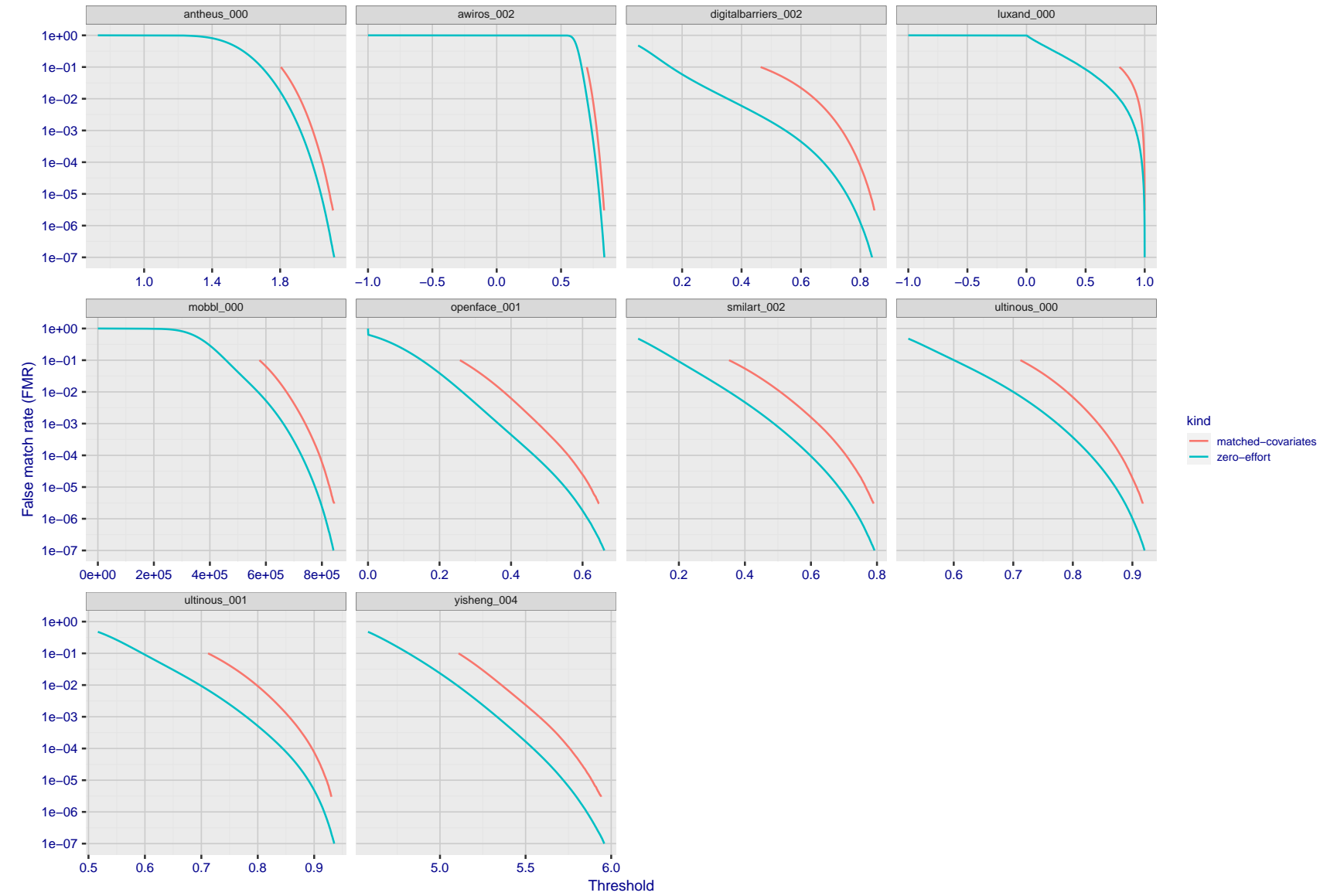


Figure 191: For the visa images, the false match calibration curves show FMR vs. threshold, T . The blue (lower) curves are for zero-effort impostors (i.e. comparing all images against all). The red (upper) curves are for persons of the same-sex, same-age, and same national-origin. This shows that FMR is underestimated (by a factor of 10 or more) by using a zero-effort impostor calculation to calibrate T . As shown later (sec. 3.6), FMR is higher for demographic-matched impostors.

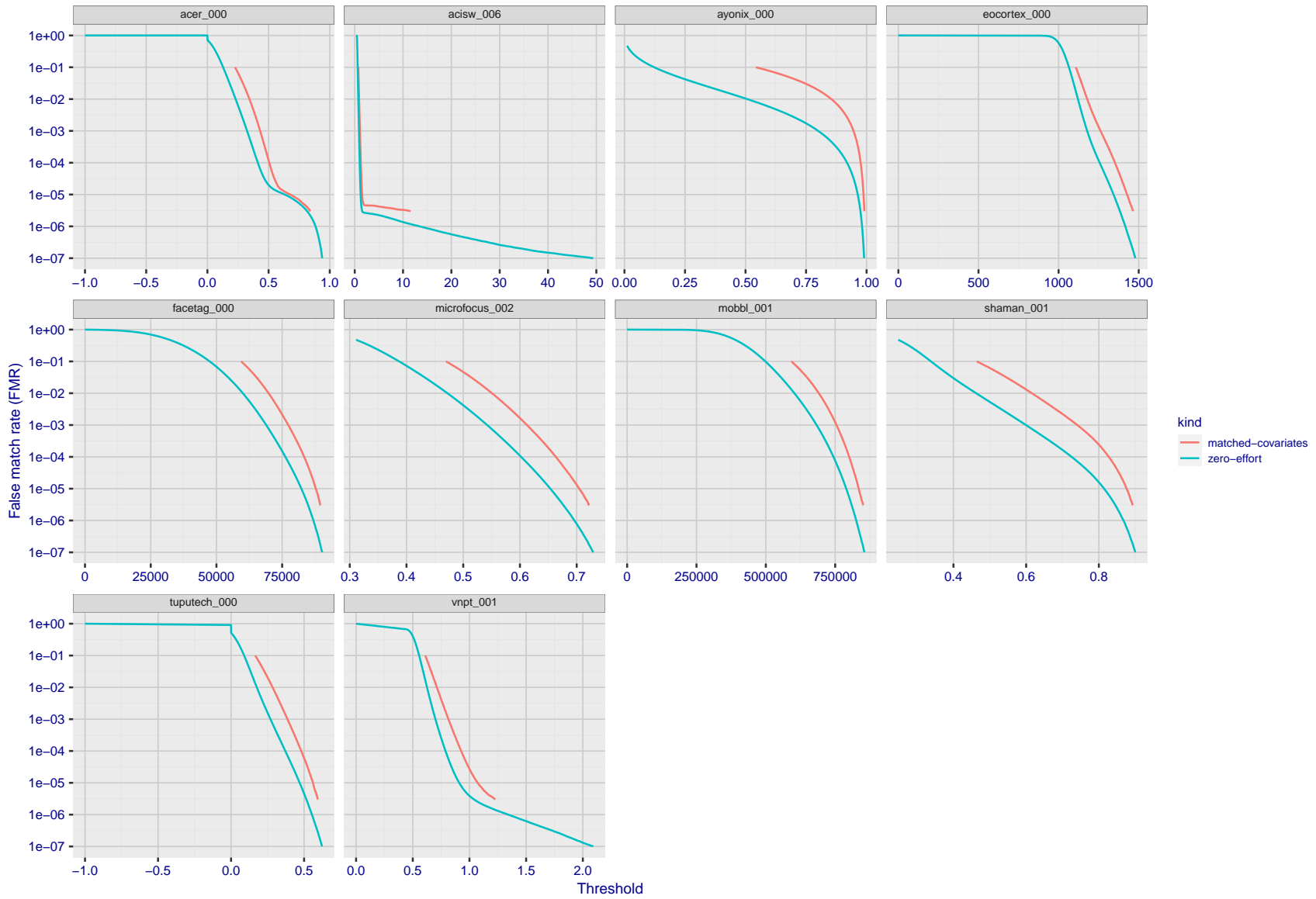


Figure 192: For the visa images, the false match calibration curves show FMR vs. threshold, T . The blue (lower) curves are for zero-effort impostors (i.e. comparing all images against all). The red (upper) curves are for persons of the same-sex, same-age, and same national-origin. This shows that FMR is underestimated (by a factor of 10 or more) by using a zero-effort impostor calculation to calibrate T . As shown later (sec. 3.6), FMR is higher for demographic-matched impostors.

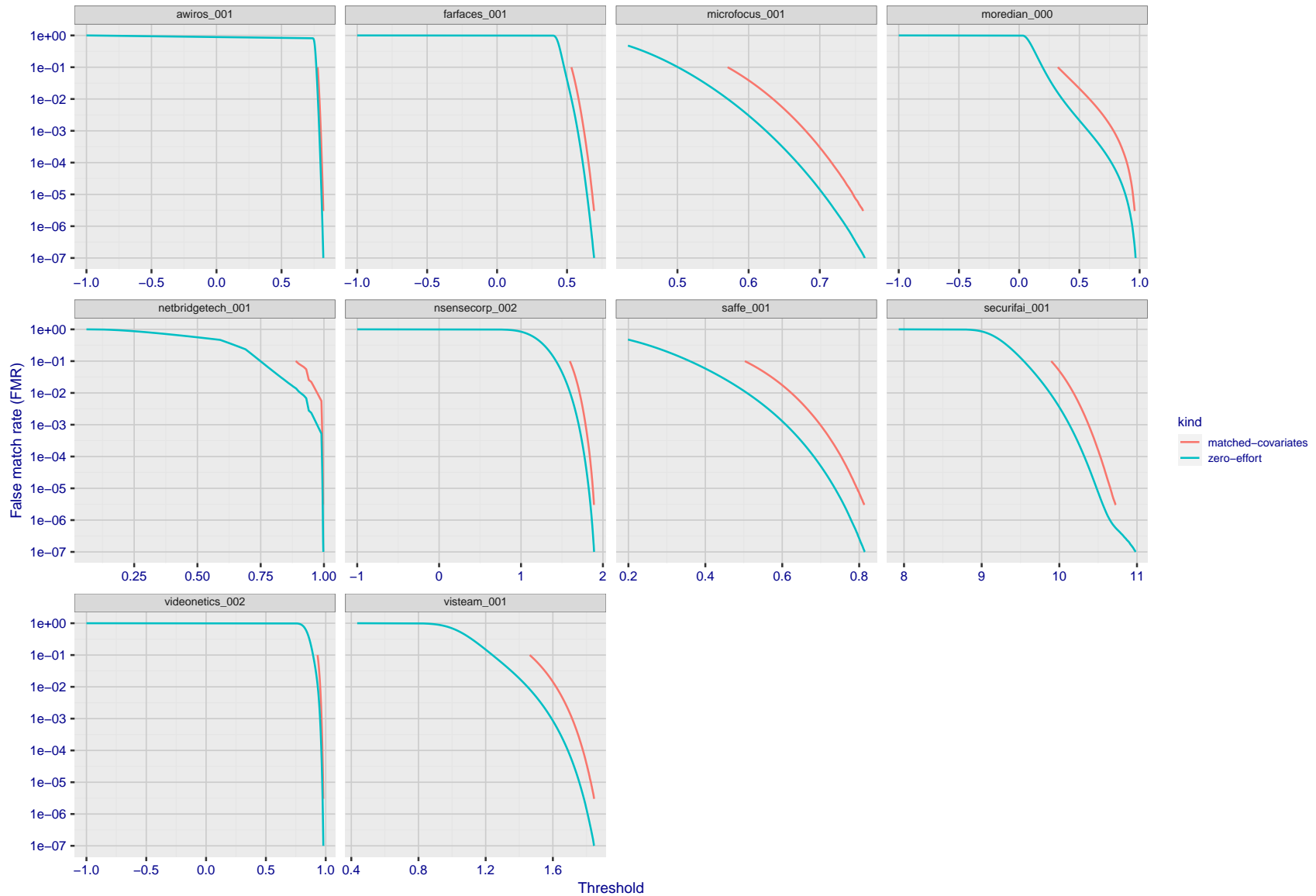


Figure 193: For the visa images, the false match calibration curves show FMR vs. threshold, T . The blue (lower) curves are for zero-effort impostors (i.e. comparing all images against all). The red (upper) curves are for persons of the same-sex, same-age, and same national-origin. This shows that FMR is underestimated (by a factor of 10 or more) by using a zero-effort impostor calculation to calibrate T . As shown later (sec. 3.6), FMR is higher for demographic-matched impostors.

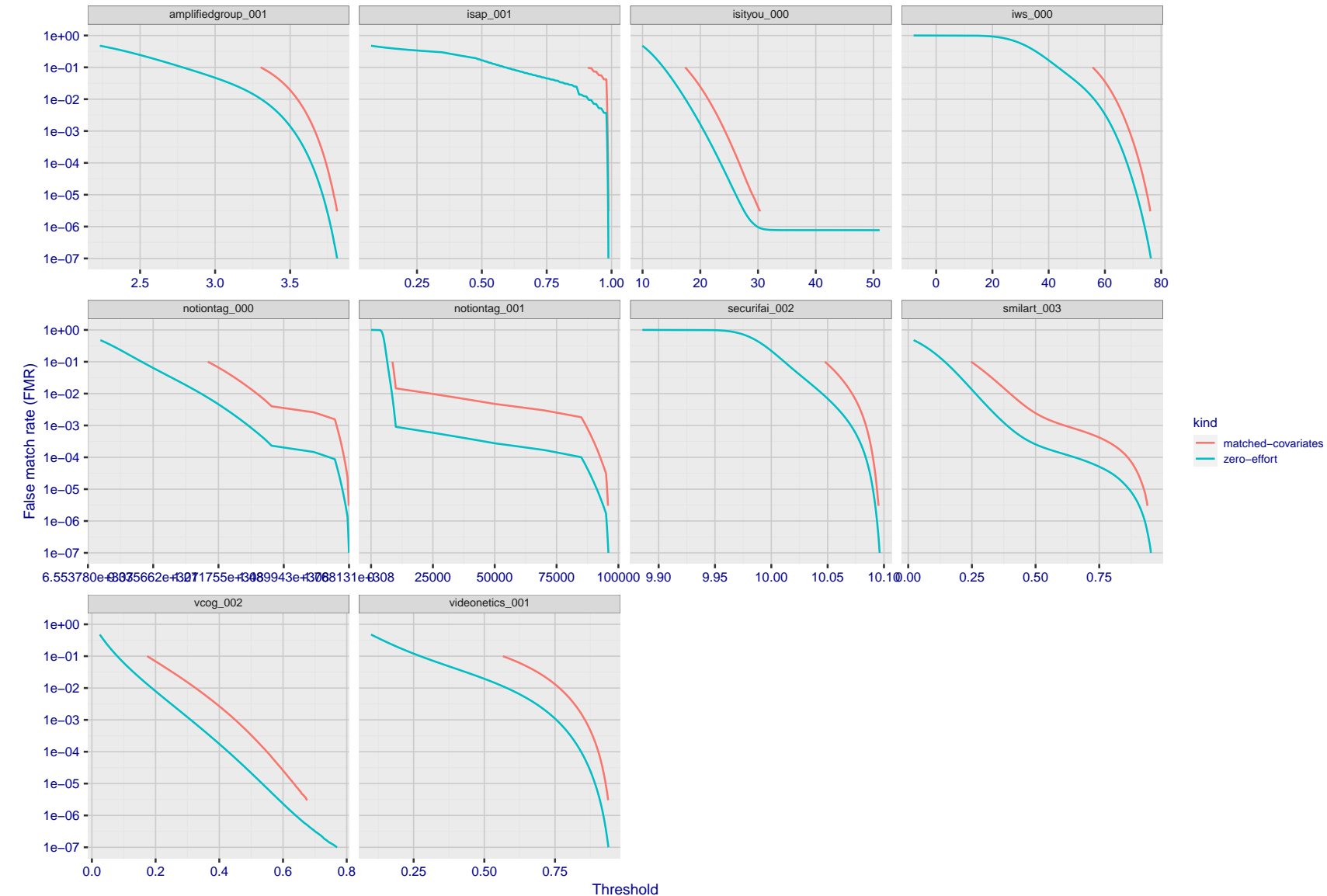


Figure 194: For the visa images, the false match calibration curves show FMR vs. threshold, T . The blue (lower) curves are for zero-effort impostors (i.e. comparing all images against all). The red (upper) curves are for persons of the same-sex, same-age, and same national-origin. This shows that FMR is underestimated (by a factor of 10 or more) by using a zero-effort impostor calculation to calibrate T . As shown later (sec. 3.6), FMR is higher for demographic-matched impostors.

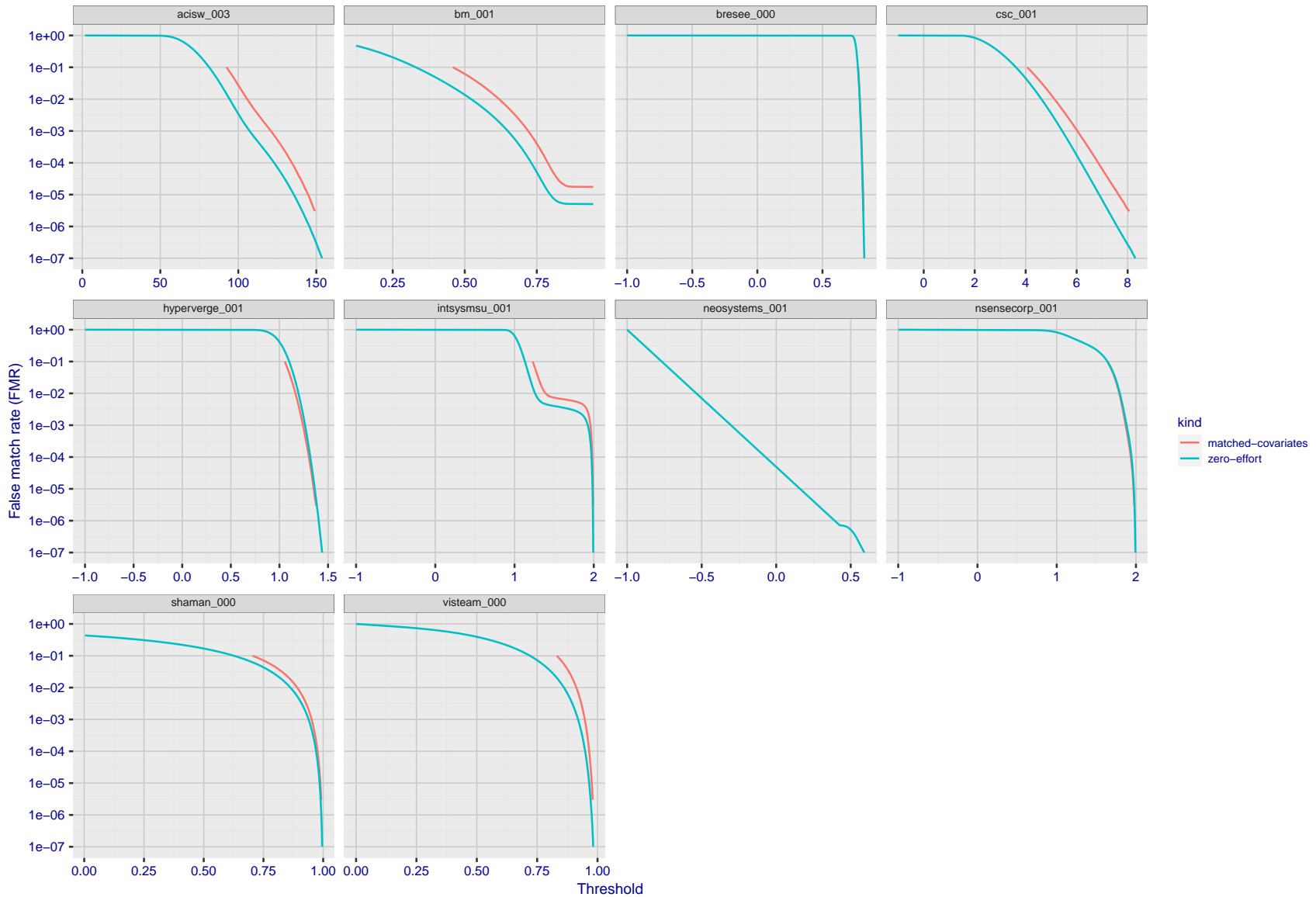


Figure 195: For the visa images, the false match calibration curves show FMR vs. threshold, T . The blue (lower) curves are for zero-effort impostors (i.e. comparing all images against all). The red (upper) curves are for persons of the same-sex, same-age, and same national-origin. This shows that FMR is underestimated (by a factor of 10 or more) by using a zero-effort impostor calculation to calibrate T . As shown later (sec. 3.6), FMR is higher for demographic-matched impostors.

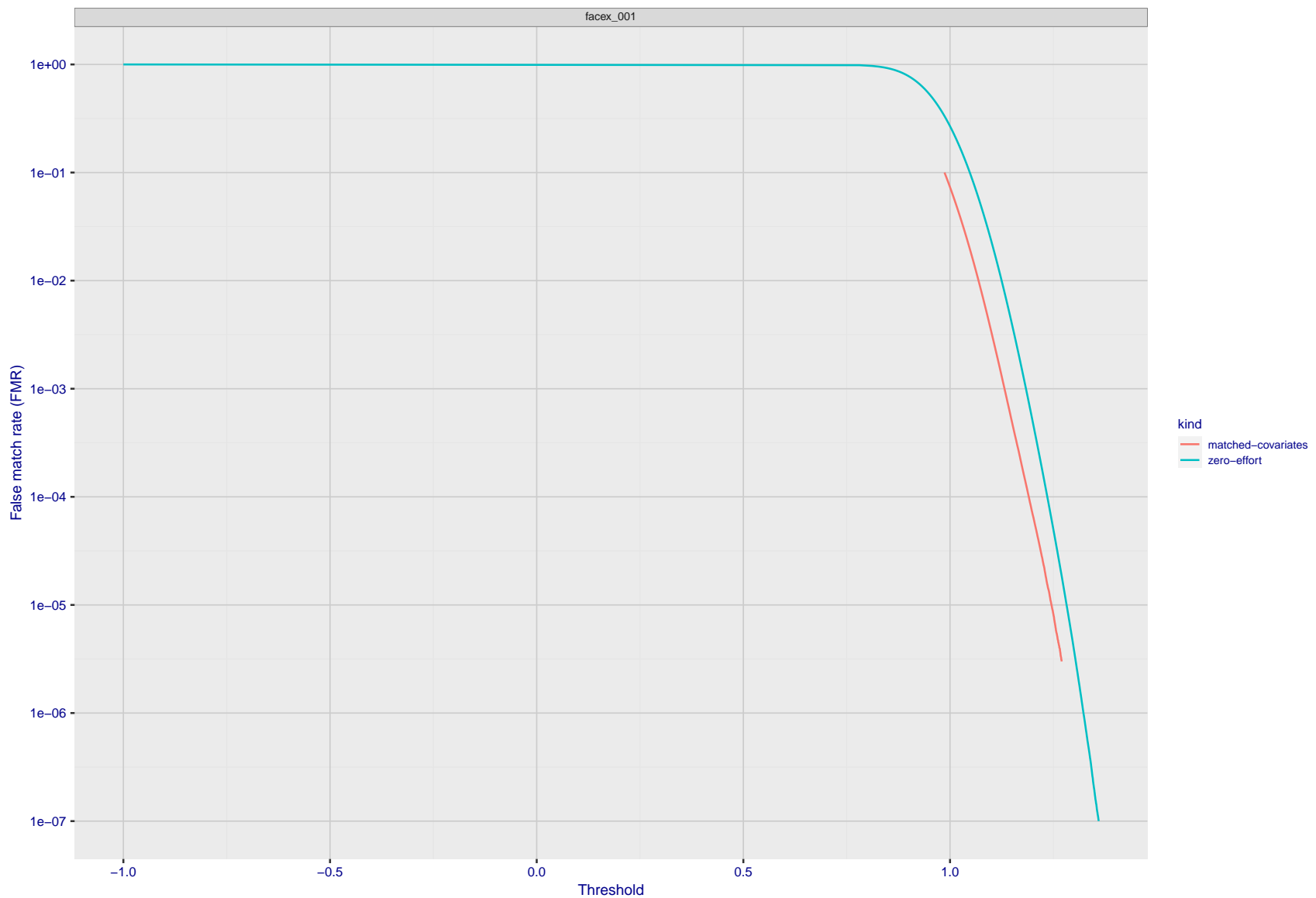


Figure 196: For the visa images, the false match calibration curves show FMR vs. threshold, T . The blue (lower) curves are for zero-effort impostors (i.e. comparing all images against all). The red (upper) curves are for persons of the same-sex, same-age, and same national-origin. This shows that FMR is underestimated (by a factor of 10 or more) by using a zero-effort impostor calculation to calibrate T . As shown later (sec. 3.6), FMR is higher for demographic-matched impostors.

3.5 Genuine distribution stability

3.5.1 Effect of birth place on the genuine distribution

Background: Both skin tone and bone structure vary geographically. Prior studies have reported variations in FNMR and FMR.

Goal: To measure false non-match rate (FNMR) variation with country of birth.

Methods: Thresholds are determined that give $FMR = \{0.001, 0.0001\}$ over the entire impostor set. Then FNMR is measured over 1000 bootstrap replications of the genuine scores. Only those countries with at least 140 individuals are included in the analysis.

Results: Figure 223 shows FNMR by country of birth for the two thresholds.

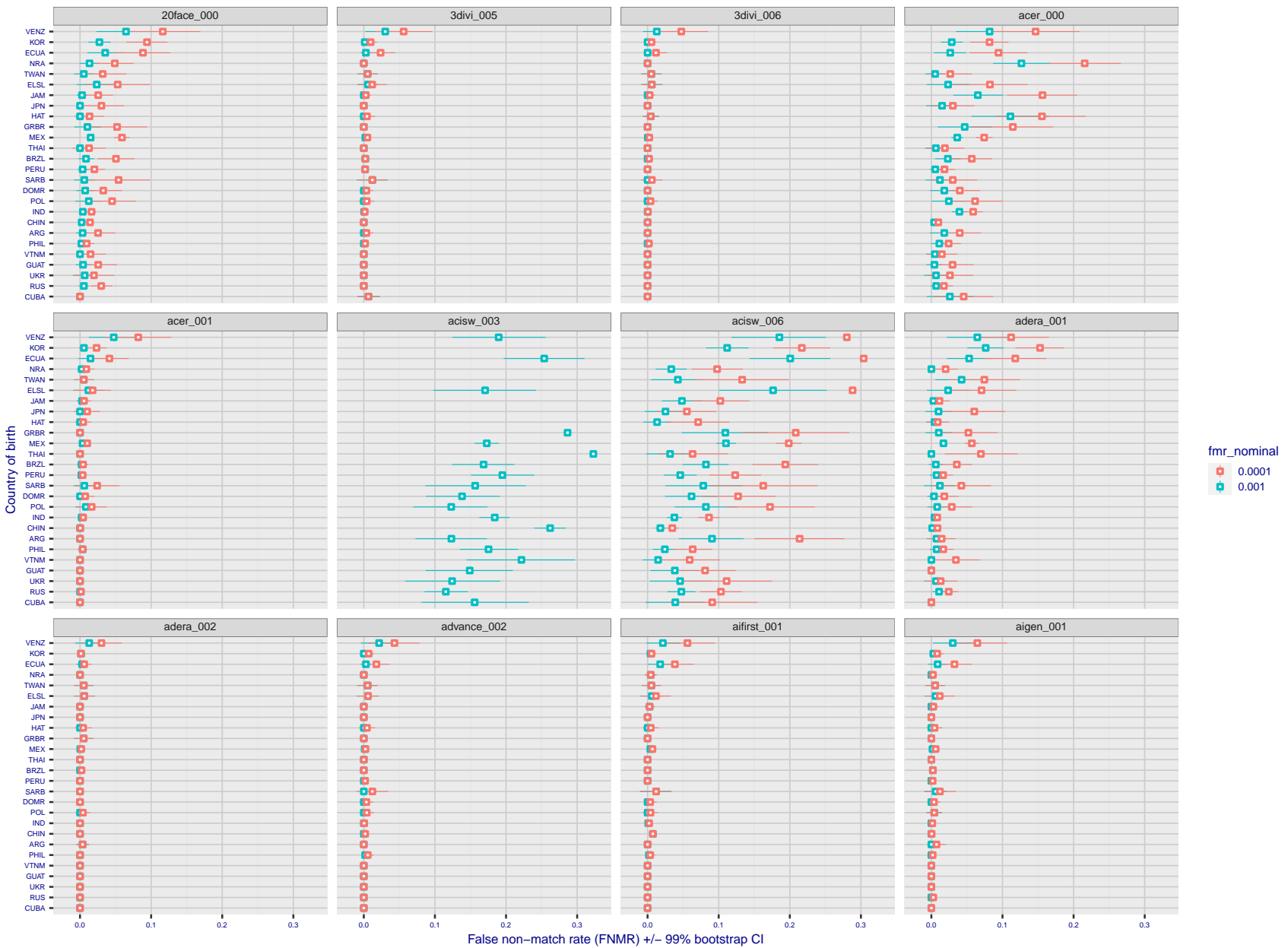


Figure 197: For the visa images, the dots show FNMR by country of birth for two globally set operating thresholds corresponding to $FMR = \{0.001, 0.0001\}$ computed over all on the order of 10^{10} impostor scores. The FMR in each bin will vary also - see subsequent impostor heatmaps in sec. 3.6.1. The figures shows an order of magnitude variation in FNMR across country of birth; these effects are likely due quality variations, then demographics like age and race. The error rates in some cases are zero, and in others the DET is flat so the error rates at the two thresholds are identical. The lines span 1% and 99% of bootstrap replicated FNMR estimates.

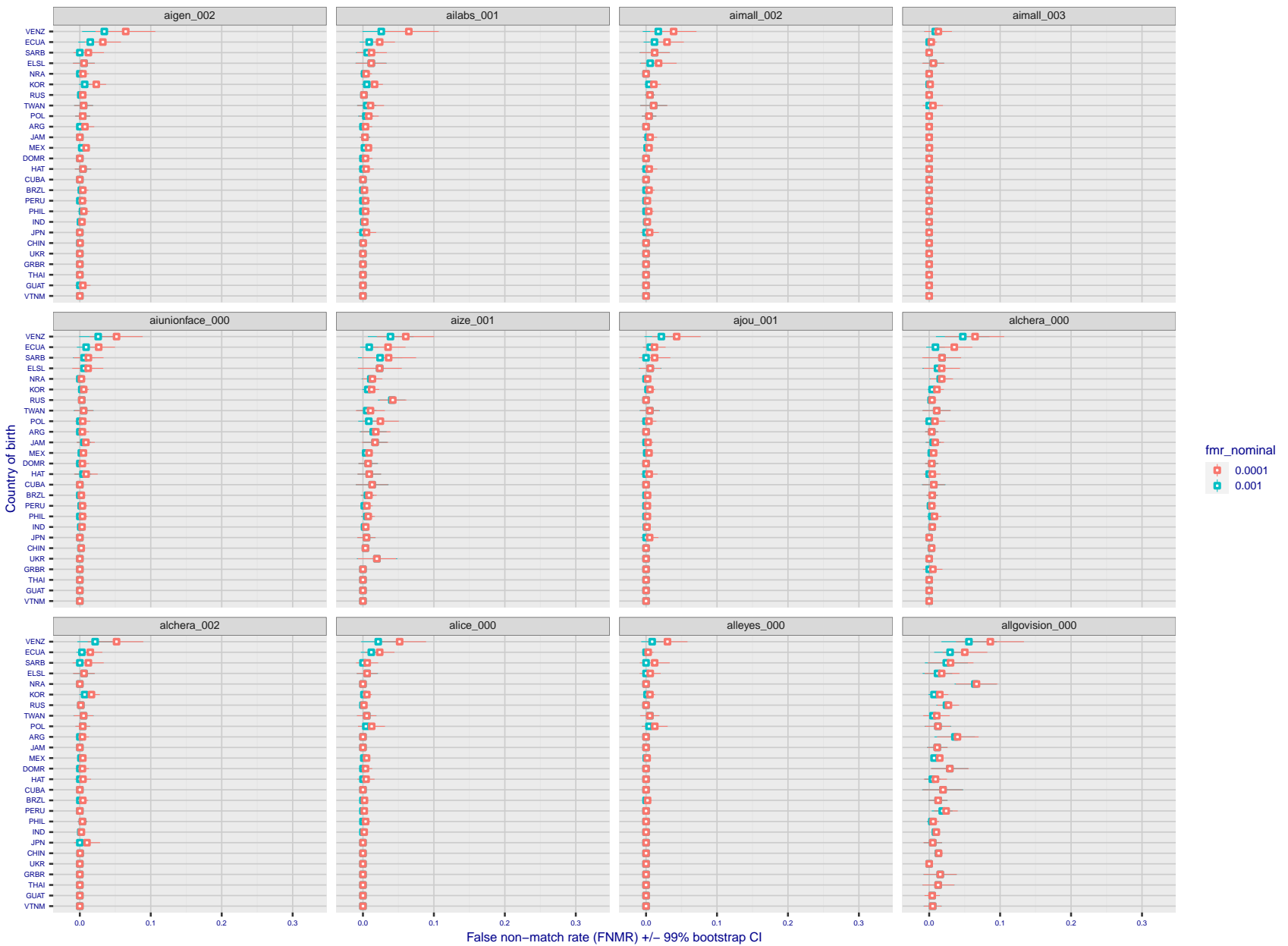


Figure 198: For the visa images, the dots show FNMR by country of birth for two globally set operating thresholds corresponding to $FMR = \{0.001, 0.0001\}$ computed over all on the order of 10^{10} impostor scores. The FMR in each bin will vary also - see subsequent impostor heatmaps in sec. 3.6.1. The figures shows an order of magnitude variation in FNMR across country of birth; these effects are likely due quality variations, then demographics like age and race. The error rates in some cases are zero, and in others the DET is flat so the error rates at the two thresholds are identical. The lines span 1% and 99% of bootstrap replicated FNMR estimates.

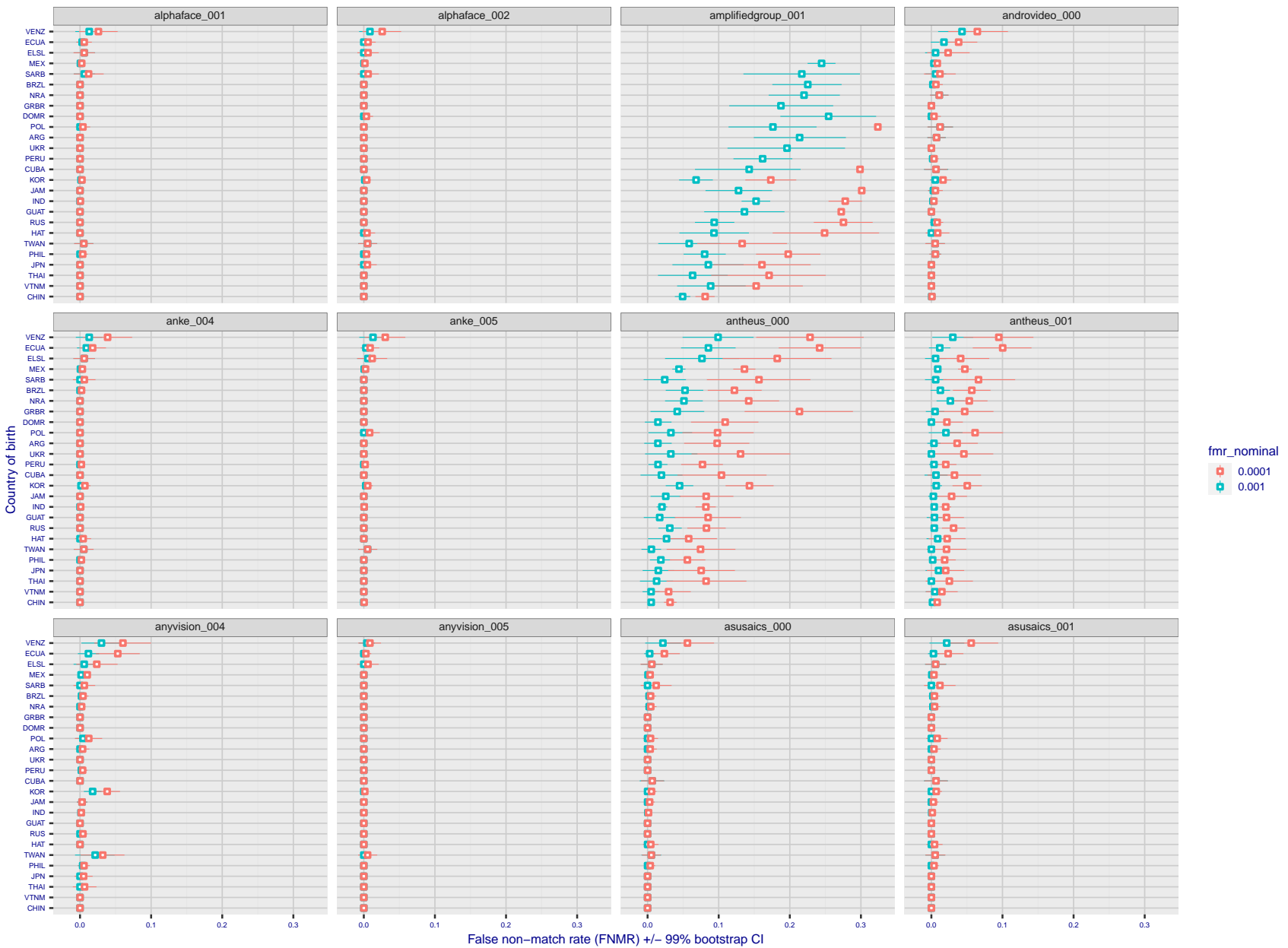


Figure 199: For the visa images, the dots show FNMR by country of birth for two globally set operating thresholds corresponding to $FMR = \{0.001, 0.0001\}$ computed over all on the order of 10^{10} impostor scores. The FMR in each bin will vary also - see subsequent impostor heatmaps in sec. 3.6.1. The figures shows an order of magnitude variation in FNMR across country of birth; these effects are likely due quality variations, then demographics like age and race. The error rates in some cases are zero, and in others the DET is flat so the error rates at the two thresholds are identical. The lines span 1% and 99% of bootstrap replicated FNMR estimates.

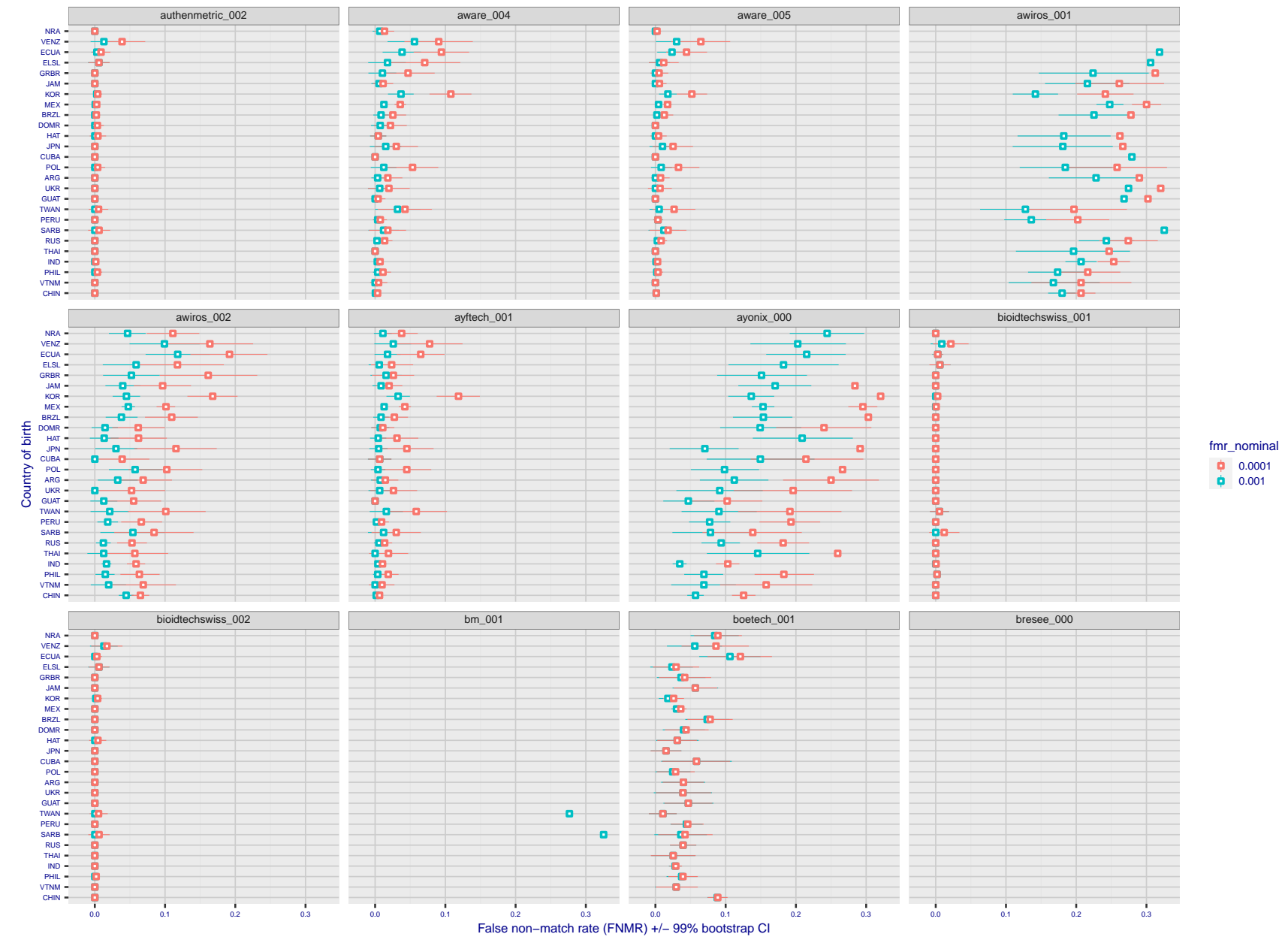


Figure 200: For the visa images, the dots show FNMR by country of birth for two globally set operating thresholds corresponding to $FMR = \{0.001, 0.0001\}$ computed over all on the order of 10^{10} impostor scores. The FMR in each bin will vary also - see subsequent impostor heatmaps in sec. 3.6.1. The figures shows an order of magnitude variation in FNMR across country of birth; these effects are likely due quality variations, then demographics like age and race. The error rates in some cases are zero, and in others the DET is flat so the error rates at the two thresholds are identical. The lines span 1% and 99% of bootstrap replicated FNMR estimates.

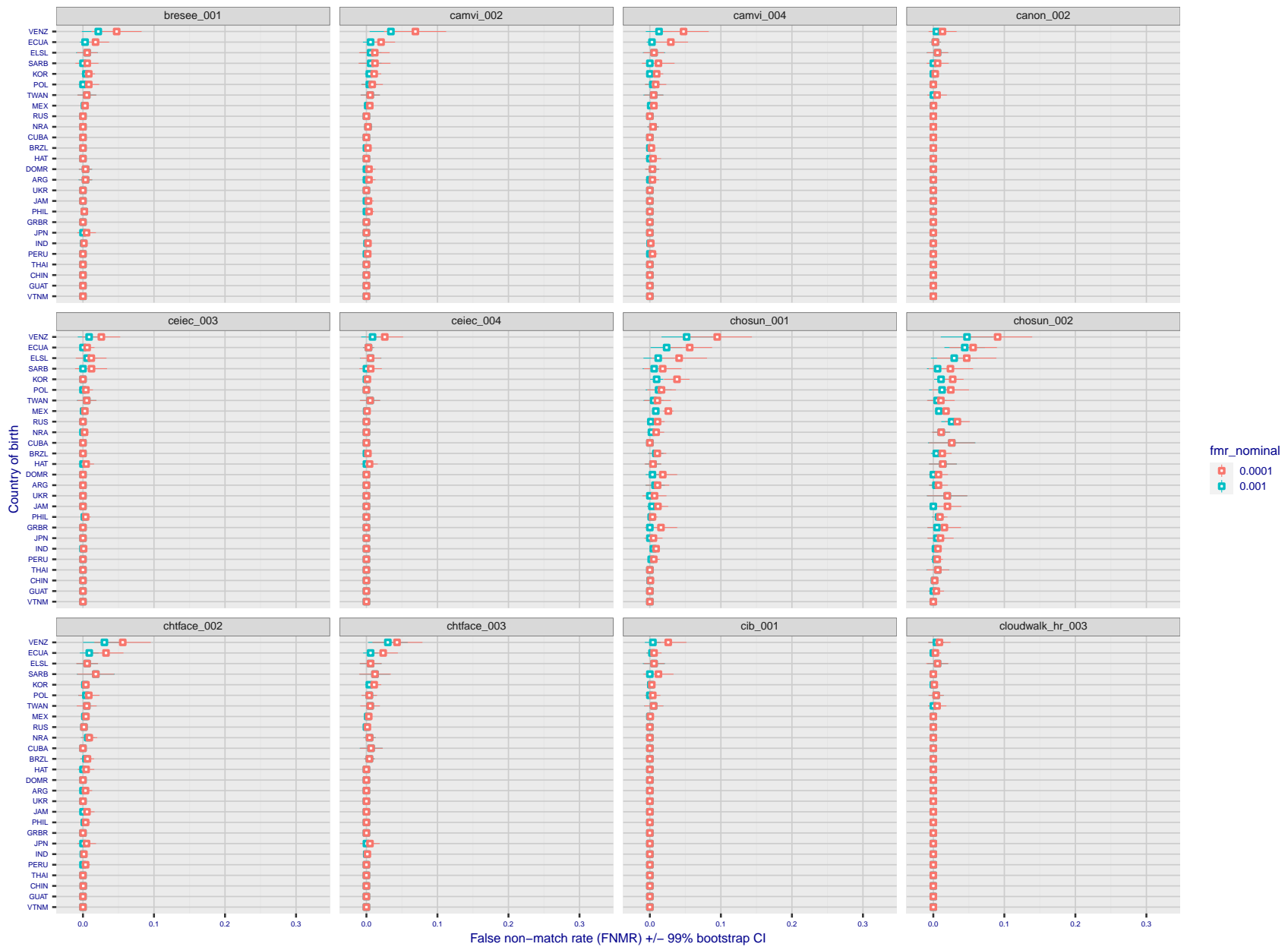


Figure 201: For the visa images, the dots show FNMR by country of birth for two globally set operating thresholds corresponding to $FMR = \{0.001, 0.0001\}$ computed over all on the order of 10^{10} impostor scores. The FMR in each bin will vary also - see subsequent impostor heatmaps in sec. 3.6.1. The figures shows an order of magnitude variation in FNMR across country of birth; these effects are likely due quality variations, then demographics like age and race. The error rates in some cases are zero, and in others the DET is flat so the error rates at the two thresholds are identical. The lines span 1% and 99% of bootstrap replicated FNMR estimates.

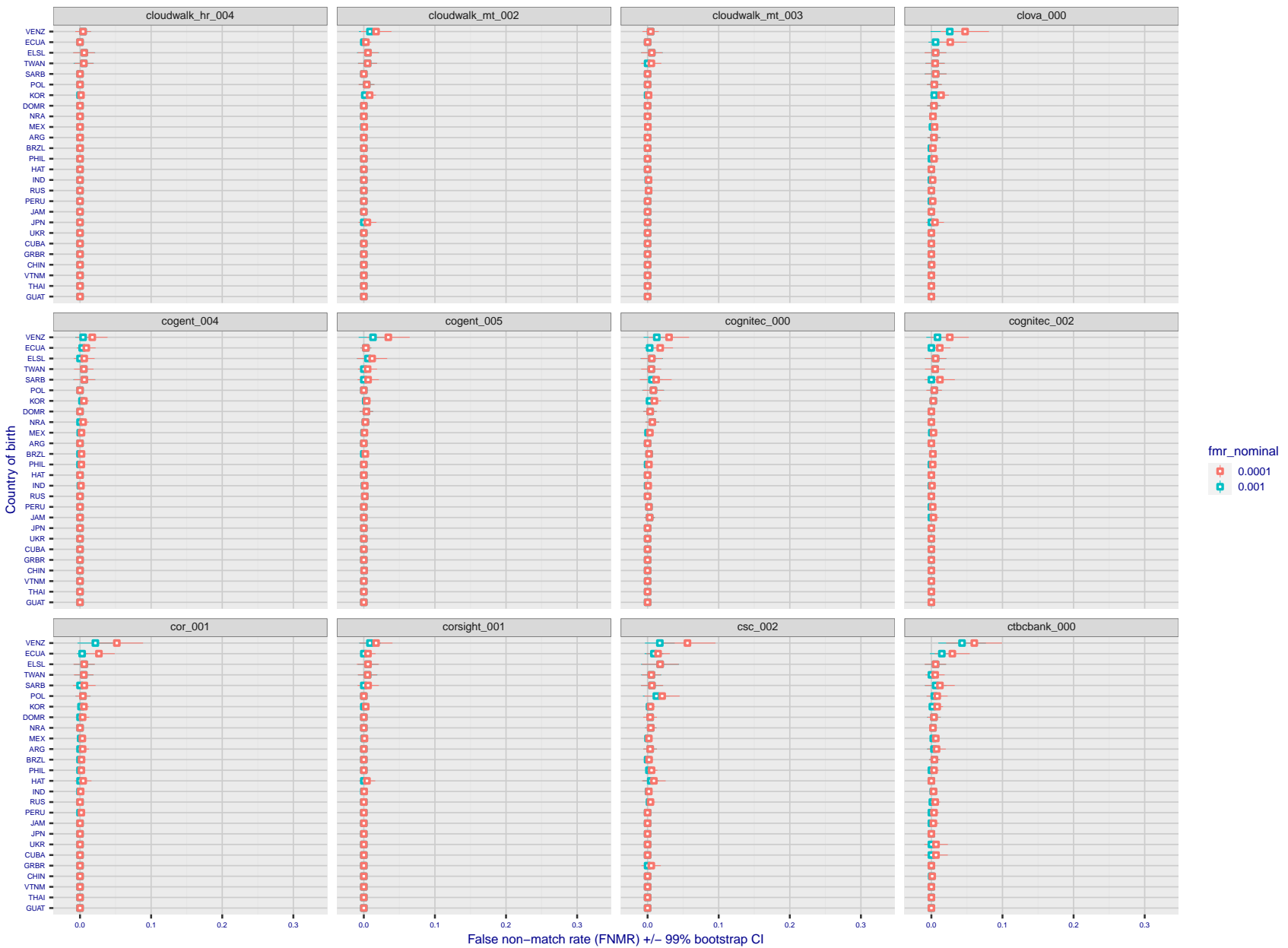


Figure 202: For the visa images, the dots show FNMR by country of birth for two globally set operating thresholds corresponding to $FMR = \{0.001, 0.0001\}$ computed over all on the order of 10^{10} impostor scores. The FMR in each bin will vary also - see subsequent impostor heatmaps in sec. 3.6.1. The figures shows an order of magnitude variation in FNMR across country of birth; these effects are likely due quality variations, then demographics like age and race. The error rates in some cases are zero, and in others the DET is flat so the error rates at the two thresholds are identical. The lines span 1% and 99% of bootstrap replicated FNMR estimates.

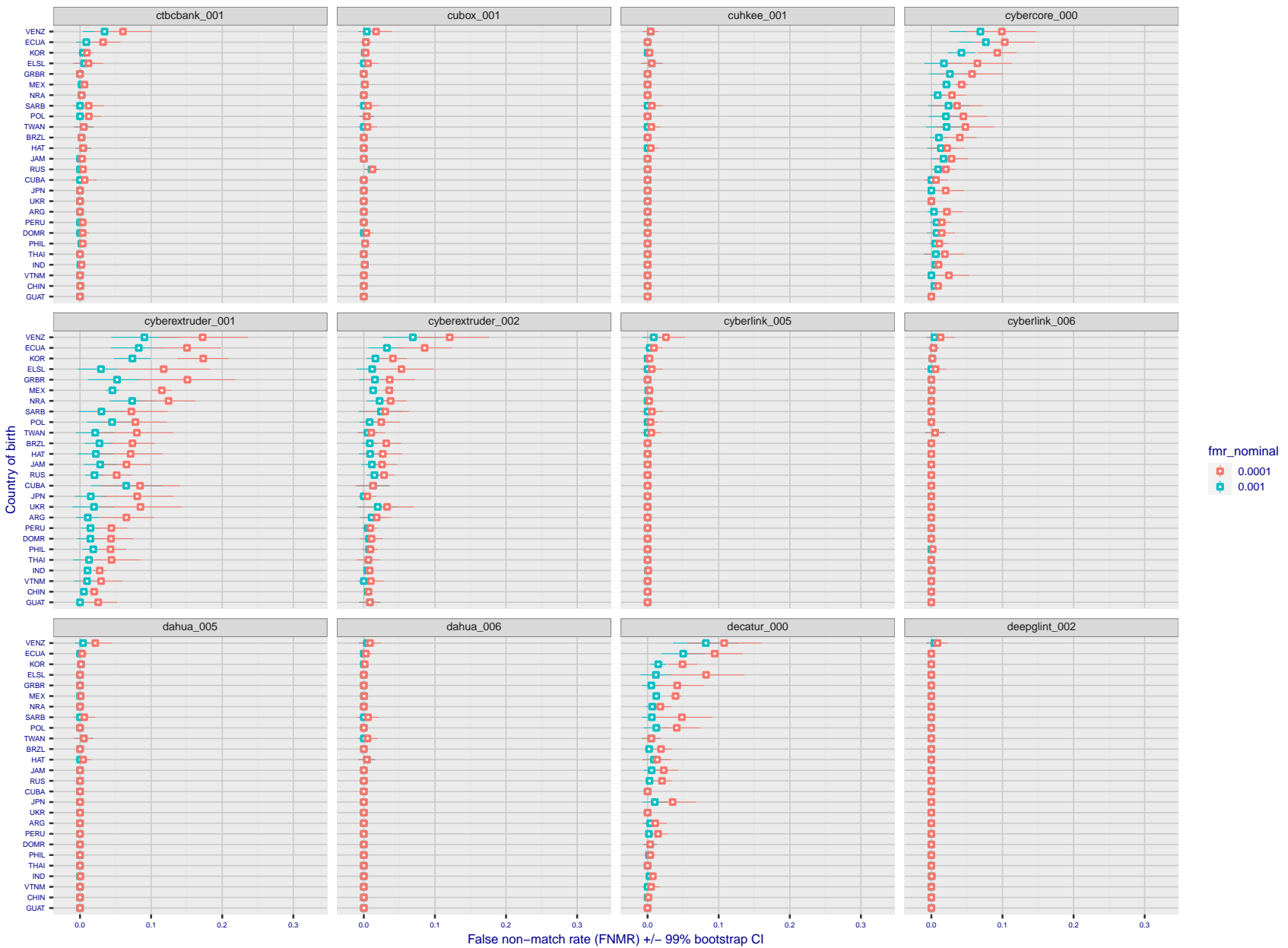


Figure 203: For the visa images, the dots show FNMR by country of birth for two globally set operating thresholds corresponding to $FMR = \{0.001, 0.0001\}$ computed over all on the order of 10^{10} impostor scores. The FMR in each bin will vary also - see subsequent impostor heatmaps in sec. 3.6.1. The figures shows an order of magnitude variation in FNMR across country of birth; these effects are likely due quality variations, then demographics like age and race. The error rates in some cases are zero, and in others the DET is flat so the error rates at the two thresholds are identical. The lines span 1% and 99% of bootstrap replicated FNMR estimates.

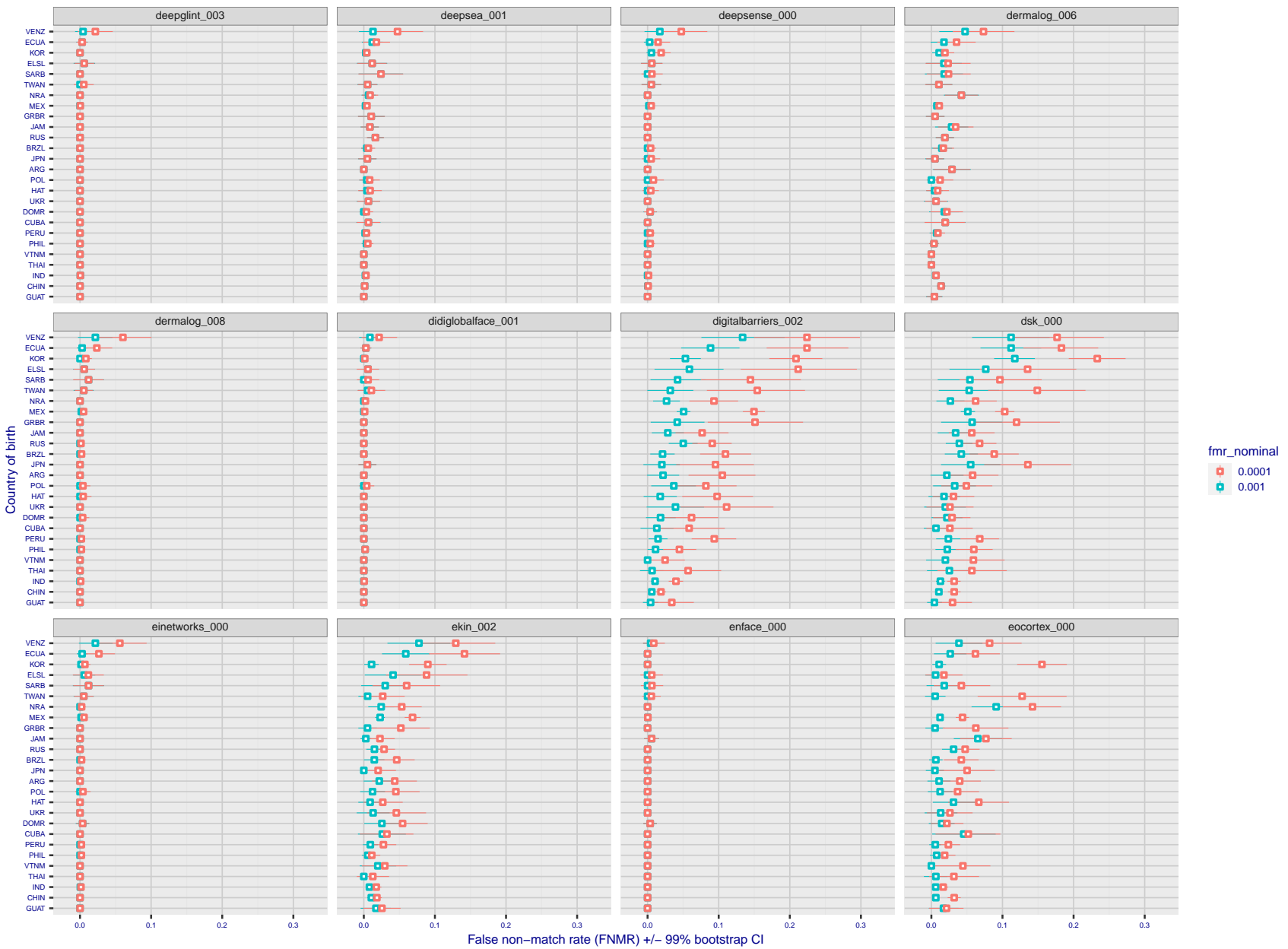


Figure 204: For the visa images, the dots show FNMR by country of birth for two globally set operating thresholds corresponding to $FMR = \{0.001, 0.0001\}$ computed over all on the order of 10^{10} impostor scores. The FMR in each bin will vary also - see subsequent impostor heatmaps in sec. 3.6.1. The figures shows an order of magnitude variation in FNMR across country of birth; these effects are likely due quality variations, then demographics like age and race. The error rates in some cases are zero, and in others the DET is flat so the error rates at the two thresholds are identical. The lines span 1% and 99% of bootstrap replicated FNMR estimates.

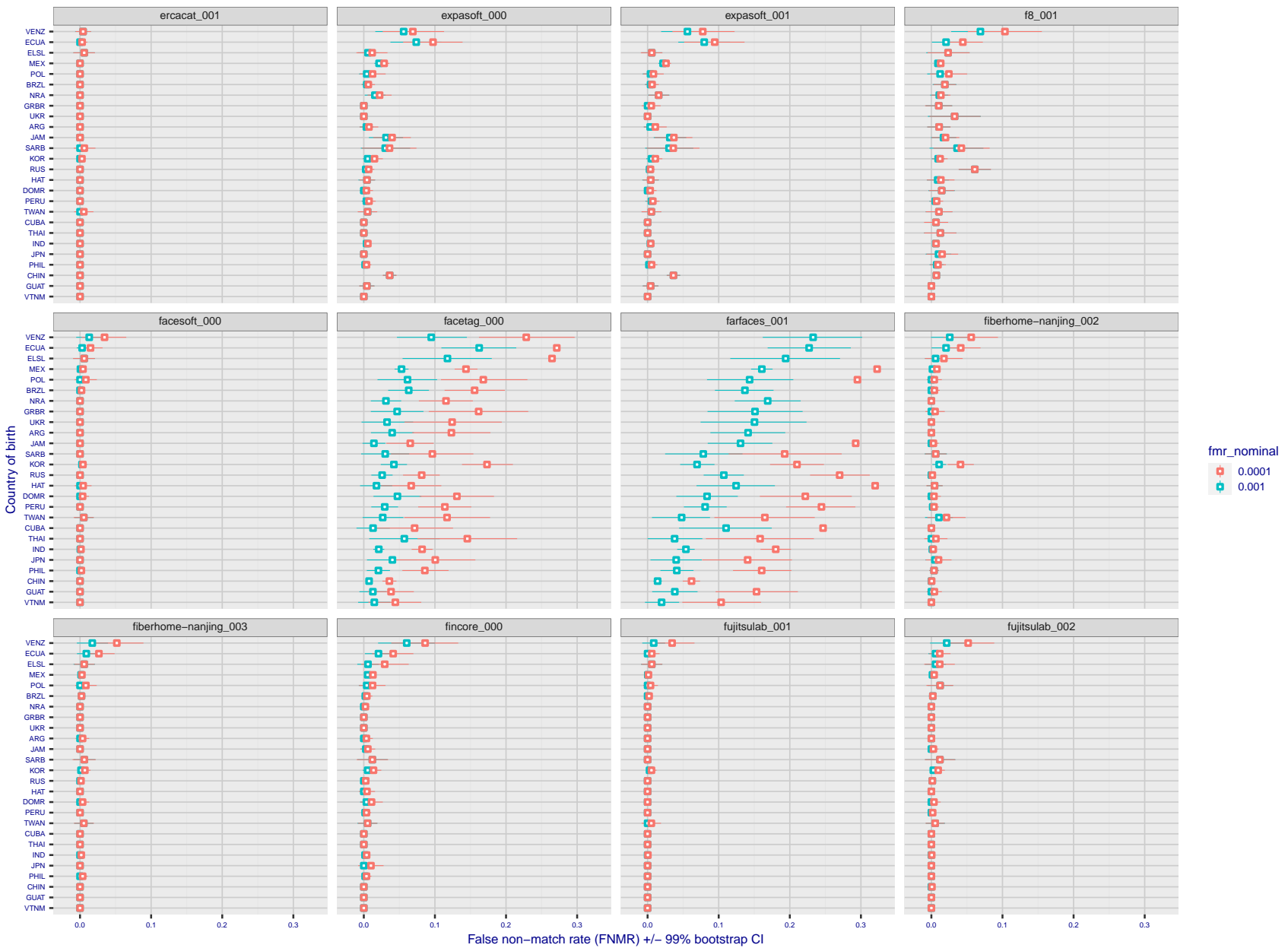


Figure 205: For the visa images, the dots show FNMR by country of birth for two globally set operating thresholds corresponding to $FMR = \{0.001, 0.0001\}$ computed over all on the order of 10^{10} impostor scores. The FMR in each bin will vary also - see subsequent impostor heatmaps in sec. 3.6.1. The figures shows an order of magnitude variation in FNMR across country of birth; these effects are likely due quality variations, then demographics like age and race. The error rates in some cases are zero, and in others the DET is flat so the error rates at the two thresholds are identical. The lines span 1% and 99% of bootstrap replicated FNMR estimates.

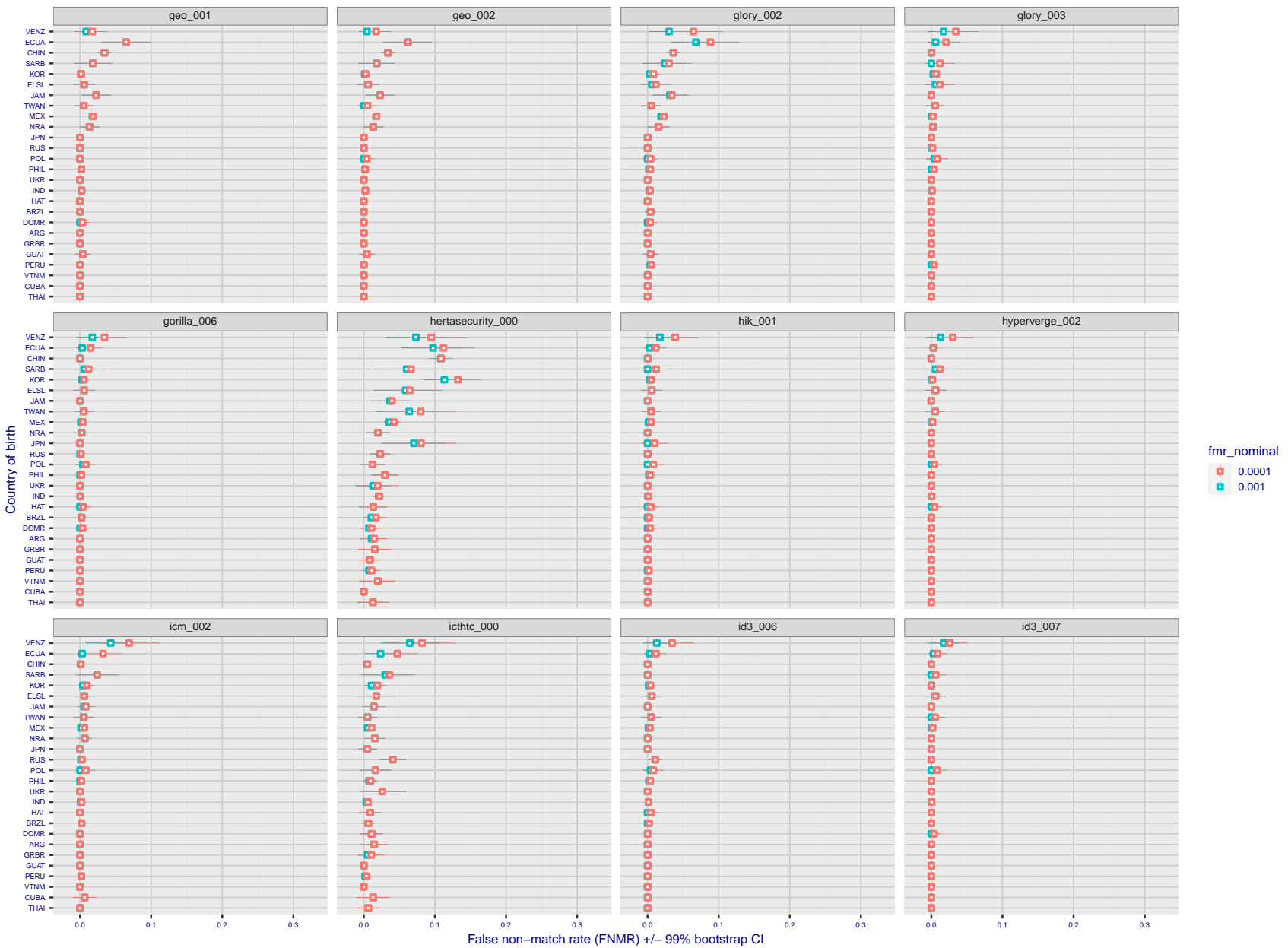


Figure 206: For the visa images, the dots show FNMR by country of birth for two globally set operating thresholds corresponding to $FMR = \{0.001, 0.0001\}$ computed over all on the order of 10^{10} impostor scores. The FMR in each bin will vary also - see subsequent impostor heatmaps in sec. 3.6.1. The figures shows an order of magnitude variation in FNMR across country of birth; these effects are likely due quality variations, then demographics like age and race. The error rates in some cases are zero, and in others the DET is flat so the error rates at the two thresholds are identical. The lines span 1% and 99% of bootstrap replicated FNMR estimates.

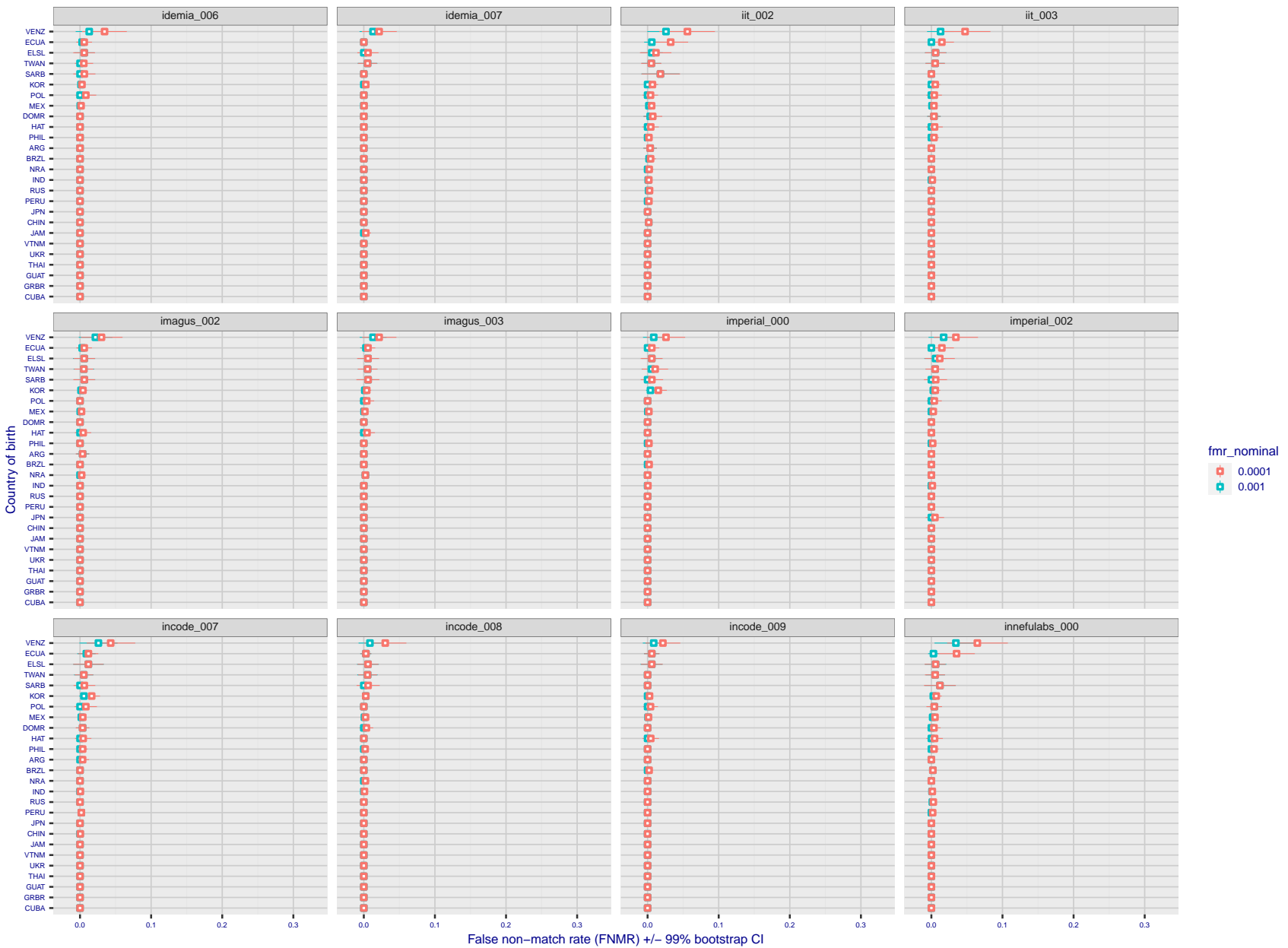


Figure 207: For the visa images, the dots show FNMR by country of birth for two globally set operating thresholds corresponding to $FMR = \{0.001, 0.0001\}$ computed over all on the order of 10^{10} impostor scores. The FMR in each bin will vary also - see subsequent impostor heatmaps in sec. 3.6.1. The figures shows an order of magnitude variation in FNMR across country of birth; these effects are likely due quality variations, then demographics like age and race. The error rates in some cases are zero, and in others the DET is flat so the error rates at the two thresholds are identical. The lines span 1% and 99% of bootstrap replicated FNMR estimates.

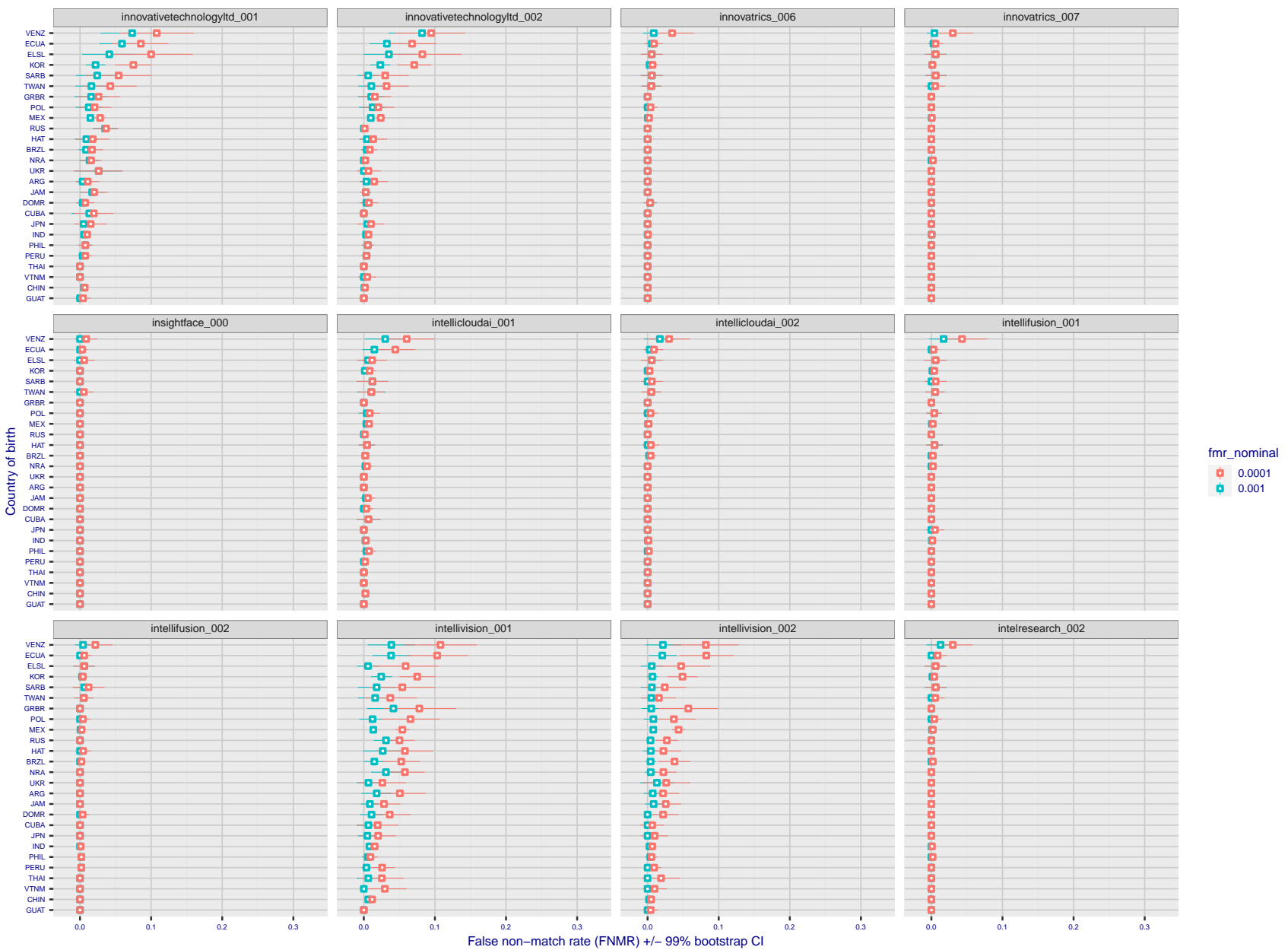


Figure 208: For the visa images, the dots show FNMR by country of birth for two globally set operating thresholds corresponding to $FMR = \{0.001, 0.0001\}$ computed over all on the order of 10^{10} impostor scores. The FMR in each bin will vary also - see subsequent impostor heatmaps in sec. 3.6.1. The figures shows an order of magnitude variation in FNMR across country of birth; these effects are likely due quality variations, then demographics like age and race. The error rates in some cases are zero, and in others the DET is flat so the error rates at the two thresholds are identical. The lines span 1% and 99% of bootstrap replicated FNMR estimates.

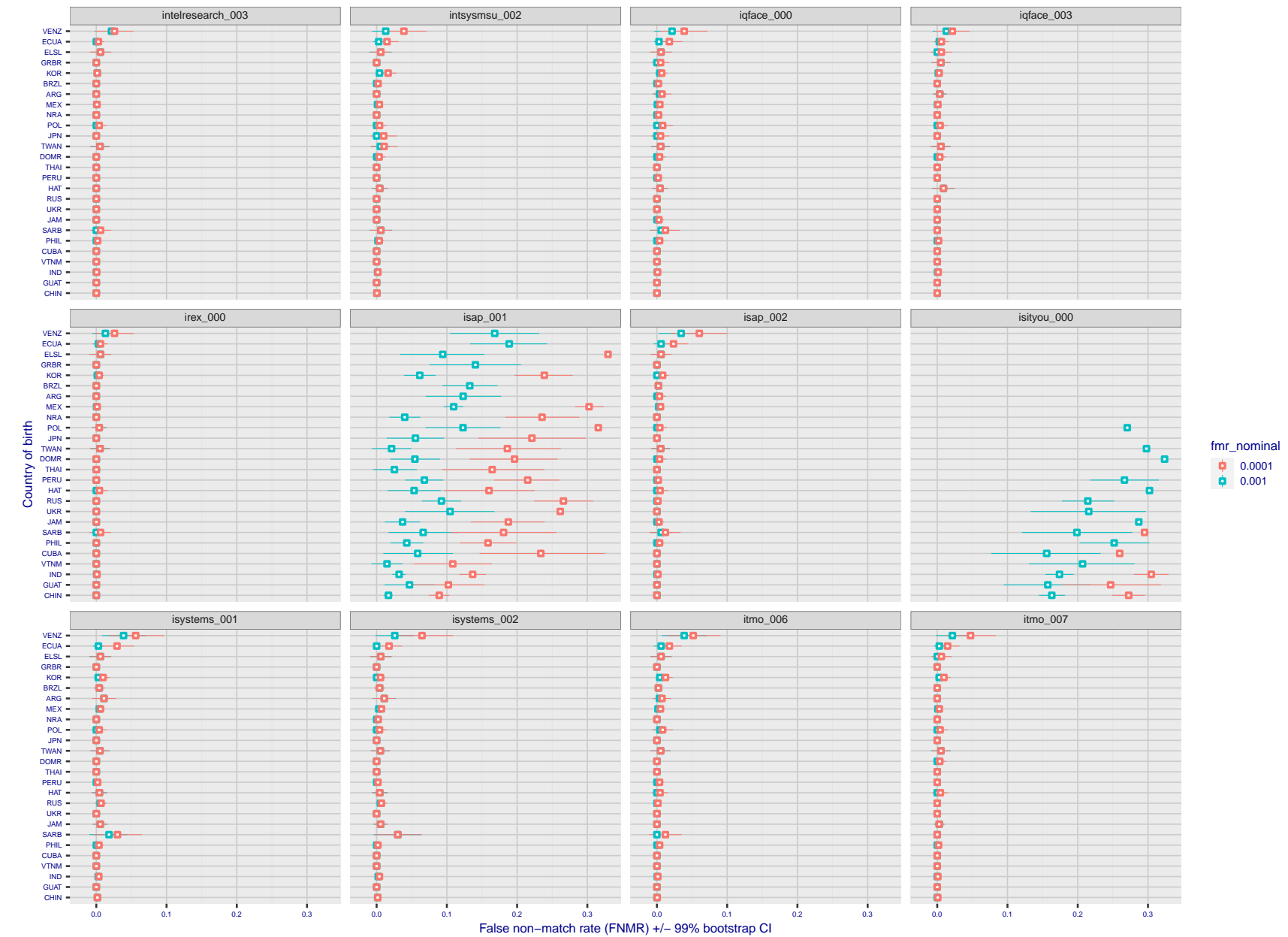


Figure 209: For the visa images, the dots show FNMR by country of birth for two globally set operating thresholds corresponding to $FMR = \{0.001, 0.0001\}$ computed over all on the order of 10^{10} impostor scores. The FMR in each bin will vary also - see subsequent impostor heatmaps in sec. 3.6.1. The figures shows an order of magnitude variation in FNMR across country of birth; these effects are likely due quality variations, then demographics like age and race. The error rates in some cases are zero, and in others the DET is flat so the error rates at the two thresholds are identical. The lines span 1% and 99% of bootstrap replicated FNMR estimates.

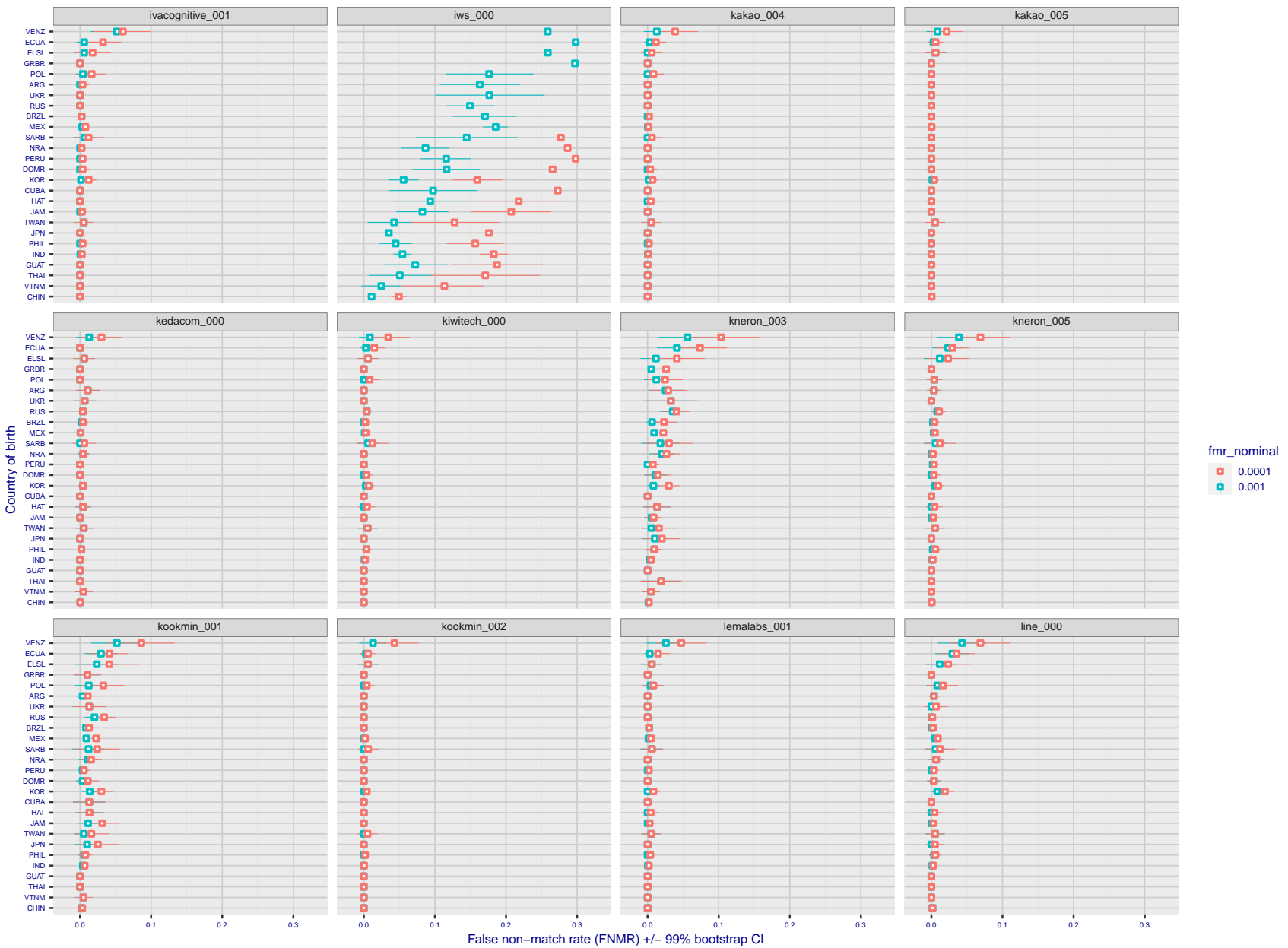


Figure 210: For the visa images, the dots show FNMR by country of birth for two globally set operating thresholds corresponding to $FMR = \{0.001, 0.0001\}$ computed over all on the order of 10^{10} impostor scores. The FMR in each bin will vary also - see subsequent impostor heatmaps in sec. 3.6.1. The figures shows an order of magnitude variation in FNMR across country of birth; these effects are likely due quality variations, then demographics like age and race. The error rates in some cases are zero, and in others the DET is flat so the error rates at the two thresholds are identical. The lines span 1% and 99% of bootstrap replicated FNMR estimates.

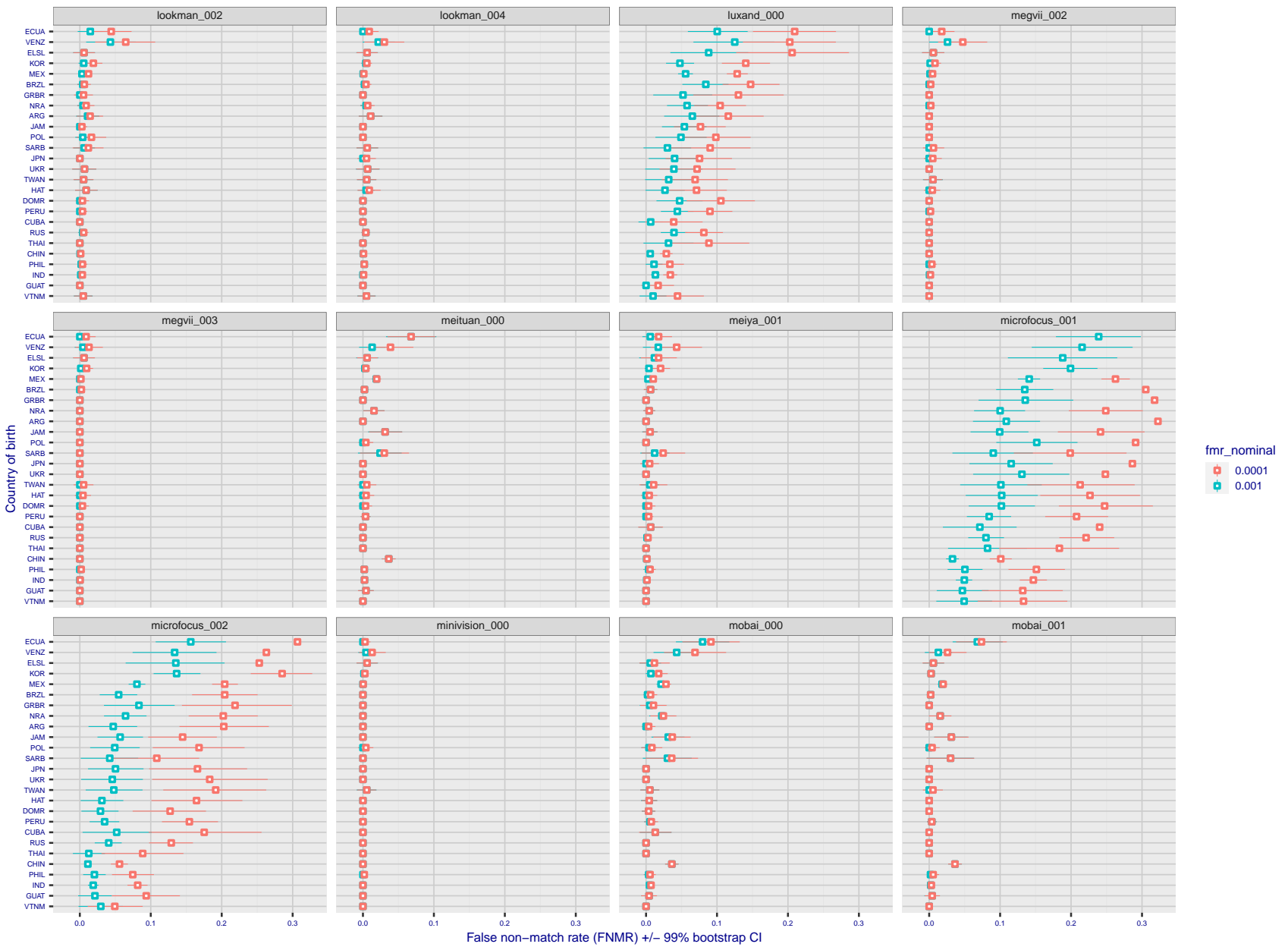


Figure 211: For the visa images, the dots show FNMR by country of birth for two globally set operating thresholds corresponding to $FMR = \{0.001, 0.0001\}$ computed over all on the order of 10^{10} impostor scores. The FMR in each bin will vary also - see subsequent impostor heatmaps in sec. 3.6.1. The figures shows an order of magnitude variation in FNMR across country of birth; these effects are likely due quality variations, then demographics like age and race. The error rates in some cases are zero, and in others the DET is flat so the error rates at the two thresholds are identical. The lines span 1% and 99% of bootstrap replicated FNMR estimates.

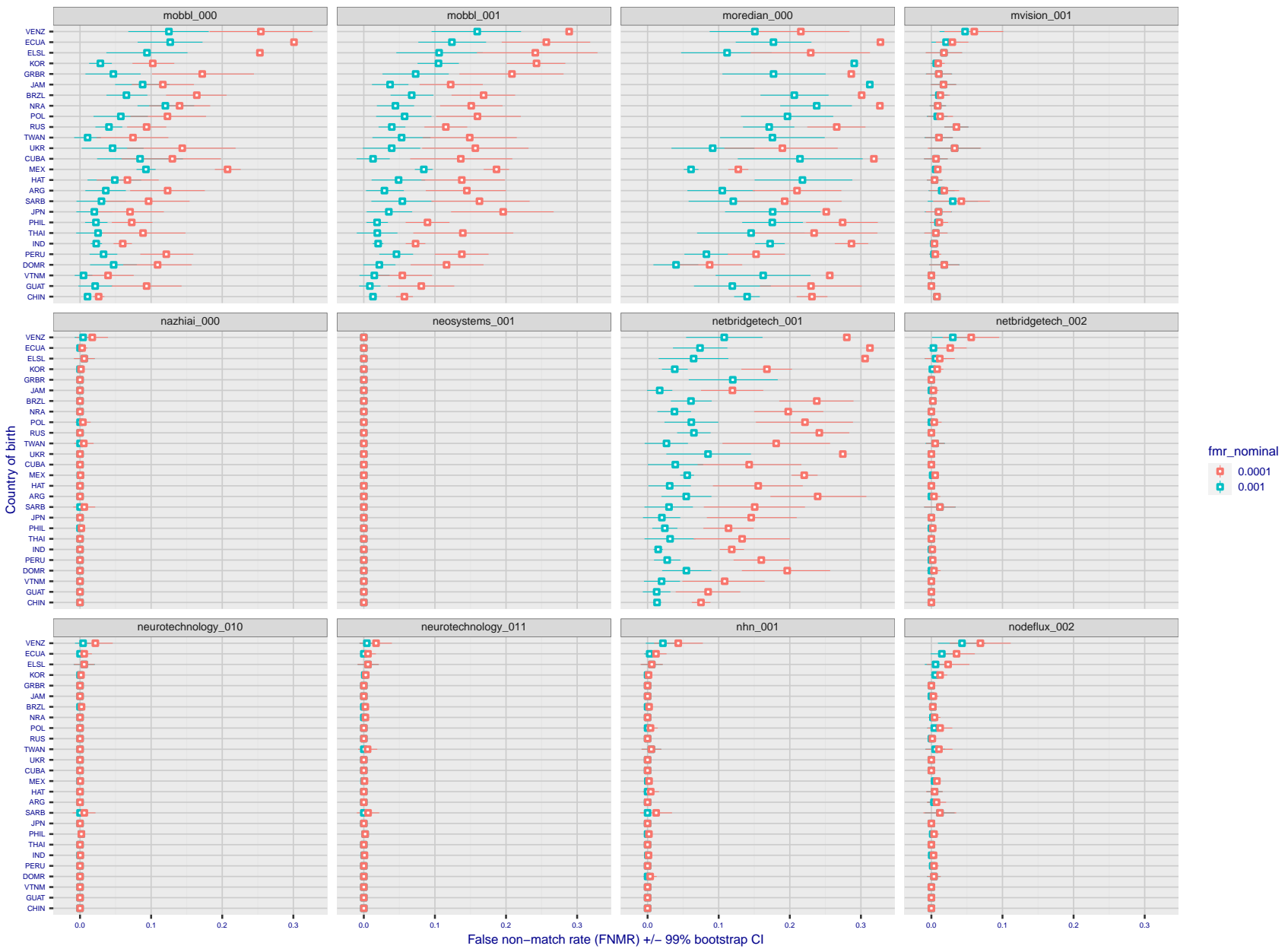


Figure 212: For the visa images, the dots show FNMR by country of birth for two globally set operating thresholds corresponding to $FMR = \{0.001, 0.0001\}$ computed over all on the order of 10^{10} impostor scores. The FMR in each bin will vary also - see subsequent impostor heatmaps in sec. 3.6.1. The figures shows an order of magnitude variation in FNMR across country of birth; these effects are likely due quality variations, then demographics like age and race. The error rates in some cases are zero, and in others the DET is flat so the error rates at the two thresholds are identical. The lines span 1% and 99% of bootstrap replicated FNMR estimates.

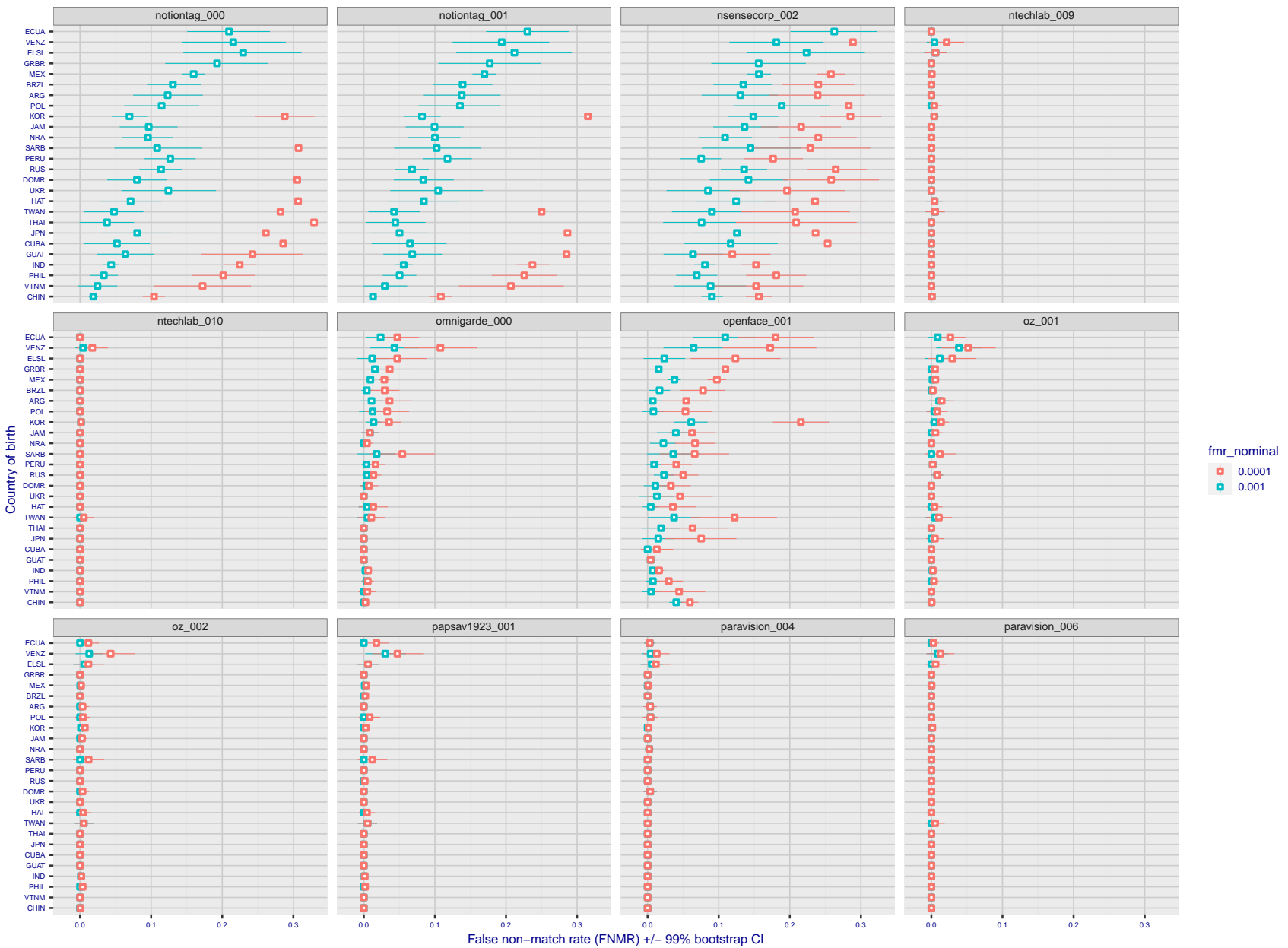


Figure 213: For the visa images, the dots show FNMR by country of birth for two globally set operating thresholds corresponding to $FMR = \{0.001, 0.0001\}$ computed over all on the order of 10^{10} impostor scores. The FMR in each bin will vary also - see subsequent impostor heatmaps in sec. 3.6.1. The figures shows an order of magnitude variation in FNMR across country of birth; these effects are likely due quality variations, then demographics like age and race. The error rates in some cases are zero, and in others the DET is flat so the error rates at the two thresholds are identical. The lines span 1% and 99% of bootstrap replicated FNMR estimates.

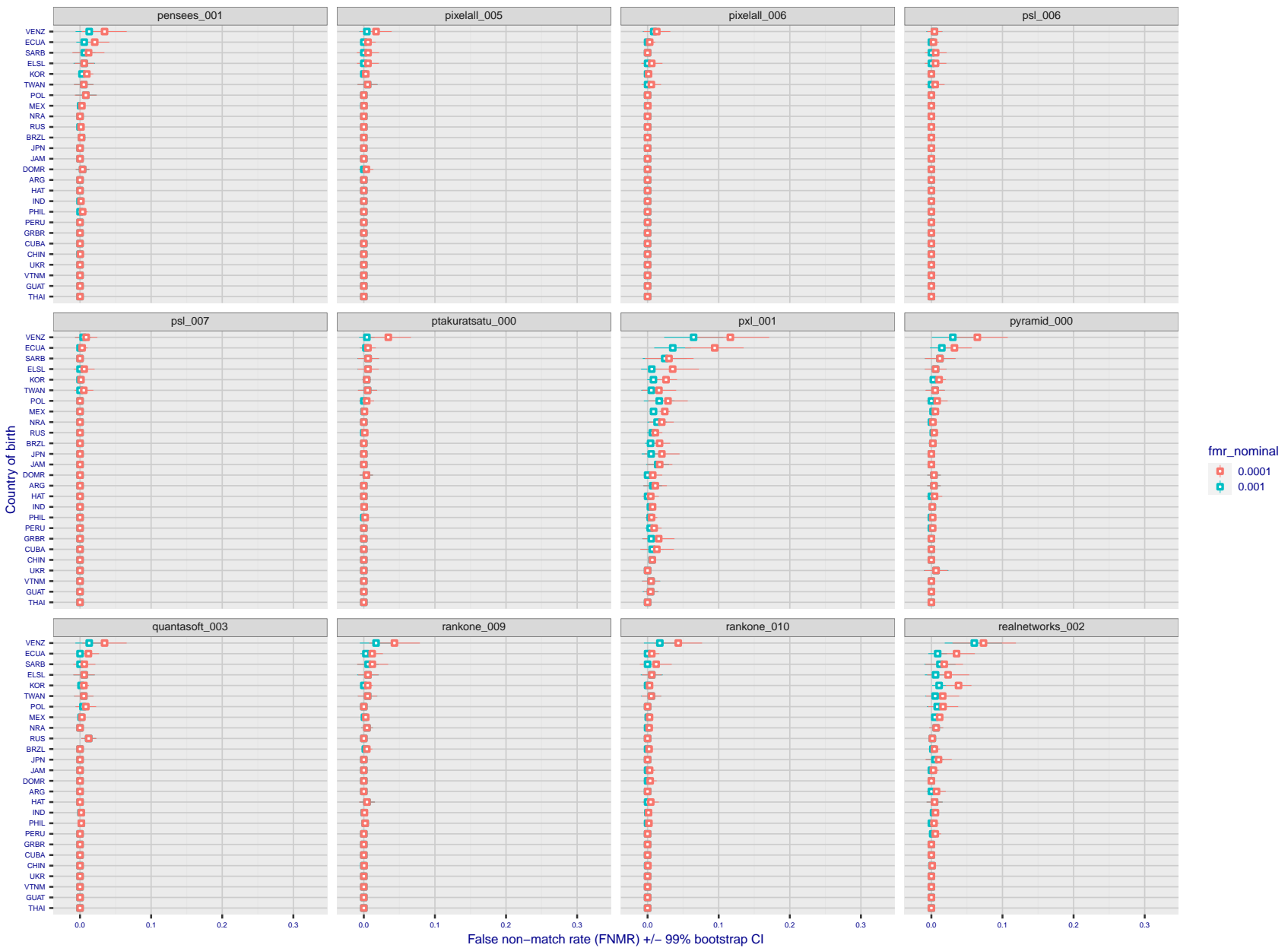


Figure 214: For the visa images, the dots show FNMR by country of birth for two globally set operating thresholds corresponding to $FMR = \{0.001, 0.0001\}$ computed over all on the order of 10^{10} impostor scores. The FMR in each bin will vary also - see subsequent impostor heatmaps in sec. 3.6.1. The figures shows an order of magnitude variation in FNMR across country of birth; these effects are likely due quality variations, then demographics like age and race. The error rates in some cases are zero, and in others the DET is flat so the error rates at the two thresholds are identical. The lines span 1% and 99% of bootstrap replicated FNMR estimates.

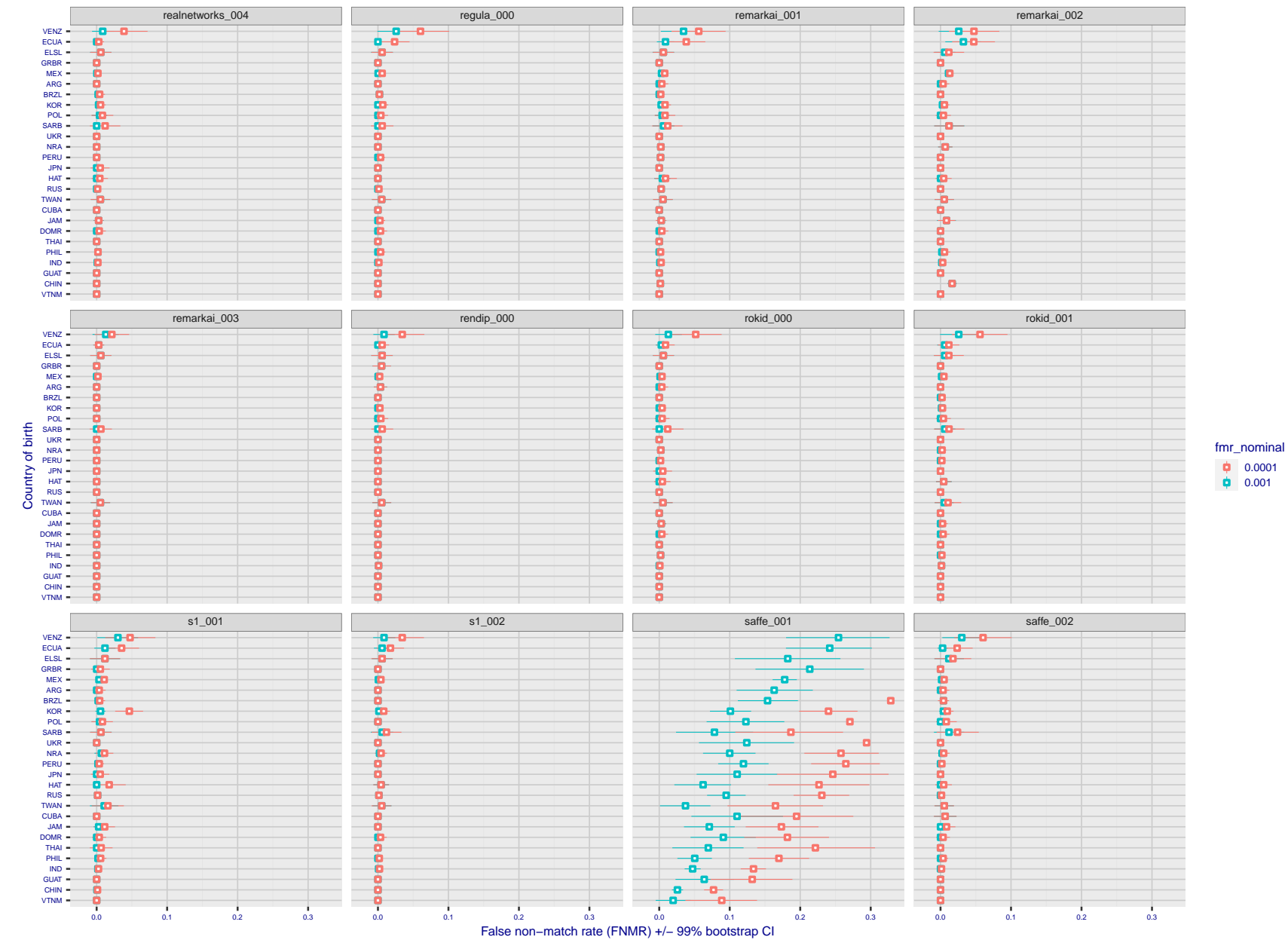


Figure 215: For the visa images, the dots show FNMR by country of birth for two globally set operating thresholds corresponding to $FMR = \{0.001, 0.0001\}$ computed over all on the order of 10^{10} impostor scores. The FMR in each bin will vary also - see subsequent impostor heatmaps in sec. 3.6.1. The figures shows an order of magnitude variation in FNMR across country of birth; these effects are likely due quality variations, then demographics like age and race. The error rates in some cases are zero, and in others the DET is flat so the error rates at the two thresholds are identical. The lines span 1% and 99% of bootstrap replicated FNMR estimates.

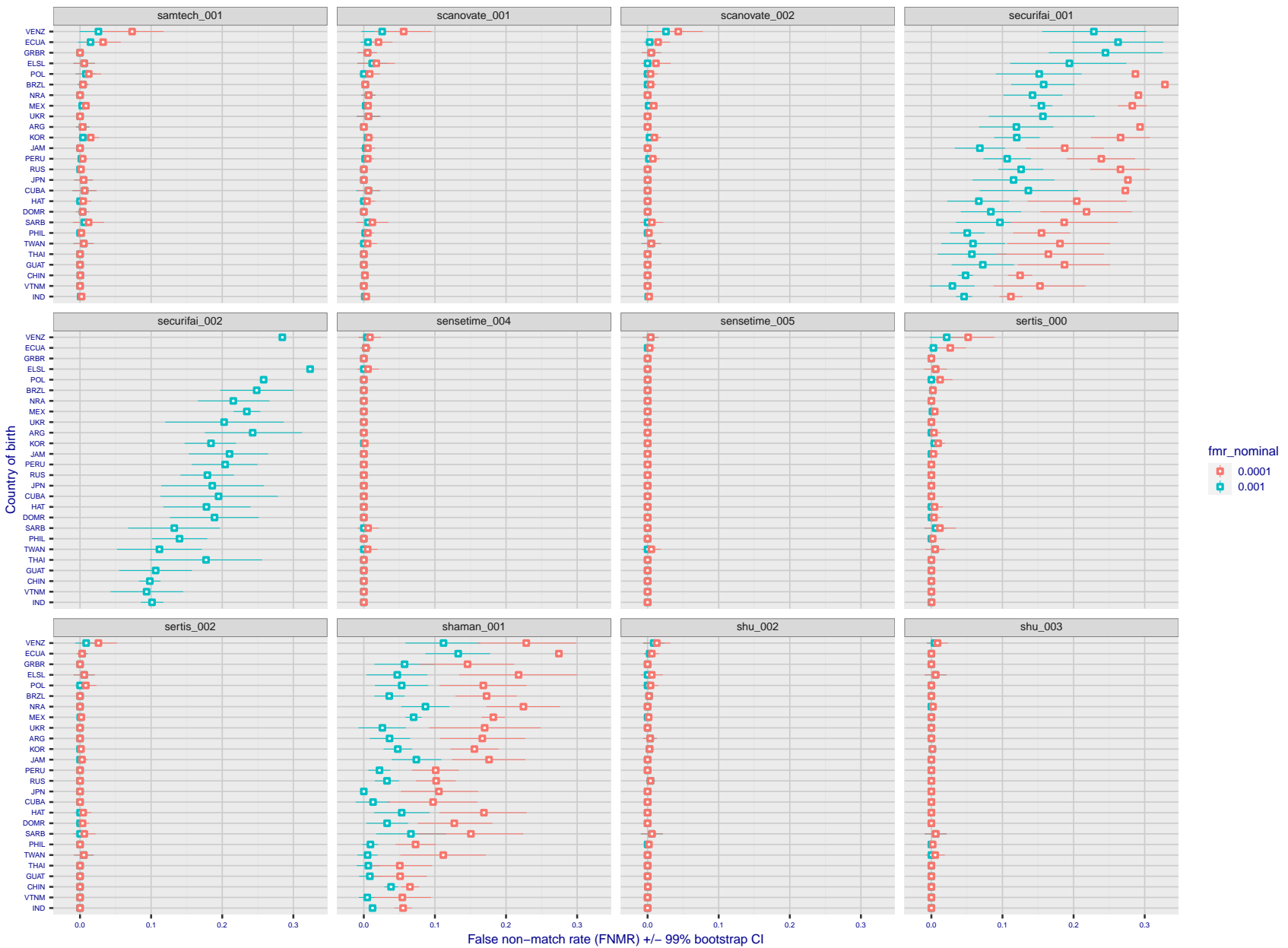


Figure 216: For the visa images, the dots show FNMR by country of birth for two globally set operating thresholds corresponding to $FMR = \{0.001, 0.0001\}$ computed over all on the order of 10^{10} impostor scores. The FMR in each bin will vary also - see subsequent impostor heatmaps in sec. 3.6.1. The figures shows an order of magnitude variation in FNMR across country of birth; these effects are likely due quality variations, then demographics like age and race. The error rates in some cases are zero, and in others the DET is flat so the error rates at the two thresholds are identical. The lines span 1% and 99% of bootstrap replicated FNMR estimates.

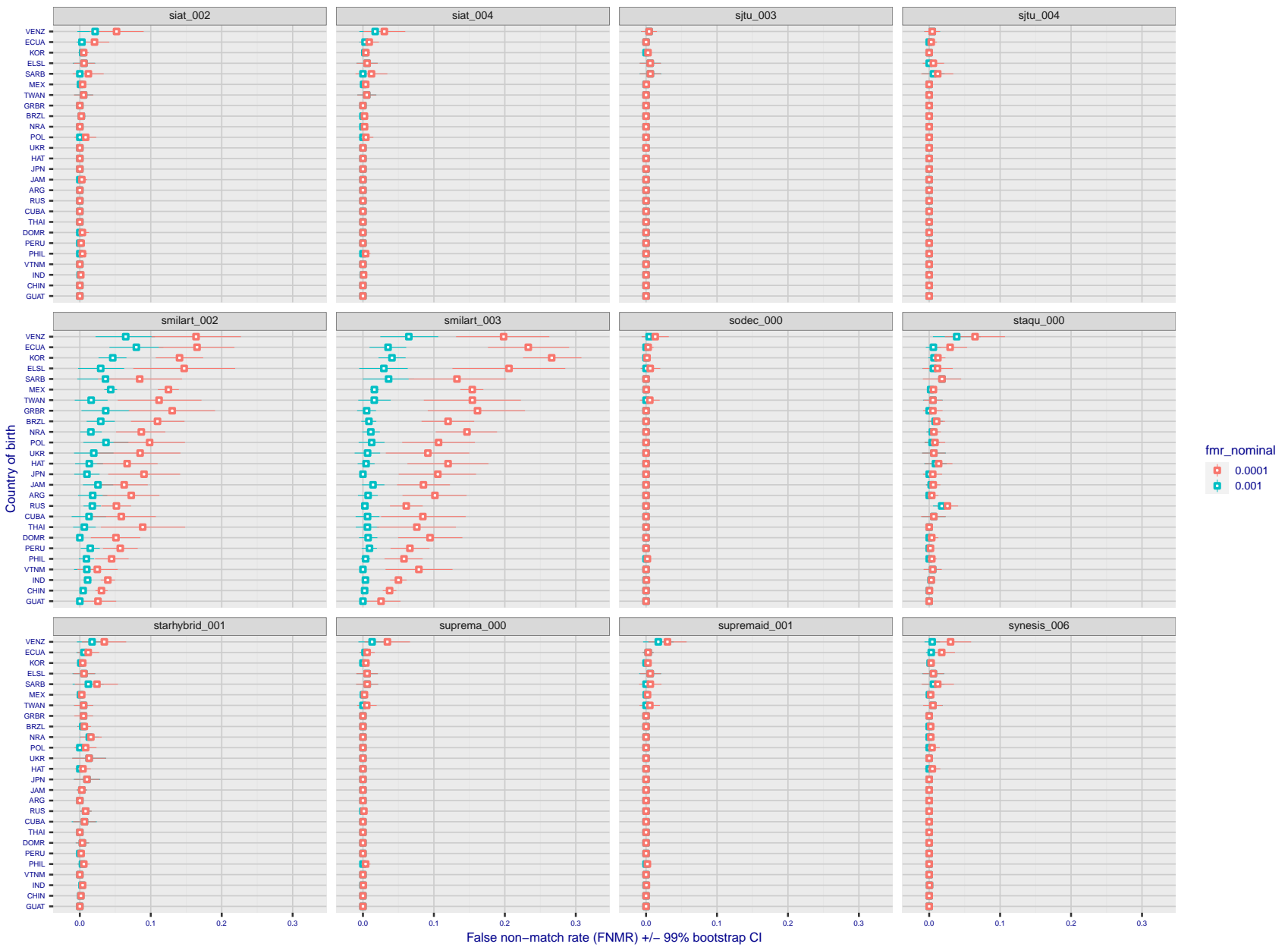


Figure 217: For the visa images, the dots show FNMR by country of birth for two globally set operating thresholds corresponding to $FMR = \{0.001, 0.0001\}$ computed over all on the order of 10^{10} impostor scores. The FMR in each bin will vary also - see subsequent impostor heatmaps in sec. 3.6.1. The figures shows an order of magnitude variation in FNMR across country of birth; these effects are likely due quality variations, then demographics like age and race. The error rates in some cases are zero, and in others the DET is flat so the error rates at the two thresholds are identical. The lines span 1% and 99% of bootstrap replicated FNMR estimates.

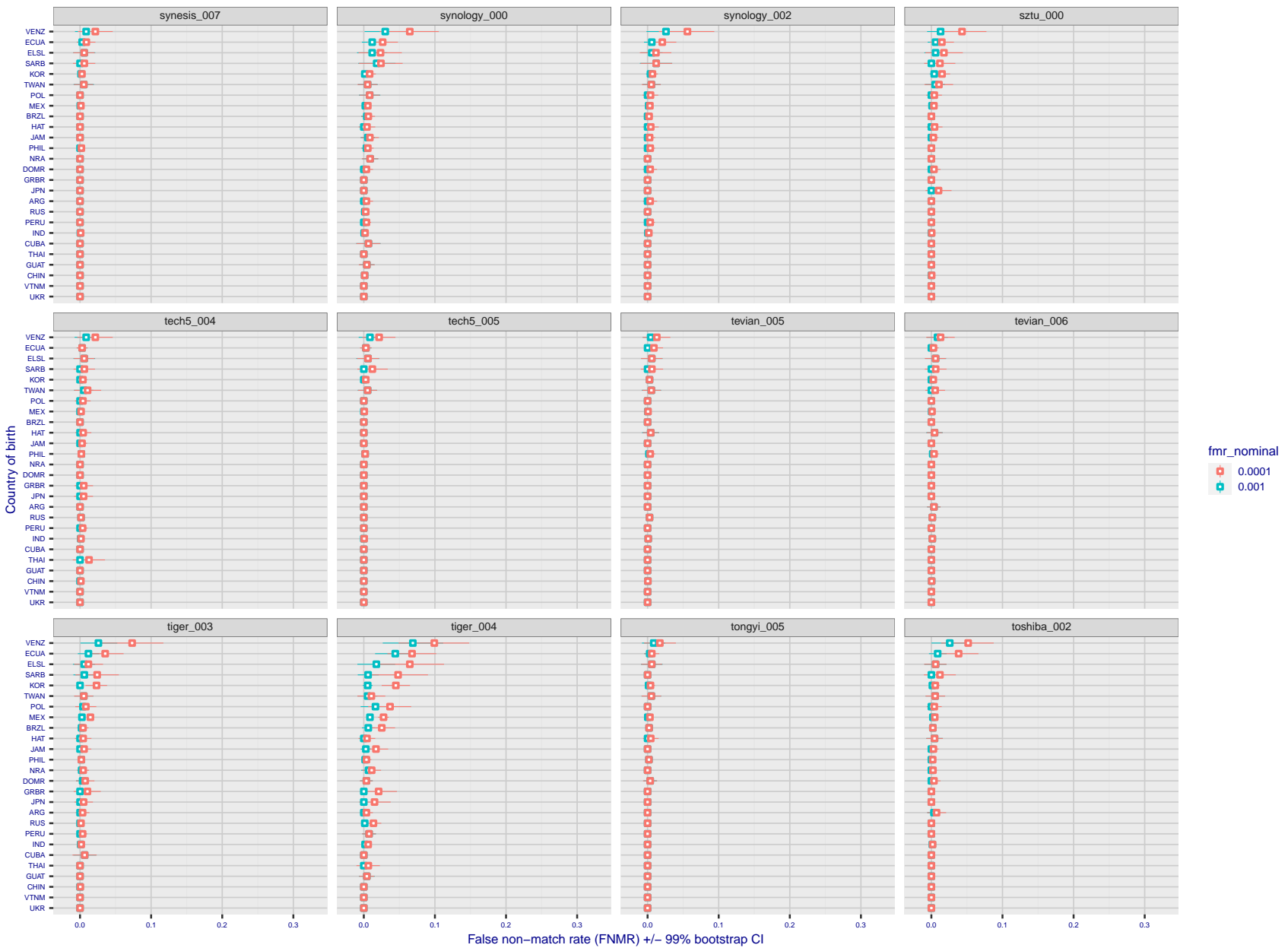


Figure 218: For the visa images, the dots show FNMR by country of birth for two globally set operating thresholds corresponding to $FMR = \{0.001, 0.0001\}$ computed over all on the order of 10^{10} impostor scores. The FMR in each bin will vary also - see subsequent impostor heatmaps in sec. 3.6.1. The figures shows an order of magnitude variation in FNMR across country of birth; these effects are likely due quality variations, then demographics like age and race. The error rates in some cases are zero, and in others the DET is flat so the error rates at the two thresholds are identical. The lines span 1% and 99% of bootstrap replicated FNMR estimates.

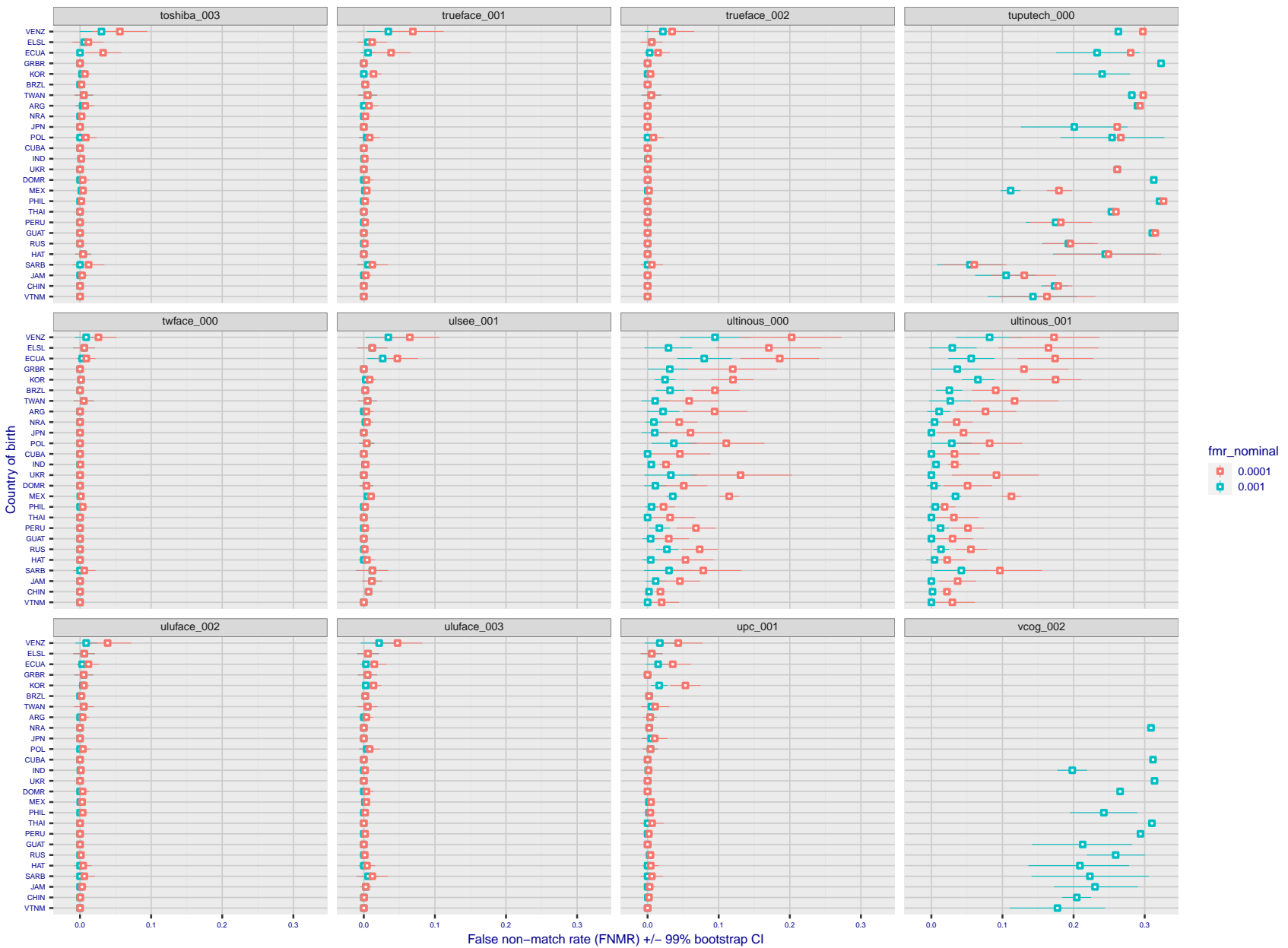


Figure 219: For the visa images, the dots show FNMR by country of birth for two globally set operating thresholds corresponding to $FMR = \{0.001, 0.0001\}$ computed over all on the order of 10^{10} impostor scores. The FMR in each bin will vary also - see subsequent impostor heatmaps in sec. 3.6.1. The figures shows an order of magnitude variation in FNMR across country of birth; these effects are likely due quality variations, then demographics like age and race. The error rates in some cases are zero, and in others the DET is flat so the error rates at the two thresholds are identical. The lines span 1% and 99% of bootstrap replicated FNMR estimates.

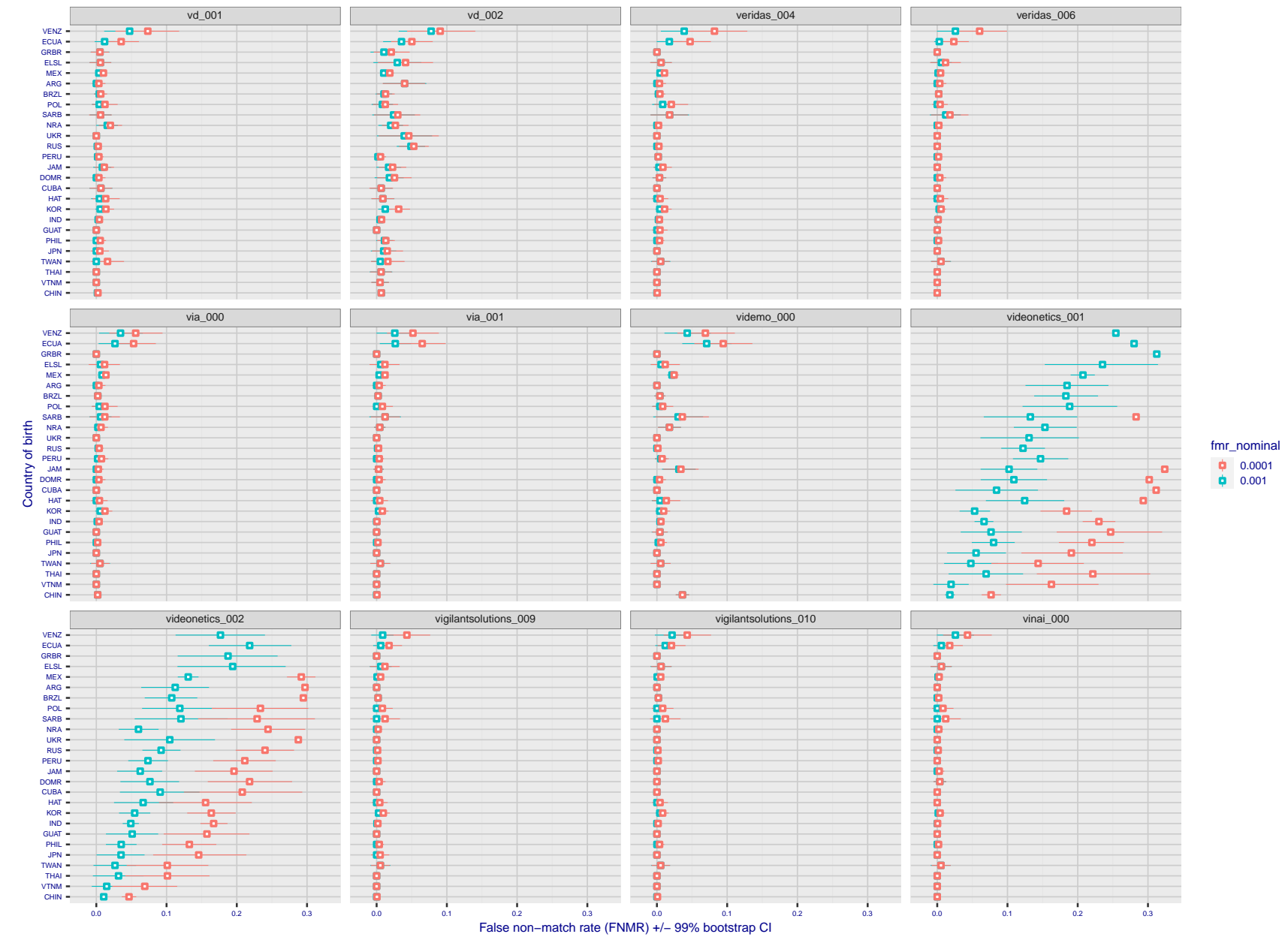


Figure 220: For the visa images, the dots show FNMR by country of birth for two globally set operating thresholds corresponding to $FMR = \{0.001, 0.0001\}$ computed over all on the order of 10^{10} impostor scores. The FMR in each bin will vary also - see subsequent impostor heatmaps in sec. 3.6.1. The figures shows an order of magnitude variation in FNMR across country of birth; these effects are likely due quality variations, then demographics like age and race. The error rates in some cases are zero, and in others the DET is flat so the error rates at the two thresholds are identical. The lines span 1% and 99% of bootstrap replicated FNMR estimates.

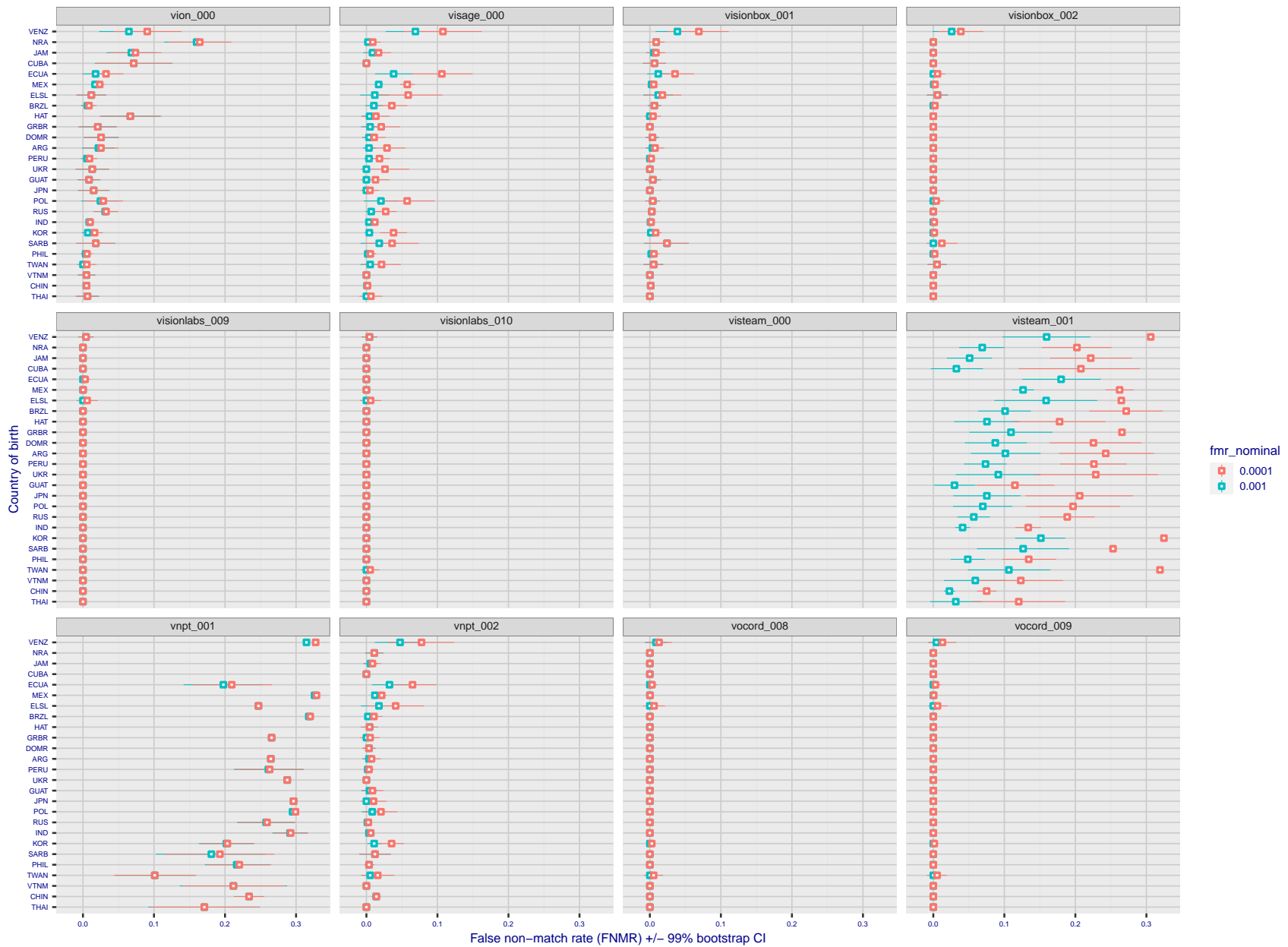


Figure 221: For the visa images, the dots show FNMR by country of birth for two globally set operating thresholds corresponding to $FMR = \{0.001, 0.0001\}$ computed over all on the order of 10^{10} impostor scores. The FMR in each bin will vary also - see subsequent impostor heatmaps in sec. 3.6.1. The figures shows an order of magnitude variation in FNMR across country of birth; these effects are likely due quality variations, then demographics like age and race. The error rates in some cases are zero, and in others the DET is flat so the error rates at the two thresholds are identical. The lines span 1% and 99% of bootstrap replicated FNMR estimates.

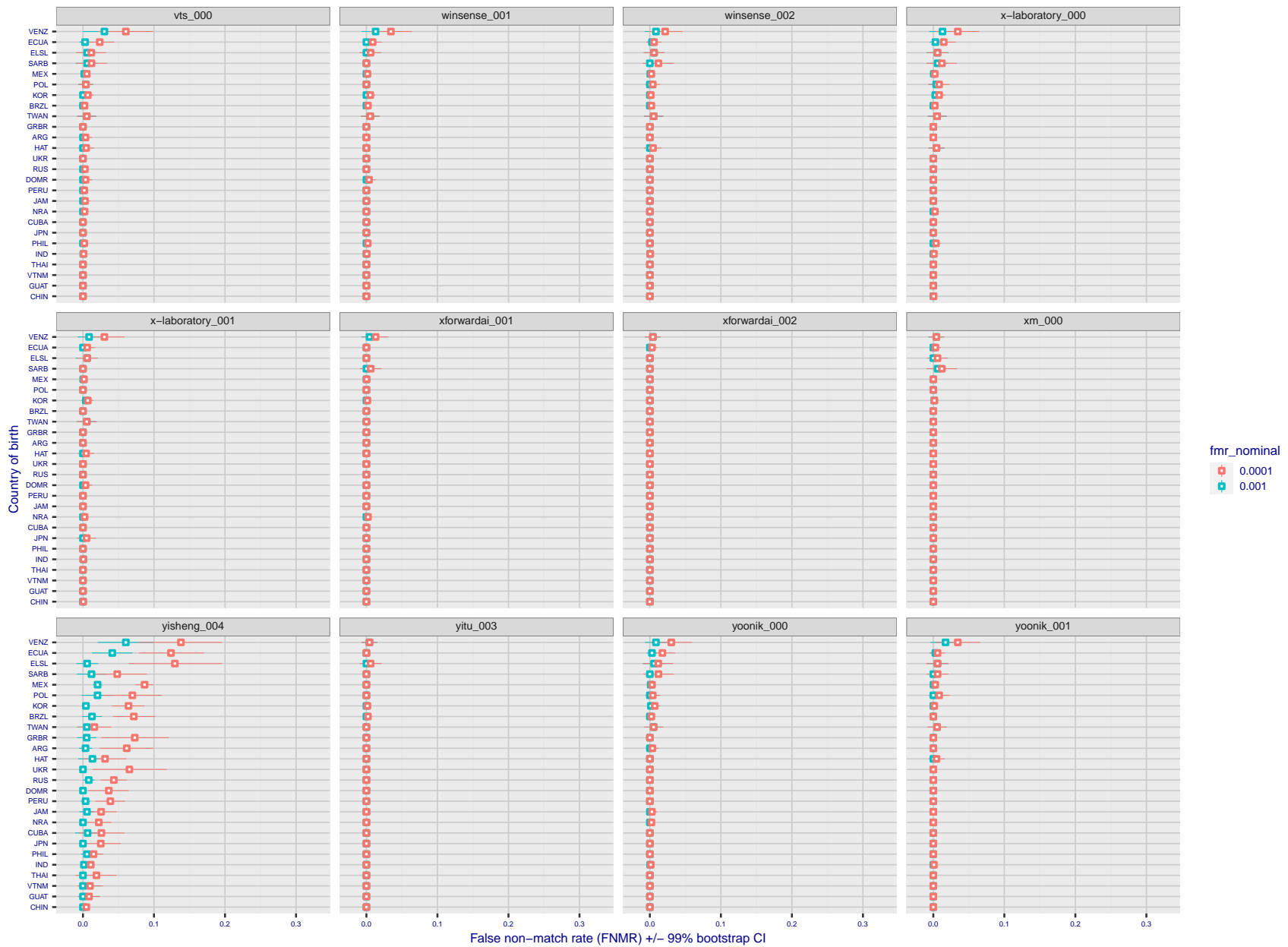


Figure 222: For the visa images, the dots show FNMR by country of birth for two globally set operating thresholds corresponding to $FMR = \{0.001, 0.0001\}$ computed over all on the order of 10^{10} impostor scores. The FMR in each bin will vary also - see subsequent impostor heatmaps in sec. 3.6.1. The figures shows an order of magnitude variation in FNMR across country of birth; these effects are likely due quality variations, then demographics like age and race. The error rates in some cases are zero, and in others the DET is flat so the error rates at the two thresholds are identical. The lines span 1% and 99% of bootstrap replicated FNMR estimates.

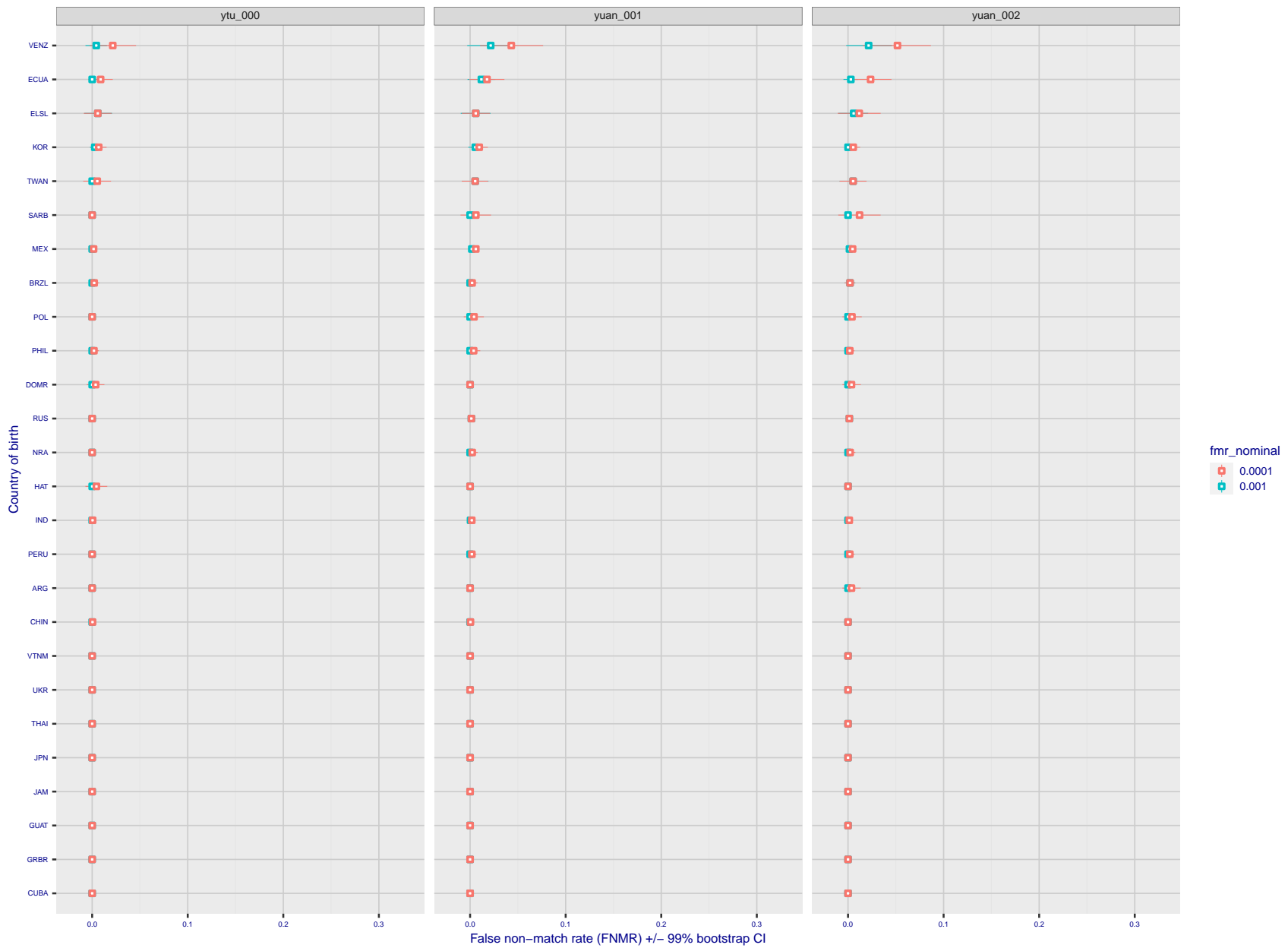


Figure 223: For the visa images, the dots show FNMR by country of birth for two globally set operating thresholds corresponding to $FMR = \{0.001, 0.0001\}$ computed over all on the order of 10^{10} impostor scores. The FMR in each bin will vary also - see subsequent impostor heatmaps in sec. 3.6.1. The figures shows an order of magnitude variation in FNMR across country of birth; these effects are likely due quality variations, then demographics like age and race. The error rates in some cases are zero, and in others the DET is flat so the error rates at the two thresholds are identical. The lines span 1% and 99% of bootstrap replicated FNMR estimates.

Caveats: The results may not relate to subject-specific properties. Instead they could reflect image-specific quality differences, which could occur due to collection protocol or software processing variations.

3.5.2 Effect of ageing

Background: Faces change appearance throughout life. This change gradually reduces similarity of a new image to an earlier image. Face recognition algorithms give reduced similarity scores and more frequent false rejections.

Goal: To quantify false non-match rates (FNMR) as a function of elapsed time in an adult population.

Methods: Using the mugshot images, a threshold is set to give FMR = 0.00001 over the entire impostor set. Then FNMR is measured over 1000 bootstrap replications of the genuine scores.

Results: For the visa images, Figure 243 shows how false non-match rates for genuine users, as a function of age group.

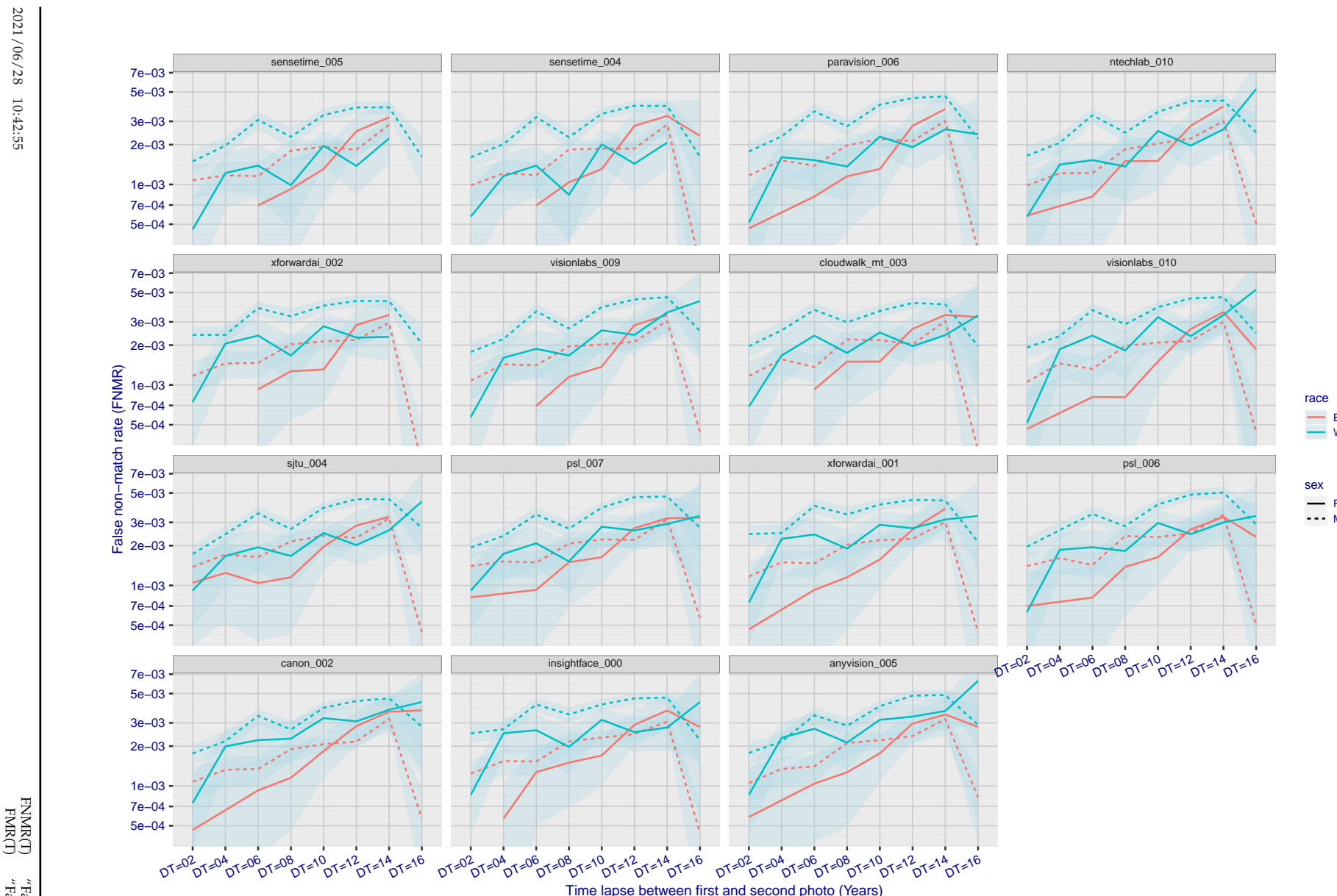


Figure 224: For the mugshot images, FNMR as a function of elapsed time between initial enrollment and second verification images. The panels appear most accurate first, and vertical scale changes on each page. The four traces correspond to images annotated with codes for black female, black male, white female, white male. The threshold is fixed for each algorithm to give FMR = 0.00001 over all (10^8) impostor comparisons. For short time-lapses, the most accurate algorithms give very few errors (FNMR < 0.001) so that the uncertainty estimates are high.

2021/06/28 10:42:55

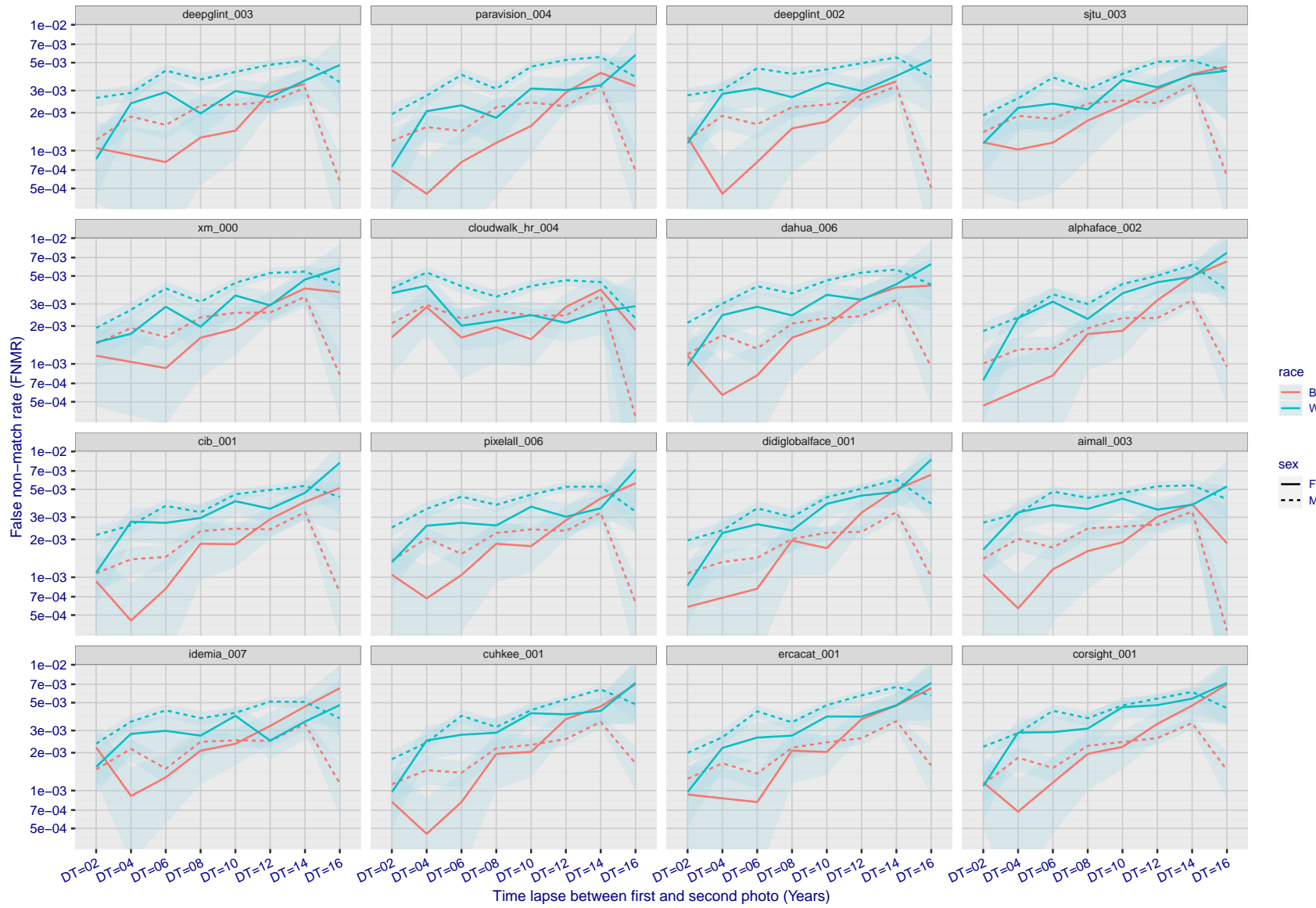


Figure 225: For the mugshot images, FNMR as a function of elapsed time between initial enrollment and second verification images. The panels appear most accurate first, and vertical scale changes on each page. The four traces correspond to images annotated with codes for black female, black male, white female, white male. The threshold is fixed for each algorithm to give $FMR = 0.00001$ over all (10^8) impostor comparisons. For short time-lapses, the most accurate algorithms give very few errors ($FNMR < 0.001$) so that the uncertainty estimates are high.

FNMR(T)
"False match rate"
"False non-match rate"

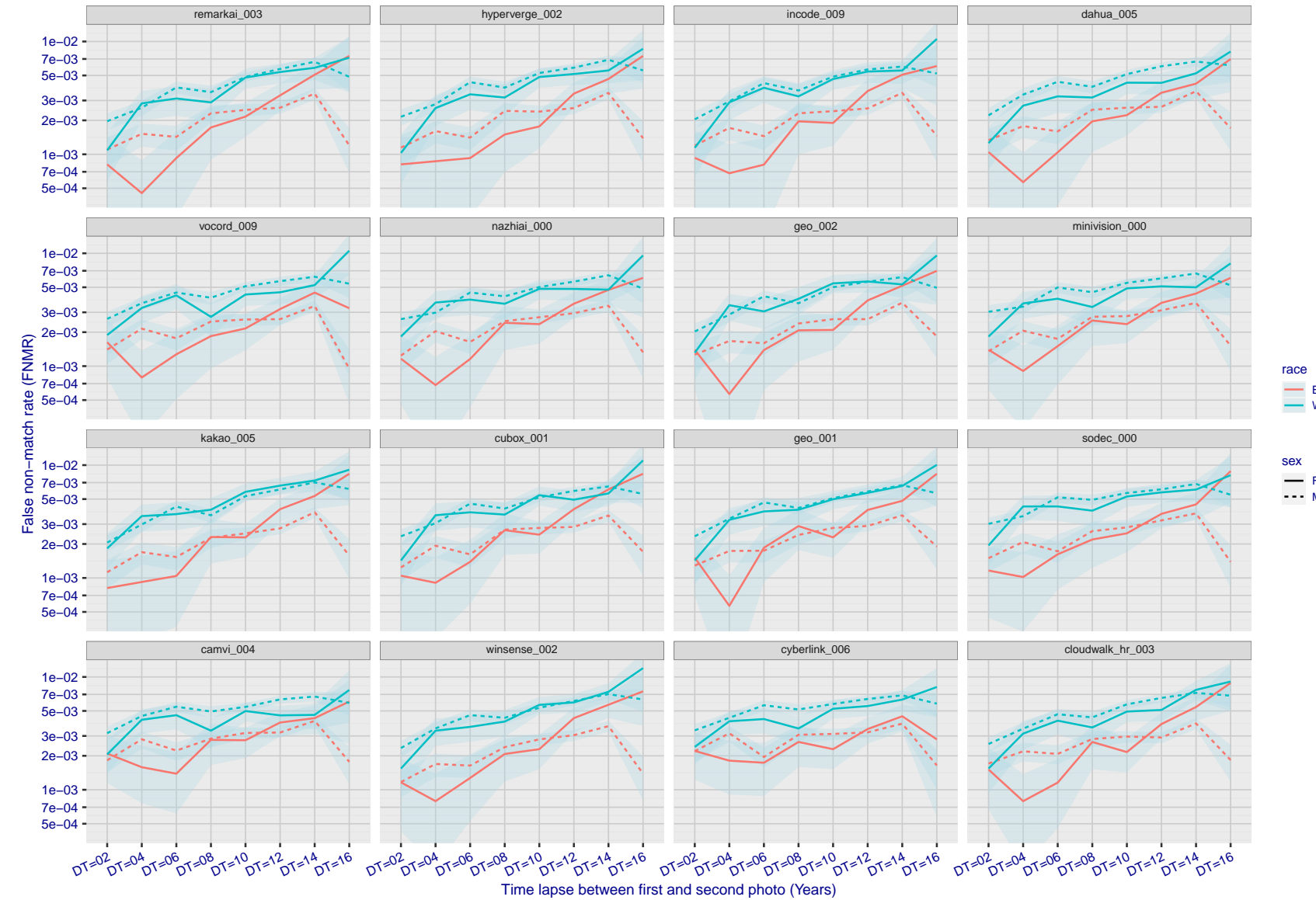


Figure 226: For the mugshot images, FNMR as a function of elapsed time between initial enrollment and second verification images. The panels appear most accurate first, and vertical scale changes on each page. The four traces correspond to images annotated with codes for black female, black male, white female, white male. The threshold is fixed for each algorithm to give $\text{FMR} = 0.00001$ over all (10^8) impostor comparisons. For short time-lapses, the most accurate algorithms give very few errors ($\text{FNMR} < 0.001$) so that the uncertainty estimates are high.

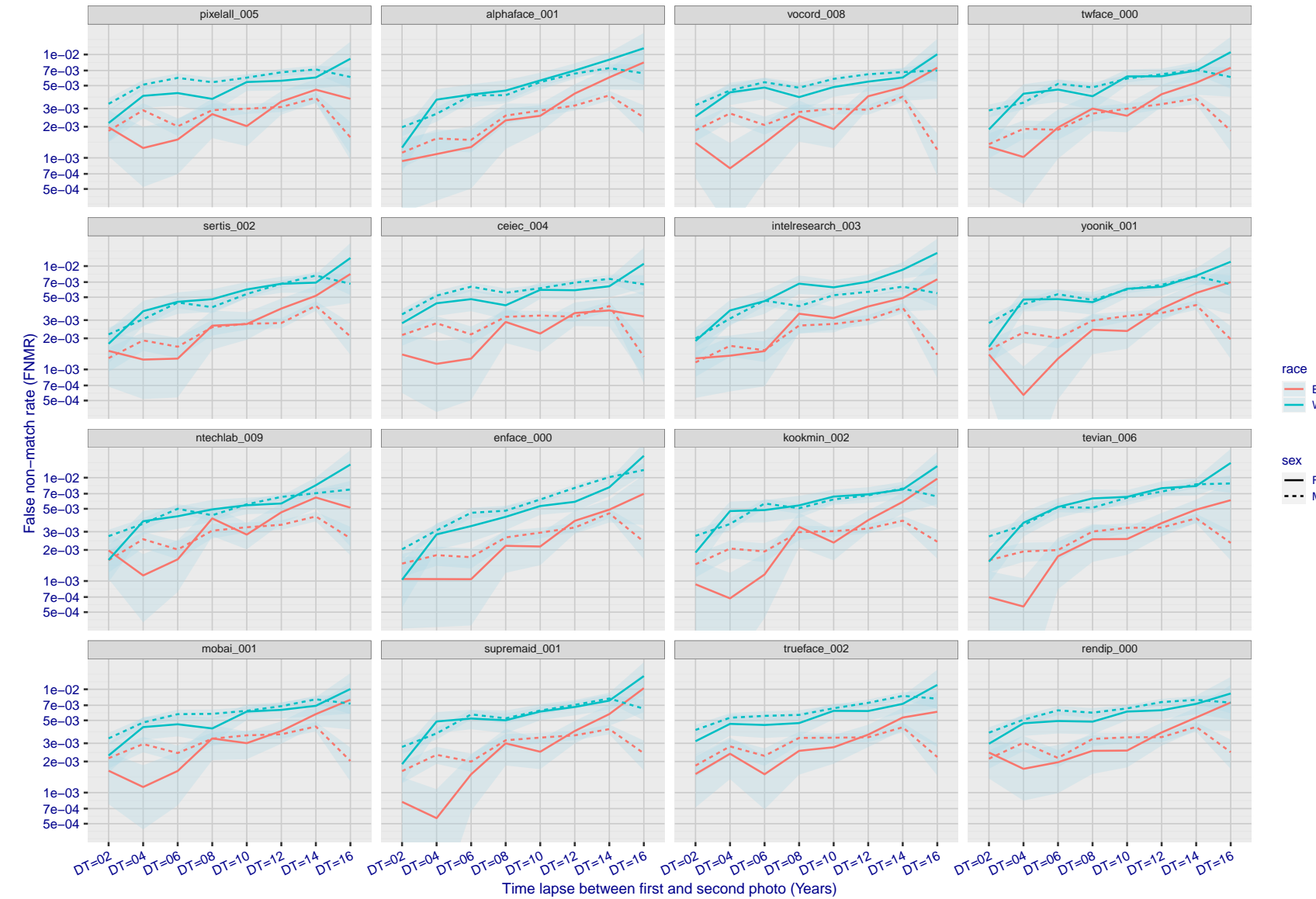


Figure 227: For the mugshot images, FNMR as a function of elapsed time between initial enrollment and second verification images. The panels appear most accurate first, and vertical scale changes on each page. The four traces correspond to images annotated with codes for black female, black male, white female, white male. The threshold is fixed for each algorithm to give FMR = 0.00001 over all (10^8) impostor comparisons. For short time-lapses, the most accurate algorithms give very few errors (FNMR < 0.001) so that the uncertainty estimates are high.

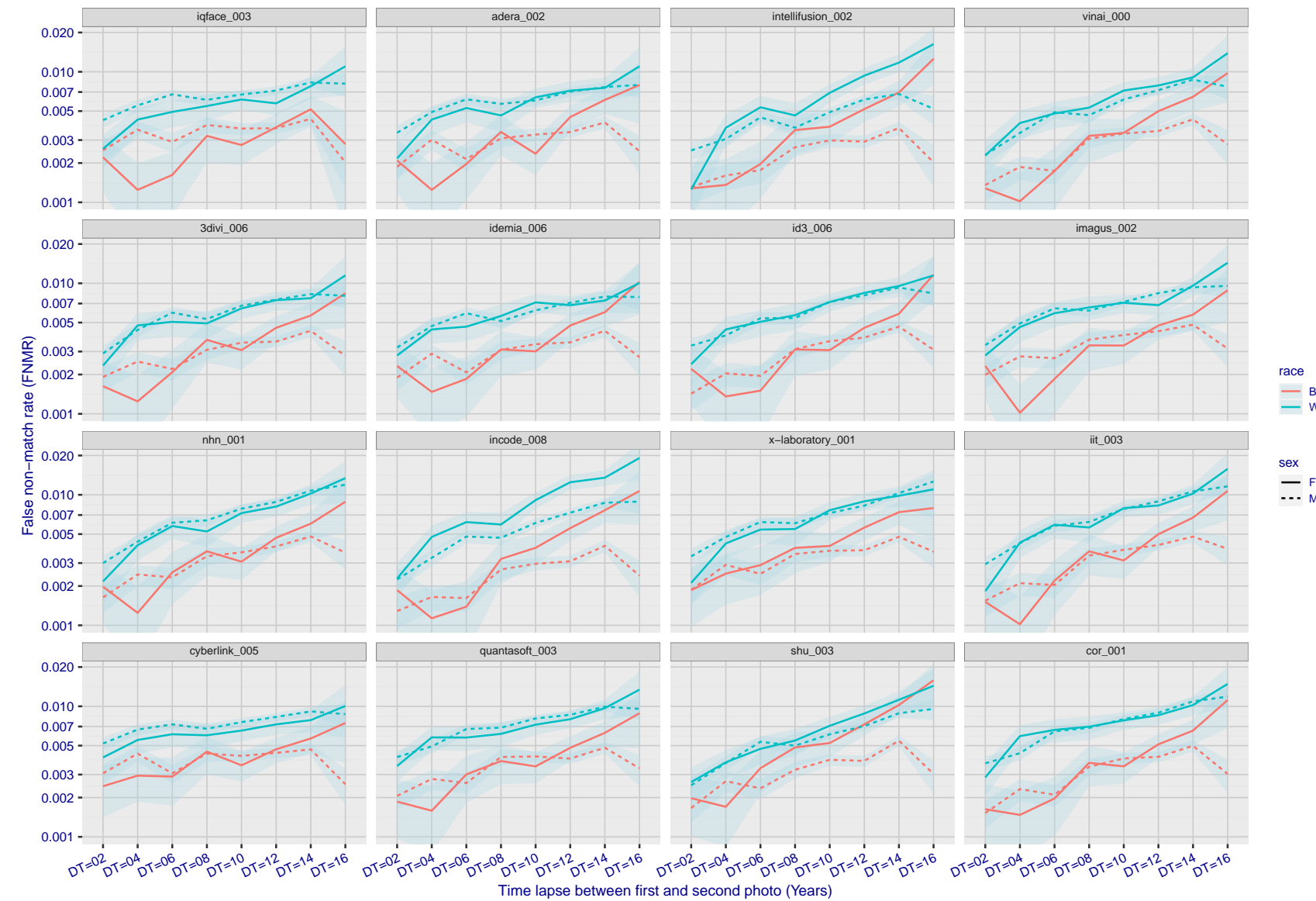


Figure 228: For the mugshot images, FNMR as a function of elapsed time between initial enrollment and second verification images. The panels appear most accurate first, and vertical scale changes on each page. The four traces correspond to images annotated with codes for black female, black male, white female, white male. The threshold is fixed for each algorithm to give $FMR = 0.00001$ over all (10^8) impostor comparisons. For short time-lapses, the most accurate algorithms give very few errors ($FNMR < 0.001$) so that the uncertainty estimates are high.

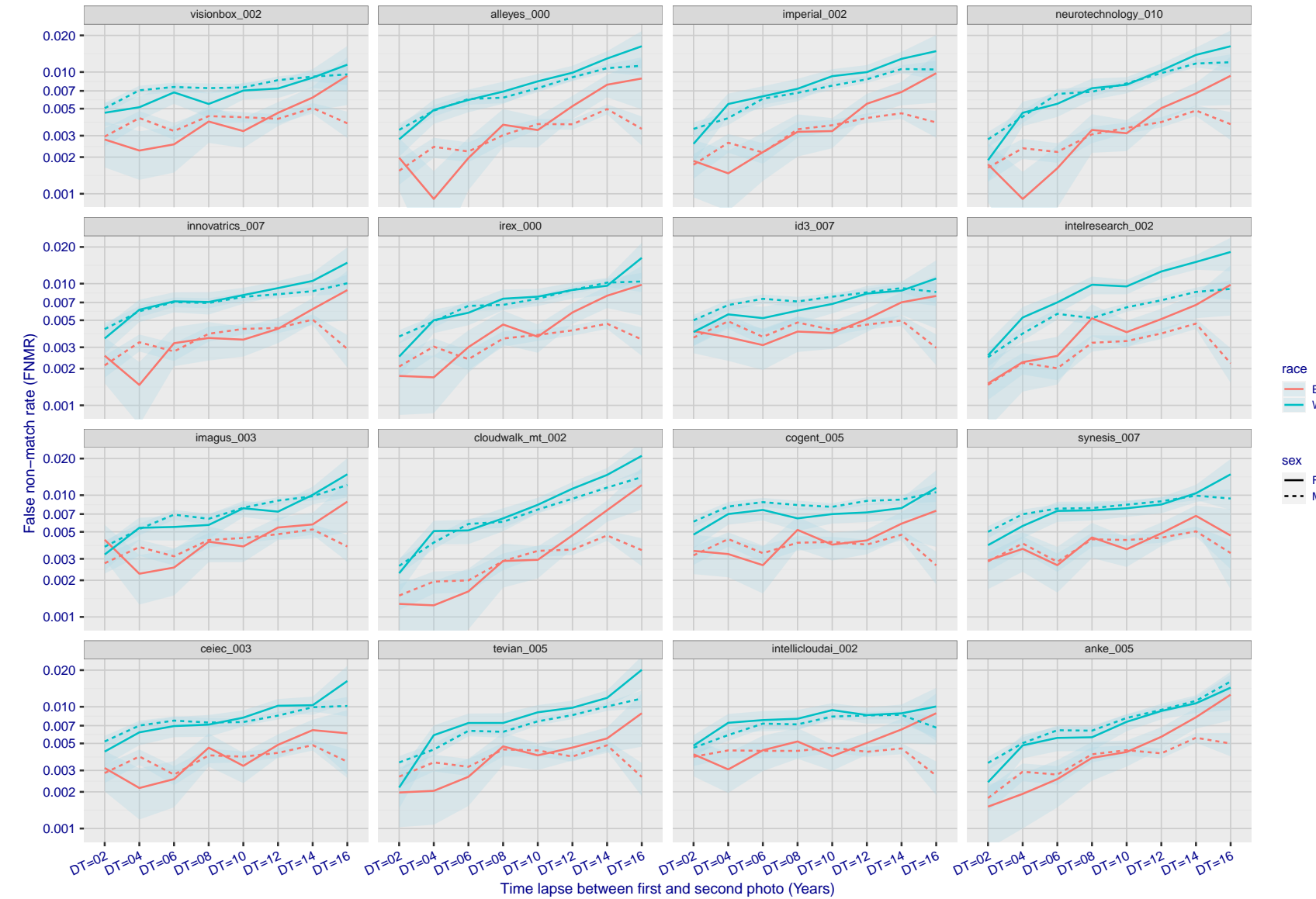


Figure 229: For the mugshot images, FNMR as a function of elapsed time between initial enrollment and second verification images. The panels appear most accurate first, and vertical scale changes on each page. The four traces correspond to images annotated with codes for black female, black male, white female, white male. The threshold is fixed for each algorithm to give FMR = 0.00001 over all (10^8) impostor comparisons. For short time-lapses, the most accurate algorithms give very few errors (FNMR < 0.001) so that the uncertainty estimates are high.

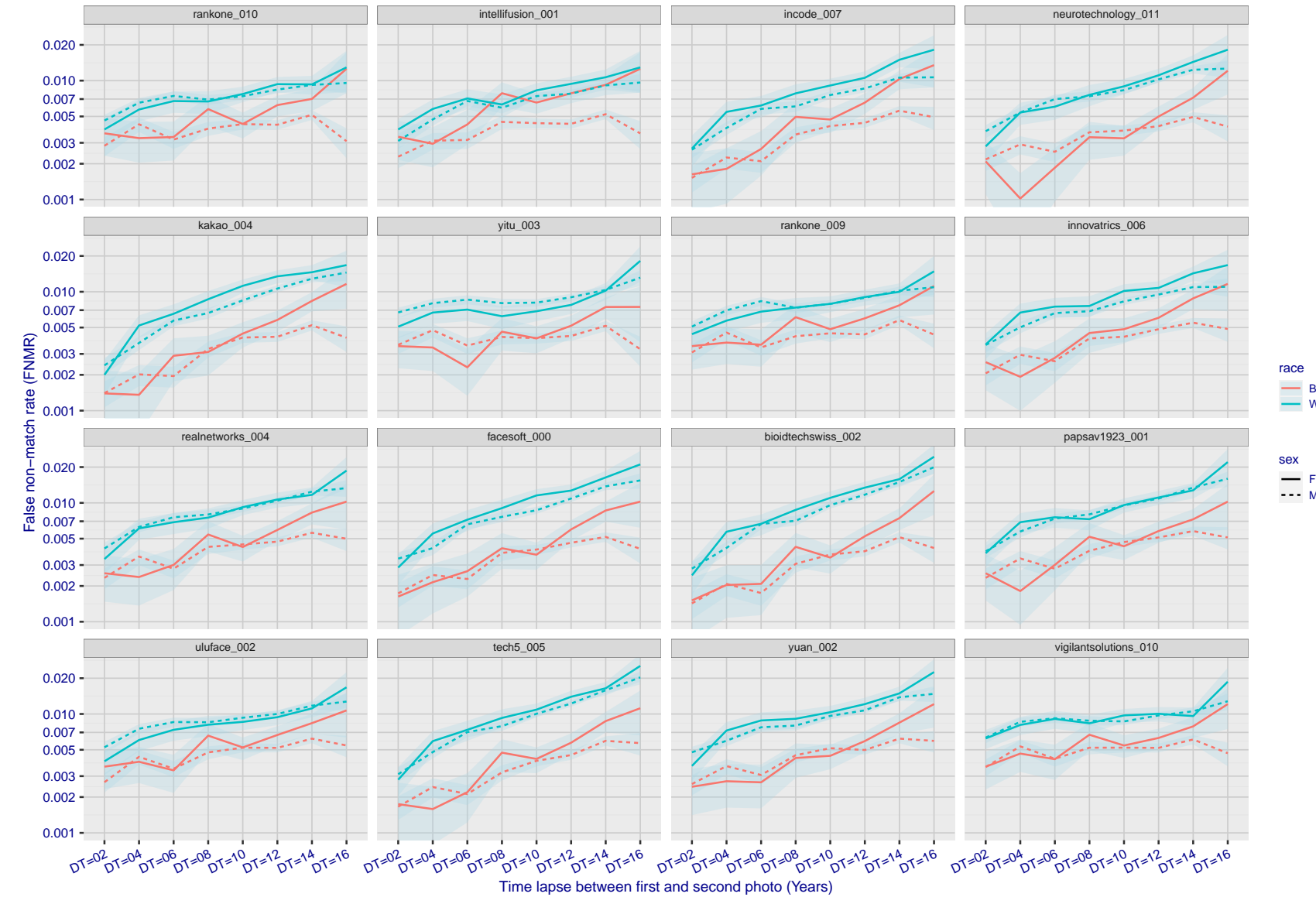


Figure 230: For the mugshot images, FNMR as a function of elapsed time between initial enrollment and second verification images. The panels appear most accurate first, and vertical scale changes on each page. The four traces correspond to images annotated with codes for black female, black male, white female, white male. The threshold is fixed for each algorithm to give FMR = 0.00001 over all (10^8) impostor comparisons. For short time-lapses, the most accurate algorithms give very few errors (FNMR < 0.001) so that the uncertainty estimates are high.

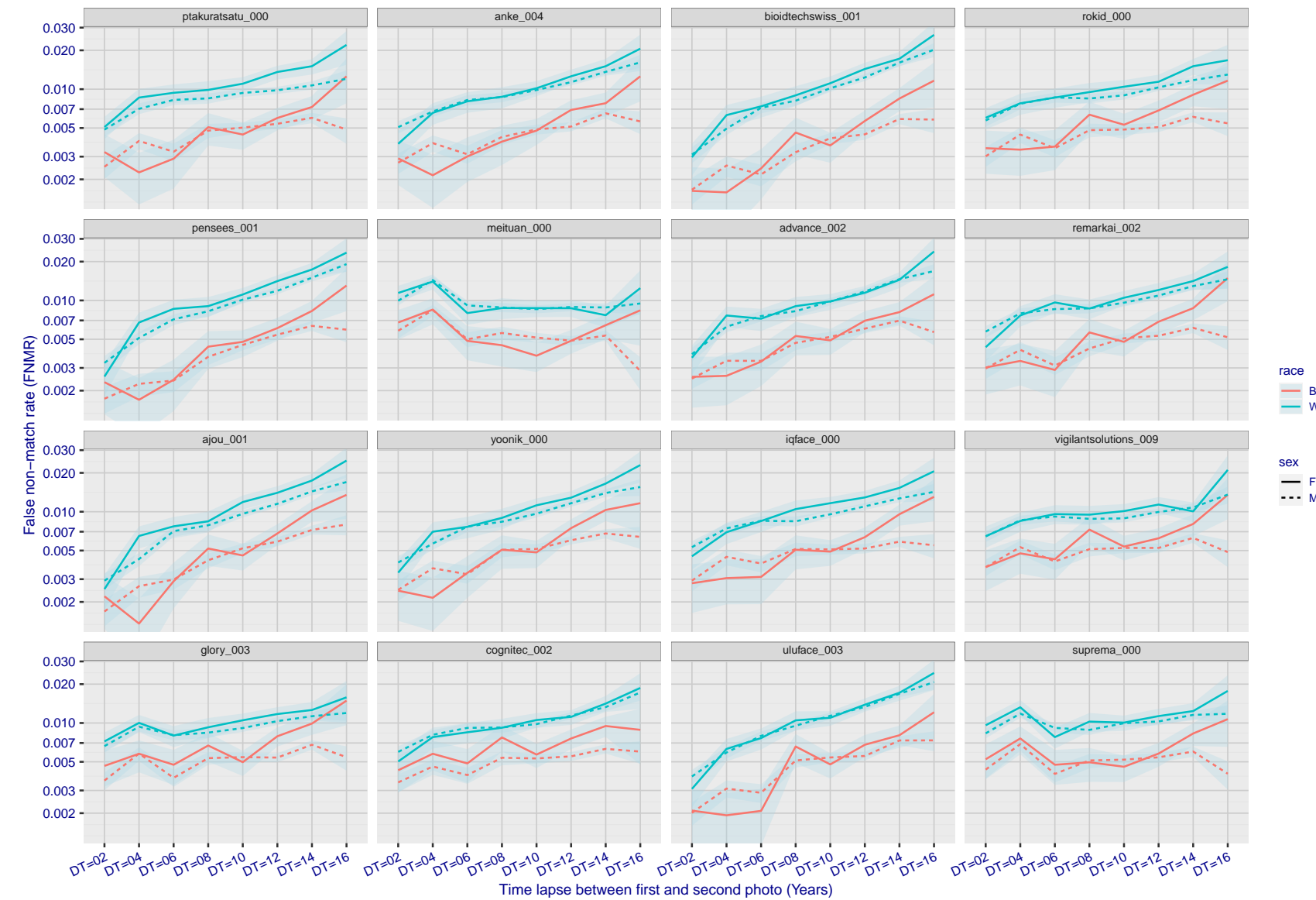


Figure 231: For the mugshot images, FNMR as a function of elapsed time between initial enrollment and second verification images. The panels appear most accurate first, and vertical scale changes on each page. The four traces correspond to images annotated with codes for black female, black male, white female, white male. The threshold is fixed for each algorithm to give FMR = 0.00001 over all (10^8) impostor comparisons. For short time-lapses, the most accurate algorithms give very few errors (FNMR < 0.001) so that the uncertainty estimates are high.

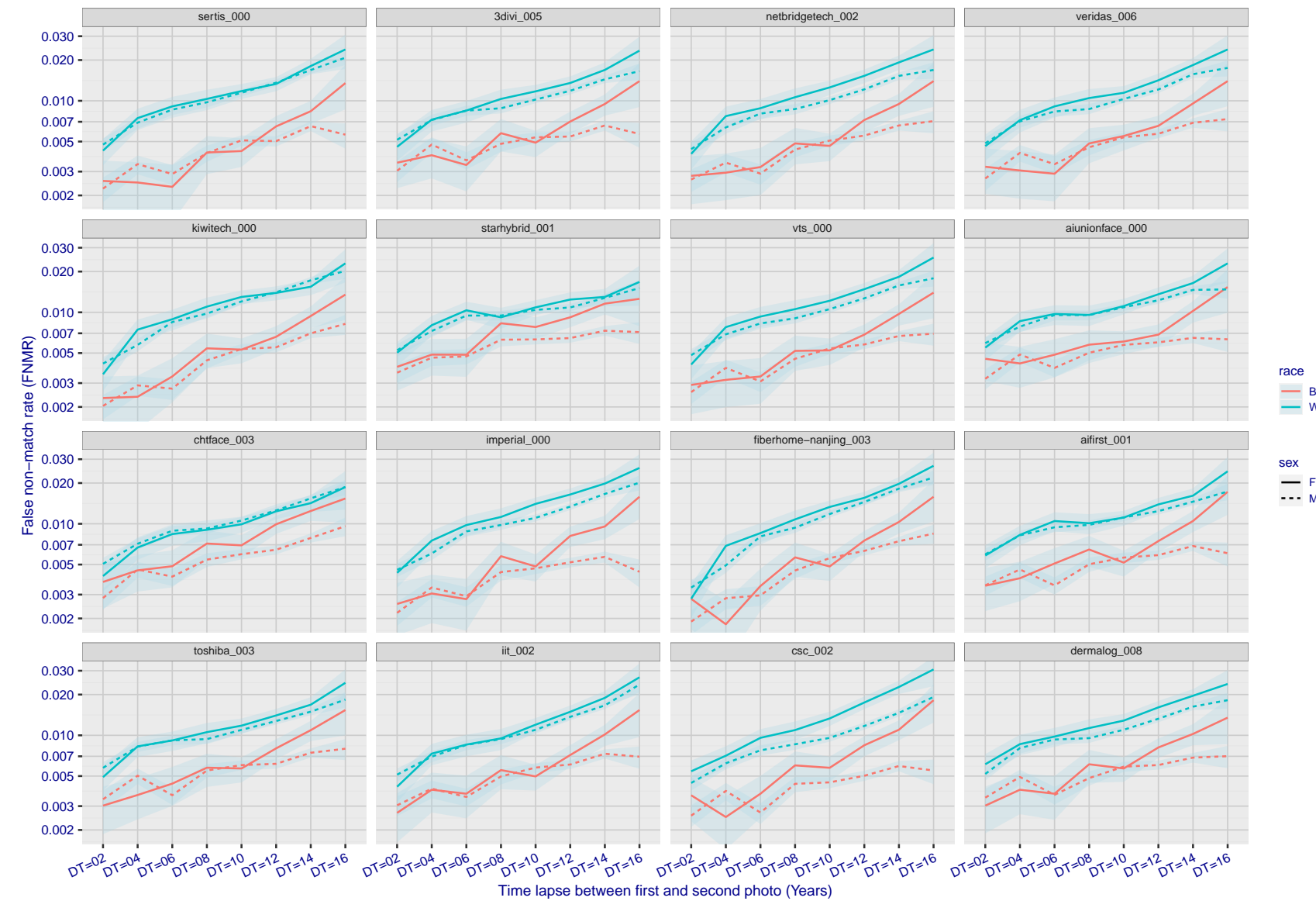


Figure 232: For the mugshot images, FNMR as a function of elapsed time between initial enrollment and second verification images. The panels appear most accurate first, and vertical scale changes on each page. The four traces correspond to images annotated with codes for black female, black male, white female, white male. The threshold is fixed for each algorithm to give FMR = 0.00001 over all (10^8) impostor comparisons. For short time-lapses, the most accurate algorithms give very few errors (FNMR < 0.001) so that the uncertainty estimates are high.

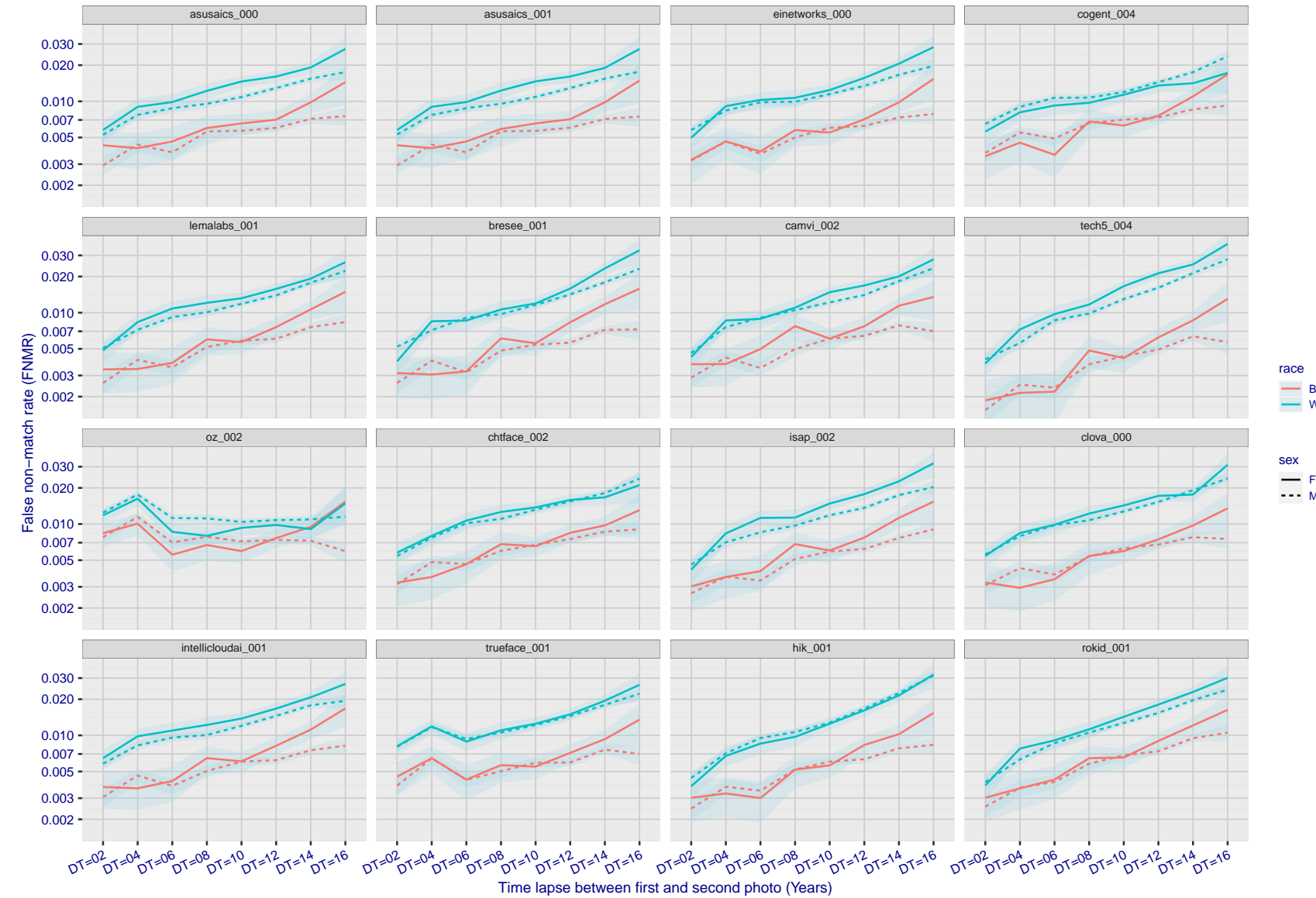


Figure 233: For the mugshot images, FNMR as a function of elapsed time between initial enrollment and second verification images. The panels appear most accurate first, and vertical scale changes on each page. The four traces correspond to images annotated with codes for black female, black male, white female, white male. The threshold is fixed for each algorithm to give FMR = 0.00001 over all (10^8) impostor comparisons. For short time-lapses, the most accurate algorithms give very few errors (FNMR < 0.001) so that the uncertainty estimates are high.

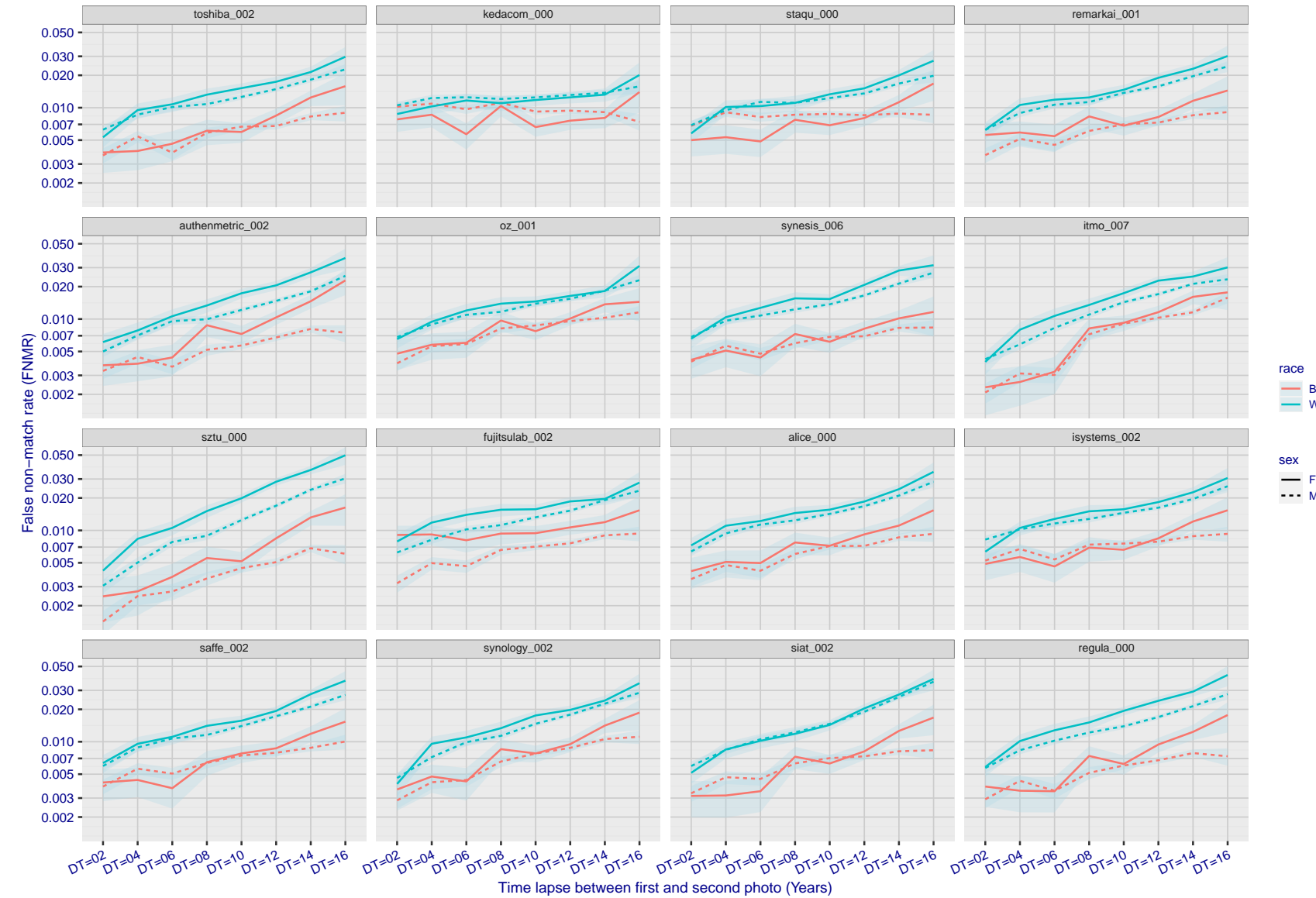


Figure 234: For the mugshot images, FNMR as a function of elapsed time between initial enrollment and second verification images. The panels appear most accurate first, and vertical scale changes on each page. The four traces correspond to images annotated with codes for black female, black male, white female, white male. The threshold is fixed for each algorithm to give FMR = 0.00001 over all (10^8) impostor comparisons. For short time-lapses, the most accurate algorithms give very few errors (FNMR < 0.001) so that the uncertainty estimates are high.

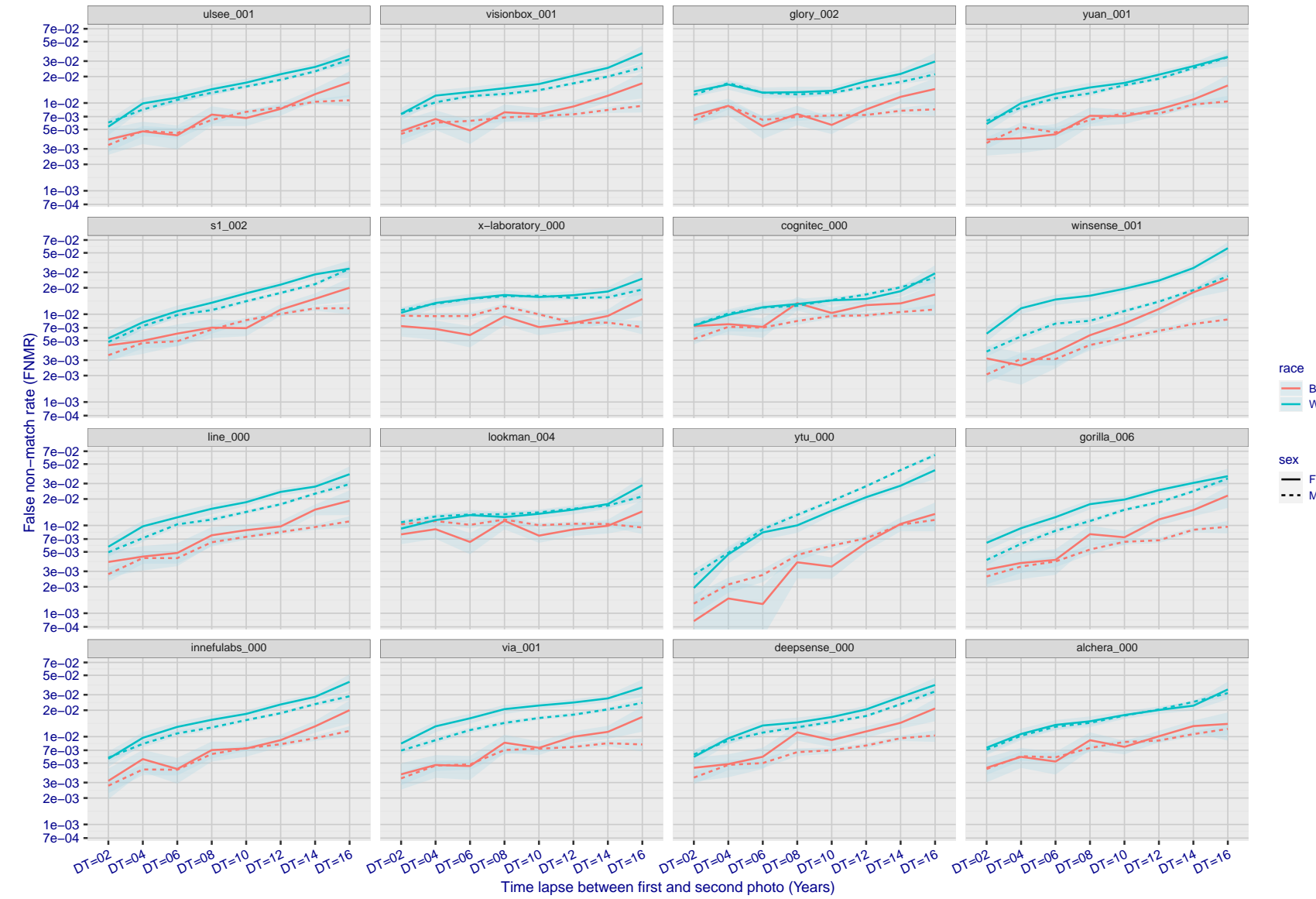


Figure 235: For the mugshot images, FNMR as a function of elapsed time between initial enrollment and second verification images. The panels appear most accurate first, and vertical scale changes on each page. The four traces correspond to images annotated with codes for black female, black male, white female, white male. The threshold is fixed for each algorithm to give $FMR = 0.00001$ over all (10^8) impostor comparisons. For short time-lapses, the most accurate algorithms give very few errors ($FNMR < 0.001$) so that the uncertainty estimates are high.

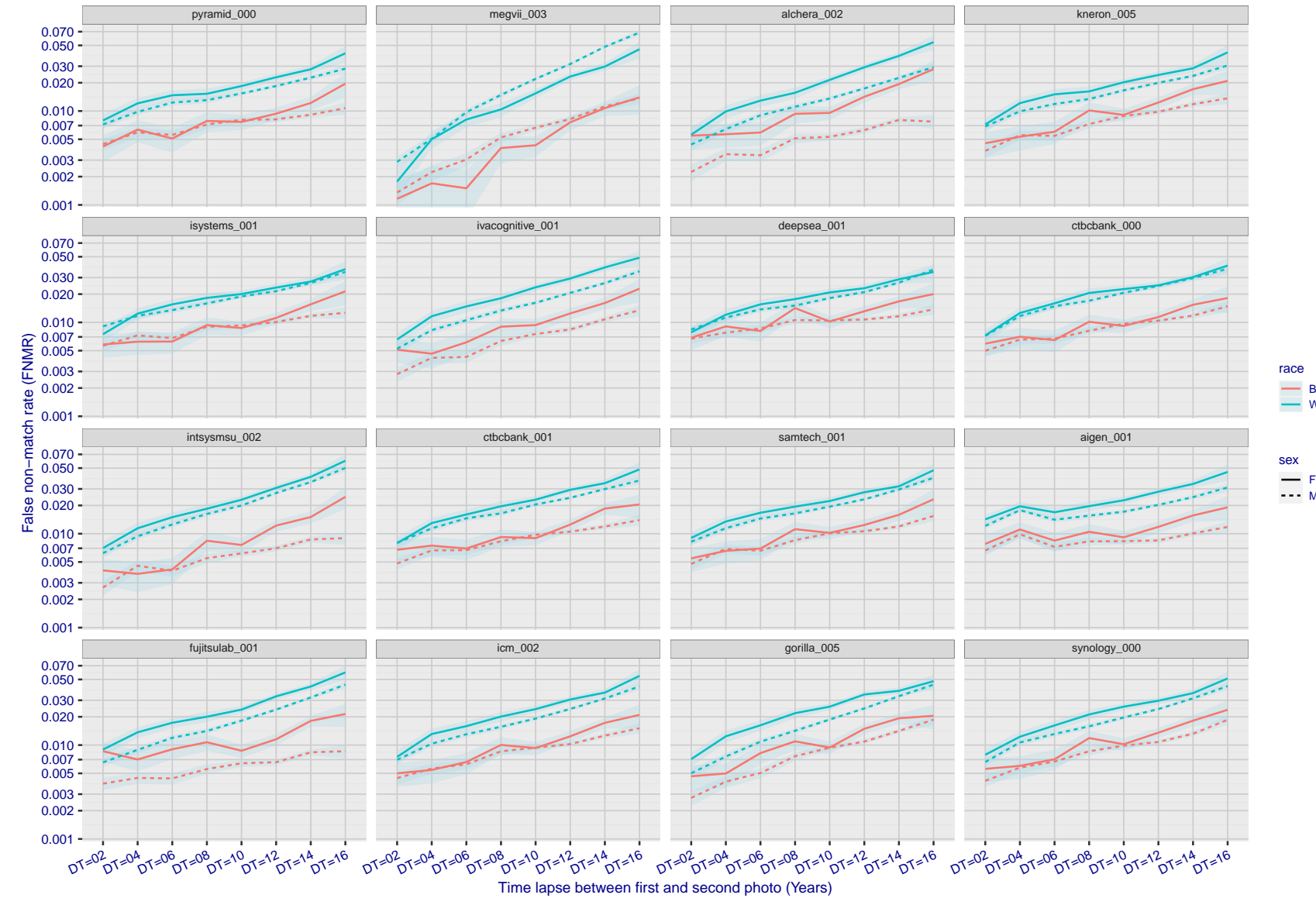


Figure 236: For the mugshot images, FNMR as a function of elapsed time between initial enrollment and second verification images. The panels appear most accurate first, and vertical scale changes on each page. The four traces correspond to images annotated with codes for black female, black male, white female, white male. The threshold is fixed for each algorithm to give FMR = 0.00001 over all (10^8) impostor comparisons. For short time-lapses, the most accurate algorithms give very few errors (FNMR < 0.001) so that the uncertainty estimates are high.

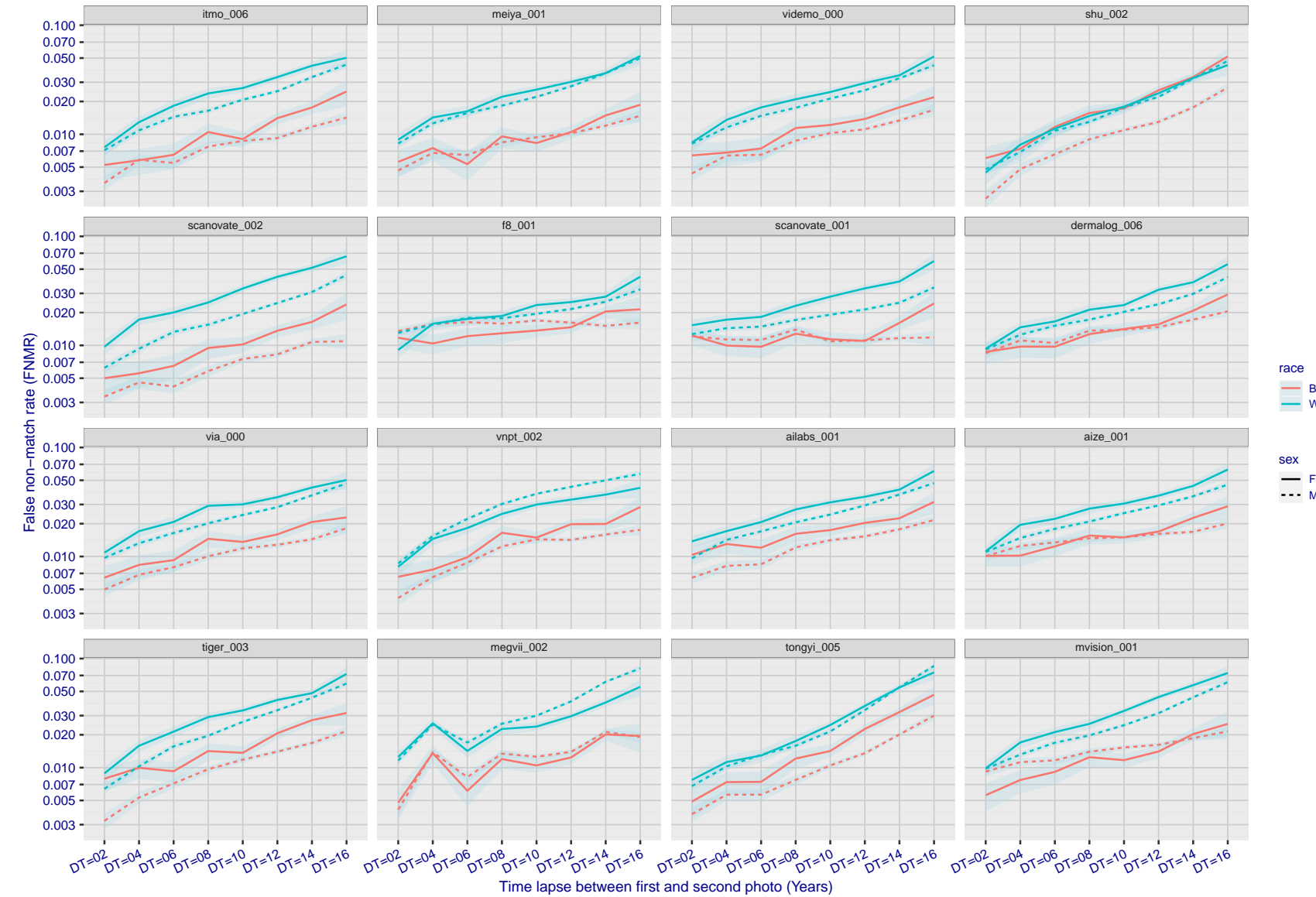


Figure 237: For the mugshot images, FNMR as a function of elapsed time between initial enrollment and second verification images. The panels appear most accurate first, and vertical scale changes on each page. The four traces correspond to images annotated with codes for black female, black male, white female, white male. The threshold is fixed for each algorithm to give FMR = 0.00001 over all (10^8) impostor comparisons. For short time-lapses, the most accurate algorithms give very few errors (FNMR < 0.001) so that the uncertainty estimates are high.

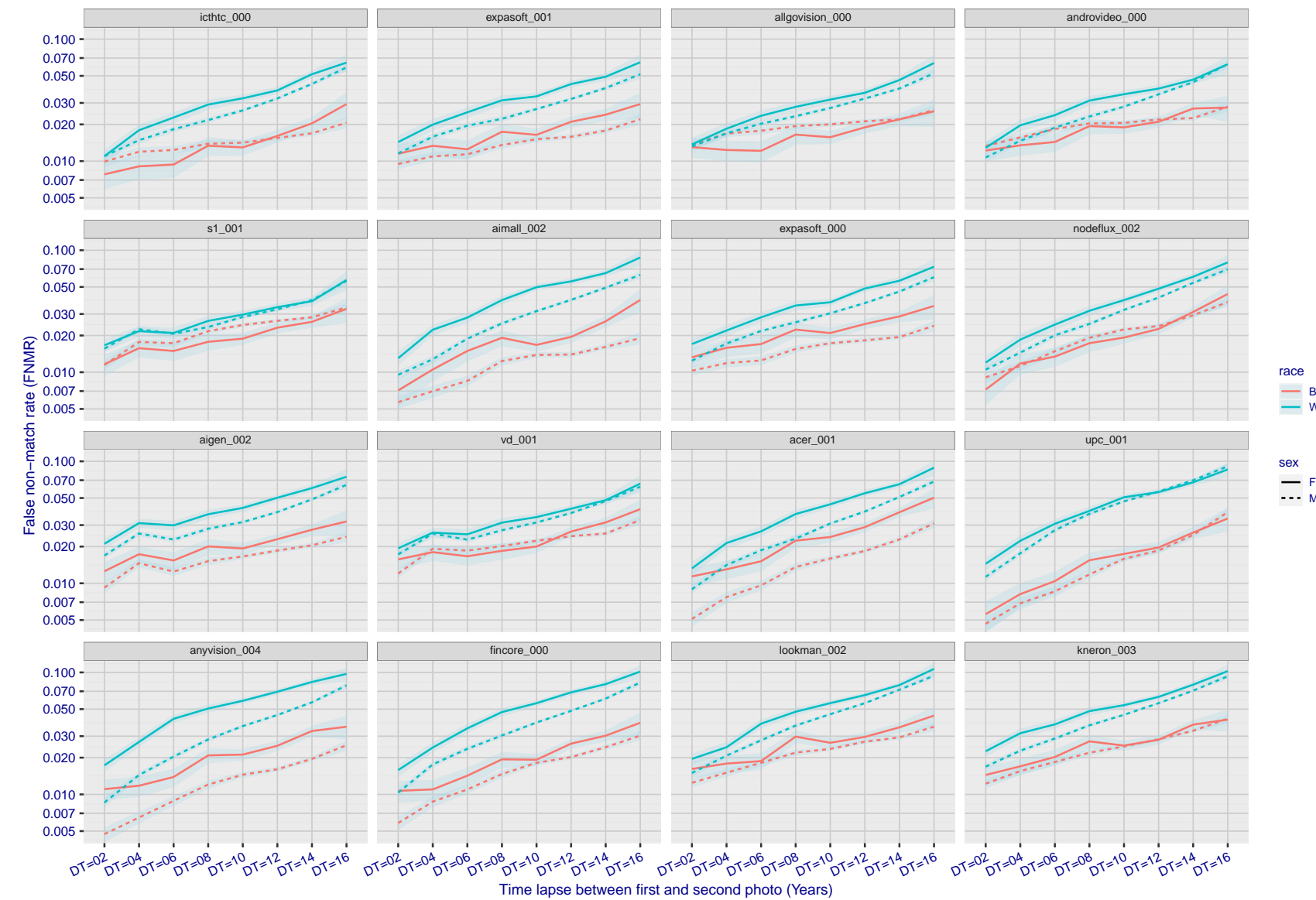


Figure 238: For the mugshot images, FNMR as a function of elapsed time between initial enrollment and second verification images. The panels appear most accurate first, and vertical scale changes on each page. The four traces correspond to images annotated with codes for black female, black male, white female, white male. The threshold is fixed for each algorithm to give $FMR = 0.00001$ over all (10^8) impostor comparisons. For short time-lapses, the most accurate algorithms give very few errors ($FNMR < 0.001$) so that the uncertainty estimates are high.

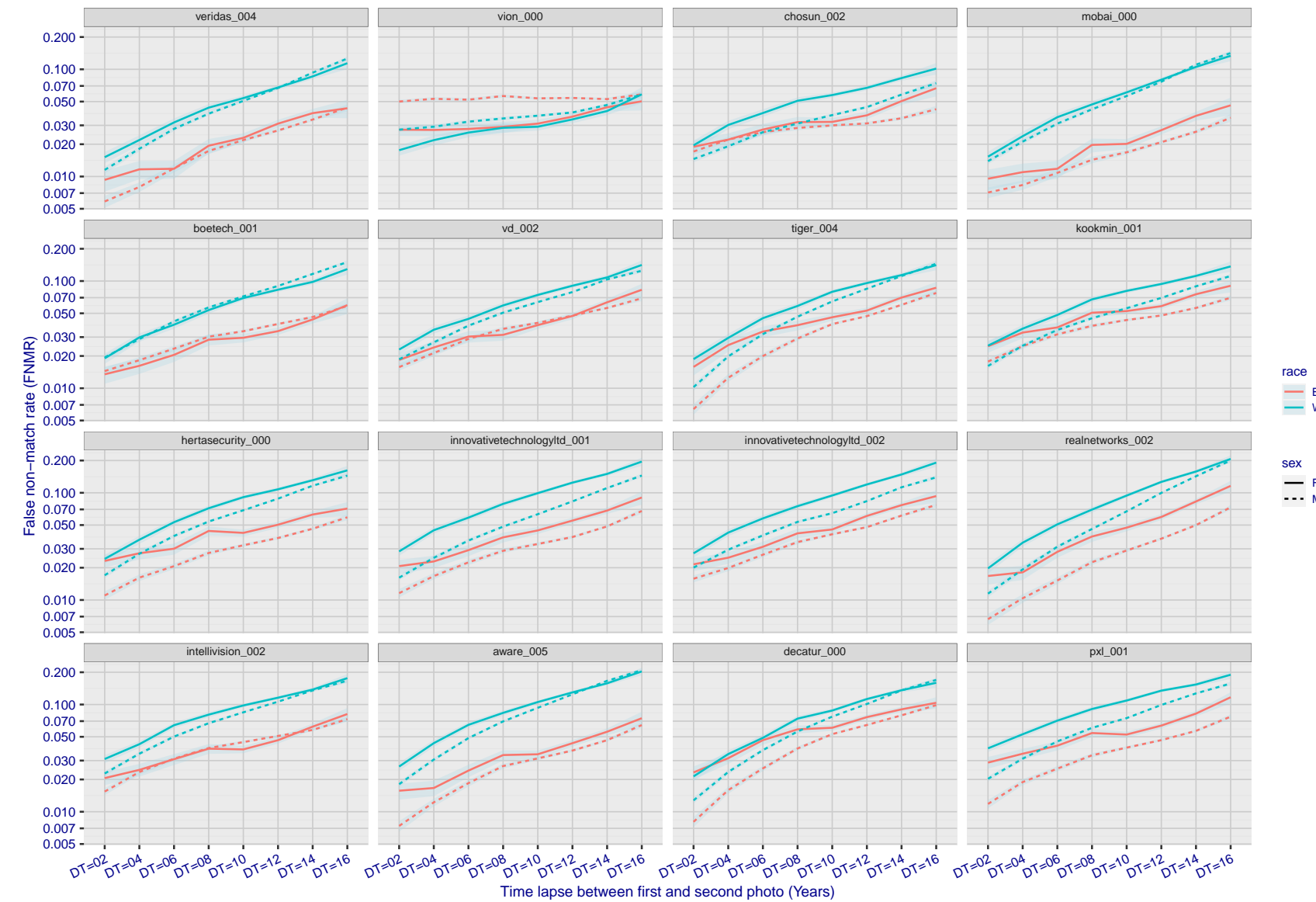


Figure 239: For the mugshot images, FNMR as a function of elapsed time between initial enrollment and second verification images. The panels appear most accurate first, and vertical scale changes on each page. The four traces correspond to images annotated with codes for black female, black male, white female, white male. The threshold is fixed for each algorithm to give FMR = 0.00001 over all (10^8) impostor comparisons. For short time-lapses, the most accurate algorithms give very few errors (FNMR < 0.001) so that the uncertainty estimates are high.

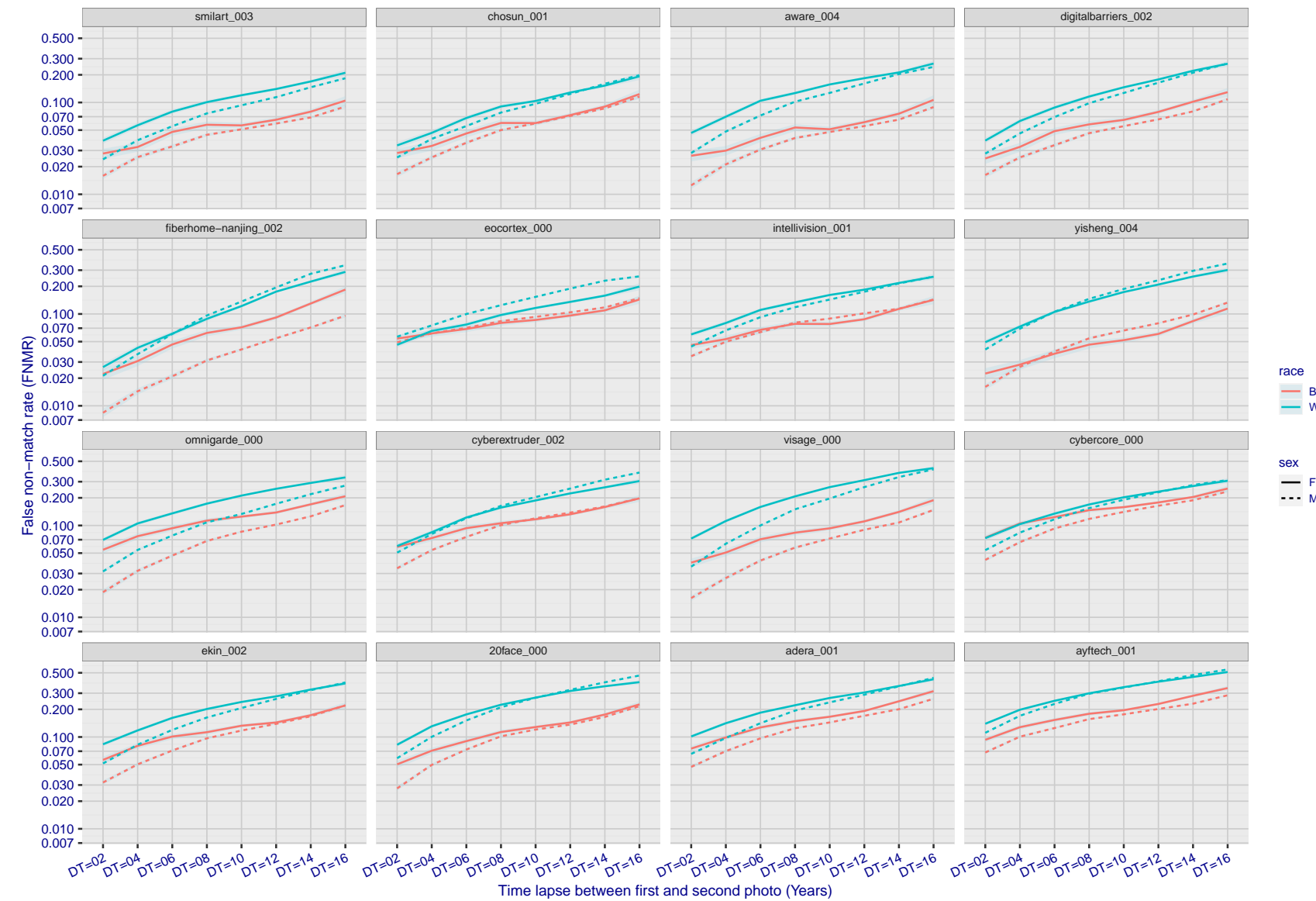


Figure 240: For the mugshot images, FNMR as a function of elapsed time between initial enrollment and second verification images. The panels appear most accurate first, and vertical scale changes on each page. The four traces correspond to images annotated with codes for black female, black male, white female, white male. The threshold is fixed for each algorithm to give FMR = 0.00001 over all (10^8) impostor comparisons. For short time-lapses, the most accurate algorithms give very few errors (FNMR < 0.001) so that the uncertainty estimates are high.

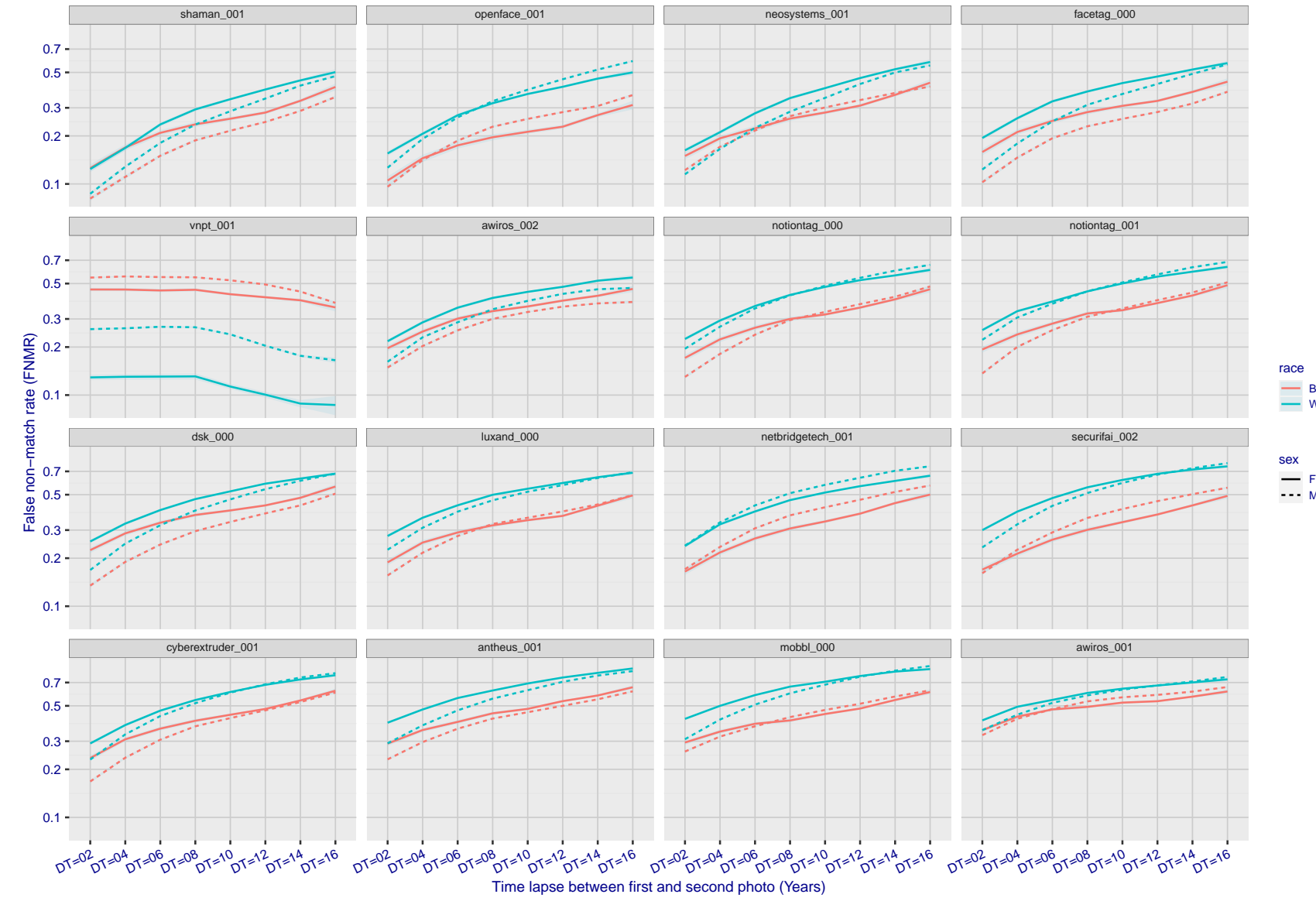


Figure 241: For the mugshot images, FNMR as a function of elapsed time between initial enrollment and second verification images. The panels appear most accurate first, and vertical scale changes on each page. The four traces correspond to images annotated with codes for black female, black male, white female, white male. The threshold is fixed for each algorithm to give $FMR = 0.00001$ over all (10^8) impostor comparisons. For short time-lapses, the most accurate algorithms give very few errors ($FNMR < 0.001$) so that the uncertainty estimates are high.

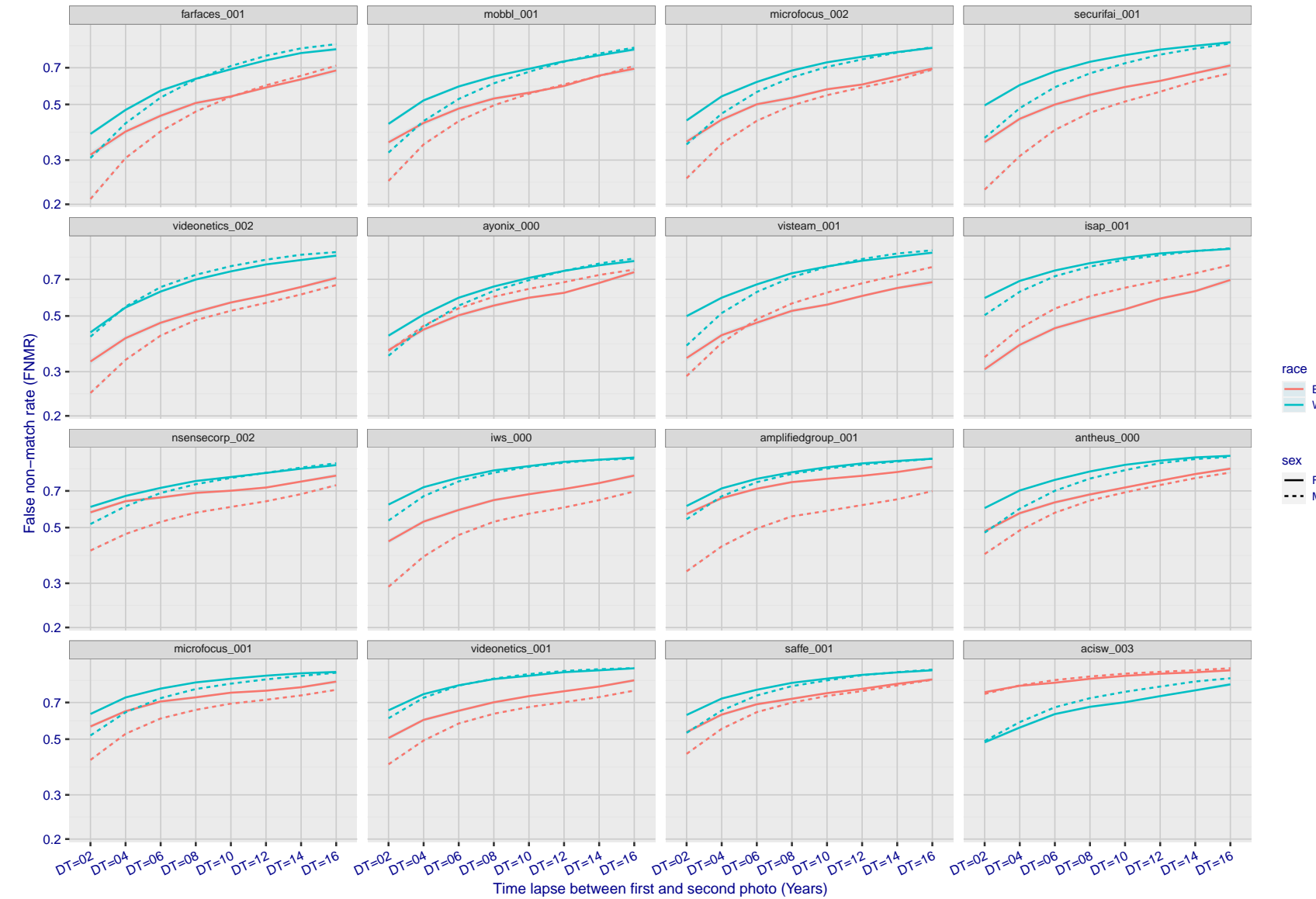


Figure 242: For the mugshot images, FNMR as a function of elapsed time between initial enrollment and second verification images. The panels appear most accurate first, and vertical scale changes on each page. The four traces correspond to images annotated with codes for black female, black male, white female, white male. The threshold is fixed for each algorithm to give FMR = 0.00001 over all (10^8) impostor comparisons. For short time-lapses, the most accurate algorithms give very few errors (FNMR < 0.001) so that the uncertainty estimates are high.

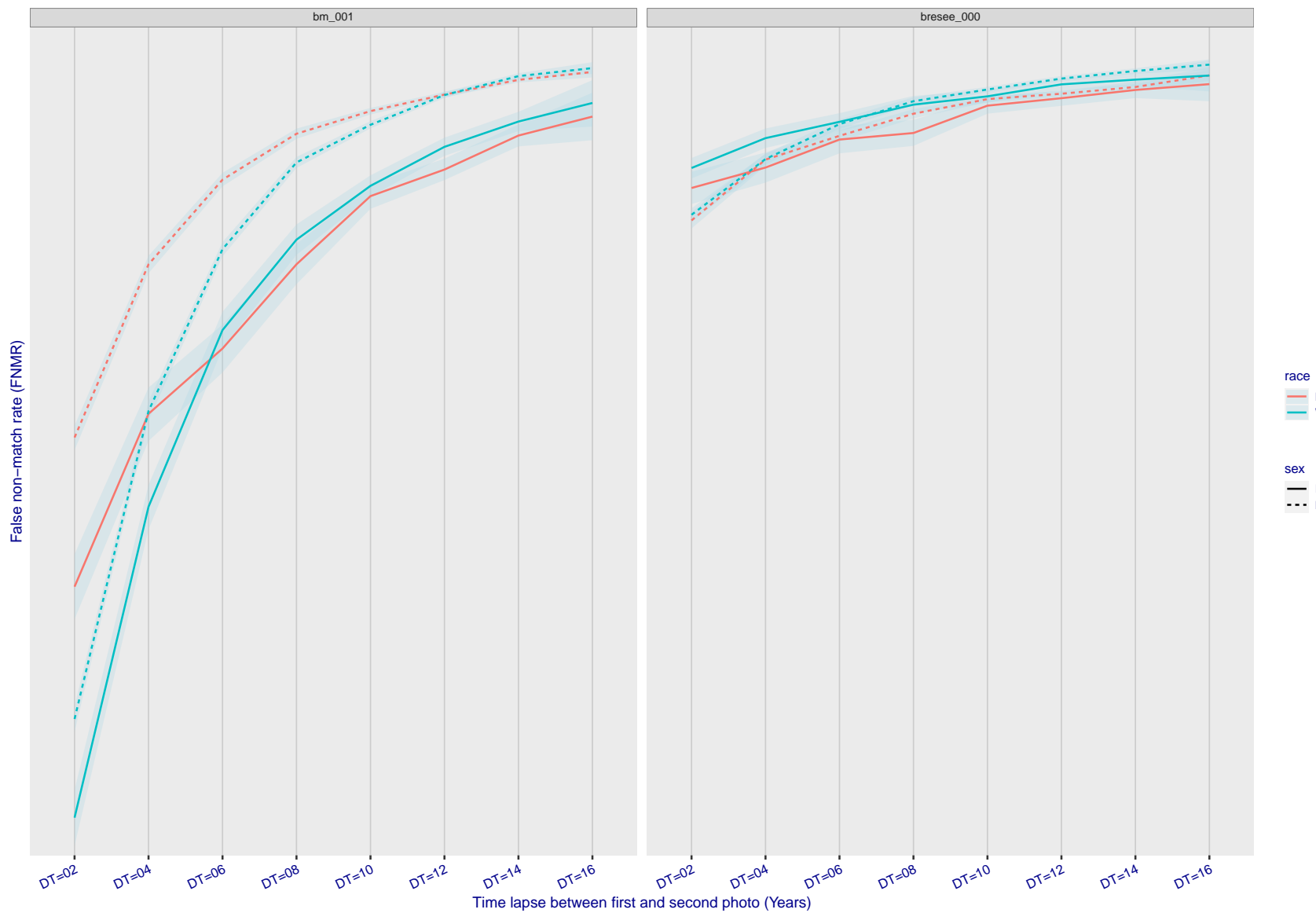


Figure 243: For the mugshot images, FNMR as a function of elapsed time between initial enrollment and second verification images. The panels appear most accurate first, and vertical scale changes on each page. The four traces correspond to images annotated with codes for black female, black male, white female, white male. The threshold is fixed for each algorithm to give $FMR = 0.00001$ over all (10^8) impostor comparisons. For short time-lapses, the most accurate algorithms give very few errors ($FNMR < 0.001$) so that the uncertainty estimates are high.

3.5.3 Effect of age on genuine subjects

Background: Faces change appearance throughout life. Face recognition algorithms have previously been reported to give better accuracy on older individuals (See NIST IR 8009).

Goal: To quantify false non-match rates (FNMR) as a function of age, without an ageing component.

Methods: Using the visa images, which span fewer than five years, thresholds are determined that give FMR = 0.001 and 0.0001 over the entire impostor set. Then FNMR is measured over 1000 bootstrap replications of the genuine scores.

Results: For the visa images, Figure 270 shows how false non-match rates for genuine users, as a function of age group.

The notable aspects are:

- ▷ Younger subjects give considerably higher FNMR. This is likely due to rapid growth and change in facial appearance.
- ▷ FNMR trends down throughout life. The last bin, AGE > 72, contains fewer than 140 mated pairs, and may be affected by small sample size.



Figure 244: For the visa images, the dots show FNMR by age group for two operating thresholds corresponding to $FMR = \{0.001, 0.0001\}$ computed over all on the order of 10^{10} impostor scores. The FMR in each bin will vary also - see subsequent impostor heatmaps in sec. 3.6.2. Given a pair of face images taken at different times, we assign the comparison to the bin that is the arithmetic average of the subject's ages. This plot shows only the effect of age, not ageing. The number of comparisons in each bin is generally in the thousands, however the first and last bins are computed over 149 and 124 respectively. The error rates in some (adult) cases are zero, and in others the DET is flat so the error rates at the two thresholds are identical. The lines span 1% and 99% of bootstrap replicated FNMR estimates.

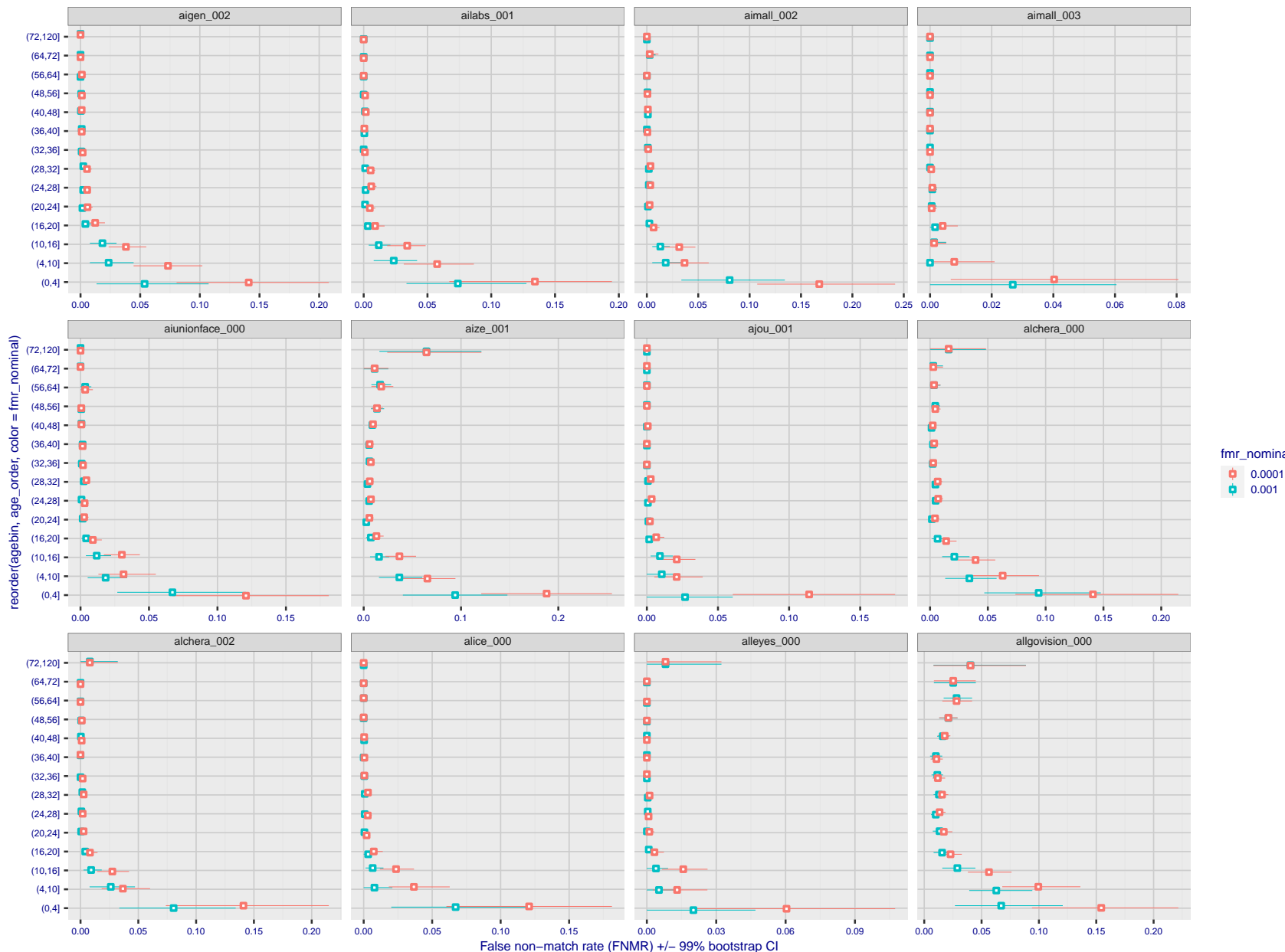


Figure 245: For the visa images, the dots show FNMR by age group for two operating thresholds corresponding to $FMR = \{0.001, 0.0001\}$ computed over all on the order of 10^{10} impostor scores. The FMR in each bin will vary also - see subsequent impostor heatmaps in sec. 3.6.2. Given a pair of face images taken at different times, we assign the comparison to the bin that is the arithmetic average of the subject's ages. This plot shows only the effect of age, not ageing. The number of comparisons in each bin is generally in the thousands, however the first and last bins are computed over 149 and 124 respectively. The error rates in some (adult) cases are zero, and in others the DET is flat so the error rates at the two thresholds are identical. The lines span 1% and 99% of bootstrap replicated FNMR estimates.

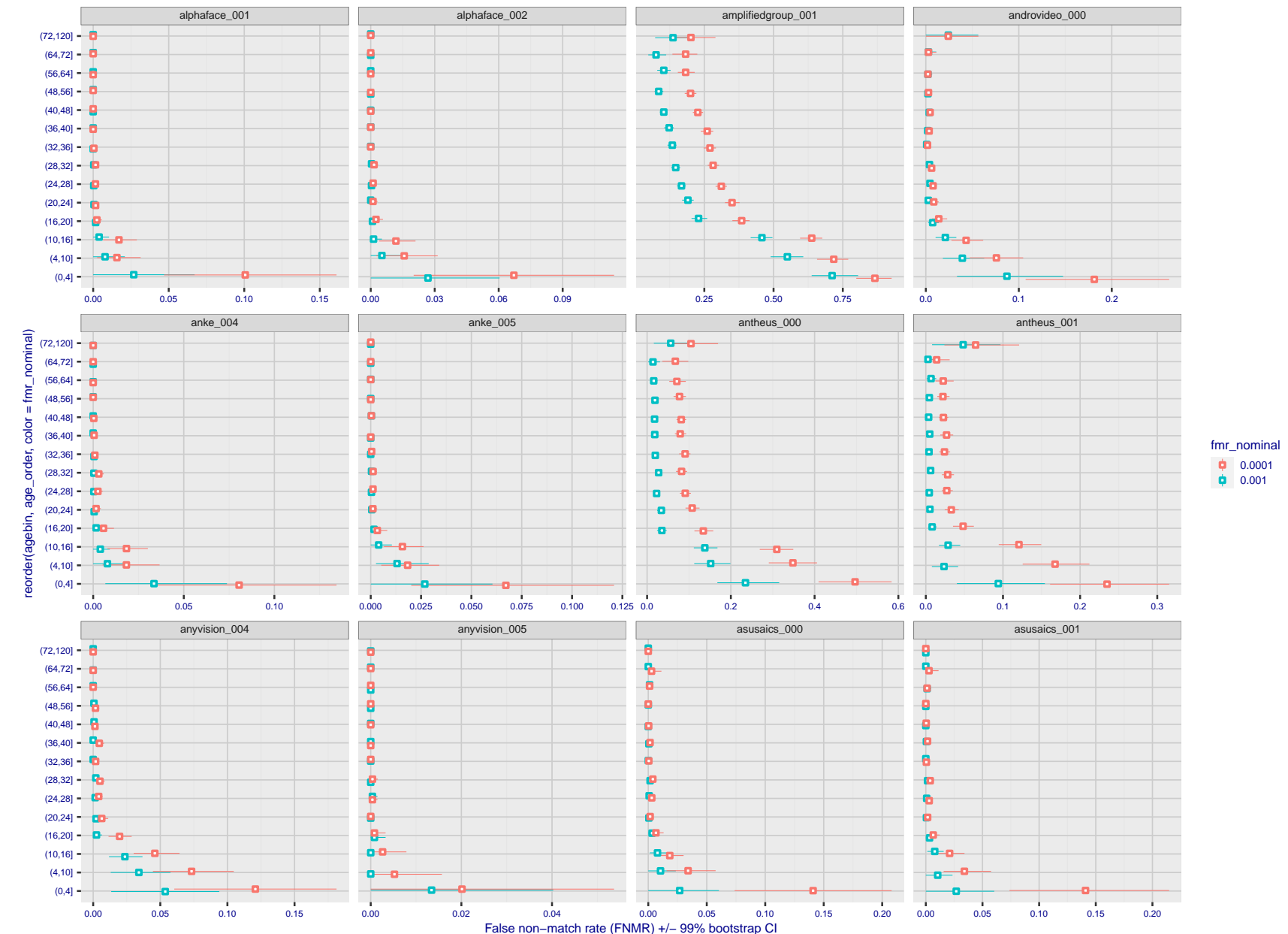


Figure 246: For the visa images, the dots show FNMR by age group for two operating thresholds corresponding to $FMR = \{0.001, 0.0001\}$ computed over all on the order of 10^{10} impostor scores. The FMR in each bin will vary also - see subsequent impostor heatmaps in sec. 3.6.2. Given a pair of face images taken at different times, we assign the comparison to the bin that is the arithmetic average of the subject's ages. This plot shows only the effect of age, not ageing. The number of comparisons in each bin is generally in the thousands, however the first and last bins are computed over 149 and 124 respectively. The error rates in some (adult) cases are zero, and in others the DET is flat so the error rates at the two thresholds are identical. The lines span 1% and 99% of bootstrap replicated FNMR estimates.

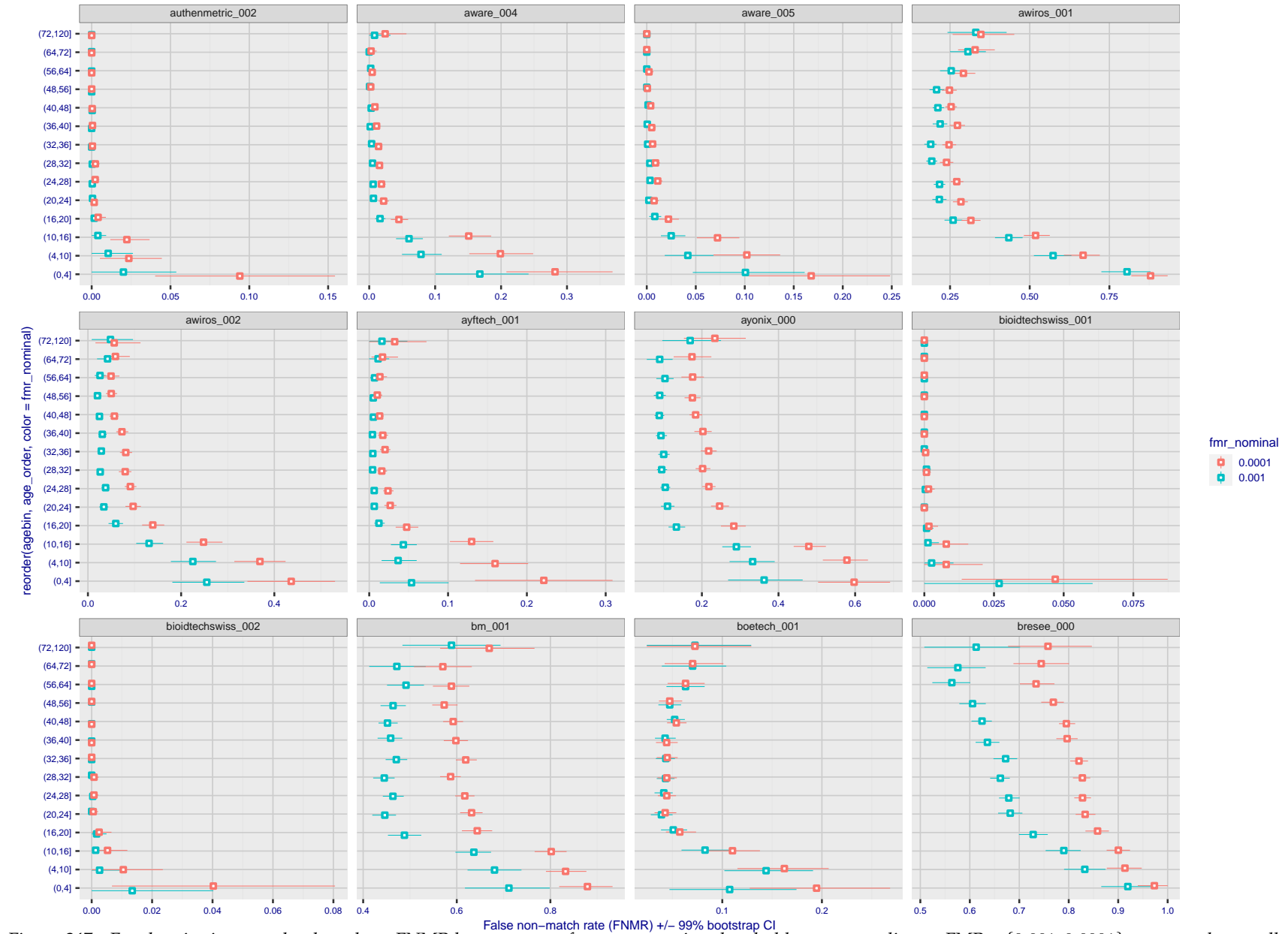


Figure 247: For the visa images, the dots show FNMR by age group for two operating thresholds corresponding to $FMR = \{0.001, 0.0001\}$ computed over all on the order of 10^{10} impostor scores. The FMR in each bin will vary also - see subsequent impostor heatmaps in sec. 3.6.2. Given a pair of face images taken at different times, we assign the comparison to the bin that is the arithmetic average of the subject's ages. This plot shows only the effect of age, not ageing. The number of comparisons in each bin is generally in the thousands, however the first and last bins are computed over 149 and 124 respectively. The error rates in some (adult) cases are zero, and in others the DET is flat so the error rates at the two thresholds are identical. The lines span 1% and 99% of bootstrap replicated FNMR estimates.



Figure 248: For the visa images, the dots show FNMR by age group for two operating thresholds corresponding to $FMR = \{0.001, 0.0001\}$ computed over all on the order of 10^{10} impostor scores. The FMR in each bin will vary also - see subsequent impostor heatmaps in sec. 3.6.2. Given a pair of face images taken at different times, we assign the comparison to the bin that is the arithmetic average of the subject's ages. This plot shows only the effect of age, not ageing. The number of comparisons in each bin is generally in the thousands, however the first and last bins are computed over 149 and 124 respectively. The error rates in some (adult) cases are zero, and in others the DET is flat so the error rates at the two thresholds are identical. The lines span 1% and 99% of bootstrap replicated FNMR estimates.

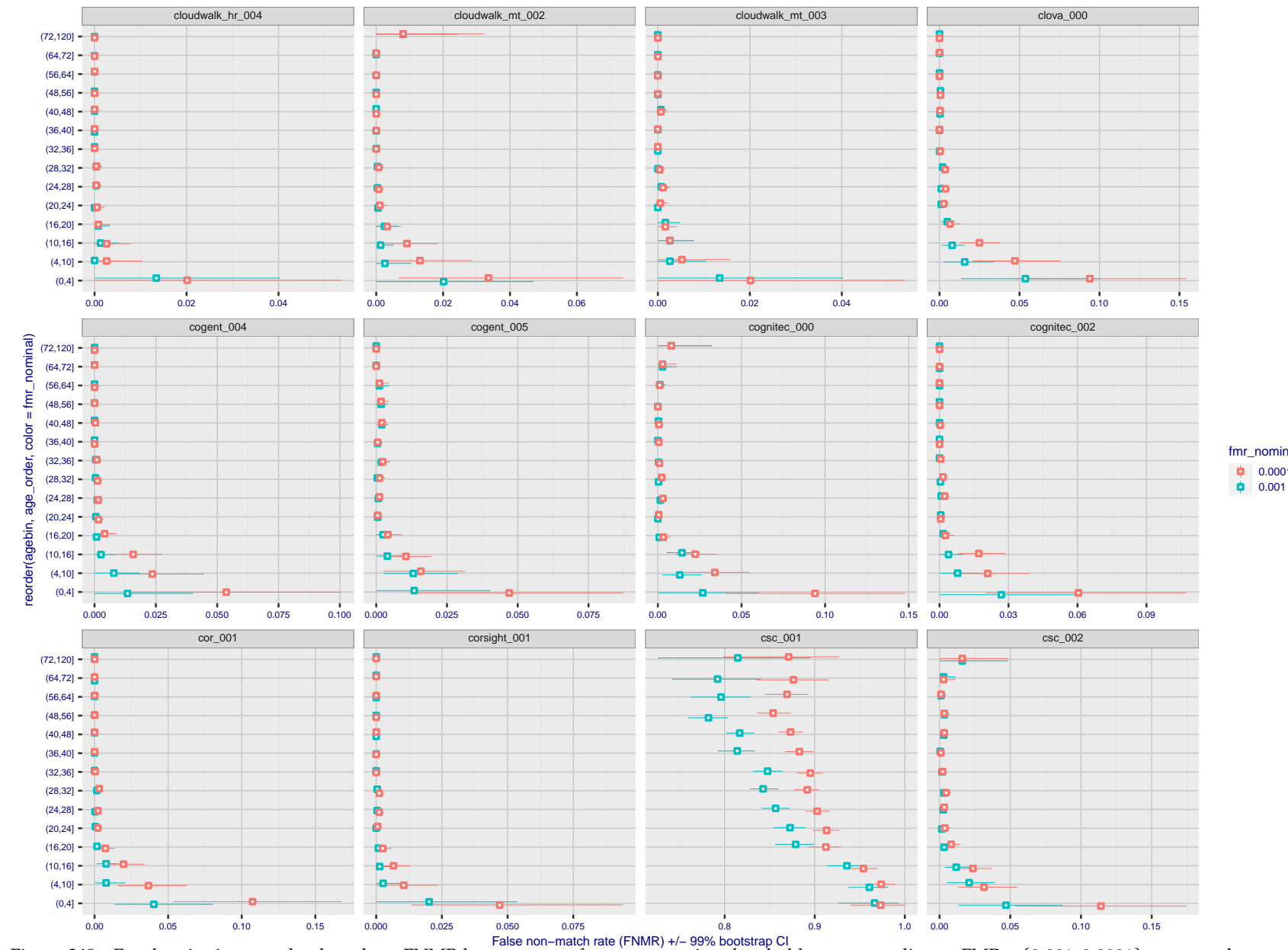


Figure 249: For the visa images, the dots show FNMR by age group for two operating thresholds corresponding to $FMR = \{0.001, 0.0001\}$ computed over all on the order of 10^{10} impostor scores. The FMR in each bin will vary also - see subsequent impostor heatmaps in sec. 3.6.2. Given a pair of face images taken at different times, we assign the comparison to the bin that is the arithmetic average of the subject's ages. This plot shows only the effect of age, not ageing. The number of comparisons in each bin is generally in the thousands, however the first and last bins are computed over 149 and 124 respectively. The error rates in some (adult) cases are zero, and in others the DET is flat so the error rates at the two thresholds are identical. The lines span 1% and 99% of bootstrap replicated FNMR estimates.



Figure 250: For the visa images, the dots show FNMR by age group for two operating thresholds corresponding to $FMR = \{0.001, 0.0001\}$ computed over all on the order of 10^{10} impostor scores. The FMR in each bin will vary also - see subsequent impostor heatmaps in sec. 3.6.2. Given a pair of face images taken at different times, we assign the comparison to the bin that is the arithmetic average of the subject's ages. This plot shows only the effect of age, not ageing. The number of comparisons in each bin is generally in the thousands, however the first and last bins are computed over 149 and 124 respectively. The error rates in some (adult) cases are zero, and in others the DET is flat so the error rates at the two thresholds are identical. The lines span 1% and 99% of bootstrap replicated FNMR estimates.



Figure 251: For the visa images, the dots show FNMR by age group for two operating thresholds corresponding to $FMR = \{0.001, 0.0001\}$ computed over all on the order of 10^{10} impostor scores. The FMR in each bin will vary also - see subsequent impostor heatmaps in sec. 3.6.2. Given a pair of face images taken at different times, we assign the comparison to the bin that is the arithmetic average of the subject's ages. This plot shows only the effect of age, not ageing. The number of comparisons in each bin is generally in the thousands, however the first and last bins are computed over 149 and 124 respectively. The error rates in some (adult) cases are zero, and in others the DET is flat so the error rates at the two thresholds are identical. The lines span 1% and 99% of bootstrap replicated FNMR estimates.

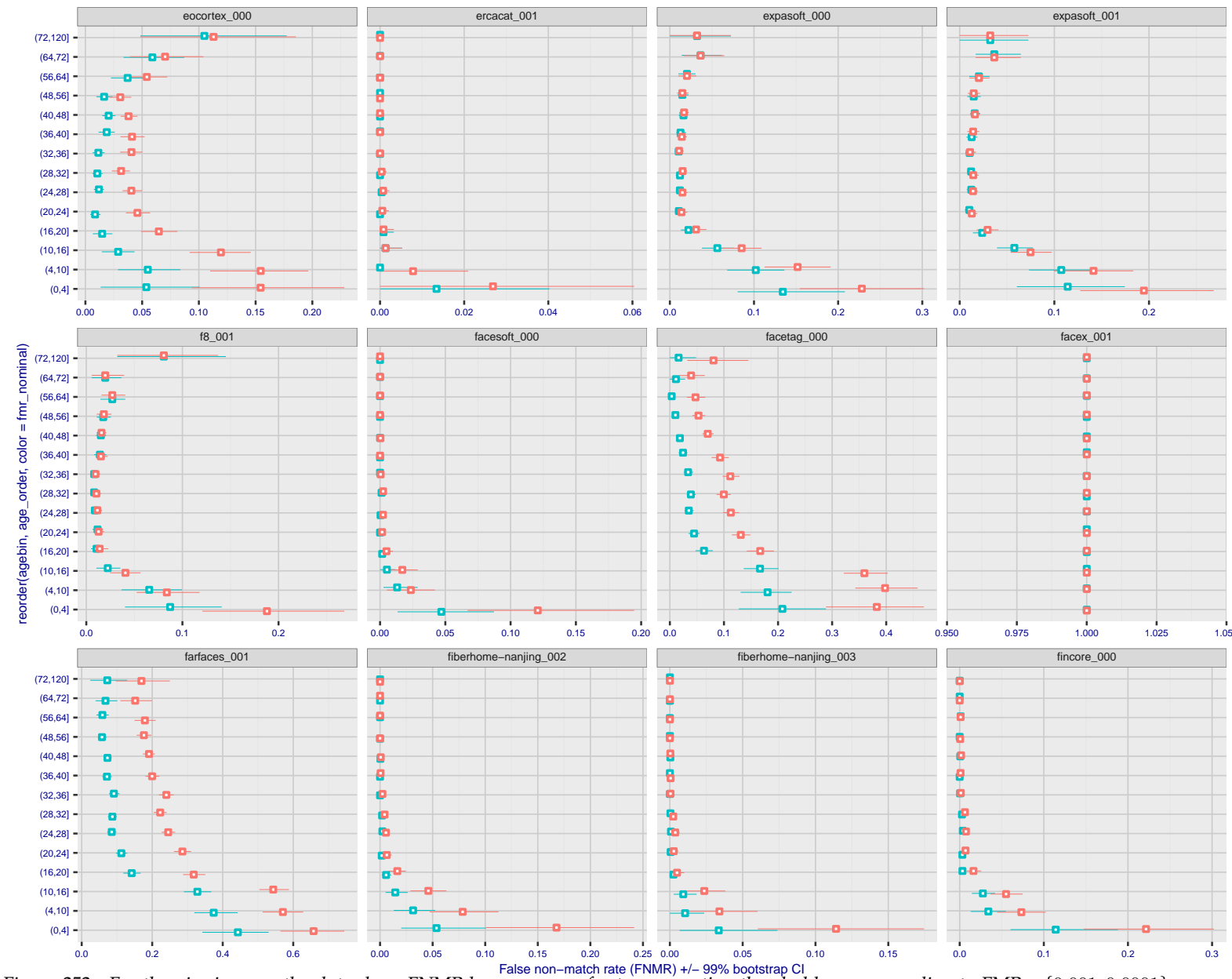


Figure 252: For the visa images, the dots show FNMR by age group for two operating thresholds corresponding to $FMR = \{0.001, 0.0001\}$ computed over all on the order of 10^{10} impostor scores. The FMR in each bin will vary also - see subsequent impostor heatmaps in sec. 3.6.2. Given a pair of face images taken at different times, we assign the comparison to the bin that is the arithmetic average of the subject's ages. This plot shows only the effect of age, not ageing. The number of comparisons in each bin is generally in the thousands, however the first and last bins are computed over 149 and 124 respectively. The error rates in some (adult) cases are zero, and in others the DET is flat so the error rates at the two thresholds are identical. The lines span 1% and 99% of bootstrap replicated FNMR estimates.



Figure 253: For the visa images, the dots show FNMR by age group for two operating thresholds corresponding to $FMR = \{0.001, 0.0001\}$ computed over all on the order of 10^{10} impostor scores. The FMR in each bin will vary also - see subsequent impostor heatmaps in sec. 3.6.2. Given a pair of face images taken at different times, we assign the comparison to the bin that is the arithmetic average of the subject's ages. This plot shows only the effect of age, not ageing. The number of comparisons in each bin is generally in the thousands, however the first and last bins are computed over 149 and 124 respectively. The error rates in some (adult) cases are zero, and in others the DET is flat so the error rates at the two thresholds are identical. The lines span 1% and 99% of bootstrap replicated FNMR estimates.



Figure 254: For the visa images, the dots show FNMR by age group for two operating thresholds corresponding to $FMR = \{0.001, 0.0001\}$ computed over all on the order of 10^{10} impostor scores. The FMR in each bin will vary also - see subsequent impostor heatmaps in sec. 3.6.2. Given a pair of face images taken at different times, we assign the comparison to the bin that is the arithmetic average of the subject's ages. This plot shows only the effect of age, not ageing. The number of comparisons in each bin is generally in the thousands, however the first and last bins are computed over 149 and 124 respectively. The error rates in some (adult) cases are zero, and in others the DET is flat so the error rates at the two thresholds are identical. The lines span 1% and 99% of bootstrap replicated FNMR estimates.



fmr_nominal
0.0001
0.001

Figure 255: For the visa images, the dots show FNMR by age group for two operating thresholds corresponding to $FMR = \{0.001, 0.0001\}$ computed over all on the order of 10^{10} impostor scores. The FMR in each bin will vary also - see subsequent impostor heatmaps in sec. 3.6.2. Given a pair of face images taken at different times, we assign the comparison to the bin that is the arithmetic average of the subject's ages. This plot shows only the effect of age, not ageing. The number of comparisons in each bin is generally in the thousands, however the first and last bins are computed over 149 and 124 respectively. The error rates in some (adult) cases are zero, and in others the DET is flat so the error rates at the two thresholds are identical. The lines span 1% and 99% of bootstrap replicated FNMR estimates.

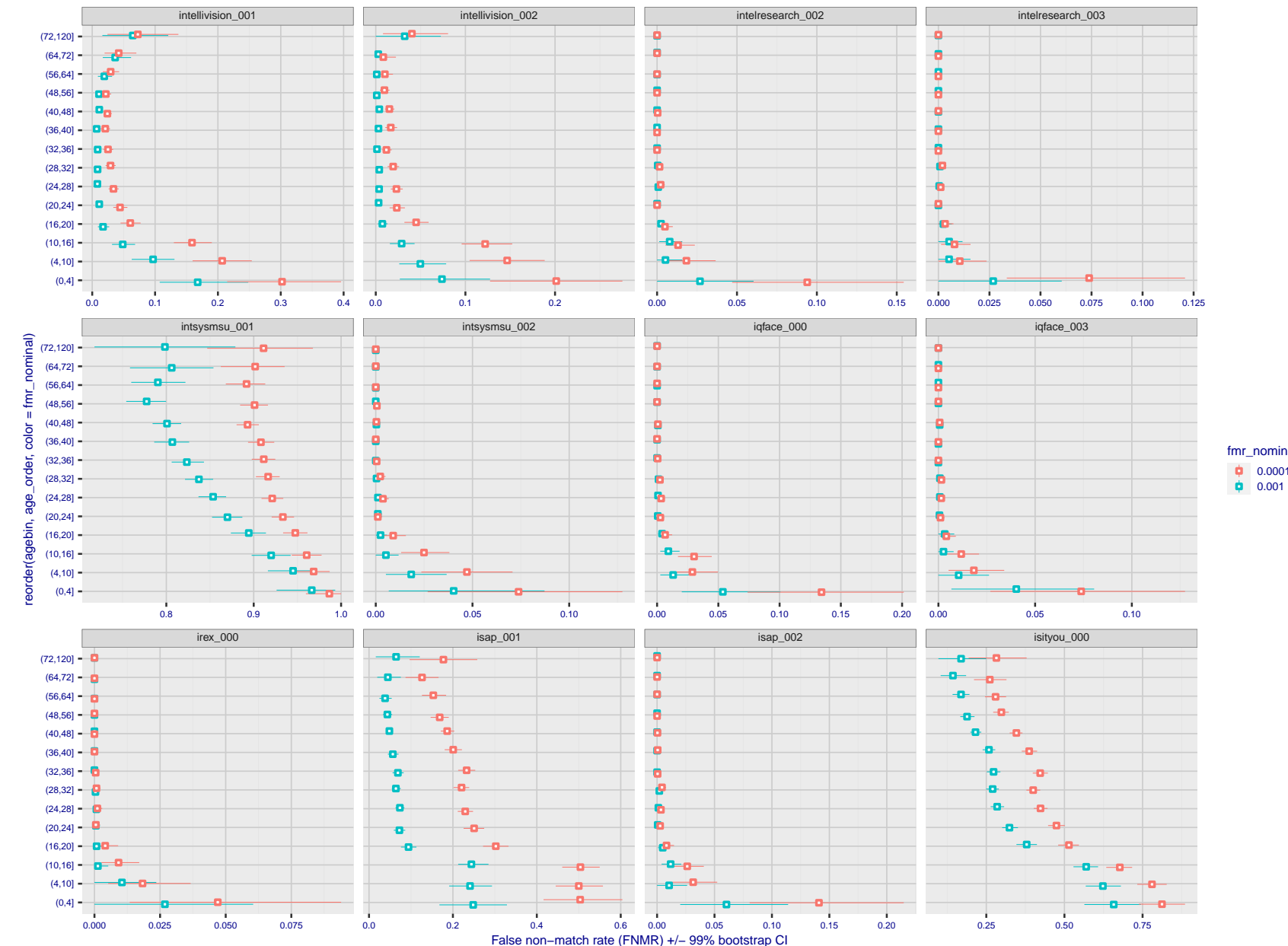


Figure 256: For the visa images, the dots show FNMR by age group for two operating thresholds corresponding to $FMR = \{0.001, 0.0001\}$ computed over all on the order of 10^{10} impostor scores. The FMR in each bin will vary also - see subsequent impostor heatmaps in sec. 3.6.2. Given a pair of face images taken at different times, we assign the comparison to the bin that is the arithmetic average of the subject's ages. This plot shows only the effect of age, not ageing. The number of comparisons in each bin is generally in the thousands, however the first and last bins are computed over 149 and 124 respectively. The error rates in some (adult) cases are zero, and in others the DET is flat so the error rates at the two thresholds are identical. The lines span 1% and 99% of bootstrap replicated FNMR estimates.

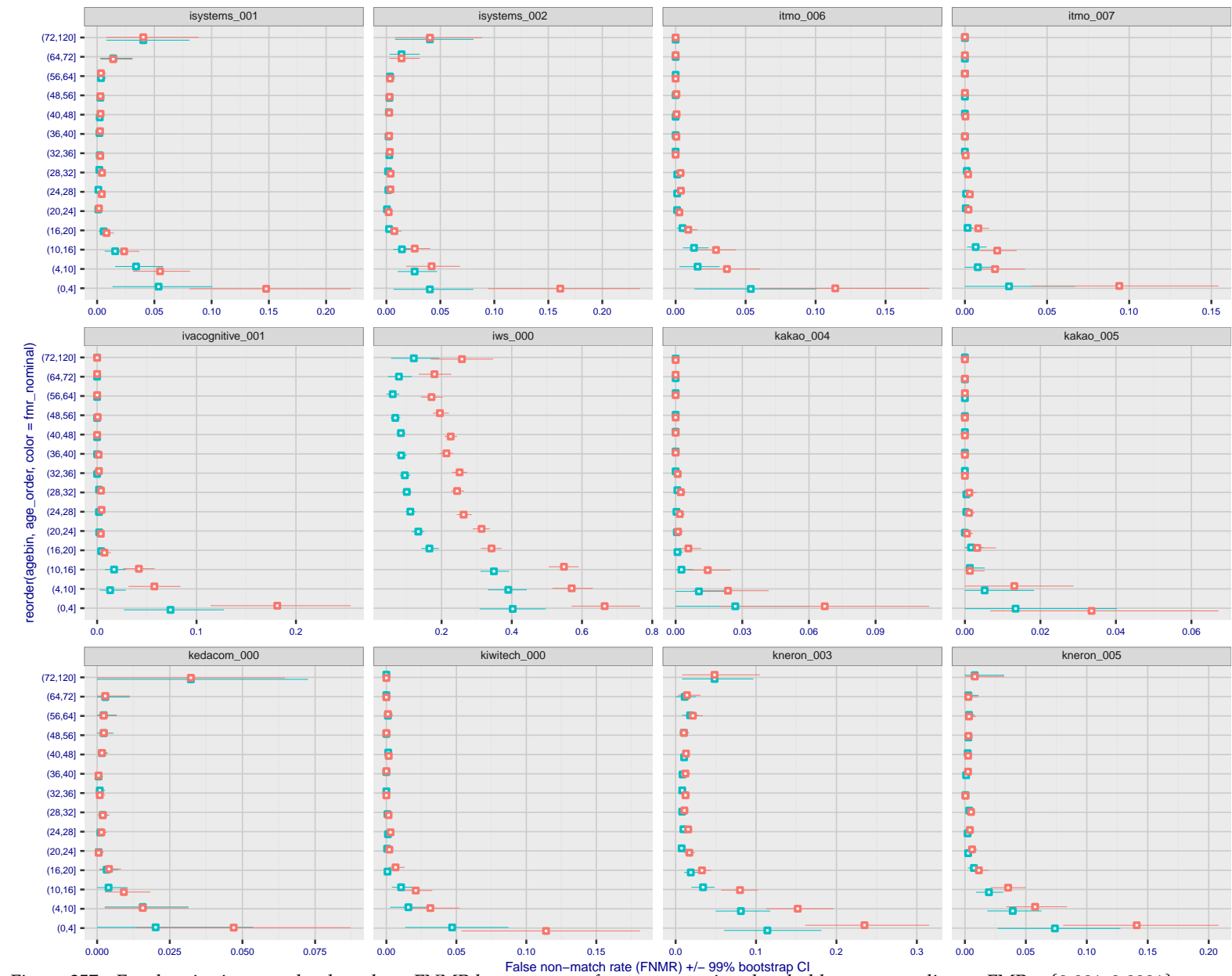
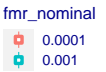


Figure 257: For the visa images, the dots show FNMR by age group for two operating thresholds corresponding to $FMR = \{0.001, 0.0001\}$ computed over all on the order of 10^{10} impostor scores. The FMR in each bin will vary also - see subsequent impostor heatmaps in sec. 3.6.2. Given a pair of face images taken at different times, we assign the comparison to the bin that is the arithmetic average of the subject's ages. This plot shows only the effect of age, not ageing. The number of comparisons in each bin is generally in the thousands, however the first and last bins are computed over 149 and 124 respectively. The error rates in some (adult) cases are zero, and in others the DET is flat so the error rates at the two thresholds are identical. The lines span 1% and 99% of bootstrap replicated FNMR estimates.

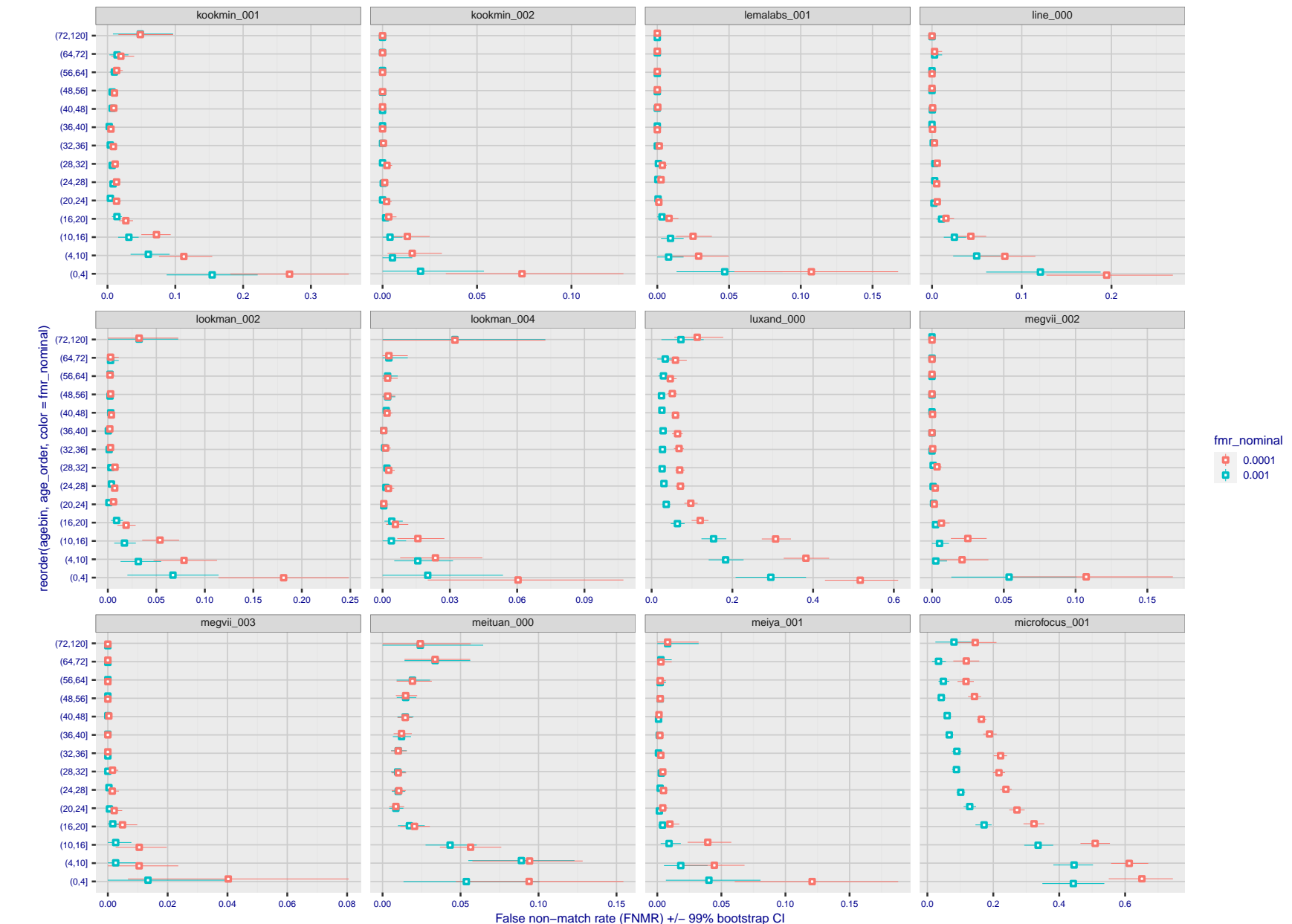


Figure 258: For the visa images, the dots show FNMR by age group for two operating thresholds corresponding to $FMR = \{0.001, 0.0001\}$ computed over all on the order of 10^{10} impostor scores. The FMR in each bin will vary also - see subsequent impostor heatmaps in sec. 3.6.2. Given a pair of face images taken at different times, we assign the comparison to the bin that is the arithmetic average of the subject's ages. This plot shows only the effect of age, not ageing. The number of comparisons in each bin is generally in the thousands, however the first and last bins are computed over 149 and 124 respectively. The error rates in some (adult) cases are zero, and in others the DET is flat so the error rates at the two thresholds are identical. The lines span 1% and 99% of bootstrap replicated FNMR estimates.

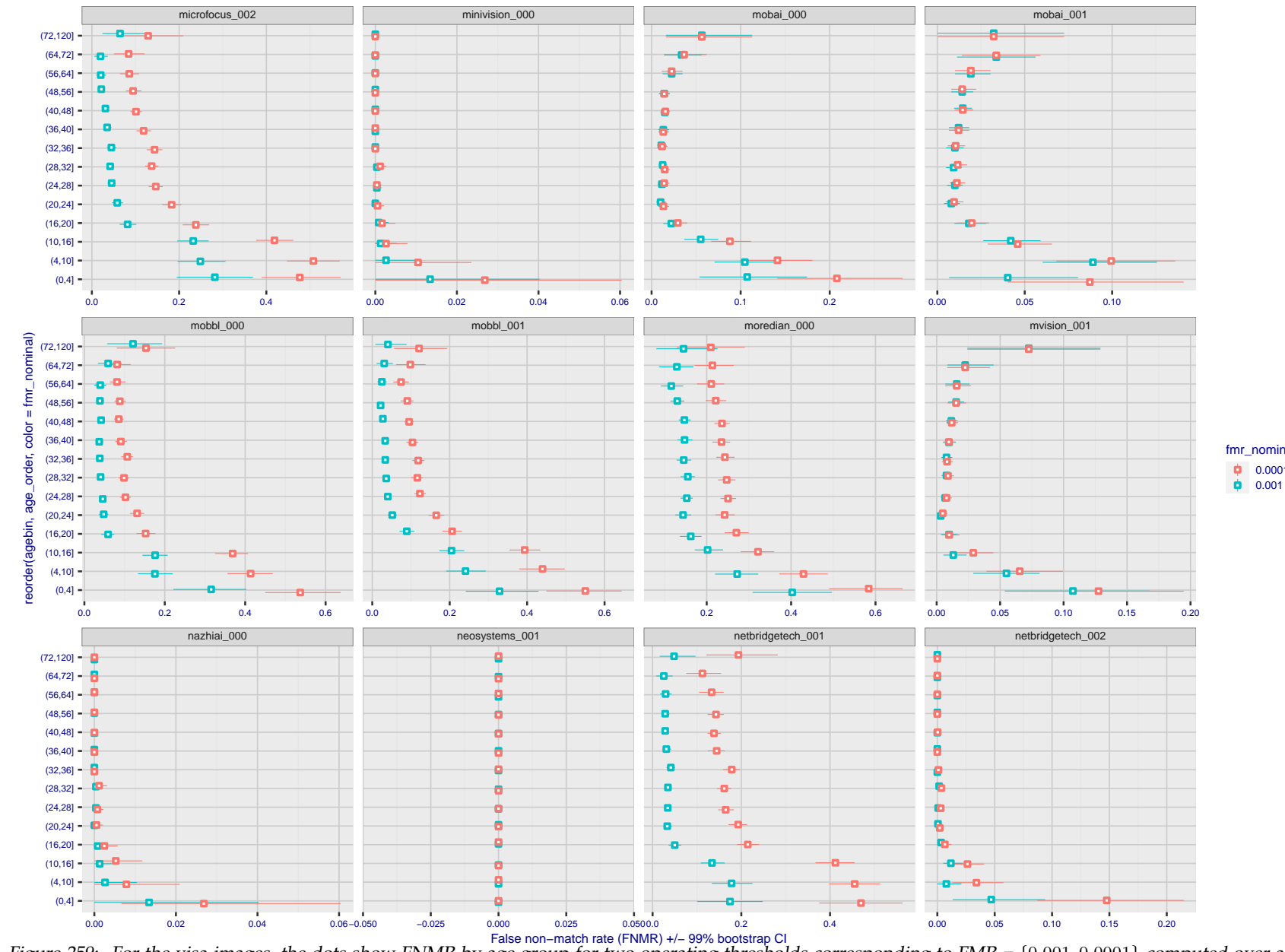


Figure 259: For the visa images, the dots show FNMR by age group for two operating thresholds corresponding to $FMR = \{0.001, 0.0001\}$ computed over all on the order of 10^{10} impostor scores. The FMR in each bin will vary also - see subsequent impostor heatmaps in sec. 3.6.2. Given a pair of face images taken at different times, we assign the comparison to the bin that is the arithmetic average of the subject's ages. This plot shows only the effect of age, not ageing. The number of comparisons in each bin is generally in the thousands, however the first and last bins are computed over 149 and 124 respectively. The error rates in some (adult) cases are zero, and in others the DET is flat so the error rates at the two thresholds are identical. The lines span 1% and 99% of bootstrap replicated FNMR estimates.

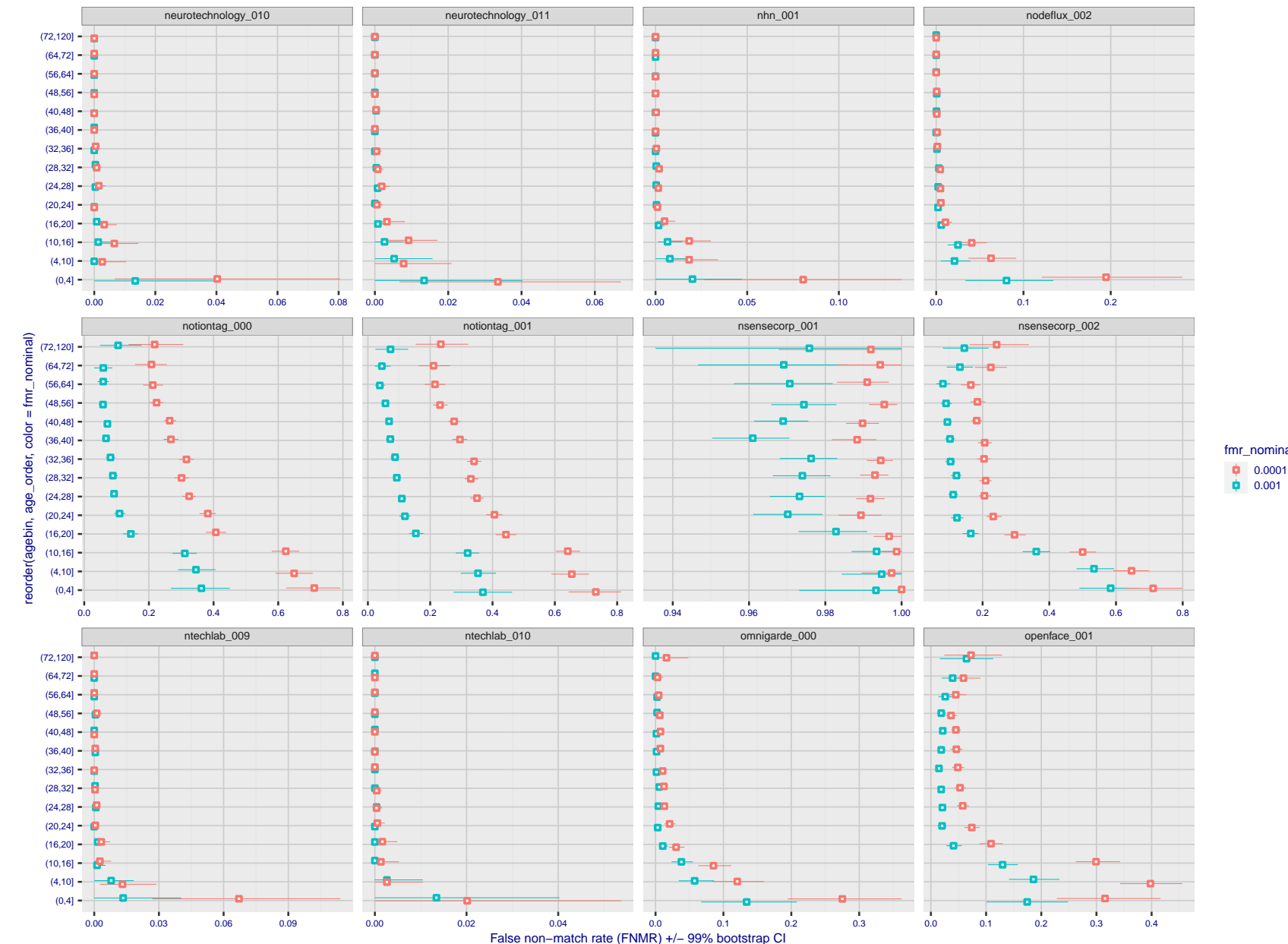


Figure 260: For the visa images, the dots show FNMR by age group for two operating thresholds corresponding to $FMR = \{0.001, 0.0001\}$ computed over all on the order of 10^{10} impostor scores. The FMR in each bin will vary also - see subsequent impostor heatmaps in sec. 3.6.2. Given a pair of face images taken at different times, we assign the comparison to the bin that is the arithmetic average of the subject's ages. This plot shows only the effect of age, not ageing. The number of comparisons in each bin is generally in the thousands, however the first and last bins are computed over 149 and 124 respectively. The error rates in some (adult) cases are zero, and in others the DET is flat so the error rates at the two thresholds are identical. The lines span 1% and 99% of bootstrap replicated FNMR estimates.

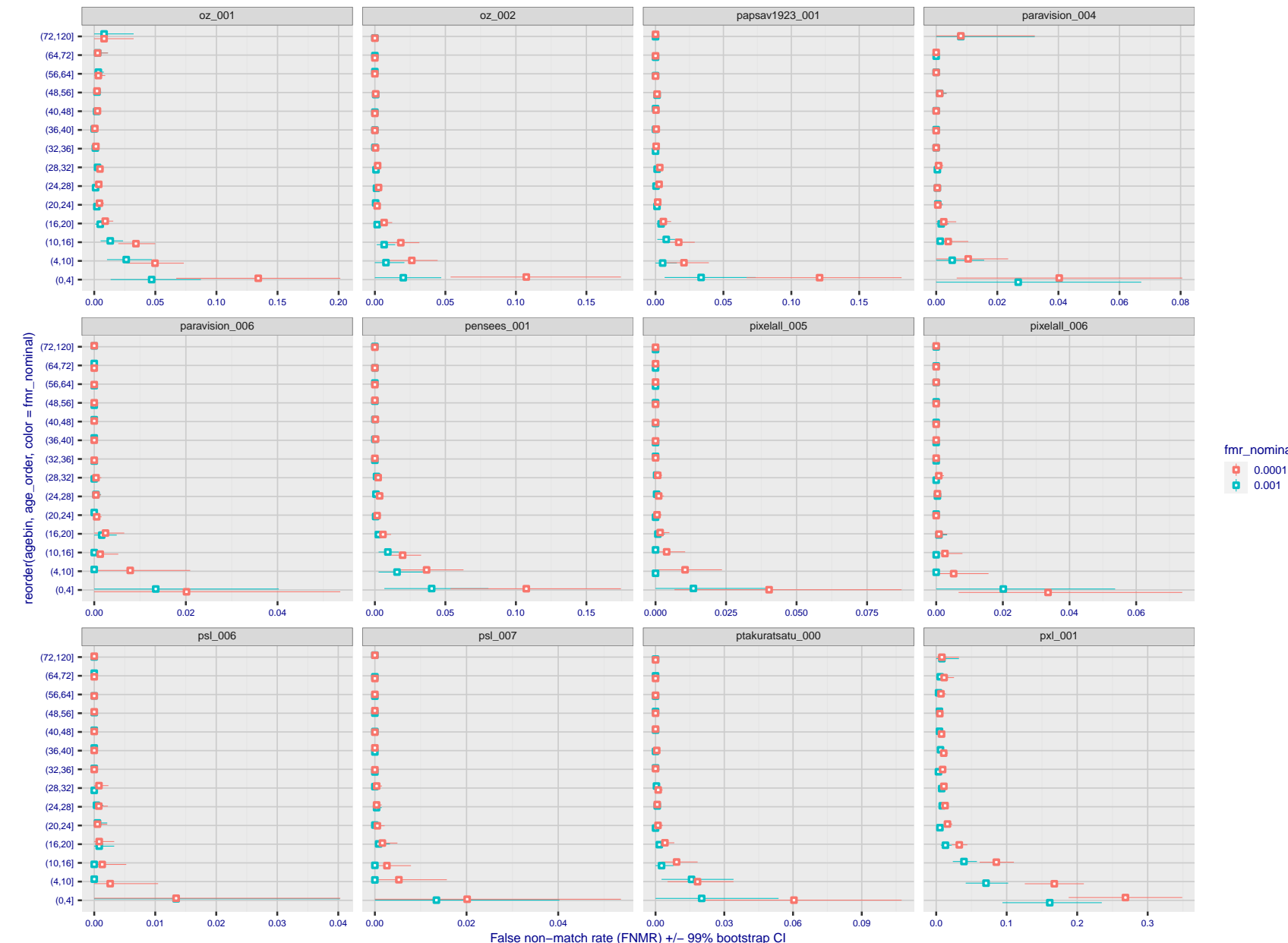


Figure 261: For the visa images, the dots show FNMR by age group for two operating thresholds corresponding to $FMR = \{0.001, 0.0001\}$ computed over all on the order of 10^{10} impostor scores. The FMR in each bin will vary also - see subsequent impostor heatmaps in sec. 3.6.2. Given a pair of face images taken at different times, we assign the comparison to the bin that is the arithmetic average of the subject's ages. This plot shows only the effect of age, not ageing. The number of comparisons in each bin is generally in the thousands, however the first and last bins are computed over 149 and 124 respectively. The error rates in some (adult) cases are zero, and in others the DET is flat so the error rates at the two thresholds are identical. The lines span 1% and 99% of bootstrap replicated FNMR estimates.

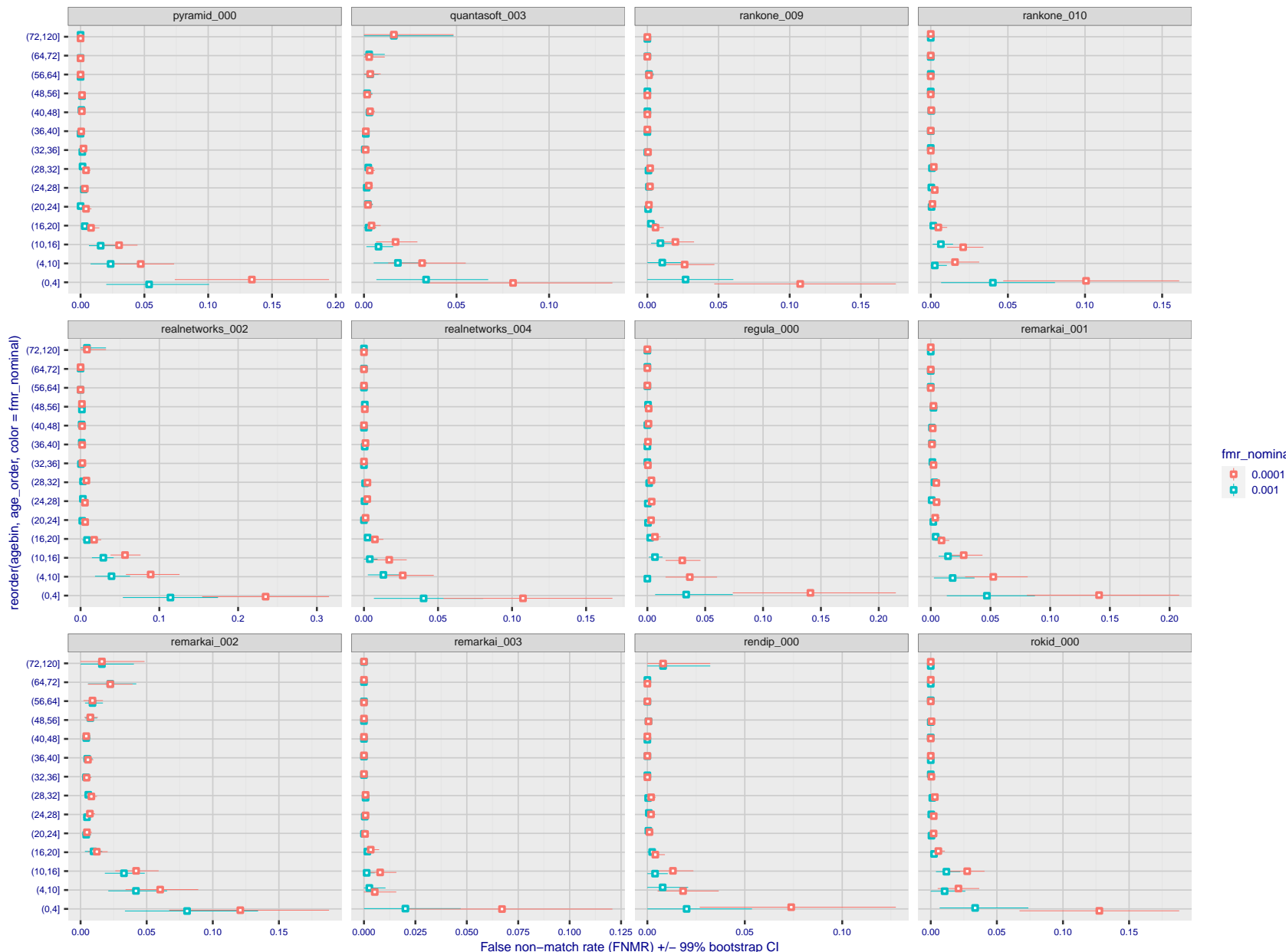
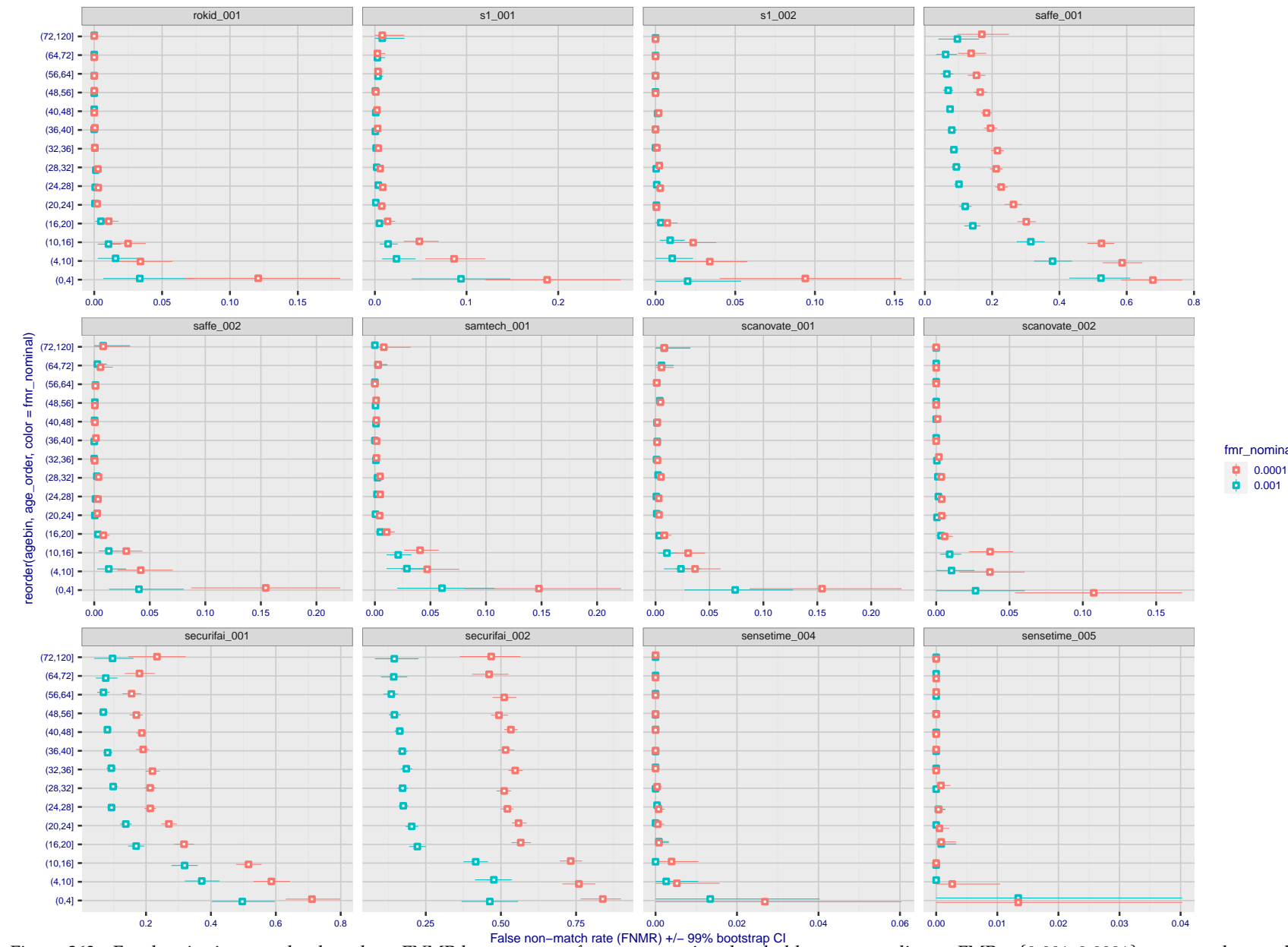


Figure 262: For the visa images, the dots show FNMR by age group for two operating thresholds corresponding to $FMR = \{0.001, 0.0001\}$ computed over all on the order of 10^{10} impostor scores. The FMR in each bin will vary also - see subsequent impostor heatmaps in sec. 3.6.2. Given a pair of face images taken at different times, we assign the comparison to the bin that is the arithmetic average of the subject's ages. This plot shows only the effect of age, not ageing. The number of comparisons in each bin is generally in the thousands, however the first and last bins are computed over 149 and 124 respectively. The error rates in some (adult) cases are zero, and in others the DET is flat so the error rates at the two thresholds are identical. The lines span 1% and 99% of bootstrap replicated FNMR estimates.



fmr_nominal
0.0001
0.001

Figure 263: For the visa images, the dots show FNMR by age group for two operating thresholds corresponding to $FMR = \{0.001, 0.0001\}$ computed over all on the order of 10^{10} impostor scores. The FMR in each bin will vary also - see subsequent impostor heatmaps in sec. 3.6.2. Given a pair of face images taken at different times, we assign the comparison to the bin that is the arithmetic average of the subject's ages. This plot shows only the effect of age, not ageing. The number of comparisons in each bin is generally in the thousands, however the first and last bins are computed over 149 and 124 respectively. The error rates in some (adult) cases are zero, and in others the DET is flat so the error rates at the two thresholds are identical. The lines span 1% and 99% of bootstrap replicated FNMR estimates.

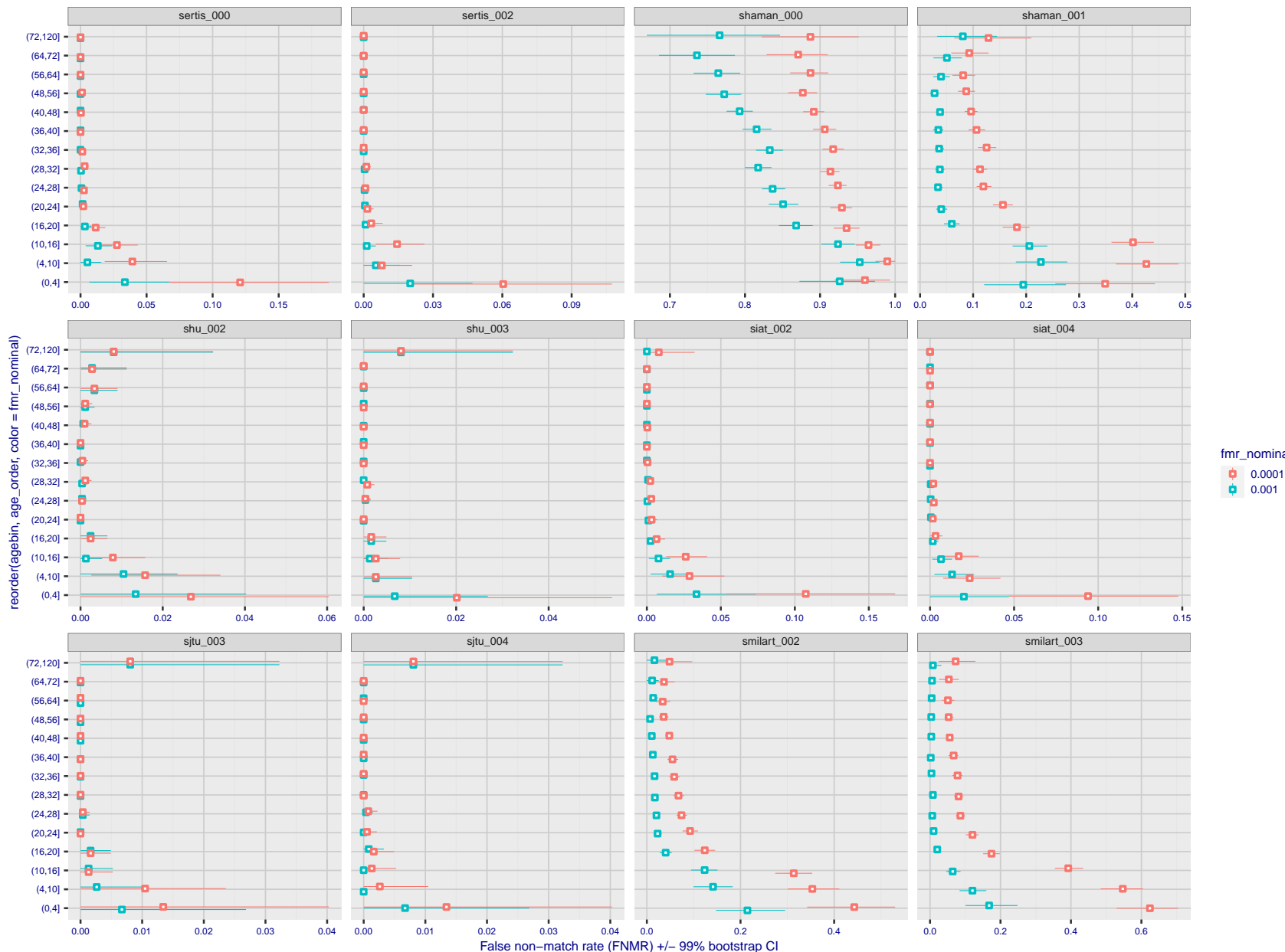


Figure 264: For the visa images, the dots show FNMR by age group for two operating thresholds corresponding to $FMR = \{0.001, 0.0001\}$ computed over all on the order of 10^{10} impostor scores. The FMR in each bin will vary also - see subsequent impostor heatmaps in sec. 3.6.2. Given a pair of face images taken at different times, we assign the comparison to the bin that is the arithmetic average of the subject's ages. This plot shows only the effect of age, not ageing. The number of comparisons in each bin is generally in the thousands, however the first and last bins are computed over 149 and 124 respectively. The error rates in some (adult) cases are zero, and in others the DET is flat so the error rates at the two thresholds are identical. The lines span 1% and 99% of bootstrap replicated FNMR estimates.



Figure 265: For the visa images, the dots show FNMR by age group for two operating thresholds corresponding to $FMR = \{0.001, 0.0001\}$ computed over all on the order of 10^{10} impostor scores. The FMR in each bin will vary also - see subsequent impostor heatmaps in sec. 3.6.2. Given a pair of face images taken at different times, we assign the comparison to the bin that is the arithmetic average of the subject's ages. This plot shows only the effect of age, not ageing. The number of comparisons in each bin is generally in the thousands, however the first and last bins are computed over 149 and 124 respectively. The error rates in some (adult) cases are zero, and in others the DET is flat so the error rates at the two thresholds are identical. The lines span 1% and 99% of bootstrap replicated FNMR estimates.

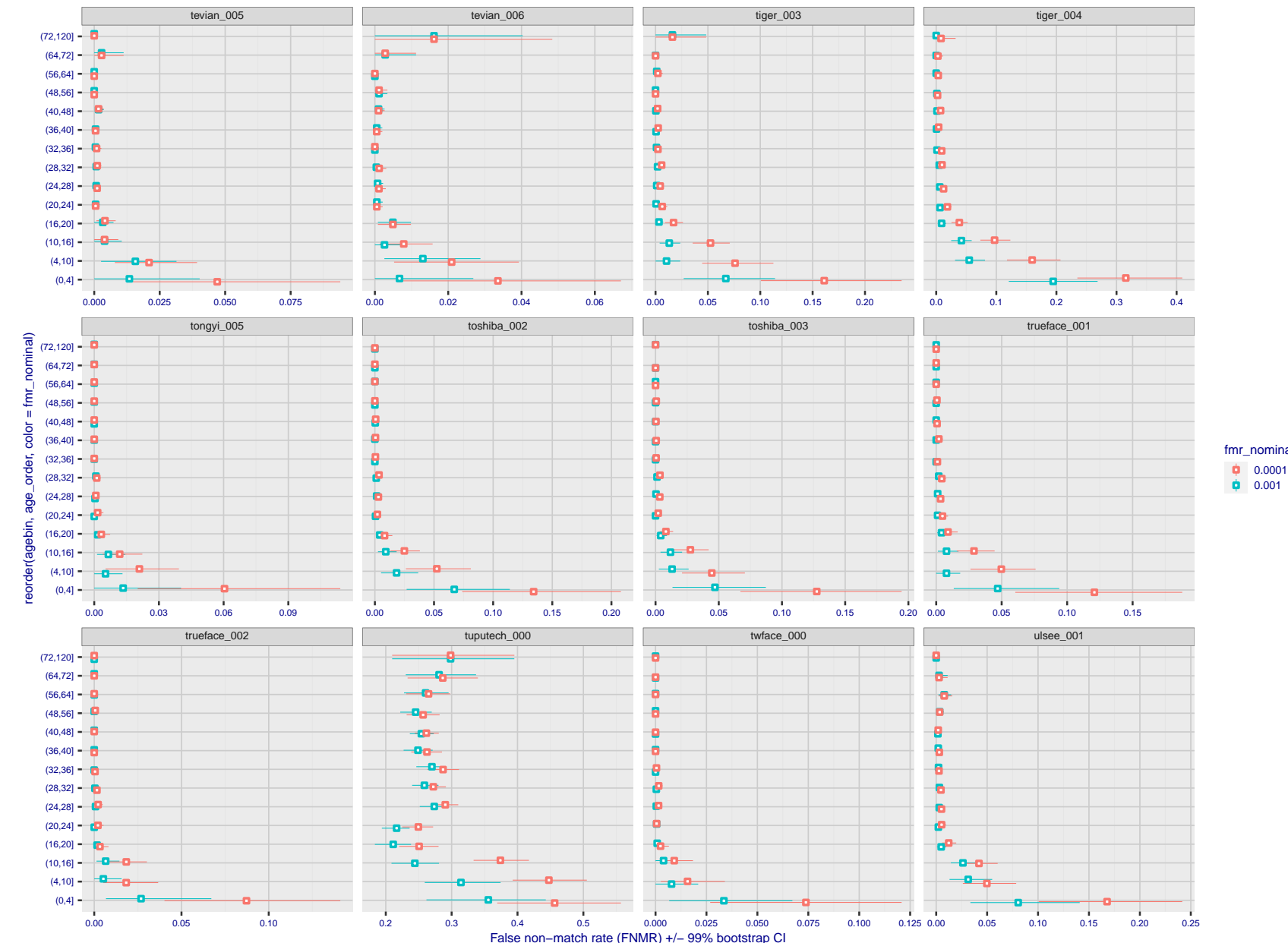


Figure 266: For the visa images, the dots show FNMR by age group for two operating thresholds corresponding to $FMR = \{0.001, 0.0001\}$ computed over all on the order of 10^{10} impostor scores. The FMR in each bin will vary also - see subsequent impostor heatmaps in sec. 3.6.2. Given a pair of face images taken at different times, we assign the comparison to the bin that is the arithmetic average of the subject's ages. This plot shows only the effect of age, not ageing. The number of comparisons in each bin is generally in the thousands, however the first and last bins are computed over 149 and 124 respectively. The error rates in some (adult) cases are zero, and in others the DET is flat so the error rates at the two thresholds are identical. The lines span 1% and 99% of bootstrap replicated FNMR estimates.

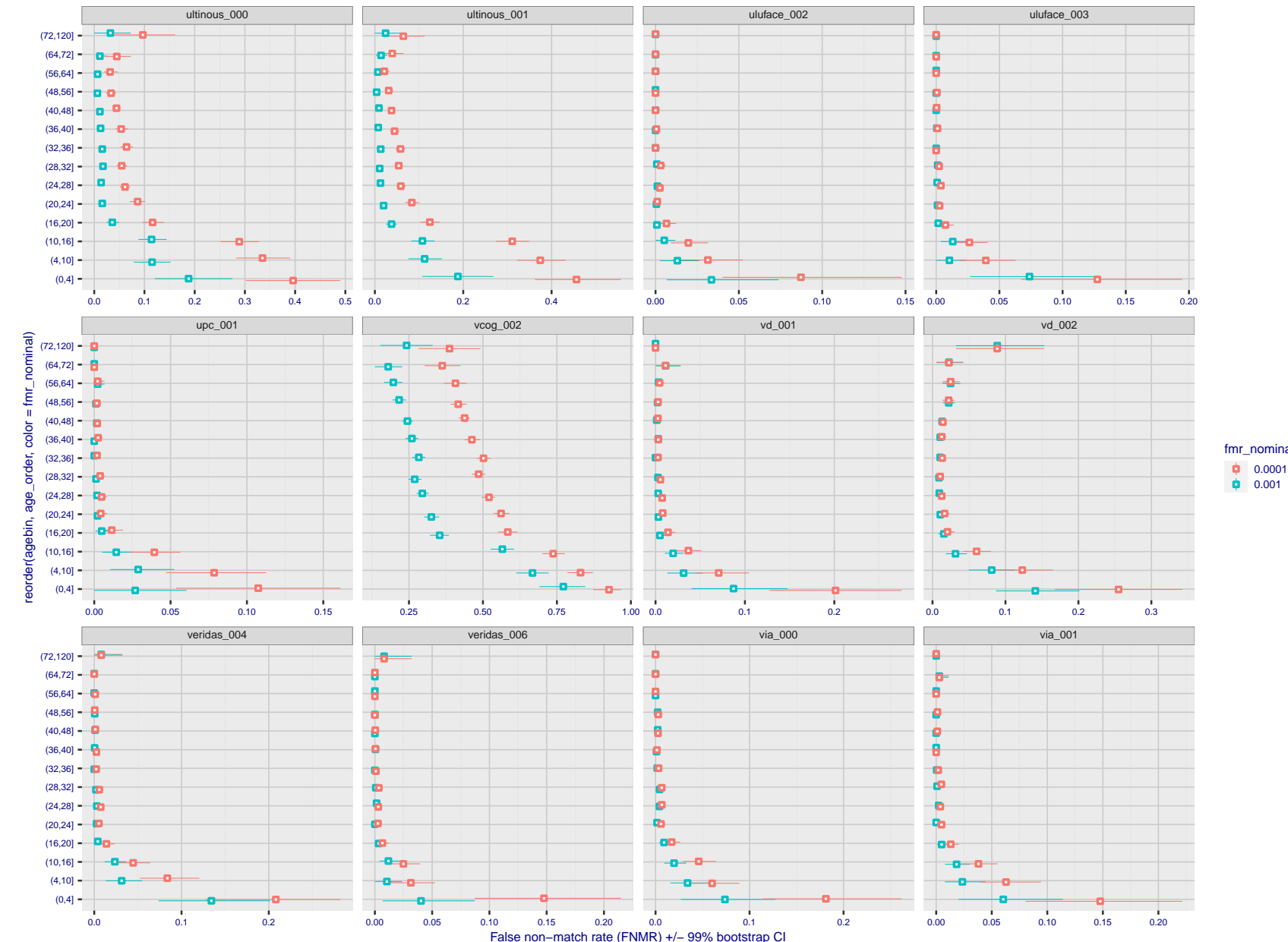


Figure 267: For the visa images, the dots show FNMR by age group for two operating thresholds corresponding to $FMR = \{0.001, 0.0001\}$ computed over all on the order of 10^{10} impostor scores. The FMR in each bin will vary also - see subsequent impostor heatmaps in sec. 3.6.2. Given a pair of face images taken at different times, we assign the comparison to the bin that is the arithmetic average of the subject's ages. This plot shows only the effect of age, not ageing. The number of comparisons in each bin is generally in the thousands, however the first and last bins are computed over 149 and 124 respectively. The error rates in some (adult) cases are zero, and in others the DET is flat so the error rates at the two thresholds are identical. The lines span 1% and 99% of bootstrap replicated FNMR estimates.

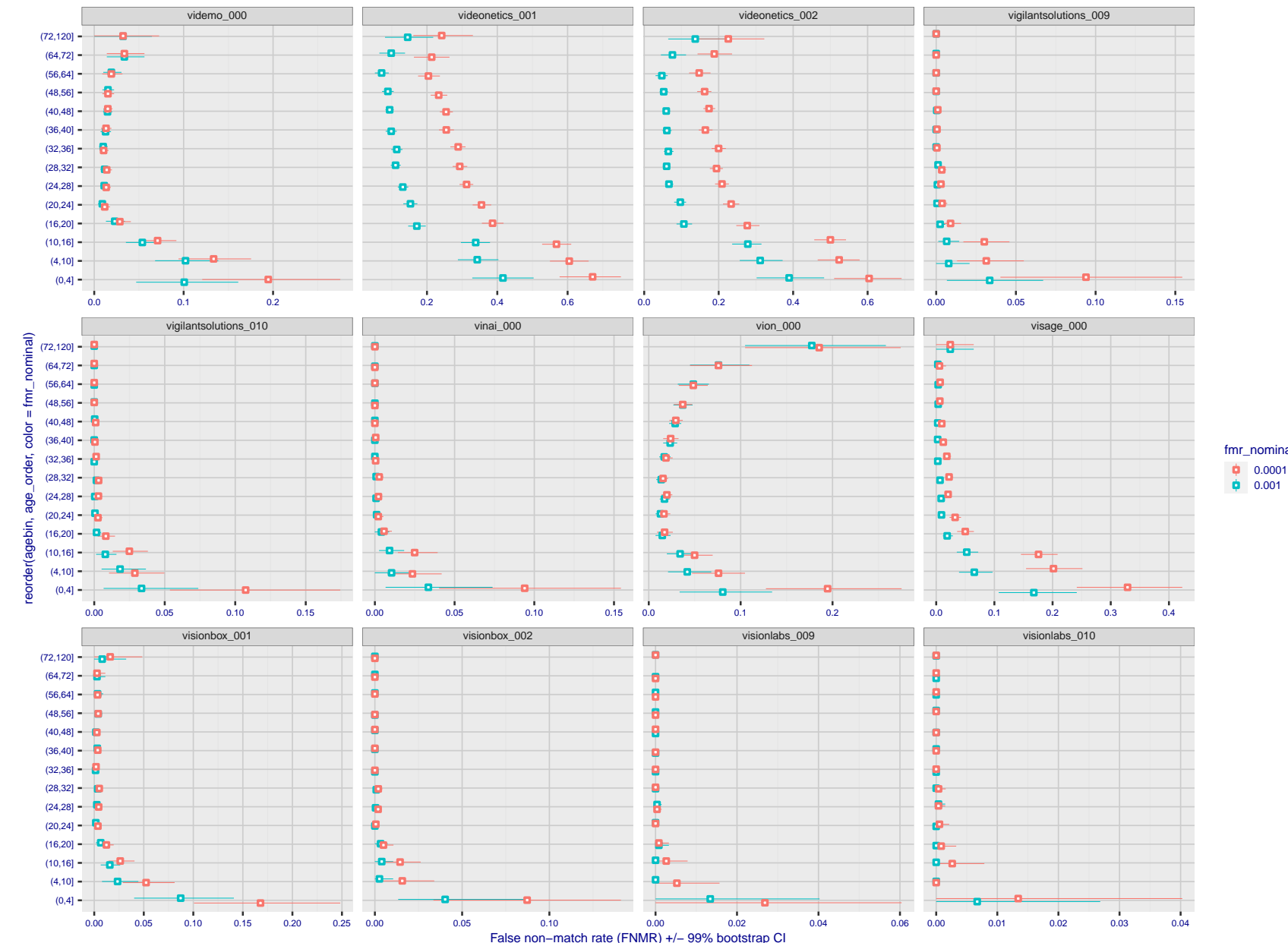


Figure 268: For the visa images, the dots show FNMR by age group for two operating thresholds corresponding to $FMR = \{0.001, 0.0001\}$ computed over all on the order of 10^{10} impostor scores. The FMR in each bin will vary also - see subsequent impostor heatmaps in sec. 3.6.2. Given a pair of face images taken at different times, we assign the comparison to the bin that is the arithmetic average of the subject's ages. This plot shows only the effect of age, not ageing. The number of comparisons in each bin is generally in the thousands, however the first and last bins are computed over 149 and 124 respectively. The error rates in some (adult) cases are zero, and in others the DET is flat so the error rates at the two thresholds are identical. The lines span 1% and 99% of bootstrap replicated FNMR estimates.

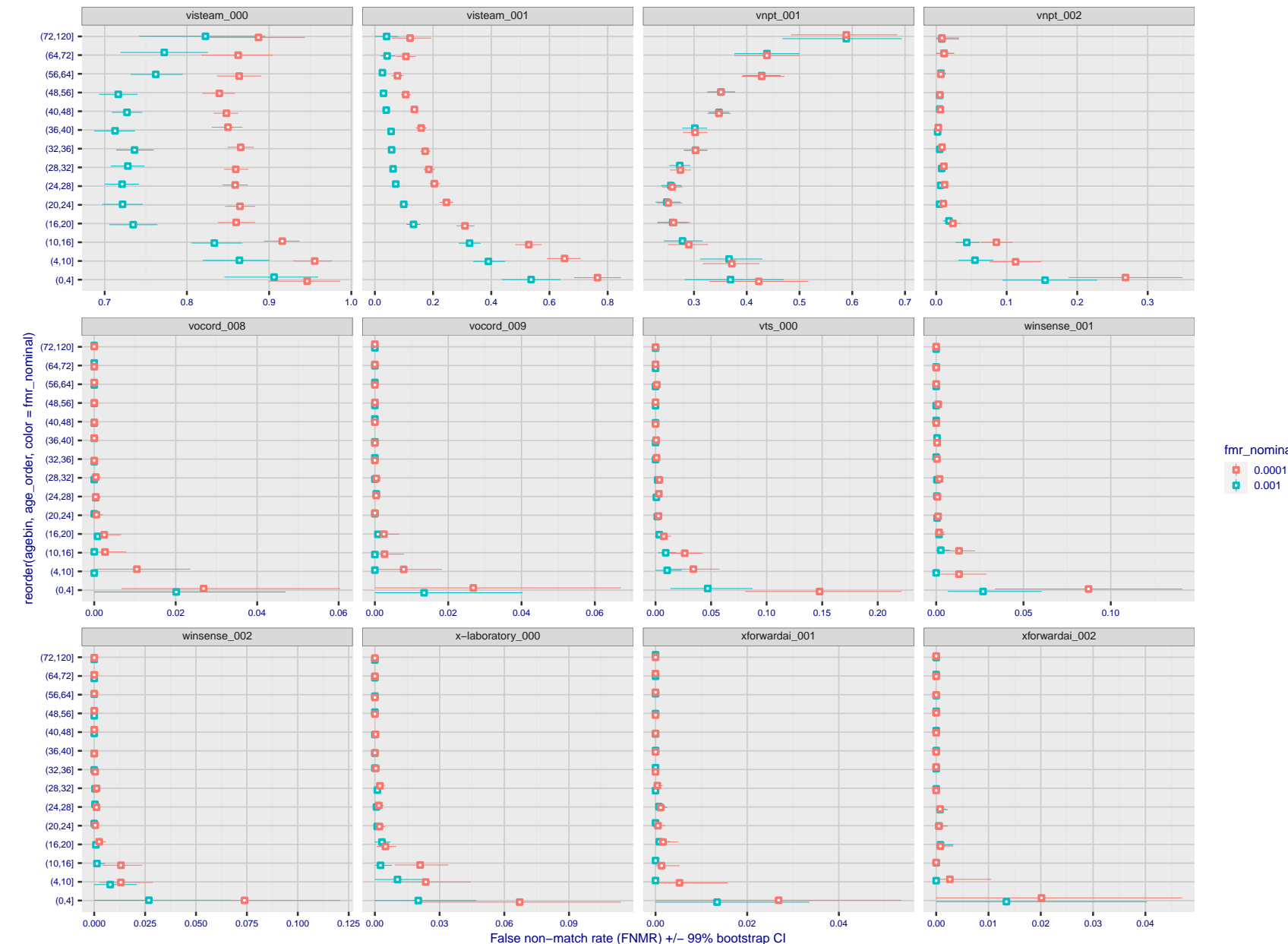


Figure 269: For the visa images, the dots show FNMR by age group for two operating thresholds corresponding to $FMR = \{0.001, 0.0001\}$ computed over all on the order of 10^{10} impostor scores. The FMR in each bin will vary also - see subsequent impostor heatmaps in sec. 3.6.2. Given a pair of face images taken at different times, we assign the comparison to the bin that is the arithmetic average of the subject's ages. This plot shows only the effect of age, not ageing. The number of comparisons in each bin is generally in the thousands, however the first and last bins are computed over 149 and 124 respectively. The error rates in some (adult) cases are zero, and in others the DET is flat so the error rates at the two thresholds are identical. The lines span 1% and 99% of bootstrap replicated FNMR estimates.

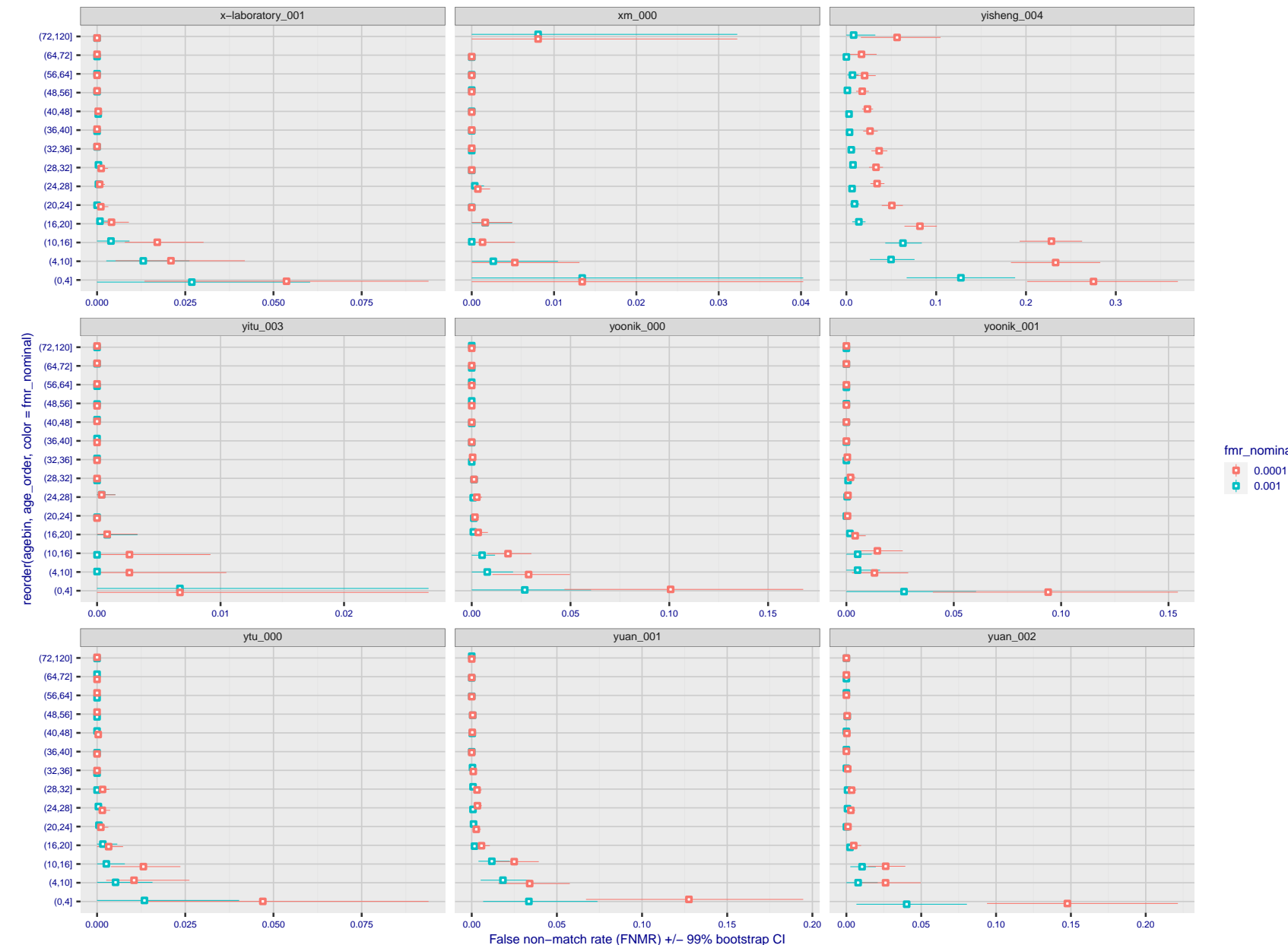


Figure 270: For the visa images, the dots show FNMR by age group for two operating thresholds corresponding to $FMR = \{0.001, 0.0001\}$ computed over all on the order of 10^{10} impostor scores. The FMR in each bin will vary also - see subsequent impostor heatmaps in sec. 3.6.2. Given a pair of face images taken at different times, we assign the comparison to the bin that is the arithmetic average of the subject's ages. This plot shows only the effect of age, not ageing. The number of comparisons in each bin is generally in the thousands, however the first and last bins are computed over 149 and 124 respectively. The error rates in some (adult) cases are zero, and in others the DET is flat so the error rates at the two thresholds are identical. The lines span 1% and 99% of bootstrap replicated FNMR estimates.

Caveats: None.

3.6 Impostor distribution stability

3.6.1 Effect of birth place on the impostor distribution

Background: Facial appearance varies geographically, both in terms of skin tone, cranio-facial structure and size. This section addresses whether false match rates vary intra- and inter-regionally.

Goals:

- ▷ To show the effect of birth region of the impostor and enrollee on false match rates.
- ▷ To determine whether some algorithms give better impostor distribution stability.

Methods:

- ▷ For the visa images, NIST defined 10 regions: Sub-Saharan Africa, South Asia, Polynesia, North Africa, Middle East, Europe, East Asia, Central and South America, Central Asia, and the Caribbean.
- ▷ For the visa images, NIST mapped each country of birth to a region. There is some arbitrariness to this. For example, Egypt could reasonably be assigned to the Middle East instead of North Africa. An alternative methodology could, for example, assign the Philippines to *both* Polynesia and East Asia.
- ▷ FMR is computed for cases where all face images of impostors born in region r_2 are compared with enrolled face images of persons born in region r_1 .

$$\text{FMR}(r_1, r_2, T) = \frac{\sum_{i=1}^{N_{r_1, r_2}} H(s_i - T)}{N_{r_1, r_2}} \quad (5)$$

where the same threshold, T , is used in all cells, and H is the unit step function. The threshold is set to give $\text{FMR}(T) = 0.001$ over the entire set of visa image impostor comparisons.

- ▷ This analysis is then repeated by country-pair, but only for those country pairs where both have at least 1000 images available. The countries¹ appear in the axes of graphs that follow.
- ▷ The mean number of impostor scores in any cross-region bin is 33 million. The smallest number of impostor scores in any bin is 135000, for Central Asia - North Africa. While these counts are large enough to support reasonable significance, the number of individual faces is much smaller, on the order of $N^{0.5}$.
- ▷ The numbers of impostor scores in any cross-country bin is shown in Figure ??.

Results: Subsequent figures show heatmaps that use color to represent the base-10 logarithm of the false match rate. Red colors indicate high (bad) false match rates. Dark colors indicate benign false match rates. There are two series of graphs corresponding to aggregated geographical regions, and to countries. The notable observations are:

- ▷ The on-diagonal elements correspond to within-region impostors. FMR is generally above the nominal value of $\text{FMR} = 0.001$. Particularly there is usually higher FMR in, Sub-Saharan Africa, South Asia, and the Caribbean. Europe and Central Asia, on the other hand, usually give FMR closer to the nominal value.
- ▷ The off-diagonal elements correspond to across-region impostors. The highest FMR is produced between the Caribbean and Sub-Saharan Africa.
- ▷ Algorithms vary.

¹These are Argentina, Australia, Brazil, Chile, China, Costa Rica, Cuba, Czech Republic, Dominican Republic, Ecuador, Egypt, El Salvador, Germany, Ghana, Great Britain, Greece, Guatemala, Haiti, Hong Kong, Honduras, Indonesia, India, Israel, Jamaica, Japan, Kenya, Korea, Lebanon, Mexico, Malaysia, Nepal, Nigeria, Peru, Philippines, Pakistan, Poland, Romania, Russia, South Africa, Saudi Arabia, Thailand, Trinidad, Turkey, Taiwan, Ukraine, Venezuela, and Vietnam.

Figure 271: For the visa images, the dots show FMR for impostor comparisons of individuals of the same sex and same age group for the region of the world that gives the worst (highest) FMR when the threshold is set to give $FMR = 0.001$ (red vertical line) over all on the order of 10^{10} impostor scores i.e. zero-effort. The shift of the dots to right shows massive increases in FMR when impostors have the same sex, age, and region of birth. The color code indicates which region gives the worst case FMR. If the observed variation is due to the prevalence of one kind of images in the training imagery, then algorithms developed on one kind of data might be expected to give higher FMR on other kinds.

- ▷ We computed the same quantities for a global FMR = 0.0001. The effects are similar.

Caveats:

- ▷ The effects of variable impostor rates on one-to-many identification systems may well differ from what's implied by these one-to-one verification results. Two reasons for this are a) the enrollment galleries are usually imbalanced across countries of birth, age and sex; b) one-to-many identification algorithms often implement techniques aimed at stabilizing the impostor distribution. Further research is necessary.
- ▷ In principle, the effects seen in this subsection could be due to differences in the image capture process. We consider this unlikely since the effects are maintained across geography - e.g. Caribbean vs. Africa, or Japan vs. China.

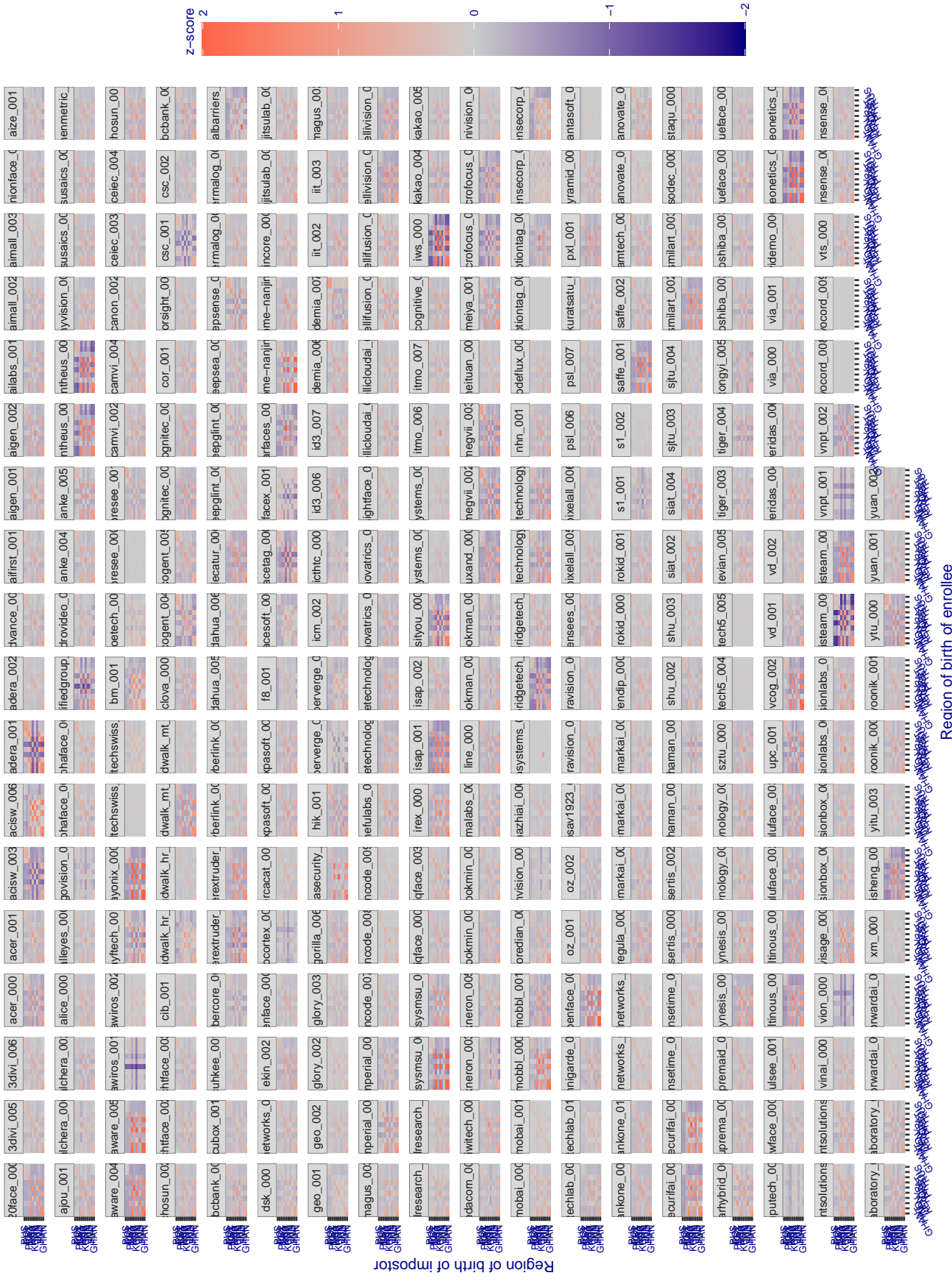


Figure 272: For visa images, the heatmap shows how the mean of the impostor distribution for the country pair (a,b) is shifted relative to the mean of the global impostor distribution, expressed as a number of standard deviations of the global impostor distribution. This statistic is designed to show shifts in the entire impostor distribution, not just tail effects that manifest as the anomalously high (or low) false match rates that appear in the subsequent figures. The countries are chosen to show that skin tone alone does not explain impostor distribution shifts. The reduced shift in Asian populations with the Yitu and Tong YiTrans algorithms, is accompanied by positive shifts in the European populations. This reversal relative to most other algorithms, may derive from use of nationally weighted training sets. The figure is computed from same-sex and same-age impostor pairs.

3.6.2 Effect of age on impostors

Background: This section shows the effect of age on the impostor distribution. The ideal behaviour is that the age of the enrollee and the impostor would not affect impostor scores. This would support FMR stability over sub-populations.

Goals:

- ▷ To show the effect of relative ages of the impostor and enrollee on false match rates.
- ▷ To determine whether some algorithms have better impostor distribution stability.

Methods:

- ▷ Define 14 age group bins, spanning 0 to over 100 years old.
- ▷ Compute FMR over all impostor comparisons for which the subjects in the enrollee and impostor images have ages in two bins.
- ▷ Compute FMR over all impostor comparisons for which the subjects are additionally of the same sex, and born in the same geographic region.

Results:

The notable aspects are:

- ▷ Diagonal dominance: Impostors are more likely to be matched against their same age group.
- ▷ Same sex and same region impostors are more successful. On the diagonal, an impostor is more likely to succeed by posing as someone of the same sex. If $\Delta \log_{10} \text{FMR} = 0.2$, then same-sex same-region FMR exceeds the all-pairs FMR by factor of $10^{0.2} = 1.6$.
- ▷ Young children impostors give elevated FMR against young children. Older adult impostor give elevated FMR against older adults. These effects are quite large, for example if $\Delta \log_{10} \text{FMR} = 1.0$ larger than a 32 year old, then these groups have higher FMR by a factor of $10^1 = 10$. This would imply an FMR above 0.01 for a nominal (global) FMR = 0.001.
- ▷ Algorithms vary.
- ▷ We computed the same quantities for a global FMR = 0.0001. The effects are similar.

Note the calculations in this section include impostors paired across all countries of birth.

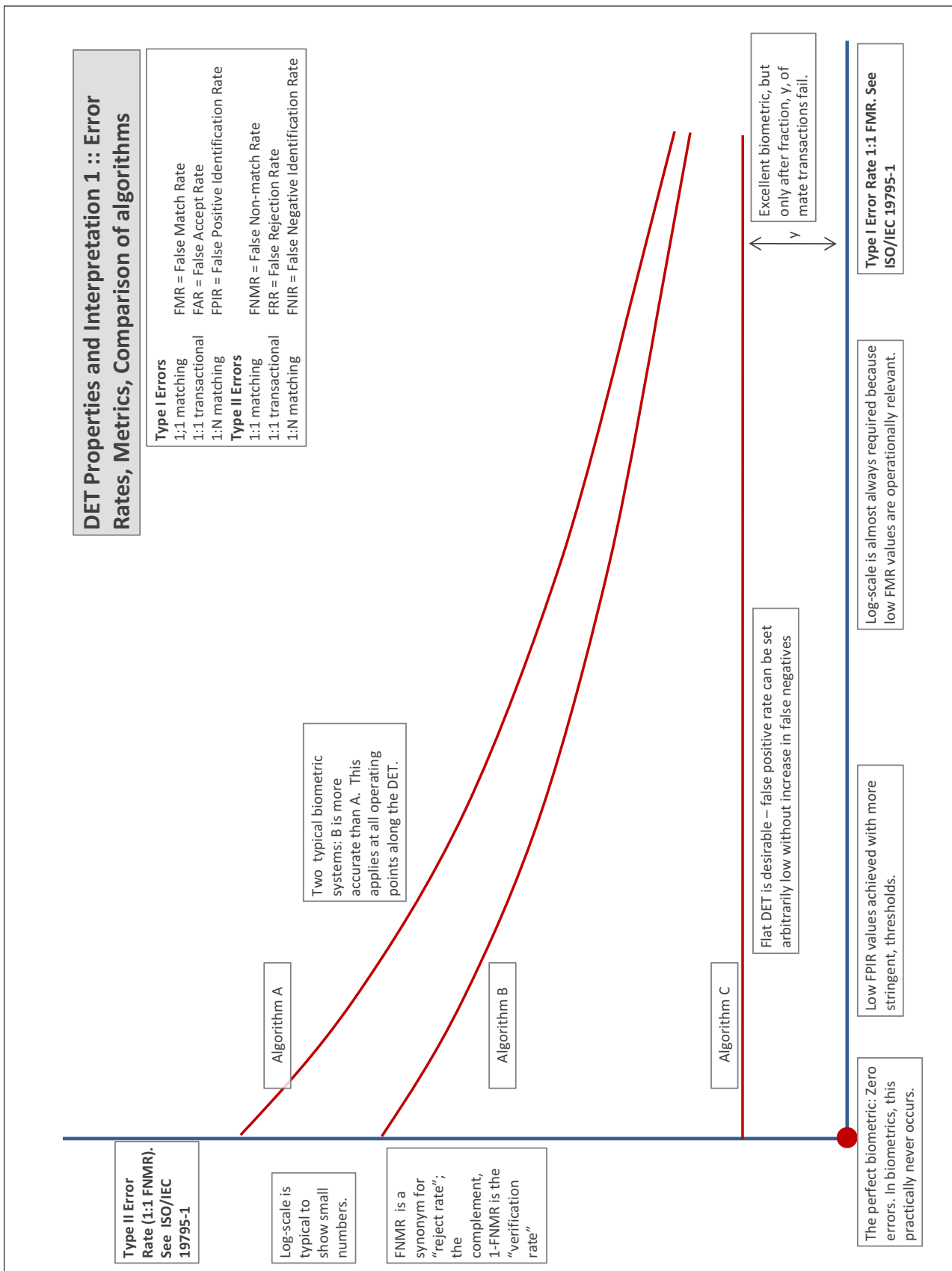
Accuracy Terms + Definitions

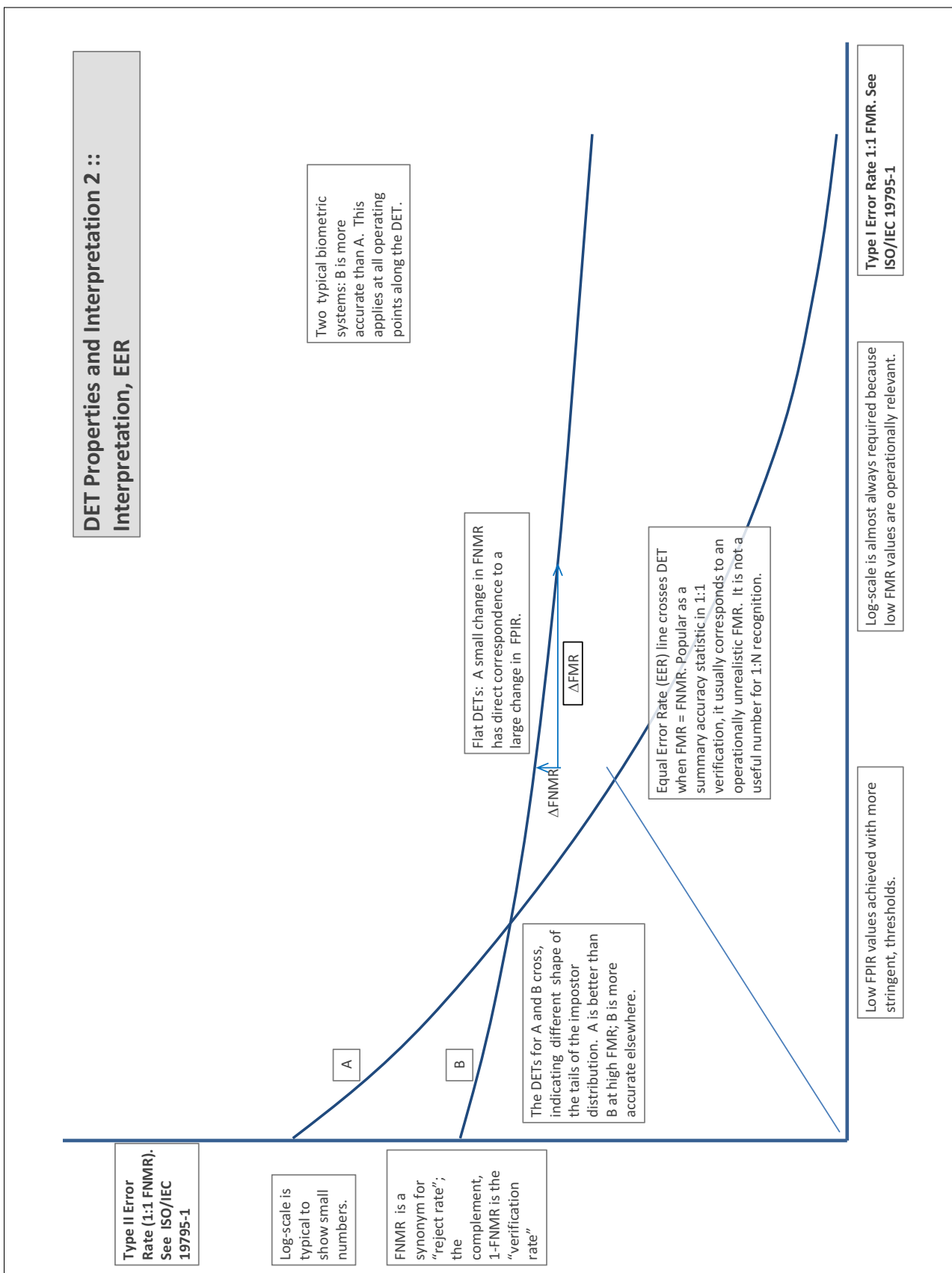
In biometrics, Type II errors occur when two samples of one person do not match – this is called a **false negative**. Correspondingly, Type I errors occur when samples from two persons do match – this is called a **false positive**. Matches are declared by a biometric system when the native comparison score from the recognition algorithm meets some **threshold**. Comparison scores can be either **similarity scores**, in which case higher values indicate that the samples are more likely to come from the same person, or **dissimilarity scores**, in which case higher values indicate different people. Similarity scores are traditionally computed by **fingerprint** and **face** recognition algorithms, while dissimilarities are used in **iris recognition**. In some cases, the dissimilarity score is a distance; this applies only when **metric** properties are obeyed. In any case, scores can be either **mate** scores, coming from a comparison of one person's samples, or **nonmate** scores, coming from comparison of different persons' samples. The words **genuine** or **authentic** are synonyms for mate, and the word **impostor** is used as a synonym for nonmatch. The words mate and nonmatch are traditionally used in identification applications (such as law enforcement search, or background checks) while genuine and impostor are used in verification applications (such as access control).

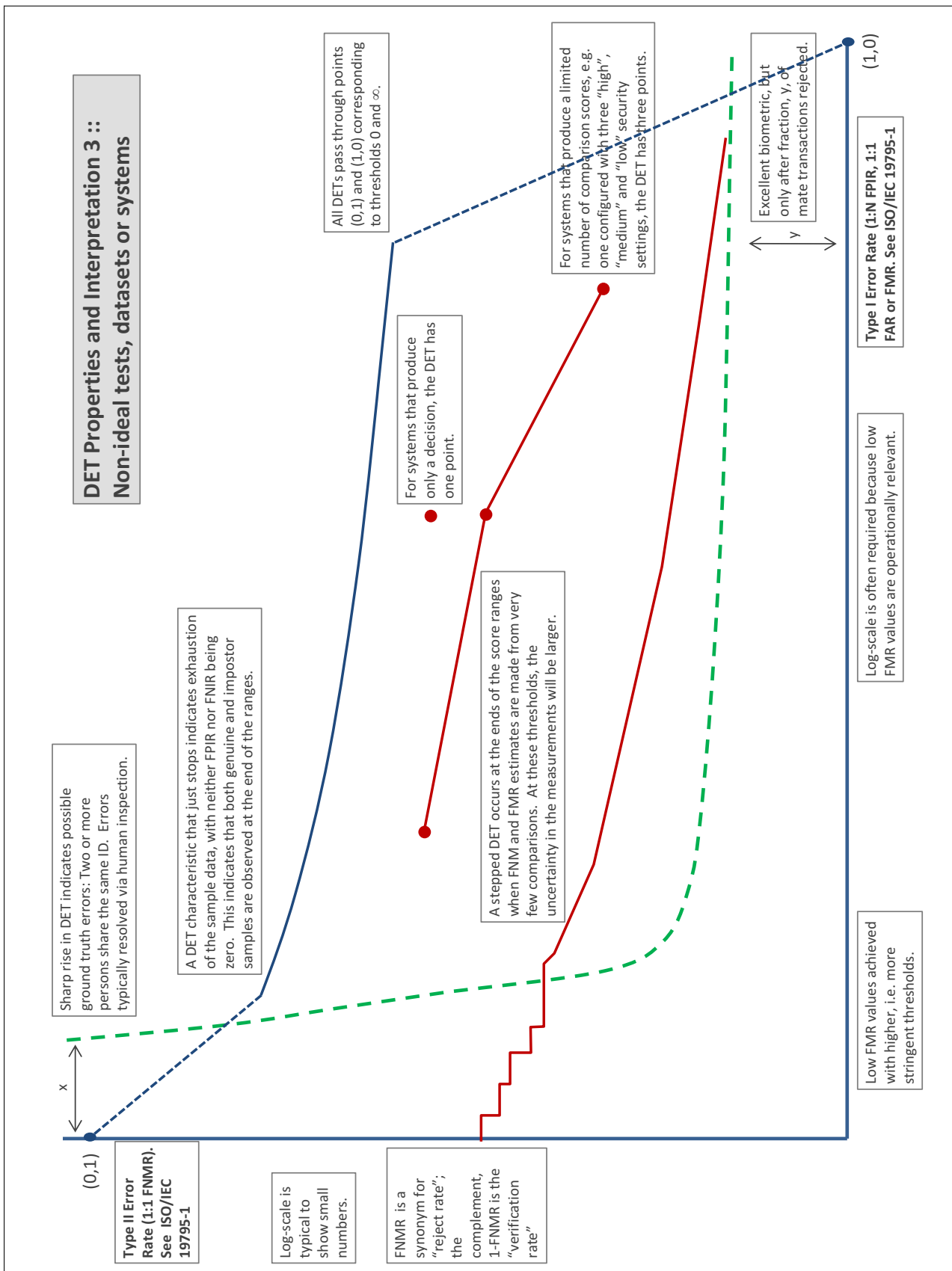
A **error tradeoff** characteristic represents the tradeoff between Type II and Type I classification errors. For verification this plots false non-match rate (FNMR) vs. false match rate (FMR) parametrically with T.

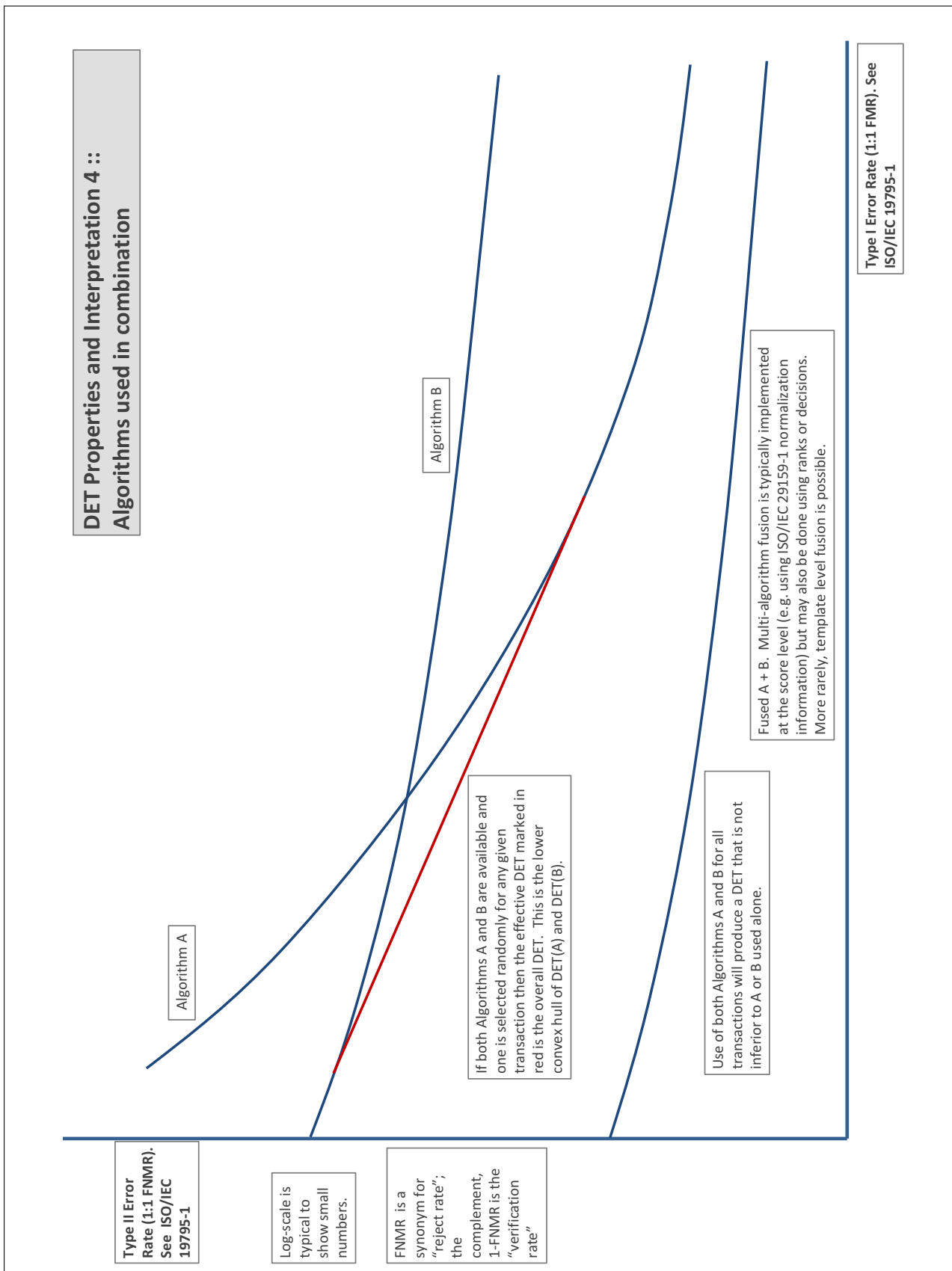
The error tradeoff plots are often called **detection error tradeoff (DET)** characteristics or **receiver operating characteristic (ROC)**. These serve the same function but differ, for example, in plotting the complement of an error rate (e.g., $TMR = 1 - FNMR$) and in transforming the axes most commonly using logarithms, to show multiple decades of FMR. More rarely, the function might be the inverse Gaussian function.

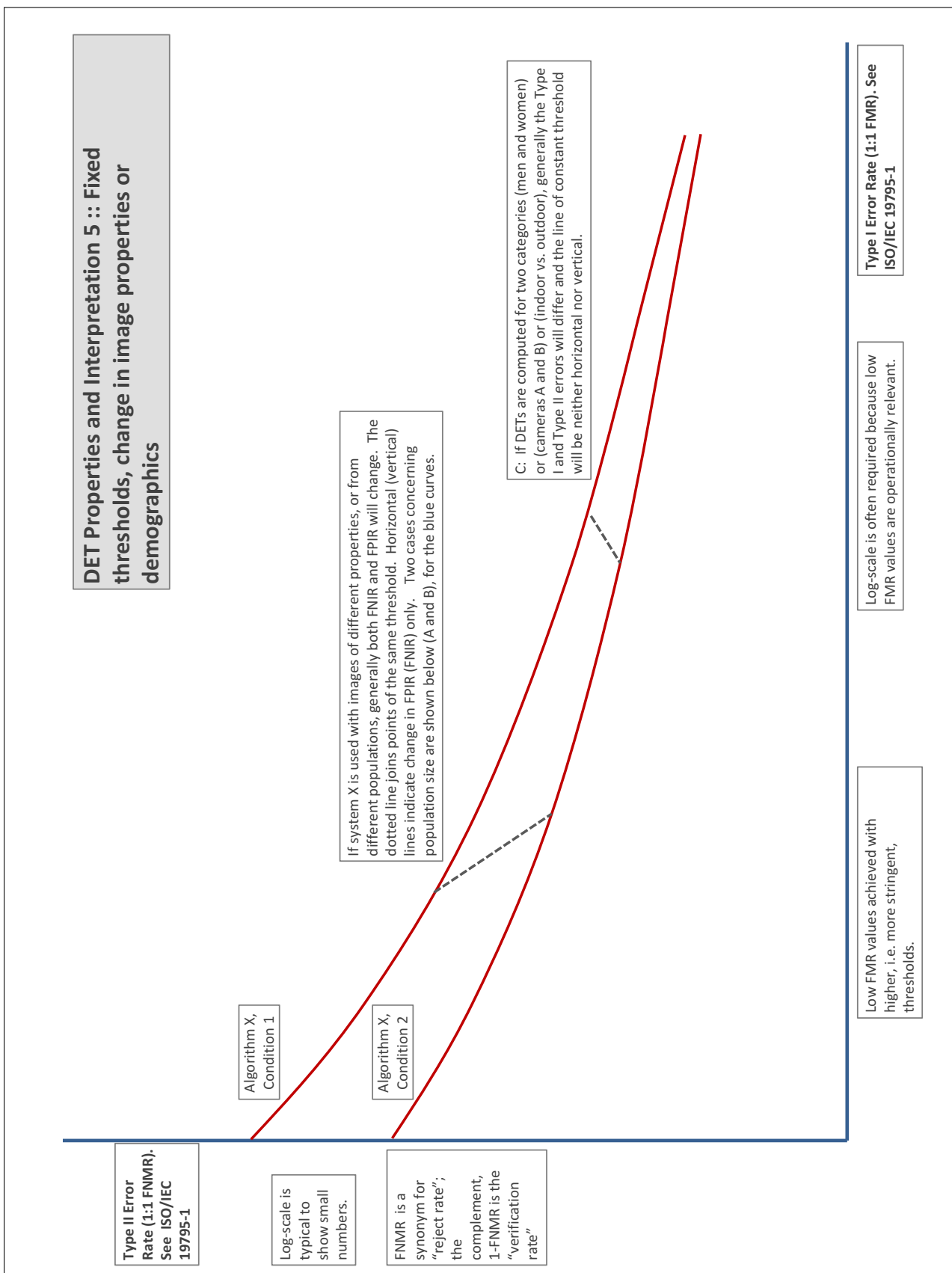
More detail and generality is provided in formal biometrics testing standards, see the various parts of [ISO/IEC 19795 Biometrics Testing and Reporting](#). More terms, including and beyond those to do with accuracy, see [ISO/IEC 2382-37 Information technology -- Vocabulary -- Part 37: Harmonized biometric vocabulary](#)











References

- [1] P. Jonathon Phillips, Amy N. Yates, Ying Hu, Carina A. Hahn, Eilidh Noyes, Kelsey Jackson, Jacqueline G. Cavazos, Géraldine Jeckeln, Rajeev Ranjan, Swami Sankaranarayanan, Jun-Cheng Chen, Carlos D. Castillo, Rama Chellappa, David White, and Alice J. O'Toole. Face recognition accuracy of forensic examiners, superrecognizers, and face recognition algorithms. *Proceedings of the National Academy of Sciences*, 115(24):6171–6176, 2018.